PACIFIC EARTHQUAKE ENGINEERING RESEARCH CENTER

The Third U.S.-Japan Workshop on Performance-Based Earthquake Engineering Methodology for Reinforced Concrete Building Structures

16–18 August 2001
Seattle, Washington

Sponsors:

Japan Ministry of Education, Science, Sports and Culture
Pacific Earthquake Engineering Research Center
U.S. National Science Foundation

PEER 2002/02
JULY 2002

The Third U.S.-Japan Workshop on Performance-Based Earthquake Engineering Methodology for Reinforced Concrete Building Structures

16–18 August 2001
Seattle, Washington

Organizers

Toshimi Kabeyasawa
Earthquake Research Institute
University of Tokyo

Jack P. Moehle
Pacific Earthquake Engineering Research Center
University of California, Berkeley

Sponsors

Japan Ministry of Education, Science, Sports and Culture
Pacific Earthquake Engineering Research Center
U.S. National Science Foundation

Research Report

PEER Report 2002/02
Pacific Earthquake Engineering Research Center
College of Engineering
University of California, Berkeley

July 2002

PREFACE

Considerable research is under way throughout the world to establish performance-based assessment and design methodology for buildings. Japan and the United States are at the forefront of this research effort, as well as the efforts to implement the research results. The U.S.-Japan Cooperative Research in Urban Earthquake Disaster Mitigation, sponsored in Japan by the Ministry of Education, Science, Sports and Culture, and in the U.S. by the National Science Foundation, is funding collaborative research in Japan and the U.S. The Pacific Earthquake Engineering Research Center in the U.S. has established the development of performance-based earthquake engineering methodology as its primary mission. Because of the importance of this topic, it is timely for researchers and practitioners from the U.S. and Japan to meet to exchange technical data and ideas as well as to identify issues of mutual concern and opportunities for cooperative study.

The Third U.S.-Japan Workshop on Performance-Based Earthquake Engineering Methodology for Reinforced Concrete Building Structures was organized to meet the needs and opportunities for research and practice in performance-based engineering. The objectives of the workshop were threefold: (1) to discuss different perspectives on performance-based engineering as it is applied to new and existing concrete buildings in Japan and the United States; (2) to exchange the latest findings related to the same subject; and (3) to enhance communications and promote opportunities for new and continuing collaboration.

The third workshop was held 16 to 18 August 2001 in Seattle, Washington. It was attended by 15 Japanese and 14 U.S. participants, as well as 2 from Taiwan, 5 from the Fédération Internationale du Béton (FIB) working group, and several observers.

U.S. SIDE	JAPAN SIDE
Mark Aschheim, U Illinois Anil Chopra, UC Berkeley Craig Comartin, Comartin-Reis Gregory Deierlein, Stanford U Marc Eberhard, U Washington Wilfred D. Iwan, California Inst. of Technology James Jirsa, U Texas Mervyn Kowalsky, North Carolina SU Dawn Lehman, U Washington Eduardo Miranda, Stanford U Jack Moehle, UC Berkeley Julio Ramirez, Purdue U Michael Valley, Skilling, Ward & Magnusson Sharon Wood, U Texas	Toshikatsu Ichinose, Nagoya IT Toshimi Kabeyasawa, ERI, U Tokyo Daisuke Kato, Niigata U Kazuhiro Kitayama, Tokyo Metro U Koichi Kusunoki, BRI Kanging Li, EDM, NIED Masaki Maeda, Tohoku U Minehiro Nishiyama, Kyoto U Shunsuke Otani, U Tokyo Hitoshi Shiohara, U Tokyo Hitoshi Tanaka, DPRI, Kyoto U Akira Tasai, Yokohama NU Masaru Teraoka, Fujita Corp Masaomi Teshigawara, BRI Manabu Yoshimura, Tokyo Metro U

Taiwan	FIB Group
Chin-Hsiung Loh, NCREE Keh-Chyuan Tsai, National Taiwan U	Michele Calvi Matej Fishinger Peter Fajfar, U Ljubljana Michael Fardis, U Patris, Greece Mario Rodriquez, National U Mexico

Front row: Toshikatsu Ichinose, Mario Rodriguez, Hitoshi (Jin) Tanaka, Kangning Li, Eduardo Miranda, Matej Fishinger, Masaru Teroaka, Shunsuke Otani, and Dawn Lehman

Middle row: Minehiro Nishiyama, Chin-Hsiung Loh, Daisuke Kato, and Masaki Maeda

Back row: Hitoshi Shiohara, Michele Calvi, Peter Fajfar, Paulo Pinto, Jack Moehle, Michael Valley, Keh-Chyuan Tsai, Manabu Yoshimura, Marc Eberhard, Craig Comartin, Gregory Deierlein, Marc Aschheim, Wilfred Iwan, James Jirsa, Masaomi Teshigawara, Mervyn Kowalsky, Sharon Wood, Toshimi Kabeyasawa, Michael Fardis, Julio Ramirez, Kazuhiro Kitayama, Akira Tasai, and Koichi Kusunoki

HOST ORGANIZATIONS AND SPONSORS

The workshop was organized under the auspices of the U.S.-Japan Cooperative Research in Earthquake Disaster Mitigation program, with funding by the Ministry of Education, Science, Sports and Culture in Japan, the U.S. National Science Foundation, the Pacific Earthquake Engineering Research Center, and the State of California.

The technical program was developed by Professor Toshimi Kabeyasawa, Division of Disaster Mitigation Science, Earthquake Research Institute, University of Tokyo, and Professor Jack P. Moehle, Director of the Pacific Earthquake Engineering Research Center, University of California, Berkeley.

The efforts of Professor Marc Eberhard, of the University of Washington, and Mr. Michael Valley, of Skilling, Ward & Magnusson, in making local arrangements for the workshop and in arranging the construction site visit in Seattle are especially appreciated. Ms. Veronica Padilla organized the submission of manuscripts.

ACKNOWLEDGMENTS

On the U.S. side, this work was supported in part by the Pacific Earthquake Engineering Research Center through the Earthquake Engineering Research Centers Program of the National Science Foundation under award number EEC-9701568.

On the Japan side, the work was supported as part of Development of Performance-Based Design Methodologies, subtheme (2-1) of the U.S.-Japan Cooperative Research in Earthquake Disaster Mitigation program under grant number 11209203, a grant-in-aid for Scientific Research on Priority Area, Category B, by the Ministry of Education, Science, Sports and Culture, in Japan.

CONTENTS

RESOLUTIONS

Recent urban earthquakes have caused significant economic losses, injuries, and fatalities in both the U.S. and Japan. This was evident in the U.S. during the 1994 Northridge earthquake, and in Japan during the 1995 Hyogo-ken Nambu earthquake. These and other earthquakes such as recent earthquakes in Turkey, Taiwan, and Seattle point out the need for effective and practical methods for evaluating and rehabilitating existing hazardous buildings and designing new buildings for more reliable and improved performance.

While great progress previously has been made in engineering for earthquake resistance, suggested frameworks for performance-based earthquake engineering will accelerate progress by focusing efforts and bridging gaps. This will lead to a future of earthquake engineering that will include increased emphasis on quantitative measures of performance over qualitative measures, precision over approximation, reliability over uncertainty, and intelligent engineering and life-cycle cost design over minimum capital cost design.

Papers presented at the First, Second, and Third U.S.-Japan Workshop on Performance-Based Earthquake Engineering Methodology for Reinforced Concrete Building Structures demonstrate progress being made in performance-based earthquake engineering. In the third workshop presentations in the plenary session described new developments in performance-based design in Japan, Taiwan, and the U.S. Two working group sessions covered the most recent research findings related to analysis and performance assessment in support of performance-based design. Two special theme sessions provided an opportunity to debate methods for nonlinear analysis as well as procedures for establishing acceptance criteria. Discussion of the presented papers enhanced understanding and advanced the state of the art in performance-based earthquake engineering. Involvement of leading researchers from Greece, Italy, Mexico, Taiwan, and Slovenia, in addition to those from Japan and the U.S., enhanced the technical discussion.

Important outcomes of the workshop include

- better understanding of the present state of knowledge and practice of performance-based earthquake engineering, especially the requirements of the recently revised Building Code of Japan, the seismic codes in Taiwan, and design practice being adopted in the U.S.;
- detailed understanding of seismic demands, especially the use of analysis methods for performance-based earthquake engineering of reinforced concrete buildings;
- detailed understanding of seismic capacities of structures and members, especially reinforced concrete columns and beam-column joints; and
- identification of common areas of concern, areas of needed advancement, and areas that would benefit from joint study.

The topic of performance-based earthquake engineering is a particularly effective one for workshop discussion because it brings together and promotes common focus of experts in ground motion, analysis, and design, and because its format is not constrained by prescriptive code requirements that vary from one country to another. Understanding of the work of individuals with different expertise was achieved in ways that would not be possible without meeting in this format.

The workshop was a successful continuation of progress made through more than two decades of cooperative U.S.-Japan research in earthquake engineering. The success at this workshop suggests that the two countries will benefit from continued cooperation. Reasons for continued cooperation include

- the two countries have a shared need to develop improved methods for seismic design and evaluation;
- in both countries, there is a need for integrated analytical and experimental approaches, which is promoted in this meeting format; and

- each side brings unique data, experience, knowledge, and facilities, the sharing of which benefits all.

These discussions are best accomplished through face-to-face meetings of extended duration such as occur in a workshop format.

Therefore, the following recommendations are offered:

(1) Because of the rapid rate at which new information and applications are being achieved, the importance of advances to Japan and the U.S., and the success of the first, second, and third workshops, the participants recommend that the Fourth U.S.-Japan Workshop on Performance-Based Seismic Engineering Methodology for Reinforced Concrete Building Structures be organized by the Japan side in about one year. Consideration also should be given to convening or participating in a major international workshop on the theme subject around one year later.

(2) At future workshops, several topics for focused discussion should be considered. A reduced number of these should be the focus of the fourth workshop:

  (a) simplified and rigorous methods for predicting seismic demands:

    (i) identification of damaging features of earthquakes

    (ii) continuation of the topic on inelastic displacement demands for SDOF and MDOF systems

    (iii) practical application of advanced analysis methods

    (iv) use of probabilistic bases for PBEE incorporating uncertainty and variability

    (v) performance of strength-degrading structures

  (b) simplified and rigorous methods for predicting seismic capacities:

    (i) definitions and measures of performance, including operations

    (ii) modeling of damage, including cumulative effects

(iii) modeling of loss of lateral and gravity load capacity of members and systems

(iv) data archive methods, and exchange of data base on test results

(v) behavior of nonstructural component

(vi) improved understanding of scale effects and variable loading histories

(c) design methodology to bring these together:

(i) validation of performance-based earthquake engineering methods

(ii) assessment of system performance on the basis of component performance

(iii) evaluation of performance in terms of costs, functionality, and casualties

(iv) development of performance-derived design criteria

(3) At the fourth workshop, the following format should be considered:

(a) focus on two to four topics, emphasizing presentation of papers on those topics coupled with special theme sessions to examine topics in greater detail; and

(b) participation of researchers, professional engineers, representatives of code-writing organizations, representatives of national organizations responsible for construction, and leading international participants.

Cooperative activities between individual participants from the U.S. and Japan are encouraged to address problems of mutual concern. Efforts should be undertaken to facilitate exchange of personnel, including students, faculty, and professional researchers and practitioners, as well as of information on technical issues and applications. Funding agencies are encouraged to support these activities.

PLENARY SESSION I: WELCOME, INTRODUCTIONS, AND KEYNOTE REPORTS

Chaired by

♦ Jack Moehle and Toshimi Kabeyasawa ♦

JAPANESE STATE OF PRACTICES IN SEISMIC DESIGN OF HIGH-RISE REINFORCED CONCRETE BUILDINGS

Shunsuke Otani

ABSTRACT

Building Standard Law of Japan was revised in 1998 with objectives partly to introduce performance-based design regulations. Building Standard Law Enforcement Order was revised in 2000 to introduce additional technical requirements for the law revision. Notification No. 1461 of Ministry of Construction was issued to define performance requirements for high-rise buildings. This paper briefly introduces new requirements and the state of practices in the design of high-rise buildings for gravity loads, snow loads, wind forces and earthquake forces with emphasis on design of reinforced concrete structures.

1. INTRODUCTION

Building Standard Law, a national law to regulate the construction of buildings and the use of land, was significantly revised in 1998 partly to introduce performance-based requirements, especially in the requirements about fire resistance of construction materials and emergency evacuation. The Article 20 of the law requires "the building shall be constructed safe against dead and live loads, snow loads, wind forces, soil and water pressures, and earthquake and other vibration forces and impacts." The methods of construction necessary to ensure the safety are referred to the cabinet order.

Building Standard Law Enforcement Order, a cabinet order issued for the enforcement of the Building Standard Law, was revised in 2000 to introduce additional technical requirements to meet the 1998 revision of the law. The order requires that the construction of high-rise buildings, taller than 60 m, must satisfy various requirements for durability, and must be approved to be safe by the Minister of Construction in accordance with the structural calculation standard outlined by the Minister of Construction (Article 36, Part 4). The structural calculation of high-rise buildings shall be carried out in conformance with the standard, outlined by the Minister of Construction, capable of evaluating the safety of structures by examining the action and deformation of structural parts caused by loads and forces taking into consideration the

Department of Architecture, Graduate School of Engineering, University of Tokyo
Email: otani@sake.t.u-tokyo.ac.jp

construction method and vibrational and other characteristics of the structure (Article 81, Part 2). The structural calculation is outlined in Ministry of Construction Notification No. 1461, issued in 2000.

The conformity of the notification in design calculation and documents is normally examined by a committee of private agencies authorized by the Ministry of Construction. The committee consists of university researchers representing various structural and geotechnical fields and of structural engineers. The review will normally take one to two months. The report of the committee is sent to the Minister of Construction for approval.

2. MINISTRY OF CONSTRUCTION NOTIFICATION No. 1461

Ministry of Construction issued Notification No. 1461 on May 31, 2000, which outlined the structural calculation standard for evaluation of structural safety of high-rise buildings. Followings are not official translation, and the reader is advised to refer to the original Japanese document. The notification is written in a performance-based format consisting of eight articles;

Article 1: No structural members shall be damaged under the dead and live loads, and other loads and forces representing actual conditions acting on all parts of the building.

Article 2: Structural calculation shall be made for snow loads on the building.

(a) Snow load shall be determined in accordance with Building Standard Law Enforcement Order. If an expected value associated with a 50-year return period is obtained for the construction site by special study or investigation, such a value can be used.

(b) No structural members shall be damaged under snow load defined in (a).

(c) The structure shall not collapse under the snow load equal to 1.4 times the value defined in (a).

Article 3: Following structural calculation shall be made for wind forces acting on the building. The effect of structural vibration normal to the wind direction and torsional vibration in the horizontal plane, and the effect of vertical vibration on the roof shall be appropriately taken into consideration in the structural calculation.

(a) No structural members shall be damaged under strong winds which produce a wind velocity equal to or higher than the average wind velocity at 10 m above ground level taking into consideration ground roughness defined by the Building Standard Law Enforcement

Order.

(b) The structure shall not collapse by strong winds which produce an average wind velocity 1.25 times the value defined in (a) at 10 m above ground level.

Article 4: Following structural calculation shall be made for earthquake forces acting on the building. The effect of vertical ground motion considering the size and configuration of the building, the effect of ground motion normal to the principal ground motion concerned, the effect of phase difference of ground motion, and the effect of vertical loads under horizontal sway shall be appropriately taken into consideration in the structural calculation.

(a) The ground motion acting on structures in the horizontal direction is defined in parts 1) to 4) below. If the ground motion is determined taking into consideration the effect of faults near the construction site, epicentral distance and other characteristics of seismic motions and the influence on structural response, the followings may not be satisfied.

1) Acceleration response spectrum (a curve representing acceleration response characteristics of structural systems with respect to periods and at a 5 % damping factor) of the ground motion on the open engineering bedrock (engineering bedrock is defined as a layer located in depth with sufficient thickness and rigidity having a shear wave velocity larger than 400 m/sec, and open engineering bedrock is a bedrock free from the effect of surface soil layers above) shall be defined in Table 1, and the amplification of ground motion by surface geology should be considered in defining the design ground motion.

Table 1: Design acceleration spectrum at engineering bedrock

Period, sec	Acceleration response spectral value, m/sec2	
	Rare ground motion	Extraordinary rare ground motion
T<0.16	(0.64+6T)Z	Five times the acceleration response values defined for the rare ground motion
0.16<T<0.64	1.6Z	
0.64<T	(1.024/T)Z	

T: period of structure, sec.

Z: seismic zone factor defined in Article 88, Part 1 of Building Standard Law Enforcement Order.

2) The duration of motion shall be longer than 60 sec.

3) The ground motion (acceleration, velocity or displacement or their combination) shall be digitally defined at appropriate time intervals.

4) The number of ground motions shall be large enough to verify the safety of the

structure under the effect of earthquake motion.

(b) Structural members shall be examined to be non-damaged under the rare ground motions defined in (a) using the equation of motion. Structural vibration control members are exempted from this requirement.

(c) The structure shall be examined to non-collapse under the extraordinary rare ground motions defined in (a) using the equation of motion.

Article 5: Loads defined in Article 1 shall be used in the structural calculation specified in Articles 2 through 4.

Article 6: The deformation and vibration of structural members under loads and forces defined in Article 1 shall not interfere the use of the building.

Article 7: Roofing elements, external facing materials and external curtain walls shall be structurally safe under the wind forces, earthquake forces and other impact forces.

Article 8: In a building located within a land failure warning zone, external walls shall not fail under the forces caused by the land failure of slope considering the types of natural hazards. The loads and forces defined in Article 1 shall be considered in the examination.

3. DESIGN FOR VERTICAL LOADS

The performance requirement under gravity loading is expressed in Article 1 of Notification No. 1461. The stresses at critical sections of structural members are calculated by a linearly elastic analysis method under the dead and live loads, representing actual conditions acting on all parts of the building. Structural members may be judged non-damaged when the stresses are smaller than "allowable stresses of materials specified for long-term loading."

Typical allowable compressive stress of concrete for long-term loading is one-third of the specified concrete strength and allowable shear and tensile stresses are one-thirtieth of the specified concrete strength. Typical allowable stress of reinforcement is two-third of the specified yield stress; the allowable stress shall not be larger than 215 MPa for bars of nominal diameter smaller or equal to 28 mm, and shall not be larger than 195 MPa for bars of nominal diameter larger than 28 mm. The allowable tensile stress of shear reinforcement shall not be larger than 195 MPa. The allowable bond stress between reinforcing bars and concrete is 0.7

MPa.

The performance requirement under snow loading is expressed in Article 2 of Notification No. 1461. The Building Standard Law Enforcement Order states that vertical snow depth for design shall be specified by the local jurisdiction. The snow depth expected under snow fall for consecutive days at a 50-year return period (annual probability of exceedance of 0.02) can be used if a special study is conducted for the construction site.

Structural members are thought to be non-damaged if maximum stresses at critical sections under the combined effect of dead, live and snow loads are less than "allowable stresses of materials for short term loading." Allowable compressive and shear stresses of concrete for short term loading are twice the corresponding allowable stresses for long term loading; i.e., allowable compressive stress of concrete is two-third of the specified compressive strength and allowable shear stress is one-fifteenth of the specified compressive strength. Allowable stress of reinforcement for short-term loading is equal to the specified yield stress, but allowable tensile stress of shear reinforcement must be not greater than 390 MPa. The level of these allowable stresses for short-term loading corresponds to the elastic limits of materials.

When the snow load corresponding to 1.4 time the design snow load is combined with the dead and live loads, the structure shall not collapse. There exists very low probability (corresponding to a return period of 500 years) for this additional snow load to occur during the life time of the building. Collapse can be examined if a collapse mechanism might be formed under the specified loading. In the reinforced concrete building, in which the dead load is large compared with live and snow loads, stresses at critical sections of structural members can be shown smaller than the allowable stresses of materials for short term loading if the structural members are dimensioned to satisfy the allowable stresses of materials for long term loading under the combined dead and live loads.

4. DESIGN FOR WIND FORCES

The performance requirement of a building under design wind forces is expressed in Article 3 of Notification No. 1461. The Building Standard Law Enforcement Order specifies the design wind pressure q under rare (Level 1) strong wind events as follows;

$$q = 0.6\, E\, V_0^2 \tag{1}$$

where, E : coefficient representing the influence of neighboring structures and trees at the roof level on the amplitudes of wind pressure, and V_0: average wind velocity over 10 minutes at 10.0 m from the ground at a return period of 100 years, defined taking into consideration the past history of typhoons and wind disasters in the region. The method to estimate coefficient E and the value of design wind velocity V_0, varying from 30 m/sec to 46 m/sec in the country, are specified in Notification No. 1454 of the Ministry of Construction.

The wind velocity of extraordinary rare (Level 2) events, corresponding to a return period of 1000 years, is 1.25 times that of rare (Level 1) events. Therefore, the level-2 design wind pressure is 1.56 (=1.25x1.25) times the level-1 design wind pressure.

In a reinforced concrete building, where the dead load is large, the story shear under level-2 wind events is shown much smaller than that under design earthquake loading (Level 1) for damage control; i.e., stresses at critical sections of structural members under damage-control earthquake loading are less than allowable stresses of materials for short term loading. Therefore, story shears caused by level-2 wind forces are shown to be much smaller than that developed by level-1 earthquake forces and the examination of member actions is exempted.

For a building taller than 100 m, if an aspect ratio ($H/\sqrt{BD}$, where H: height of building, B, D: width and depth in building plan) is greater than 3.0, the wind pressure acting normal to the wind and the torsional vibration must be examined. If the following equation is satisfied, this examination can be exempted;

$$\eta_0 \sqrt{BD} / U_H \leq 0.4 \qquad (2)$$

where, η_0: fundamental frequency of building normal to wind direction or of torsional vibration, U_H : design wind velocity.

5. DESIGN FOR EARTHQUAKE FORCES

The performance of a building under earthquake motions is outlined in Article 4 of Notification No. 1461, and must be examined by earthquake response calculation.

5.1 Design Earthquake Motions

For rare (Level 1) earthquake events, artificial ground motions compatible with a response acceleration spectrum specified by the Notification at the open engineering bedrock must be generated. The engineering bedrock is defined as a thick soil layer at which shear wave velocity is larger than 400 m/sec; the engineering bedrock is typically a soil layer which is selected to support the pile foundation or mat foundation of a high-rise building.

For extraordinary rare (Level 2) earthquake events, artificial earthquake ground motions either (a) compatible with response acceleration spectrum specified at the engineering bed rock or (b) generated taking into consideration the effect of faults near the construction site, magnitude, epicentral distance and other characteristics of seismic motion.

The intensity levels ground motions at levels 1 and 2 earthquake events are compatible with those specified for the normal building less than 60 m in height. The intensity of level 1 ground motions is believed by some engineers to be too small for the damage control of important facilities as high-rise buildings. At design reviewing agencies, therefore, the use of additional observed earthquake records is recommended in design calculation. The maximum velocity of observed ground motions is normalized to 250 mm/sec for level-1 earthquake events, and 500 mm/sec for level-2 events.

More than two ground motion records must be prepared each for level-1 and level-2 earthquake events. The duration of motion must be longer than 60 sec.

Spectrum compatible ground motions are generated either of the following methods;

(a) Composition by Random Phase Angle

Acceleration time history of a ground motion is expanded by Fourier series

$$\ddot{y}(t) = e(t) \sum_{i=1}^{n} A_i \cos(\omega_i t + \phi_i) \tag{3}$$

in which $e(t)$: an envelope function, A_i, ω_i, ϕ_i: Fourier amplitude, circular frequency and phase angle. The following envelope functions are often used after Jennings et al (1969).

For level-2 earthquake events;

$$\begin{aligned} e(t) &= (\frac{t}{5})^2 && 0 \le t < 5 \\ e(t) &= 1.0 && 5 \le t < 35 \\ e(t) &= \exp\{-0.027(t-35)\} && 35 \le t < 120 \end{aligned} \tag{4}$$

For level-1 earthquake events;

$$\begin{aligned} e(t) &= (\frac{t}{5})^2 && 0 \le t < 5 \\ e(t) &= 1.0 && 5 \le t < 25 \\ e(t) &= \exp\{-0.066(t-25)\} && 25 \le t < 60 \end{aligned} \tag{5}$$

Phase angle ϕ_i is taken random in a range of 0 to 2π for each circular frequency ω_i. Fourier amplitude A_i at frequency ω_i is revised iteratively until (i) the pseudo-velocity spectrum amplitudes of generated motion become more than 85 % of the target response spectrum at each frequency, (ii) the covariance of error in generated response spectrum relative to the target spectrum is less than 0.05, and (iii) average error becomes less than 0.02 over the entire frequency range. The initial values for Fourier amplitudes may be taken from the target pseudo-velocity spectrum because velocity spectrum ordinates at zero damping are similar to Fourier spectrum amplitudes of the motion.

(b) Composition using Phase Differences of Observed Motions

It is empirically observed that the distribution of ground motion amplitudes over the duration resembles to the distribution of phase differences $\Delta\phi_i$ between 0 to 2π of the Fourier expansion of a ground motion. The probability density function of phase angle differences is assumed similar to the envelope curve of an observed ground motion. A random number between 0 and 1.0 is transformed to a phase angle difference between 0 to 2π using an accumulated probability density function of the amplitudes of an observed ground motion. A phase angle ϕ_i for circular frequency ω_i is determined by adding phase difference $\Delta\phi_i$ to a previous phase angle ϕ_{i-1}.

$$\ddot{y}(t) = \sum_j A_j \cos(\omega_j t + \phi_j) \qquad (6)$$

The amplitude of Fourier components is iteratively revised until the response spectral amplitudes of a generated signal becomes close to the target spectral shape using the procedure similar to method (a) above.

Recent development in engineering seismology makes it possible to generate artificial earthquake motions including fracture propagation at earthquake faults. Pure theoretical calculation tends to underestimate short period components of a ground acceleration waveform. Therefore, semi-empirical methods are suggested to define Green's function for the propagation of earthquake motion (Fig. 1) from an epicenter to the engineering bedrock under a construction site (Kobayashi and Midorikawa, 1982 and Irikura, 1983).

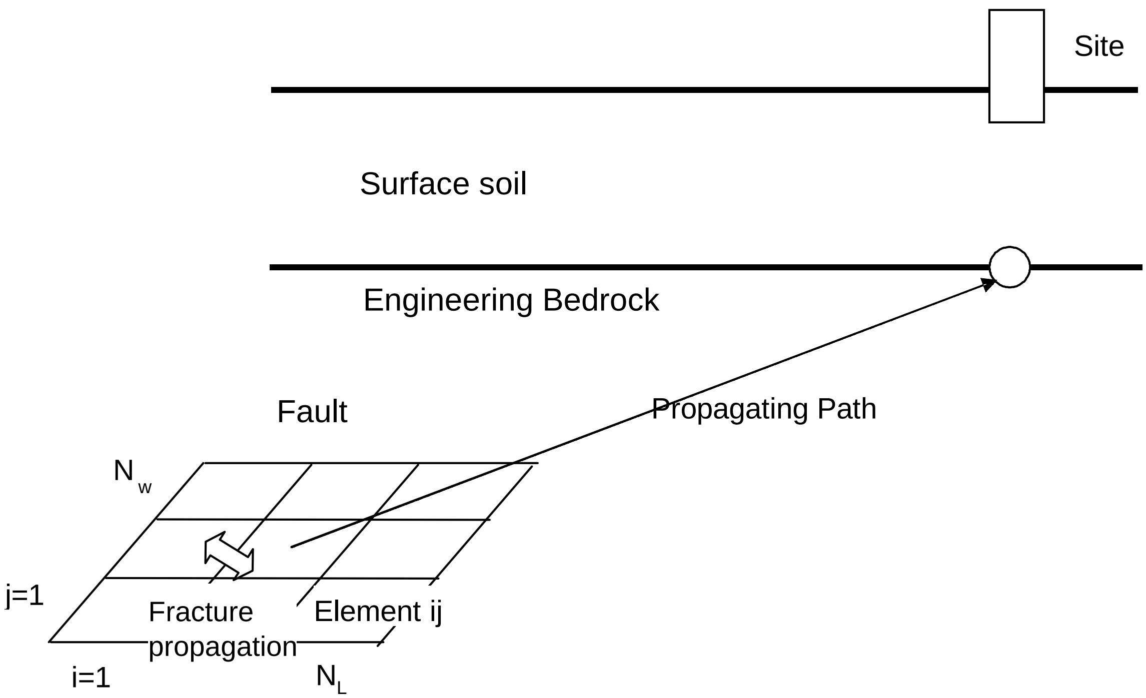

Fig. 1: Generation of ground motion from fault movements

The generated earthquake motions at the engineering bedrock are amplified to take into consideration the effect of surface geology above the engineering bedrock. One-dimensional response analysis is carried out using an iterative equivalent linearization method revising shear modulus and damping factor with calculated shear strain of each soil layer. Complex transfer function of motions is defined after convergence. Complex Fourier amplitudes of ground motion at the structure's base are calculated by multiplying complex Fourier amplitudes of ground motion at the engineering bedrock by complex transfer functions of the surface soil layers at each frequency. Time history of a ground motion at the structure's base is constructed from the complex Fourier amplitudes at each frequency.

5.2 Structural Modeling

The method of structural modeling for response analysis is not specified in the notification. A structure as designed is normally analyzed under monotonically increasing lateral forces considering member stiffness changes at cracking and flexural yielding; shear deformation is normally assumed to be elastic because high resistance is provided against shear failure in design. The distribution of lateral forces is normally taken same as that specified for normal buildings (less than 60 m); higher mode effect is considered in the distribution. Story shear and story drift relation is obtained for each story to construct a multi-mass multi-spring model. Mass is assumed to concentrate at each floor level; i.e., dead load combined with reduced live load for earthquake loading is used to evaluate the floor mass. Story drift is divided into an elastic flexural component and a nonlinear shear component (Fig. 2).

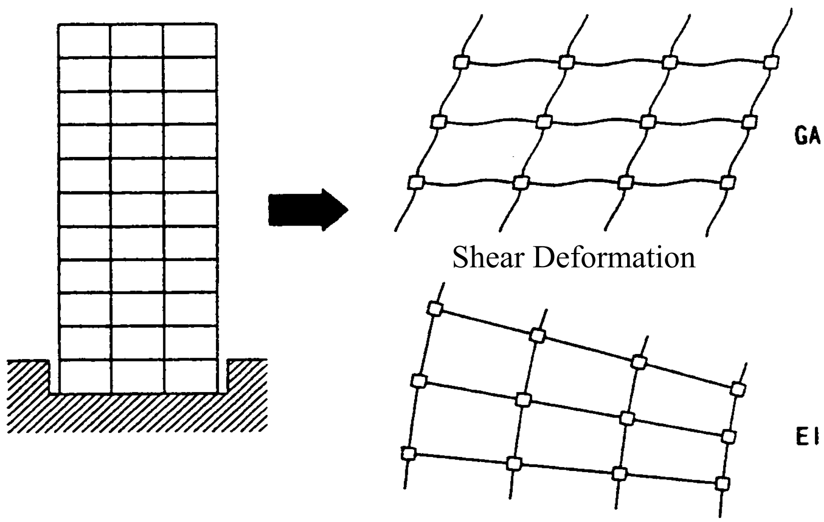

Fig. 2: Bending and shear deformation of a frame

The flexural stiffness of a story is evaluated by assuming the linear distribution of vertical displacement at a floor level. The strain energy is equated to determine story rotation $\Delta\theta_i$ of floor level i (Fig. 3) ;

$$\frac{1}{2}\sum_{j=1}^{N}\Delta N_{ij}\,\Delta v_{ij}=\frac{1}{2}\sum_{j=1}^{N}EA_{ij}\,\frac{\ell_{ij}\Delta\theta_i}{h_i}\,\ell_{ij}\Delta\theta_i \tag{7}$$

where, ΔN_{ij} and Δv_{ij}: axial force and axial deformation of $j-th$ column in story i, ℓ_{ij}: distance from the center to $j-th$ column, $\Delta\theta_i$: equivalent rotation at story i, EA_{ij}: axial rigidity of $j-th$ column.

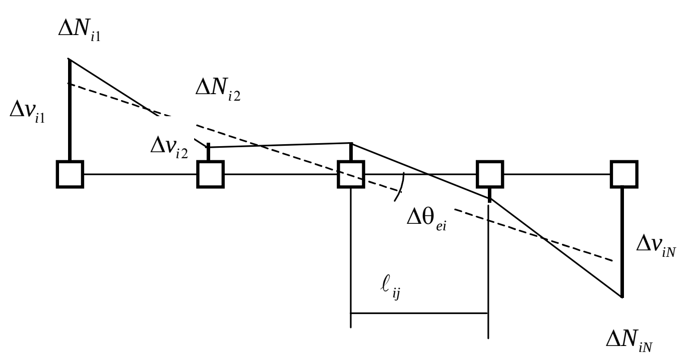

Fig. 3: Distribution of vertical floor displacements and axial forces in columns

After solving the relation for floor rotation, the equivalent flexural rigidity EI_{ei} of a story is evaluated assuming linear moment distribution between two adjacent floors;

$$\frac{EI_{ei}}{h_i} = \frac{\Delta M_i + \Delta M_{i-1}}{2\Delta\theta_i} \tag{8}$$

where, h_i: inter-story height at story i, ΔM_i: overturning moment at the base of story i.

The story drift after removing flexural deformation is assigned to the deformation of a story shear spring. The story-shear and shear-spring-deformation relation is idealized by a trilinear backbone with Takeda hysteresis rules (Takeda et al., 1970).

If the effect of foundation deformation is judged to be important, sway and rocking springs are considered at the base. The story shear response of a structure normally decreases with the use of soil springs although displacement response may be amplified.

Damping is normally assumed proportional to instantaneous stiffness of the structure;

$$[c] = \frac{2h_1}{\omega_1}[k^*] \tag{9}$$

where, $[c]$: damping matrix, $[k^*]$: instantaneous stiffness matrix, h_1, ω_1: damping factor and circular frequency of the first mode at the initial elastic stage.

5.3 Damage Control of Structure

The performance requirement of a building under level-1 ground motions is not to cause damage in structural members. The linear story shear response of a multi-mass-spring model under level-1 ground motions is calculated. Design earthquake story shears are determined as the envelope of maximum story shears calculated for all ground motions. Static linearly elastic analysis of the structure as designed is carried out under the design story shears. Structural members are judged undamaged if the stress at critical sections under member actions are less than allowable stresses of materials for short-term loading.

The story drift calculated for the mass-spring system must be less than 1/200 so that nonstructural elements should not be damaged by level-1 earthquake motions.

Normally, the intensity of level-1 ground motions specified in Notification No. 1461 is by far too small to cause any inelastic stresses in structural members. Observed earthquake records normalized to 250 mm/sec, recommended by review agencies, develops response much larger than the level-1 earthquake motions specified in the notification.

5.4 Structural Safety

The performance requirement of a building under level- 2 ground motions is not to collapse. It is generally controlled to make the maximum story ductility factor of any shear springs less than two and the maximum story drift at any stories less than 1/100.

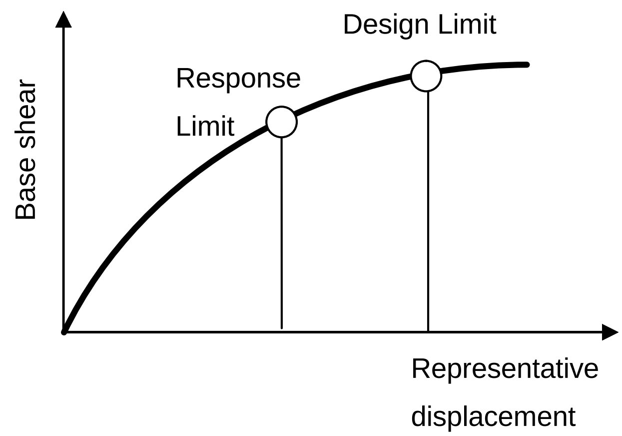

Fig. 4: Response limit and design limit points

The response analysis, however, of a multi-mass-spring system under level-2 earthquake motions cannot define the status of structural members. Therefore, a pushover analysis is used to examine the state of damage in structural members. A displacement at the geometrical centroid of the lateral forces during a static push-over analysis is called a “representative displacement” of the building. Maximum representative displacement of the multi-mass-spring model under the level-2 ground motions is called as a “response limit displacement (Fig. 4)”.

Design limit displacement is defined at a point on the representative displacement-base shear curve, where the area under the curve is twice as much as that at the response limit point (Fig. 4). The member response of the pushover analysis is examine at the design limit point to examine (a) location of plastic hinges, (b) rotational ductility factors at plastic hinges, (c) safety margin against plastic hinge formation at column ends, (d) safety margin against brittle failure in all members, and (e) maximum axial force level of columns. The formation of plastic hinges is normally accepted at the ends of girders, at the bottom of the first-story columns, and at the top of top-story columns, and at the ends of columns subjected to tensile forces under lateral loading. The rotational ductility factor must be less than 4.0 at girder ends and 2.0 at column ends. The safety margin against brittle failure and the acceptable level of axial forces in columns vary by engineers.

The examination of member response at "design limit point" is necessary because the pushover analysis is carried out under a given distribution of lateral forces ignoring the phase difference of higher mode response in the distribution and because there exists uncertainty in the definition of ground motion characteristics.

If the maximum response of a mass-spring system is limited to a ductility factor of 2.0, maximum story drifts, story shears and overturning moments of the mass-spring system have been shown to be comparable to those obtained by the nonlinear earthquake response analysis of the corresponding frame structure.

5.5 Additional Studies

The notification requires the examination of following four effects on the earthquake response of a structure; i.e.,

- Effect of vertical ground motion,
- Effect of orthogonal ground motions,
- Effect of phase difference of ground motions, and
- Effect of vertical load through horizontal sway.

(1) Effect of Vertical Ground Motion

Vertical component of artificial ground motions is generated taking into account the response spectrum of vertical ground motions and frequency amplification of vertical motion by the surface geology above the engineering bedrock.

A building structure is idealized by a linearly elastic multi-mass-spring system. A spring of a story represents the sum of axial stiffness of columns in the story. Maximum story axial force of a story is distributed to constituent columns proportional to axial stiffness. Calculated axial forces of columns are combined with those of the pushover analysis at the design limit displacement either by algebraic sum or by square root of sum of squares. Maximum level of axial forces is examined for columns.

In some rare occasions, the linearly elastic response analysis of a three dimensional frame is carried out to find column axial forces under vertical ground motions. In rare cases of long span structures, distributed masses are considered along girders to include the effect of vertical vibration of slabs.

(2) Effect of Orthogonal Ground Motions

A pushover analysis of frames is carried out in a direction diagonal to the principal axes in the structural plan. The design limit displacement for diagonal loading is defined using response limit point on the basis of either the maximum nonlinear response in the diagonal direction or the maximum response in the principal directions.

In some cases, a building is subjected to a level-2 earthquake motion in one principal direction and a level-1 earthquake motion in the other principal direction using a three-dimensional nonlinear frame analysis program.

Axial force level in corner columns is a critical design issue under loading in the orthogonal directions because the corner columns are subjected to axial forces generated by loadings in the two principal directions.

(3) Effect of Phase Difference of Ground Motions

When a horizontal ground motion propagates at a shear wave velocity with an inclination from the vertical axis, the arrival time of such ground motion varies along the length of structural base. Therefore, the base of a structure is subjected to ground motion of different amplitudes and directions. This is called the phase difference of ground motion (Fig. 5).

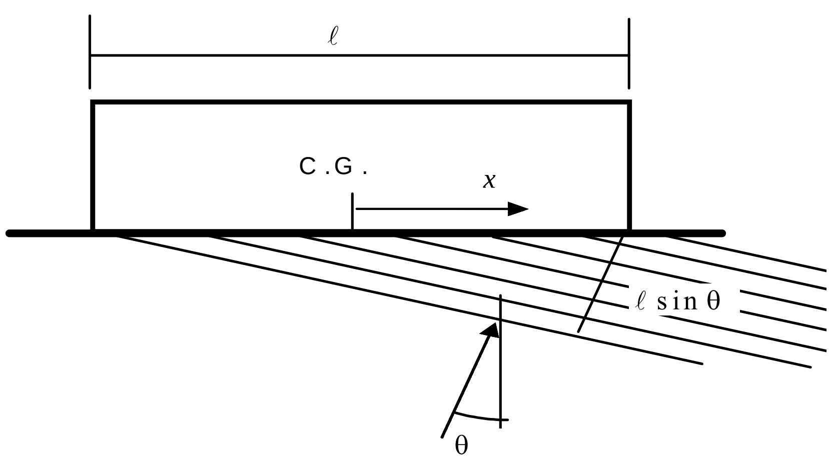

Fig. 5: Phase difference of ground motion

The phase difference will excite torsional response of a structure even in the symmetric case. The effective torsional acceleration may be estimated by the following equation;

$$a_\theta(t) = \frac{\int \rho \; a(t,x)\; x\; dx}{\int \rho \; a(t,x)\; x^2 \; dx} \tag{10}$$

where, ρ : mass per unit length along the length of a structural base, $a(t,x)$: horizontal acceleration at time t and distance x from the center of mass. The response of a structure can be calculated under the torsional ground motion and combined with the response under horizontal motion.

The effect of phase difference is important when the inclination θ of ground motion is large and when the length of structural base is long. The inclination angle is normally small when ground motion propagates upward reflecting and refracting at boundaries of soil layers (Snell's Law) (Fig. 6) because the shear wave velocity of soil is smaller near the surface. Therefore, the effect of phase difference is believed to be relatively small when the length of base is shorter than 100 m.

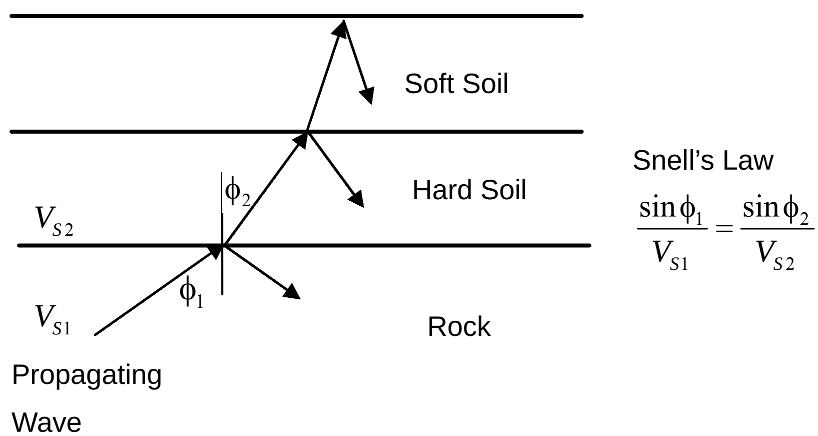

Fig. 6: Reflection and Refraction of Propagating Wave

(4) Effect of Vertical Load through Horizontal Sway (P-Δ effect)

The effect of vertical load through horizontal sway is normally ignored in the structural analysis. Therefore, the story drift was examined less than 1/100 so that the effect could be ignored in the structural analysis. However, this effect was recently realized important in evaluating the safety margin against shear failure or flexural yielding in columns in lower stories because the effect increases bending moment and shear in columns subjected to high axial forces especially in external columns where overturning moment by lateral forces causes large variation of axial forces.

6. DESIGN OF EXTERNAL FINISHING

The stresses of external finishing and curtain walls caused by out-of-plane pressure and inertia forces as well as in-plane forces are examined under wind and earthquake forces. The fasteners of curtain walls should be able to resist stresses caused by winds and earthquake motions or should be capable of following the story drift caused by earthquake motions.

There should not be damage in external finishing under level-1 winds and earthquake motions. The falling and breakage of external finishing must be examined for level-2 winds and earthquake motions.

7. SUMMARY

Japanese design requirements and the state of practices in design of high-rise reinforced concrete buildings are briefly introduced. Nonlinear dynamic analysis of equivalent multi-mass-spring models is carried out to estimate the maximum structural response. Pushover analysis is used to examine the state of structural members under strong earthquake motions.

REFERENCES

1. Architectural Institute of Japan (1993), Recommendations for Loads on Buildings and Commentary (in Japanese), 512 pp.
2. Irikura, K. (1983), "Semi-empirical estimation of strong ground motion during large earthquakes," Bulletin, Disaster Prevention Research Institute, Kyoto University, Vol. 32.
3. Jennings, P. C., G. W. Housner and N.C. Tsai (1969) "Simulated Earthquake Motions for Design Purpose," Proceedings, Fourth World Conference on Earthquake Engineering, Santiago,. Chile, Vol. 1, A-1, pp. 145-160.
4. Kobayashi, H. and S. Midorikawa (1982), "A Semi-empirical Method for Estimating Response Spectra of Near-field Ground Motions with Regard to Fault Rupture," Proceedings, Seventh European Conference on Earthquake Engineering, Vol. 2, pp. 161-168.
5. Takeda, T., M. A. Sozen and N. N. Nielsen (1970), "Reinforced Concrete Response to Simulated Earthquakes," Journal, Structural Division, ASCE, Vol. 96, No. ST12, pp. 2557-2573.

THE CURRENT DEVELOPMENT OF SEISMIC DESIGN CODE IN TAIWAN

C. H. LOH [1], J.-F. CHAI [1], W.-I LIAO [1] and T.-J. TENG [1]

ABSTRACT

After the Chi-Chi earthquake, the revised seismic design force and other related requirements in the seismic design code are developed in Taiwan. In addition to the conventional force based design, a capacity checking level is considered by limiting the ultimate capacity to exceed the maximum possible seismic demand. In this paper, the development of seismic design base shear, the seismic demand at checking level and the checking requirements are briefly introduced.

1. INTRODUCTION

The requirement of lateral force resistance of a structure is specified by the seismic design code. In general, the lateral force must take into account the following issues: (a) seismic hazard, (b) soil condition at construction site, (c) structure period, (d) anticipated ductility and acceptable level of damage of a structure, and (e) structural irregularity. It should be noted that the seismic design code normally outlines the minimum standard requirement in the society. The expected performance of structures varies from a country to another because each country has its own consideration on different levels of (a) seismic risk, (b) hazard tolerance, (c) economic background, and (d) technical development. The historical development of earthquake resistant building design and the seismic lateral force requirements in Taiwan are listed in Table 1.

On September 21, 1999, a devastating earthquake was occurred in the central part of Taiwan (Chi-Chi earthquake). After the earthquake, according to the investigations of structural damages, we learned that the current seismic design provisions have some inadequacies and need to be revised. It includes the development of design spectral response acceleration and structure system seismic reduction factor to determine the seismic design base shear, the static and dynamic analysis methods, the detail requirements of structural systems, and other requirements for seismically isolated structural systems and passive energy dissipation systems.

[1] *National Center for Research on Earthquake Engineering*
Email: lohc@ncree.gov.tw Fax: +886-2-2732-2223

Since the 1960s, it has been believed that it is not feasible to design a building structure to remain elastic under intense ground motions. The seismic design has aimed to ensure that (a) the structure should not suffer any structural damage from frequently minor earthquakes, (b) the repaired structure should be usable after an infrequent earthquake of major intensity, and (c) the structure should not collapse (life safety limit state) for the safety of occupants during the largest possible earthquake at the construction site. Therefore, in this study besides the modification on the requirements for conventional force based design, a capacity checking level to protect the occupant′s life by limiting the building capacity to exceed the required demand caused by the maximum possible earthquakes is also added. It is noted that the two-level design is requested only for the near-fault sites because the maximum seismic demand caused by the near-fault effect is much larger than that caused by other potential sources at general sites.

In the following sections, the development of seismic design base shear, the seismic demand at checking level for near-fault sites, and the checking requirements which are developed in the current revised seismic design code are briefly introduced.

2. SEISMIC DESIGN BASE SHEAR

For the current development of seismic design code in Taiwan, the elastic seismic demand is represented by the design spectral response acceleration S_{aD} corresponding to a uniform seismic hazard level of 10% probability of exceedance within 50 years (return period of 475 years). Based on the uniform hazard analysis, the mapped design 5% damped spectral response acceleration at short periods (S_S^D) and at 1 second (S_1^D) are determined and prepared for each administration unit of village, town or city level. These spectral response acceleration parameters should be modified by site coefficients to include local site effects, and the site adjusted spectral response acceleration at short periods (S_{DS}) and at 1 second (S_{D1}) are expressed as

$$S_{DS} = F_a S_S^D \quad ; \quad S_{D1} = F_v S_1^D \tag{1}$$

where site coefficients F_a and F_v are defined in Table 2, and they are functions of site class and ground shaking level. Based on the soil structures in the upper 30 meters below the ground surface, the site can be classified into three classes by using $\overline{V}_s$-method, $\overline{N}$-method or

$\bar{s}_u$-method as shown in Table 3. The site class parameters $\overline{V}_s$ and $\overline{N}$ are defined as the averaged shear wave velocity and averaged standard penetration resistance for all soil layers in the top 30 m, respectively. On the other hand, if the $\bar{s}_u$-method is adopted, $\overline{N}_{ch}$ is the averaged standard penetration resistance for cohesionless soil layers (PI<20) while $\bar{s}_u$ being the averaged undrained shear strength for cohesive soil layers (PI>20) in the top 30 m.

Based on S_{DS} and S_{D1}, the design spectral response acceleration S_{aD} can be developed by

$$S_{aD} = \begin{cases} S_{DS}\left(0.4 + 3T/T_0\right) & ;\quad T \le 0.2T_0 \\ S_{DS} & ;\quad 0.2T_0 < T \le T_0 \\ S_{D1}/T^{2/3} & ;\quad T > T_0 \end{cases} \quad \text{with} \quad T_0 = \left(\frac{S_{D1}}{S_{DS}}\right)^{1.5} \tag{2}$$

where T is the structure period in the unit of second, and the associated design response spectrum curve is indicated in Figure 1. Furthermore, if the structure with an effective critical damping ratio other than 5% is considered, two parameters B_S and B_1 were introduced to modify the design spectrum. The spectral response acceleration parameters S_{DS} and S_{D1}, as shown in Eq.(2), are modified to become S_{DS}/B_S and S_{D1}/B_1, respectively, and hence, the associated design spectral response acceleration S_{aD} can be modified from Eq. (2) as

$$S_{aD} = \begin{cases} S_{DS}\left[0.4 + \left(1/B_S - 0.4\right)T/\left(0.2T_0\right)\right] & ;\quad T \le 0.2T_0 \\ S_{DS}/B_S & ;\quad 0.2T_0 < T \le T_0 \\ S_{D1}/\left(B_1 T^{2/3}\right) & ;\quad T > T_0 \end{cases} \quad \text{with} \quad T_0 = \left(\frac{S_{D1}B_S}{S_{DS}B_1}\right)^{1.5} \tag{3}$$

The values of damping coefficients B_S and B_1 are defined in Table 4.

The structure system ductility capacity R for some basic types of seismic-force-resisting system can be found in the seismic design code, and further, the allowable ductility capacity R_a can be defined by

$$R_a = 1 + (R-1)/1.5 \tag{4}$$

Based on the equal displacement principle between elastic and elastic-plastic systems for long period range and equal energy principle for short periods, the structure system seismic reduction factor F_u can be defined by the allowable ductility capacity R_a and structure period T as

$$F_u = \begin{cases} R_a & ; \quad T \geq T_0 \\ \sqrt{2R_a - 1} + \left(R_a - \sqrt{2R_a - 1}\right) \times \dfrac{T - 0.6T_0}{0.4T_0} & ; \quad 0.6T_0 \leq T \leq T_0 \\ \sqrt{2R_a - 1} & ; \quad 0.2T_0 \leq T \leq 0.6T_0 \\ \sqrt{2R_a - 1} + \left(\sqrt{2R_a - 1} - 1\right) \times \dfrac{T - 0.2T_0}{0.2T_0} & ; \quad T \leq 0.2T_0 \end{cases} \tag{5}$$

where T_0 is the corner period of the design response spectrum as defined by Eq. (2) or Eq. (3), and the linear interpolation is adopted between long and short periods. It is noted that the reduction factor becomes 1 if the period approaches zero for a rigid body.

Finally, the seismic design base shear can be expressed as

$$V = \frac{S_{aD} IW}{1.4\alpha_y F_u} \quad \text{(for Buildings)} \quad ; \quad V = \frac{S_{aD} IW}{1.2\alpha_y F_u} \quad \text{(for Bridges)} \tag{6}$$

where I is the important factor, W is the total gravity load of the structures, α_y is the first yield seismic force amplification factor that is dependent on the structure types and design method. The constant 1.4 (for buildings) or 1.2 (for bridges) means the over strength factor between the ultimate and first yield forces, and it is dependent on the redundancy of the structural system. The procedures to determine the seismic design base shear are resumed in Figure 2.

Furthermore, a vertical component response spectrum is also introduced. It may be constructed by taking one half (general site) or two third (near-fault site) of the spectral ordinates, at each period, obtained for the horizontal response spectrum (Eq. (2) or (3)).

3. SEISMIC DEMAND AT CHECKING LEVEL FOR NEAR-FAULT SITES

In order to define the seismic demand at the checking level, the maximum possible earthquake should be taken into account. For the general sites in Taiwan, the maximum possible earthquake is defined at a uniform seismic hazard level of 2% probability of exceedance within 50 years (return period of 2500 years). At these general sites, it can be found that the multiplication of the design force by a factor of $1.4\alpha_y$ (for buildings) or $1.2\alpha_y$ (for bridges) is always larger than the maximum seismic demand estimated at a return period of 2500 years, and hence, it implies that no additional capacity check procedure is needed. However, it is not true for the near-fault sites because of the much larger seismic demand caused by the near-fault effect.

To consider the effect of near-fault ground motion in seismic design, both the probabilistic analysis based on the seismic hazard analysis at a return period of 2500 years and the deterministic analysis based on the attenuation law corresponding to the maximum potential magnitude of the fault are implemented. Then, as shown in Figure 3, the fault-affected sites can be identified as the region where the seismic demand determined by the attenuation law is larger than that determined by the probabilistic analysis, because the seismic demand outside the range is dominated by other potential sources and hence the fault effect can be ignored.

Based on the maximum potential magnitude of an active fault, the attenuation relations $S_{S,Att}(r)$ and $S_{1,Att}(r)$ for the median 5% damped spectral acceleration demands at short periods (e.g. 0.3 second period) and at 1 second are determined firstly. Compared with the mapped spectral response acceleration at short periods (S_S^M) and at 1 second (S_1^M) that are determined based on the uniform hazard analysis at a return period of 2500 years, the near-fault factors $N_A(r)$ and $N_V(r)$ can be defined as

$$N_A(r) = 1.5\, S_{S,Att}(r) \big/ S_S^M \quad ; \quad N_V(r) = 1.5\, S_{1,Att}(r) \big/ S_1^M \tag{7}$$

The factor of 1.5 implies the consideration of 1σ deviation of uncertainty of fault movement and the component effect (fault-normal). The site with either $N_A(r)$ or $N_V(r)$ larger than 1.0 is defined as the effect of near-fault ground motion, and hence the two-level design should be implemented within this site. The required spectral response acceleration S_{aM} at the checking level can be defined by

$$S_{aM} = \begin{cases} S_{MS}\left[0.4 + \left(1/B_S - 0.4\right)T\big/\left(0.2T_0^M\right)\right] & ;\ T \le 0.2T_0^M \\ S_{MS}/B_S & ;\ 0.2T_0^M < T \le T_0^M \\ S_{M1}\big/\left(B_1 T^{2/3}\right) & ;\ T > T_0^M \end{cases} \quad \text{with} \quad T_0^M = \left(\frac{S_{M1} B_S}{S_{MS} B_1}\right)^{1.5} \tag{8}$$

The values of damping coefficients B_S and B_1 can be found in Table 4, and the site-adjusted spectral response acceleration parameters S_{MS} and S_{M1} are determined by

$$S_{MS} = F_a N_A S_S^M \quad ; \quad S_{M1} = F_v N_V S_1^M \tag{9}$$

It is noted that the site coefficients F_a and F_v should be evaluated based on the ground shaking level of $N_A S_S^M$ and $N_V S_1^M$, respectively. The spectral acceleration S_{MS} and S_{M1} are used for the ultimate checking level.

4. CAPACITY CHECK FOR BRIDGES AT NEAR-FAULT SITES

Consider a RC bridge located at a near-fault site where the second level of capacity check is requested. Based on the reinforcement details and stress-strain curves of both concrete and steel reinforcing bars, the yielding and ultimate curvatures (ϕ_y and ϕ_u) and the corresponding moments (M_y and M_u) of the pier can be determined by the moment-curvature method. The yielding condition is defined as the reinforcing bar reaches its maximum elastic range, and the ultimate condition is define as the compressive strain of concrete reaches its ultimate condition. The ultimate flexural capacity P_u and ultimate displacement δ_u can be defined by

$$P_u = M_u / h \quad ; \quad \delta_u = \delta_y + (\phi_u - \phi_y) L_p (h - L_p / 2) \tag{10}$$

where L_p is the plastic hinge length, h is the total height of the pier. On the other hand, the shear capacity V_n of the RC pier can be evaluated by $V_n = V_s + V_c$. Herein, V_s and V_c are the shear capacity shared by the reinforcement and concrete, respectively, and they are evaluated by

$$V_s = A_v f_{yh} d / s \quad ; \quad V_c = 0.53(k + F)\sqrt{f_c'} A_e \tag{11a}$$

with

$$F = N / (140 A_g) \ \text{ and } \ k = \begin{cases} 1.0 & \text{(outside the plastic hinge zone)} \\ (R_a - 1.0)/3.0 & \text{(inside the plastic hinge zone)} \end{cases} \tag{11b}$$

where A_v and d are the sectional area and height of the tie reinforcement, s is the spacing of the tie reinforcement, A_e(=0.8A_g) and A_g are the effective shear area and total cross section area, f_{yh} and f_c' are the design strength of reinforcement and concrete, and k and F are the adjustment factors related to the allowable ductility ratio R_a and axial force N, respectively.

Based on the ultimate flexure capacity and the shear capacity of a RC pier, the failure modes are categorized to be flexural failure ($P_u \le V_s$), flexural to shear failure ($V_s < P_u \le V_{n0}$) and shear failure ($V_{n0} < P_u$), and V_{n0} is the shear capacity with k=1.0. Figure 4 shows the condition of the flexural to shear failure mode. Therefore, the allowable lateral capacity P_a and the associated allowable ductility capacity R_a of a pier can be defined by

$$P_a = \begin{cases} P_u & \text{: for flexural failure and flexural to shear failure} \\ V_{n0} & \text{: for shear failure} \end{cases} \tag{12}$$

and

$$R_a = \begin{cases} 1.0 + \left(\delta_u - \delta_y\right)/1.25\delta_y & \text{: for flexural failure } (R_a \le 4.0) \\ 4.0 - 3(P_u - V_s)/\left(V_{n0} - V\right) & \text{: for flexural to shear failure} \\ 1.33 & \text{: for shear failure} \end{cases} \tag{13}$$

In above equation for the flexural failure, the allowable ductility capacity is defined as 80% of the ductility capacity and limits the maximum value up to 4.0. Furthermore, based on the near-fault ground motions recorded in Taiwan Chi-Chi earthquake, the structure system seismic reduction factor F_u should be determined under the equal energy principles as (Liao *et al*, 2001)

$$F_u = \sqrt{2R_a - 1} \tag{14}$$

The criteria for the capacity check for a RC pier is that the allowable lateral capacity should exceed the shear force demand, i.e.

$$P_a > \frac{S_{aM} IW}{F_u} \tag{15}$$

and the required spectral response acceleration S_{aM} at the checking level is defined by Eq. (8). The procedures for the ultimate capacity check is resumed in Figure 5.

5. CONCLUSIONS

Based on the uniform hazard analysis at a return period of 475 years, the mapped design 5% damped spectral response acceleration at short periods and at 1 second are prepared for the specified administration unit. Furthermore, by considering the local site effect, the site-adjusted design spectral response acceleration parameters can be defined through the site coefficients and then to develop the design spectral response acceleration. Together with the system reduction factor and the first yield amplification factor, the seismic design base shear can be well defined. The two-level design for the bridges located at a near-fault site is considered in the current revised code in Taiwan. The seismic demand caused by the near-fault effect at checking level, the estimation of ultimate capacity of a RC bridge pier and the checking requirements are developed in the current revised seismic design code.

6. REFERENCES

1. BSSC, (1997). NEHRP Guidelines for the Seismic Rehabilitation of Buildings, 1997 Edition, prepared by the Applied Technology Council for the Building Seismic Safe Council (Report No. FEMA 273). Washington, D.C.
2. CALTRANS, (1999). CALTRANS Seismic Design Criteria, Version 1.1
3. ICBO, (2000). "International Building Code," 2000 Edition, Whittier, CA.
4. Japan Road Association (1995). Design Specification of Highway Bridges Part V. Seismic Design, translated and edited by S. Unjoh and T. Terayma..
5. Liao, W. I., C.H. Loh, and S. Wan, (2001). Earthquake responses of RC frames subjected to near-fault ground motions, *Structural Design of Tall Buildings* (accepted).
6. MOTC, (1995). Highway Bridge Seismic Design Criteria.
7. Otani, S. (2001), Earthquake Resistant Design of Reinforced Concrete Buildings, *Proc. 1st International Conference on Concrete & Development*: 65-75.

7. ACKNOWLEDGEMENTS

This research work was partially supported by Ministry of Interior (Building Research Institute) and Ministry of Transportation, Taiwan, Republic of China.

Table 1: The evolution of the seismic force requirements in Taiwan

Year	Seismic Base Shear	Remarks	
1974	$V_w=ZKCW$	Z=1.25, 1.0, 0.75; C_{max}=0.10, $W=D$+0.25L	K=0.67, 0.8, 1.0,1.33
1982	$V_w=ZKCIW$	Z=1.0, 0.8, 0.6; C_{max}=0.15, $W=D$	K=0.67, 0.8, 1.0,1.33 I=1.0, 1.25, 1.5;
1997	$V=\dfrac{ZICW}{1.4\alpha_y F_u}$	Z=0.33, 0.28, 0.23, 0.18; C_{max}=2.5, $W=D$ α_y=1.2(WSD), 1.5 (USD)	I=1.0, 1.25, 1.5 $F_u\approx$2.9, 2.5 2.1

Table 2: Values of site coefficients F_a and F_v

Site Class	Values of F_a				Values of F_v			
	$S_S^D \le 0.5$	$S_S^D = 0.75$	$S_S^D = 1.0$	$S_S^D \ge 1.25$	$S_1^D \le 0.2$	$S_1^D = 0.3$	$S_1^D = 0.4$	$S_1^D \ge 0.5$
S1 (Hard Site)	1.0	1.0	1.0	1.0	1.0	1.0	1.0	1.0
S2 (Normal site)	1.2	1.1	1.0	1.0	1.5	1.4	1.3	1.2
S3 (Soft Site)	1.4	1.2	1.1	1.0	1.8	1.6	1.5	1.4

Table 3: Site classification

Site Class	$\overline{V}_s$ -method	$\overline{N}$ -method	$\overline{s}_u$ -method	
	$\overline{V}_s$ (m/s)	$\overline{N}$	$\overline{N}_{ch}$	$\overline{s}_u$ (kPa)
Type 1 (Hard site)	$\overline{V}_s > 400$	$\overline{N} > 55$	$\overline{N}_{ch} > 55$	$\overline{s}_u > 100$
Type 2 (Normal site)	$200 \le \overline{V}_s \le 400$	$15 \le \overline{N} \le 55$	$15 \le \overline{N}_{ch} \le 55$	$50 \le \overline{s}_u \le 100$
Type 3 (Soft site)	$\overline{V}_s < 200$	$\overline{N} < 15$	$\overline{N}_{ch} < 15$	$\overline{s}_u < 50$

NOTE: If the $\overline{s}_u$ -method is used and the $\overline{N}_{ch}$ and $\overline{s}_u$ criteria differ, select the category with the softer soils

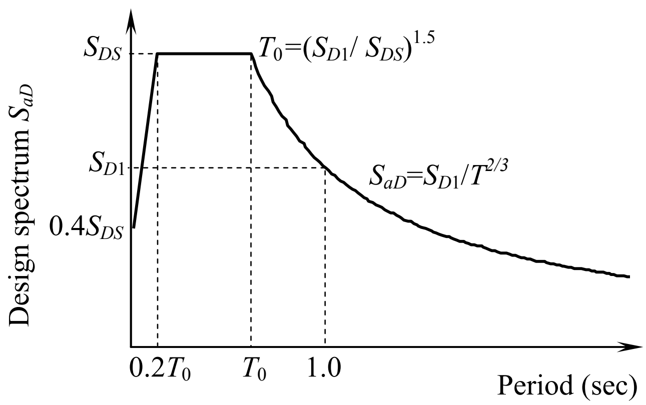

Figure 1: Design Response Spectrum

Table 4: Damping coefficients B_s and B_1

Effective Damping ξ (%)	B_S	B_1
<2	0.8	0.8
5	1.0	1.0
10	1.3	1.2
20	1.8	1.5
30	2.3	1.7
40	2.7	1.9
>50	3.0	2.0

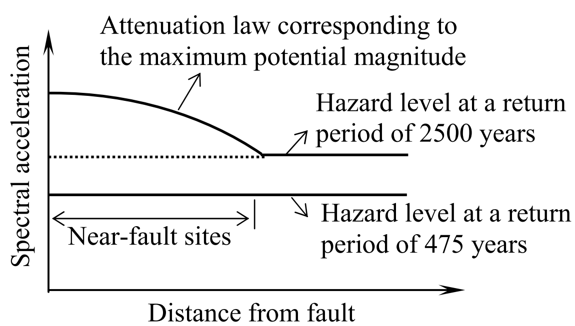

Figure 3: Seismic demand for the checking level at near-fault sites

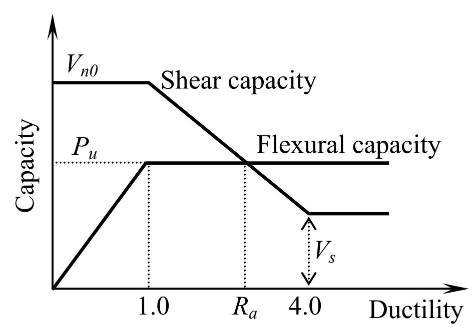

Figure 4: Configuration of flexural to shear failure mode and associated ductility

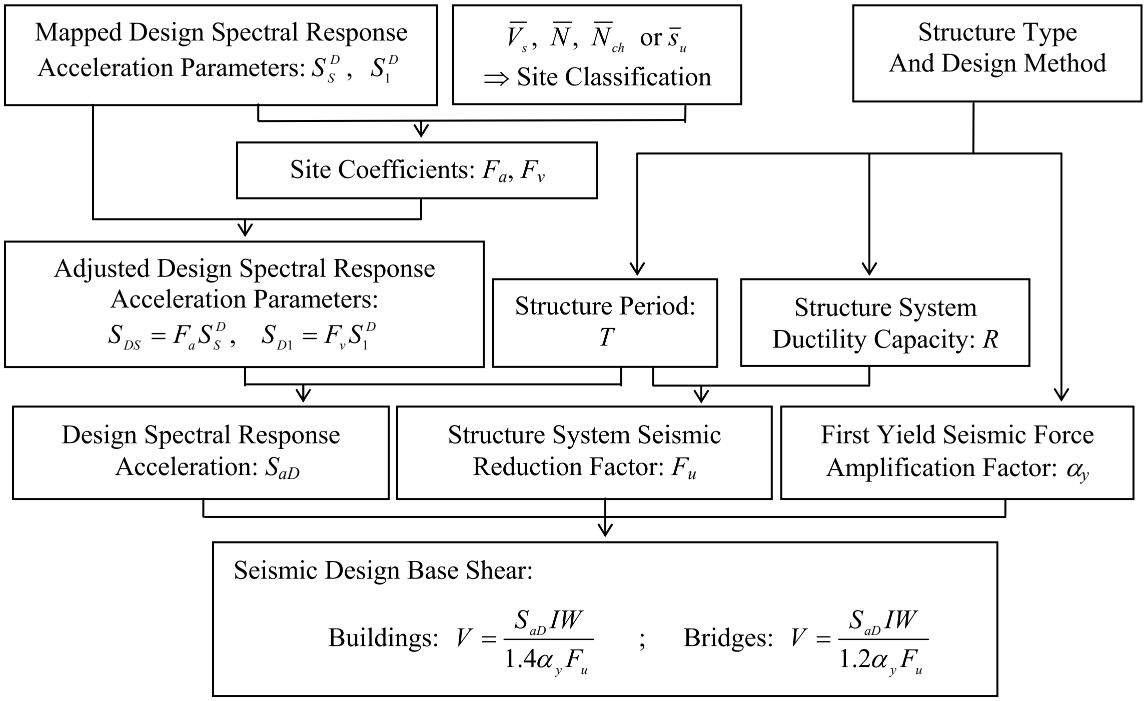

Figure 2: Procedures to determine the seismic design base shear for buildings and bridges

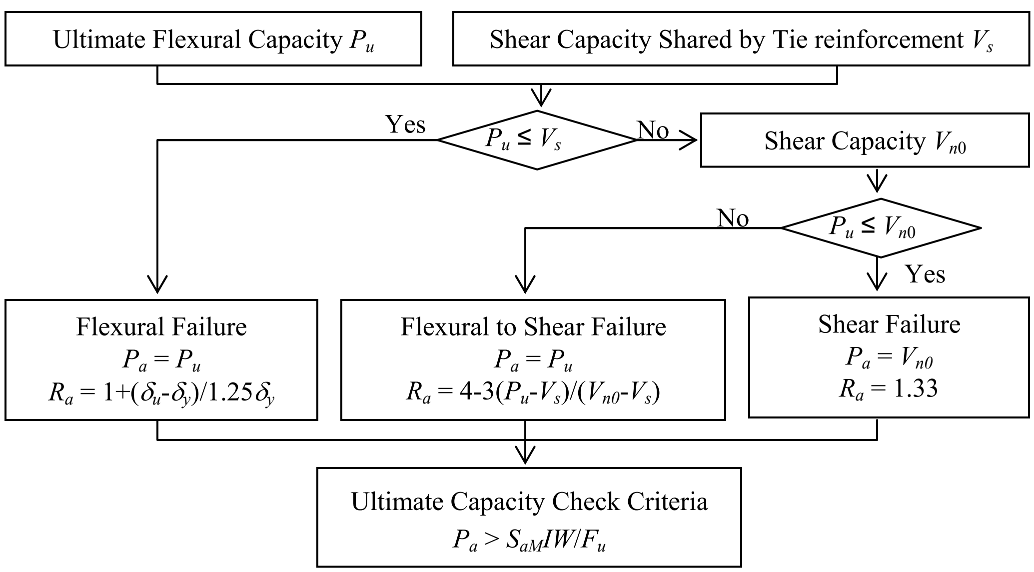

Figure 5: Procedures for the ultimate capacity check

Keywords: two-level seismic design, uniform hazard analysis, site classification, near-fault effect, design spectral response acceleration, seismic demand at checking level, ultimate capacity, and capacity check requirement

DISPLACEMENT-BASED SEISMIC DESIGN FOR HIGH-RISE CONCRETE BUILDINGS

Michael VALLEY, Jeff DRAGOVICH, and John HOOPER[1]

ABSTRACT

A displacement-based design approach applicable to high-rise concrete shear wall buildings is described. The approach includes traditional code-based procedures and features of the capacity design method. Structural performance for two levels of ground shaking is explicitly addressed. Elements are designed and detailed both to produce the desired structural behavior and to meet economic and constructability objectives.

1. BACKGROUND

Seismic design of new buildings in the U.S. typically begins with the selection of a lateral-force-resisting system from a list of many "defined" systems. The same building codes that define these systems impose limits on their use and provide corresponding analysis, design, and detailing requirements. U.S. codes limit the use of reinforced concrete shear wall systems to buildings no taller than 240 feet (73 m) unless a backup moment resisting frame is also provided (to form a "dual system").

Where designers wish to employ a structural system that does not satisfy the prescriptive requirements of the building code, substantiating "cyclic test data and analyses" must be provided. Since the code-based procedures are not directly applicable under these circumstances, "alternative lateral-force procedures using rational analyses based on well-established principles of mechanics" are applied (ICBO, 1997). Regardless of the technical merit of the methods used, the final design must be approved by the building official. The burden of proving the adequacy of an "undefined" structural system rests squarely on the designer.

In recent years several high-rise concrete buildings that exceed the code-imposed 240 feet height limit have been designed by the engineers of Skilling Ward Magnusson Barkshire (Skilling). Six

[1] *Skilling Ward Magnusson Barkshire, Seattle, Washington, U.S.A.*
Email: mtv@skilling.com

such projects have been completed in the Seattle area; key information concerning these projects is presented in Table 1. This paper describes the structural design approach that was used.

Table 1: Seattle-Area Projects

Project	Height	Aspect ratios	Use
Elliott Hotel	330 ft (101 m)	6 and 10	Hotel, exhibit
Key Center	305 ft (93 m)	6 and 7	Office, parking
Millennium Tower	241 ft (73 m)	6 and 8	Residential, office, retail, parking
Terry Avenue Condos	245 ft (75 m)	8 and 12	Residential, parking
1700 Seventh Avenue	320 ft (98 m)	11 and 5	Office, retail, parking
IDX Tower	450 ft (137 m)	5 and 15	Office, parking

2. DESIGN APPROACH

The design approach that is prescribed in U.S. building codes includes explicit consideration of only one level of ground shaking. The intent of the codes is to provide life safe performance for buildings subjected to design-level ground shaking. Generally code writers have assumed that buildings which satisfy the requirements for this single level of design will also have reduced damage in smaller earthquakes and avoid collapse in larger earthquakes. However, none of these performance goals is explicitly considered in the typical U.S. design approach.

2.1 Two-Level Design

The design approach used by Skilling for the previously cited projects was developed with the goals of (1) assuring acceptable performance for the range of anticipated ground motions and (2) putting to rest the concerns of building officials who are used to the traditional design approach. The fundamental decision in the design is the selection of the "fuse," or plastic hinge location, for the building, where the inelastic action will be concentrated. The flexural strength in the hinge region is derived from code-level design forces based on a design earthquake (DE). This portion of the design is consistent with traditional practice and includes application of building code provisions to provide a building strength compatible with the code as well as to satisfy the building official. The subsequent steps in the design process center on a performance evaluation that is used to ensure appropriate controlling behavior, establish the required levels of detailing, demonstrate the suitability of the system, and satisfy the "rational analysis" clause in the building code. This performance evaluation is performed for the maximum considered earthquake (MCE) ground shaking.

2.1.1 Ground shaking hazard

The design is based on mode superposition dynamic analysis, using elastic acceleration response spectra. Two spectra are required, representing the DE and MCE levels of ground shaking. The MCE response spectrum is taken as the MCE spectrum defined in the *International Building Code* (ICC, 2000) or a site-specific response spectrum with a 2 percent probability of exceedance in 50 years. The DE response spectrum is taken as the design response spectrum defined in the *Uniform Building Code* (*UBC*, ICBO, 1997), two-thirds of the MCE response spectrum, or a site-specific response spectrum with a 10 percent probability of exceedance in 50 years. For both levels of analysis, the spectra that produce the most conservative results in the period range of interest are used.

2.2 Modeling and Analysis

To implement the two-level design, two analyses are required–one each for DE and MCE levels of ground shaking. To reflect the differences in behavior that are expected, some of the modeling assumptions differ.

2.2.1 Modeling assumptions

A three-dimensional computer model of the building is created for the analysis. Mode superposition dynamic analysis using elastic response spectra is employed for both levels of ground shaking. The analyses are in general conformance with the dynamic analysis procedures outlined in Section 1631 of the *UBC*. The effective seismic mass is based on the criteria of Section 1630.1.1 of the *UBC*. Element stiffnesses are modeled as linearly elastic, where the assumed stiffness properties are intended to reflect the effective response at the performance level of interest. Table 2 shows the properties that are used in the two analyses. For both levels of analysis, the stiffness properties are achieved by scaling the modulus of elasticity.

Table 2: Stiffness Assumptions for Analysis

Item	Code-Level [DE]	Performance Evaluation [MCE]
Walls, above hinge	$0.8E_c$	$0.75E_c$
Walls, at hinge	$0.8E_c$	$0.5E_c$
Walls, below hinge	$0.8E_c$	$0.75E_c$
Coupling beams	$0.1E_c$ to $0.5E_c$ (Paulay, 1992)	Same as code-level

For some of the projects cited in Table 1, the building official mandated an independent peer review, requiring subsequent nonlinear response history analysis. The response history analyses for DE ground shaking indicated essentially elastic response of the walls, which is consistent with the values indicated in Table 2.

2.2.2 Code-level analysis

The analysis and design procedures implemented for code-level checks are practically identical to the traditional methods used to design concrete shear wall buildings in accordance with the *UBC*. The code-level analysis addresses the following items:

- Regularity checks are performed,
- The redundancy factor, ρ, is applied,
- Both actual and "accidental" torsion are included,
- Torsional effects are amplified as indicated in the *UBC*,
- Directional effects are considered,
- Required strengths are calculated using R equal to 5.5 as for code-compliant concrete shear wall buildings (the forces used in design are described in Section 2.3.1),
- Appropriate load combinations are used,
- Axial load limits are checked, and
- Story drift limits are satisfied.

2.2.3 Performance evaluation analysis

The performance evaluation analysis focuses on determination of the level of roof displacement expected due to occurrence of the maximum considered earthquake, in order to satisfy two main objectives as follows.

- Establish required strengths to limit inelastic response to flexural hinging in coupling beams and in a "hinge zone" near the base of the shear walls.
- Determine the levels of concrete strain in the hinge zone and at locations of abrupt stiffness changes so as to provide appropriate amounts of confinement reinforcement.

The maximum roof displacement during inelastic response to MCE ground shaking is estimated using elastic response spectrum analysis as described above. There are several methods available to compute this value, but elastic response spectrum analysis is relatively simple to implement and has been shown to produce reasonably accurate estimates of displacement. For concrete structures whose fundamental period is larger than the characteristic period of the earthquake, T_g, the nonlinear displacement may be approximated using elastic response spectrum analysis with appropriate stiffness modifications (Shimazaki, 1984). The basic procedure used is as follows.

- Estimate the maximum roof displacement, Δ_u, in each principal building direction using elastic response spectrum analysis with the reduced flexural stiffness properties and unreduced MCE spectrum.
- Determine the roof displacement corresponding to yield of the hinge zone, Δ_y. This is determined using integration of the elastic curvatures over the height of the structure and an estimate of the yield curvature in the hinge zone. The yield curvature in the hinge zone is initially taken as $0.0025/L_w$ and subsequently refined using moment-curvature analysis.
- Calculate the ultimate curvature demand in the hinge zone, ϕ_u, based on the ultimate and yield roof displacements, the geometry of the wall, the yield curvature, and an assumed hinge length ($L_p = L_w/2$).
- Determine the maximum probable moment in the hinge zone, M_{pr}, based on the calculated ultimate curvature and the moment-curvature relation developed for the controlling section using realistic material properties that include the effects of overstrength, strain hardening, and confinement of concrete. The moment-curvature analysis is performed assuming an axial load level of $1.0D + 0.5L$, where D is the dead load and L is the reduced live load.
- Define the system overstrength factor, Ω_0, as the ratio of M_{pr} to M_{code}, where M_{code} is the moment in the hinge zone predicted by the code-level analysis.

2.3 Design

2.3.1 Strength Design

This section describes the force levels used for design of the various elements of the lateral-force-resisting system. The Skilling design approach is based on the capacity design method (Paulay, 1992), whereby elements that are intended to dissipate energy through inelastic response are provided with appropriate strength and ductility and all other elements are made strong enough to remain elastic so that the assumed inelastic mechanism is valid. The components in question include coupling beams throughout the height of the building and shear walls which may be considered to have three distinct regions–above the hinge zone, at the hinge zone itself, and below the hinge zone.

Code-level design forces are used to select the flexural reinforcement for the shear wall hinge zone, which is the primary energy-dissipating element, and for the coupling beams, which are secondary energy-dissipating elements. To alleviate congestion and to promote flexurally dominated response, uniformly spaced longitudinal reinforcement is used to provide flexural capacity in the shear walls. The arrangement of reinforcement in coupling beams (diagonally reinforced or reinforced as beams of a moment frame, depending on the span-to-depth ratio) is in accordance with current U.S. codes (ACI, 1999). For repetition in design and detailing, redistribution of coupling beam forces (up to 20 percent) is allowed between beams in the same bay, so long as the total capacity of all of the coupling beams exceeds the total demand. Flexural and shear design strengths for all elements are calculated as indicated in the *UBC*.

For regions above the hinge zone, the capacity design method proposed by Paulay is used. The goal of the method is to ensure that wall hinging occurs only where assumed (near the base of the structure), and not elsewhere over the height. The essential feature of the method is that a linear variation of moment over the height of the structure is assumed, and the design bending moment envelope above the hinge zone is amplified to ensure that the hinge forms at the assumed location (Paulay, 1992).

For regions below the hinge zone, where the moment diagram drops off due to the transfer of lateral loads from the wall, the hinge zone flexural reinforcement is kept constant to the foundation. That is, the design moment is not reduced from the value at the hinge zone. The diaphragms that transfer loads from the core to basement walls are designed for code-level forces multiplied by the overstrength factor. Where the hinge zone is supported by a discontinuous lateral system, the design forces are based on the code-level forces times the overstrength factor. Where the calculated overstrength factor is less than the code mandated value for discontinuous systems, the code value is used.

Design of wall shear reinforcement is based on the results of the code-level analysis multiplied by the system overstrength factor. This results in a design where flexural hinging precludes shear failure.

2.3.2 Wall Detailing

The arrangement of confinement reinforcement provided in these shear walls is generally consistent with that provided for columns of moment frames. Because this includes cross ties for longitudinal bars throughout the length and height of the walls, the performance of the walls is expected to be better than that provided by typical shear wall detailing. Confinement reinforcement is provided based on recommendations by Wallace (Wallace, 1996). Using the computed maximum compression strain and the depth of the compression zone, three general levels of detailing are used as follows.

Level 1, High level: Where $\varepsilon_{cu} > 0.004$, the requirements of *UBC* Section 1921.6.6.6 (subparagraphs 2.1 through 2.5) are satisfied and the maximum spacing of transverse reinforcement does not exceed 6 inches or 6 longitudinal bar diameters. The walls are proportioned to assure that the maximum compression strain does not exceed 0.01, although the *UBC* allows strains up to 0.015.

Level 2, Moderate level: Where $0.002 < \varepsilon_{cu} \leq 0.004$, the requirements of (ACI, 1999) Section 7.10.5 are satisfied and the maximum spacing of transverse reinforcement does not exceed 8 inches or 8 longitudinal bar diameters. Moderate level details are intended to suppress buckling of longitudinal bars as well as to provide moderate toughness to the wall.

Level 3, Low level: Where $\varepsilon_{cu} \leq 0.002$, the requirements of (ACI, 1999) Section 7.10.5 are satisfied and the maximum spacing of transverse reinforcement does not exceed 12 inches or 12 longitudinal bar diameters.

3. ADDITIONAL ISSUES

3.1 Displacement Calculations

Many researchers (including those participating in this workshop) have proposed methods to calculate the roof displacement of structures subjected to strong ground shaking. However, those more involved calculations are based on many of the same simplifying assumptions used in the approach described above. It is not clear that the additional effort required to implement those calculations would produce meaningful improvements to the design. Nonlinear response history analysis is a possibility, but it is not the most design-friendly method and the results tend to be highly sensitive to minor changes in the modeling assumptions.

3.2 Coupling Beams

The main assumption in the design approach is that the inelastic behavior is concentrated in the wall sections. Although the coupling beams are detailed to sustain large inelastic rotations, they are not assumed to provide the primary energy dissipation mechanism. Some other designers have used an approach where inelastic action is concentrated in the coupling beams and wall sections are designed to remain elastic (CSA, 1994). Both approaches are equally valid if adequate toughness is provided. However, a major disadvantage of concentrating inelastic action in the coupling beams is that coupled wall sections have to be provided in each principal building direction. The resulting reduction of the wall section in each principal direction can diminish the overall structural torsional stiffness, which may not be desirable. Also as compared to C-shaped walls, L-shaped wall sections at corners could then be subjected to increased axial loads and compressive strains, which arise due to directional effects.

3.3 Foundation Design

For the projects described in this paper, a mat foundation was used. To preclude punching shear failures, the foundation shear design is based on the forces from the code-level analysis multiplied by the structural overstrength factor. The flexural strength of the mat is based on DE forces, and the mat is detailed to provide sufficient ductility to accommodate the MCE curvature demands.

4. REFERENCES

ACI Committee 318. (1999). *Building Code Requirements for Structural Concrete*. American Concrete Institute.

CSA Committee A23.3. (1994). *Design of Concrete Structures*. Canadian Standards Association.

ICBO. (1997). *Uniform Building Code*. International Conference of Building Officials.

ICC. (2000). *International Building Code*. International Code Council.

Paulay, T., and M. J. N. Priestley. (1992). *Seismic Design of Reinforced Concrete and Masonry Buildings*. New York: John Wiley & Sons.

Shimazaki K., and M. A. Sozen. (1984). *Seismic Drift of Reinforced Concrete Structures.* Research Reports, Mazama-Gumi, Ltd., Tokyo.

Wallace, J. W. (1996). *A Designer's Guide to Displacement-Based Design of RC Structural Walls*. Final Report to Skilling Ward Magnusson Barkshire.

Wallace, J. W. (1997). *Performance-Based Design of RC Core Wall Systems*. Final Report to Skilling Ward Magnusson Barkshire.

Whittaker et al., "Displacement Estimates for Performance-Based Seismic Design," Journal of Structural Engineering, August 1998.

SESSION A-1: ANALYSIS OF STRUCTURES

Chaired by

♦ W. D. Iwan and Manabu Yoshimura ♦

PUSHOVER ANALYSIS OF RC SHEAR-WALL STRUCTURE WITH CONCRETE SOFTENING

Kangning Li[1], Xilin Lu[2] and Tetsuo Kubo[3]

ABSTRACT

Pushover analysis of reinforced concrete shear-wall structure using fixed load pattern may cause the analysis results to be unstable even divergent, when the concrete of the lower story shear-walls undergoes large compression strain and starts to soften. That is, the concrete softening may result in strength deterioration in the lower stories and the balance between the restoring force and the external load, according to a given load pattern, may not be maintained. The case is studied by analyzing an ultra high-rise building and a RC shear-wall structural model. The method of improving the analysis results is then shown. The method simply allows for the change of load pattern when the concrete softens (it is estimated that the softening begins when the lateral stiffness becomes less than five percent of the initial stiffness). Applying this method, the pushover analysis can be carried out to find the ultimate behavior of the RC shear wall structure and to stabilize the analysis results.

INTRODUCTION

Pushover analysis is a simple and effective method to obtain the nonlinear force-displacement relations, and to find the load-carrying capacity and yielding mechanism of structures. Pushover analysis is usually conducted by gradually increasing the external lateral load according to a set of give load pattern, not by applying displacement (displacement pattern is unknown before the analysis). It is a familiar analysis method to engineers and a useful method in earthquake-resistant structural design. However, in some cases it may have the problem of unstable analysis results or even failure in obtaining the results because of divergence. This case could be met in the analysis of reinforced concrete shear wall structures. It is because the concrete in lower story shear walls tends to undergo large compression strain and softening, and causes significant unbalance between the structural resistance and the external load by the given load pattern.

This paper studies the case using the analysis examples of an ultra high-rise building and a RC shear wall structural model, and shows the method to improve the analysis results and avoid divergence.

1 *Earthquake Disaster Mitigation Research Center (EDM), National Research Institute for Earth Science and Disaster Prevention, Miki, Japan. Email: Kangning@edm.bosai.go.jp, Fax: +81 (794) 83 6695*

2 *College of Civil Engineering, Tongji University, Shanghai, China. Email: lxlries@online.sh.cn*

3 *Department of Architecture, Nagoya Institute of Technology, Nagoya, Japan. Email: kubo@archi.ace.nitech.ac.jp*

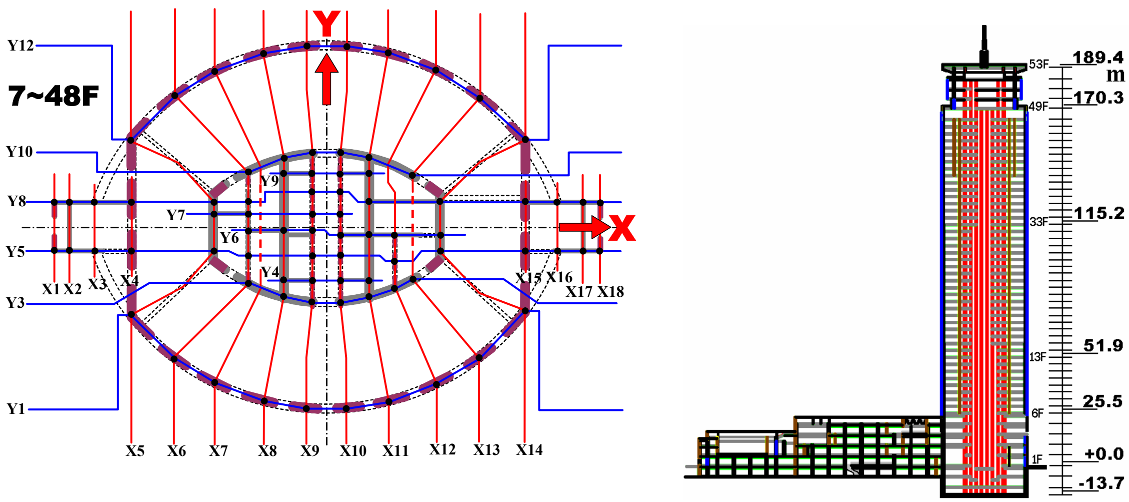

Fig. 1 The Shaanxi IT tower building: Left: main tower typical floor plan; Right: elevation view.

ANALYSIS OF AN ULTRA HIGH-RISE BUILDING

The building is designed and constructed in Xian (Shaanxi-province, China), 190 meters high (52-story) above ground, 3-story basement, double-tube RC shear-wall structure. The main tower typical floor plan and elevation view are shown in Fig. 1. According to the Chinese new seismic design requirements, nonlinear analysis must be carried out to double-check the safety against earthquake load. The analysis uses three-dimensional structural model and bases on the nonlinear force-displacement relations of individual structural members (frame model). The effect of axial load fluctuation in the shear walls and other vertical structural members due to overturning moment is considered using multi-spring model (or fiber model, as shown in Fig. 2). The idealized force-displacement relations (or stress-strain relations) shown in Fig. 3 are assumed for the steel and concrete materials. The concrete of shear walls is treated as unconfined concrete and allowed for concrete softening after the maximum compression strength. Pushover and dynamic response analyses are carried out (the first project in China to carry out such sophisticated analysis). The pushover analysis results are examined and discussed in this paper. The detail of the building structure and other analysis results can be found in the reference (Xu et al. 2001).

The load pattern used in the pushover analysis is simply decided as the weight-and-height proportional pattern (anti-triangle pattern), and the load pattern is kept throughout the analysis process. Other commonly used load patterns are considered to have little difference to the analysis results. Fig. 4 shows the results in the building transverse Y-direction, in the relations of relative inter-story displacement vs. story shear factor. It shows unstable results for the lower stories after large stiffness degradation. In fact, the analysis had to be terminated owing to the divergence when the displacement angle of some lower stories reaches 1/100. It was considered that the concrete of shear walls in lower stories has undergone large deformation over the maximum compression strength and started descending (softening), resulting in unbalance between the internal restoring force and external load and the unbalance could not be corrected. To confirm again the problem, the analysis using simple model of shear-wall structure is carried out as shown in the following section.

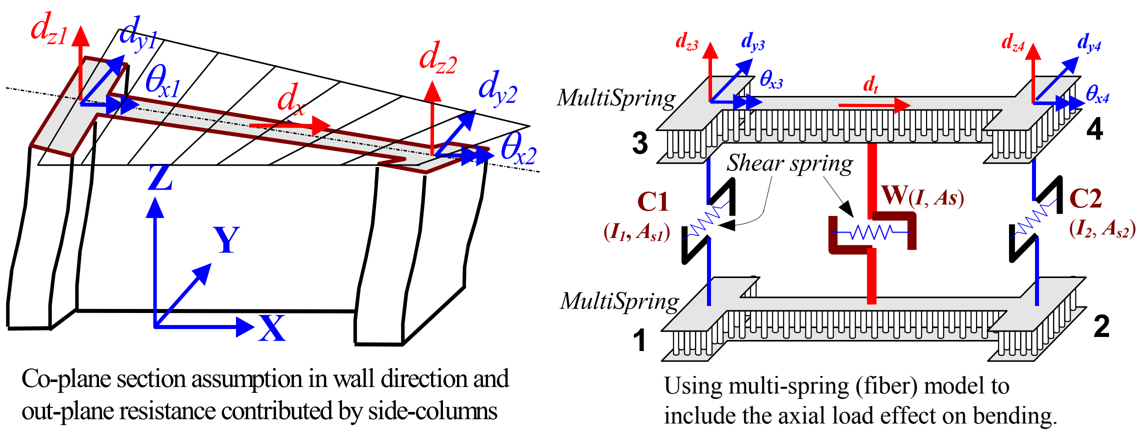

Fig. 2 Three-dimensional analysis model of shear wall

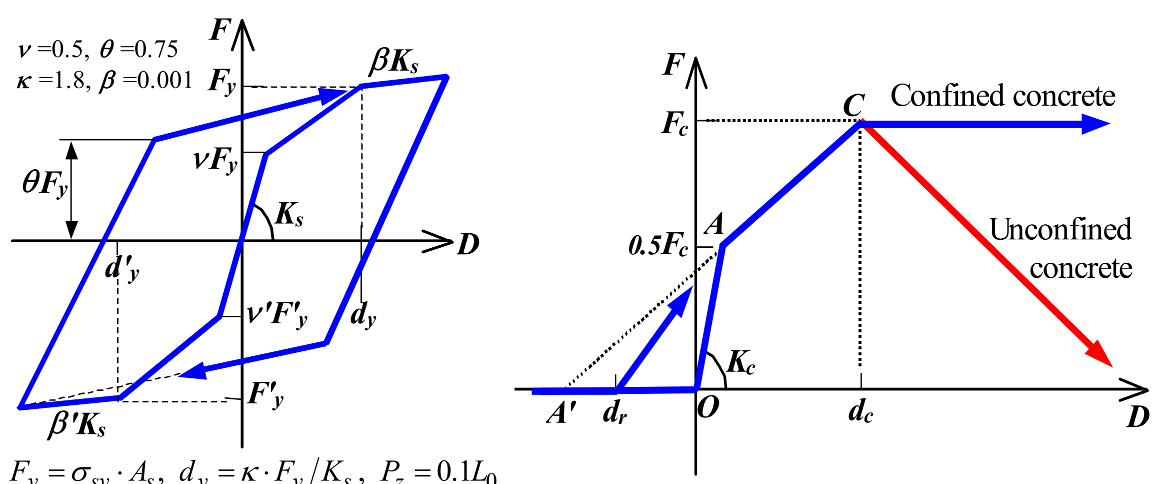

$$F_y = \sigma_{sy} \cdot A_s,\ d_y = \kappa \cdot F_y / K_s,\ P_z = 0.1 L_0$$

$$K_s = \frac{E_s A_s}{\varepsilon_{sy} \cdot P_z},\ \kappa = 1 + \frac{h_0/D - 1}{h_0/D}\ (\kappa \geq 1)$$

(a) Steel material

$$K_c = \frac{E_c A_{ci}}{\varepsilon_c \cdot P_z},\quad F_c = \sigma_c \cdot A_{ci},\ d_c = \varepsilon_c \cdot P_z$$
$$F_t = \sigma_t \cdot A_{ci},\ d_t = \varepsilon_t \cdot P_z$$

(b) Concrete material

Fig. 3. Idealized material force-displacement relations (stress-strain relations)

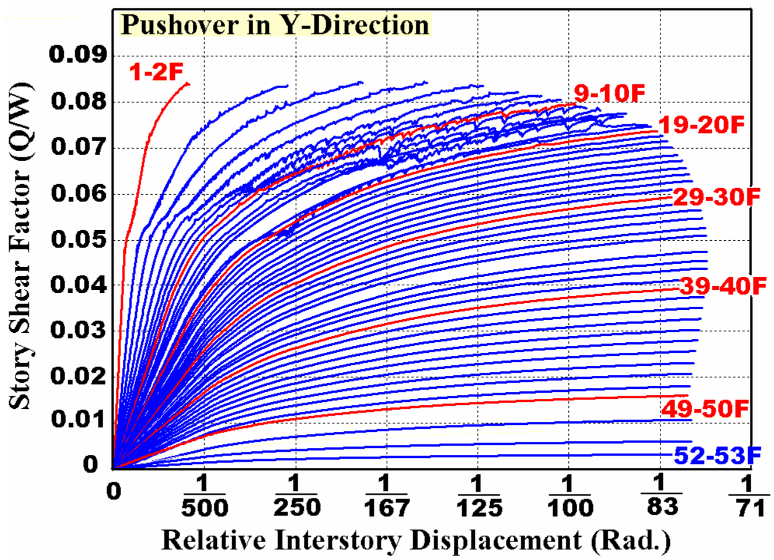

Fig. 4 Analysis results of ultrahigh-rise RC shear-wall building using constant load pattern

ANALYSIS OF SIMPLE MODEL OF SHEAR-WALL STRUCTURE

The simple structural model is shown in Fig. 5, one-span 12-story shear-wall plane frame. The shear-wall span is made equal to 12 or 6 meters. The strength of concrete is assumed to be 35 MPa, and of steel bar is 425 MPa (D35) and 295 MPa (D13). The structural model is treated as a multi-story cantilever column with a deep I-shape section, and the multi-spring model is used to represent the stiffness of the section steel and concrete materials. The section concrete is finely discretized into a large number of small concrete areas, each represented by a concrete spring (using total numbers of 700 and 500 concrete springs for the structural models with span L = 12 m and L = 6 m, respectively).

The analysis results of the structural model are shown in Fig. 6. These results confirmed again the unstable analysis results in lower stories after yielding. However, by comparing the results of the span L = 12 m and L = 6m, it can be seen that the tendency of the unstableness is weakened in the shorter span shear-wall model. The shorter span model is expected to have less concrete softening (smaller deformation). Therefore, for beam-column frame structure having columns in square or short rectangular sections, the column would be almost tension yielding, and then it would not have the unstable analysis results or divergence.

IMPROVING THE PUSHOVER ANALYSIS

Since the unstable results or divergence is caused by the unbalance between the restoring force and external load, the idea of improving is to allow for the change of load pattern when concrete softening occurs. That is, before the yielding, balance is maintained between the internal restoring force and the external load corresponding to the given load pattern, while after yielding the unbalance between the internal force and external load is ignored (the balance among the internal restoring forces is still maintained). This is equivalent to giving a displacement pattern for pushover analysis after yielding. Here the yielding is considered as the story lateral stiffness degradation reaching a certain small value (e.g., 5 % to the initial stiffness).

Thus the analysis results are improved to be even stable against large displacement over 1/100 relative to the story height (Fig. 7 and Fig. 8). Observing and comparing the load patterns at the beginning and final steps, the load pattern change occurs only in the lower stories and the effect to the shear force of each story is expected to be subtle.

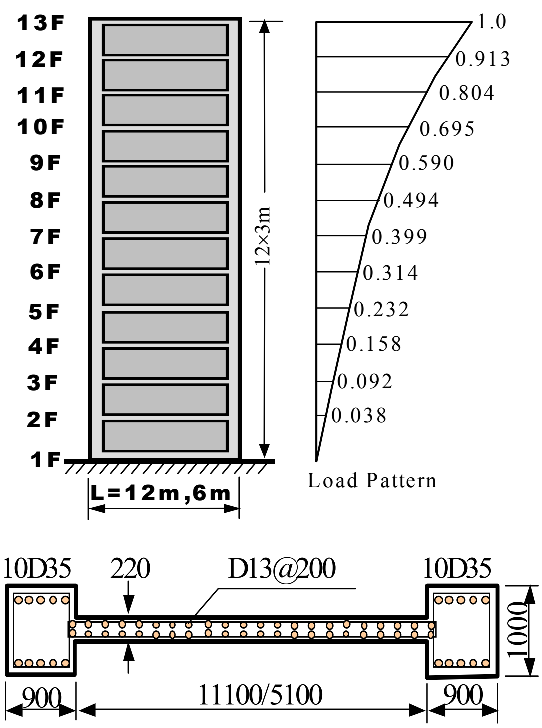

Concrete strength 35 MPa
Steel D35: 425 MPa; D13 295 Mpa.

Fig. 5. Model RC shear-wall structure

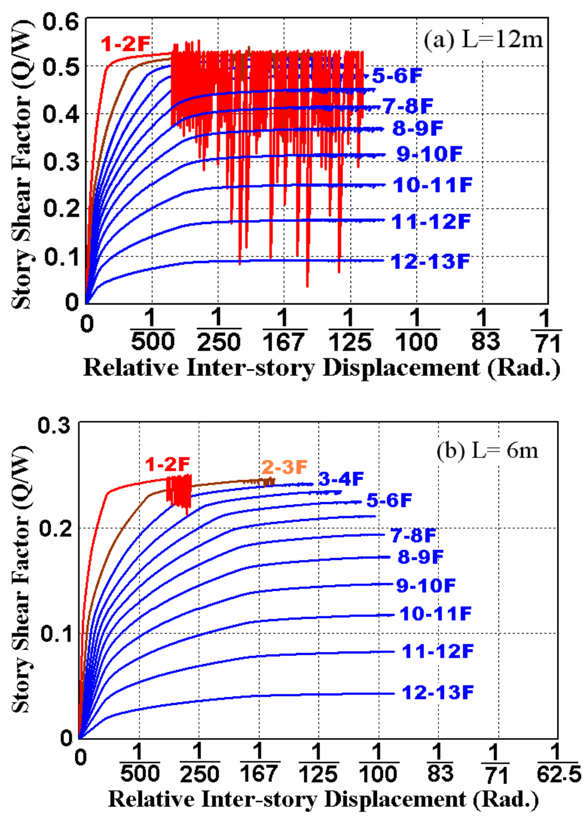

Fig. 6. Analysis results of model structure

CONCLUDING REMARKS

Finding the ultimate force-displacement relations of RC shear-wall structure by pushover analysis using constant load pattern may lead to the problem of unstable results or divergence, when the concrete of shear walls in lower stories undergoes large compression deformation and has concrete softening. To avoid the problem, change of the load pattern may have to be allowed for after a certain small stiffness (e.g., 5% to the initial stiffness) is reached.

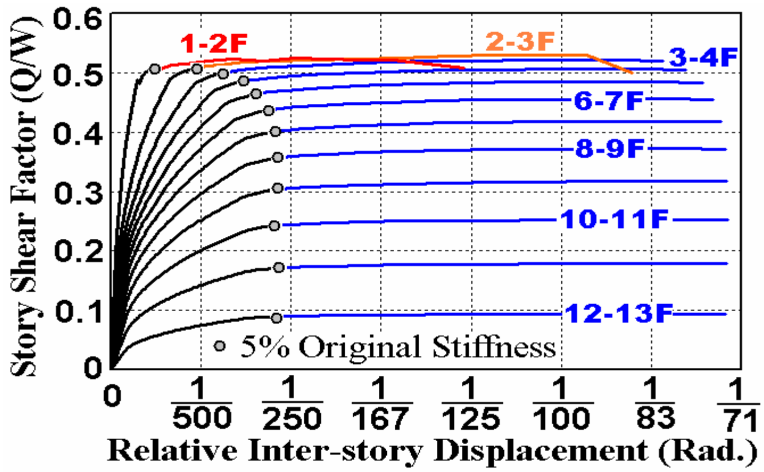

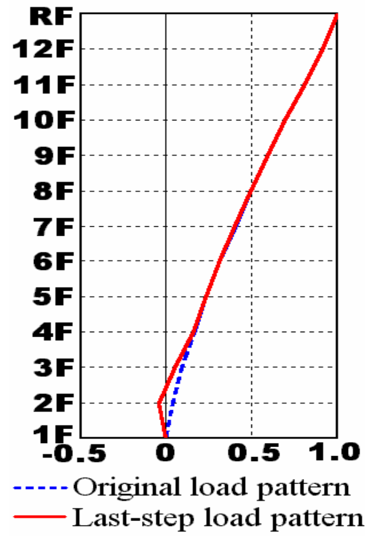

Fig. 7. Pushover analysis results (L = 12 m)
allowed for load pattern change (left) after stiffness ≤ 5 %

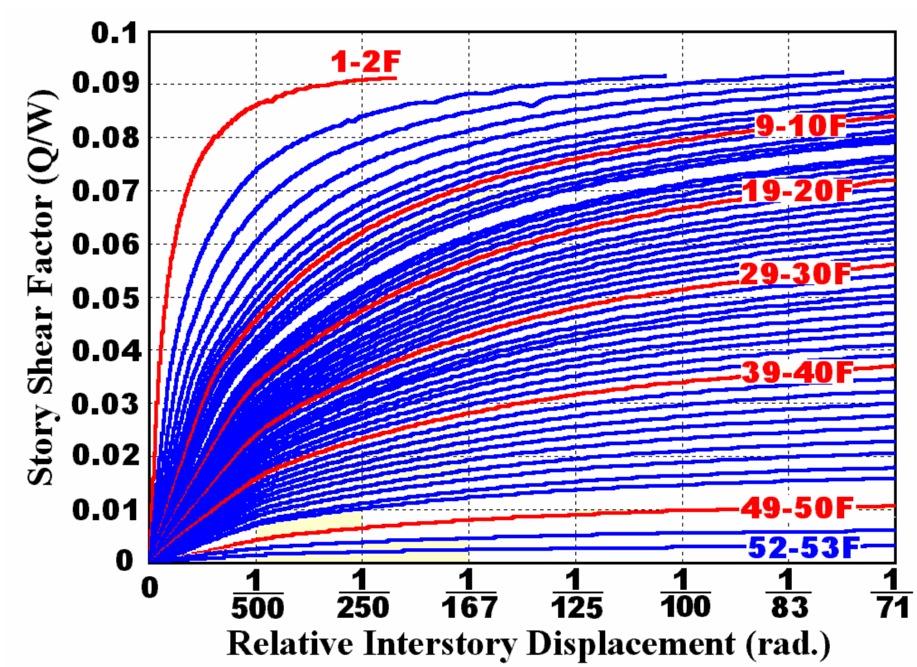

Fig. 8. Pushover analysis results (ultrahigh-rise building) allowed for load pattern change after stiffness degraded to equal or less than five percent of initial stiffness.

REFERENCES

Xu Yongji et al. (2001). Structural Design and Safety analysis of Shaanxi Provincial IT Tower (in Chinese). Proceedings of Sino-Japan Conference on Structural Technologies, June 2001, Xian, China.

PERFORMANCE-BASED SEISMIC DESIGN OF A STRUCTURAL WALL BUILDING BASED ON YIELD DISPLACEMENT

Tjen N. TJHIN and Mark A. ASCHHEIM[1]

John W. WALLACE[2]

ABSTRACT

This paper puts forward a displacement-based design method for reinforced concrete structural wall buildings using yield displacement as the primary design parameter. The method employs an "equivalent" single-degree-of-freedom (ESDOF) system representation of the structure in conjunction with Yield Point Spectra (YPS), to determine the base shear strength required to limit drift and ductility demands to satisfy multiple seismic performance objectives. Simple graphical procedures allow design to be done for only the governing performance objective. Each performance level is expressed in terms of roof drift and plastic hinge rotation at the base of the member having the smallest displacement capacity. The plastic hinge rotation limit is determined based on the axial force level, shear stress level, and boundary confinement provided. Once the base shear coefficient is obtained, standard procedures are used to distribute the lateral forces over the height of the structure and to determine vertical and horizontal reinforcement and details for each member. A six-story structural wall building is used to illustrate the technique; nonlinear static and dynamic analyses of the building demonstrate the simplicity and accuracy of the design methodology.

1. INTRODUCTION

Recent experience with performance-based design has led to the notion that the yield displacement of a structure responding in its predominant mode is nearly invariant even as the lateral strength is adjusted to control the peak response of the system (Aschheim and Black, 2000; Paulay, 2000; Priestley, 2000). Changing the base shear strength of the structure in design normally affects the lateral stiffness and periods of vibration. This was demonstrated by Black and Aschheim (2000) in the performance-based design of 4- and 12-story moment resistant steel frames. The yield displacement was found to be a relatively stable parameter that is more useful for performance-based seismic design than the period of vibration (see Aschheim, 2000).

This paper presents a simple method for the design of reinforced concrete structural wall systems. The method employs an "equivalent" single-degree-of-freedom (ESDOF) system representation of the structure in conjunction with Yield Point Spectra (YPS) to determine the base shear coefficient required to satisfy multiple performance objectives. A six-story structural wall building is used to illustrate the technique; nonlinear static and dynamic analyses of the building are presented to demonstrate the accuracy of the design methodology. The present

[1] *Department of Civil and Environmental Engineering, University of Illinois, Urbana, USA*

[2] *Department of Civil and Environmental Engineering, University of California, Los Angeles, USA*

discussion is limited to full-height prismatic cantilever wall systems of uniform length exhibiting ductile structural response; extensions to treat systems with varied wall lengths are discussed elsewhere (Tjhin et al., 2001). All members in these systems are assumed to be interconnected to each other by floor slabs and to have fixed-based foundations. Buildings are assumed to be regular; torsional conditions are not addressed.

2. IDEALIZED BEHAVIOR OF DUCTILE STRUCTURAL WALLS

The behavior of a prismatic wall in an *n*-story building is idealized in this section for purposes of design. The wall, having height h_w, length l_w, and thickness t_w, is subjected to lateral inertial forces associated with the floor masses (Figures 1(a) and (b)). Assuming response is predominantly in the first mode, the forces along the height of the wall are proportional to the fundamental mode shape and floor masses. Associated with the lateral forces are story shears, wall moments, and the deflected shape shown in Figures 1(c), (d), and (f), respectively.

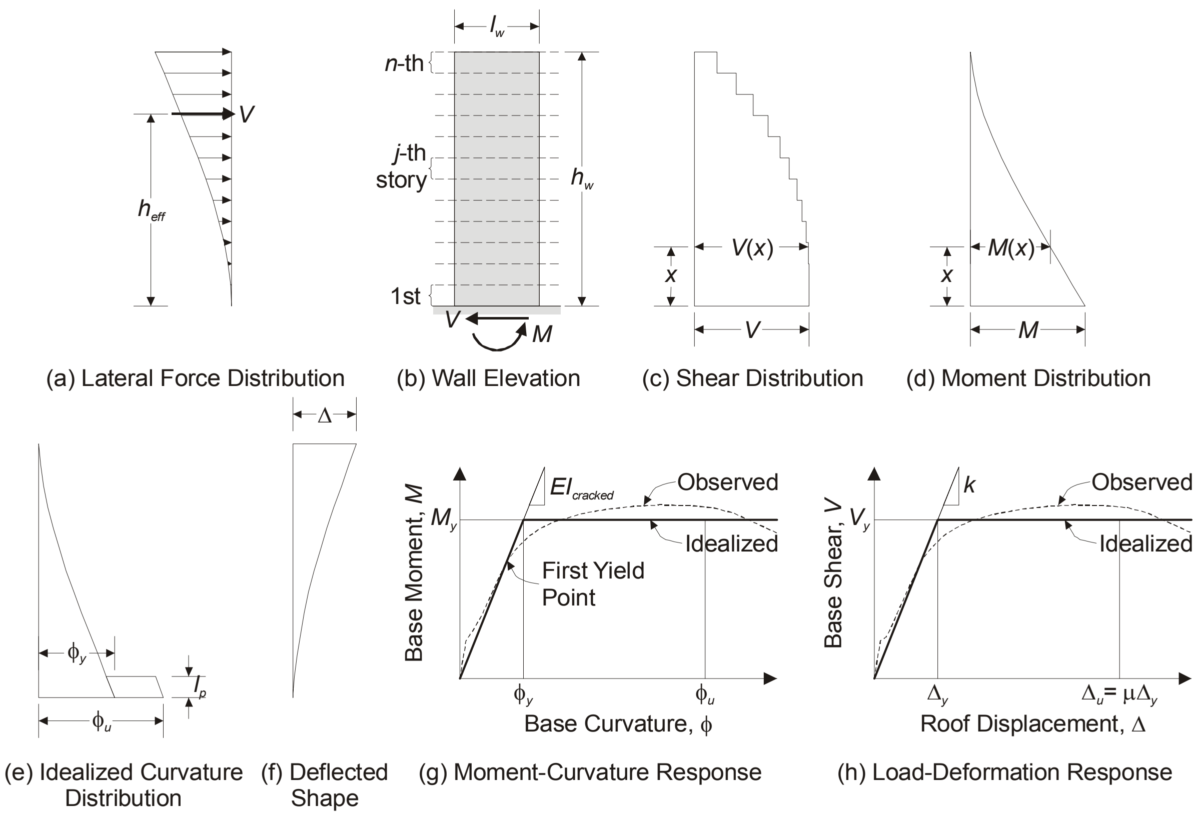

Figure 1: Behavior of a Single Wall System

The sum of the lateral forces is the base shear *V*, equilibrated by a resultant located at a distance h_{eff} from the base. The corresponding overturning moment at the base is $M = Vh_{eff}$. If the wall is designed to yield in flexure at the base and has the moment-curvature relationship shown in Figure 1(g), the moments associated with the predominant mode (Figure 1(d)) give rise to deformations throughout the height of the wall. Based on these deformations, the relationship between roof displacement, Δ, and base shear, *V*, may be derived (Figure 1(h)). Although concrete cracking, concrete softening, and yielding and strain hardening of reinforcing steel influence the response, for design purposes, the load-deformation relationship is idealized as elasto-plastic with stiffness degradation. Similarly, the moment-curvature relationship is idealized as elasto-plastic, with the idealized flexural strength, M_y, set equal to the nominal strength, M_n, calculated according to ACI 318 (1999).

Curvatures over the height of the wall can be estimated by invoking simple beam theory as $M(x)/EI(x)$, where $M(x)$ = moment at a section x from the base and $EI(x)$ = the elastic flexural stiffness of the cross section. Assuming the base of the wall yields in flexure, the yield displacement at the top of the wall, Δ_y, may be estimated based on flexural deformation as

$$\Delta_y = \kappa_\Delta \phi_y h_w^2 \tag{1}$$

where κ_Δ = yield displacement coefficient and ϕ_y = yield curvature of the wall section at the base when the base moment reaches M_y. Values of κ_Δ, computed assuming uniform $EI(x)$ over the height of the wall, uniform floor masses, and response in the fundamental mode, are given in Table 1. The yield curvature, ϕ_y, ideally corresponds to $M_n/EI_{cracked}$. Various definitions of yield curvature, ϕ_y, have been proposed (e.g. Priestley and Kowalsky, 1998; Wallace and Moehle, 1992); these often have the form

$$\phi_y = \frac{\kappa_\phi}{l_w} \tag{2}$$

where κ_ϕ = a yield curvature coefficient that depends primarily on the cross-sectional shape of the wall, axial load level, and the amount, configuration, and yield strength of the longitudinal reinforcement. For rectangular cross sections, κ_ϕ is often in the range of 0.0025 to 0.0035 for Grade 60 steel and for typical levels of axial load and reinforcement ratio (Wallace and Moehle, 1992); a value of 0.0033 is recommended by Paulay and Priestley (1992). The yield curvature for other cross sections, such as flanged or bar-bell sections, can be obtained from a moment-curvature analysis by linearly extrapolating the yield curvature corresponding to the first yield of longitudinal reinforcement to the idealized flexural strength, M_y (Figure 1(g)).

The flexural stiffness of the wall, k, of the idealized load-deformation relationship can be defined in terms of the base shear strength, V_y, corresponding to the flexural strength at the base and the yield displacement at roof, Δ_y, as

$$k = \frac{V_y}{\Delta_y} \tag{3}$$

Ductility in structural walls is best achieved by plastic flexural deformation at and near the base of the wall. The maximum displacement at the roof, or roof drift, Δ_u, includes flexural components associated with deformation of the plastic hinge at the base of the wall and elastic deformations over the height of the wall. According to well-accepted models (Park and Paulay, 1975), the curvature over the height of the wall can be idealized as shown in Figure 1(e). Corresponding to this curvature distribution,

$$\Delta_u = \Delta_y + \theta_p \left(h_w - \frac{l_p}{2} \right) \tag{4}$$

where l_p = plastic hinge length of the wall at the base, θ_p = plastic hinge rotation at the base, and Δ_y is calculated per Equation (1). The plastic hinge length, l_p, typically ranges between $0.5l_w$ and l_w; a value of $0.5l_w$ is recommended for design purposes (Wallace and Moehle, 1992). Based on Figure 1(e), the plastic hinge rotation, θ_p, is

$$\theta_p = (\phi_u - \phi_y) l_p \tag{5}$$

where ϕ_u = ultimate curvature of the wall section at the base. Like ϕ_y, ϕ_u has different definitions (e.g. Priestley and Kowalsky, 1998; Wallace and Moehle, 1992) and is often expressed in the form of Equation (2), except now κ_ϕ becomes the ultimate curvature coefficient, which depends primarily on the cross-sectional shape of the wall, axial load level, confinement level at the boundary, and the amount, configuration, and yield strength of the longitudinal reinforcement. In general, ϕ_u may be obtained from a moment-curvature analysis.

Table 1: Properties of Uniform Walls Responding in the Fundamental Mode

Number of Stories	Γ_1	α_1	κ_Δ	h_{eff}/h_w
1	1.000	1.000	0.333	1.000
2	1.197	0.791	0.316	0.879
3	1.291	0.727	0.308	0.833
4	1.347	0.696	0.303	0.809
6	1.410	0.667	0.297	0.783
10	1.467	0.645	0.293	0.761
15	1.498	0.634	0.290	0.750
20	1.514	0.629	0.289	0.744

Displacement ductility demands and capacities of the system, μ, are defined by

$$\mu = \frac{\Delta_u}{\Delta_y} \tag{6}$$

where μ = displacement ductility, Δ_u = maximum displacement demand or capacity at roof, and Δ_y = yield displacement at roof.

3. ESDOF SYSTEM FOR ESTIMATING INELASTIC SEISMIC DEMANDS

The use of "equivalent" SDOF (ESDOF) systems for estimating the displacement response of multistory buildings is becoming widely accepted. The resistance of the ESDOF system to deformation is calibrated to represent the resistance of the multistory building responding in its predominant mode of response. While ESDOF systems are often used for estimating the displacement response of a multistory building with known properties, they are used here to determine the strength required to assure that the response of the building nominally satisfies its performance objectives. The ESDOF formulation used here is based on ATC-40 (1996) and is summarized in Figure 2. The formulation employs the elastic first mode shape, resulting in a match between the fundamental period of the ESDOF system, T^*, and that of the wall system, T. An elasto-plastic model with stiffness-degrading hysteresis property is used to determine the response of the ESDOF system to design-level ground motions. Alternatively, estimates of the response to a smoothed design spectrum may be obtained with suitable R-μ-T relationships (e.g. Nassar and Krawinkler, 1991).

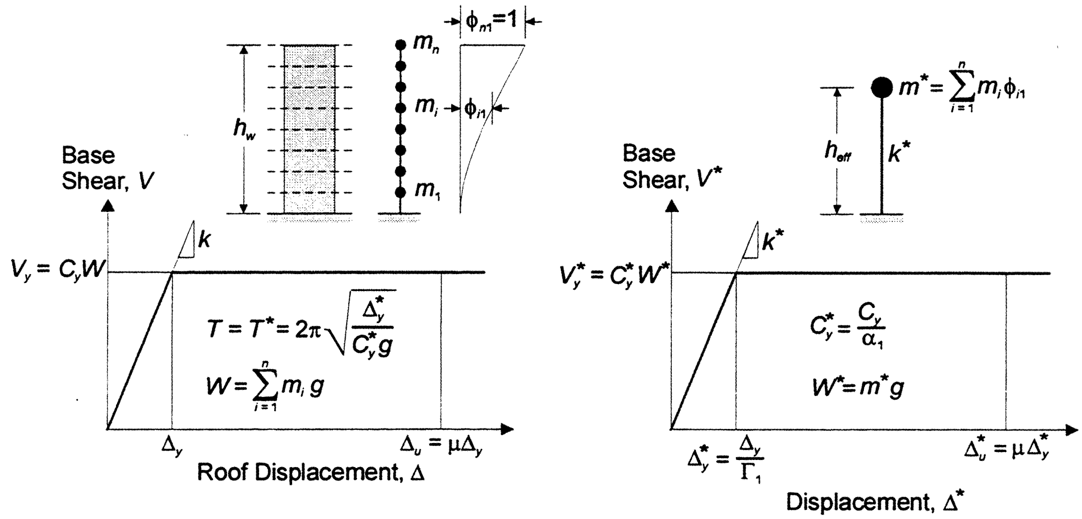

Figure 2: Idealized Load-Deformation Responses of a Wall System and the Equivalent SDOF System

Given an estimate of the yield displacement, Δ_y, the corresponding yield displacement of the ESDOF system, Δ^*_y, is

$$\Delta^*_y = \frac{\Delta_y}{\Gamma_1} \tag{7}$$

where Γ_1 = first mode participation factor, calculated with the mode shape amplitude at roof, ϕ_{n1}, set to unity.

The yield strength coefficient of the ESDOF system, C^*_y, required to satisfy the design objectives is determined using Yield Point Spectra as described in the next section. Once C^*_y is established, the required yield strength coefficient, C_y, and the base shear, V_y, corresponding to developing M_n at the base of the wall are determined as

$$C_y = \alpha_1 C_y^* \tag{8}$$

and $V_y = C_y W$ (9)

where: α_1 = first mode mass coefficient. For buildings with uniform story heights and floor masses, with prismatic walls dominated by flexural deformation, the first mode participation factor, Γ_1, and mass coefficient, α_1, have the values given in Table 1. For nonuniform conditions, Γ_1 and α_1 may be established according to conventional formulas, such as those in ATC-40.

4. YIELD POINT SPECTRA FOR ANALYSIS AND DESIGN

Yield Point Spectra (YPS) are constant displacement ductility spectra plotted on the axes of yield strength coefficient and yield displacement, computed for SDOF oscillators having a range of periods, a specified load-deformation relationship, and a level of damping. YPS may be computed for specific ground motion records (e.g. using USEE (Inel et al., 2001)) or may be estimated by applying R-μ-T relationships to elastic design response spectra. Figure 3 shows an example of YPS for the 1997 Uniform Building Code (ICBO 1997) response spectrum for a rock site, derived using the Nassar and Krawinkler (1991) R-μ-T relationship, for elasto-plastic non-degrading SDOF oscillators having 5% damping ratio.

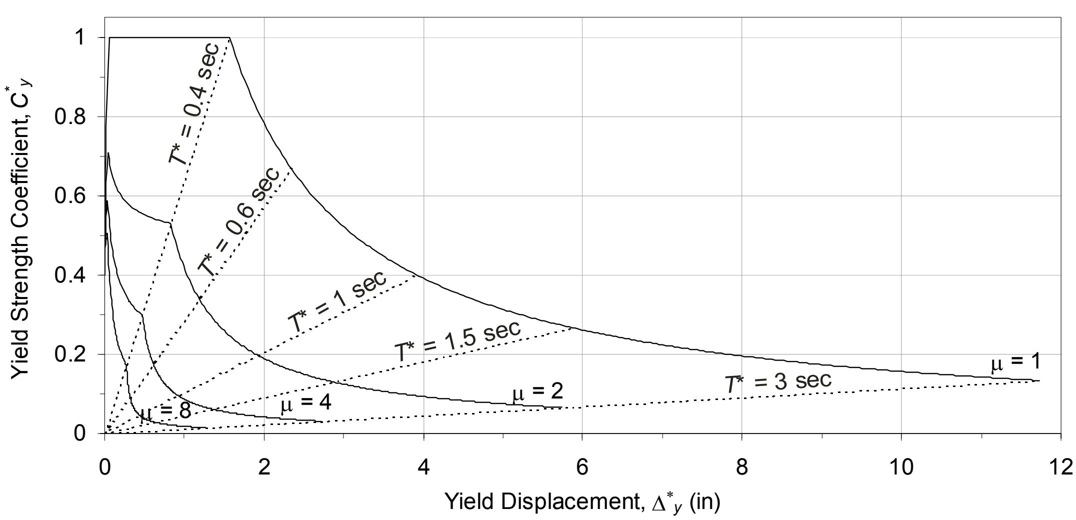

Figure 3: Example of YPS Using Smoothed Design Response Spectra

YPS may be used to estimate the peak response of a SDOF system (or an "equivalent" SDOF system). Given the yield displacement, Δ_y^*, and the yield strength coefficient, C_y^*, an estimate of the ductility demand, μ, may be determined by interpolating between the constant ductility curves. The corresponding drift demand is $\Delta_u^* = \mu\Delta_y^*$. For design, graphical procedures are available to determine admissible combinations of strength and stiffness (or strength and yield displacement) that satisfy one or more performance objectives (see Aschheim and Black, 2000). Given an estimate of the yield displacement, the yield strength coefficient required to satisfy the performance objectives is determined and then is used for design.

5. DESIGN PROCEDURE

The design method explicitly considers various levels of damage, preferably expressed in terms of roof drift and plastic hinge rotation at the base of the walls (Seneviratna and Krawinkler, 1994). Plastic hinge rotation limits associated with different performance levels have been quantified based on axial force level, shear stress level, and boundary confinement (e.g. FEMA 273/274, 1997). Such information is used in the design procedure as follows:

1. Establish performance objectives, wall materials, and wall dimensions.
2. Estimate the yield displacement of the typical wall, Δ_y, using Equation (1). For rectangular cross sections, the yield curvature, ϕ_{yi}, can be estimated using Equation (2) with κ_ϕ value between 0.0025 and 0.0035 for Grade 60 steel. For reasonably regular wall systems, the value of κ_Δ may be estimated using Table 1.
3. For each performance objective, determine the allowable displacement ductility for the system. This value is the minimum of (1) the ratio of the roof drift limit and the yield displacement, and (2) the ratio of the drift limit associated with plastic hinge rotation at the base of the wall (Equation (4)) and the yield displacement.
4. Determine the participation factor for the first mode, Γ_1, and the modal mass coefficient, α_1, or estimate these values using Table 1. Estimate the ESDOF yield displacement, Δ_y^*, using Equation (7).
5. For each performance objective, determine the ESDOF yield coefficient, C_y^*, required to limit the ductility demand of the ESDOF system to the value determined in Step 3. This may be done graphically by constructing admissible regions on a YPS or algebraically by direct calculation. Retain the largest yield coefficient for design.
6. Calculate the required base shear strength, V_y, using Equations (8) and (9). Distribute the base shear over the height of the structure and to various walls of the lateral force resisting system using standard code provisions. Design each plastic hinge region to have the nominal strength, M_n, required to resist the applied lateral forces.
7. Because the development of flexural overstrength in the plastic hinge regions and higher modes will increase wall shears and alter the distribution of moments over the height of the wall, the shear strength over the height of the wall and the flexural strength outside of the plastic hinge region must be increased relative to first mode values (Figures 1(c) and (d)), to ensure that the predominant mode of response consists of the intended flexural mechanism. An approach is recommended by Paulay (1986).

While limited experience suggests the method is reliable for regular buildings, designers may wish to conduct pushover analyses to refine the design or may wish to perform nonlinear dynamic analyses to develop statistics on performance, particularly for irregular buildings.

6. DESIGN EXAMPLE

A six-story structural wall building was designed to illustrate the technique. The typical floor plan is shown in Figure 4; story heights are 12 ft. Space constraints limit discussion to the design of the four W1 walls in the N-S direction. Design of the N-S and E-W walls is described in greater detail in Tjhin et al. (2001). Preliminary dimensions for the walls are also shown in Figure 4. A concrete compressive strength of 5 ksi and a steel yield strength of 60 ksi were used in design. Floor dead and live loads were 175 and 50 psf, respectively. Performance objectives were obtained from FEMA 273/274 (1997), and FEMA 302 (1997) was used to distribute the base shear vertically. Proportioning and detailing of the walls followed ACI 318 (1999).

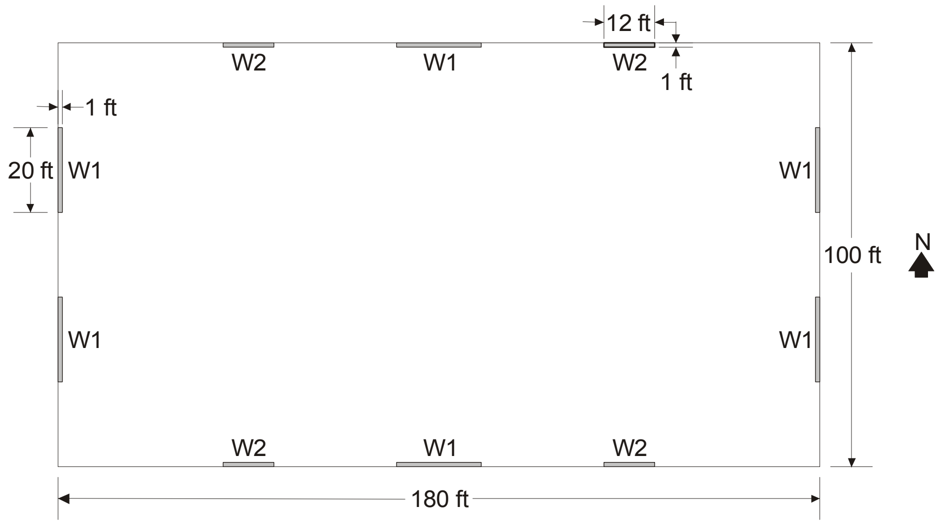

Figure 4: Typical Floor Plan

The building was designed to satisfy three performance objectives as shown in Table 2. Damage levels associated with each performance level were obtained from FEMA 273, for illustrative purposes (Table 3). The plastic hinge rotation limits in Table 3 strictly apply to existing construction only, and are based on unconfined concrete, an axial force level of less than $0.1t_w l_w f_c'$, and a shear force level of less than $3t_w l_w \sqrt{f_c'}$ (psi units).

Table 2: Assumed Performance Objectives

Earthquake Hazard Level	Building Performance Level
50 % Exceedance in 50 Years	Immediate Occupancy (IO)
10 % Exceedance in 50 Years	Life Safety (LS)
5 % Exceedance in 50 Years	Collapse Prevention (CP)

Table 3: Assumed Damaged Levels per FEMA 273

Limit	Building Performance Level		
	IO	LS	CP
Roof Drift (% of Building Height)	0.5	1	2
Plastic Hinge Rotation (rad)	0.002	0.004	0.008

Smoothed design spectra would normally be used for design. In this example, actual earthquake records are used so that the performance of the design can be assessed by nonlinear dynamic analysis using the design records. The 1987 Whittier Narrows, the 1940 N-S El Centro, and the 1985 Chile (N10E Llolleo) records were selected somewhat arbitrarily to represent IO, LS, and CP design earthquakes, respectively.

The properties of wall W1 are summarized in Table 4. The yield curvature, ϕ_y, was estimated as $0.003 / l_w$; the κ_Δ value for estimating the yield displacement, Δ_y, was obtained from Table 1. The plastic hinge rotation, l_p, was estimated as $0.5 l_w$. The first mode participation factor and mass coefficient were also determined from Table 1, as 1.410 and 0.667, respectively. The ESDOF yield displacement, Δ^*_y, is 2.78/1.410 = 1.97 in.

Table 4: Wall W1 Properties

Wall ID	t_w (in)	l_w (in)	h_w (in)	l_p (in)	ϕ_y (10^{-6} rad/in)	Δ_y (in)
W1	12	240	864	120	12.5	2.78

Table 5 summarizes the allowable system displacement ductilities corresponding to the performance levels. As shown in the shaded cells of the table, the roof drift limit controls design for the IO performance level whereas the plastic hinge rotation limit controls for the LS and CP performance levels.

Table 5: Drift and Ductility Limits

Limit	Building Performance Level		
	IO	LS	CP
Drift-Controlled			
Roof Drift (% of Building Height)	0.5	1	2
Roof Drift (in)	4.32	8.64	17.28
System Displacement Ductility	1.56	3.11	6.23
Plastic-Hinge-Controlled			
Plastic Hinge Rotation (rad)	0.002	0.004	0.008
Roof Drift (in)	4.38	5.99	9.21
Curvature (10^{-6} rad/in)	29.2	45.8	79.2
System Displacement Ductility	1.58	2.16	3.32

The use of admissible design regions for design is illustrated in Figure 5. Consider first the LS performance objective. The YPS for the LS design earthquake, i.e., the El Centro motion, is shown in Figure 5(b). The drift and plastic hinge rotation limits result in a valley-shaped curve denoted by the thick line in the figure. The curve to the right of point *A* represents oscillators that just satisfy the drift limits, and the curve to the left of point *A* represents oscillators that just satisfy the plastic hinge rotation limits. This curve defines the boundary of an admissible design region and is termed the "Life Safety Demand Curve." Oscillators with yield points that lay above the Life Safety Demand Curve have better performance than those required for this performance objective. For the CP performance objective, none of the oscillator responses shown in Figure 5(c) reach the roof drift limit of 17.28 in. As a result, only the plastic hinge rotation limit constrains the admissible design region. For the IO performance objective, the oscillator responses shown in Figure 5(a) can neither reach the drift nor the plastic hinge rotation limits; thus the entire region is admissible. Demand curves for all performance objectives are superimposed in Figure 5(d). In this example, the LS Demand Curve controls over all other performance objectives. Entering Figure 5(d) with the ESDOF yield displacement of 1.97 in. establishes a minimum value of C_y^* of 0.0907 to satisfy the three performance objectives; the corresponding base shear coefficient is C_y = 0.667(0.0907) = 0.0605. Thus, the design base shear is V_y = 0.0605W = 1140 kips. The fundamental period of the building (and the ESDOF system) can be determined from $T = 2\pi\sqrt{\Delta_y^* / C_y^* g}$ = 1.49 sec.

FEMA 302 was used to distribute the base shear over the height of the building. For T = 1.49 sec, a nearly parabolic distribution (k = 1.75) is used. If the base shear were distributed in the fundamental mode, h_{eff} equals $0.783h_w$ according to Table 1, and the corresponding required M_y for each wall is 16,100 k-ft. Using the FEMA distribution, $h_{eff} = 0.790h_w$, and the corresponding required M_y is 16,300 k-ft. The walls were proportioned to have M_n = 16,400 k-ft, satisfying both distributions. Wall shears and moments were amplified for design of the remaining portions of the walls using the approach suggested by Paulay (1986). Code provisions for accidental torsion were not applied. The final design is shown in Figure 6.

To validate the method, nonlinear static (pushover) and nonlinear dynamic analyses were done using Drain-2DX (Prakash et al., 1993). The wall system was modeled using fiber beam-column (Type 15) elements (Powell, 1993). Each wall consisted of six elements, one element per story. Each element was divided into six segments along the element axis. The cross section of each segment was divided into 20 fibers. The model employed unconfined concrete and a bilinear stress-strain relationship for the longitudinal steel. The mass was lumped at the ends of the element. A damping ratio of 5% was applied to modes 1 and 3. Figure 7 compares the load-deformation curve used for design and that obtained from the nonlinear static analysis. Figure 8 compares the roof displacement response history of the ESDOF system used for design and response of the MDOF model computed using Drain 2DX. Both figures confirm the design method.

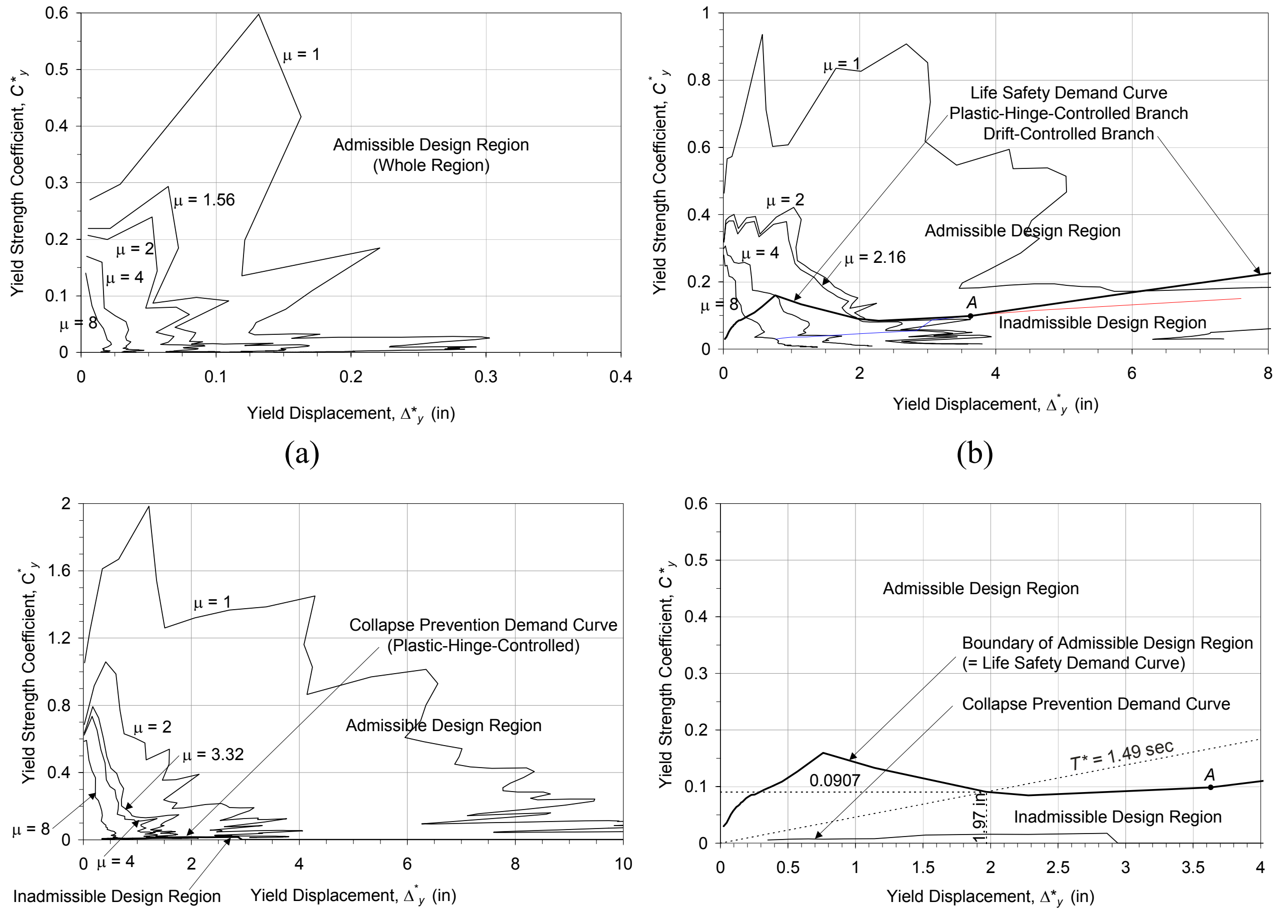

Figure 5: Admissible Design Regions for (a) IO Performance Objective, (b) LS Performance Objective (c) CP Performance Objective, and (d) All Performance Objectives

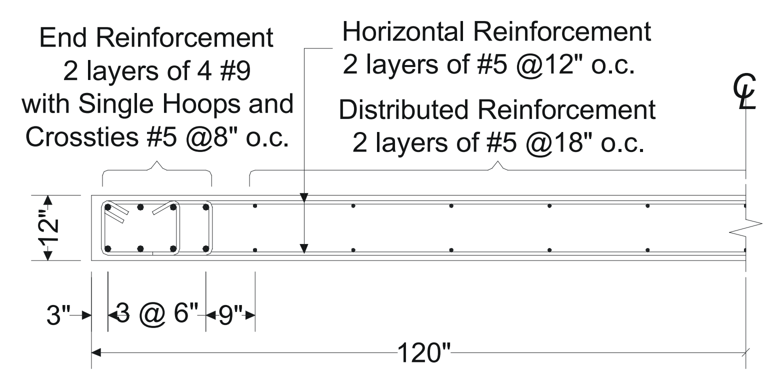

Figure 6: Reinforcing Details at the Base of Wall W1

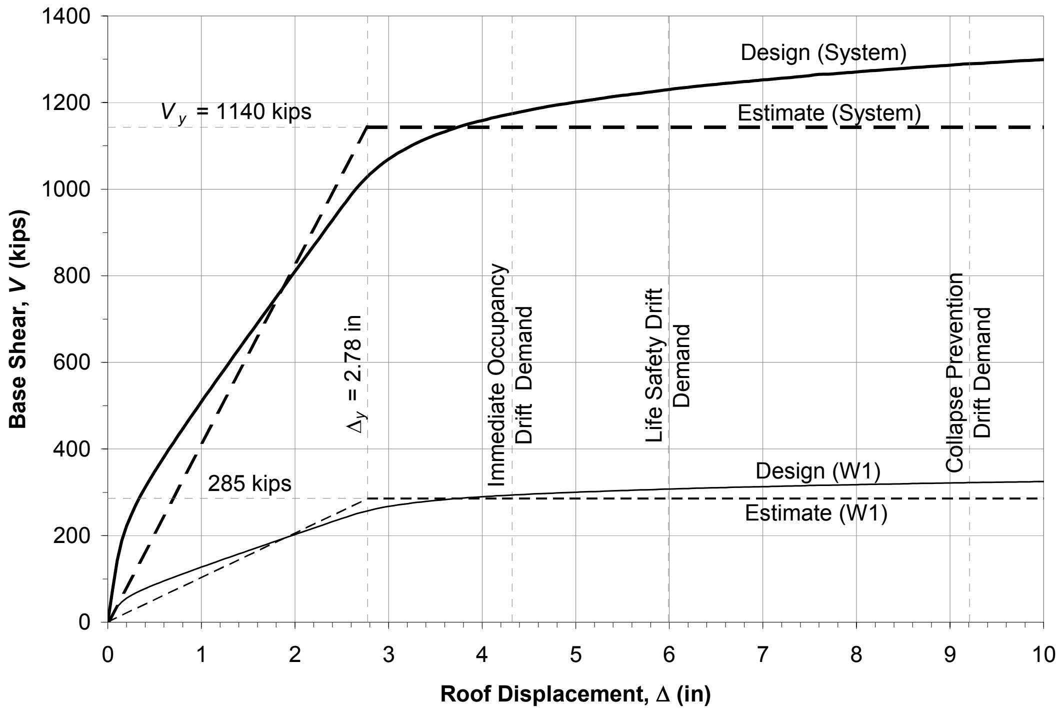

Figure 7: Capacity Curves Determined from Pushover Analysis

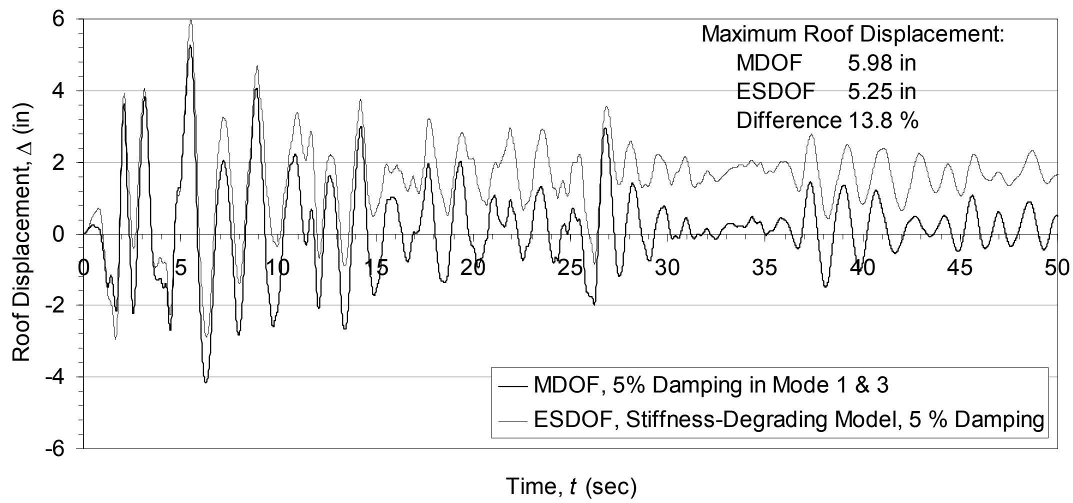

Figure 8: Displacement Histories under Life Safety Design Earthquake

7. CONCLUSIONS

While other techniques for the design of structural wall buildings based on ESDOF systems have been suggested recently, none appear to be as simple, straightforward, and accurate as the one described here. The method emphasizes design based on yield displacement rather than period. The yield displacement is stable and can be estimated easily given the initial geometry and material properties. Limited experience suggests that the yield displacement estimate is sufficiently accurate that design iterations are usually not required. A further advantage of the method is the ability to simultaneously consider multiple performance objectives, with a single design being developed only for the most critical performance objective.

8. ACKNOWLEDGMENTS

This work was supported in part by the Earthquake Engineering Research Centers Program of the National Science Foundation under Award Number EEC-9701785.

9. REFERENCES

American Concrete Institute Committee 318 (ACI 318) (1999). *Building Code Requirements for Structural Concrete (ACI 318-99) and Commentary (ACI 318R-99)*. Farmington Hills, MI: American Concrete Institute.

Aschheim, M., (2000). The Primacy of the Yield Displacement in Seismic Design. *Second US-Japan Workshop on Performance Based Design of Reinforced Concrete Buildings*.

Aschheim, M. A., and Black, E. F. (2000). Yield Point Spectra for Seismic Design and Rehabilitation. *Earthquake Spectra* 16(2): 317-335.

ATC-40 (1996). *Seismic Evaluation and Retrofit of Concrete Buildings* (Report No. SSC 96-01). Redwood City, CA: Applied Technology Council.

Black, E. F., and Aschheim, M. A. (2000). *Seismic Design and Evaluation of Multistory Buildings Using Yield Point Spectra* [CD-ROM Release 00-04]. Urbana, IL: Mid-America Earthquake Center, University of Illinois.

FEMA 273 (1997). *NEHRP Guidelines for the Seismic Rehabilitation of Buildings* (Report No. FEMA 273). Washington, DC: Federal Emergency Management Agency.

FEMA 274 (1997). *NEHRP Commentary on the Guidelines for the Seismic Rehabilitation of Buildings* (Report No. FEMA 274). Washington, DC: Federal Emergency Management Agency.

FEMA 302 (1997). NEHRP Recommended Provisions for Seismic Regulations for New Buildings and Other Structures, Part 1 - Provisions (Report No. FEMA 302). Washington, DC: Federal Emergency Management Agency.

FEMA 303 (1997). NEHRP Recommended Provisions for Seismic Regulations for New Buildings and Other Structures, Part 2 - Commentary (Report No. FEMA 303). Washington, DC: Federal Emergency Management Agency.

Inel, M., Black, E. F., Bretz, E. M., Aschheim, M. A., and Abrams, D. P. (2000). *Utility Software for Earthquake Engineering (USEE) Version 1.0* [Computer program and manual]. Urbana, IL: Mid-America Earthquake Center, University of Illinois. Available: http://mae.ce.uiuc.edu/.

International Conference of Building Officials (ICBO) (1997). *Uniform Building Code*. Whittier, CA.

Nassar, A. A., and Krawinkler, H. (1991). *Seismic Demands for SDOF and MDOF Systems* (Report No. 95). Stanford, CA: John A. Blume Earthquake Engineering Center, Stanford University.

Park, R., and Paulay, T. (1975). *Reinforced Concrete Structures*. New York: John Wiley & Sons.

Paulay, T. (1986). The Design of Ductile Reinforced Concrete Structural Walls for Earthquake Resistance. *Earthquake Spectra* 2(4): 783-823.

Paulay, T. (2000). A Simple Displacement Compatibility-Based Seismic Design Strategy for Reinforced Concrete Buildings (Paper No. 0062). *Proceeding of the 12th World Conference on Earthquake Engineering*.

Paulay, T., and Priestley, M. J. N. (1992). *Seismic Design of Reinforced Concrete and Masonry Buildings*. New York: John Wiley & Sons.

Powell, G. H. (1993). *Drain-2DX Element Description and User Guide for Element Type01, Type02, Type04, Type06, Type09, and Type15 Version 1.10* (Report No. UCB/SEMM-93/18). Berkeley, CA: Structural Engineering Mechanics and Materials, University of California.

Prakash, V., Powell, G. H., and Campbell, S. (1993). *Drain-2DX Base Program Description and User Guide Version 1.10* (Report No. UCB/SEMM-93/17). Berkeley, CA: Structural Engineering Mechanics and Materials, University of California.

Priestley, M. J. N. (2000). Performance-Based Seismic Design (Paper No. 2831). *Proceeding of the 12th World Conference on Earthquake Engineering*.

Priestley, M. J. N, and Kowalsky, M. J. (1998). Aspects of Drift and Ductility Capacity of Rectangular Cantilever Structural Walls. *Bulletin NZNSEE* 31(2): 73-85.

Seneviratna, G. D. P. K., and Krawinkler, H. (1994). Strength and Displacement Demands for Seismic Design of Structural Walls. *Proceedings of the 5th National Conference on Earthquake Engineering*.

Tjhin, T. N., Aschheim, M. A., and Wallace, J. W. (2001). *Performance-Based Seismic Design of Ductile Reinforced Concrete Wall Buildings* (Report in preparation). Urbana, IL: University of Illinois.

Wallace, J. W., and Moehle, J. P. (1992). Ductility and Detailing Requirements of Bearing Wall Buildings. *Journal of Structural Engineering* 118(6): 1625-1644.

Keywords

reinforced concrete structural wall; shear wall; seismic design; performance-based design; displacement-based design; yield displacement; yield point spectra.

COMPARISON OF SIMPLIFIED PROCEDURES FOR NONLINEAR SEISMIC ANALYSIS OF STRUCTURES

Dan Zamfirescu[1] and Peter Fajfar[2]

ABSTRACT

In the paper, six simplified procedures for nonlinear seismic analysis and/or performance evaluation of building structures, based on pushover analysis and response spectrum approach, are briefly described and employed for analysis of a regular multi-story frame structure. Two simple procedures, that do not require the pushover analysis, are also included. The results of simplified procedures are compared with the results of nonlinear dynamic analyses. The comparison indicates that the employed procedures generally yield results of adequate accuracy. However, they differ in regard to simplicity, transparency and the clarity of the theoretical background.

INTRODUCTION

The structural engineering community has developed a new generation of design and seismic evaluation procedures that incorporates performance-based engineering concepts. It has been recognized that damage control must become a more explicit design consideration. This aim can be achieved only by introducing some kind of nonlinear analysis into the seismic design methodology. In a short term, the most appropriate approach seems to be a combination of the nonlinear static (pushover) analysis and the response spectrum approach. Examples of such an approach are the capacity spectrum method, applied in *ATC 40* (ATC, 1996) in Trisevices' manual (Freeman, 1998), and in Japanese Building Standard Law (Otani et al, 2000), the nonlinear static procedure, applied in *FEMA 356* (FEMA, 2000), the N2 method developed at the University of Ljubljana (Fajfar, 2000) and implemented in the draft Eurocode 8 (EC8, 2001), and the Modal Pushover Analysis (Chopra and Goel, 2001a). All methods combine the pushover analysis of a multi-degree-of-freedom (MDOF) model with the response spectrum analysis of an equivalent single-degree-of-freedom (SDOF) system. Inelastic spectra or elastic spectra with equivalent damping and period are applied. As an alternative representation of inelastic spectrum the Yield point spectrum has been developed (Aschheim and Black, 1998). Some other simplified procedures based on deformation-controlled design have been developed, e.g. the approaches developed by Priestley (Priestley,

[1] *Technical University of Civil Engineering Bucharest*
[2] *University of Ljubljana*
Contract/grant sponsors: European Commission through the SAFERR project (for the first author) and Ministry for Education, Science and Sport of the Republic of Slovenia (for the second author).

1997, Priestley 2000) and by Panagiotakos and Fardis, 1998).

The aim of the paper is to evaluate the suitability of the above procedures for practical application based on accuracy, simplicity, transparency and clarity of theoretical background. First, a typical procedure based on pushover analysis is summarized and its implementation in the N2 method is described. Then a summary of other methods is presented with the emphasis on differences to the reference (N2) method. All methods have been applied for analysis of a five-story regular reinforced concrete frame. The main results are compared with the results of nonlinear dynamic analyses. Finally, some conclusions are drawn. The limitations of the procedures should be observed. All of them are, for the time being, limited to planar structures vibrating predominantly in the first mode.

SUMMARY OF A TYPICAL PROCEDURE AND ITS IMPLEMENTATION IN THE N2 METHOD (for details, see Fajfar, 2000)

Step 1: Data

As a rule, a planar MDOF structural model is used. Seismic demand is traditionally defined in the form of an elastic (pseudo)-acceleration spectrum S_{ae}. The specified damping coefficient is taken into account in the spectrum. For an elastic SDOF system, the acceleration (S_{ae}) and displacement spectrum (S_{de}) are related. They can be plotted in the same plot if the acceleration – displacement (AD) format is used.

Step 2: Pushover analysis

Using a pushover analysis, a characteristic nonlinear force - displacement relationship of the MDOF system can be determined. Usually, base shear and roof (top) displacement have been used as representative of force and displacement, respectively. The selection of an appropriate lateral load distribution is an important step within the pushover analysis. In the N2 method, the lateral load distribution is related to the assumed displacement shape. The lateral force in the i-th level is proportional to the component Φ_i of the assumed displacement shape, i.e. to the assumed displacement in the i-th level, weighted by the story mass m_i:

$$P_i = p\, m_i\, \Phi_\mathrm{i} \qquad (1)$$

where p is the proportionality factor. Consequently, the assumed load and displacement shapes are not mutually independent as in the majority of other pushover analysis approaches. Note that Equation (1) does not present any restriction regarding the distribution of lateral loads. Usually, this distribution is assumed directly. In the N2 method, the distribution is assumed indirectly, by assuming the displacement shape. Such an approach for the determination of the distribution of lateral loads has a physical background: if the assumed displacement shape was exact and constant during ground shaking, then the distribution of lateral forces would be equal to the distribution of effective earthquake forces. Moreover, by using lateral forces according to Equation (1), the transformation from the MDOF to the equivalent SDOF system and vice-versa (Steps 3 and 6) follows from simple mathematics. No additional approximations are required, as in the case of some other procedures.

In code procedures, some guidelines for the selection of the distribution of lateral forces have to be provided. According to the new draft of Eurocode 8 (EC8, 2001), in which the N2 method has been implemented, at least two vertical distributions of lateral loads should be applied: a "uniform" pattern, based on lateral forces proportional to story masses, and a "modal" pattern, proportional to lateral force distribution determined in elastic analysis (based on equivalent static procedure or modal analysis). In the case of the "modal" pattern, the assumed displacement shape is equal to the first mode shape if only the first mode is taken into account. If higher modes are accounted for, the distribution of lateral forces is determined from the story shears, computed by the SRSS or CQC combination rule, and the displacement shape is determined from Equation (1). In the comparative study, reported in this paper, both "uniform" and "modal" pattern will be used.

Step 3: Equivalent SDOF model and capacity diagram

In the simplified methods, seismic demand is determined by using response spectra. Consequently, the structure should, in principle, be modeled as a SDOF system. Different procedures have been used to determine the characteristics of an equivalent SDOF system. Unless an "adaptive" pushover procedure is used, it is assumed that the displacement shape is constant, i.e. that it does not change during the structural response to ground motion. This is the basic and the most critical assumption within the procedure. In the N2 method, both forces and displacements are transformed using the same equivalence factor Γ, which is a function of masses and assumed displacement shape. This follows from a mathematical derivation (Fajfar 2000) and is a consequence of lateral loads pattern which is related to the assumed displacement shape. Γ is usually called the modal participation factor. Note, however, that any reasonable shape can be used as displacement shape. The elastic first mode shape is just a special case. Γ is equivalent (but, in general, not equal) to PF_1 in capacity spectrum method, and to C_0 in the displacement coefficient method (*ATC 40* and *FEMA*). Since the same constant Γ applies for the transformation of both displacements and forces, the initial (elastic) stiffness of the equivalent SDOF system remains the same as that defined by the base shear – top displacement diagram of the MDOF system.

The capacity diagram in AD format is obtained by dividing the forces in the force - deformation (F^* - D^*) diagram by the equivalent mass. Alternatively, the acceleration coordinate of the capacity diagram can be obtained directly from the base shear of the MDOF system by dividing it by the effective (modal) mass. This alternative procedure is used for example in ATC-40 and BSL. However, it is restricted to the first mode shape.

Step 4: Bilinear idealization of the capacity diagram
In all procedures, which employ initial (elastic) stiffness and/or any measure of ductility, a bilinear idealization of the pushover or capacity diagram is needed. In order to determine a simplified bilinear acceleration (or force) – displacement relationship for the equivalent SDOF system, engineering judgement has to be used. In principle, there is no restriction regarding the idealization. However, in regulatory documents some guidelines may be given. In the draft of the EC8 (EC8 2001), where a simple version of the N2 method has been implemented, it is suggested (in the informative Annex B) to use an elastic – perfectly plastic (without post-yield stiffness) idealization. The yield force of the idealized system is equal to the force at the formation of the plastic mechanism. The initial (elastic) stiffness of the idealized system is defined in such a way that areas under the actual and idealized force-deformation curves are equal. This approach is employed also in the comparative study reported in this paper. Other procedures, applied in this paper, employ different approaches. For example, FEMA 356 and Chopra and Goel make the idealization dependant on the target displacement. Such an approach, although generally more accurate, requires an iterative computational procedure.

Step 5: Displacement demand for SDOF system (target displacement)
Two basically different approaches are used for the determination of the target displacement of the equivalent SDOF system. The first one uses equivalent elastic systems and elastic spectra, whereas the second one is based on inelastic spectra.

a) Target displacement based on equivalent elastic system: In this approach, a value of the target displacement has to be assumed. Based on this assumed value, the equivalent elastic period and equivalent viscous damping of the SDOF system are determined. The equivalent stiffness, used for the determination of the equivalent period, is usually equal to the secant stiffness to the assumed target displacement, while different approaches are used for the determination of equivalent damping. The new value for target displacement is determined from the elastic spectrum for the equivalent damping as a function of the equivalent period. An iterative procedure is needed which is supposed to converge to the final value of the target displacement. The details of the procedures for the determination of target displacement based on equivalent elastic system will not be discussed here. The reader is referred to a recent overview paper (Miranda & Ruiz-Garcia, 2001).

b) Target displacement based on inelastic spectrum: Inelastic demand spectra are determined either by a rigorous procedure by using nonlinear dynamic analysis, or from a typical smooth elastic design spectrum by using force (and/or displacement) reduction factors. The reduction factors, which relate inelastic spectra to the basic elastic spectrum, should be consistent with the elastic spectrum. Several proposals have been made for the reduction factor R_μ. In the simple version of the N2 method, a bilinear spectrum for the reduction factor R_μ is used:

$$R_\mu = (\mu - 1)\frac{T}{T_C} + 1 \text{, for } T < T_C \text{; } R_\mu = \mu \text{, for } T \geq T_C \qquad (2);(3)$$

where μ is ductility, T is the period of the structure, and T_C is the characteristic period of the ground motion. It is typically defined as the transition period where the constant acceleration segment of the response spectrum (the short-period range) passes to the constant velocity segment of the spectrum (the medium-period range). Equation 3 suggests that, in the medium- and long-period ranges, the equal displacement rule applies, i.e., the displacement of the inelastic system is equal to the displacement of the corresponding elastic system with the same period. The demand spectrum for a constant ductility is shown in Figure 1. Note that any other inelastic spectrum can be employed.

Steps 6 and 7: Global and local seismic demand for the MDOF model

The displacement demand for the SDOF model is transformed into the maximum top displacement of the MDOF system (target displacement for the MDOF system) by using the transformation factor Γ determined in Step 3. The local seismic demands (e.g., story drifts, joint rotations) can be determined by a pushover analysis. Under monotonically increasing lateral loads with a fixed pattern (as in Step 2), the structure is pushed to its target top displacement determined in Step 5.

Step 8: Performance evaluation (Damage analysis)

In the last step, expected performance can be assessed by comparing the seismic demands, determined in Step 7, with the capacities for the relevant performance level.

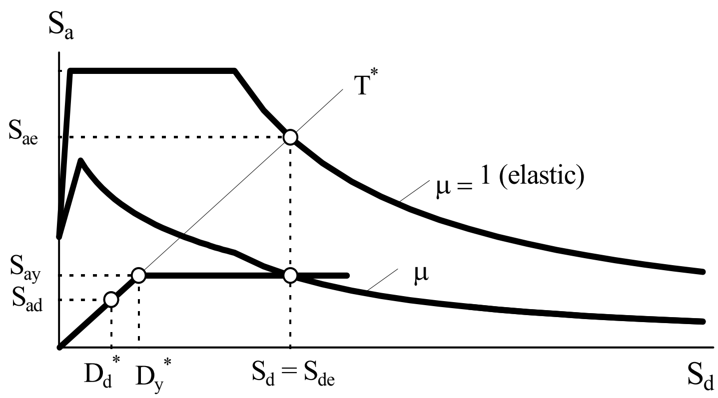

Figure 1: Elastic and inelastic demand spectra versus capacity diagram.

Step 9: Graphical presentation

If the procedure is formulated in the acceleration - displacement (AD) format, the visual interpretation of the procedure and of the relations between the basic quantities controlling the seismic response is possible. Some approaches (e.g. ATC-40) use graphical procedures for the determination of the "performance point", which represents seismic demand. The graphical presentation of the basic parameters (of the equivalent SDOF system) in the N2 method (simple variant, as implemented in EC8) for medium- and long-period structures, for which the "equal displacement rule" applies, is given in Figure 1. The intersection of the radial line corresponding to the elastic period T^* of the idealized bilinear system with the elastic demand spectrum defines the acceleration demand (strength) required for elastic behavior S_{ae} and the corresponding elastic displacement demand S_{de}. The yield acceleration S_{ay} represents both the acceleration demand and the capacity of the inelastic system. The reduction factor R_μ represents the ratio between the accelerations corresponding to the elastic and inelastic systems. If the elastic period T^* is larger than or equal to T_C (i.e., if the period of the structure is in the medium- or long-period range), the inelastic displacement demand S_d is equal to the elastic displacement demand S_{de} ("equal displacement rule"). From triangles in Figure 1 it follows that the ductility demand is equal to the ratio between S_{ae} and S_{ay}, i.e. to R_μ. S_{ad} represents a typical design strength, i.e. strength required by codes for ductile structures, and D_d* is the corresponding displacement obtained by linear analysis. The inelastic demand in terms of accelerations and displacements corresponds to the intersection point of the capacity diagram with the demand spectrum corresponding to the ductility demand μ. At this point, the ductility factor determined from the capacity diagram and the ductility factor associated with the intersecting demand spectrum are equal. Note that all steps in the procedure can be performed numerically without using the graph. However, visualization of the procedure may help in better understanding the relations between the basic quantities.

SHORT DESCRIPTION OF THE PROCEDURES

The common features of the typical simplified procedures were pointed out in the previous chapter together with the presentation of N2 method. The only exceptions are the procedures proposed by Priestley and Fardis & Panagiotakos. Consequently, the short description of the methods will be focused only on the differences in: (a) used response spectrum, (b) the elastic stiffness of structural components, (c) the distribution of lateral forces for pushover, (d) the assumed displacement shape along the height, (e) MDOF to SDOF transformation, and (f) the idealization of pushover curve.

FEMA 356 - Guidelines for the seismic rehabilitation of buildings

- Two lateral load distributions are used for the pushover analysis. The first one is based on the modal shapes of the structure and the other one is the uniform distribution.
- Iteration is needed for the bilinear idealization rules recommended by FEMA 356. The initial stiffness and yielding point depend on the target displacement. The resulting curve is bilinear with post-yield stiffness, though the positive post-yield stiffness has no influence on the target displacement.
- The MDOF to SDOF transformation is theoretically inconsistent. FEMA allows partial or no association between the lateral load pattern, MDOF to SDOF equivalence coefficients for top displacement and base shear, and assumed displacement shape.
- Target displacement is determined using simplified nonlinear spectra (the same as in the N2 method). For $T > T_c$ the equal displacement rule with possible correction is provided, for $T < T_c$ the elastic displacement is amplified in order to obtain the inelastic target displacement.
- No graphical representation is provided.

Chopra-Goel – Modal Pushover Analysis (Chopra & Goel 2001a)

- The Modal Pushover Analysis is proposed in order to take into account the effect of higher modes by combining several individual peak modal responses obtained from a pushover procedure.
- The pushover procedure is iterative due to the proposed bilinear idealization of the

pushover curve (same as FEMA 356).

- Advocates the use of computed or simplified (Newmark-Hall) inelastic spectra.

ATC 40 & TriServices' Manual (Freeman 1998) **- Capacity Spectrum Method (CSM)**

- The lateral load distribution and the MDOF to SDOF transformation coefficients are determined according to the first elastic mode (basic variant).
- The target displacement (called performance point) is assessed using equivalent elastic spectrum by a graphical iterative procedure. The equivalent damping of the elastic spectrum is determined from:
    - Dissipated energy based on idealized hysteretic loops (ATC 40). In this study, type A structural behavior was considered.
    - Newmark-Hall reduction factors for inelastic spectra (TriServices' manual). Equivalent damping was derived by equating the peak deformation of the equivalent linear system, determined from the elastic design spectrum, to the peak deformation of the yielding system, determined from the inelastic (Newmark-Hall) design spectrum. Consequently, the equivalent elastic spectrum is computed based on the already determined inelastic spectrum.

Japanese Building Standard Law (BSL 2000) - Variant of CSM (Otani et. al 2000)

- The lateral load pattern for pushover is not correlated to the first mode shape used for the determination of the MDOF to SDOF transformation coefficients.
- The equivalent damping is estimated as the weighted average (with respect to strain energy) of equivalent damping ratios of structural members that are assessed based on rotational ductility. For large structures this procedure should be very laborious, imposing the need of special software. Alternatively, for common structures, the equivalent damping can be determined as a function of the global ductility of the equivalent SDOF system.
- No explicit bilinear idealization of the pushover curve is required in the case of regular structures. Nevertheless, the yield displacement has to be specified if the global ductility of the equivalent SDOF is used.
- Based on personal communication (Otani), the iteration is not applied in practice when the method is used for checking design. However, iteration is needed if the displacement demand is to be found.

Yield Point Spectra (Aschheim & Black 2000)

The yield point spectrum represents seismic demand in terms of yield displacement. The same results as in any other procedure based on inelastic spectra can be obtained. The difference is in graphic representation.

Priestley (Priestley 1997, Priestley 2000)

The method is based only on displacement acceptance criteria, and no analysis is needed. The main steps of the procedure are shortly presented:

- The plastic mechanism of the structure is assumed, based on simple calculations.
- The elastic stiffness of structural components is assessed based on empirical relations proposed by Priestley (Priestley 2000). For common RC frames designed according Eurocodes, the resulting global cracked stiffness is about 15% of the stiffness computed based on gross concrete section properties.
- The global displacement and ductility capacity of the structure is determined, based on simplified formulas for yield and ultimate element rotations, assumed (predetermined) displacement shape, and drift limit values.
- The displacement demand is established using the substitute structure (equivalent elastic) method. The characteristics of the substitute structure are based on ductility capacity.
- The displacement demand is compared with the capacity.
- Iteration is needed if the actual displacement demand is to be found. For direct displacement-based design (new buildings), no iteration is required.

Fardis-Panagiotakos (Panagiotakos & Fardis 1998)

The objective of the procedure is to estimate the inelastic chord rotations of the structural elements through linear analysis. The procedure is to some extent similar to the FEMA 356 Liner Static Procedure (LSP) and to the NZ code procedure. The main steps of the method are:

- Determine secant stiffness (at yielding) of components using empirical relations for chord rotations. The values of the resulting cracked stiffness amount to about 15-20% and to about 10-15% of those computed based on gross concrete section properties, for columns and for beams, respectively. The global stiffness is comparable to the one resulting from Priestleys' method.
- Estimate the peak inelastic chord rotations from linear analysis using the equal displacement rule.

The method is appropriate for structures having moment diagram in the inelastic range similar to the elastic one. Its application is restricted for structures having $T > T_c$.

COMPARATIVE STUDY

The methods described above were applied to a regular two bay reinforced concrete frame structure with five stories. The design was conducted according to Eurocodes (EC2 and EC8) for subsoil class B, PGA = 0.2g, and high ductility class. Capacity design was applied and all the structural elements are flexure-dominated. The seismic demands in terms of top displacements, story drifts, rotations, and ductilities of components were determined by all the investigated procedures using the EC8 acceleration spectra, and by nonlinear time-history analysis, using 11 European ground motions recorded on stiff soil. The ground motions were normalized to the EC8 spectral acceleration value for the fundamental period of the structure (0.95 s) which amounts to .31 g. All computations were repeated using the increased intensity of ground motion (twice the design value). Static and dynamic nonlinear analyses were performed with a modified version of DRAIN – 2DX using the trilinear Takeda model. For N2 and FEMA procedures two lateral load patterns were adopted, modal and uniform, respectively. In the case of Chopra & Goel (MPA) procedure the target displacement was computed using two different inelastic spectra. The first one is the computed mean inelastic displacement spectrum of the 11 considered accelerograms (Chopra (ICS)), and the second one is Newmark-Hall spectrum (Chopra (N-H)). Note that the effect of the higher modes is not important for the analyzed structure.

Selected results are presented in Figures 2-7. Figures 2 and 3 present the period of the equivalent SDOF system, and the MDOF to SDOF equivalence factor for displacements. Seismic demands for the two levels of ground intensity, obtained from the investigated methods, are compared with the mean and mean plus one standard deviation values computed by time history nonlinear analyses (Figures 4-7). Note that the standard deviation of the results obtained by nonlinear dynamic analysis is small because the ground motions were normalized to the same first period spectral acceleration.

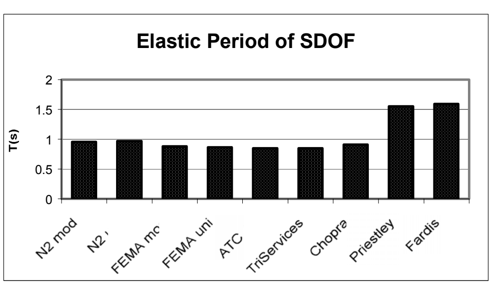

Figure 2

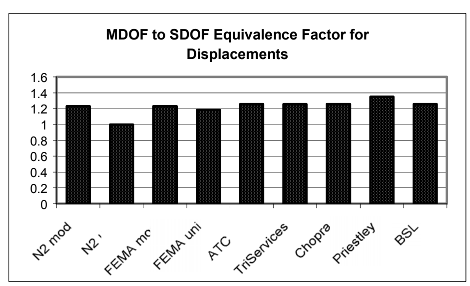

Figure 3

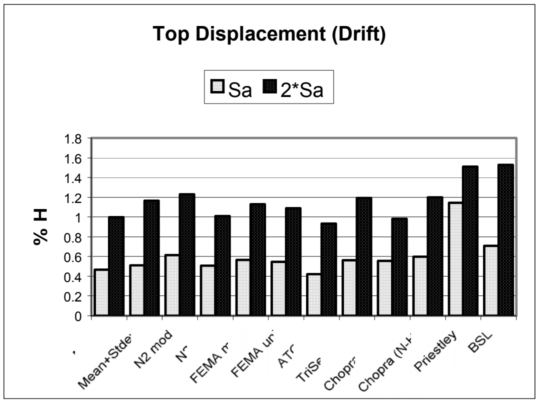

Figure 4

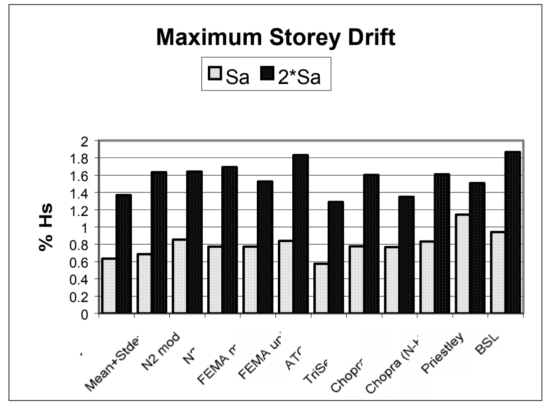

Figure 5

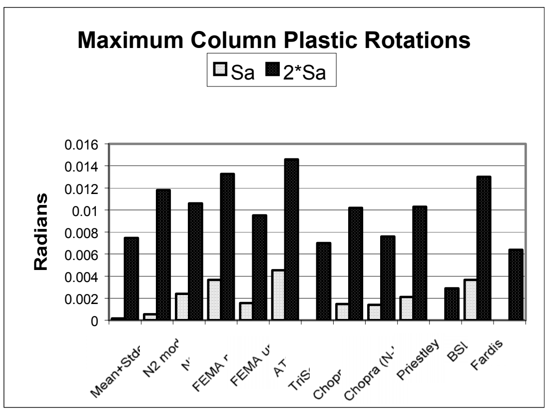

Figure 6

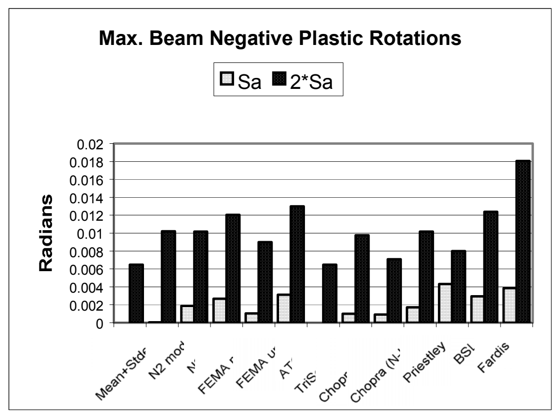

Figure 7

CONCLUSIONS

The comparison of results indicates that the employed simplified procedures generally yield, for a regular planar structure with the first period in the medium-period range, results of adequate accuracy. The global quantities (like top displacement) are generally more accurate than the local ones (like rotations at member ends). Due to the use of the mean inelastic displacement spectrum, Chopra & Goel (Chopra (ICS)) approach yields results very close to the mean values obtained from dynamic analysis. The ATC 40 (type A structural behavior was considered) appears to be unconservative, particularly in respect to the mean plus one standard deviation values. Furthermore, ATC 40 algorithm that requires iteration for the assessment of the displacement demand is considered to be unnecessarily complex taking into account the accuracy of the method. It should be also noted that some problems in the convergence of ATC-40 procedure have been reported in the literature (e.g. Chopra and Goel

1999). On the other side, BSL, N2 with uniform load pattern, and FEMA using uniform load pattern are conservative in the case of the studied structure. The results obtained by Priestley and Fardis-Panagiotakos procedures cannot be directly compared to other results due to significantly different assumptions regarding the elastic stiffness of the structural elements. According to these assumptions the initial elastic period of the frame structure is 2.5 times greater than the period computed based on gross concrete sections and 1.6 times greater than the period based on the equivalent stiffness computed according to other procedures (Figure 2). In the case of the investigated structure, higher mode effects are not important. An improved accuracy can be expected if the Chopra-Goel method is used for structures with considerable higher mode effects.

The procedures, based on pushover analysis, which can be directly compared, differ in regard to simplicity, transparency, and the clarity of the theoretical background. The essential difference is related to the determination of the displacement demand (target displacement). If an equivalent elastic spectrum is used, displacement demand is determined based on equivalent stiffness and equivalent damping. Both quantities depend on the displacement demand. Consequently, the three quantities are interrelated and iteration is needed. (Note that iteration is not needed if a procedure based on equivalent elastic spectrum is used for direct displacement based design in which the target displacement is fixed. Often, iteration is not performed if the procedure is used for checking if displacement demand is smaller than displacement capacity.) The quantitative values of equivalent damping, suggested by different authors, differ considerably. It is interesting to note that Freeman, the author of the "Capacity spectrum method", derived the equivalent damping (employed in Triservices' manual procedure) by equating the peak deformation of the equivalent linear system, determined from the elastic spectrum, to the peak deformation of the inelastic system, determined from the inelastic (Newmark-Hall) spectrum. The question arises, why this detour? The inelastic design spectra can be used directly and they do not require iteration. Inelastic spectra can be used not only for analysis and performance evaluation, but also for direct displacement based design as indicated by Fajfar (Fajfar 1999) (see also Figure 1), and demonstrated by Chopra and Goel (Chopra & Goel 2001b). The above arguments suggest the superiority of the procedures based on inelastic spectra to those based on equivalent elastic spectra.

Different procedures differ also in the assumed lateral load pattern, used in pushover analysis, and in the displacement shape, used for the transformation from the MDOF to the SDOF system (and vice versa). Only if the two vectors are related, i.e. if the lateral load pattern is determined from the assumed displacement shape, the transformation from the MDOF to the SDOF system is based on a mathematical derivation. This feature leads to a transparent transformation. If the two vectors are independent, additional approximations are implicitly introduced, and the clarity of the theoretical background and the transparency are lost, although the accuracy of results may be adequate. The use of lateral load pattern, which is related to the assumed displacement shape, does not present any restriction, because any displacement shape can be used.

Bilinear idealization of the pushover curve is required for the methods using inelastic spectra. The procedures employing equivalent elastic spectra do not need initial stiffness. However, the equivalent damping is usually based on the ductility, therefore a bilinear idealization is needed also for these procedures (partial exception BSL). If the bilinear idealization depends on the displacement demand, than the computational procedure becomes iterative even in the case when inelastic spectrum is used. It is questionable if this complication is warranted.

Table 1: Basic Features of Simplified Procedures

Procedure	Analysis	Spectrum	Iteration	Consistency of MDOF→SDOF	Graphic Presentation
ATC 40	Pushover	Equiv. El.	Yes	Yes (1st Mode)	Yes
TriServices	Pushover	Equiv. El.	Yes	Yes (1st Mode)	Yes
FEMA	Pushover	Inelastic	Yes[1]	No	No
BSL	Pushover	Equiv. El.	Yes	No	Yes
N2	Pushover	Inelastic	No	Yes	Yes
Yield Spectra	Pushover	Inelastic	No	NA	Yes
Chopra & Goel	Pushover (Several)	Inelastic	Yes[1]	Yes (El. Modal Shapes)	No/Yes[2]
Priestley (A)	-	Equiv. El.	Yes/No[3]	No	No
Fardis & Panagiotakos (B)	Linear	Equal Disp.	No	Yes (Elastic)	No

(A) - Predetermined plastic mechanism and displacement shape. Appropriate for regular structures.
(B) - Fundamental period T > Tc. Predetermined elastic displacement shape (global plastic mechanism).
[1] Due to bilinear idealization
[2] For each mode
[3] For new structures (direct displacement-based design)

For practical applications and for educational purposes a graphical representation of the procedure is extremely important. A breakthrough of the simplified methods was possible when the acceleration – displacement format was implemented, which allows a visualization of important demand and capacity parameters (even if all results can be obtained numerically). It seems that the use of this format is essential for the appreciation of the procedure in practice.

REFERENCES

Aschheim, M.A., Black, E.F. (2000), *Yield point spectra for seismic design and rehabilitation*, Earthquake Spectra, Vol.16, May 2000.

ATC 40, *Seismic Evaluation and Retrofit of Concrete Buildings*, Applied Technology Council, 1996.

Chopra, A. K., Goel, R. K. (1999), *Capacity-demand-diagram methods for estimating seismic deformation of inelastic structures: SDF systems,* Report PEER 1999/2, April 1999.

Chopra, A. K., Goel, R. K. (2001a), *A modal pushover analysis procedure to estimate seismic demands for buildings,* Report PEER 2001/3, January 2001.

Chopra, A. K., Goel, R. K. (2001b), *Direct displacement-based design: use of inelastic vs. elastic design spectra,* Earthquake Spectra, Vol.17, February 2001.

EC8 (2001), *Eurocode 8 -Design of structures for earthquake resistance,* May 2001 draft.

Fajfar, P. (1999), *Capacity spectrum method based on inelastic demand spectra*, Earthquake Engineering and Structural Dynamics, Vol. 28, 979-993.

Fajfar, P. (2000), *A nonlinear analysis method for performance-based seismic design*, Earthquake Spectra, Vol.16, August 2000.

FEMA 356, *Prestandard and Commentary for the Seismic Rehabilitation of Buildings*, Federal Emergency Management Agency, November 2000.

Freeman, S. A. (1998), *Development and use of capacity spectrum method*, 6USNCEE.

Miranda E., Ruiz-Garcia, J. (2001), *Evaluation of approximate methods to estimate maximum inelastic displacement demands*, Earthquake Engineering and Structural Dynamics, accepted for publication.

Otani, S., Hiraishi, H., Midorikawa, M., Teshigawara, M. (2000), *New seismic design provisions in Japan*, 2000 Fall ACI Convention, Toronto.

Panagiotakos, T. B., Fardis, M. N. (1998), *Deformation-controlled seismic design of RC structures*, 11ECEE.

Priestley, M. J. N. (1997), *Displacement-based seismic assessment of reinforced concrete buildings*, JEE, Vol.1, January 1997.

Priestley, M. J. N. (2000), *Performance based seismic design*, 12WCEE.

EXPERIMENTAL STUDY ON DYNAMIC RESPONSE CHARACTERISTICS OF FRAME STRUCTURES WITH ECCENTRICITY

Koichi KUSUNOKI[1], Hiroto KATO[2], Toshibumi FUKUTA[3] and Fumitoshi KUMAZAWA[4]

ABSTRACT

Torsional response can destructively effect the seismic capacity of structures. Many damaged buildings due to torsional response were observed after sever earthquakes. However, it cannot be said that the mechanism of damage due to torsional response had been clearly investigated. The main purpose of this paper is to reproduce the torsional response with the pseudo-dynamic testing technique. One-span-one-bay-two-story steel column structure was tested, and six structures that had different eccentric factors were designed. Furthermore, shaking table tests on three structures were conducted to verify the validity of pseudo-dynamic test. From the shaking table and pseudo-dynamic tests, it was confirmed that the pseudo-dynamic testing technique can reproduce the response of structure with eccentricity; eccentricity was not as effective on the maximum horizontal displacement at gravity center, but the maximum rotational angle was increased according to its eccentricity.

1 INTRODUCTION

There have been many buildings damaged due to torsional response during big earthquakes. However, it cannot be said that the mechanism of damage due to torsional response has been clearly investigated. One of the main purposes of this paper is to reproduce the torsional response of structures with the pseudo-dynamic testing technique, and to investigate the mechanism of damage due to torsional response. In order to verify the validity of pseudo-dynamic testing technique, shaking table tests were also conducted.

2 JAPANESE STANDARD CODE RELATED TO THE TORSIONAL RESPONSE

The Building Standard Law if Japan chooses to increase the necessary horizontal ultimate resistance force on each floor Q_{un} according to the eccentric factor for each floor R_e.The ultimate horizontal resistant force Q_u should be larger than Q_{un}. Q_{un} and R_e can be calculated with following equations [JBC2001].

1Research engineer, Building Research Institute E-mail kusunoki@kenken.go.jp

2 Senior research engineer, ditto

3 Director of International Institute of Seismology and Earthquake Engineering, ditto

4 Associate Professor, Shibaura Institute of Technology

$Q_{un} = D_s \cdot F_{es} \cdot Q_{ud}$

$Q_{ud} = Z \cdot R_t \cdot A_i \cdot C_0 \cdot W$

where D_s Deformability and damping factor of structure

F_{es} Shape factor $= F_e \cdot F_s$

F_e Horizontal shape factor

F_s Vertical shape factor

Z Zone coefficient

R_t Coefficient for response in term of period

A_i Vertical distribution for story shear coefficient

C_0 Standard shear coefficient (≥ 1.0)

W Mass of upper portion than a floor

$$R_e = \frac{e}{r_e}$$

e Eccentric distance. The distance between center of gravity and rigidity

r_e Radius of spring force. $r_{ex} = \sqrt{K_R / K_x}$, $r_{ey} = \sqrt{K_R / K_y}$

K_R Torsional stiffness

K_x, K_y Horizontal stiffness to the direction of X and Y

Eccentric factor represents how easily a structure can vibrate torsionally. One component of the shape factor, F_e, changes gradually from 1.0 to 1.5 according to eccentric factor R_e. The relationship between F_e and R_e is shown in Fig. 1. Q_{un} will be increased linearly from Q_{ud} with R_e of 0.15, to $1.5 \cdot Q_{ud}$ with R_e of 0.30. Q_{un} is constant as Q_{ud} with R_e of less than 0.15, and Q_{un} is constant as $1.5 \cdot Q_{ud}$ with R_e of more than 0.3.

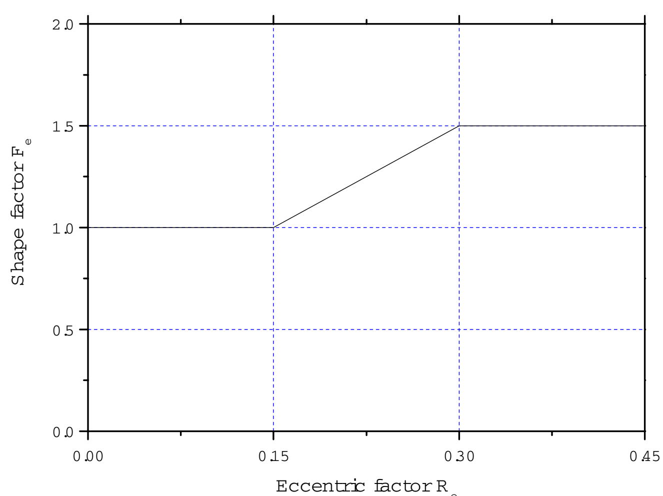

Fig. 1 Relationship between F_e and R_e

3 OUTLINE OF TEST STRUCTURE

The test structure was a 1-span-1-bay-2-story structure as shown in Fig. 2. The structure was scaled down by 1/2. Rigid slabs made of reinforced concrete provided inertia force on the shaking table, and were used as loading beam for the pseudo-dynamic test. The mass of each floor was 76.9kN for the first floor and 78.0kN for the second floor. Torsional response was provided only on the first story by mass eccentricity as shown in Fig. 2 a). Two of four columns were located closer to the center of slab than others to provide mass eccentricity. There are three types of eccentricity that can be raised, mass, stiffness and strength eccentricity. Natural period of the structures need to be nearly the same to neglect the effects of frequency characteristics of the input motion. Since it is not easy to provide steel columns with specific stiffness or strength, it is not easy to provide structures with various stiffness or strength eccentricity that have the same natural period. Therefore mass eccentricity was applied for our test in order to make the natural periods of test structures almost constant.

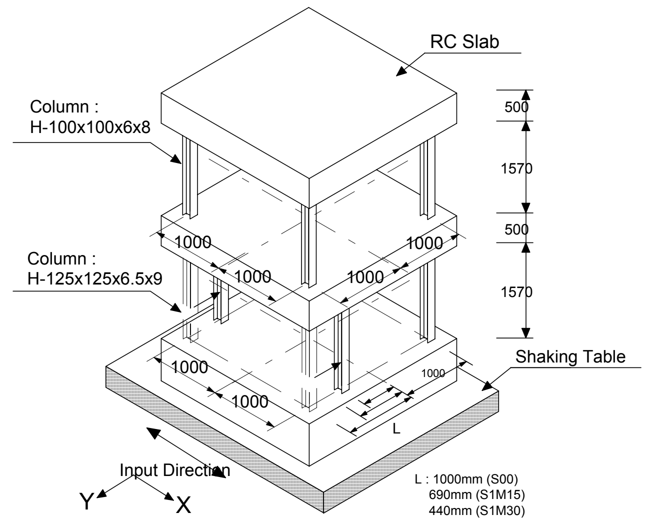

a) Shaking table test

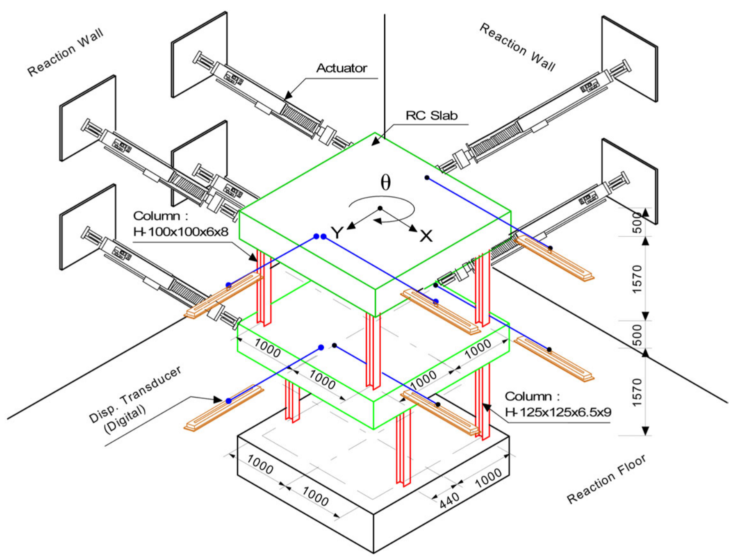

b) Pseudo-dynamic test

Fig. 2 Setup of structure

H-Shaped steel was used for columns ($H-125\times125\times6.5\times9$ for the first floor and $H-100\times10\times6\times8$ for the second floor). The length of column between top and bottom base plates was 1,500mm as shown in Fig. 3. Material test results are shown in Table 1. Table 2 shows strength of column, story shear and story shear coefficients. Story shear coefficient for the first story is 1.43 and 1.85 for the second story.

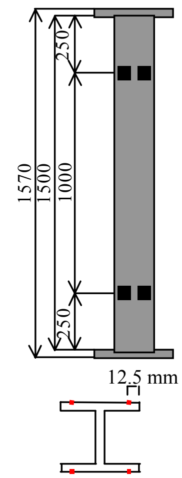

Fig. 3 Column

Test parameters are the values of the eccentric factor in the direction of both X and Y. X axis is the direction of input motion, and Y axis is perpendicular to the X axis as shown in Fig. 2. The eccentric factors of 0.0, 0.15 and 0.30 were applied in the X direction, and those of 0.0 and 0.15 were applied in the Y direction. An eccentric factor of zero means that the structure has no eccentricity, while 0.15 is the maximum value until which horizontal external force need not to be increased (Fe=1.0), and horizontal external force should be amplified by 1.5 for a structure of which the eccentric factor is 3.0. The test parameters are shown in Table 3. The number of structures are eight, three with eccentricity only in the X direction (P00, P1M15 and P1M30), and two with eccentricity in the both directions (P2M1515 and P2M3015). In addition, three structures (S00, S1M15 and S1M30) were used for shaking table test in order to compare the reproduced behaviors between the pseudo-dynamic test and those of the shaking table tests.

In order to achieve the specific eccentricity, columns were shifted by the distance shown in Table 4 from the location for the structure without eccentricity.

Table 1 Material test results

	H125 (First story)	H100 (Second story)
Yield strength (N/mm^2)	304.4/301.7	347.8/340.1
Tensile strength (N/mm^2)	431.9/435.5	475.6/473.6
Strain fracture(%)	26.4/27.3	25.8/25.5

Left-side value is for flange, right-side value for web

Table 2 Strength of test structure

	Yielding moment (kN*m)	Story shear at yielding (kN)
First story	41.4/14.3 [2.9]	220.8/76.3 (1.43)
Second story	26.6/9.3 [2.9]	141.9/49.5 (1.85)

Left-side value is for X Direction, right-side value for Y Direction
[] the ratio of yielding moment on X Direction to Y Direction
() Story Shear Coefficient

Table 3 Test parameters

		Eccentric factor in the Y direction		
		0.0		0.15
Eccentric factor in the X direction.	0.0	S00	P00	-
	0.15	S1M15	P1M15	P2M1515
	0.30	S1M30	P1M30	P2M3015
Testing Method		Shaking table test	Pseudodynamic test	

Table 4 Shifted distance from uniform arrange (mm)

.		Eccentric factor in the Y direction		
		0.0	0.15	
		Y Direction	Y Direction	X Direction
Eccentric factor in the X direction	0.00	0	0	0
	0.15	310	290	490
	0.30	560	520	440

4 SCALE FACTOR

The test structure was assumed to be 1/2 scaled-down model of a real size structure. However, no prototype structure in real size was designed because the main purpose of this research was to observe the effect of torsional response on structural damage, not to observe the response of a specific structure. Because of this, horizontal strength of columns were assumed simply to be proportional to the area of section.

To simplify the problem, a one-story structure was considered to calculate the vibration modes of the scale model. Since Young's modulus cannot be scaled-down, stiffness can be shown in fashions as follows.

Stiffness	Unit	Scale factor
$K_{xx} = \sum K_x = \sum \frac{12EI_x}{L^3}$	$[\mathrm{kN/cm}]$	1/2
$K_{yy} = \sum K_y = \sum \frac{12EI_y}{L^3}$	$[\mathrm{kN/cm}]$	1/2
$K_{x\theta} = \sum K_x \cdot \ell_y = \sum \frac{12EI_x}{L^3} \cdot \ell_y$	$[\mathrm{kN}]$	1/4
$K_{y\theta} = \sum K_y \cdot \ell_x = \sum \frac{12EI_y}{L^3} \cdot \ell_x$	$[\mathrm{kN}]$	1/4

$$K_{\theta\theta} = \sum K_x \cdot \ell_y^2 + \sum K_y \cdot \ell_x^2 \qquad [\mathrm{kN \cdot cm}] \qquad 1/8$$

$$K_{xy} = 0.0$$

Eigen-value equations for real size and scale model structure can be shown as Equation 1 and Equation 2. Dashed values mean the values of the scale model.

$$\left(-\omega^2 \begin{bmatrix} \mathrm{m_1} & & \\ & \mathrm{m_2} & \\ & & \mathrm{I} \end{bmatrix} + \begin{bmatrix} \mathrm{K_{xx}} & 0 & \mathrm{K_{x\theta}} \\ 0 & \mathrm{K_{yy}} & \mathrm{K_{y\theta}} \\ \mathrm{K_{x\theta}} & \mathrm{K_{y\theta}} & \mathrm{K_{\theta\theta}} \end{bmatrix} \right) \{\mathrm{u}\} = \{0\} \qquad \text{Equation 1}$$

$$\left(-\omega'^2 \begin{bmatrix} \frac{1}{8}\mathrm{m_1} & & \\ & \frac{1}{8}\mathrm{m_2} & \\ & & \frac{1}{32}\mathrm{I} \end{bmatrix} + \begin{bmatrix} \frac{1}{2}\mathrm{K_{xx}} & 0 & \frac{1}{4}\mathrm{K_{x\theta}} \\ 0 & \frac{1}{2}\mathrm{K_{yy}} & \frac{1}{4}\mathrm{K_{y\theta}} \\ \frac{1}{4}\mathrm{K_{x\theta}} & \frac{1}{4}\mathrm{K_{y\theta}} & \frac{1}{8}\mathrm{K_{\theta\theta}} \end{bmatrix} \right) \{\mathrm{u'}\} = \{0\} \qquad \text{Equation 2}$$

Determinants of Equation 1 and Equation 2 can be calculated as Equation 3 and Equation 4.

$$\left(\mathrm{K_{xx}} - \mathrm{m_1}\omega^2\right)\left(\mathrm{K_{yy}} - \mathrm{m_2}\omega^2\right)\left(\mathrm{K_{\theta\theta}} - \mathrm{I}\omega^2\right) - \mathrm{K_{x\theta}^2}\left(\mathrm{K_{yy}} - \mathrm{m_1}\omega^2\right) - \mathrm{K_{y\theta}^2}\left(\mathrm{K_{xx}} - \mathrm{m}\omega^2\right) = 0$$

Equation 3

$$\left(\mathrm{K_{xx}} - \mathrm{m_1}\left(\frac{\omega'}{2}\right)^2\right)\left(\mathrm{K_{yy}} - \mathrm{m_2}\left(\frac{\omega'}{2}\right)^2\right)\left(\mathrm{K_{\theta\theta}} - \mathrm{I}\left(\frac{\omega'}{2}\right)^2\right) - \mathrm{K_{x\theta}^2}\left(\mathrm{K_{yy}} - \mathrm{m_1}\left(\frac{\omega'}{2}\right)^2\right) - \mathrm{K_{y\theta}^2}\left(\mathrm{K_{xx}} - \mathrm{m_2}\left(\frac{\omega'}{2}\right)^2\right) = 0$$

Equation 4

With Equation 3 and Equation 4, the scale factor of the natural period can be calculated as 1/2. With the scale factor of natural period, Equation 5 can be lead from Equation 2

$$\left(-\omega^2 \begin{bmatrix} \mathrm{m_1} & & \\ & \mathrm{m_2} & \\ & & \mathrm{I} \end{bmatrix} + \begin{bmatrix} \mathrm{K_{xx}} & 0 & \mathrm{K_{x\theta}} \\ 0 & \mathrm{K_{yy}} & \mathrm{K_{y\theta}} \\ \mathrm{K_{x\theta}} & \mathrm{K_{y\theta}} & \mathrm{K_{\theta\theta}} \end{bmatrix} \right) \begin{Bmatrix} 2\mathrm{u'_x} \\ 2\mathrm{u'_y} \\ \mathrm{u'_\theta} \end{Bmatrix} = \{0\} \qquad \text{Equation 5}$$

Equation 5 shows the relationship of eigenvectors as Equation 6.

$$\begin{Bmatrix} \mathrm{u'_x} \\ \mathrm{u'_y} \\ \mathrm{u'_\theta} \end{Bmatrix} = \begin{Bmatrix} \frac{1}{2}\mathrm{u_x} \\ \frac{1}{2}\mathrm{u_y} \\ \mathrm{u_\theta} \end{Bmatrix} \qquad \text{Equation 6}$$

Equation 6 shows that horizontal response displacement at gravity center of the scale model is half of the real size structure. On the other hand, torsional response angle of the scale model is the same as the real size structure. Horizontal response displacement of each frame of the scale model is also half of real size structure as shown in Fig. 4. However, because torsional response angle is not affected by scaling, twisting strain of each column of the scale model becomes double of real size structure.

Scale factors for each item are listed in Table 5 (Kumazawa 1996). Single underlined items are the items that cannot be scaled down, and double underlined items are the items of which scale factor does not have proper relationship with the real size structure.

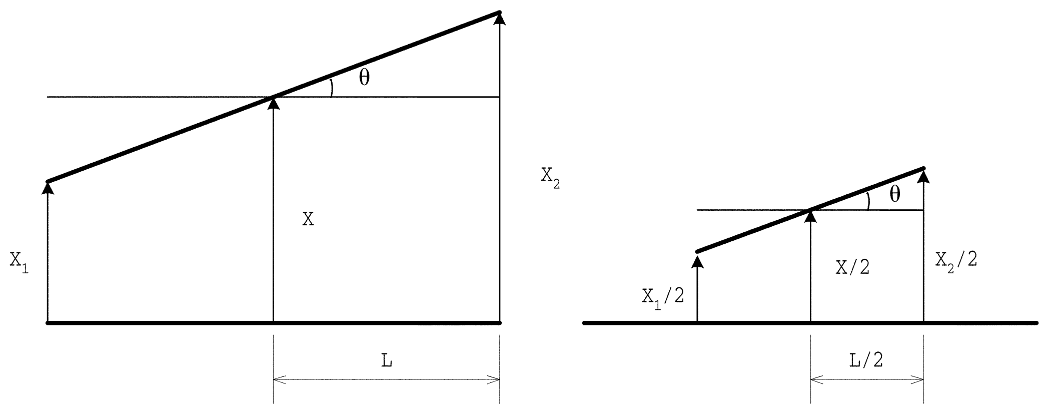

Real size structure Scale model

Fig. 4 Relationship of horizontal response

Table 5 Scale factors

Physical phenomenon			
Length	1/2	Area	1/4
Volume	1/8	Gravity Acceleration	1.0
Specific gravity	1.0	Mass	1/8
Rotational inertia	1/32	Time	1/2
Column			
Young's modulus	1.0	Axial strain	1.0
Curvature	2.0	**Twisting strain**	2.0
Horizontal strength	1/4	Horizontal stiffness	1/2
Yield deformation	1/2	Rotational stiffness	1/8
Response of structure			
Natural period	1/2	Horizontal acceleration	2.0
Horizontal velocity	1.0	Horizontal deformation	1/2
Rotational acceleration	1.0	Rotational velocity	1.0
Rotational deformation	1.0		

5 INPUT MOTION

North-South component of JMA (Japan Meteorological agency) KOBE recorded at the Hyogo-Ken-Nambu earthquake in 1995 was used for input motion. As mentioned in Chapter

4, time axis was scaled down by 1/2. The input wave is shown in Fig. 5, and response acceleration magnification is shown in Fig. 6. Five different PGAs of 200, 450, 900, 1640 and 2400 gal were inputted in order of level. PGAs in real size are 100, 225, 400, 820 and 1200 gal because of scale factors (Table 5). Shaking table tests were conducted with these input motions prior to the pseudo-dynamic tests, and recorded acceleration at the basement of structure was used for the input motion to the pseudo-dynamic test. Since a shaking table test with the structure that has the eccentricities in both X and Y directions was not carried out, the acceleration recorded at S00 was used for the input motion to P2M3015 and P2M1515. The input motion was inputted in a direction to 10 degrees rotated from X for P2M3015 and P2M1515.

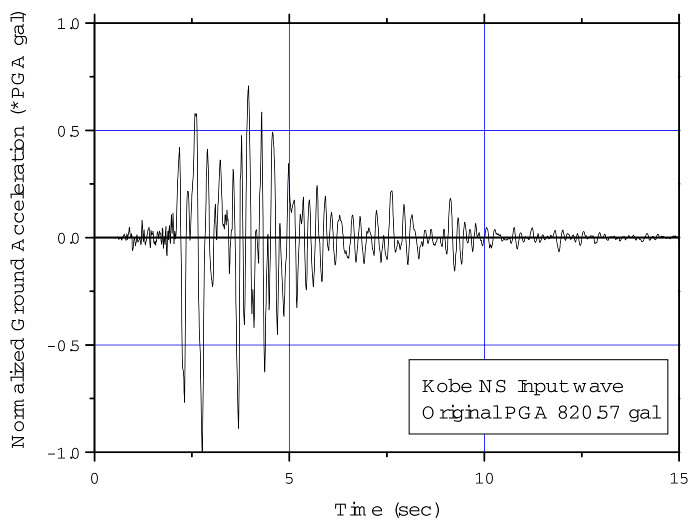

Fig. 5 Input wave

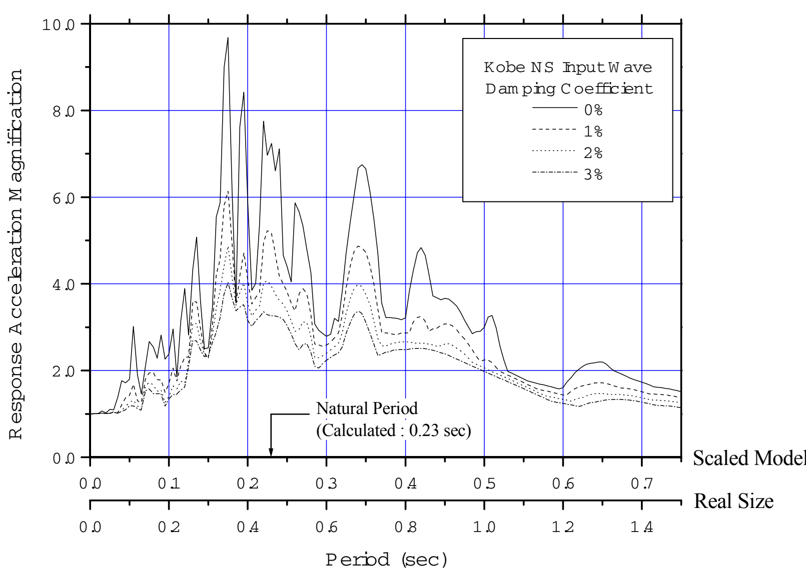

Fig. 6 Response Acceleration Magnification

6 DATA ACQUISITION SYSTEM

Strains of steel columns were measured with strain gauges put on the flange at both ends of columns as shown in Fig. 3 (black rectangular marks show strain gauge locations). Four strain gauges were put at one end, eight gauges were used for one column, and totally strains at 64 different points were measured during shaking table tests and pseudo-dynamic tests.

Three transducers were used to measure response bi-directional horizontal displacement and rotational angle of each floor as shown in Fig. 2 (b) and Fig. 7. Two transducers were for X-direction and rotation, and one was for Y-direction. Two additional transducers were used to measure slip displacement at bottom of basement during shaking table test.

Three accelerometers were used to measure response acceleration during each floor at shaking table test. Two were for Y-direction and rotation, and one was for X-direction. One accelerometer was placed on the center of basement to measure actual input motion to structure.

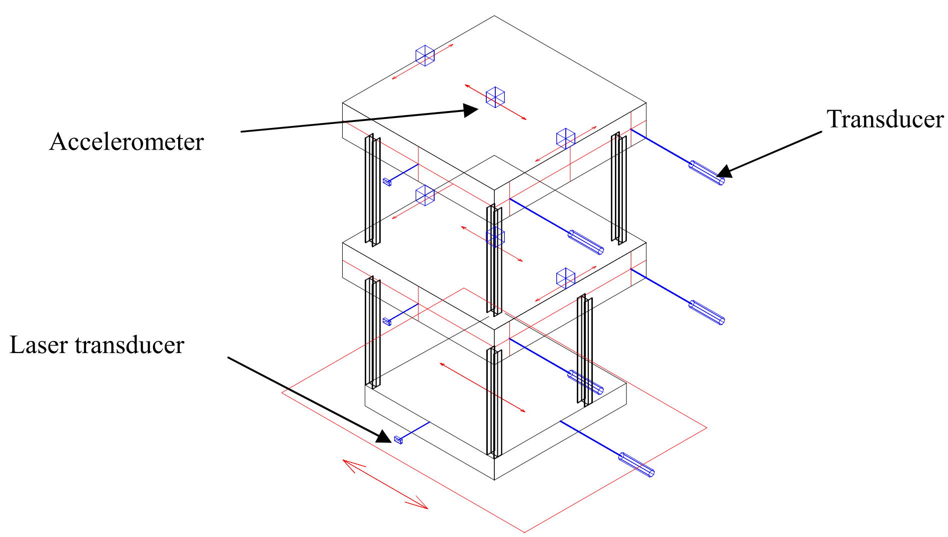

Fig. 7 Measuring equipments set-up

7 TEST RESULTS AND DISCUSSION

Shaking table tests were conducted from July 2000 to September 2000, and pseudo-dynamic tests were conducted from October 2000 to July 2001. In order to measure natural periods and damping coefficient of structures, responses with white noise input were measured at shaking table tests. On the other hand, a stiffness matrix was needed for pseudo-dynamic tests to assume a damping matrix. To get the stiffness matrix, small amount of force was loaded at each floor, and in each direction just after setting up the structure. Then, all responses for each force were measured, and a flexibility matrix was generated. The natural periods were calculated with the flexibility matrix and mass matrix for each structure. Measured natural periods were listed in Table 6. Damping coefficients could be assumed as 1% from shaking table test with white noise. Damping coefficients of 1% proportional to initial stiffness were assumed for pseudo-dynamic tests.

The natural periods in both X and Y direction of shaking table and pseudo-dynamic tests are almost the same, however, those of torsional response are a little different. Since natural periods of shaking table tests were calculated with transfer function at white noise input, the accuracy of natural period of torsional response is not so high because it is higher modes.

Table 6 Natural periods

	X Direction	Y Direction	Torsion
S00	0.26	0.41	0.22
S1M15	0.28	0.41	0.24
S1M30	0.28	0.41	0.25
P00	0.266	0.381	0.145
P1M15	0.273	0.398	0.178
P1M30	0.267	0.389	0.163
P2M1515	0.281	0.422	0.233
P2M3015	0.280	0.416	0.239

7.1 Comparison of pseudo-dynamic test result with shaking table test results

The relationship between inter-story drift and story shear in the first story of shaking table tests and pseudo-dynamic tests are shown in Fig. 8 to Fig. 10. The input level was 1640 gal. The behaviors of P1M15 and P1M30 agreed well with those of shaking table tests, however, the behavior of P00 was different from that of S00, especially the initial stiffness of the shaking table test was a little higher than that of pseudo-dynamic test. Because of the difference of stiffness, the response of the pseudo-dynamic test did not agree with that of the shaking table test. The reason why the stiffness of S00 and P00 were different needs further investigation.

The response displacement in the X direction of P1M15 and P1M30 agreed with those of S1M15 and S1M30 very well. The response displacement in the X direction of P1M15 and S1M15, of which the input level was 1640 gal, was shown in Fig. 11. It can be said that pseudo-dynamic test results agreed very well with shaking table test results especially during 1.0 to 3.5 sec., which includes maximum response displacement. From these results, it can be concluded that the pseudo-dynamic testing technique can reproduce the dynamic response of a structure very well if the stiffness of structure can be reproduce well.

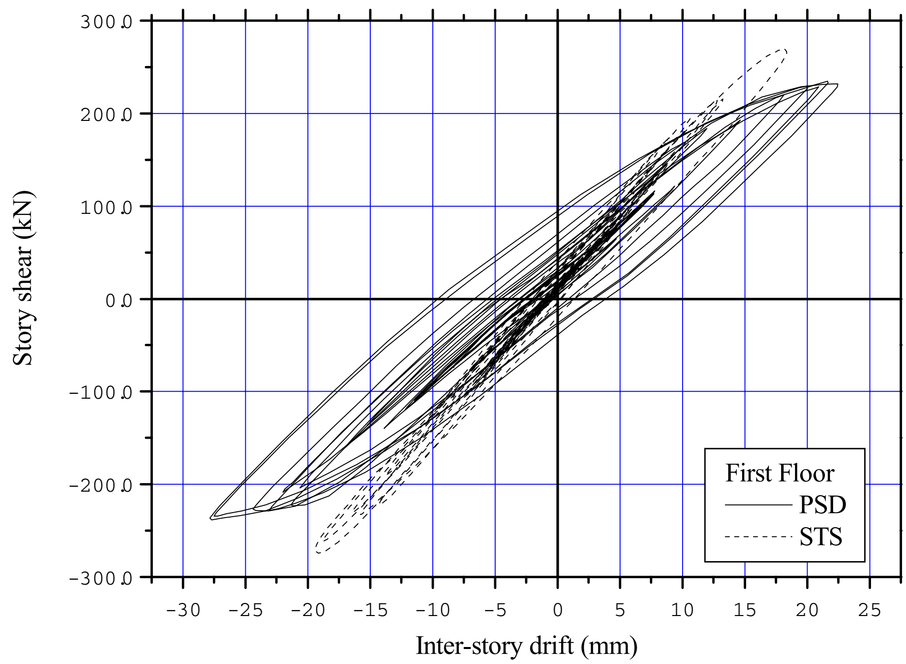

Fig. 8 Relationship between story shear and inter-story displacement (S00 and P00, First story)

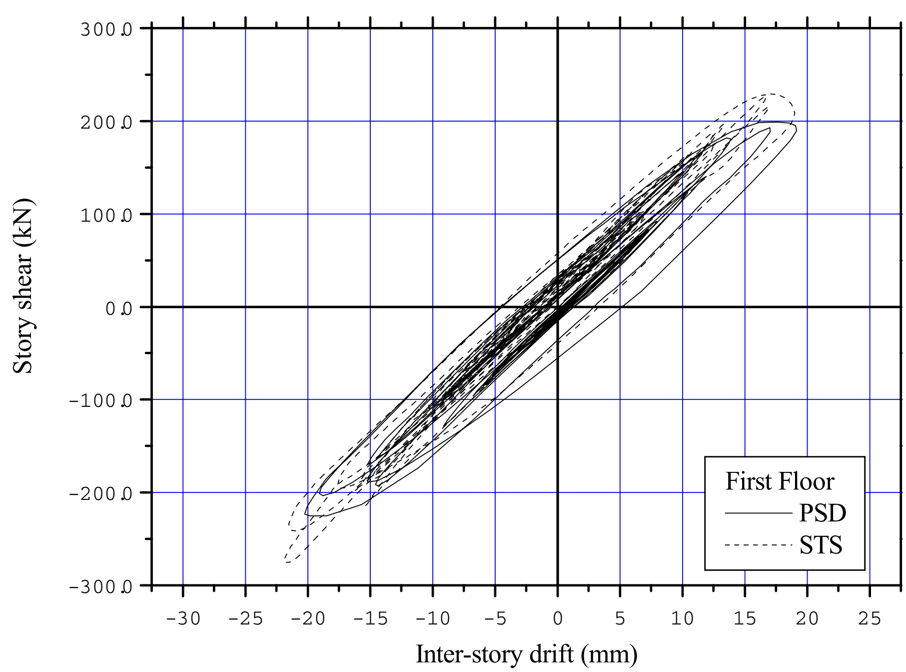

Fig. 9 Relationship between story shear and inter-story displacement (S1M15 and P1M15, First story)

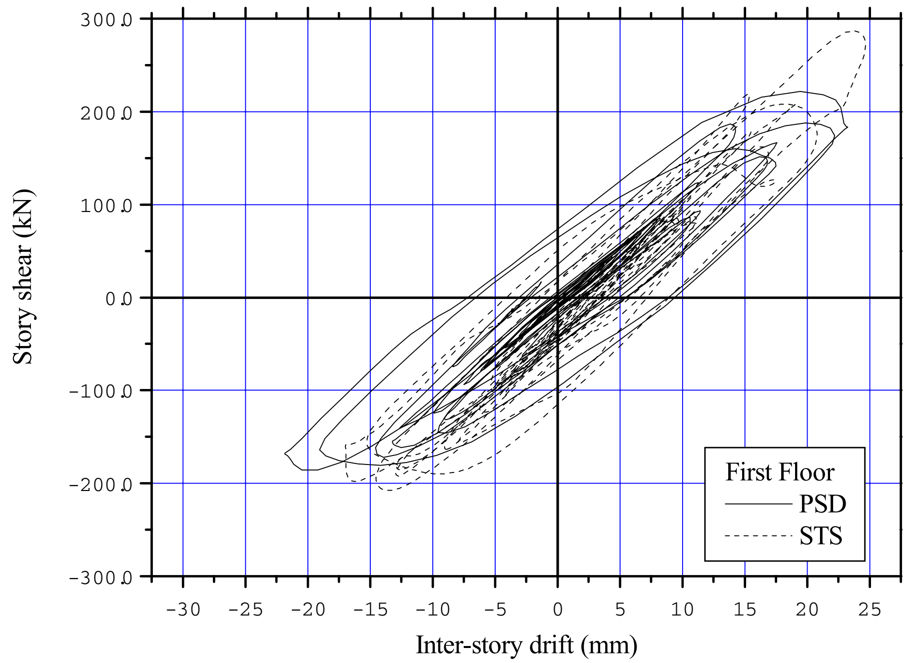

Fig. 10 Relationship between story shear and inter-story displacement (S1M30 and P1M30, First story)

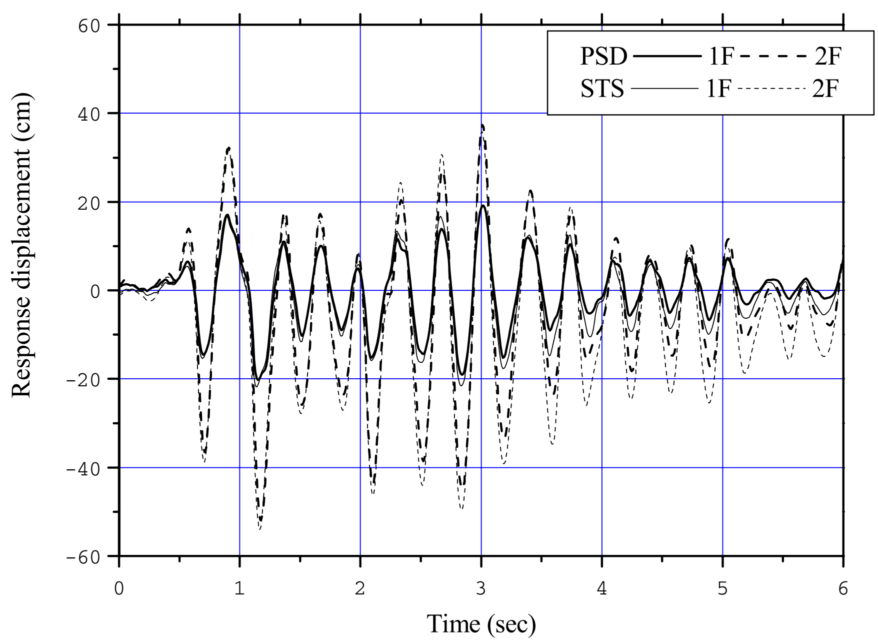

Fig. 11 Response displacements (S1M15 and P1M15)

7.2 Maximum responses

Fig. 12 shows maximum response displacements at gravity center of the second floor in the X direction for each input level. As mentioned before, P00 and S00 are quite different especially for relatively large input levels. P1M15 and P1M30 agree well with S1M15 and S1M30 regardless of input level. It can be seen that there is the tendency to slightly increase the maximum response displacement at gravity center according to the eccentric factor.

Fig. 13 shows maximum torsional response angle of the second floor for each input level. Maximum torsional response angle of P1M30 at an input level of 1640 gal was 28% smaller than that of S1M30. Maximum torsional response angle is the relative angle to the basement and residual torsional angle could be accumulated. Maximum angle of P1M30 at input level of 2400 gal was also 27% smaller than that of S1M30.

Maximum torsional response angle increased according to the eccentric factor. For example, the ratios of maximum angle to P1M15 at input level of 1640 gal were 1.15 (P1M30), 1.55 (P2M1515) and 1.72 (P2M3015).

8 CONCLUDING REMARKS

In order to investigate the mechanism of damage due to torsional response, pseudo-dynamic tests with the five structures that had mass eccentricity were conducted. Furthermore, in order to verify the validity of the pseudo-dynamic test, shaking table tests with three structures were conducted. Following remarks can be pointed out.

1. Pseudo-dynamic testing technique with torsional response with a scale model was developed.
2. If the stiffness can be reproduced properly, pseudo-dynamic test can reproduce the dynamic response very well.
3. Torsional response angle increases according to the eccentric factor. The ratios of maximum torsional angle to P1M15 at input level of 1640 gal were measured as 1.15 (P1M30), 1.55 (P2M1515) and 1.72 (P2M3015).

Pseudo-dynamic test with a structure that has strength eccentricity will be conducted this fall, and substructuring pseudo-dynamic test will be done this winter. Finally, columns will be changed to reinforced concrete next year.

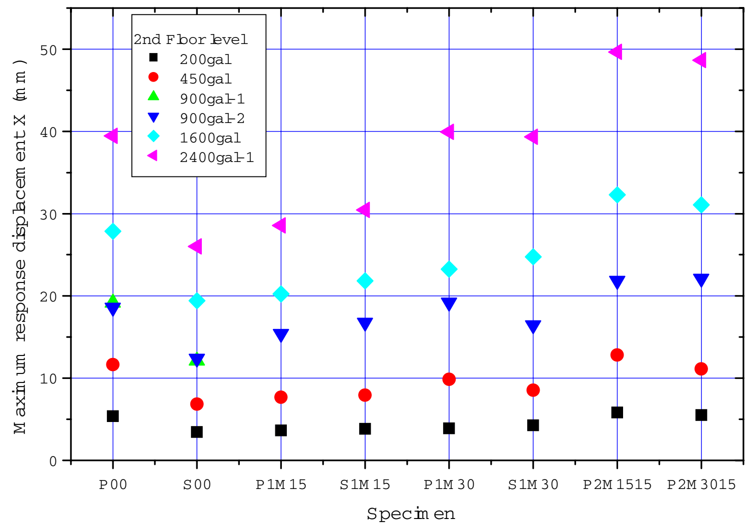

Fig. 12 Maximum response displacement on the direction of X (first story)

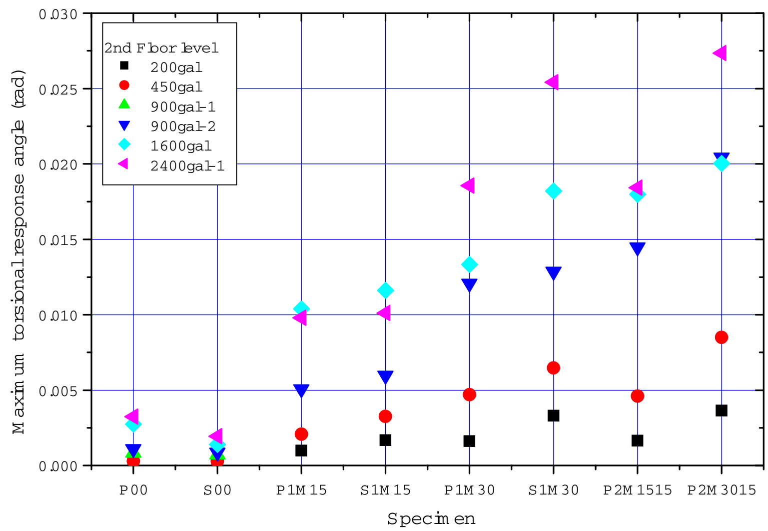

Fig. 13 Maximum torsional response angle (first story)

9 REFERENCES

Fumitoshi KUMAZAWA (1996), "*Study on response characteristics of small scaled reinforced concrete structures*", Ph. D thesis, University of Tokyo (in Japanese)

JBC/Japan Building Center (2001), "*Guideline for technical standard related to building structure*" (in Japanese)

Koichi KUSUNOKI, et al., (2001) "*Study on earthquake response characteristics of frame structures with eccentricity part 1 – 3*", Summaries of technical papers of AIJ annual meeting (in Japanese, to be published)

SESSION A-2: INTERSTORY DRIFT DEMANDS

Chaired by

♦ Gregory Deierlein and Hitoshi Shiohara ♦

MODAL PUSHOVER ANALYSIS OF SAC BUILDINGS*

Anil K. CHOPRA[1]

Rakesh K. GOEL[2]

ABSTRACT

Evaluated is the accuracy of the modal pushover analysis in estimating the seismic demands for six SAC buildings. These results are compared with those obtained by nonlinear response history analysis and three force distributions in FEMA-273.

1. INTRODUCTION

The nonlinear static procedure (NSP) or pushover analysis in FEMA-273 [FEMA, 1997] has become a standard procedure in current structural engineering practice. Seismic demands are computed by nonlinear static analysis of the structure, which is subjected to monotonically increasing lateral forces with an invariant height-wise distribution until a target displacement is reached. None of the current invariant force distributions can account for the contribution of higher modes—higher than the fundamental mode—to the response or for redistribution of inertial forces because of structural yielding. To overcome these limitations several researchers have proposed adaptive force distributions that follow more closely the time-variant distributions of inertia forces (Fajfar and Fischinger, 1988; Bracci et al., 1997; Gupta and Kunnath, 2000). Others have tried to address this issue by considering more than the fundamental vibration mode in standard pushover analysis (Paret et al., 1996; Sasaki et al, 1998, Gupta and Kunnath, 2000; Kunnath and Gupta, 2000; Matsumori et al., 2000).

Recently, a modal pushover analysis (MPA) procedure has been developed that includes the contributions of several modes of vibration (Chopra and Goel, 2001). This paper demonstrates the accuracy of the MPA procedure in estimating the seismic demands for SAC buildings and

---

* This paper will also appear in the *Proceedings* of the SEAOC Convention to be held in San Diego, California, 2001.

[1] *University of California, Dept. of Civil & Environmental Engineering, Berkeley, Calif. 94720*

[2] *California Polytechnic State University, Dept. of Civil & Environmental Engineering, San Luis Obispo, Calif. 93407*

compares these results with those obtained for the same buildings by pushover analysis using three force distributions in FEMA-273.

2. MODAL PUSHOVER ANALYSIS PROCEDURE: SUMMARY

Summarized below are a series of steps used to estimate the peak inelastic response of a symmetric-plan, multistory building about two orthogonal axes to earthquake ground motion along an axis of symmetry using the MPA procedure developed by Chopra and Goel (2001):

1. Compute the natural frequencies, ω_n and modes, $\boldsymbol{\phi}_n$, for linearly elastic vibration of the building (Fig. 1).

2. For the *n*th-mode, develop the base shear-roof displacement, $V_{bn} - u_{rn}$, pushover curve for force distribution

$$s_n^* = \mathbf{m}\phi_n$$

where **m** is the mass matrix of the structure. These force distributions for the first three modes are shown schematically in Fig. 2 and the pushover curves for the first two modes in Fig. 3. For the first mode, gravity loads, including those present on the interior (gravity) frames, were applied prior to the pushover analysis. The resulting P-delta effects lead to negative post-yielding stiffness of the pushover curve (Fig. 3a). The gravity loads were not included in the higher mode pushover curves, which generally do not exhibit negative post-yielding stiffness (Fig. 3b).

3. Idealize the pushover curve as a bilinear curve (Fig. 4). If the pushover curve exhibits negative post-yielding stiffness, idealize the pushover curve as elastic-perfectly-plastic.

4. Convert the idealized pushover curve to the force-displacement, $F_{sn} / L_n - D_n$, relation (Fig. 4b) for the *n*th -“mode” inelastic SDF system by utilizing

$$\frac{F_{sny}}{L_n} = \frac{V_{bny}}{M_n^*} \qquad D_{ny} = \frac{u_{rny}}{\Gamma_n \phi_{rn}}$$

in which M_n^* is the effective modal mass, ϕ_{rn} is the value of ϕ_n at the roof, and $\Gamma_n = \phi_n^T \mathbf{m} 1 / \phi_n^T \mathbf{m} \phi_n$.

5. Compute peak deformation D_n of the nth-"mode" inelastic SDF system defined by the force-deformation relation of Fig. 4b and damping ratio ζ_n. The elastic vibration period of the system is

$$T_n = 2\pi \left(\frac{L_n D_{ny}}{F_{sny}} \right)^{1/2}$$

For an SDF system with known T_n and ζ_n, D_n can be computed by nonlinear response history analysis (RHA) or from the inelastic design spectrum (Chopra, 2001, Section 7.11).

6. Calculate peak roof displacement u_{rn} associated with the nth-"mode" inelastic SDF system from

$$u_{rn} = \Gamma_n \phi_{rn} D_n$$

7. From the pushover database (Step 2), extract values of desired responses r_n : floor displacements, story drifts, plastic hinge rotations, etc.

8. Repeat Steps 3-7 for as many modes as required for sufficient accuracy. Typically, the first two or three "modes" will suffice.

9. Determine the total response (demand) by combining the peak "modal" responses using the SRSS rule:

$$r \approx \left(\sum_n r_n^2 \right)^{1/2}$$

3. SAC BUILDINGS AND GROUND MOTIONS

SAC commissioned three consulting firms to design 3-, 9-, and 20-story model buildings according to the local code requirements of three cities: Los Angeles (UBC 1994), Seattle (UBC, 1994), and Boston (BOCA, 1993). Described in detail in Gupta and Krawinkler (1999), the structural systems of these model buildings consisted of perimeter steel moment-resisting frames (SMRF). The N-S perimeter frames of 9- and 20-story buildings are analyzed in this paper.

For all three locations, sets of 20 ground motion records were assembled representing probabilities of exceedance of 2% and 10% in 50 years (return periods of 2475 and 475 years, respectively) (Somerville et al., 1997). The 2/50 set of records are used in the subsequent analysis.

4. STORY DRIFT DEMANDS-NONLINEAR RESPONSE HISTORY ANALYSIS

The dynamic performance characteristics of SAC buildings were evaluated in a comprehensive study of story drift demand predictions through nonlinear RHA (Gupta and Krawinkler, 1999). Studied were the distribution of story drift demands over the height of the structures, the relation between story drift and roof drift, and the effect of modeling accuracy. Shown in Fig. 5 are the median values of story drift demands over the height of the buildings for Pre-Northridge M1 models of the structures. "Median" refers to the exponent of the mean of the natural log of the demand values due to 20 ground motions.

The distribution of story drift demands over the height of the structure (Fig. 5) is strongly dependent on the structural characteristics; increases in upper stories of Boston (BO) structures, especially in the 20-story building because higher modes dominate the response; is more-or-less uniform in lower half of Seattle (SE) structures and concentrated in the upper five stories; and is more-or-less uniform in the upper half of Los Angeles (LA) structures, however, increases in the lower part of the buildings with the strongest concentration in the lowest 6 stories in 20-story buildings.

The story drifts presented cover a wide range of response from slightly beyond yielding—in the case of Boston structures—to very large demands—in the case of Los Angeles buildings—that represent response far into the inelastic range.

5. COMPARISON OF MPA AND NONLINEAR RHA RESULTS

The MPA procedure was implemented for each of the six buildings and for each of the 20 ground motions. Contributions of the first three “modes” or the first five “modes” were considered for the 9-story buildings and 20-story buildings, respectively. The combined values of story drifts were computed for the 9-story building including one, two, or three “modes” and for the 20-story building including one, three, or five “modes.” Figure 6 shows these median values of story drift demands together with the results of nonlinear RHA obtained from Fig. 5.

Figure 6 shows that the first “mode” alone is inadequate in estimating story drifts. However, by including the response contributions due to the second “mode” for the 9-story buildings and second and third “modes” for 20-story buildings the numbers are more accurate. With sufficient number of “modes” included, the height-wise distribution of story drifts estimated by MPA is generally similar to the trends noted from nonlinear RHA observed in the preceding section.

6. ACCURACY OF MPA PROCEDURE

Figure 7 shows the errors in the story drift demands estimated by the MPA procedure, including contributions of sufficient number of modes: three modes for 9-story buildings and five modes for 20-story buildings. These results permit the following observations: the MPA procedure underestimates seismic demands in most stories of the Boston structures by about 20%; in few upper stories, the error may approach 30%; the MPA procedure estimates to acceptable accuracy seismic demands in the lower stories of the 9-story and 20 Seattle buildings, but underestimates demand near the top of the building by up to 30%; and the MPA procedure is least accurate in estimating seismic demands for the LA buildings.

Errors in the MPA procedure for inelastic systems arise from several assumptions and approximations, but principally from: (1) neglecting coupling among modal coordinates associated with the modes of the corresponding linear system arising from yielding of the system; and (2) estimating the total response by combining the peak “modal” responses using the SRSS rule. The modal coordinates are indeed uncoupled for elastic buildings, and the MPA procedure is equivalent to standard response spectrum analysis (RSA). The RSA procedure, implemented in most commercial software, has become a standard analytical tool for the structural engineering profession. The principal source of approximation in this procedure is in using modal combination rules to combine the peak modal responses to estimate the total response. As these errors are considered acceptable by the profession, we compare next the errors in the MPA procedure with those in the RSA procedure.

For this purpose, elastic analysis of each building was implemented by RSA and RHA methods. The relative errors in story drift demands determined by the RSA procedure, also shown in Fig. 7, lead to the following observations: depending on the structure and its location, RSA (with three modes for the 9-story buildings and five modes for 20-story buildings) underestimates the elastic response by 15% to 30%. The RSA errors are essentially uniform over the height of the structures; the errors in MPA are essentially the same as in RSA for the 9-story Boston structure because it remains essentially within the elastic range; the MPA errors are larger than RSA in the case of the 20-story Boston building because modest yielding occurs in upper stories; the MPA errors are larger than RSA in upper stories but smaller in lower stories in the case of Seattle buildings that undergo significant yielding; and the MPA errors vary irregularly over height and are much larger than RSA errors for the Los Angeles buildings because near-fault ground motions drive their response far into the inelastic range.

7. COMPARISON OF MODAL AND FEMA PUSHOVER ANALYSES

FEMA-273 Force Distributions

We consider only one step in the nonlinear static procedure in the FEMA-273 document (FEMA, 1997). The pushover curve, a plot of base shear versus roof displacement, is determined by nonlinear static analysis of the structure subjected to lateral forces with invariant distribution over height but gradually increasing values until a target value of roof displacement is reached. The gravity load is applied prior to the pushover analysis. The floor displacements, story drifts, joint rotations, plastic hinge rotations, etc., computed at the target displacement represent the seismic demands on the structure.

FEMA-273 specifies three distributions for lateral forces:

1. "Uniform" distribution: $s_j^* = m_j$, the mass at the jth floor level (where the floor number $j = 1, 2...N$);

2. Equivalent lateral force (ELF) distribution: $s_j^* = m_j h_j^k$ where h_j is the height of the jth floor above the base, and the exponent k = 1 for fundamental period $T_1 \leq 0.5\,\text{sec}, k = 2$ for $T_1 \geq 2.5\,\text{sec}$; and varies linearly in between; and

3. SRSS distribution: $\mathbf{s}^*$ is defined by the lateral forces back-calculated from the story shears determined by response spectrum analysis of the structure, assumed to be linearly elastic.

Comparative Evaluation

Compared next are the story drift demands for each building determined by five analyses: pushover analysis using the three force distributions in FEMA-273, MPA considering three or five "modes," and nonlinear RHA. The target roof displacement in the analyses using FEMA force distributions was taken as equal to its value determined by the MPA procedure to achieve a meaningful comparison of the two methods, as shown in Fig. 8.

As clearly demonstrated in the figure, the height-wise variation of story drifts determined from the FEMA force distributions differs considerably from nonlinear RHA. Clearly, the FEMA force distribution procedure is inadequate; it does not predict the increasing drifts in the upper stories of Boston structures; the concentration of large story drifts in the upper stories of Seattle structures (especially in the 20-story building); and the complex variation of story drifts over the height of the 20-story Los Angeles building.

Obviously, the MPA procedure performs much better than FEMA force distributions in estimating story drift demands.

8. ACKNOWLEDGMENTS

This research investigation is funded by the National Science Foundation under Grant CMS-9812531, a part of the U.S. Japan Cooperative Research in Urban Earthquake Disaster Mitigation. This financial support is gratefully acknowledged. Our research has benefited from discussions with Helmut Krawinkler of Stanford University, and Chris Poland, Jon Heintz, and Kent Yu of Degenkolb Engineers, Inc.

9. REFERENCES

BOCA (1993). *National Building Code*, *12th Edition*, Building Officials and Code Administration International Inc., Country Club Hills, Illinois.

Bracci, J.M., Kunnath, S.K. and Reinhorn, A.M. (1997). Seismic performance and retrofit evaluation for reinforced concrete structures. ASCE, *J. Struc. Engrg.*, 123(1):3-10.

Building Seismic Safety Council (1997). *NEHRP Guidelines for the Seismic Rehabilitation of Buildings FEMA-273*. Federal Emergency Management Agency, Washington, D.C.

Chopra, A.K. (2001). *Dynamics of Structures: Theory and Applications to Earthquake Engineering*. 2nd Edition, New Jersey: Prentice Hall.

Chopra, A.K. and Goel, R.K. (2001). A modal pushover analysis procedure to estimate seismic demands for buildings: Theory and preliminary evaluation. *Report No. PEER 2001/03*, PEER, Univ. of Calif., Berkeley, Calif.

Fajfar, P. and Fischinger, M. (1988). N2—a method for nonlinear seismic analysis of regular structures. *Proc.*, 9th World Conf. Earthq. Engrg., 5:111-116, Tokyo-Kyoto, Japan.

Gupta, A. and Krawinkler, H. (1999). Seismic demands for performance evaluation of steel moment resisting frame structures (SAC Task 5.4.3), *Report No. 132*, John A. Blume Earthq. Engrg. Center, Stanford Univ., Stanford, Calif.

Gupta, B. and Kunnath, S.K. (2000). Adaptive spectra-based pushover procedure for seismic evaluation of structures," *Earthq. Spectra*, 16(2):367-392.

ICBO, 1994, *Uniform Building Code*, International Conference of Building Officials, Whittier, Calif.

Kunnath, S.K. and Gupta, B. (2000). Validity of deformation demand estimates using nonlinear static procedures. *Proc.*, U.S. Japan Workshop on Performance-Based Engrg., Sapporo, Hokkaido, Japan.

Matsumori, T., Otani, S., Shiohara, H. and Kabeyasawa, T. (1999). Earthquake member deformation demands in reinforced concrete frame structures. *Proc.*, U.S.-Japan Workshop on Performance-Based Earthq. Engrg., pp. 79-94, Maui, Hawaii.

Paret, T.F., Sasaki, K.K., Eilbekc, D.H., and Freeman, S.A. (1996). Approximate inelastic procedures to identify failure mechanisms from higher mode effects. *Proc.*, 11th World Conf. on Earthq. Engrg., Paper No. 966, Acapulco, Mexico.

Sasaki, K.K., Freeman, S.A., and Paret, T.F. (1998). Multimode pushover procedure (MMP)—A method to identify the effects of higher modes in a pushover analysis. *Proc.*, 6th U.S. Nat. Conf. on Earthq. Engrg., Seattle, Washington.

Somerville, P. et al. (1997). Development of ground motion time histories for phase 2 of the FEMA/SAC steel project," *SAC Background Document Report No. SAC/BD-9/04*, SAC Joint Venture, 555 University Ave., Sacramento, Calif.

Keywords

Building Design, Building Evaluation, Nonlinear Static Procedure, Pushover Analysis, Seismic Demands

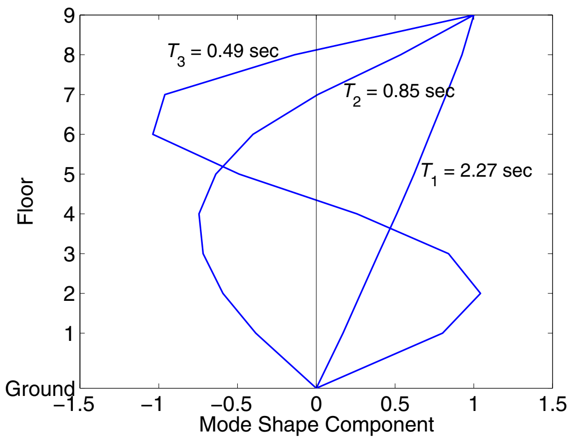

Fig. 1: First Three Natural-Vibration Periods and Modes of the 9-story SAC-Los Angeles Building

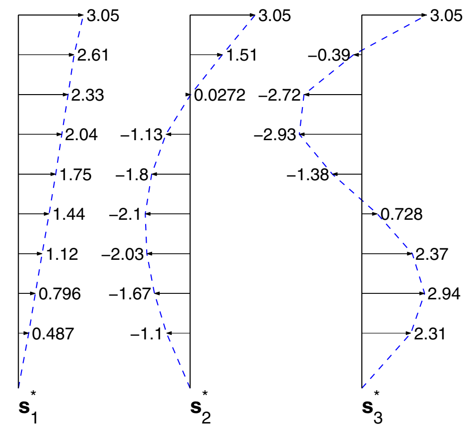

Fig. 2: Force Distributions $\mathbf{s}_n^* = \boldsymbol{m\phi}_n$, n = 1, 2, and 3 for the 9-story SAC-Los Angeles Building

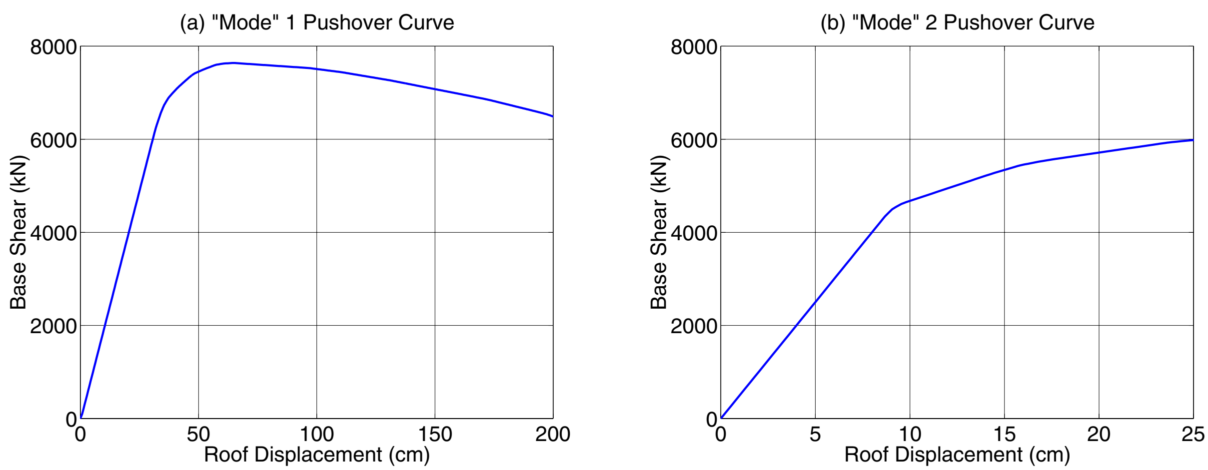

Fig. 3: “Modal” pushover curves for the 9-story SAC-Los Angeles Building

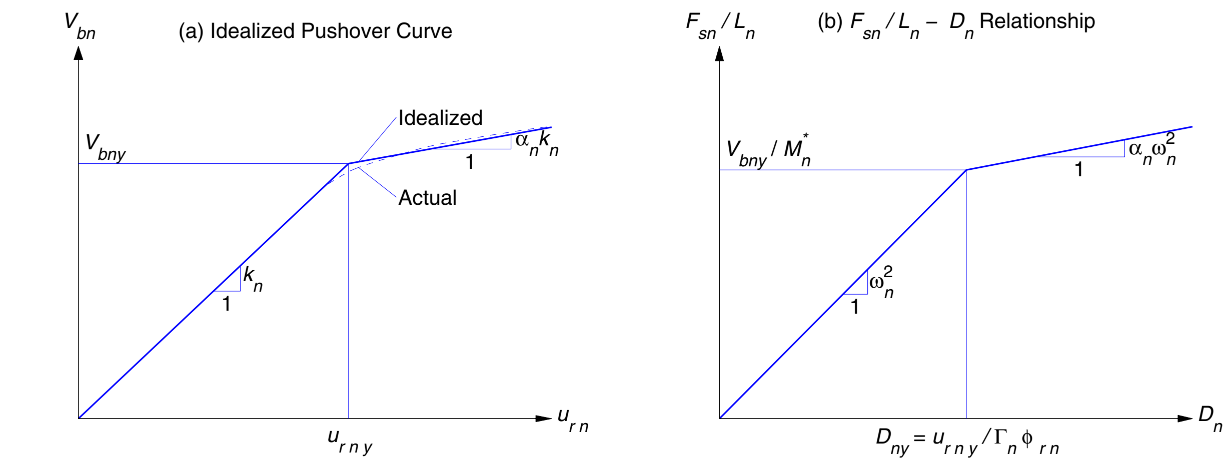

Fig. 4: Properties of the nth-"Mode" Inelastic SDF System from the Pushover Curve

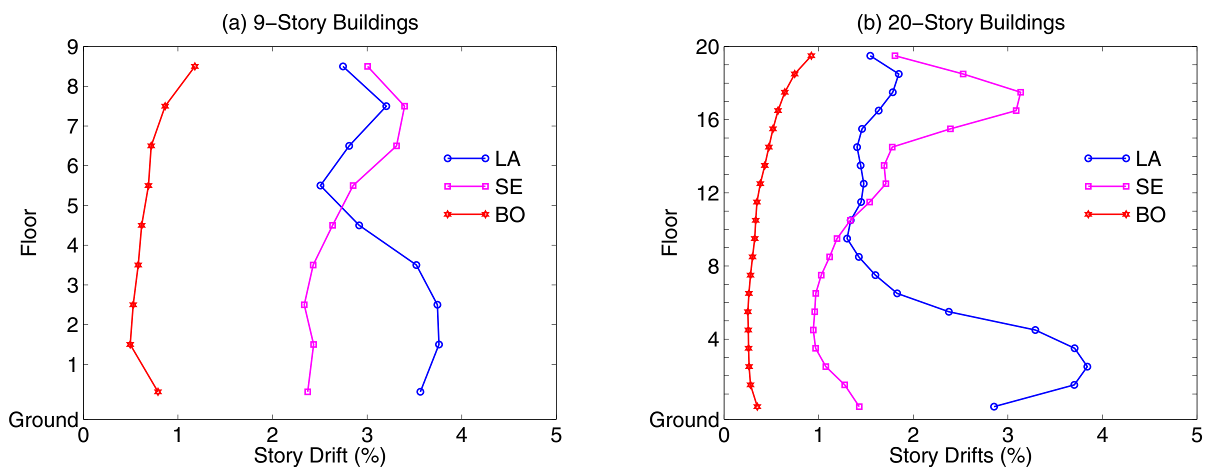

Fig. 5: Median Story Drift Demands determined by Nonlinear RHA: (a) 9-story Buildings; (b) 20-story Buildings (adapted from Gupta and Krawinkler, 1999)

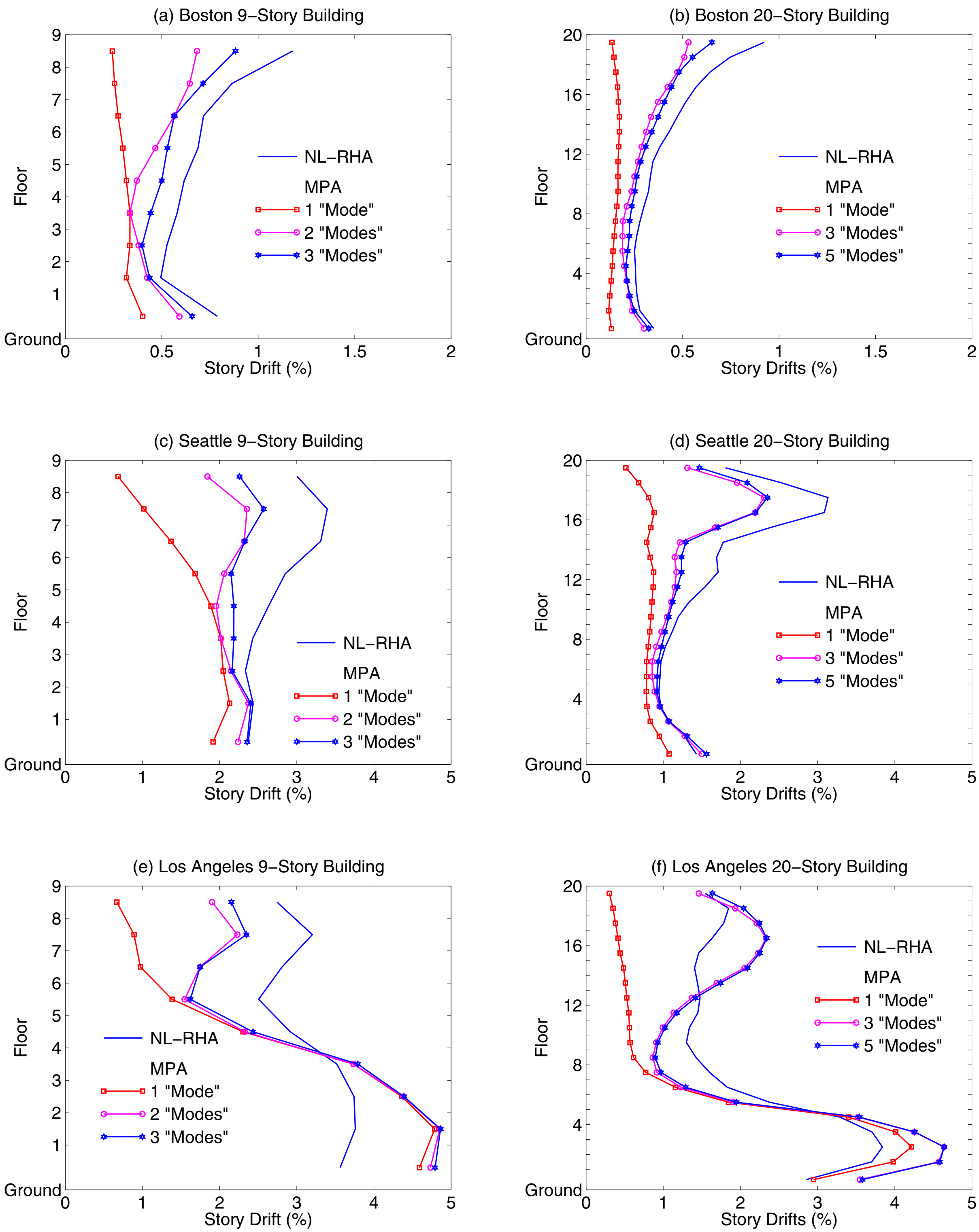

Fig. 6: Median Story Drift Demands Determined by MPA with Variable Number of "Modes" and Nonlinear RHA

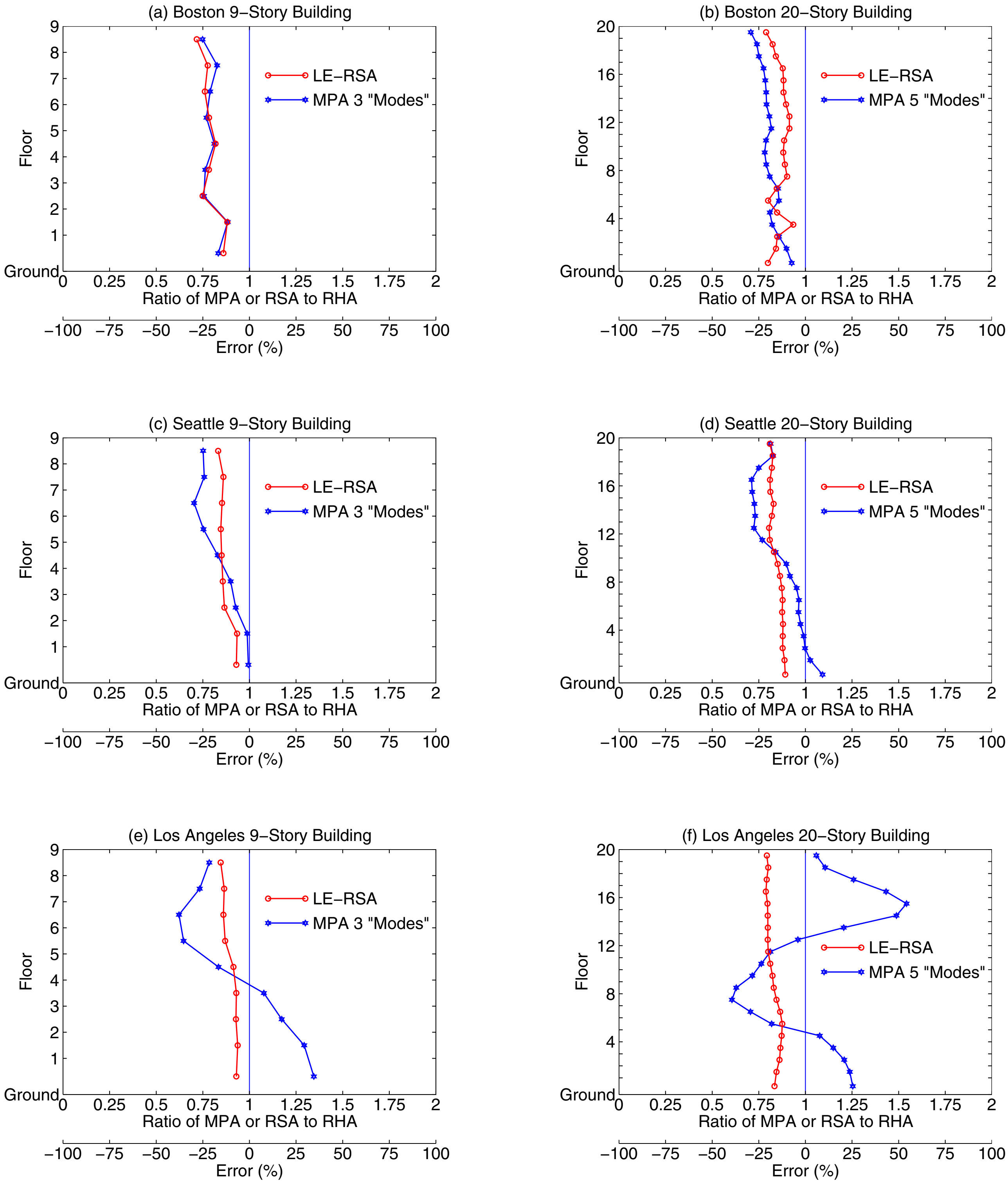

Fig. 7: Errors in the Median Story Drift Demands Estimated by (1) MPA Procedure for Inelastic Systems, and (2) RSA Procedure for Elastic Systems

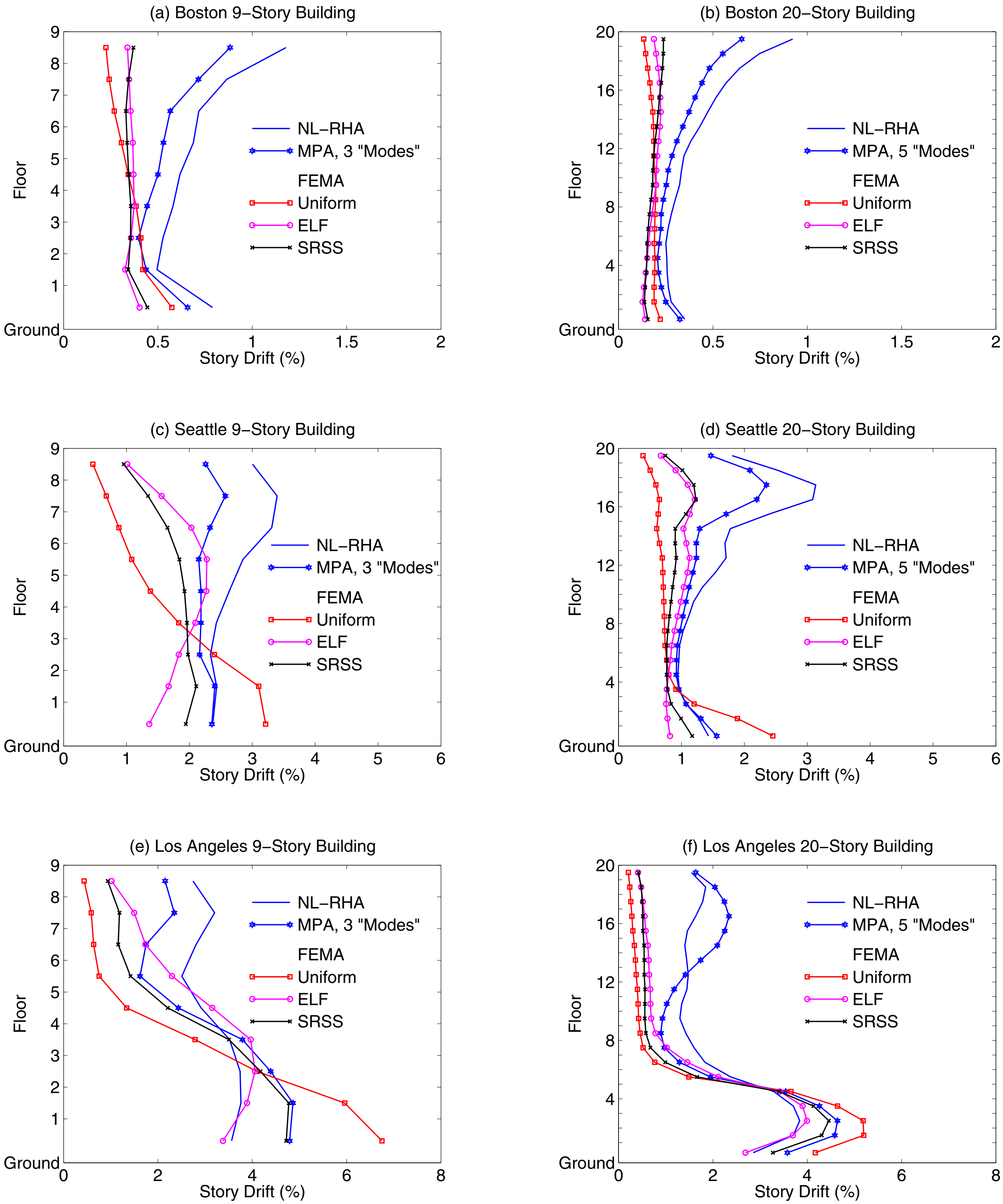

Fig. 8: Comparison of Median Story-Drift Demands Determined by Five Procedures: Pushover Analysis using Three Force Distributions in FEMA-273, MPA, and Nonlinear RHA

INTERMEDIATE-STORY COLLAPSE OF CONCRETE BUILDINGS

M. Yoshimura[1] and T. Nakamura[2]

ABSTRACT

What drew the most attention among various types of the damages to concrete buildings during the 1995 Kobe earthquake was collapse at an intermediate story for buildings with around ten stories. The intermediate-story collapse was studied by the dynamic analysis based on the test results. The major findings from the study are, (1) the analysis presented here can, though roughly, describe the scenario of the intermediate-story collapse considering ground motions with the order of the intensity level of the record from the highest seismic area, and (2) the collapse story is considered to have been relatively weaker in lateral strength probably by 10 to 30 % than the other stories.

1. INTRODUCTION

During the 1995 Kobe earthquake, a number of concrete buildings suffered heavy damages including collapse. What drew the most attention among various types of the damages was collapse at an intermediate story for buildings with around ten stories (Architectural Institute of Japan, 1998). The special feature of the intermediate-story collapse was that only a single story collapsed and damages to the other stories remained light. Most of these buildings were designed according to the old building code (before 1971), which was the allowable stress design method. But since there are still many buildings designed according to the old code, it is essential to identify the reason of such collapse and grasp the seismic performance of similar buildings.

2. COLUMN BEHAVIOR UP TO COLLAPSE

The intermediate-story collapse occurred due to that columns at a certain story underwent

[1]*Department of Architecture, Tokyo Metropolitan University, Hachioji, Japan*
Email: myoshim@arch.metro-u.ac.jp

[2]*Department of Architecture, Tokyo Metropolitan University, Hachioji, Japan*
Email: takaya@ecomp.metro-u.ac.jp

severe shear failure and eventually came to be unable to sustain their gravity load. A test was planned to simulate the column behavior up to the collapse or loss of axial load carrying capacity (Ryu, Nakamura and Yoshimura, 2001). Shear-failing RC columns with height/depth of 3 were designed and tested under the constant axial stress of 0.18 f_c, the value of which was determined as a gravity load level of the intermediate-story columns. The specimens were tested under the double curvature loading condition.

Figure 1 shows lateral load vs. lateral drift relations of the specimen subjected to monotonic loading. It is believed the column behavior at the collapse is greatly affected by the previous loading history. The monotonic loading was selected by considering the dynamic analysis results for the Kobe earthquake records. This will be discussed later. The ♦ mark denotes maximum load point and ● mark does collapse point. Lateral drift at the two points were 0.8% and 10.3% respectively. The load vs. drift relations idealized from the test result are used in the dynamic analysis. Note that although lateral load was negative at the collapse point, shear force, defined as force in the direction perpendicular to the column axis, at that point was near zero because of the contribution of the vertical load to this direction. The photo after the collapse is shown in Fig. 2.

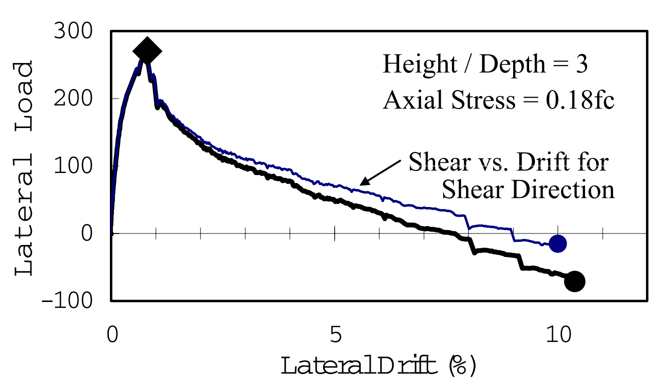

Fig. 1 Lateral Load vs. Lateral Drift


Lateral Drift = 10.3%
Fig.2 Photo after Collapse

3. ANALYSIS METHOD

A ten story building is analyzed (Kamino, Yoshimura and Nakamura, 2001). The building was represented by an equivalent shear building model, as shown in Fig. 3. Conventional member to member analysis can not be used for this case because it is impossible at present to represent the column axial behavior at and after the collapse realistically. Story height and story mass were assumed uniform, 300 cm and 753 KN, respectively. Story stiffness was so determined that the period for the fundamental mode might result in 0.6 sec., where linear distribution of the story stiffness was assumed with 1.0 for the first story and 0.5 for the tenth story. The story stiffness is shown as K_1 in Table 1. Lateral strength of story shear spring was determined in such that it might be 1.5 times as much as the design shear force as prescribed in the old building code (design base shear = 20% of total weight). However, considering the construction practice that a column size for the top two or three stories are in general not changed, lateral strength of the ninth and tenth stories was assumed same as the eighth story. Figure 4 compares the lateral strength of the analytical model and the lateral strength required by the current code for usual concrete buildings. The analytical model is less in strength at the intermediate story than the current requirements. This is a reason of the intermediate-story collapse of old buildings. The lateral strength of the analytical model is shown as Q_y in Table 1.

Table 1 Structural Properties of Analytical Model

Story	Weight (KN)	K_1 (KN/cm)	Q_y (KN)	δ_u (%)
10	753	2300	745	10.0
9	753	2560	745	10.0
8	753	2820	745	10.0
7	753	3070	959	9.4
6	753	3330	1160	8.9
5	753	3580	1350	8.3
4	753	3840	1580	7.7
3	753	4090	1810	7.1
2	753	4350	2030	6.6
1	753	4610	2260	6.0

The idealized story shear vs. interstory (IS) drift relations are shown in Fig. 5(a). The lateral load vs. lateral drift relations from the test are also shown. Story shear vs. IS drift relations were represented by a quadrilinear function. IS drift at the maximum shear, δ_y, was assumed uniform for all stories to be 0.8%. IS drift at the collapse, δ_u, was assumed 10% for the eighth story and above, and 6% for the first story. The interpolation was used to determine for the other stories. Such a way to determine δ_u was intended to reflect that it might decrease with the increase of axial load. IS drift at the third break point, δ_b, was assumed uniform for all stories to be 5%. Other structural properties including the stated above are shown in Fig. 5(a). Stiffness after δ_u , K_0, was assumed to be 1/10,000 of the initial stiffness. Takeda slip model was used to represent hysteresis rules of the shear spring (Fig. 5(b)).

Viscous damping proportional to the initial stiffness was assumed because if viscous damping proportional to the instantaneous stiffness was assumed, accelerating (not damping) force resulted in the region of negative instantaneous stiffness. Damping ratio was set 2%. The effect of damping will be discussed later. Two ground motion records from the Kobe earthquake were used for the analysis: FKI recorded at the highest seismic (Intensity 7) area and JMA recorded at the next to the highest seismic (Intensity 6) area. Response acceleration spectra of the two records are shown in Fig. 6. The dynamic analysis was continued till the end of the ground motion records even after the collapse of a story to study whether another story might or might not collapse.

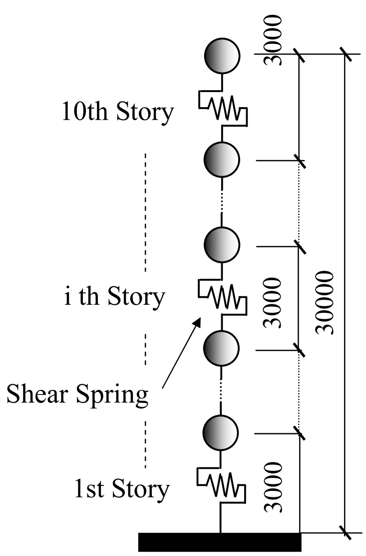

Fig. 3 Analytical Model

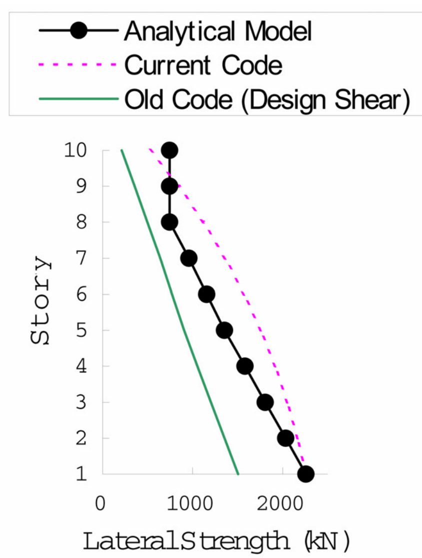

Fig. 4 Lateral Strength

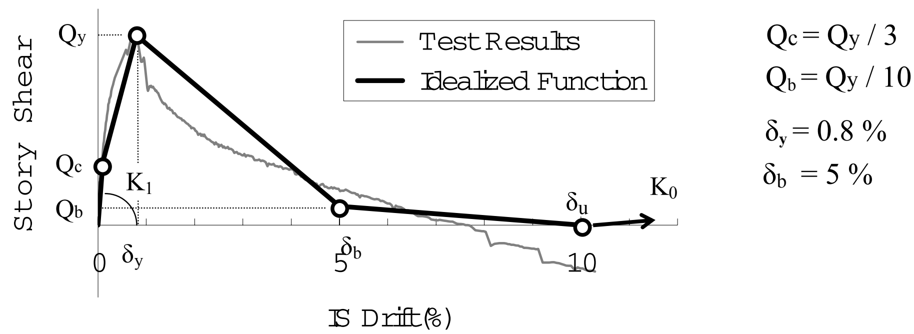

(a) Envelope Curve

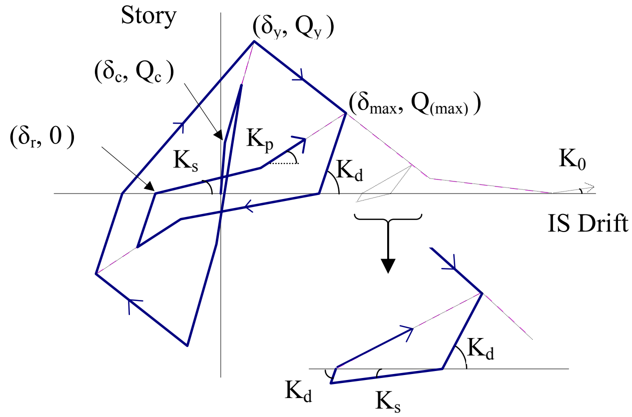

(b) Hysteresis Rules

Fig. 5 Hysteresis Model

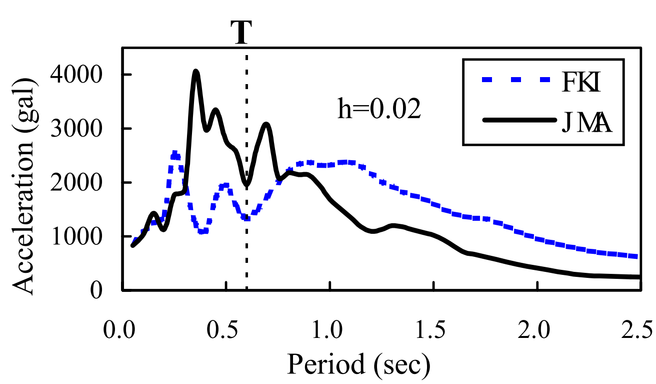

Fig. 6 Acceleration Spectra

4. ANALYTICAL RESULTS

4.1 Standard Case

The dynamic analysis was done for various intensity levels of the ground motion records. The intensity level of the ground motion records was expressed by a parameter A (A=1 for the original level). The introduction of this parameter enabled us to evaluate the intensity level of ground motions to have worked on the collapse buildings.

Maximum IS drift is schematically depicted in Fig. 7, where each story is classified into the four groups depending on the maximum response: for example the ■ mark denotes the collapse. For FKI, when A = 0.7, the sixth story underwent drift more than $1/2\delta_u$ but any story did not collapse. When A = 0.8, the sixth story collapsed, and When A = 0.9 and 1.0, the fifth and sixth stories collapsed. When A ≥1.1, more than two stories collapsed. For JMA, when A = 1.4, the seventh and eighth stories underwent drift more than $1/2\delta_u$ but any story did not collapse. When A = 1.5, the seventh story collapsed. And when A ≥ 1.6, the seventh and eighth stories collapsed. These results indicate the ground motions with the intensity level of 80 % of FKI or 150 % of JMA worked on the collapse buildings. The value of A for FKI being near 1.0 and that for JMA being considerably larger than 1.0 are believed to be due to the fact that FKI was in the Intensity 7 area while JMA was in the Intensity 6 area.

Maximum IS drift for A = 0.8 of FKI and A =1.5 of JMA are shown in Figs. 8. Both cases correspond to the minimum intensity level to induce the collapse. The dotted line in the figure shows δ_u. For FKI the stories immediately above and below the collapse story (sixth story) underwent near 5 % drift, and for JMA the story immediately above the collapse story (seventh story) did near collapse drift. But, as stated before, in reality damages to the stories except the collapse story were rather light. It is apparent there are some discrepancies between the analytical results and observations. This will be discussed later.

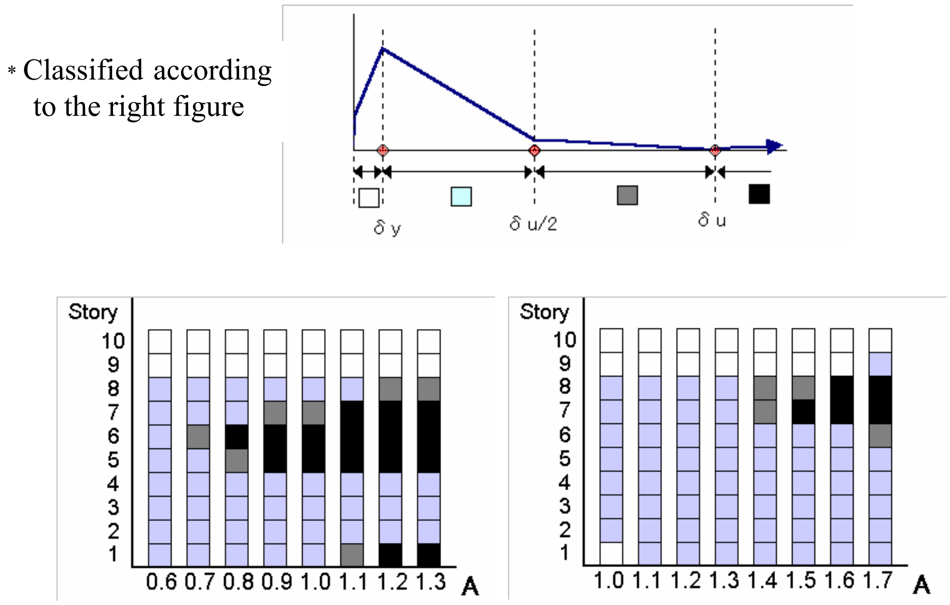

(a) FKI **(b) JMA**

Fig. 7 Maximum IS Drift (Standard Case)

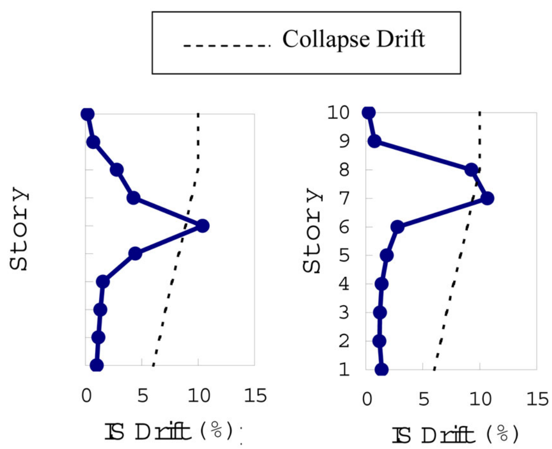

(a) FKI, A=0.8 **(b) JMA, A=1.5**

Fig. 8 Maximum IS Drift

Time history of IS drift and story shear vs. IS drift relations are shown in Fig. 9. They are for the sixth story for A = 0.8 of FKI. IS drift is observed to drift to one direction, indicating the monotonic loading used for the test was appropriate. Similar results were obtained from the JMA analysis as well.

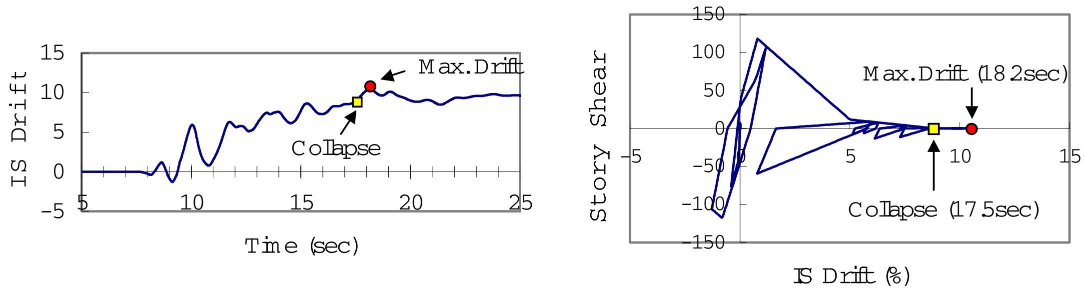

(a) Time History of IS Drift **(b) Story Shear vs. IS Drift**

Fig.9 Response Results (FKI, A=0.8, 6th Story)

Story shear vs. IS drift relations are shown in Fig. 10. They are for the fifth and sixth stories for A = 1.0 of FKI. For this case the fifth story first collapsed and 1.7 sec. later the sixth story did. The graph is shown until the time of the fifth story collapse. When the fifth story reached the collapse, the sixth story was also just before the collapse. I can be said that when plural stories collapsed, strength deterioration happened almost simultaneously for those stories and the collapse occurred at nearly same time.

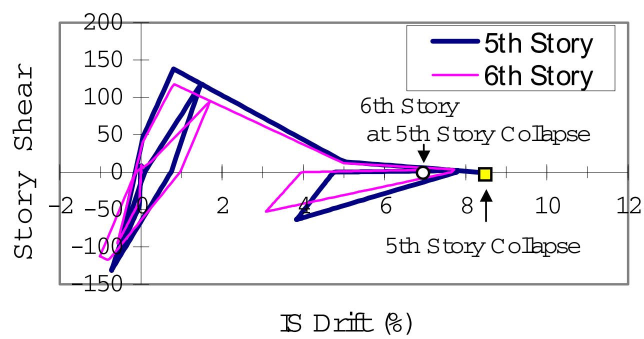

Fig. 10 Story Shear vs. IS Drift (FKI, A=1.0, 5th and 6th Stories)

Up to now the damping ratio was assumed to be 2 %. A case of zero damping was computed to study the effect of damping. Figure 11 shows time history of IS drift for the sixth story for A =0.8 of FKI. This story, after the collapse at 9.5 sec. (δ_u = 8.9 %), keeps vibrating with a very long period, which corresponds to the assumed post-collapse stiffness, 1/10,000 of the initial stiffness. For a reference a case of zero damping and zero post-collapse stiffness was computed. For this case the response diverged after the collapse. In reality the collapse buildings did not keep vibrating or keep moving to one direction after the collapse, suggesting it is not rational to assume zero damping.

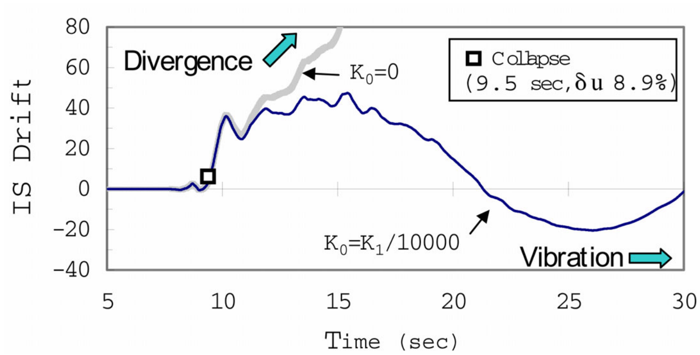

Fig. 11 Effect of Damping (h=0, FKI, A=0.8, 6th Story)

4.2 Case with Partially Reduced Strength

The analysis for the standard case produced larger response for the stories except the collapse story than the observations. This implies the collapse story was relatively weaker in strength than the other stories, therefore, resulting in the damage concentration on this story. To study this, cases with partially reduced strength at a story were considered. Lateral strength of the sixth story was reduced to 90 % or 70% of the standard case. Initial stiffness, δ_y, δ_b, and δ_u were left unchanged. FKI was used for this study.

Maximum IS drift is depicted in Fig. 12. It is observed while the collapse occurred at A = 0.8 for the standard case, it occurred at A = 0.6 for the reduced strength case (smaller than the former case). It is also noted that while plural stories collapsed frequently for the standard case, the collapse tends to concentrate on the sixth story for the reduced strength case. And such trend is more pronounced for the 70 % strength case.

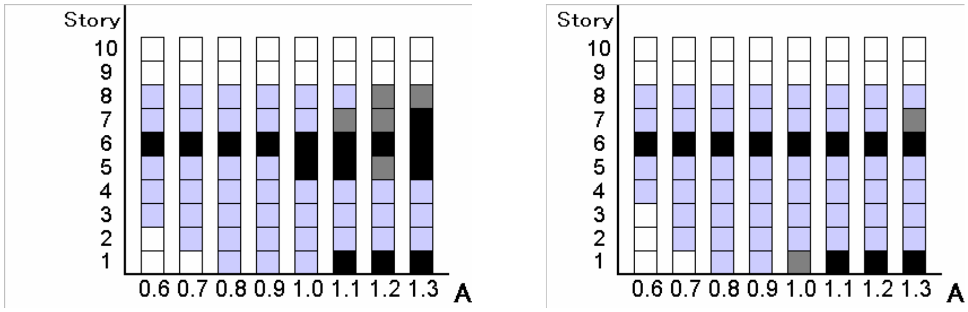

(a) 6th Story with 90% Strength (b) 6th Story with 70% Strength

Fig. 12 Maximum IS Drift (FKI, Case with Partially Reduced Strength)

Maximum IS drift is compared with the standard case in Fig.13 for A = 0.8 and 1.0. A = 0.8 and 1.0 are the intensity levels of single story collapse and plural story collapse for the standard case. In case of A = 0.8, for the 90 % strength the sixth IS drift was almost identical with the standard, and the fifth and seventh IS drift was considerably smaller than for the standard. For the 70 % strength the sixth IS drift became larger than for the standard and the fifth and seventh story drift did further smaller than for the 90 % strength. In case of A =1.0, while for the standard case the fifth and sixth story collapsed, for the reduced strength cases only the sixth story collapsed. The sixth IS drift increased and the fifth and seventh story drift decreased with the decrease of the sixth story strength, which was the same trend as A = 0.8. These results strongly support that the reduced strength case is more agreeable with the observations. It is likely that the collapse occurred at the story, which was weaker in strength than the other stories for some reasons.

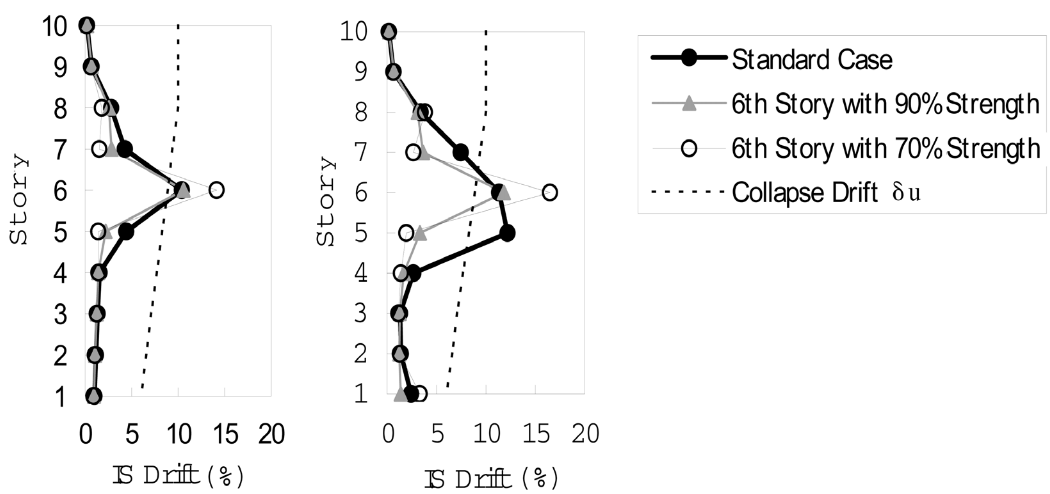

(a) A=0.8 (b) A=1.0

Fig. 13 Maximum IS Drift (FKI)

Story shear vs. IS drift relations of the fifth and sixth stories are shown in Fig. 14 for A = 0.8 for the 70 % strength case. The graph is depicted up to the time of the sixth story collapse. The graph for the standard case was shown in Fig. 10. For the standard case the sixth story shear was almost zero at the time of the fifth story collapse, but for the reduced strength case the fifth story did not lose the lateral strength much at the time of the sixth story collapse. This comparison also indicates that if there is a story relatively weaker in strength than the other stories, damages concentrate on this story.

4.3. Case with Uniformly Increased Strength

There were a number of buildings with light damages though they were similar to the collapse buildings in the structural properties and were in the highest seismic area. It is likely these buildings had lateral strength larger than the standard case defined here. To study this, cases with uniformly increased strength were considered. A parameter B, as defined as a multiplication factor of the lateral strength over the standard case for all stories was considered. The parameter B was varied from 1.0 to 1.5 (B = 1.0 for the standard case). FKI was used and A was set as 0.8. Remember A = 0.8 is the minimum intensity level to induce the collapse for the standard case. Maximum IS drift is depicted in Fig. 15. While the sixth story collapsed for B = 1.0 and 1.1, the story collapse did not occur for B ≥ 1.2. But even for B = 1.5 maximum response was more than $1/2\delta_u$.

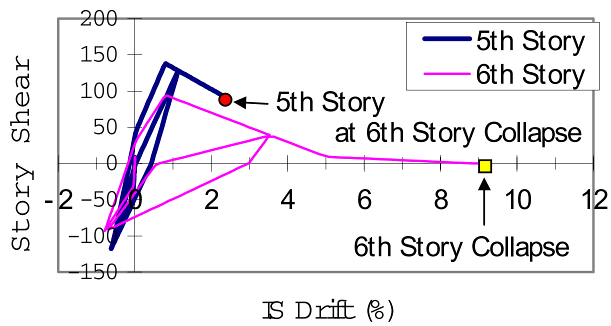

Fig. 14 Story Shear vs. IS Drift (FKI, A=1.0, 6th Story with 70% Strength)

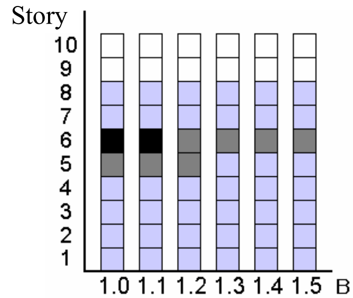

Fig. 15 Maximum IS Drift (FKI, A=0.8, Case with Uniformly Increased Strength)

5. CONCLUSIONS

The intermediate-story collapse of concrete buildings was studied by the dynamic analysis based on the test results. The major findings from the study are as follows:

(1) The analysis presented here can, though roughly, describe the scenario of the intermediate-story collapse considering ground motions with the intensity level of the record from the highest seismic area, and

(2) The collapse story is considered to have been relatively weaker in lateral strength probably by 10 to 30 % than the other stories.

REFERENCES

Architectural Institute of Japan. (1998). *Recommendation to RC structural design after Hanshin-Awaji earthquake disaster – Cause of particularly noticed damages and corresponding RC structural design details*

Ryu, Y., Nakamura, T. and Yoshimura, M. (2001), Axial load carrying capacity of RC columns subjected to seismic actions. Proceedings of the Japan Concrete Institute. Vol.23. No.3. 217-222

Kamino, T., Yoshimura, M. and Nakamura, T. (2001), Collapse of building at intermediate story during Hyogoken-Nanbu earthquake. Proceedings of the Japan Concrete Institute. Vol.23. No.3. 1201-1206

KEYWORDS

Collapse, Intermediate Story, Shear, Earthquake, Dynamic Analysis, Interstory Drift, Column, Test

COMPUTING STORY DRIFT DEMANDS FOR RC BUILDING STRUCTURES DURING THE 1999 CHI-CHI TAIWAN EARTHQUAKE

K. C. Tsai and Yuan-Tao Weng[1]

Abstract

The 921 Chi-Chi earthquake caused very significant amount of building collapses or damages of various degrees. Many collapsed buildings had a pedestrian corridor and open front at the ground floor. Using a modified modal participation factor and the generalized shape function computed from the nonlinear push over analysis, story drift demands imposed on soft first story building systems are studied in this paper. Generalized shape functions are constructed from the nonlinear static push over analysis of shear buildings having specific distributions of story stiffness and strength. Nonlinear response spectrum analyses were performed on the ground acceleration recorded from 62 sites in Taichung Region. Analytical results indicate that soft first story buildings are likely to have a story drift demands significantly greater than regular buildings of short fundamental period. Results of the nonlinear dynamic analysis of a 6-story structure indicate that the maximum story drift demand can be satisfactorily predicted by the story spectral drift constructed from the generalized shape functions.

1. INTRODUCTION

On 1:47a.m. of September 21, 1999, a magnitude $M_L = 7.3$ earthquake struck the central region of Taiwan. Survey data indicates that approximately 3,000 buildings totally collapsed as a result of the earthquakes, with more than 10,000 others partially collapsed and countless others damaged to various degrees (ABRI, 1999). Many collapsed buildings had a pedestrian corridor and open front at the ground floor, and only one wall at the back of the building along the street direction. Due to the long raining season in Taiwan, the Taiwanese developers commonly construct the buildings with the pedestrian corridor, and this popular style becomes a local practice and is prescribed in the building codes. Thus, the pedestrian corridor buildings represent a large portion of the failed structures, and experienced different level of damages. Figure 1 indicates that approximately 84% of the RC damaged structures are the pedestrian corridor buildings, and roughly 45% of the pedestrian corridor buildings are classified as severely damaged or worse. In the affected area, more than two dozen modern 10-to-20 story apartment buildings overturned or collapsed. These were reinforced concrete moment resisting frames, most of them constructed with cast-in-place 15cm thick exterior wall and 12cm thick partition walls. Seismic force requirements of building designs in Taiwan for the past 25 years are given in Table 1. In this research (Tsai et al, 2001), the story drift demands imposed on the building systems having various strength and stiffness distributions are studied by analyzing the drift spectra constructed from the generalized shape functions.

[1]*Department of Civil Engineering, National Taiwan University, Taipei, Taiwan. Email: kctsai@ce.ntu.edu.tw*

2. RESPONSE SPECTRA ANALYSIS FOR SOFT FIRST STORY BUILDING SYSTEMS

As noted above, the extensive vulnerability of the existing building inventory, as revealed by this earthquake, must be addressed before other equally destructive earthquakes strike again in the country. A particular attention is paid to buildings having soft stories and open front. In particular, this paper discuss the spectral responses for soft first story building systems using the free-field ground motion records obtained in the EW direction from 62 sites in Taichung Region.

3. RECORDED GROUND MOTIONS IN TAICHUNG REGION

Figure 2 shows the shake contour map for the Chi-Chi earthquake using geometric mean of two horizontal PGA values. For Taichung region, 62 free field ground motion records were chosen in this study. The epicentral distances of these 62 sites range from about 20km to 50km. The average of the 62 PGAs in EW direction is about 164gal. Their averaged acceleration response spectra and the COVs are shown in Figure 3. Many reinforced concrete buildings in Taichung region suffered damages of various degrees ranging from cracks in in-fill partitions or external window walls to collapse of ground floor or overturn of entire multi-story buildings.

4. SEISMIC FORCE REQUIREMENTS AND INELASTIC RESPONSE SPECTRA

As shown in Table 1, there are four major editions of seismic building codes adopted during the past 25 years. In general, seismic design forces increased as newer versions of building code were adopted. Due to a large amount of building constructions took place during the 80s and the early 90, it is believed that a significant amount of building were constructed based on the 1982 seismic building codes. Therefore, elastic and inelastic response spectra were critically assessed for regular and soft first story building systems designed and constructed using the 1982 seismic force requirements. Using Z=1.0, I=1.0 and K=1.0, the design base shear is V_{code}=1.0CW, where C varies as given in Table 1. As the ultimate strength method has been widely adopted, the governing load combination involving the seismic force is Q=0.75(1.4D+1.7L+1.87EQ). When the strength factor is governed by flexural yielding of the beam members (i.e. $\Phi M_n=0.9M_n$) as in the case of strong column weak beam design, then the yield strength of the system, $R_y=\Omega V_{code}$, can be characterized with a strength factor $\Omega=0.75\times1.87/0.9=1.55$. Thus, a properly designed reinforced concrete structure generally possesses a lateral yield strength of at least about 1.50 times the code prescribed seismic base shear. An idealized bilinear base shear versus roof displacement relationship showing the Ω ratio of yielding strength R_y and V_{code} is schematically given in Figure 4a. Figure 5a shows the spectral yield strength for building systems constructed in Taichung Region, in terms of system weight based on the 1982 seismic force requirements for five different Ω values. An Ω value of 3.0 or 4.5 represents a conservative or very strong system where as an Ω value of 0.75 or 0.5 can be viewed as a substandard structure due to poor workmanship or low concrete strength. Using the Ω as the key parameter, the displacement spectra for 5% damped systems with an elasto-plastic and cyclically degrading force-deformation characteristics (Mahin and Lin, 1983) given in Figure 4b are shown in Figure 5b for Taichung Region. These averaged spectra were constructed using the responses computed for the main shocks recorded in the EW direction from 62 sites for Taichung Region. For substandard structures (Ω values smaller than 1.5) designed by using the 1982 seismic force requirements, the ductility demands imposed by the Ch-Chi earthquakes can be significantly greater than 4.0 as shown in Figure 6 for short period structures in Taichung Region. As shown in Table 2, the Fu factor is a function of the prescribed structural ductility capacities ranging from 1.6 to 4.8 for various structural systems. Figure 7 compares the force reduction factors derived from the spectral force response ratios and that prescribed in the Taiwan building code. In Figure 7, the curves of R_μ are constructed by dividing the elastic shear demand (μ=1.0) of each SDOF system by the inelastic shear demand of the corresponding SDOF having the same vibration period and a specific ductility demand (μ=2.0 or 4.0). The shaded margins in Figure 7 indicate that Fu values in Taichung Region are larger than R_μ for certain short period ranges. This somewhat suggests that some of the code prescribed force reduction factors, Fu, may be too large to control the ductility demand in these ranges of buildings.

5. STORY DRIFT DEMANDS IMPOSED ON MDOF BUILDING SYSTEMS

In order to compute inelastic deformation demands imposed on the building structures, simplified analytical procedures have been proposed by many researchers (Krawinkler and Seneviratna, 1996; Fajfar, 1999) and given in model seismic design specifications (ATC 1996; BSSC, 1997). The “capacity spectrum method” assumes an MDOF is responding essentially in the first mode. It incorporates results of the push over analysis into the nonlinear spectral acceleration versus spectral displacement curve in order to find the peak lateral floor displacements of an MDOF building system. Following the same logic (Fajfar and Fischinger, 1987), in this research it is assumed that the building maximum lateral displacement demands imposed by the earthquake can be estimated by multiplying the inelastic spectral displacement

S_d of a specific elasto-plastic SDOF, a modified first mode participation factor Γ_1 and a participation factor-consistent deformed shape function $\phi_1(y)$. That is, the peak lateral displacement u(y) along the height of the MDOF system, and its spectral first story drift angle θ_1 can be computed from :

$$u_1(y) = S_d \cdot \Gamma_1 \cdot \phi_1(y) \tag{1}$$

$$\theta_1 = S_d \cdot \Gamma_1 \cdot \phi_1(h_1) / h_1 \tag{2}$$

where the modified first modal participation factor is computed from the same shape function $\phi_1(y)$:

$$\Gamma_1 = \frac{\sum m_i \phi_{i1}}{\sum m_i \phi_{i1}^2} \tag{3}$$

The computation of the shape functions and the accuracy of the proposed method in estimating the nonlinear story drift demands for soft or weak story building systems are presented in the following sections.

6. GENERALIZED VERTICALLY REGULAR AND IRREGULAR BUILDING SYSTEMS

It is noted that many of the severely damaged buildings appear to have tall floor and open plaza features in the ground level. It is found from the modal analyses that the fundamental mode shapes, for the regular building can be approximated by an inverted triangle having a linear shape function while for the soft first story building, it can be characterized by a bi-linear shape function (Tsai et al., 2001). In this paper, using an iterative procedure, the shape functions computed from nonlinear push over analysis of inelastic frame models are adopted. The effects of the vertical irregularity on the first mode shapes were investigated by constructing 2- to 20-story inelastic building models. It is assumed that:

- the mass distribution over the building height is uniform and the vertical distribution of the design lateral forces is an inverted triangle;
- the ground floor height is 4 meters and typical floor height is 3 meters;
- the lateral stiffness distribution for regular building is approximately uniform over the full height;
- the definition of soft story and weak story follows those given for the irregular buildings in the model building codes (Building Technology Standards, 1989, 1997). A soft first story building is when the lateral stiffness ratio, R_{soft} between the first and second story is smaller than 0.8. Likewise, the weak first story building is when the ratio, of the yield strength to the design shear ratio between the first and second floor, R_{weak} is smaller than

0.8.

- if H_n is the building height (in meter), the fundamental period, T (in second) of the buildings follows (Building Technology Standards, 1997):

$$T=0.07(H_n)^{3/4} \tag{4}$$

7. DRIFT SPECTRA INCORPORATING THE GENERALIZED SHAPE FUNCTIONS

The story drift spectra for the regular or irregular building systems were constructed using the following procedures:

1. assume the buildings range from 2- to 20-story with the floor-to-floor height noted above,
2. compute the fundamental period from Eq. 4 for a given building height, find the corresponding spectral displacement S_d for a specific Ω value from results like those shown Figures 5b,
3. predict a modal participation factor Γ', a value of about 1.3 is a good starting point,
4. construct an inelastic structural model having the same fundamental period, story and building heights as that given in step 2, but with a specific set of R_{soft} and R_{weak} values,
5. perform a nonlinear pushover analysis until the roof displacement of the structure reaches $\Gamma' \times S_d$, obtain the maximum structural lateral displacement pattern, set the normalized structural lateral deformation shape as the fundamental deformed shape function,
6. compute the corrected participation factor from Eq. 3 using the shape function obtained in step 5,
7. repeat steps 3 through 6 until the corrected participation factor converges to a specified tolerance, set the final deformed shape as the participation factor-consistent shape function,
8. repeat steps 2 through 7 for the range of building heights interested,

It is found that the story drift spectra can then be conveniently and satisfactorily constructed from Eq. 2, if the regression analysis is performed on the shape functions for the whole range of building heights having a specific set of R_{soft} and R_{weak} values. The specification of the story mass in step 4 is required only when a dynamic analysis of the MDOF system is desired. The modified participation factor spectra computed for the regular and irregular buildings are shown in Figure 8. These are computed from the participation factor-consistent deformations given in Table 3. It is noted that the modal participation factors for the regular and the soft story buildings are quite different. For regular buildings, it is about 1.5 regardless the heights of the building. The modified first mode participation factor of the soft first story cases is generally smaller than that of the regular buildings of the same height or period, but approaching 1.5 as the building height increases. However, the proposed method failed to differentiate the regular systems from the irregular systems having the strength irregularity of R_{weak}=0.8 alone (no soft story) on the participation factor. This is because both systems will yield at the same level of lateral loads for a given system Ω value, and reach essentially the same lateral displacement. It is found in Figure 8 that the effects of irregularity indices, R_{soft} and R_{weak}, in reducing the value of the participation factors are more pronounced in the systems having a lower strength factor Ω. Using the ground motion records noted previously, the mean and the corresponding mean plus one standard deviation (1.0σ) of the first story drift spectra are computed and shown in Figures 9 for Taichung Region. Similarly, Figure 10 shows the averaged first story drift spectra for the R_{soft} and R_{weak} values equal to 0.7 or 0.9.

8. ACCURACY ASSESSMENTS

In order to examine the accuracy of the proposed method in predicting the maximum seismic responses of the MDOF building systems, dynamic analyses were performed on a 6-story structure. The overall height of the structure is 19m and the corresponding first mode period is 0.637 sec. The story mass, the typical story and the first story stiffnesses for the 6-story structure of various irregularities are given in Table 4. Using the TCU095 EW direction ground accelerations (PGA=0.367g), the maximum roof and ground floor displacements and the first story drift angle computed from the nonlinear dynamic analyses using the DRAIN2D+ (Tsai and Li, 1994) computer program with the bilinear elements are given in Table 5. The modified modal participation factors, the shape functions and the lateral displacements computed from the proposed method are given in Table 6. It is found that the error is less than 26% for the four models studied.

9. DISCUSSION OF ANALYTICAL RESULTS

Based on the analyses noted above, it appears that the maximum seismic story drift spectra for building systems vibrating essentially in the first mode can be predicted using the proposed procedures. It is found that the shapes of the first story drift spectrum for the regular (not shown here) and irregular (Figure 9) buildings are about the same, but the magnitudes of the spectral first story drift demand on the irregular buildings are significantly greater than the regular ones. It is evident in Figure 9 that the equal displacement theory can be extended to story drift analysis for structures having normal or strong lateral strength (Ω > 1.5). However, for substandard structures (Ω < 1.5) having a weak story (R_{weak} = 0.8), the story drift demand is significantly greater than that of the normal or strong structures across the full range of periods. Comparing Figures 9b with 9a, it is apparent that the effects of the first-story weakness on the story drift demand is much more pronounced than the effects of softness of the first floor. For story drift demands imposed on the buildings in Taichung Region during the Chi-Chi main shocks (averaged PGA=0.164g), Figure 9 indicates that the mean and the mean plus one standard deviation (1.0σ) of the first story drift demand for irregular buildings are greater than 0.01 radian for substandard structures. These large story drift demands could be fatal if non-ductile details of reinforcing steel ties or bar splices exist in the ground floor columns.

10. DESIGN IMPLICATIONS

For long period structures having a normal or strong lateral strength in Taichung, Figures 10(a)~(c) indicate that the averaged first story drift demand for irregular buildings with R_{soft} and R_{weak} values equal to 0.7 are significantly greater than those of R_{soft} and R_{weak} values equal to 0.8. And in many cases, their first story drifts exceed 0.01 radian. But if the R_{soft} and R_{weak} value is raised up to 0.9, as shown in Figures 10(d)~(f), the averaged first story drift demands can be significantly reduced for the intermediate and long period structures. Thus, before further data becomes available, it appears that the lower limit of the R_{soft} and R_{weak} ratios for the soft or weak story prescribed in the Taiwan seismic building code could be raised from 0.8 to 0.9 for damage control, especially for structural rehabilitation design of existing old buildings.

11. SUMMARY AND CONCLUSIONS

Using the ground accelerations recorded during the 1999 Chi-Chi Taiwan Earthquake, the story drift response spectra were constructed by using the displacement response spectra, the lateral floor displacements obtained from the nonlinear frame push over analysis, and a deformation-consistent modal participation factor. It is confirmed that the dynamic peak story drift angle can be satisfactorily predicted using the proposed procedures. Analytical results indicate that the effects of first story weakness on the story drift demand are much more pronounced than the effects of softness of the first story for substandard structures.

12. REFERENCES

Applied Technology Council (ATC), (1996). Seismic Evaluation and Retrofit of Concrete Buildings. Vols. 1 and 2, *ATC-40*, Applied Technology Council, Redwood City.

ABRI (1999). Preliminary reconnaissance report for the 921 Chi-Chi earthquake. Architecture and Building Research Institute, Ministry of Interior, R.O.C. (in Chinese)

BSSC (1997), NEHRP guidelines for the seismic rehabilitation of buildings, *FEMA-273*,

developed by ATC for FEMA, Washington D.C.
Building Technology Standards (1974, 1982, 1989, 1997), Ministry of Interior, R.O.C.
Fajfar, P. and Fischinger, H.(1987). Nonlinear seismic analysis of RC buildings: Implications of a case study. *Eur. Earthquake eng.* 1, pp.31-43.
Fajfar, P.(1999). Capacity Spectrum Method Based On Inelastic Demand Spectra. *Earthquake Engng. Struct. Dyn.*(28), pp.979-939.
Krawinkler, H. and Seneviratna, G. D. P. K.(1996). Pros and cons of a pushover analysis for seismic performance evaluation. *Engng Struct.*(20), pp.452-464.
Mahin, S. A. and Lin, J.(1983). "Construction of Inelastic Response Spectra for Single Degree of Freedom System", *Report No.UCB/EERC-83/17*, University of California, Berkeley.
Tsai, K. C. and Li, J. W.(1994). DRAIN2D+ , A General Purpose Computer Program for Static and Dynamic Analysis of Inelastic 2D Structures, Supplemented with a Graphic Processor VIEW2D ,User's Guide. *CEER/R83-03,* Center for Earthquake Engineering Research ,National Taiwan University.
Tsai, K.C., Weng, Y.T., Jang, L.C. and Lai, J.W. (2000). Spectral Responses and Building Damages in 1999 Chi-Chi Taiwan Earthquake. Proceedings, *International Conference on Advances in Structural Dynamics*, Hong Kong, December.
Tsai, K.C., Weng, Y.T., Jang, L.C., Lai, J.W., Liu, J.G. and Lin, Y.H. (2001). Response Spectrum Analyses using Chi-Chi Earthquake Ground Accelerations. Center for Research on Earthquake Engineering, College of Engineering, National Taiwan University, CEER Report. (in Chinese)

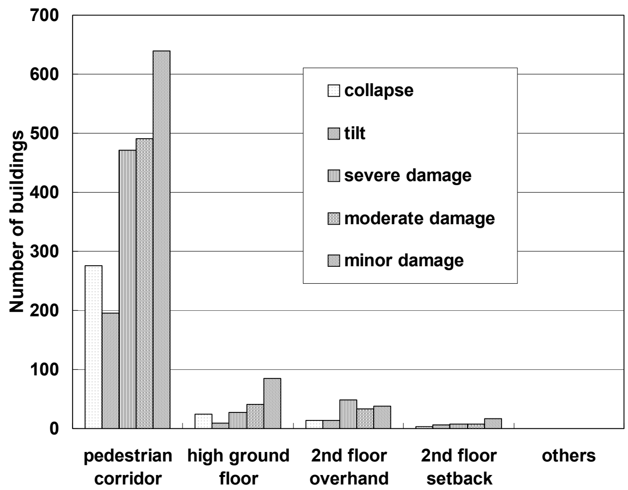

Figure 1. Number of damaged RC structures with respect to vertical configuration

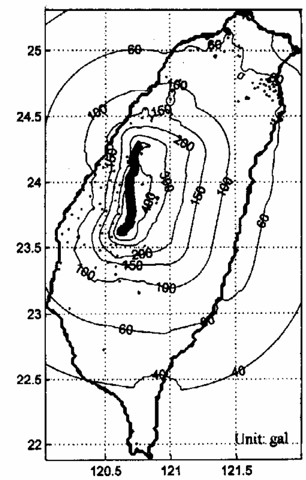

Figure 2. Shake contour map for the Chi-Chi earthquake (using geometric mean of both two horizontal components, adopted by Central Weather Bureau in 1999

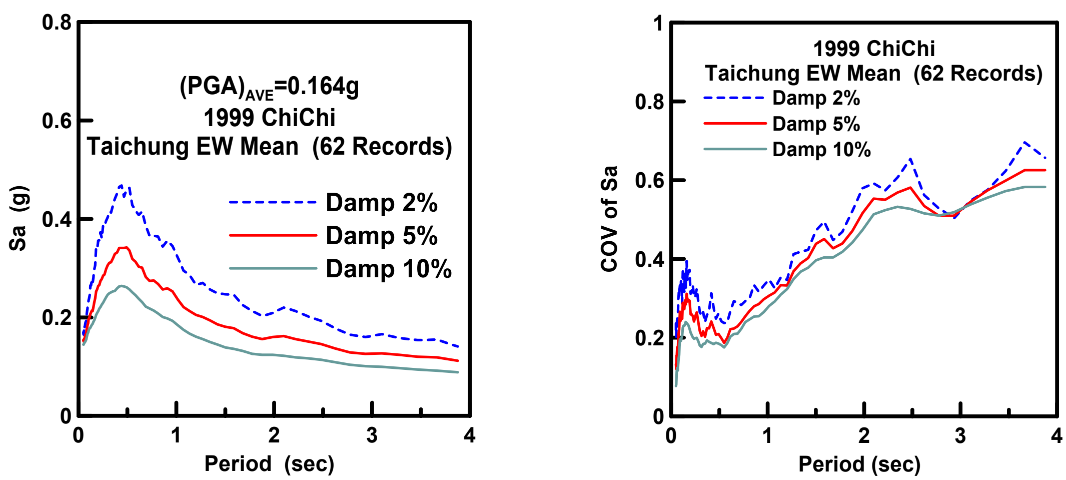

Figure 3. Averaged elastic acceleration response spectra and COVs computed for 62 stations in Taichung Region

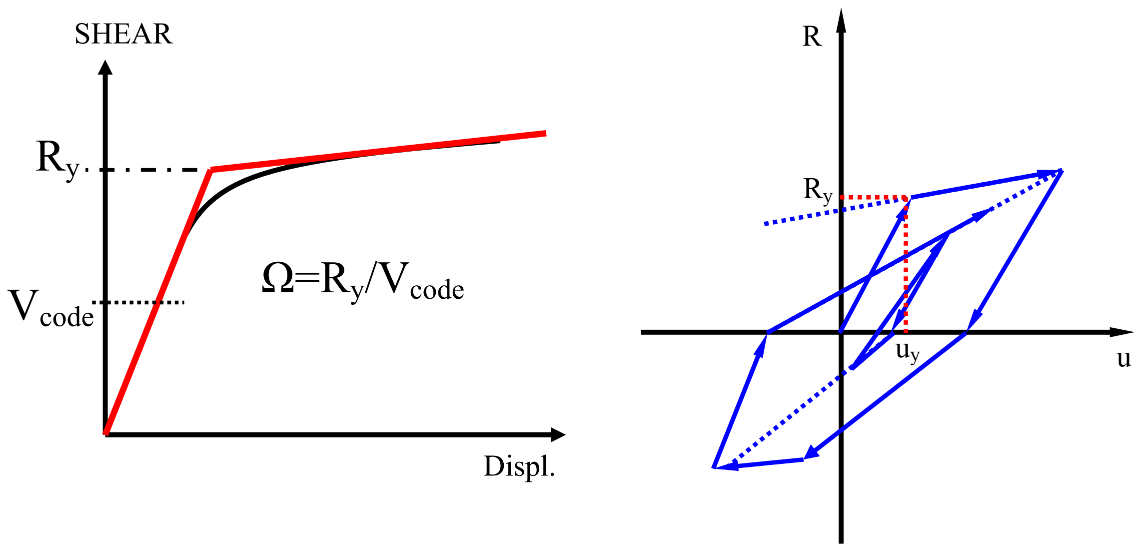

(a) Bilinear Relationship (b) Stiffness Degrading Model

Figure 4. Lateral force versus displacement relationship

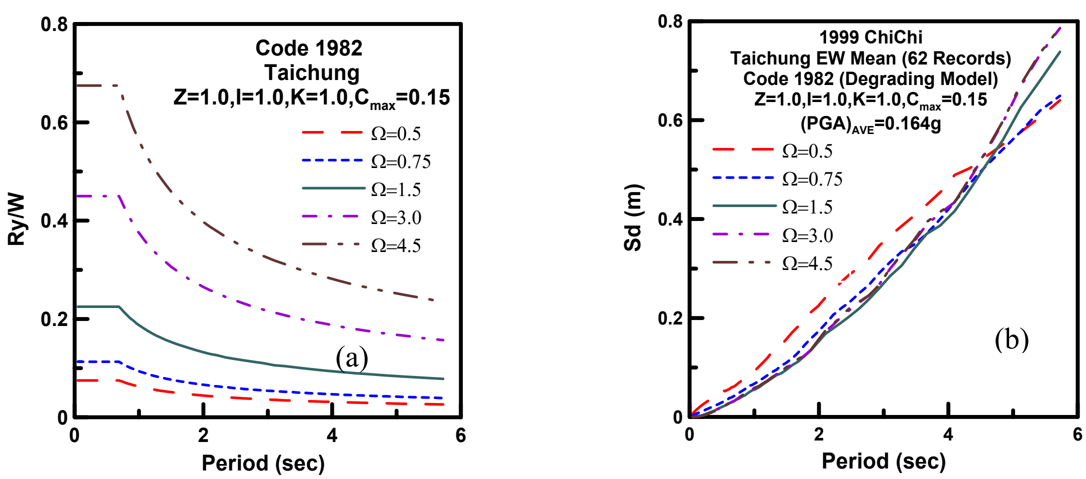

Figure 5. Spectral yield capacities and the corresponding inelastic displacement spectra for Taichung Region

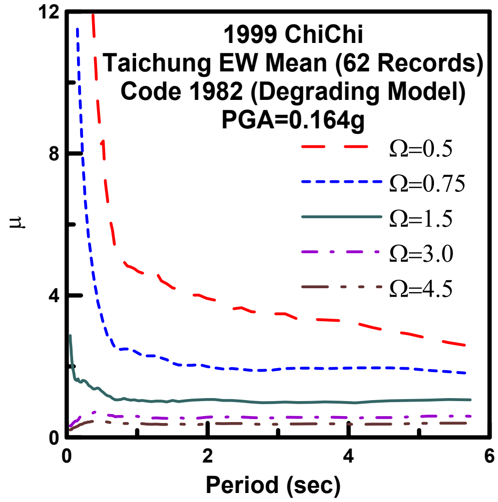

Figure 6. Ductility demand spectra for Taichung Region

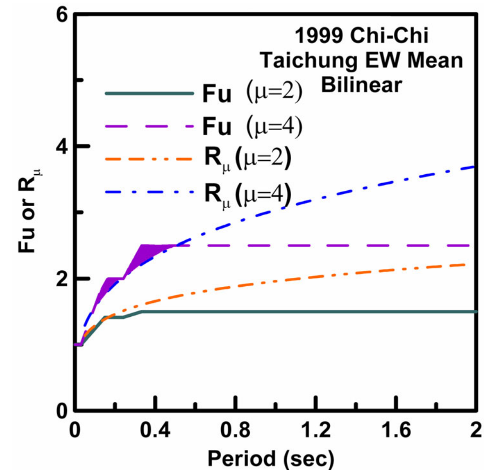

Figure 7. Comparing Fu with R_{μ} for Taichung Region

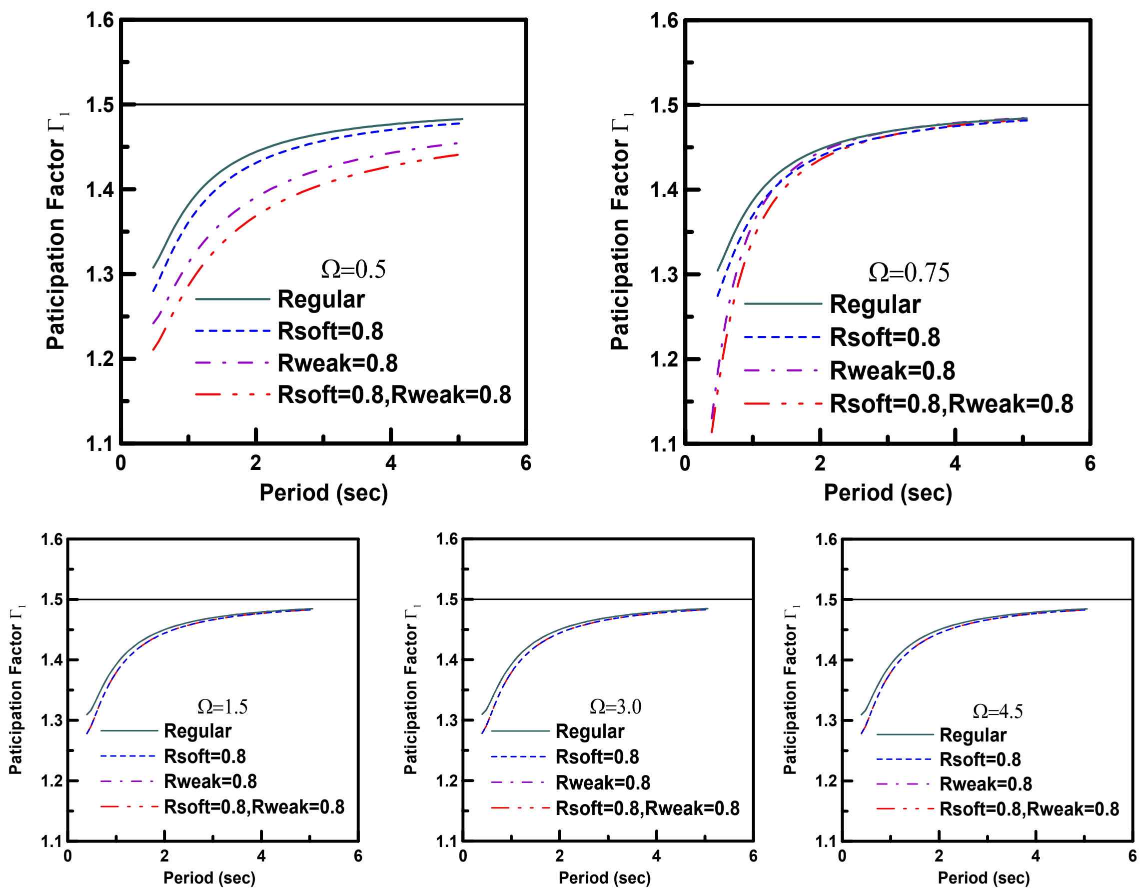

Figure 8. Modified modal participation factors for systems having various vertical irregularities and spectral yield capacity in Taichung Region

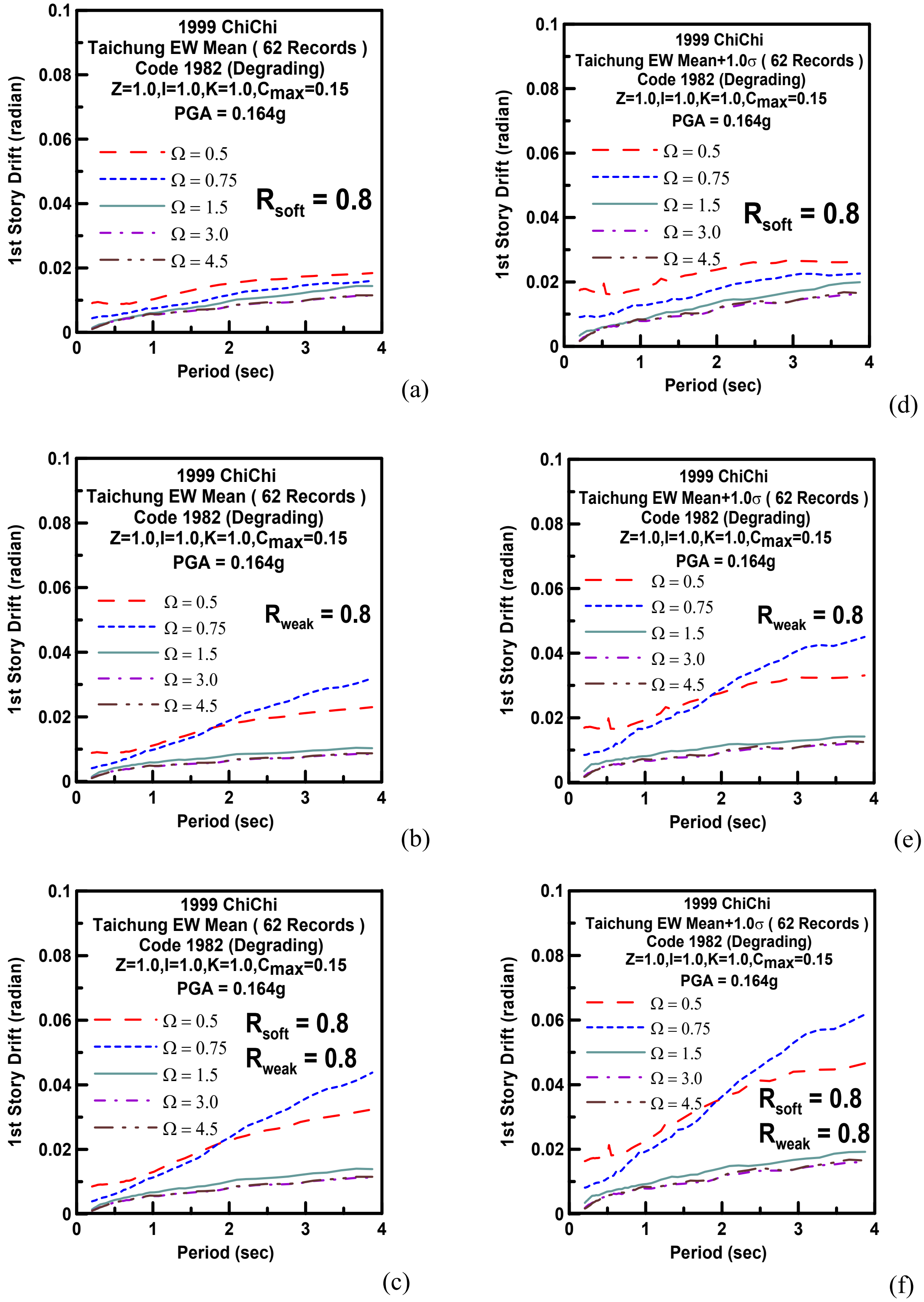

Figure 9. The mean and mean plus one standard deviation (1.0σ) of the first story drift spectra for irregular buildings with the R_{soft} and R_{weak} values equal to 0.8 in Taichung Region

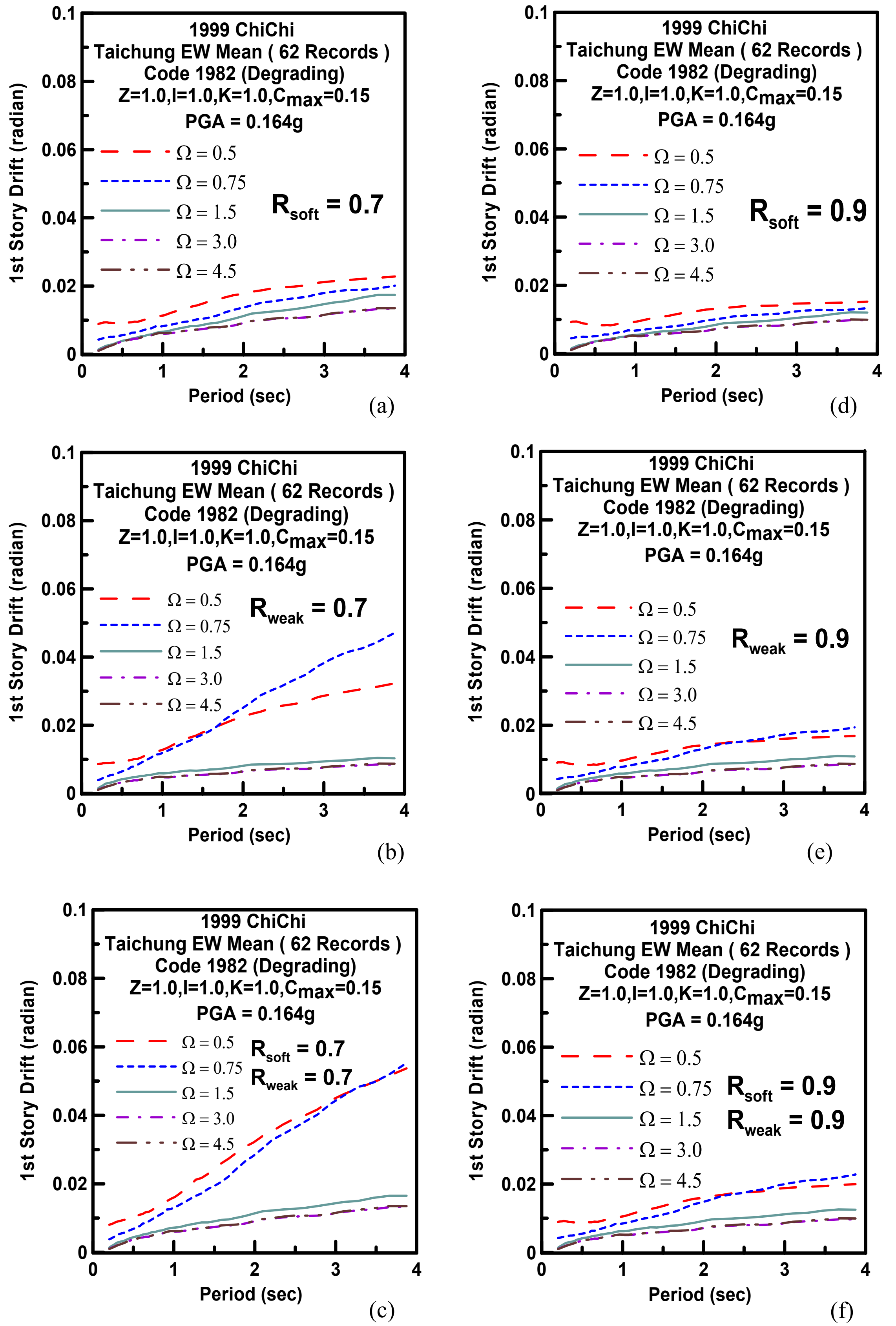

Figure 10. Averaged first story drift spectra for irregular buildings with the R_{soft} and R_{weak} values equal to 0.7 or 0.9 in Taichung Region

Table 1: Seismic Force Requirements in Taiwan

Year	Seismic Base Shear	Remarks
1974	Vw = Z K C W	Z = 1.25, 1.0, 0.75 K = 0.67, 0.8, 1.0, 1.33 $C=0.1/0.3\sqrt{T}$, $C_{max} = 0.10$; W = D + 0.25 L
1982	Vw = Z K C I W	Z = 1.0, 0.8, 0.6 K = 0.67, 0.8, 1.0, 1.33 I = 1.0, 1.25, 1.5; $C=1/8\sqrt{T}$, $C_{max} = 0.15$; W = D
1989	Vw = Z K C I W	Same as 1982, except $0.248/T$ for Taipei Basin; $C=1/8\sqrt{T}$ for elsewhere
1997	$V = \dfrac{Z\ I\ C\ W}{1.4\ \alpha_y\ F_u}$	Z = 0.33, 0.28, 0.23, 0.18 I = 1.0, 1.25, 1.5; $C_{max} = 2.5$; W = D $\alpha_y = 1.2$ (WSD), $\alpha_y = 1.5$ (USD); $F_u \approx 2.9, 2.5, 2.1$

Table 2: List of the normalized spectra acceleration coefficient C and structural seismic force reduction factor Fu for hard rock site (1999)

T	Shortest	Shorte	Short	Medium	Long
C	$T \le 0.03$ sec C=1.0	$0.03\ sec \le T \le 0.15\ sec$ C=12.5T+0.625	$0.15sec \le T \le 0.333\ sec$ C=12.5T+0.625	$0.333\ sec \le T \le 1.315\ sec$ $C=1.2T^{2/3}$	$1.315sec \le T$ C=1.0
Fu	$T \le 0.03$ sec Fu=1.0	$0.03\ sec \le T \le 0.15\ sec$ $Fu = \sqrt{2R_a - 1} + \left(\sqrt{2R_a - 1} - 1\right)\left(T - 0.15\right)/0.12$	$0.15sec \le T \le 0.242\ sec$ $Fu = \sqrt{2R_a - 1}$	$0.242\ sec \le T \le 0.333\ sec$ $Fu = \sqrt{2R_a - 1} + \left(R_a - \sqrt{2R_a - 1}\right)\left(T - 0.242\right)/0.091$	$0.333\ sec \le T$ $Fu=R_a$
$R_a = 1 + \left(\mu - 1\right)/2$, $\mu = 1.6$ to 4.8					

Table 3: Generalized first and top story drift angles, θ_1 and θ_{TOP} for various Ω, R_{soft} and R_{weak} values (Taichung Region)

$K_1/K_2 = R_{soft}$	$R_1/R_2 = R_{weak}$	Ω	θ_1	θ_{TOP}
1.0	1.0	0.5	$\theta_1 = 2.31T^{0.396}$	$\theta_{TOP} = 0.180T^{-0.988}$
0.7	0.7	0.5	$\theta_1 = 4.76T^{0.990}$	$\theta_{TOP} = 0.114T^{-1.06}$
0.7	1.0	0.5	$\theta_1 = 3.15T^{0.616}$	$\theta_{TOP} = 0.157T^{-0.917}$
1.0	0.7	0.5	$\theta_1 = 3.60T^{0.782}$	$\theta_{TOP} = 0.145T^{-1.05}$
0.8	0.8	0.5	$\theta_1 = 3.68T^{0.771}$	$\theta_{TOP} = 0.143T^{-0.965}$
0.8	1.0	0.5	$\theta_1 = 2.81T^{0.535}$	$\theta_{TOP} = 0.167T^{-0.958}$
1.0	0.8	0.5	$\theta_1 = 3.06T^{0.643}$	$\theta_{TOP} = 0.160T^{-1.01}$
0.9	0.9	0.5	$\theta_1 = 2.89T^{0.580}$	$\theta_{TOP} = 0.164T^{-0.970}$
0.9	1.0	0.5	$\theta_1 = 2.53T^{0.470}$	$\theta_{TOP} = 0.174T^{-1.00}$
1.0	0.9	0.5	$\theta_1 = 2.65T^{0.518}$	$\theta_{TOP} = 0.171T^{-0.993}$
1.0	1.0	1.5	$\theta_1 = 2.27T^{0.370}$	$\theta_{TOP} = 0.187T^{-0.946}$
0.7	0.7	1.5	$\theta_1 = 3.38T^{0.437}$	$\theta_{TOP} = 0.150T^{-0.303}$
0.7	1.0	1.5	$\theta_1 = 3.06T^{0.555}$	$\theta_{TOP} = 0.165T^{-0.819}$
1.0	0.7	1.5	$\theta_1 = 2.70T^{0.248}$	$\theta_{TOP} = 0.171T^{-0.440}$
0.8	0.8	1.5	$\theta_1 = 3.12T^{0.368}$	$\theta_{TOP} = 0.158T^{-0.355}$
0.8	1.0	1.5	$\theta_1 = 2.75T^{0.487}$	$\theta_{TOP} = 0.174T^{-0.867}$
1.0	0.8	1.5	$\theta_1 = 2.70T^{0.249}$	$\theta_{TOP} = 0.171T^{-0.449}$
0.9	0.9	1.5	$\theta_1 = 2.88T^{0.349}$	$\theta_{TOP} = 0.169T^{-0.633}$
0.9	1.0	1.5	$\theta_1 = 2.49T^{0.426}$	$\theta_{TOP} = 0.181T^{-0.908}$
1.0	0.9	1.5	$\theta_1 = 2.69T^{0.299}$	$\theta_{TOP} = 0.175T^{-0.684}$
1.0	1.0	4.5	$\theta_1 = 2.05T^{0.280}$	$\theta_{TOP} = 0.201T^{-0.931}$
0.7	0.7	4.5	$\theta_1 = 2.65T^{0.419}$	$\theta_{TOP} = 0.181T^{-0.795}$
0.7	1.0	4.5	$\theta_1 = 2.65T^{0.419}$	$\theta_{TOP} = 0.181T^{-0.795}$
1.0	0.7	4.5	$\theta_1 = 2.05T^{0.280}$	$\theta_{TOP} = 0.201T^{-0.931}$
0.8	0.8	4.5	$\theta_1 = 2.42T^{0.366}$	$\theta_{TOP} = 0.189T^{-0.846}$
0.8	1.0	4.5	$\theta_1 = 2.42T^{0.366}$	$\theta_{TOP} = 0.189T^{-0.846}$
1.0	0.8	4.5	$\theta_1 = 2.05T^{0.280}$	$\theta_{TOP} = 0.201T^{-0.931}$
0.9	0.9	4.5	$\theta_1 = 2.22T^{0.320}$	$\theta_{TOP} = 0.196T^{-0.893}$
0.9	1.0	4.5	$\theta_1 = 2.22T^{0.320}$	$\theta_{TOP} = 0.196T^{-0.893}$
1.0	0.9	4.5	$\theta_1 = 2.05T^{0.280}$	$\theta_{TOP} = 0.201T^{-0.931}$

Table 4: Story mass, lateral stiffness for typical and ground floors for a 6-story frame in Taichung

	Regular	R_{soft} =0.8	R_{weak} =0.8	R_{soft} =0.8, R_{weak} =0.8
(ton)	17.68	15.67	17.68	15.67
EI(kN-m^2)	121275	121275	121275	121275
$(EI)_1$(kN-m^2)	121275	97020	121275	97020

Table 5: Maximum roof and ground floor displacements, and first story drifts for a 6-story frame having various R_{soft} values (TCU095)

	Regular	R_{soft}=0.8	R_{weak}=0.8	R_{soft} =0.8, R_{weak} =0.8
u_{roof}(cm)	24.551	24.871	22.831	23.235
u_1(cm)	20.627	21.122	19.776	20.368
θ_1 (rad.)	0.0331	0.0372	0.0361	0.0397

Table 6: Generalized shape function, modified participation factor, spectral first story drift and error for a system having a fundamental period of 0.637 second and with various R_{soft} values (TCU095)

	Regular		R_{soft}=0.8		R_{weak}=0.8		R_{soft} =0.8, R_{weak} =0.8	
Γ_1	1.226		1.208		1.212		1.192	
	ϕ_{i1}	$\Gamma_1 S_d \phi_{i1}$	ϕ_{i1}	$\Gamma_1 S_d \phi_{i1}$	ϕ_{i1}	$\Gamma_1 S_d \phi_{i1}$	ϕ_{i1}	$\Gamma_1 S_d \phi_{i1}$
6F	1.000	39.135	1.000	38.563	1.000	38.698	1.000	38.062
5F	0.953	37.277	0.957	36.905	0.956	37.007	0.961	36.566
4F	0.864	33.809	0.877	33.823	0.874	33.830	0.888	33.799
3F	0.740	28.956	0.766	29.551	0.760	29.426	0.787	29.951
2F	0.588	23.004	0.630	24.306	0.620	23.993	0.663	25.239
1F	0.415	16.237	0.476	18.340	0.461	17.847	0.523	19.902
θ_1(rad.)		0.0406		0.0459		0.0446		0.0498
Error of θ_1		22.66%		23.25%		23.71%		25.33%

A STUDY OF THE ACCURACY OF THE CAPACITY SPECTRUM METHOD IN ENGINEERING ANALYSIS

W. D. IWAN and A. C. GUYADER[1]

ABSTRACT

This paper describes an ongoing investigation of possible approaches to improving the accuracy of the Capacity Spectrum Method (CSM) as employed in Performance Based Engineering design and analysis of structures subjected to strong earthquake ground motions. The paper discusses the response prediction errors associated with the conventional CSM approach and an alternate approach based more directly on theories of equivalent linearization. A methodology is outlined for determining a set of optimal effective linear period and damping parameters for use in the CSM approach. Example results are given to illustrate the basic concepts presented. The results suggest that improvements can be made in the conventional CSM approach.

1. BACKGROUND AND MOTIVATION

The Capacity Spectrum Method (CSM) is appealing for Performance Based Engineering design and analysis because it is based on the intuitive idea that earthquake ground motion places a certain "Demand" on a structure while the structure itself has a certain "Capacity" to absorb this demand. Therefore, it is reasoned, when the Demand exceeds the assumed Capacity, the response must be increased to achieve a balance, and when the assumed Capacity exceeds the Demand, the response of the structure must be decreased to achieve a balance. When the Demand is equal to the Capacity, the system can be thought of as being in a state of dynamic equilibrium that corresponds to the actual response or "Performance" of the structure under the applied ground motion.

As currently set forth in ATC-40, the conventional CSM approach consists of the following steps and assumptions:

1. Assume an initial response ductility, μ, for the structure.
2. Based on this value of μ, calculate an effective viscous damping, β_{eff}, using an empirical formula that has been provided.

---

[1] *Earthquake Engineering Research Laboratory, California Institute of Technology, Pasadena, California 91125, USA*

3. Using β_{eff}, and possibly a set of rules for spectral reduction as a function of β_{eff}, determine an approximate nonlinear Acceleration Displacement Response Spectrum (ADRS). It is assumed that this spectrum gives the Demand of the ground motion.
4. Use a static pushover analysis to obtain a representation (surrogate) of the structural Capacity of the structure.
5. Determine the intersection of the Capacity and Demand curves. This point corresponds to an effective linear stiffness that is the secant stiffness of the structural capacity.
6. If the intersection point on the Capacity curve corresponds to the assumed value of ductility, the "Performance Point" has been determined and the procedure is complete. If not, the process is iterated by assuming different values of ductility until the Demand and Capacity are equal for a particular value of ductility.

There are clearly a number of issues associated with implementation of the conventional CSM approach that could benefit from further study. These include:

1. An obvious potential weakness of the current approach lies in the fact that it is well known from theories of equivalent linearization that the secant stiffness provides only a lower bound on the effective linear stiffness of an inelastic system and is usually not a very good measure of the most favorable effective stiffness.
2. The effective linear system parameters that are obtained from linearization methods are generally inter-dependent, so adoption of any effective linear period will affect the most favorable value of the effective linear damping and vice versa.
3. There is questionable theoretical and numerical basis for adoption of the current formulas for β_{eff} when using the secant stiffness. Therefore, there is a valid concern whether the conventional combination of effective linear parameters is most favorable.
4. Further investigation is needed into the adequacy of using the static pushover relationship as a surrogate for structural capacity of MDOF structures.

2. PURPOSE AND METHODOLOGY OF THE PRESENT INVESTIGATION

The purpose of the present investigation is to determine whether it is possible to achieve any significant improvement in the results of the CSM approach by applying concepts from the theory of equivalent linearization in a more consistent manner.

The methodology that is being employed is as follows:

1. Determine the response amplitude error for the current CSM approach for SDOF systems using real earthquakes and the specified effective linear damping value without employing any spectral reduction rules. This will eliminate any possible sources of error in the spectral reduction rules that are employed for smoothed design spectra.
2. Determine the response amplitude error using an equivalent linearization technique that employs *both* an effective linear damping *and* stiffness (not the secant stiffness as assumed in the current CSM approach).
3. Compare the results from steps one and two as a guide for further work.
4. Numerically determine a set of "optimal" effective linear viscous damping and period that are functions of ductility over a range of different types of earthquakes.
5. Derive empirical relations for these optimal linear viscous damping and period parameters as a function of ductility and type of earthquake.
6. Verify any new empirical relations by determining the response amplitude error for SDOF systems and comparing these results to those for the current CSM approach.
7. Extend the optimal approach to MDOF structures.

3. SOME PRELIMINARY RESULTS

Figure 1 shows the general concepts of the CSM. A family of linear (viscous damped) Response Spectra are shown in ADRS format. These curves represent different Demand curves for the specific earthquake in question. For the conventional CSM approach, the effective linear stiffness of the inelastic system is the secant stiffness, and the value of effective damping is a function of ductility. Each of the demand curves is therefore associated with a corresponding value of ductility. Also shown is a bilinear Capacity curve (the backbone curve of the bilinear hysteretic restoring force diagram) For an assumed ductility, the Demand curve will intersect the Capacity curve at some point and this gives a tentative Performance Point. However, this point will not, in general, correspond to the assumed value of ductility on the Capacity curve. The process is therefore iterated until the assumed ductility is equal to the ductility given by the Capacity curve of the system. In light of the above, a logical measure of the error in the approximate linear procedure will be the percentage difference between the predicted Performance Point ductility and the true ductility obtained from an inelastic time history analysis. This error will be referred to as the Performance Point Error.

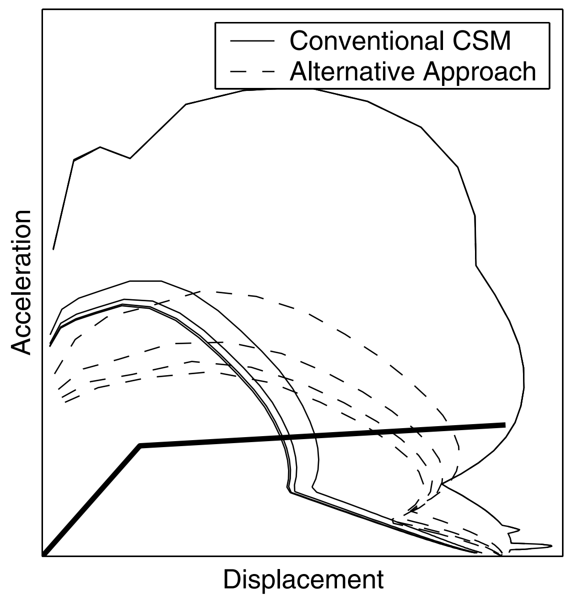

Figure 1. General Concepts of the CSM

In order to examine the effects of using an alternative set of linear parameters in place of those specified by the conventional ATC-40 CSM approach, the equivalent linear parameters determined in an earlier study by one of the authors will be used (Iwan, 1980). These parameters are based on a best fit of the inelastic Pseudo-Velocity Response Spectrum using a linear Response Spectrum that is shifted in frequency and damping value. The effective period and damping for this alternative approach can be expressed as:

$$T_{eff} / T_0 = 1 + 0.121(\mu - 1)^{0.939} \tag{1}$$

$$\zeta_{eff} - \zeta_0 = 5.87(\mu - 1)^{0.371} \tag{2}$$

where ζ_0 is the nominal linear viscous damping in the system and T_0 is the small amplitude linear period (that is, the damping and period when $\mu = 1$). A family of Demand curves for the alternative approach is also shown in Figure 1. It is seen that these Demand curves are no longer merely a reduction of the original linear spectrum along essentially radial lines, but that the period axes have also been noticeably rotated. This effective rotation is the result of projecting the peak displacement of the equivalent linear system onto the secant stiffness line.

Figure 2 shows the effective linear period and damping as a function of ductility for both the conventional and alternative approaches. For all cases considered, ζ_0=5% and the second slope ratio is 5%. It is clear that the two approaches give quite different values for effective linear parameters. In general, the conventional CSM provides estimates of the period and damping that are substantially greater than those provided by the alternative approach. The differences can be of the order of 100%. It is not surprising therefore that the two approaches should produce significantly different predictions for the Performance Point.

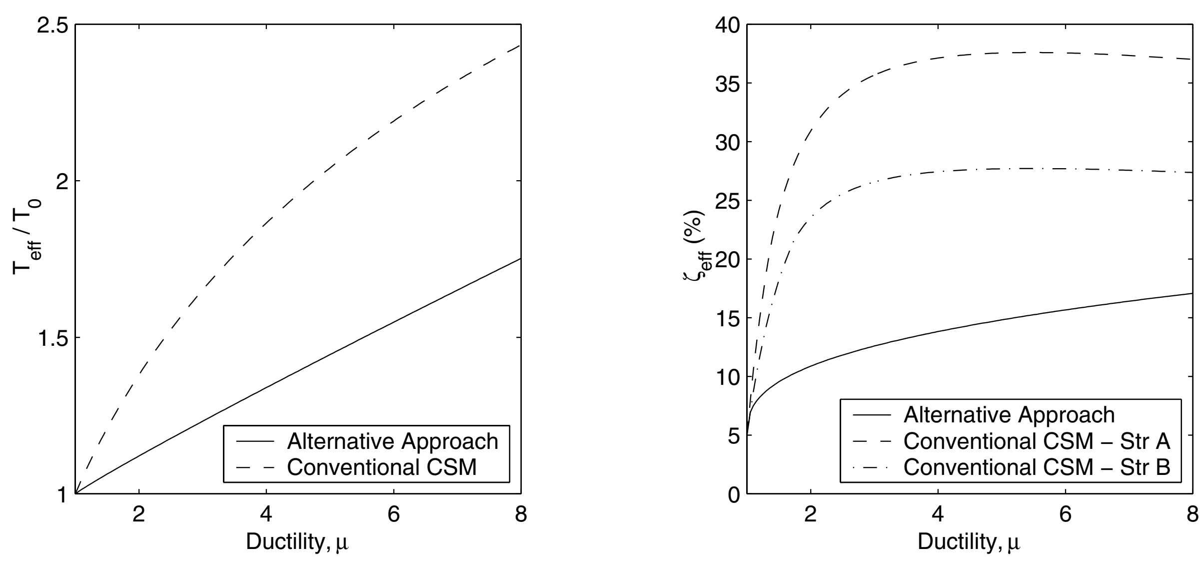

Figure 2. Effective Linear Parameters

Table I gives statistical results for the Performance Point Error both the conventional CSM approach and the alternative approach. The four (4) so-called "near field" earthquake ground motions considered are the maximum velocity direction components from Rinaldi Receiving Station, Sylmar County Hospital, Takatori Station, and JMA Kobe Station. The seven (7) "far field" earthquake ground motions considered are the maximum peak-to-peak velocity components from El Centro, Taft, Vernon, Pacoima Dam, Caltech Athenaeum, Palmdale Fire Station, and 15250 Ventura Blvd. Thirteen (13) initial linear periods are considered ranging in value from T_0 =0.3 sec to T_0 =3.9 sec in increments of 0.3 sec Twenty-one (21) ductilities are considered ranging in value from μ =1.4 to μ =7.4 in increments of 0.3. For the conventional CSM approach, Type A structural parameters are used for near field ground motions and Type B parameters are used for far field motions.

Table 1: Performance Point Error

Earthquake	Initial period, T_0 (sec)	Ductility, μ	Performance Point Error Mean (Std. Dev.), %	
			Conventional CSM Approach	Alternative Approach
All (11)	All (13)	All (21)	-5.8 (38.5)	3.6 (25.7)
Near Field (4)	All (13)	All (21)	-7.8 (33.0)	3.4 (22.7)
Far Field (7)	All (13)	All (21)	-4.7 (41.4)	3.7 (27.3)
All (11)	0.3	All (21)	39.5 (75.7)	-7.2 (29.2)
All (11)	1.5	All (21)	-5.4 (28.9)	11.7 (24.7)
All (11)	2.7	All (21)	-16.1 (12.5)	2.1 (20.4)
All (11)	3.9	All (21)	-11.9 (26.5)	2.9 (26.9)
All (11)	All (13)	2.0	-15.6 (30.5)	-1.4 (19.8)
All (11)	All (13)	3.5	-9.0 (32.7)	6.3 (27.7)
All (11)	All (13)	5.0	-2.8 (42.0)	5.0 (27.5)
All (11)	All (13)	6.5	2.1 (44.5)	6.8 (29.8)
Near Field (4)	0.3	All (21)	39.1 (63.4)	-26.2 (17.3)
Near Field (4)	1.5	All (21)	-12.8 (14.8)	16.3 (22.7)
Near Field (4)	2.7	All (21)	-15.9 (9.2)	5.2 (18.4)
Near Field (4)	3.9	All (21)	-18.0 (11.2)	-7.1 (13.3)
Near Field (4)	All (13)	2.0	-14.1 (30.8)	0.3 (19.8)
Near Field (4)	All (13)	3.5	-5.8 (36.7)	8.2 (24.0)
Near Field (4)	All (13)	5.0	-6.3 (33.7)	5.1 (24.5)
Near Field (4)	All (13)	6.5	-5.9 (31.8)	2.1 (23.8)
Far Field (7)	0.3	All (21)	39.8 (82.2)	3.7 (29.0)
Far Field (7)	1.5	All (21)	-1.1 (33.8)	9.1 (25.4)
Far Field (7)	2.7	All (21)	-16.2 (14.0)	0.3 (21.3)
Far Field (7)	3.9	All (21)	-8.4 (31.7)	8.6 (30.9)
Far Field (7)	All (13)	2.0	-16.4 (30.5)	2.3 (19.8)
Far Field (7)	All (13)	3.5	-10.8 (30.2)	5.3 (29.6)
Far Field (7)	All (13)	5.0	-0.8 (46.1)	4.9 (29.1)
Far Field (7)	All (13)	6.5	6.6 (50.0)	9.5 (32.6)

+ error is conservative, - error is non-conservative

Figure 3 shows the overall distribution of the Performance Point Error for the near and far field cases respectively. Figure 4 shows the distribution of the Performance Point Error for the near field ground motions for two specific periods, while Figure 5 shows the corresponding result for the far field ground motions.

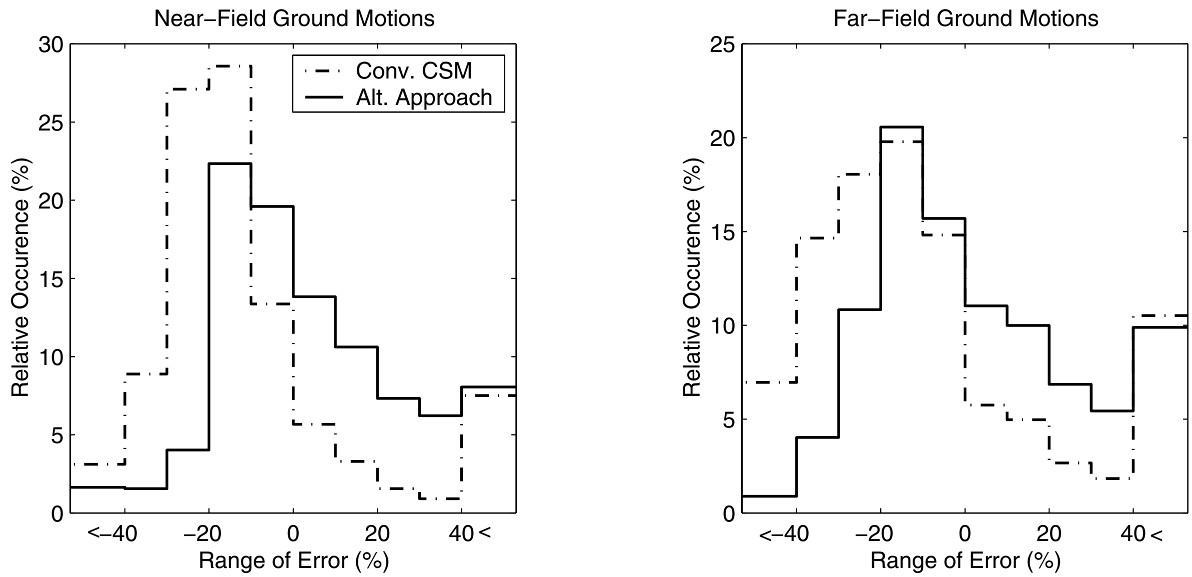

Figure 3. Distribution of Performance Point Error for Near Field and Far Field Ground motions

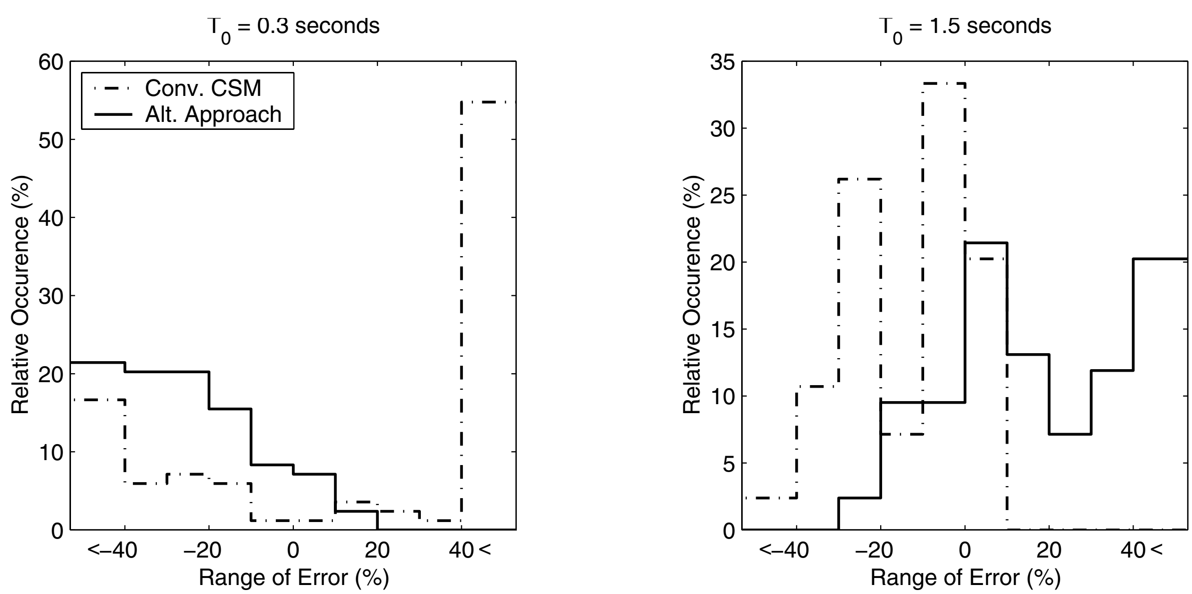

Figure 4. Distribution of Performance Point Error for Near Field Ground Motions.

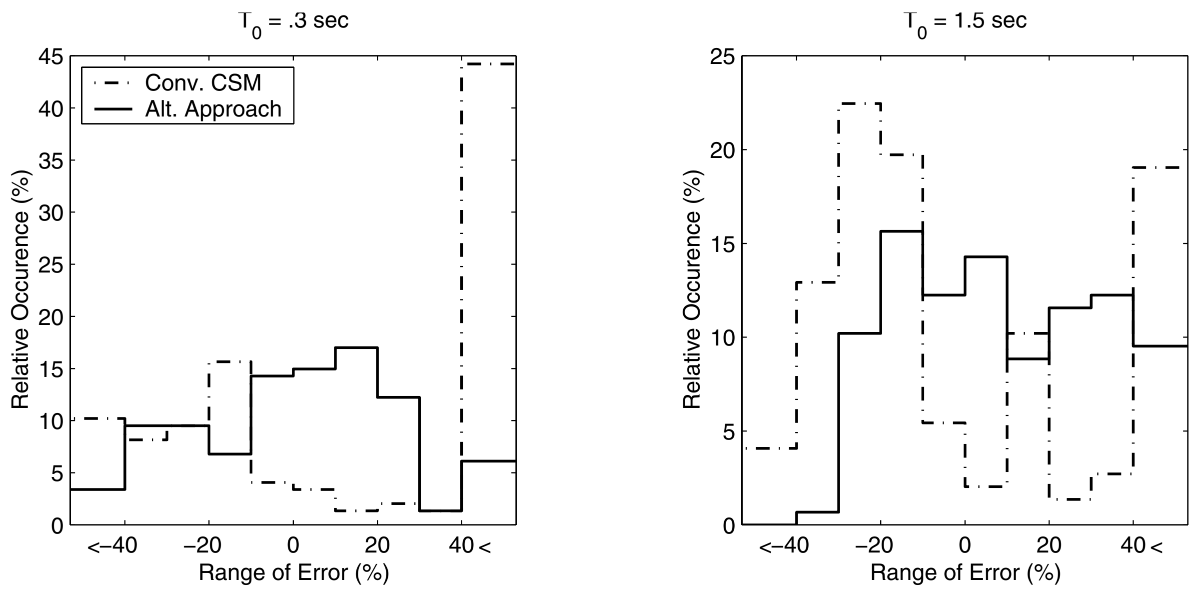

Figure 5. Distribution of Performance Point Error for Far Field Ground Motions.

It is noted from the table and figures that both of the approaches considered give mean response errors that are generally fairly small. For all cases considered, the magnitude of the mean error for the conventional CSM approach is only 5.8% while that for the alternative approach is noticeably less at 3.6%. It is observed that in the mean, the conventional CSM approach is generally somewhat non-conservative (it under predicts the response) while the alternative approach is somewhat conservative (it over predicts the response). In most cases, the variance of the response prediction, as indicated by the standard deviation, significantly exceeds the mean value of the prediction. For all cases considered, the standard deviation of the error for the conventional CSM approach is 38.5% while that for the alternative approach is considerably less at 25.7%.

The results presented above provide a useful indication of the errors associated with the use of different effective linear parameters in the CSM. However, another form of analysis can be more useful in identifying optimal values of the effective linear period and damping. Let the error in the response amplitude, D, for a *given* set of effective period, T_{eff}, and damping, ζ_{eff}, be defined as follows:

$$\varepsilon_D = D_{linear}(T_{eff}, \zeta_{eff}) / D_{inelastic}(T_0, \zeta_0, \mu) - 1 \tag{3}$$

The optimal effective linear parameters will be taken as those parameters that minimize, in some sense, the error, ε_D.

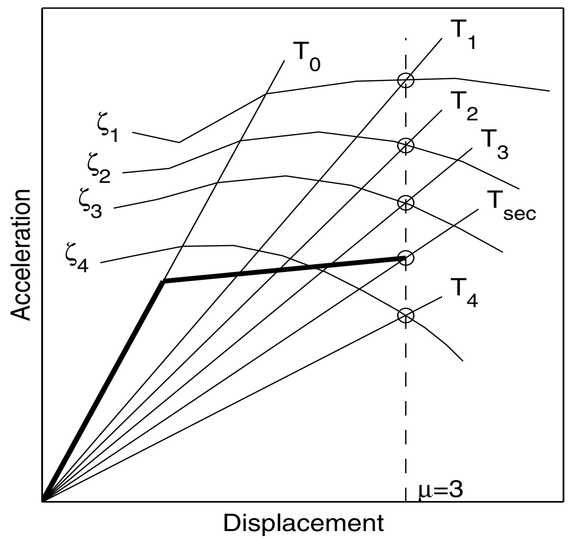

Figure 6. Different Effective Linear System Parameters Producing the Same Response Ductility

Figure 6 shows a family of linear ADRS spectra associated with different values of effective viscous damping. It is noted that there are no unique optimal values for effective period and damping for a particular earthquake, initial period, and ductility using the error definition of Equation (3). In fact, it will be seen that there is a continuous range of combinations of effective period and damping (infinite in number) for which the equivalent linear system response precisely matches that of the inelastic system. There will likewise be a continuous combination of effective linear parameters that minimize the average of the response error over any set of earthquake ground motions, periods, or ductilities. Thus, any optimal effective parameters must be determined by minimizing some measure of the absolute value of the error (Iwan and Gates, 1979).

Figure 7 shows contours of the average error and the average absolute value error for the case of μ = 3.5 for all periods and the set of near field earthquake ground motions. Figure 8 shows similar contours for the set of far field ground motions. Also indicated on each figure are the effective linear period and damping values provided by the conventional and alternative CSM approaches.

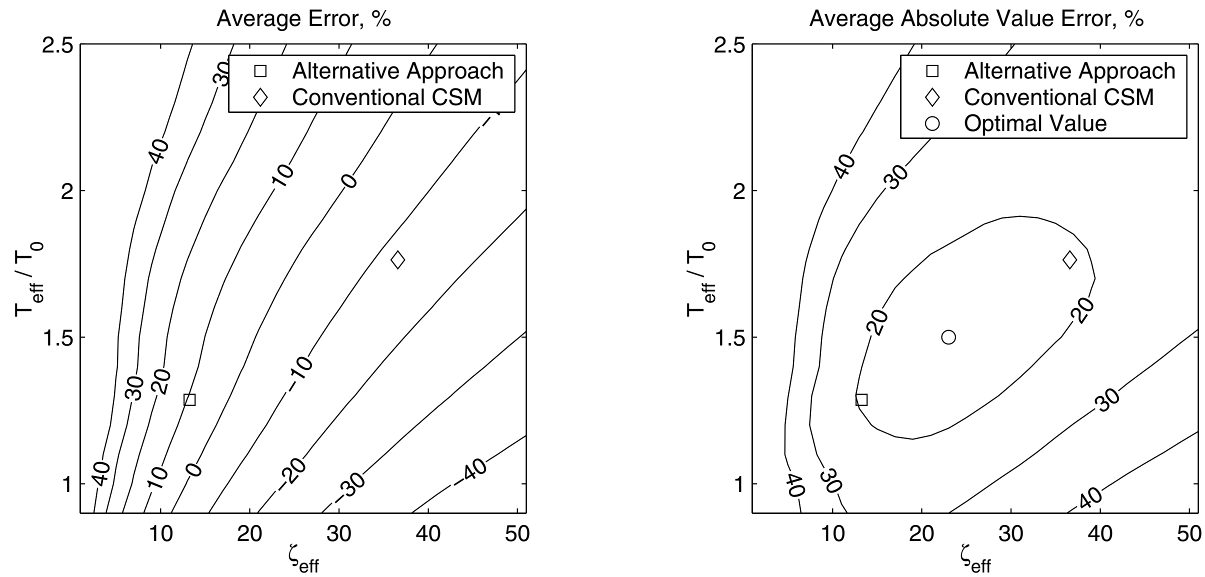

Figure 7. Contours of Response Error Averaged over All Periods – Near Field Ground Motions

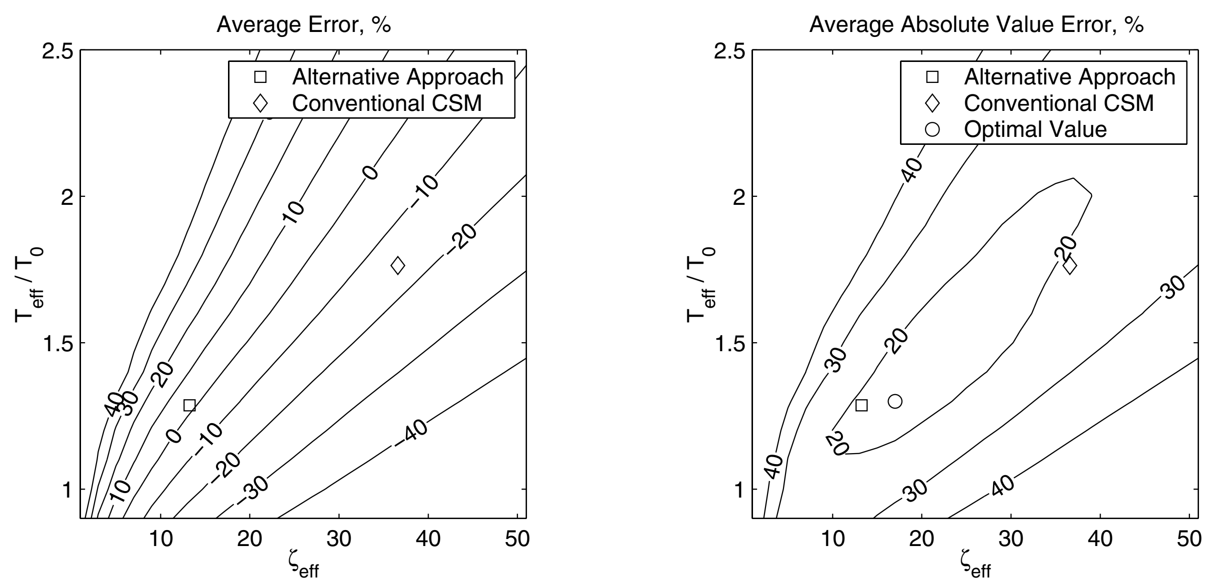

Figure 8. Contours of Response Error Averaged over All Periods – Far Field Ground Motions

It is observed that the average error yields a contour map with a range of parameters for which the error is identically zero. Both the conventional and alternative approaches yield effective linear parameters that are very close to this zero error contour. This helps to explain why both approaches produce quite modest average errors in Table 1. However, it is seen that there is a unique set of parameters that minimizes the absolute value response error. For the example cases shown, the alternative approach produces effective parameters that are much closer to this optimal set of parameters. This explains the significantly improved error variance that is obtained by using the alternative approach parameters.

It is also clear from Figures 7 and 8 that a major shortcoming of the conventional CSM approach is indeed the use of the secant period. In the cases shown here and others not shown, the conventional CSM approach consistently provides an effective period that is larger than the optimal value. This is not at all surprising in light of the results of various well-accepted equivalent linearization techniques.

It is further observed that the optimal effective linear parameters change depending on whether near field or far field ground motions are used as a basis for the analysis. This implies that a different set of optimal parameters will most likely be needed for different types of ground motion.

From the preliminary results shown here, it appears that an alternative representation for the equivalent linear period and damping parameters in a CSM analysis could result in a marked improvement in the accuracy of response results. This is true not only for the mean value of the error, but also for the variance of the error. This in turn could lead to substantial improvements in statistically based performance analysis of structural response.

4. PRELIMINARY CONCLUSIONS

Based on the results reported herein, it is concluded that it is possible to significantly improve the accuracy of the Capacity Spectrum Method by employing more appropriately selected effective linear damping and period parameters. By reducing both the mean and variance of the response error, substantial improvements can be achieved in the statistical analysis of structural performance as employed in current Performance Based Engineering analyses. The present investigation is directed toward this end. This paper has outlined a methodology for determining an optimal set of effective linear parameters for use in the CSM procedure. Further results will be presented at a future date.

5. ACKNOWLEDGEMENT

This investigation has been supported in part by a grant from the National Science Foundation. The authors gratefully acknowledge this assistance.

6. REFERENCES

Applied Technology Council (1996). Seismic evaluation and retrofit of concrete buildings. Volume 1. Report No. ATC-40.

Iwan, W. D. (1980). Estimating Inelastic response spectra from elastic spectra. *Intl. J. Earthq. Engng. and Struc. Dyn.*, 8:375-388.

Iwan, W. D. and N. C. Gates (1978). The effective period and damping of a class of hysteretic structures. *Intl. J. Earthq. Engng and Struc. Dyn.*, 7:199-211.

7. KEYWORDS

Capacity, Capacity Spectrum Method, Demand, Effective Damping, Effective Period, Equivalent Linearization, Inelastic Response, Performance Based Engineering, Performance Point, Response Error.

SESSION A-3: SEISMIC PERFORMANCE EVALUATION

Chaired by

♦ Mark Aschheim and Kangning Li ♦

PROBABILISTIC ESTIMATION OF BUILDING RESPONSE FOR PERFORMANCE BASED ENGINEERING

Eduardo MIRANDA[1], Hesameddin ASLANI[2] and Brian K. BAER[2]

ABSTRACT

An investigation of the effects of modeling assumptions on the estimation of the seismic response of reinforced concrete buildings subjected to earthquake ground motions is presented. The effects of changes in strength and stiffness are studied through three models of a seven-story moment resisting frame building using a probabilistic framework. For each model different assumptions of the strength and stiffness of structural elements that are commonly used have been adopted. The resulting models have different lateral strengths but particularly significantly different lateral stiffnesses. Effects of modeling assumptions on the probability distribution of various response parameters conditioned to the ground motion intensity and on the annual rate of exceedance of various response parameters are evaluated. Preliminary results suggest that, in the absence of stiffness and strength deterioration, relatively large changes in strength and stiffness lead only to moderate changes in the conditional probability of different response parameters at various levels of ground motion intensity. However, since the ground motion hazard intensity on the building is a function of the lateral strength and stiffness of the structure, then the annual rate of exceedance of specific response parameters can exhibit significant variations with changes in modeling assumptions that, in general, cannot be ignored.

1. INTRODUCTION

The main objective in Performance Based Design is to be able to design, build and maintain structures capable of providing predictable performance. One of the most important elements in performance prediction is the estimation of the structural response. Assessment of the seismic response of a specific building usually involves two steps. In a first step future earthquake ground motions that can occur at the site are estimated through a seismic hazard analysis and in a second step the structural response is estimated through a structural analysis using the ground motions that were estimated in the first step. Many simplifications are usually introduced in both steps. Simplifications in the structural analysis include but are not limited to: simplifications in modeling the mechanical characteristics of the structural elements and their connections, simplifications in not considering all elements present in the buildings but only those that a priori are judge to contribute in resisting lateral forces, simplifications by assuming small deformations, simplifications on the way soil-structure interaction effects are considered, etc. In the case of reinforced concrete building additional uncertainties are introduced in modeling the

[1] *Asst. Prof., Dept. of Civil and Envir. Engrg., Stanford University, Email: miranda@ce.stanford.edu*
[2] *Graduate Student, Dept. of Civil and Envir. Engrg., Stanford University, Email haslani@ce.stanford.edu*

structure due to cracking, bar slippage due to bond deterioration, not fully understood behavior of connections between members, slab contribution, etc.

Various studies have shown that changes in structural modeling assumptions can cause important variations in the computed response of reinforced concrete buildings when subjected to earthquake ground motions (Islam, 1996; Li and Jirsa 1998; Browning, et al., 2000). However, most of these studies have been aimed at trying to reproduce the recorded response of instrumented structures that have considered the seismic excitation and seismic response as deterministic. It is well known that the largest source of uncertainty in the estimation of the performance of existing buildings is on the estimation of the characteristics of future earthquake ground motions at the site. So it is particularly important to consider this uncertainty. It has been suggested that a more rational approach is to consider a probabilistic framework (Bazzuro and Cornell, 1994; Shome and Cornell, 1999). However, these analysis procedures have not considered modeling uncertainty and have only computed the probabilistic response of a given structural model. In particular, it is important to put into perspective the dispersion in the computed response introduced by modeling uncertainty with respect to that produce by the record-to-record variability of structural response for a given ground motion intensity and for a given model, and to that produced by the uncertainty in the ground motion intensity.

The objective of this study is to study the effects of changes in modeling assumptions on the probabilistic response of reinforced concrete buildings. First the influence of changes of modeling assumptions on the overall strength and stiffness of the model are evaluated. Then the effect of modeling assumptions on the conditional probability of the structural structure for a given ground motion intensity is investigated. Finally the influence of modeling assumptions on the rate of exceedance of structural response is assessed.

2. BUILDING AND GOUND MOTIONS CONSIDERED IN THIS STUDY

The test bed building used in this research is seven-story reinforced concrete building. Figure 1 shows the plan and elevation of the building (Browning, et al., 2000). The structural system consists of a moment-resisting perimeter frame with flat slabs in the interior.

The building was subjected to a set of 80 ground motions recorded in California earthquakes with magnitudes between 5.8 and 6.9 and at epicentral distances varying from 13 km to 60 km (8 and 37.5 miles). All the ground motions were recorded at accelerographic stations whose soil

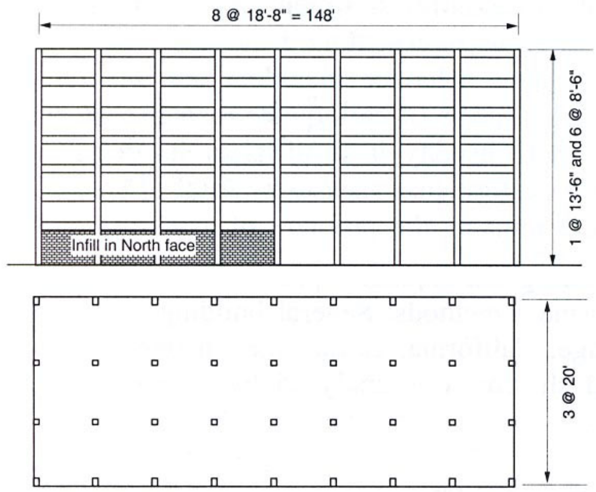

Figure 1. Plan and Elevation of the case study building (Browning et al. 2000).

conditions can be classified as site class D according to NEHRP seismic provisions. All ground motions were processed using the same processing techniques and were carefully selected from Pacific Earthquake Engineering Research (PEER) Center ground motion database (http://peer.berkeley.edu/smcat/) (Medina and Krawinkler, 2001).

3. MODELING UNCERTAINTY

There are many uncertainties in the modeling of reinforced concrete structures when subjected to earthquake ground motions. One major source of uncertainty is related to the uncertainty on the estimation of the stiffness of the elements due to the contribution of the steel reinforcement which tends to increase the stiffness of the element and cracking which reduces the stiffness.

Table 1 lists commonly used assumptions for modeling the stiffness of reinforced concrete elements. In addition to the effective stiffness of the members other sources of uncertainty are the effective width of slab contributing to the stiffness of the beams, contribution of interior frames to the response of the structure, loss of stiffness due to connection flexibility, etc. Here three models of the longitudinal direction of the building were considered. One is based on modeling recommendations included in ACI-318 (ACI model), another following using element strength and stiffness computed from detailed moment curvature relations (MCB Model) and another neglecting slab contribution and using center-line dimensions (FLX model).

Table 1. Recommended ratios for effective moments of inertia of reinforced concrete elements as a fraction of gross moment of inertia.

Reference	Beams	Columns
ACI 318	0.25 - 0.35	0.7
ATC 40	0.5	0.7
FEMA 273	0.5	0.5 - 0.7
Paulay & Priestley	0.4	0.4 - 0.8
Moehle et al.	0.5	1.0

As shown in Table 2 and Figures 2 and 3 changes in modeling assumptions produce very important changes in beam-to-column stiffness ratios and in lateral stiffness. For example, the beam-to-column stiffness ratio of the MCB model is almost twice of that of the ACI model and the lateral stiffness of the ACI model is 50% larger than that of the FLX model. Similarly the strength of some beams in the MCB model is three times those in the FLX model. However, changes in mode shapes, modal participation factors and period ratios are very small. This implies that when the response of the structure is linear elastic, for a given ground motion differences in response from these models are primarily a function of differences in the fundamental period. Modeling assumptions can also have a big influence of the lateral response of the model. As shown in figure 3, the lateral yielding strength of the MCB model is almost twice of the FLX model.

Table 2. Variation of system parameters with changes in modeling assumptions.

Type of Parameter	Parameter	ACI Model	MCB Model	FLX Model
Beam-to-Column Stiffness Ratio	ρ	0.41	0.79	0.5
Period of Vibration	T_1 [s]	1.39	1.59	1.70
	T_2 [s]	0.46	0.54	0.56
	T_3 [s]	0.26	0.32	0.33
Period Ratio	T_1/T_2	3.02	2.94	3.04
	T_1/T_3	5.33	4.97	5.15
Modal Participation Factor	Γ_1	1.29	1.30	1.28
	Γ_2	0.44	0.45	0.43
	Γ_3	0.22	0.22	0.22

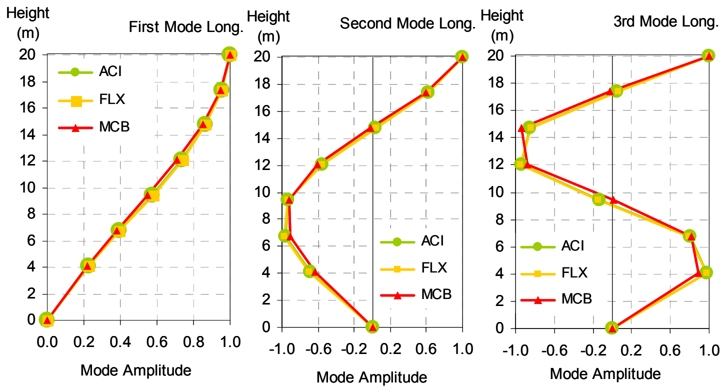

Figure 2: Variation of mode shapes with changes in modeling assumptions

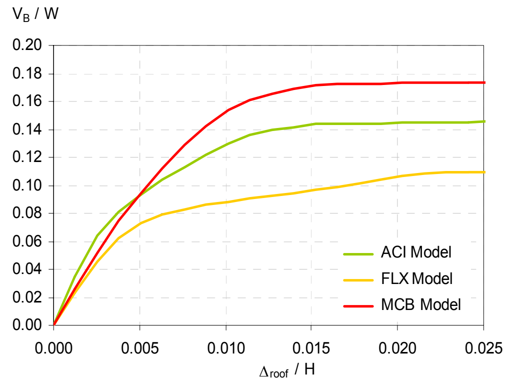

Figure 3: Variation of pushover curves with changes in modeling assumptions

3. PROBABILISTIC SEISMIC RESPONSE ANALYSIS

For a given earthquake ground motion intensity a considerable variability of structural response exist from one ground motion to another. In this study all ground motions are scaled such that they have the same linear spectral ordinate at the fundamental period of the structure. Figure 4 shows the probability distribution of the maximum interstory drift ratio (IDR) in the first story of the building conditioned to a ground motion intensity S_d=30cm (11.8 in). Also shown in this figure is a lognormal probability distribution which the same median and dispersion as the observed data. It can be seen that the probability distribution of the maximum interstory drift ratio closely follows that of the lognormal distribution.

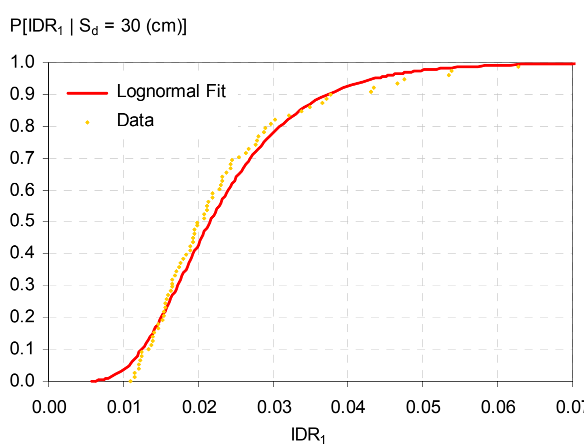

Figure 4. Verification of lognormal distribution of response, at a given level of intensity.

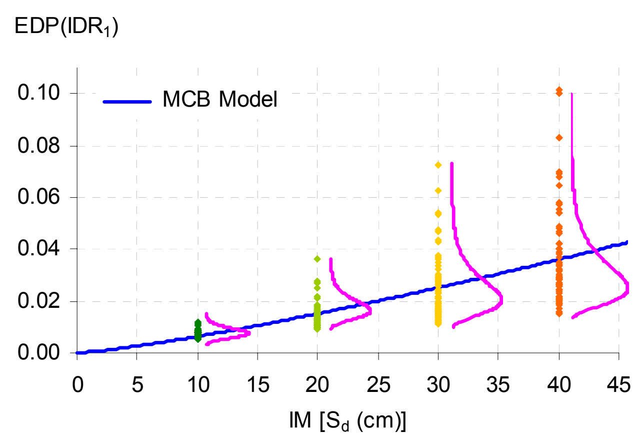

Figure 5. Response probability density function of building response at different intensity levels.

Figure 5 shows the variation of the median interstory drift ratio at the first story of the MCB model with increasing level of intensity of the ground motion. The median is one of two parameters required to compute the probability density function of the structural response. Also shown in the figure is the probability density function at four increasing levels of intensity. Nonlinear time history analyses provide information at specific levels of intensity. However, functions that describe the continuous variation of the parameters of the lognormal probability distribution as a function of the level of ground motion intensity are needed in a probabilistic response analysis. In this study both the median and dispersion have approximated by the following second-degree polynomial function:

$$\mu_{LnX} = a + b(S_d) + c(S_d)^2 \tag{1}$$

It can be seen that, as expected, the median response increases as the ground motion intensity increases (Fig. 6). In particular, up to about 20 cm (7.9 in) there is almost no difference in median response with changes in the modeling assumptions. However, differences increase as the ground motion intensity increases. Furthermore, it can also be observed that, in general, the dispersion of the response increase as the intensity of the ground motion increases, with differences in dispersion from one model to another that are not very large.

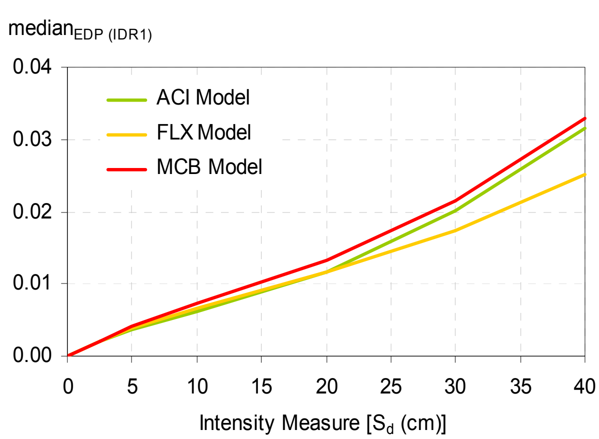

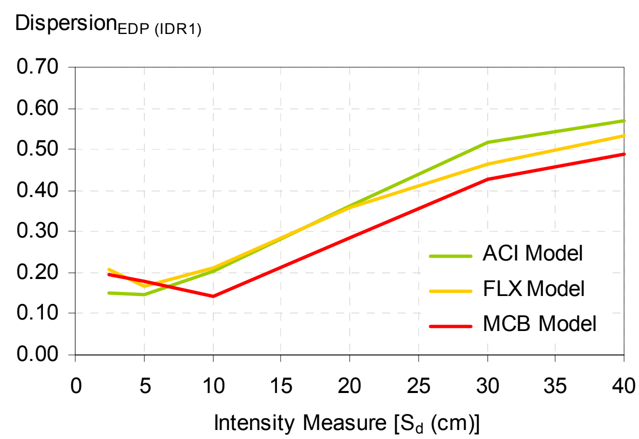

Figure 6. Variation of median and dispersion of structural response median with the changes in modeling assumptions at different levels of intensity.

Figure 7 shows changes in median interstory drift ratios in all story levels for three levels of intensity. It can be seen that models ACI and FLX, that neglect practically neglect the slab contribution have almost the same beam-to-column stiffness ratio and exhibit very similar median response. However, the MCB model that has a higher beam-to-column stiffness ratio and higher lateral strength produce a larger difference in response. Figure 8 shows differences in modeling assumptions on the conditional probability of interstory drift ratio at the first story conditioned to a given level of spectral ordinate. It can be seen that for this story and this level of intensity the differences are not very large. The FLX model shows higher probability of exceeding different levels of interstory drift than those computed by the ACI and MCB models. However, differences produced by changes in modeling assumptions are significantly smaller than changes produced by the record-to-record variability of structural response for a given level of ground motion intensity. For example, for this level of intensity the interstory drift ratio can vary from about 1% to about 6% which is a ratio of six, while the differences from one model to another are significantly smaller.

The annual rate of exceedance of a given structural response parameter (SRP) can be computed by integrating the conditional probabilities given a certain level of intensity over all ground motion intensity levels (IM). This can be computed using the total probability theorem as follows:

$$P(SRP > edp) = \int P(SRP \mid IM)\, \nu(IM)\, dIM \tag{2}$$

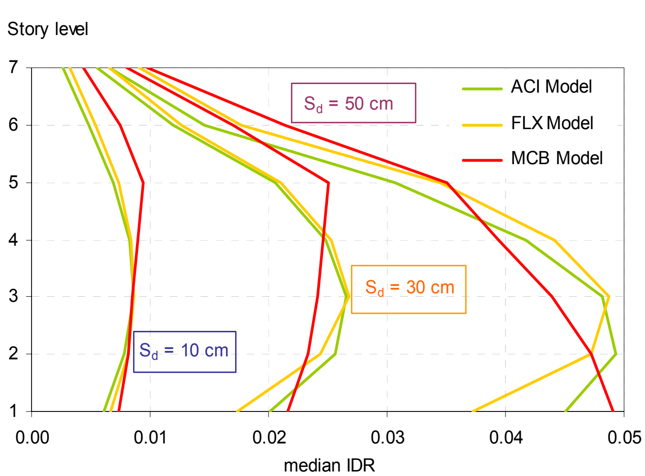

Figure 7. Comparison of the changes of median interstory drift ratio along the building height for different models at three different levels of intensity.

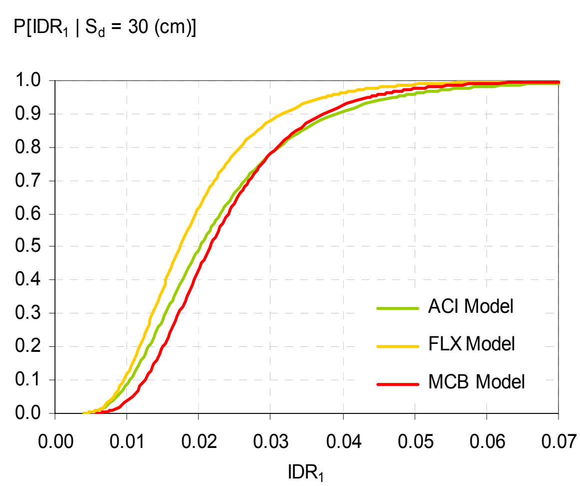

Figure 8: Changes in P(IDR| Sd) with changes in modeling assumptions.

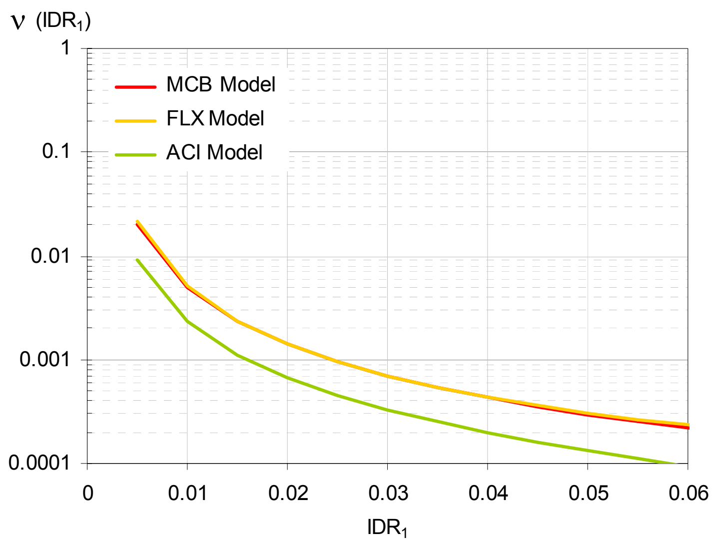

Figure 9: Changes in annual rates of exceedance of interstory drift ratios with changes in modeling assumptions.

where P(SRP|IM) is the conditional probability of exceeding a structural response parameter given a ground motion intensity IM, and ν(IM) is the annual rate of occurrence of the ground motion intensity parameter. In this investigation equation (2) is solved numerically.

Figure 9 show changes in annual rates of occurrence of various levels of interstory drift ratio at the first story of the building with changes in the modeling assumptions. It can be seen that FLX and MCB models yield practically the same probability. This is produce by observing that higher conditional probabilities of interstory drift ratios at first story shown in figure 7 are approximately compensated by lower median ground motion intensity demands for the MCB model which has smaller period of vibration. The ACI model, which is the most rigid model, leads to lower probabilities of exceedance. The response of this model is on average about 35% smaller than that of the other model.

4. CONCLUSIONS

The effect of modeling uncertainty in probabilistic seismic response analyses has been investigated in this study. Results have shown that changes in modeling assumptions can produce very large changes in strength and stiffness of the model. In particular, changes of a factor of three in the flexural capacities of some beams were computed while changes of 100% were computed on the lateral strength of the structure. However, the changes in interstory drift ratios are smaller than one would expect. In particular, the changes are smaller than those produced in the lateral stiffness and lateral strength of the building.

Both median response and dispersion tend to increase as the intensity of the ground motions increases. The variation in dispersion with changes in intensity level are very large suggesting that it is inadequate to assume that the dispersion remains constant.

In the case of linear elastic response, it has been shown that mode shapes, modal participation factors and period ratios are not significantly influenced by changes in modeling assumptions studied here. Suggesting that, for a given ground motion, differences in structural response of different models will be primarily a function of changes in the fundamental period. This very important observation means that when the response is linear, modeling uncertainty can be approximately taken into account by only considering the uncertainty in the estimation of the fundamental period of vibration of the building when computing seismic hazard curves.

For nonlinear response changes in modeling assumptions lead to changes in structural response that are larger than those on observed for linear response. However, the variations in median response are significantly smaller than the record-to-record variability of structural response for a given ground motion intensity. Changes in modeling assumptions can change median response but also the distribution of interstory drift s along the height of the structure.

5. ACKNOWLEDGEMENTS

This work was supported by the Pacific Earthquake Engineering Research (PEER) Center with support from the Earthquake Engineering Research Centers Program of the National Science Foundation under Award Number EEC-9701568. This financial support to the authors is gratefully acknowledged.

6. REFERENCES

Bazzuro P. and Cornell C. A. (1994). Seismic hazard analysis for non-linear structures. I: Methodology. *ASCE Journal of Structural Engineering*, 120(11): 3320-3344,1994.

Browning J., Li R.Y., Lynn Abraham, Moehle J. P. (2000). Performance assessment for a Reinforced concrete frame building. *Earthquake Spectra*, Volume 16, Number 3: 541-557.

Islam M. S. (1996). Analysis of the Northridge earthquake response of a damaged non-ductile concrete frame building. *The Structural Design of Tall Buildings*, Vol. 5: 151-182.

Li, Y.R. and Jirsa, J.O. (1998). Parametric studies of nonlinear time history analysis. *Proc. Sixth U.S. National Conference on Earthquake Engineering*, Earthquake Engineering Research Inst., Oakland, California.

Medina R., Krawinkler H. (2001) Seismic demands for performance-based design. Proceedings of first PEER annual meeting, Oakland, California, January 2001.

Shome, N. Cornell, C. A. (1999). Probabilistic seismic demand analysis of nonlinear structures. Report RMS-35, Reliability of Marine Structures Program, Dept. of Civil Engineering, Stanford, Calif., 320 pages.

Keywords:

Performance Based Engineering, Probabilistic Response Analysis, Reinforced Concrete Buildings, Modeling Uncertainty, Intensity Measure, Seismic Hazard Curve, Lateral Stiffness, Lateral Strength, Interstory Drift Ratio, Displacement Based Design

POST-EARTHQUAKE DAMAGE EVALUATION FOR R/C BUILDINGS BASED ON RESIDUAL SEISMIC CAPACITY IN STRUCTURAL MEMBERS

Masaki MAEDA[1]

Masahiro BUNNO[2]

ABSTRACT

This paper describes a method for post-earthquake damage evaluation for reinforced concrete buildings. A concept of residual seismic capacity ratio, which are the ratio of residual seismic capacity to the original capacity, was introduced and evaluated using experimental data and a simple analytical model. A simple post-earthquake damage evaluation method for a reinforced concrete building was proposed based on the residual seismic capacity ratio. Validity of the proposed method was examined using database of reinforced concrete buildings damaged due to 1995 Hyogo-ken-nambu Earthquake, and correlation of the residual seismic capacity and damage levels was discussed. Good agreement between the residual seismic capacity ratio and damage levels was observed.

1. INTRODUCTION

In damage investigation of building structures suffering from seismic input, estimation of residual seismic capacity is essential in order to access the safety of the building against aftershocks and to judge the necessity of repair and restoration. This paper describes a method for post-earthquake damage evaluation for reinforced concrete buildings. Residual seismic capacity in structural members was estimated through investigation of relation between structural damage (residual crack) and maximum earthquake response (displacement). An evaluation method for the damage of a building structure was proposed based on the residual seismic capacity in structural members. Validity of the proposed method was examined using database of reinforced concrete school buildings damaged due to 1995 Hyogo-ken-nambu Earthquake, and the correlation of the residual seismic capacity and observed damage levels was discussed.

[1] *Department of Architecture and Building Science, Tohoku University, Sendai, Japan*
Email: maeda@struct.archi.tohoku.ac.jp
[2] *East Japan Railway Company, Tokyo, Japan*

2. BASIC CONCEPT OF POST-EARTHQUAKE DAMAGE EVALUATION

2.1 Residual Seismic Capacity Ratio, *R*

In this paper, damage level of a building structure was evaluated by residual seismic capacity ratio *R*, which is defined as the ratio of post-earthquake seismic capacity to the original capacity. Seismic Evaluation Standard [JBPDA, 1990], which is most widely applied to existing reinforced concrete buildings in Japan, was employed to evaluate the seismic capacity of a building. In the Seismic Evaluation Standard, seismic performance index of a building is expressed by the *Is*-index. The basic concept of *Is*–index appears in **APPENDIX**. Residual seismic capacity ratio *R* is given by Eq.(1).

$$R = \frac{{}_{D}Is}{Is} \times 100 \tag{1}$$

where, Is: original seismic performance index, ${}_{D}Is$: post-earthquake seismic performance index

2.2 Estimation of Post-earthquake Seismic Capacity of Building

The original seismic performance *Is*-index of a building can be calculated from lateral resistance and deformation ductility of structural members in accordance with the Seismic Evaluation Standard. On the other hand, residual resistance and deformation ductility in the damaged structural members are needed to be evaluated in order to quantify post-earthquake seismic performance index ${}_{D}Is$. Idealized lateral force-displacement relationships for ductile and brittle columns are shown in Figure 1 with damage class defined in Table1. Table 1 shows damage classification of structural members in the Damage Level Classification Standard [JBPDA, 1991].

Table 1: Damage classification of structural members [JBPDA, 1991]

Damage Class	Observed Damage on Structural Members
I	Some cracks are found. Crack width is smaller than 0.2 mm.
II	Cracks of 0.2 - 1 mm wide are found.
III	Heavy cracks of 1 - 2 mm wide are found. Some spalling of concrete is observed.
IV	Many heavy cracks are found. Crack width is larger than 2 mm. Reinforcing bars are exposed due to spalling of the covering concrete.
V	Buckling of reinforcement, crushing of concrete and vertical deformation of columns and/or shear walls are found. Side-sway, subsidence of upper floors, and/or fracture of reinforcing bars are observed in some cases.

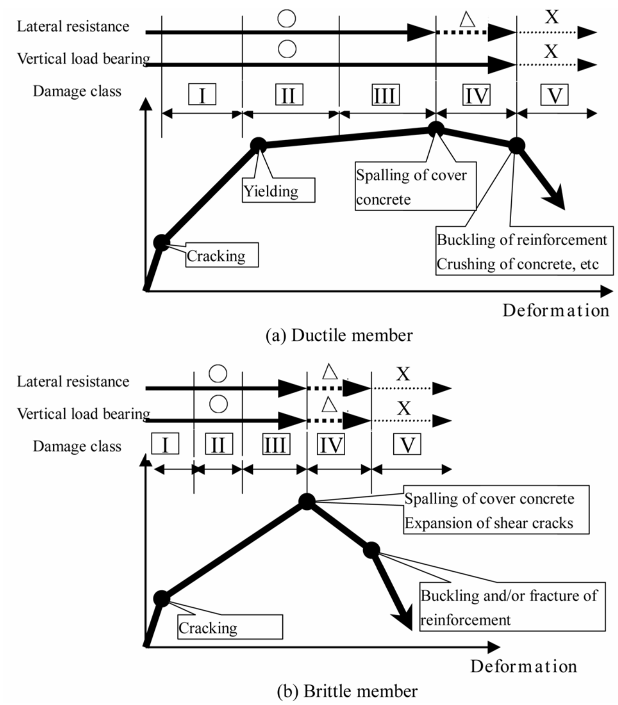

Figure 1: Idealized lateral force-displacement relationships and damage class

In the Seismic Evaluation Standard, most fundamental component for *Is*-index is E_0-index, which is basic structural seismic capacity index calculated from the product of strength index (C), and ductility index (F). Accordingly, deterioration of seismic capacity was estimated by energy dissipation capacity in lateral force- displacement curve of each member, as shown in Figure 2. Seismic capacity reduction factor η is defined by Eq.(2).

$$\eta = \frac{E_r}{E_t} \tag{2}$$

where, E_d : dissipated energy, E_r : residual energy capacity, E_t : entire energy capacity ($E_t = E_d + E_r$).

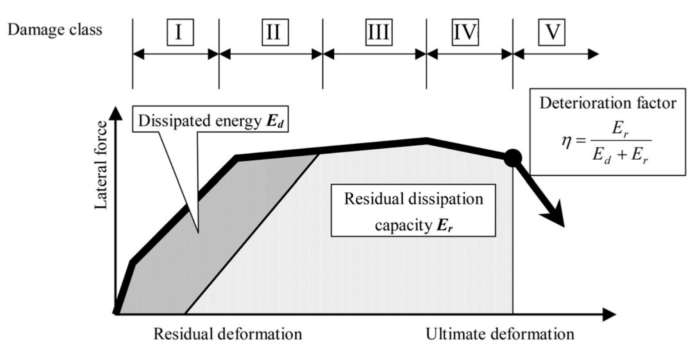

Figure 2: Seismic capacity reduction factor η

2.3 Evaluation of the seismic capacity reduction factor η based on experimental results

The seismic capacity reduction factor η for ductile flexural members was investigated using authors' test results [Bunno et al. 1999]. The details of the specimens are illustrated in Figure 3. Four beam specimens were tested under anti-symmetric bending and axial restraint force applied in proportion to the measured axial elongation. The stiffness constant for the axial force was selected as 1000 kN/cm or 4000 kN/cm, representing the lateral restraint stiffness of columns in prototype frame structures. The shear span ratio was 1.0 or 2.0. Sufficient lateral reinforcement was provided not only to prevent from brittle shear failure before flexural yielding but also to ensure adequate deformation capacity in the hinge region. The specimens were subjected to two cycles at rotation angles of 1/200, 1/100, 1/67, 1/50, 1/33 rad after the first cycle at a rotation angle of 1/400rad.

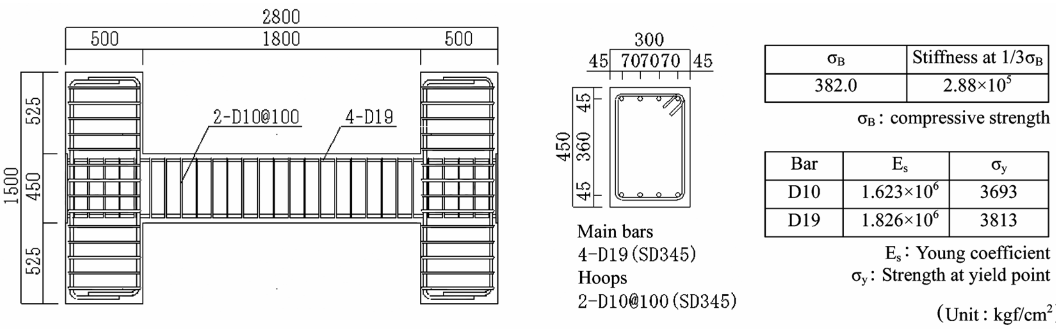

Figure 3: Details of the beam specimen

Figure 4 shows the observed shear force-lateral displacement relations. The relationship between maximum residual crack widths and the lateral displacement is shown in Figure 5. In the experiment, all the flexural crack widths were measured by crack gauges along the top and bottom surfaces of the specimen at the peak in each cycle and at the moment when the lateral force was unloaded. (see Figure 6).

Longitudinal bars yielded in each specimen at the rotation angle of the order of 1/200rad. As can be seen in Figure 5, residual crack widths were smaller than 0.2mm, which corresponds to the "damage class I (slight damage)", until flexural yielding occurred in a cycle at 1/200rad. In performance-based design point of view, the result indicates that flexural yielding may be defined as one of the criteria for the serviceability limit state in structural members of ductile flexural type. After flexural yielding, the maximum residual crack increased markedly with increase in the lateral displacement. When specimens reached maximum lateral force at the rotation angle of 2/100-3/100rad, the maximum residual crack widths were about 2mm and damage class was III or IV.

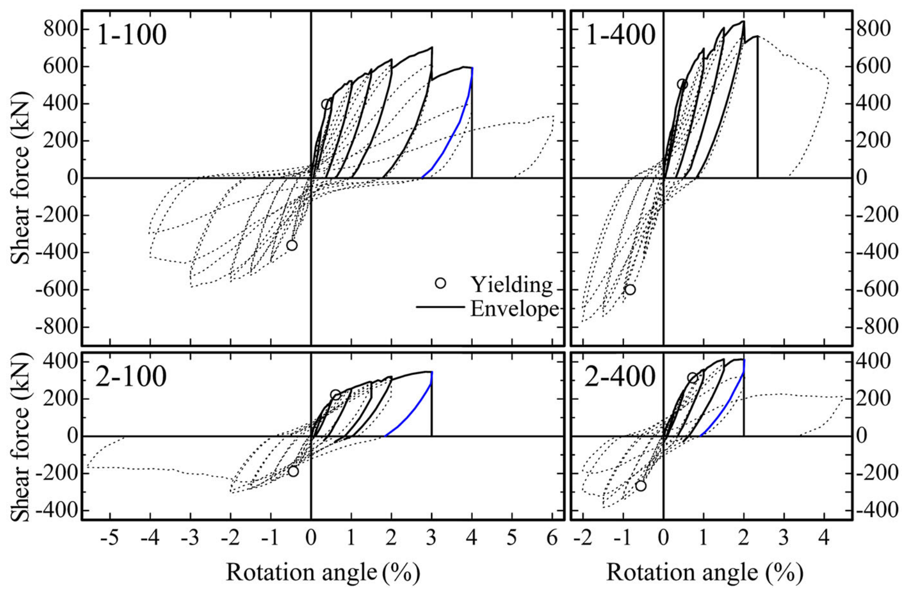

Figure 4: Shear Force-Lateral Displacement Relations

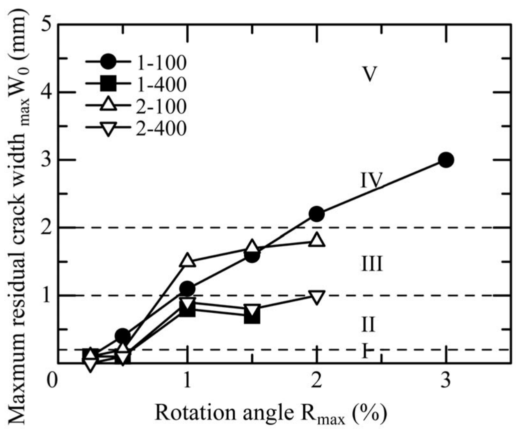

Figure 5: Maximum residual crack width vs. rotation angle

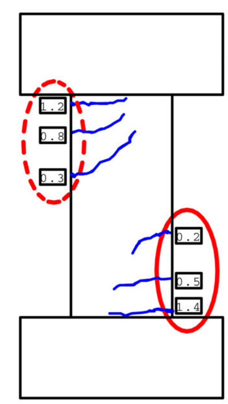

Figure 6: Measurement of crack width

From the test results, the seismic the seismic capacity reduction factor η, defined in Figure 2, was evaluated. The entire energy dissipation E_t was calculated from positive envelopes of shear force-lateral displacement curve (see Figure 4). Ultimate displacement was assumed as the rotation angle when shear force decrease to 80% of maximum force. The relationships between seismic capacity reduction factor η and maximum residual crack widths $_{max}w_0$ are shown in Figure 7. From the figure, linearly decreasing relation is observed.

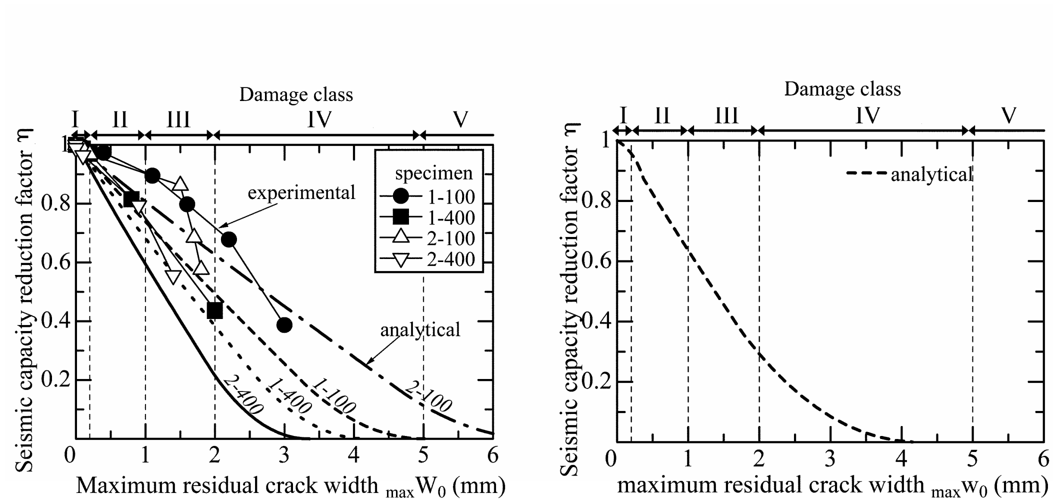

(a) Ductile member **(b)Brittle member**

Figure 7: Maximum residual crack width $_{max}w_0$ vs. seismic capacity reduction factor η

2.4 Evaluation of the seismic capacity reduction factor η based on an analytical model

A simple analytical model was introduced in order to formulate the relation of maximum residual crack width $_{max}w_0$, and the seismic capacity reduction factor η. As shown in Figure 8, deformation of a column was assumed to be consist of two components: flexural and shear deformation. If the column is idealized as a rigid body, the flexural deformation of the column can be represented by the rotation of the rigid body [Bunno et. al, 1999]. This assumption gives an estimation of flexural deformation R_f, due to total flexural crack widths $\sum w_f$ by Eq.(3).

$$R_f = \frac{\sum w_f}{D} \tag{3}$$

If shear deformation due to shear cracks is idealized as shown in Figure 8(b), shear deformation R_s due to total shear crack widths $\sum w_s$ can be formulated as Eq.(4).

$$R_s = \frac{\sum w_s \cdot \sin\theta}{h_0} \tag{4}$$

where, h_0:clear span height of a column, θ: angle of shear crack to the horizontal plane (assume θ= 45 degree).

Residual deformation of a column R_0 is obtained by the summation of two components.

$$R_0 = R_{0f} + R_{0s} = \frac{\sum w_f}{D} + \frac{\sum w_s \cdot \sin\theta}{h_0} \tag{5}$$

Rearranging Eq.(5) leads to Eqs.(6) and (7).

$$ {}_{\max} w_{0f} = \frac{\alpha \cdot D}{n_f} R_0 \tag{6} $$

$$ {}_{\max} w_{0s} = \frac{(1-\alpha)h_0}{n_s \sin\theta} R_0 \tag{7} $$

where, $\alpha = \dfrac{R_{0f}}{R_0}$, $n_f = \dfrac{\sum w_f}{{}_{\max} w_{0f}}$, $n_s = \dfrac{\sum w_s}{{}_{\max} w_{0s}}$

Substituting appropriate value into α, n_f, and n_s, the relation of maximum residual crack width ${}_{max}w_0$ with residual deformation R_0 is evaluated, although the ratio of flexural deformation α, and the ratio of total crack width to maximum crack width n_f, n_s change in accordance with failure mode, shear-span-to-depth ratio h_0/D, construction age, lateral reinforcement ratio and so on.

Analytical results for seismic capacity reduction factor η were plotted in Figure 7. From the experimental results, α=3/4, n_f=2 and n_s=4 were used for a ductile member. α=1/2, n_f=2 and n_s=2 were assumed for a brittle member. As can be seen in Figure 7(a), analytical results agreed well with experimental results. From these results, seismic capacity reduction factor η for ductile and brittle members were determined as shown in Table 2.

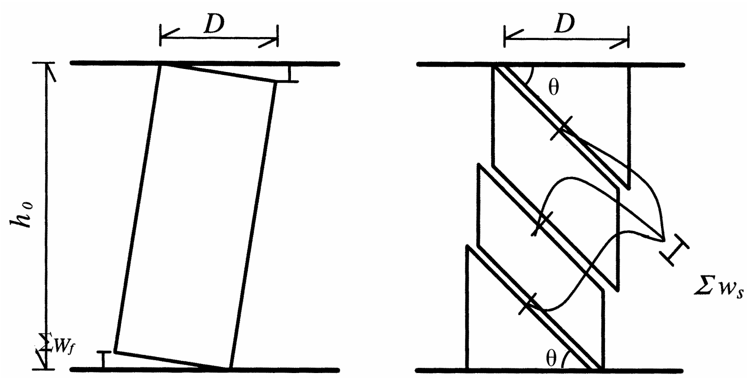

Figure 8: Analytical model

Table 2: seismic capacity reduction factor η

Damage Class	Ductile Members	Brittle Members
I	0.95	0.95
II	0.75	0.6
III	0.5	0.3
IV	0.1	0
V	0	0

3. APPLICATION TO RC BUILDINGS DAMAGED DUE TO RECENT EARTHQUAKES IN JAPAN

The proposed evaluation method was applied to reinforced concrete buildings damaged due to recent earthquakes such as 1995 Hyogo-ken-nambu Earthquake.

3.1 Approximation of lateral strength and ductility in members

One of main purposes of damage level classification is to grasp the residual seismic capacity as soon as possible just after the earthquake, in order to access the safety of the damaged building for aftershocks and to judge the necessity for repair and restoration. For this purpose, need of complicated procedure, i.e. calculation of strength and ductility of structural member based on material and sectional properties, reinforcing details etc, is inconvenient. Accordingly, a simplified method was developed by approximating the lateral strength and ductility. Following assumptions were employed in the approximation.

(1) Vertical members are categorized into five members and normalized lateral strengths $\overline{C}$ of the five categories are assumed as shown in Table 3. These values were evaluated from cross section area and average shear stress for typical low-rise reinforced concrete buildings in Japan.

(2) Ductility factor F of each vertical member is assumed 1.0.

(3) The original and residual capacities of a building are estimated by the summation of the original and residual capacities of vertical members in the damaged story. Therefore residual seismic capacity ratio R is calculated by Eq.(8).

$$R = \frac{\sum \eta \overline{C} F}{\sum \overline{C} F} \tag{8}$$

Table 3: Categories of vertical members and normalized lateral strengths $\overline{C}$

	Ductile/Brittle column	Wall without boundary column	Wing wall with column	Wall with boundary columns
Section	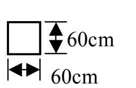	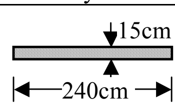	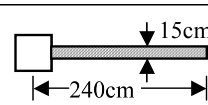	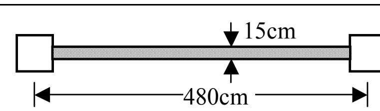
Average Shear Stress	1 N/mm^2	1 N/mm^2	2 N/mm^2	3 N/mm^2
Normalized shear strength $\overline{C}$	1	1	2	6

3.2 Application to damaged buildings

The proposed damage evaluation method was applied to reinforced concrete buildings damaged due to recent earthquakes. Objective buildings are listed in Table4. Buildings No.1-10 were beam-column moment frame structures in the longitudinal direction, in which major damage was observed. The others are wall-frame structure. First floor plan of building No.11 and No.12 are shown in Figure 9.

Table 4: Objective buildings

No.	Usage	Construction age	Number of Story	Residual seismic capacity R		Damage level
				Approximated R_1	Accurate R_2	
1	School	1972 1974	4	54.1	48.1	Severe
2	School	1972 1974	4	33.5	24.0	Severe
3	School	1972 1974	4	38.4	51.3	Severe
4	School	1976	3	80.0	81.1	Minor
5	School	1970 1976	4	71.9	76.6	Moderate
6	School	1959 1960	3	34.9	35.9	Severe
7	School	1967	3	71.3	71.5	Moderate
8	School	1967	3	16.0	13.6	Severe
9	Community center	1977	3	89.0	88.4	Minor
10	Community center	1969	3	57.6	54.3	Severe
11	Apartment	1968	10	23.5	27.5	Severe
12	Office	1969 1970	6	50.0	59.0	Severe

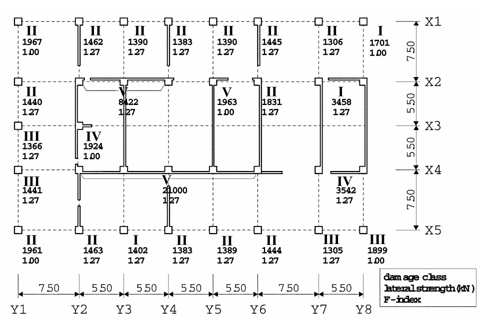

(a) Building No.11

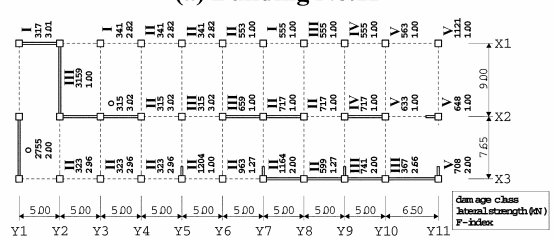

(b) Building No.12

Figure 9: First floor plan and damage class in structural members

As shown in Figure 9(a), severer damage was observed in shear walls in the building No.11 and lateral strengths of shear walls were relatively higher than the assumption in Table3. On the other hand, lateral strengths of shear walls in the building No.12 were relatively lower.

Approximated value of Residual seismic capacity ratio R_1 was compared with accurate value R_2, which was evaluated from calculated lateral strength and ductility based on material and sectional properties, reinforcing details, in Figure 10. From the figure, approximated value R_1 agrees with accurate value R_2 not only for frame structure but also for wall-frame structure.

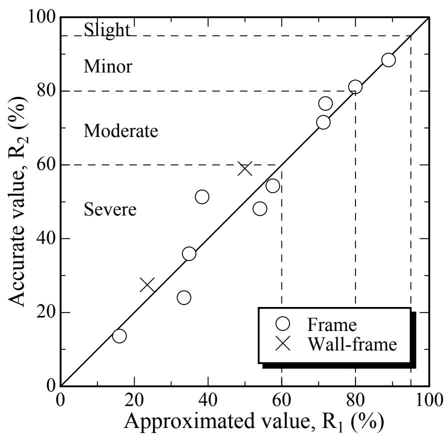

Figure 10: Comparison R_1 and R_2

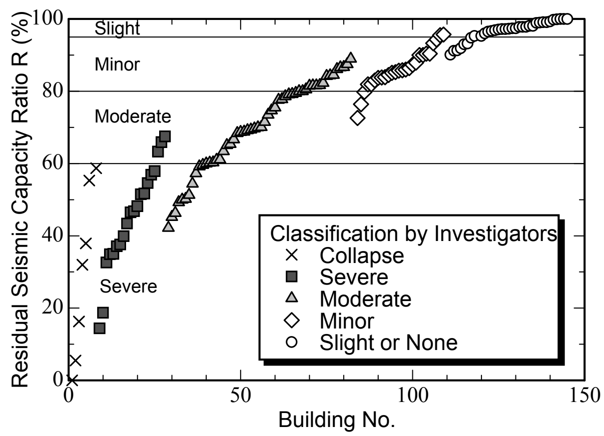

Figure 11: Residual seismic capacity ratio R and damage level classification

The residual seismic capacity ratio R of about 150 reinforced concrete school buildings, including above mentioned buildings, are shown in Figure 11 together with damage levels estimated by the engineering judgment of investigators according to Table 4. As can be seen in the figure, no significant difference between damage levels and residual seismic capacity ratio R can be found although near the border some opposite results are observed.

The horizontal lines in Figure 11 are borders between damage levels due to following definition.

[slight] $R \geq 95$ (%)

[minor] $80 \leq R < 95$ (%)

[moderate] $60 \leq R < 80$ (%)

[severe] $R < 60$ (%)

[collapse] $R \approx 0$

The border between slight and minor damage was set R=95% to harmonize “slight damage” to the serviceability limit state. Almost of severely damaged and about 1/3 of moderately damaged buildings were demolished and rebuilt after the earthquake according to the report of Hyogo Prefecture. Therefore, if the border between moderate and severe damage was set R=60%, "moderate damage" may correspond to the reparability limit state.

Table 4: Damage level classification of reinforced concrete buildings used in Japan

Damage level	Damage in members	Illustration of damage
No damage	No damage is found	---
Slight damage	Columns, shear walls or non-structural walls are slightly damaged.	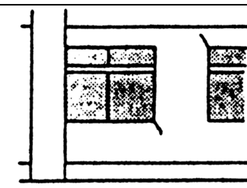
Minor damage	Columns or shear walls are slightly damaged. Some shear cracks in non-structural walls are found.	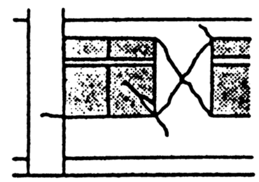
Moderate damage	Typical shear and flexural cracks in columns, shear cracks in shear walls, or severe damage in non-structural walls are found.	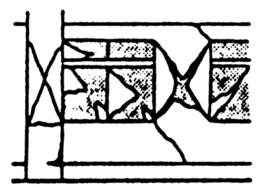
Severe damage	Spalling of concrete, buckling of reinforcement, and crushing or shear failure in columns are found. Lateral resistance of shear walls is reduced due to heavy shear cracks.	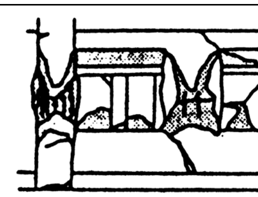
Collapse	The building is partially/totally collapsed due to severely damaged columns and/or shear walls.	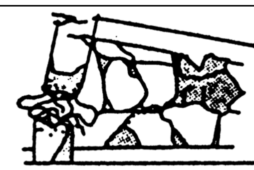

4. CONCLUDING REMARKS

In this paper a concept of residual seismic capacity ratio R, which are the ratio of residual seismic capacity to the original capacity, was introduced and evaluated using experimental data and a simple analytical model. A simple post-earthquake damage evaluation method for a reinforced concrete building was proposed based on the residual seismic capacity ratio. Good agreement between the residual seismic capacity ratio R and damage levels classified by engineering judgment was observed for relatively low-rise buildings damaged due to 1995

Hyogo-ken-nambu Earthquake. The proposed method can provide a quantitative estimation of structural damage of a building, which is essential for performance-based-design. Much work is, however, needed to estimate accurately the reparability limit state which may be determined not only by damage level of structural members but also by damage in non-structural elements and equipment and cost of repair and restoration.

5. REFERENCES

Bunno, M., Komura, N., Maeda, M., and Kabeyasawa, T. (1999), "Experimental study on behavior of reinforced concrete beams under axial restriction (in Japanese)", Proceedings of the Japan Concrete Institute, Vol. 21, No. 3, JCI, pp.517-522.

JBDPA / The Japan Building Disaster Prevention Association (1990), *Standard for Seismic Evaluation of Existing Reinforced Concrete Buildings*. (in Japanese)

JBDPA / The Japan Building Disaster Prevention Association (1991), *Standard for Damage Level Classification of Reinforced Concrete Buildings*. (in Japanese)

6. APPENDIX
BASIC CONCEPT OF JAPANESE STANDARD FOR SEISMIC PERFORMANCE EVALUATION

The Standard consists of three different level procedures; first, second and third level procedures. The first level procedure is simplest but most conservative since only the sectional areas of columns and walls and concrete strength are considered to calculate the strength, and the inelastic deformability is neglected. In the second and third level procedures, ultimate lateral load carrying capacity of vertical members or frames are evaluated using material and sectional properties together with reinforcing details based on the field inspections and structural drawings.

In the Standard, the seismic performance index of a building is expressed by the *Is*-Index for each story and each direction, as shown in Eq. (7)

$$Is = E_0 \times S_D \times T \tag{7}$$

where, E_0 : basic structural seismic capacity index calculated from the product of strength index (C), ductility index (F), and story index (ϕ) at each story and each direction when a story or building reaches at the ultimate limit state due to lateral force, i.e., $E_0 = \phi \times C \times F$.

C : index of story lateral strength, calculated from the ultimate story shear in terms of story shear coefficient.

F : index of ductility, calculated from the ultimate deformation capacity normalized by the story drift of 1/250 when a standard size column is assumed to failed in shear. F is dependent on the failure mode of structural member and their sectional properties such as bar arrangement, member proportion, shear-to-flexural-strength ratio etc. . F is assumed to vary from 1.27 to 3.2 for ductile column, 1.0 for brittle column and 0.8 for extremely brittle short column.

ϕ : index of story shear distribution during earthquake, estimated by the inverse of design story shear coefficient distribution normalized by base shear coefficient. A simple formula of $\phi = \frac{n+1}{n+i}$ is basically employed for the i-th story level of an n-storied building by assuming straight mode and uniform mass distribution.

S_D : factor to modify E_0-Index due to stiffness discontinuity along stories, eccentric distribution of stiffness in plan, irregularity and/or complexity of structural configuration, basically ranging from 0.4 to1.0

T : reduction factor to allow for the deterioration of strength and ductility due to age after construction, fire and/or uneven settlement of foundation, ranging from 0.5 to 1.0.

INVESTIGATION OF EQUIVALENT VISCOUS DAMPING FOR DIRECT DISPLACEMENT-BASED DESIGN

Mervyn J. Kowalsky[1]

John P. Ayers[2]

ABSTRACT

Concepts of equivalent viscous damping as applied to direct displacement-based design are reviewed. A series of 80 time history analysis are conducted in an effort to identify potential limitations and the range of applicability of the equivalent viscous damping concept for prediction of non linear response. The limited study indicated that for the majority of the cases, the equivalent viscous damping concept behaved as expected. However, in cases where the earthquake time history resulted in a large single pulse, the equivalent viscous damping approach failes to recognize that the peak non-linear response is no longer a function of the energy dissipated. Further studies are proposed in order to investigate the phenomena more closely.

INTRODUCTION

Simplified non-linear analysis techniques are of primary importance in development of design procedures for PBSE. In this paper, the term "Simplified Non-Linear Analysis" represents methods that are response spectrum-based. When determining the inelastic response of single degree (or equivalent) of freedom systems with a response spectrum, the analyst can use either inelastic spectra or elastic spectra combined with equivalent elastic properties representing the behavior of the inelastic system. Extensive past effort has been devoted to development of inelastic spectra. The primary benefit of inelastic spectra is that an exact spectra can be obtained for a SDOF oscillator of prescribed period and hysteretic characteristics. Unfortunately, the resulting R-μ-T relationship varies not only as a function of period and hysteretic properties, but also as a function of the earthquake.

The other method that an analyst can utilize to determine non-linear response involves the characterization of an inelastic system as an equivalent elastic system. As a result, the response of the non-linear system can theoretically be described by the more familiar elastic response spectra. The accuracy of such a method is directly related to the accuracy of the definition of the

---

[1] Assistant Professor, Department of Civil Engineering, North Carolina State University, Box 7908, Raleigh, NC

[2] Engineering Intern, Sutton-Kennerly and Associates, 300 Pomona Dr., Greensboro, NC. Formerly MS Student, NCSU.

equivalent elastic system. By definition, equivalent elastic systems are defined by an equivalent period, T_{eq}, and equivalent viscous damping, ζ_{eq}.

The concept of equivalent elastic systems to assess inelastic response was first proposed by Jacobsen in 1930. Equivalent viscous damping was analytically defined by Jacobsen by assuming a sinusoidal earthquake response in the equation of motion and integrating the resulting expression over one cycle of response and equating that to the area of a rigid perfectly plastic hysteretic response. Subsequent to Jacobsen's work various other definitions of equivalent systems were proposed as reviewed by Jennings (1968).

Iwan and Gates (1979) conducted a rigorous statistical study whose objective was to identify the combination of equivalent period and equivalent damping that would best describe the inelastic response of SDOF systems. His study did not rely on any previous definitions of equivalent systems and was solely a statistical study to assess the combination of equivalent period and damping that would minimize the error in estimating inelastic structural response with elastic spectra. Iwan and Gates conducted dynamic inelastic time history analysis on a wide range of SDOF systems and considered ductility, initial period, and ground motion as variables. The primary conclusions from their work were: (1) Optimal values of equivalent damping never exceed 14%. (2) Peak displacements are relatively insensitive to definition of equivalent period.

Gulkan and Sozen (1974), and more recently Bonacci (1994) utilized experimental results to assess the equivalent damping of non-linear systems. In each of these two cases, the equivalent period was identified from experimental results and was defined as the fictitious period that coincides with the secant stiffness to the measured maximum response point (Maximum recorded force divided by maximum recorded displacement). Equivalent damping was calculated by balancing the energy input into the SDOF system during the earthquake with a linear dashpot that would be required to bring the system to rest as shown in Eq. 1. This definition of equivalent damping relies on knowledge regarding the earthquake time history, as well as the response time history.

$$\beta_s\left(2m\omega_s\int_0^{t_f}\dot{x}^2dt\right)=-m\int_0^{t_f}\ddot{y}\dot{x}dt \qquad \text{(Eq. 1)}$$

The calculated equivalent period and equivalent damping were then utilized to determine the expected maximum response displacement from the response spectra and the results compared with the measured values. Gulkan and Sozen also utilized Jacobsen's approach to obtain a damping vs. ductility relationship for a form of the Takeda hysteretic model (Takeda et al., 1970). It is noted that Jacobsen's approach assumes sinusoidal response for one cycle of motion, which is very different from the average method initially utilized by Gulkan and Sozen. However, when the equivalent damping values with the average damping approach are plotted for Gulkan and Sozen and Bonacci's tests, they agree reasonably well with Jacobsen's approach, implying that the extra effort of calculating what may be deduced as a more accurate average damping is not warranted. Furthermore, from a design perspective, calculation of average damping requires a priori knowledge of the structural response which is contrary to the objective of simplified analysis and design techniques.

When the experimental displacements are compared with the displacements expected from the elastic spectrum and equivalent system, the following results are obtained for the tests conducted by Gulkan and Sozen and Bonacci: The scatter between the ratio of actual peak displacement to peak displacement from the elastic response spectra using equivalent properties ranged from 0.4 to 1.5. The mean value was 0.94, and the standard deviation was 0.18. A total of 59 different tests were encompassed by both studies.

Given the variation in definitions of equivalent systems, and the corresponding variation in the results that are obtained and the importance of such procedures towards achieving PBSE, it is felt to be essential to further explore the concept of equivalent elastic systems for inelastic analysis. Furthermore, it is essential to identify limitations of the procedures.

REVIEW OF DIRECT DISPLACEMENT-BASED DESIGN APPROACH

The equivalent viscous damping concept is an important component of performance-based earthquake engineering design procedures such as Direct Displacement-Based Design (DDBD) (Priestley and Kowalsky, 2000). The DDBD approach aims to design a structural system for a prescribed target displacement for a given earthquake motion characterized by linear response spectra generated for various levels of viscous damping. The basic steps of the procedure are described below.

1. **Select target displacement.** In the case of a SDOF system such as a single column bridge or structural wall, the target displacement can be readily obtained from drift or strain criteria. In the case of MDOF systems such as multi-span bridges or buildings, the target displacement is derived from a prescribed target displacement profile which is obtained from specified drift or strain limits and consideration of multiple response modes where appropriate.

2. **Calculate Level of Equivalent Viscous Damping.** Based on the chosen target displacement and the yield displacement of the system, member and/or system ductility levels are tabulated. These are then utilized to calculate the level of hysteretic damping expected. Relations between hysteretic damping and ductility are readily obtained for different materials and structural system types from consideration of the expected hysteretic response of the system. A nominal viscous damping of 0%-5% can be added to the hysteretic damping to obtain the level of equivalent viscous damping used for design.

3. **Determine Effective Period of System.** Using the target displacement from Step 1, and the equivalent viscous damping from step 2, the effective period at maximum response is obtained by entering the design spectra with the target displacement and reading across to the response curve given by the level of damping from step 2 and down to horizontal axis to evaluate the effective period. This process is shown in Fig. 1.

4. **Evaluate Effective Stiffness and Design Base Shear Force.** From consideration of a SDOF oscillator, the effective stiffness at maximum response is obtained with Eq. 2 where m_{eff} represents the effective mass. Following this, the design base shear force at maximum response is obtained with Eq. 3. As an alternative, the entire process can be reduced to one expression if the 5% damped design spectra is characterized as a straight line with corner point period and displacement of T_c and Δ_c, respectively, as shown in Fig. 1. The resulting expression is shown as Eq. 4 (Kowalsky, 1998). Eq 4 contains the EuroCode expression (1988) for relating design spectra at a damping higher than 5% to that at 5%.

$$k_{eff} = \frac{4\pi^2 m_{eff}}{T_{eff}^{\ 2}} \qquad \text{(Eq. 2)}$$

$$V_b = k_{eff}\Delta_T \qquad \text{(Eq. 3)}$$

$$V_b = \frac{4\pi^2 m_{eff}}{\Delta_T}\frac{\Delta_c^{\ 2}}{T_c^{\ 2}}\frac{7}{2+\zeta_{eff}} \qquad \text{(Eq. 4)}$$

5. **<u>Conduct Structural Analysis and Design for Moment and Deformation Demands.</u>** The base shear force from Step 4 is distributed in accordance with the prescribed displacement profile of Eq. 1 and structural analysis conducted utilizing secant stiffnesses for the structural members. Members are designed for resulting moments, and confinement details provided to reach the prescribed deformation demands from Step 1.

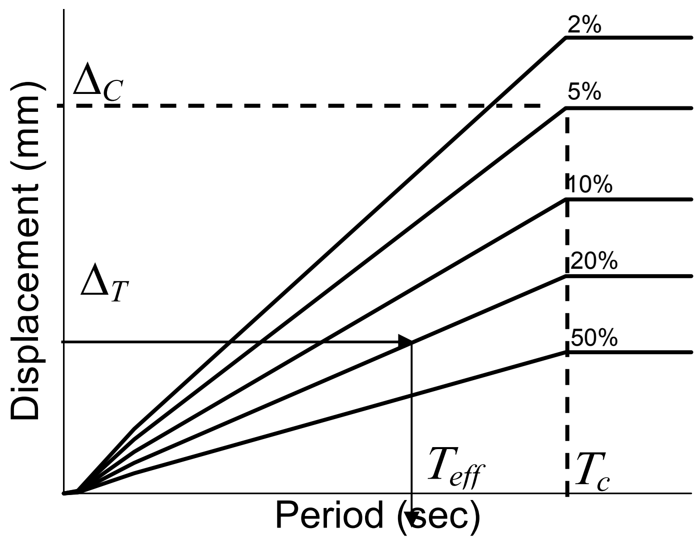

Fig. 1 Obtaining Effective Period in DDBD

DESCRIPTION OF THIS STUDY

In this study, a series of 80 DITH are conducted on SDOF systems. The variables in the study are initial period, earthquake excitation, and hysteretic parameters. The goal of the study is to investigate the behavior of equivalent viscous damping as defined by Jacobsen's approach since it is most suitable in a design setting. By varying hysteretic parameters and applying Jacobsen's approach, different damping vs. ductility relations will be developed. As a result, different responses are expected for the structures with different hysteretic characteristics. Namely, structures with higher equivalent damping at a given ductility should reach a lower peak displacement than structures with lower equivalent damping.

SDOF systems consisted of single columns supporting a mass. All columns were 1m in diameter and heights of 3m, 5m, 8m, and 12m were considered. Concrete strength was set at 30Mpa for all columns. Each column contained a longitudinal reinforcement ratio of 1.5% with a steel yield strength of 400Mpa. Each column sustained an axial load equal to $0.1f'_cA_g$, and an inertia mass equal to $0.1f'_cA_g/g$. Each column was analyzed with the Takeda degrading stiffness hysteretic response with the sole difference being parameters that describe the size of the loop, and hence damping vs. ductility relationship. Two extreme cases identified as Case A and Case B were considered in terms of the hysteretic characteristics as shown in Fig. 2. An expression between displacement ductility and hysteretic damping can be readily obtained by applying Jacobsen's approach to the Takeda hysteretic response. The resulting expression is shown as Eq. 5 (Loeding et al., 1998) where μ is the displacement ductility. Applying Eq. 5 to the two cases shown in Fig. 2 results in the damping ductility relations shown in Fig. 3.

$$\zeta_{hyst} = \frac{2}{\pi} R_{LA} \qquad \text{(Eq. 5)}$$

$$R_{LA} = 1 - \frac{3}{4}\mu^{\alpha-1}\gamma - \frac{1}{4}\left[\frac{r\beta\mu}{\gamma}\left(1-\frac{1}{\mu}\right)+1\right]\left[2-\beta\left(1-\frac{1}{\mu}\right)-\mu^{\alpha-1}\gamma\right] - \frac{1}{4}\left[\frac{r\beta^2\mu}{\gamma}\left(1-\frac{1}{\mu}\right)^2\right] \qquad \text{(Eq. 6)}$$

$$\gamma = r\mu - r + 1 \qquad \text{(Eq. 7)}$$

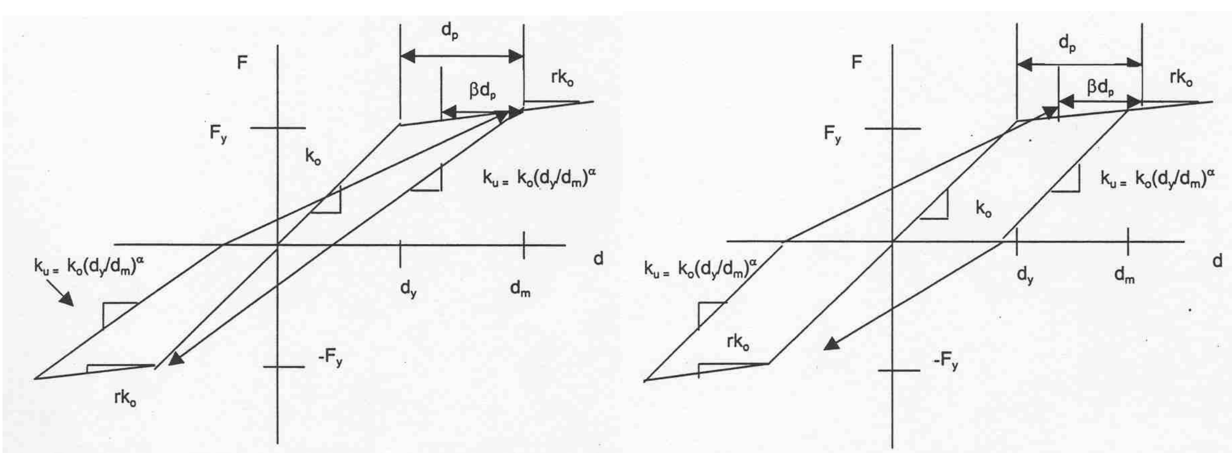

(a) Case A: α = 0.5, β = 0 **(b) Case B: α = 0, β = 0.6**

Fig. 2 Takeda Degrading Stiffness Hysteretic Response (Ayers, 2000)

Each of the four columns heights in the study were subjected to the following seven earthquake time histories: 1994 Sylmar, 1976 Tabas, 1940 El Centro EW, 1940 El Centro NS, 1971 Pacoima

Dam, 1995 Kobe EW, 1995 Kobe NS. In addition, three artificial earthquake time histories generated to fit the 1997 UBC Soil Type C spectrum were utilized (ICBO, 1997).

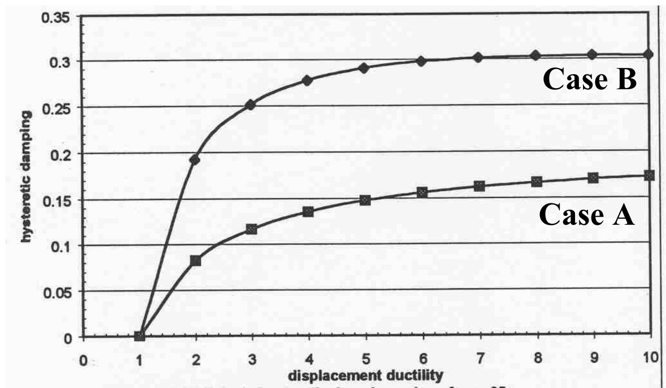

Fig. 3 Damping vs. Displacement Ductility Relations Used In Study (Ayers, 2000)

Analyses were conducted twice with the computer program Ruaumoko (Carr, 1998). Case A columns had the thinner hysteretic characteristics shown in Fig. 1a, while Case B columns followed the hysteretic response of Fig. 1b. All analyses were conducted assuming 0% viscous damping such that energy dissipation came solely from hysteretic damping. The following procedure was applied to each of the analysis results. An example calculation is shown in Fig. 4.

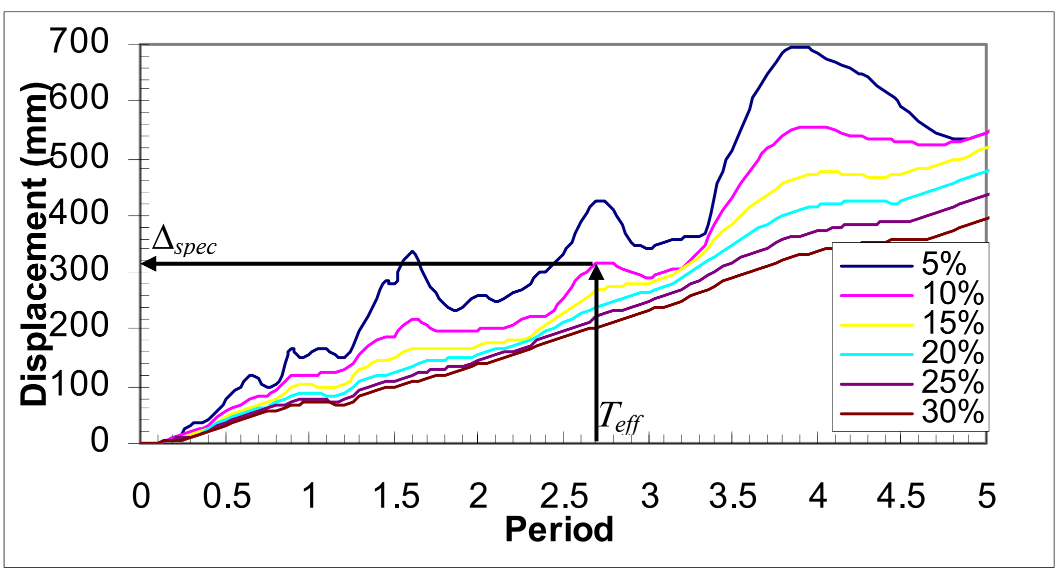

Fig. 4 Evaluating Expected Displacement

1. From the maximum recorded displacement, Δ_{th}, and force, F_{th}, from the time history analysis, evaluate the effective stiffness using Eq. 8. Using Eq. 9, evaluate the effective period.

$$K_{eff} = \frac{F_{th}}{\Delta_{th}} \quad \text{(Eq. 8)} \qquad T_{eff} = 2\pi\sqrt{\frac{m}{K_{eff}}} \quad \text{(Eq. 9)}$$

2. From the maximum recorded displacement, evaluate the displacement ductility demand with Eq. 10. Then, using Eq. 5, evaluate the expected hysteretic damping.

$$\mu = \frac{\Delta_{th}}{\Delta_y} \quad \text{(Eq. 10)}$$

3. Using the effective period, and calculated hysteretic damping, enter the displacement response spectra and evaluate the expected maximum displacement, Δ_{spec}.

4. Compare the expected maximum displacement from the response spectra, Δ_{spec}, with the maximum displacement from the dynamic inelastic time history analysis, Δ_{th}.

Analysis results are shown in Fig. 5 for the Case A columns, and Fig. 6 for the Case B columns. In each case the ratio of the displacement from the response spectra to that from the time history analysis is plotted versus effective period.

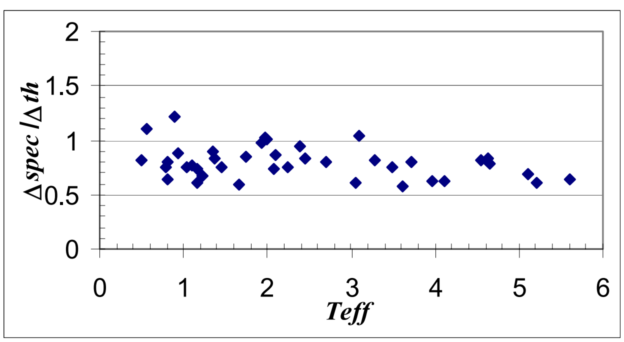

Fig. 5 Case A (Low Damping Level)

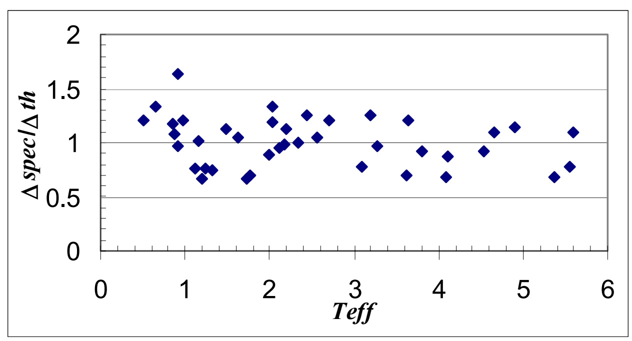

Fig. 6 Case B (High Damping Level)

For Case A columns, the average ratio was 0.796 with a standard deviation of 0.149. For Case B columns, the average was 1.006 with a standard deviation of 0.227. Overall, these results compare favorably with previous experimental results from the studies by Gulkan and Bonacci. However, in an effort to identify potential sources of error, an interesting observation is made. As an example, consider the structures subjected to the Pacoima dam record and the artificial UBC matched record (Figs. 7 and 8 respectively). The maximum recorded displacements from the time history analysis for columns 8A and 8B (as well as 12A and 12B) of the Pacoima Dam record were identical even though the calculated equivalent damping values were significantly different due to the different hysteretic characteristics shown in Fig. 2. However, when utilizing the elastic spectra and equivalent structure to determine the expected maximum response, different values for maximum displacement were obtained due to the different equivalent viscous damping values.

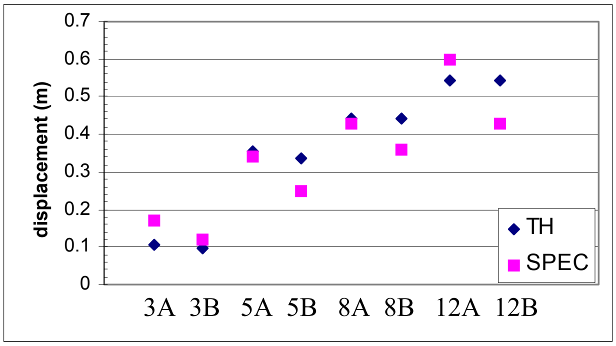

Fig. 7 Pacoima Dam Results

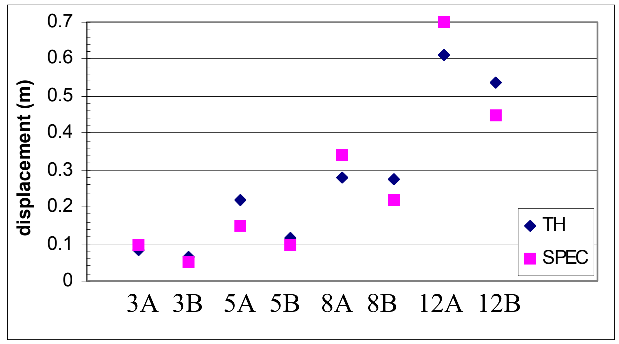

Fig. 8 Artificial UBC Record Results

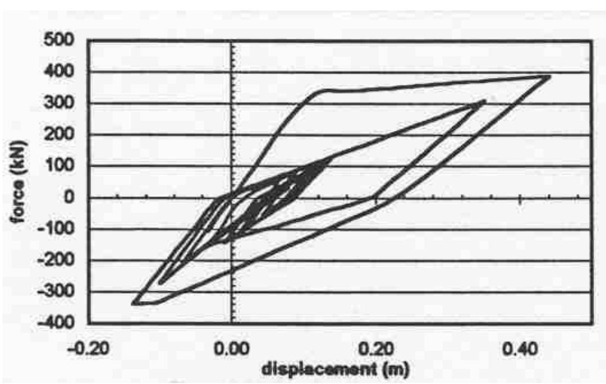

Fig. 9 Column 8A Pacoima Record

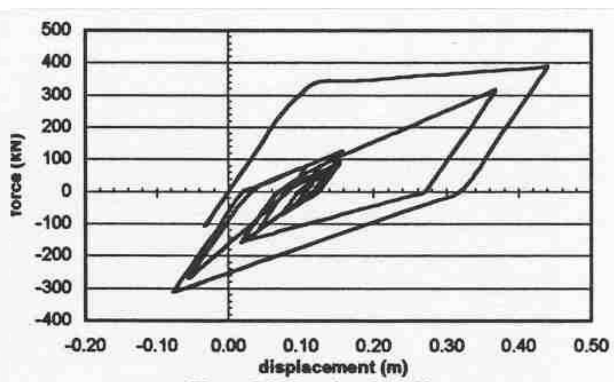

Fig. 10 Column 8B Pacoima Record

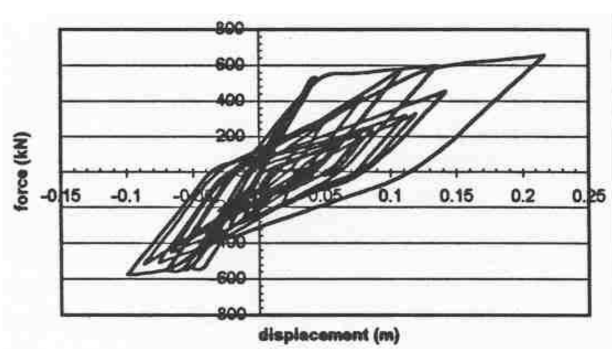

Fig. 11 Column 5A UBC Record

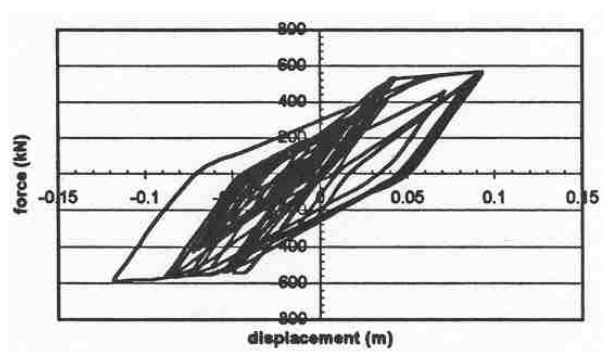

Fig. 12 Column 5B UBC Record

Upon examination of the force-displacement hysteretic responses (Figs. 9 and 10), the reason for this discrepancy is immediately apparent. For the Pacoima dam record, a large-long duration acceleration pulse occurs early on in the record, as a result, the structure reaches its maximum response without any cycling in the inelastic range. Aside from some minor elastic cycling, the structure behaves monotonically to the maximum response point. This of course does not change even if the hysteretic parameters change since the fatness of the loops is irrelevant if the energy dissipation is not mobilized in a cyclic manner. In contrast, consider the results of columns 5A and 5B from the UBC record (Fig. 8). In this case, the results of the time history analysis, as well as the results from the analysis of the equivalent structure, indicate that the case A column achieves a higher displacement than the case B column due to the lower level of hysteretic damping in case A. Upon examination of the force-deformation responses (Figs. 11 and 12), it is clear that in these cases, the structure is cycled extensively in the inelastic range before reaching maximum response, and that as a result, dissipates hysteretic energy, thus lending support to the equivalent viscous damping concept as proposed by Jacobsen.

Ultimately, this implies that the concept of equivalent viscous damping as described by Jacobsen's approach is more applicable in the case where inelastic excursions that mobilize extensive energy dissipation precede the excursion to maximum response. In the case where the earthquake is such that a large duration pulse to maximum response is not preceded by inelastic excursions, Jacobsen's approach has the potential to induce additional errors.

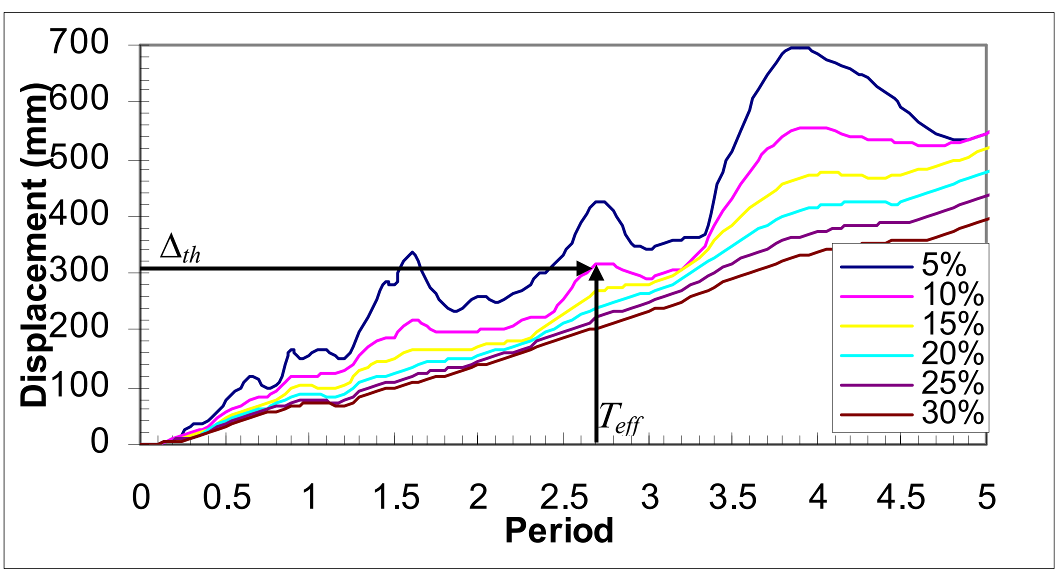

Fig. 13 Evaluating Expected Equivalent Viscous Damping

A similar set of analysis were performed from the perspective of identifying the equivalent viscous damping needed to match the time history analysis results, and comparing that value with the one obtained from Eq. 5. In these studies, the response spectra were entered with the effective period from Eq. 9 and the time history analysis displacement, Δ_{th}. The intersection of these two lines then represents the equivalent viscous damping, which is compared with the expected value form Eq. 5. Fig. 13 illustrates a sample calculation.

Results for these calculations are shown in Fig. 14 below. The average value was 0.822 with a standard deviation of 0.568. Clearly, this represents extensive scatter, some of which can be attributed to the manner in which the values were obtained, i.e., visually from the response spectra. However, there are two observations which are important to note: (1) The scatter is greatest in the lower effective period range, and (2) The scatter in evaluation of equivalent damping does not translate to scatter in prediction of maximum displacement as shown in the results of Figs. 5 and 6.

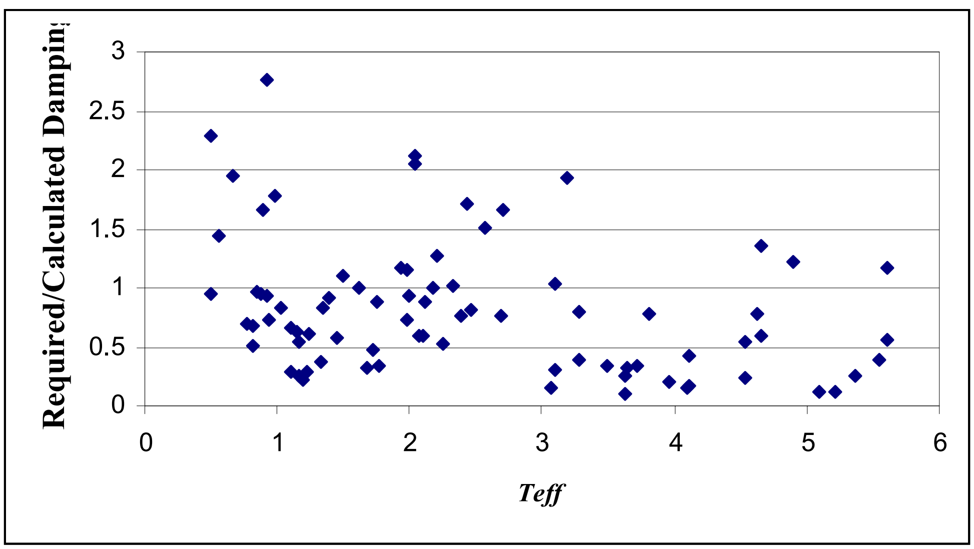

Fig. 14 Ratio of required to calculated hysteretic damping vs. effective period

FUTURE WORK

Based on the limited results presented, further studies are planned regarding the range of application of the equivalent viscous damping concept. In the study currently underway, an extensive set of SDOF oscillators will be considered under a variety of earthquake time histories. In addition to evaluating the equivalent viscous damping as described in this paper, analysis will be conducted where the most significant assumption in Jacobsen's approach is removed, that is, the assumption on sinusoidal response in establishing Eq. 5. This will be accomplished by numerically integrating each of the ground motions and obtaining a time-history specific factor to be incorporated into Eq. 5. Through consideration of a large enough number of time histories, it is expected that the variability in this factor will be estimated.

CONCLUSIONS

Based on the limited results of this study, the following conclusions are offered:

1. On average, assessment of non-linear response with equivalent linear systems defined by effective period at maximum response and equivalent damping defined by Jacobsen's approach yields good results for the majority of cases considered.

2. In some cases, the agreement between time history analysis and response spectra analysis may be fortuitous as noted by the response of systems to time histories with large early pulses such as the Pacoima Dam record.

3. Scatter in calculated equivalent viscous damping *does not* translate into proportional scatter in calculation of maximum response displacements.

4. In order to confidently utilize the concept of equivalent viscous damping for simplified performance-based earthquake engineering design procedures, further studies are needed to identify any limitations, and better determine the expected scatter in results. If nothing else, such a study will result in increased confidence in the approach based on the knowledge gained regarding its behavior.

REFERENCES

Carr A.J. (1998) *Ruaumoko Users Manual*. University of Canterbury, Christchurch, New Zealand.

EuroCode 8 (1988) ‘Structures in seismic regions - Design’ Part 1, General and Building. May 1988 Edition, *Report EUR 8849 EN*, Commission of the European Communities.

International Conference of Building Officials (1997), *1997 Uniform Building Code, Vol. 2*, 1997.

Kowalsky M.J. (2000). "Deformation Limit States and Implications on Design of Circular RC Bridge Columns", *ASCE Journal of Structural Engineering*, V126#8 pp. 869-878, August.

Priestley M.J.N. and Kowalsky M.J. (2000). "Direct Displacement-Based Seismic Design of Concrete Buildings", *Bulletin of the New Zealand National Society for Earthquake Engineering*, V33#4 pp. 421-444, December.

Takeda T., Sozen M., and Nielsen N. (1970). 'Reinforced Concrete Response to Simulated Earthquakes', *Journal of the Structural Division, ASCE,* 96(12) pp. 2557-2583.

Jacobsen L.S. (1930). "Steady Forced Vibrations as Influenced by Damping." *ASME Transactione,* 52(1), pp. 169-181

Jennings P.C. (1968). 'Equivalent Viscous Damping for Yielding Structures' *Journal of the Engineering Mechanics Division, ASCE,* 90(2) pp. 103-116.

Iwan W.D, Gates N.C. (1979). 'The Effective Period and Damping of a Class of Hysteretic Structures', *Earthquake Engineering and Structural Dynamics,* V. 7, pp. 199-211.

Gulkan P. and Sozen M. (1974). 'Inelastic Response of Reinforced Concrete Structures to Earthquake Motions', *ACI Journal*, V. 71, pp. 604-610, December 1974.

Bonacci J.F. (1994). 'Design Forces for Drift and Damage Control: A Second Look at the Substitute Structure Approach', *Earthquake Spectra*, pp. 319-331.

Ayers J.P. (2000). *Evaluation of Parameters for Limit-States Design of Masonry Walls,* M.S. Thesis, North Carolina State University, July, 2000

Loeding, S., Kowalsky, M.J., Priestley, M.J.N. (1998) *Direct Displacement-Based Design of Reinforced Concrete Building Frames.* Report #SSRP-98-08, University of California, San Diego.

KEYWORDS

Displacement-based design, equivalent viscous damping, effective stiffness.

SESSION A-4: DESIGN METHODOLOGY

Chaired by

♦ Eduardo Miranda and K. C. Tsai ♦

STRUCTURAL DEMAND SPECTRA BASED ON LIFE CYCLE ECONOMIC LOSS OF BUILDING STRUCTURES IN HIGH SEISMIC ZONE

Hitoshi SHIOHARA[1], Noriyuki TAKAHASHI[2], and Shunsuke OTANI[3]

ABSTRACT

In high seismic zones, the repairing cost of structural damage for the maintenance of buildings is more important because the cost due to moderate to major earthquake may increase the life cycle cost of the building. This paper reports the result of a study on the structural demand based on the life cycle loss and the on the effect of a repairing cost model; relation between the damage to repairing cost, on the life cycle economic loss. Buildings are modeled as single-degree-of-freedom systems with non-linear hysteresis model subjected to multiple earthquake record expected in their life cycle duration. The total repairing costs for maintain the functionality of the building were calculated using the models. Four models are arbitrarily chosen for representation of relation between the damage and repairing cost, considering the nonlinearity in the relation. Calculated results are compared in terms of the expected total economic loss, which are function of strength and ductility capacity of the structural system and length of life cycle. It is revealed how the expected total economic loss and the life cycle length effect on the structural demand It is also revealed that the total life cycle economic loss is sensitive to the repairing cost modelling. If the damage increase in earlier stage of damage, the expected life cycle economic loss become larger.

1. INTRODUCTION

One of the most important features of the performance-based earthquake engineering for building structure is that it offers selection from multiple performance objectives. The FEMA-273 document (FEMA 1997) is a milestone in the development of a performance-based earthquake engineering of building structure. It has three discrete levels of performance objectives for rehabilitation; basic safety, enhanced rehabilitation, and limited rehabilitation. To define the performance level for protecting the loss of private properties due to the damage of a building, the FEMA-273 adopts rather simple method. It is to incorporate new limit states for damage control named “immediate occupancy performance level.” The performance level is defined qualitatively

1. *Department of Architecture, Graduate School of Engineering, The University of Tokyo, Tokyo, Japan*
Email: shiohara@arch.t.u-tokyo.ac.jp
2. *Department of Architecture, Graduate School of Engineering, The University of Tokyo, Tokyo, Japan*
Email: Noriyuki.Takahashi@rcs.arch.t.u-tokyo.ac.jp
3. *Department of Architecture, Graduate School of Engineering, The University of Tokyo, Tokyo, Japan*
Email: otani@arch.t.u-tokyo.ac.jp

by a set of description of damage to building elements. So building are required to be verified by an analytical procedures that it meets the definition of performance level under specified medium seismic action.

However, the definition of the “immediate occupancy performance level” is very conceptual and abstract. Particularly, the wide gap between immediate occupancy performance level and the “operational performance level” is hard to quantify. Damage level to real buildings is not easily quantified like a damage of each building element. Because a real building is complicated system consisting of several hundreds of members and the damage to each member differs in location and severity.

An alternative method to quantify the damage to building, is to estimate damage in terms of economic loss, or to estimate expected value of repairing cost of a building. The economic loss is the cost required to repair and restore the original functionality of the building. In other words, economic loss is a kind of weighted sum of damage in a building. So it may be used as an quantitative representation of the capability to protect building functions and the properties from earthquake. Cost is meaningful enough to building owners as well as to public. In particular, insurance industry, corporate administrator and policy makers of local government need this type of information to prepare for the expenditure. In addition to that, this method is better than the first one because the reliability of the evaluation method is verifiable through assessments of actual damage in buildings and repairing work after an earthquakes.

In this paper, a concept of “expected value of annual repairing cost” is introduced as an convenient indicator of the performance of a building protecting from property loss based on the concept of the economic loss. Then simple application of the “expected value of annual repairing cost” is demonstrated. A concept of “structural demand spectra” is proposed based on life cycle economic loss. The effects of the model of relation between structural damage to repairing cost on structural demand spectra are investigated. These indicators are useful to inform the building owners the performance of the buildings in advance in terms of cost for repair works expected in the life length of a building. It significantly helps them to decide the detail of building structural system, material, which will meets their precise requirement and develop their attitude to understand the performance of building.

2. EXPECTED VALUE OF ANNUAL REPAIRING COST

In evaluating the total economic loss of a building constructed in an area with high seismic hazard, evaluation of damage due to medium to major earthquakes is not negligible, because it is probable that building suffers many earthquakes in its life length. To estimate the seismic performance of a building through its life length, "Expected value of Annual Repairing Cost (EARC)" is a good measurement to evaluate the damage control performance. EARC (unit: currency / year) is defined as a total repairing cost of a building expected in its life length, divided by the life length in year. In order to estimate the total cost, models such as (a) a model for earthquake history in the life length, (b) models for simulating non-linear structural response, (c) model for relating the structural response to damage to the component of the building, and (d) model for relating the damage of the component to repairing cost according to the properties of the building element, are necessary.

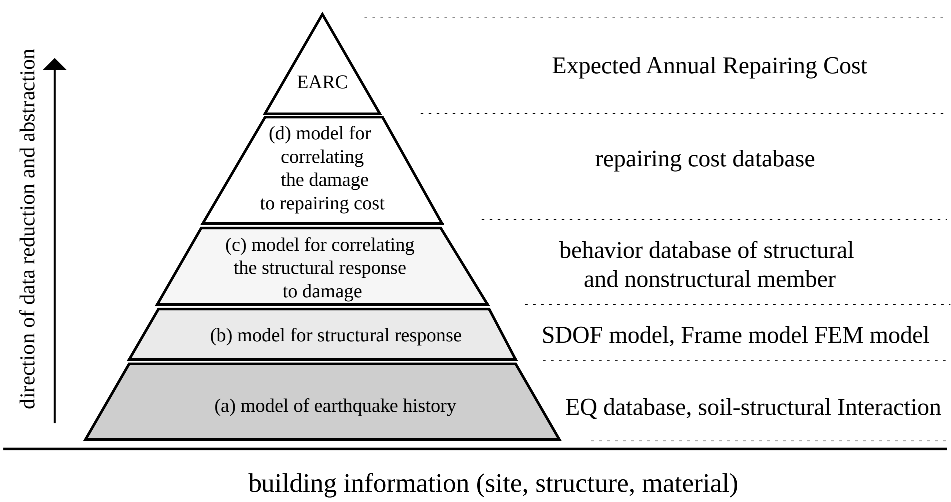

Figure 1: Layered expression of models for the process of estimation of the life cycle cost

To depict the whole set of the scheme, layered expression is effective as shown in Fig. 1. The EARC is estimated by the process from the bottom to the top. The procedure depends on many existing analytical tools and knowledge database. These tools and database are classified into several groups. Each layer is defined as a set of models substituted with each other. For an example, the layer of the models for structural response estimation varied from a simple single-degree-of-freedom model to complicated nonlinear frame analysis model. Currently, the models for structural response or models for earthquake history are implemented precisely owing to the modern development of non-linear structural analysis and seismology. However the development of models for relating structural damage to structural response, or the models relating structural damage to repairing cost are not enough. The development of the latter models is important in future.

In this study, the investigation is focused on the effect of the modelling of the fourth layer, (d) models for correlating the damage to repairing cost on the EARC using simple models for the other layer.

3. PROCEDURE TO EVALUATE ANNUAL REPAIRING COST

3.1 Input Ground Motion

To evaluate life cycle damage, a life cycle history of input ground motion is necessary. However it is not feasible to obtain exact time histories of earthquake record including multiple events in the life time length of a particular building. In this study, the following simplified method is used to synthesize an earthquake input from information available currently.

Based on the theory of probability, several types of functions applicable to evaluate expected extreme value of peak base velocity due to earthquake are proposed in the “Recommendations for Loads on Buildings” by AIJ (AIJ 1993) for different areas in Japan. One of the functions, which considers the upper and lower limits of the probability (Dan and Kanda 1986), is used to determine the target base velocities for a building in Tokyo. A series of values of peak velocity is created such that it fits the probabilistic function. The sequence of earthquake is rearranged in random order. This series of peak velocity is used as a target to modify a existing base accelerogram.

3.2 Accelerogram for non-linear response analysis

To simulate non-linear responses of a structural system, time history of base acceleration is necessary. Four accelerogram of Kobe 1995 (NS), El Centro 1940(NS), Hachinohe 1968(EW), and Tohoku Univ. 1978 (NS), are used in this study. A common time history are used for all event. It is factored such that peak ground velocity matched to the target peak velocity.

3.3 Model for Structural Response

A single-degree-of-freedom system representing a reinforced concrete building structure is used for the prediction of a displacement response time history. Responses are calculated by step-by-step integration of the equation of motion using a computer software “SDF” (Otani 1981). Tri-linear backbone curve and Takeda hysteresis model (Takeda et al. 1970) are used. Viscous damping proportional to instantaneous stiffness is assumed to be 2%. The cracking strength is assumed to be one fourth of yielding strength and the secant stiffness at yielding point was assumed to be one fourth of the linearly elastic stiffness. The period of the building based on the secant stiffness at yielding point is assumed to be 0.3 sec. These common properties are used for all cases reported in this study.

3.4 Model for Damage Accumulation

The process of the accumulation of the damage due to consecutive multiple events are not usually considered in evaluation of structural damage. However, damage such as a hysteretic fatigue of steel dissipating energy are not repaired completely. These types of damage makes it complicated to evaluate the life cycle repairability at a design stage. Thus repairing cost is evaluated considering the accumulation of damage. Park et al. (Park et al. 1985) proposed a damage model in which dissipation of hysteretic energy is considered as follows,

$$D = \frac{\delta_M}{\delta_u} + \frac{\beta}{Q_y \delta_u} \int dE \tag{1}$$

where, D: damage index, δ_M: maximum response under an earthquake event, δ_u: ultimate displacement under monotonic loading, Q_y: yield point strength, β: non-negative parameter to explain the failure of structural member subjected to cyclic loading, dE: incremental absorbed hysteretic energy. By the definition, damage index D of unity means a collapse. As Park suggested the constant value β of 0.05 showed good correlation to failure in structural tests of reinforced concrete member, so value of 0.05 is used for β value in this study. The post yield stiffness is assumed zero. Yield strength Q_y of the system and ultimate deformation δ_u were chosen as parameters.

3.5 Assumption on Repairing Policy

The first term of the damage index D defined in the Eq. 1 is related to the maximum attained displacement response. So it is assumed that this damage is reparable immediately, whereas the second term of the Eq. 1 is assumed that damage accumulates and is not reparable by repairing work except through an exchange of structural component with new one.

Thus, the assumption on repairing policy is summarized as follows. The damage represented by the first term in Eq. (1) is assumed to be repaired after an earthquake event in which the displacement exceeds the yielding point displacement. The stiffness is also recovered to linearly elastic one. If maximum response displacement is smaller than yielding point displacement, it is left unrepaired and residual degradation of stiffness remains. Hereafter, the repaired damage represented by the first term is denote Repaired Damage index D_R. As the number of earthquake events increase, the accumulated damage represented by the second term in Eq. (2) increases. If the value of damage index D exceeds unity, then the structure is totally replaced and full repair cost is added but the accumulation of damage is cancelled to zero.

3.6 Modelling of Relation between Repaired Damage Index D_R to Repairing Cost R

Four different types of monotonically increasing functions shown in Fig. 2 are used to model the relation between the damage repair index D_R and the repairing cost index R. Hereafter, the model is called “repairing cost model” in this paper. The repairing cost index R is a normalized cost by the cost for replacing building components with new one. If D_R is smaller than damage index $1/\mu$, corresponding to the yielding point, the repair cost index is zero. Once the value of D_R exceeds the $1/\mu$, the repair cost index is assumed to be calculated using one of the monotonically increasing functions as shown in Fig. 2. When the damage index D_R exceeds unity, the repairing cost index is assumed to be 1. Thus a convex curve (a) in Fig. 2 is represented by Eq. 2.

$$R = -\left(\frac{1-D_R}{1-\alpha}\right)^3 + 1 \qquad (\alpha < D_R < 1) \tag{2}$$

where, α denotes $(1/\mu)$ and μ is the ductility capacity of a SDOF system. This type of repairing cost increase immediately provided maximum displacement response exceeds the yielding point displacement. This type of curve for repairing cost may be suitable for the evaluation of repairing cost of non ductile components such as captive column which is vulnerable to brittle shear failure.

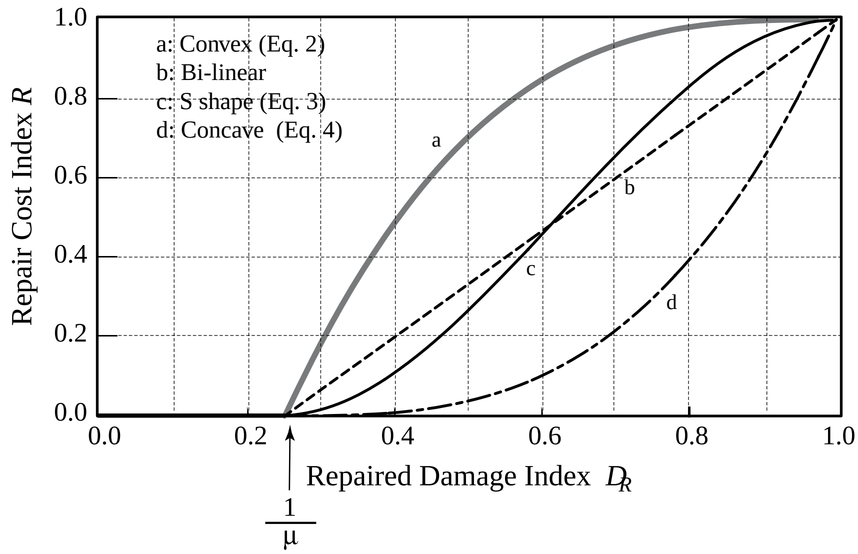

Figure 2: Repairing cost models

The bi-linear curve (b) in Fig. 2 is the simplest model which assume that the repairing cost R is linearly proportional to repairing damage index D_R, except the repairing cost remain zero as far as maximum displacement smaller than yield displacement.

The S-shape curve (c) in Fig. 2 is expressed by Eq. 3 The curve lies between the convex curve given by Eq. 2 and the concave curve given by Eq. 4

$$R = -\left(\frac{D_R - \alpha}{1 - \alpha}\right)^4 \left\{\frac{4}{3}\left(\frac{1 - D_R}{1 - \alpha}\right) + 1\right\}^3 \qquad (\alpha < D_R < 1) \qquad (3)$$

The concave curve (d) is represented by Eq. 4.

$$R = \left(\frac{D_R - \alpha}{\alpha - 1}\right)^3 + 1 \qquad (\alpha < D_R < 1) \qquad (4)$$

This curve may represent a characteristics of damage which increased rapidly just before it reach to the ultimate ductility.

3.7 Expected Value of Annual Repairing Cost Index

Finally, the total repair cost index is calculated as a sum total of the required repairing cost R through the life cycle of the building. Expected value of Annual Repair Cost Index (EARCI) is defined as the total repair cost index divided by life length of a building in year. EARCI is evaluated with respect to four cases; or 50, 100, 200, and 400 life cycle length in this study. To see the effects of the different earthquake record, four different base acceleration records are used. In each combination of life cycle length and acceleration record, non-linear responses of non-linear SDOF system are calculated and EARCI are obtained with respect to the cases with yield point strength divided by weight of the SDOF system Q_y of 0.05 to 0.65, and ductility capacity μ of 2 to 12.

3.8 EARCI Contour and Structural Demand Spectra

Contour lines of equal EARCI values are plotted on a coordinate system, with vertical axis of base yield point strength divided by the weight of SDOF system Q_y and the horizontal axis of ductility capacity μ in Fig. 3. The contour lines are obtained by an interpolation of the EARCI values at grid point., the bi-linear cost curve (b) is used in all cases to estimate repairing cost from damage index D_R, to obtained the results in Fig. 3. The contour lines for equal EARCI value represent the structural demand to achieve constant life cycle economic loss. Hence the EARCI line is regarded as structural demand spectra based on life cycle economic loss.

As shown in Fig. 3, when the life cycle length is shorter or when the EARCI is larger, the contour lines becomes flat. It means that, when the building life cycle length is shorter, good ductility capacity will not contribute to reduce the repair cost. On the other hand, when the building life cycle time is long, good ductility will be contribute to reduce the repairing cost. This property can be also applicable to every case using four different accelerogram. If the life cycle length is common, EARCI calculated by different accelerogram seem to have little difference.

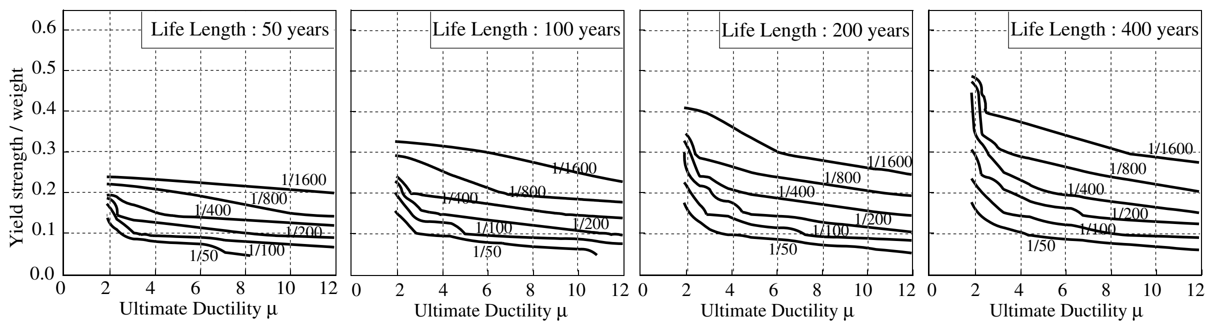

(a) Kobe1995 (NS)

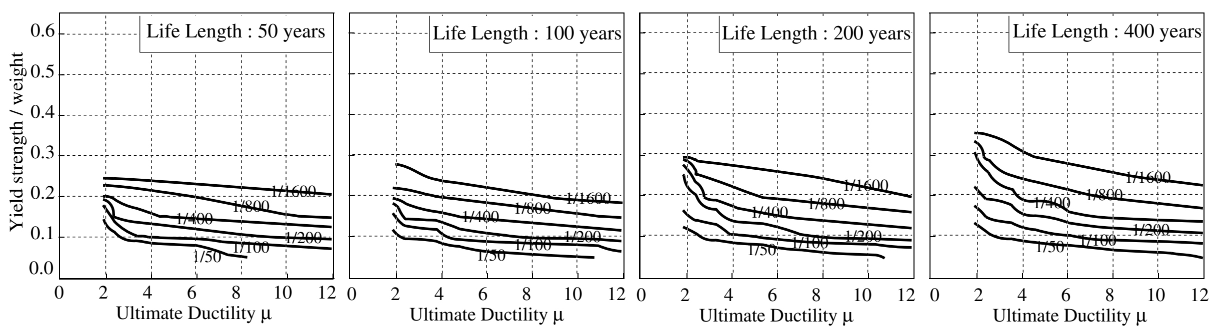

(b) El Centro1940 (NS)

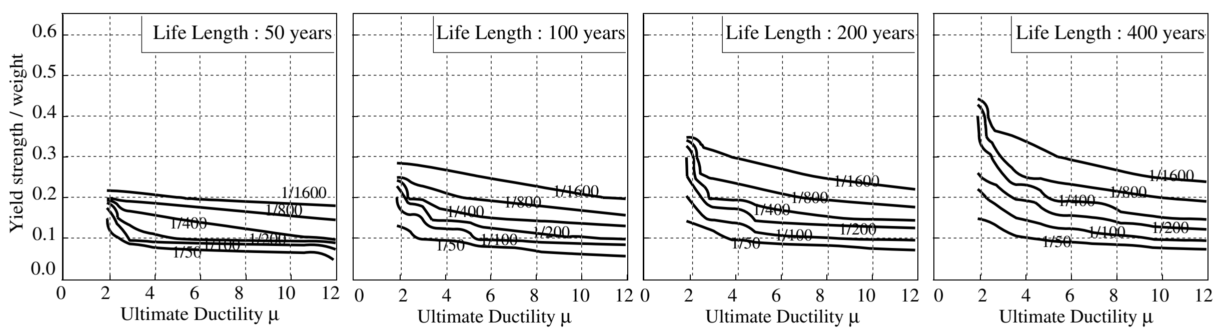

(c) Hachinohe 1968 (EW)

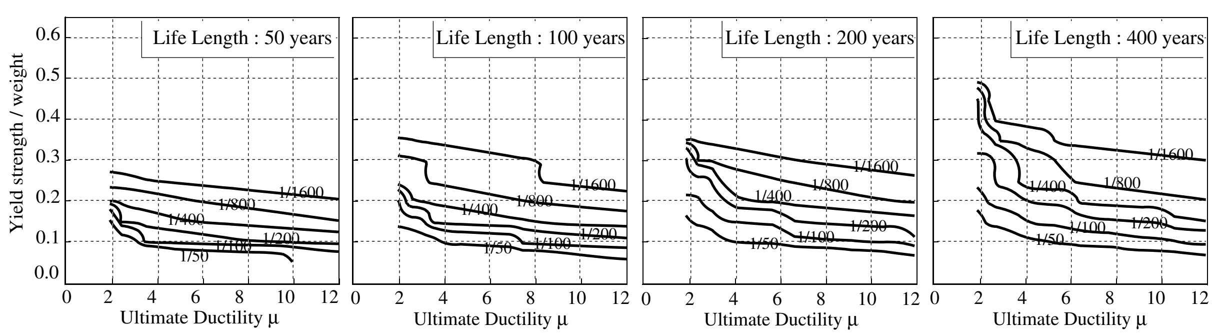

(d) Tohoku Univ.1978 (NS)

Figure 3: Structural demand spectra for equal EARCI

4. STRUCTURAL DEMAND SPECTRA DETERMINED FROM EARCI

Building should satisfy the mandate requirement of safety. The structural demand on strength and ductility determined by minimum requirement of seismic safety is compared with the structural demand determined by EARCI requirement.

In Fig. 4, EARCI contour lines for four life cycle length, 50, 100, 200 and 400 years are plotted for the Kobe 1995 (NS) records calculated using bi-linear repairing cost model (b). The structural demand for seismic safety is estimated using equal energy criterion. The maximum response of linearly-elastic response is calculated using the maximum target accelerogram with in each life cycle length and the maximum base shear coefficient Q_L is used to derive the relation between maximum ductility response μ and yielding base shear coefficient Q_Y using the Eq. 6.

$$Q_Y = \frac{1}{\sqrt{2\mu - 1}} Q_L \tag{5}$$

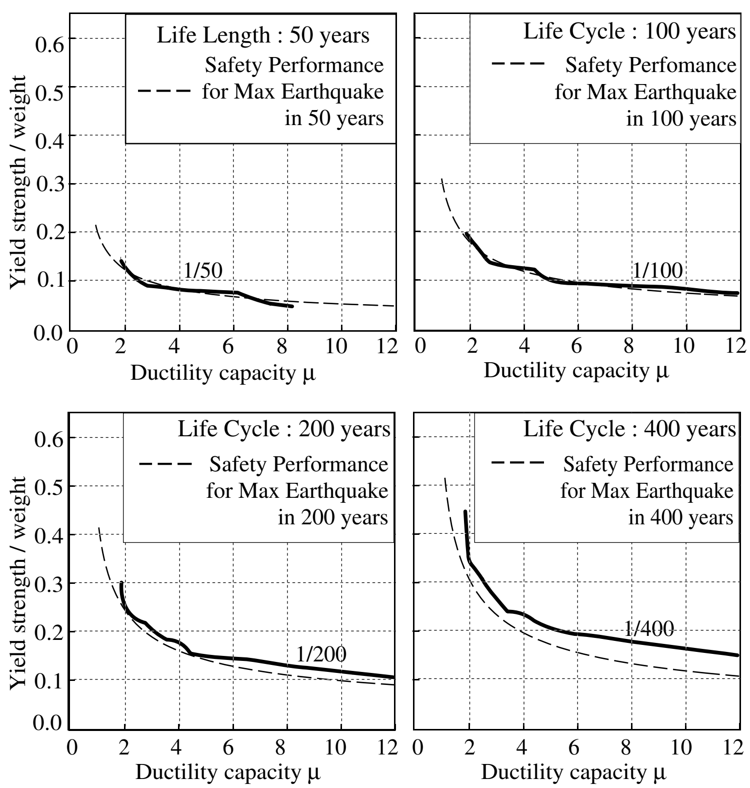

Figure 4: Comparison of structural demand spectra by life safety and EARCI

The dashed line in Fig.4 shows the structural demand by seismic safety requirement of buildings. It is observed that seismic safety requirement agree well with the requirement from the structural demand corresponding to the total repairing cost in life length is unity, or the EARCI is one *n*-th, where *n* is the life length of the building, provided the life length is shorter than 200 years. On the contrary, life cycle length increase, the continuous line lies above the dashed line, which means that structural demand from EARCI requirement is larger in this particular case. By using the EARCI, the cost effectiveness of the modification of structural components is clearly quantified.

5. STRUCTURAL DEMAND SPECTRA AND REPAIRING COST MODEL

Fig.5 shows the contour lines of the equal EARCI to compare the effect of the for repairing cost models. All the values of EARCI in Fig. 5 are calculated for life cycle length of 400 years. The solid continuos lines are the contour line of EARCI of 1/1200 and 1/2400. The dashed line is structural demand from the safety requirement according to the energy criteria represented by Eq. 6, assuming maximum base shear coefficient of linearly elastic system is 1.0, which is comparable to the standard minimum safety requirement of the Building Standard Law Cabinet Order of Japan.

As shown in Fig. 5, the structural demand from EARCI requirement is very sensitive to the model of repairing cost model. The structural demand calculated using convex curve by Eq. (2), is quite larger than the structural demand due to safety requirement as shown in Fig. 5(a), On the contrary, the concave curve gave much lower structural demand as shown in Fig. 5(d), The demand curves for EARCI calculated using bi-linear or S shape model gave intermediate results. It is also noted that from Fig. 5 that the concave curve (d) gave small difference for different EARCI of 1/1200 and 1/2400 and required yield strength is almost same for the ductile buildings, or structure with large ductility capacity μ. Therefore, it may be very effective for obtain good performance in terms of EARCI to number of the structural element with repairing cost model represented by the convex curve represented by Eq. 2.

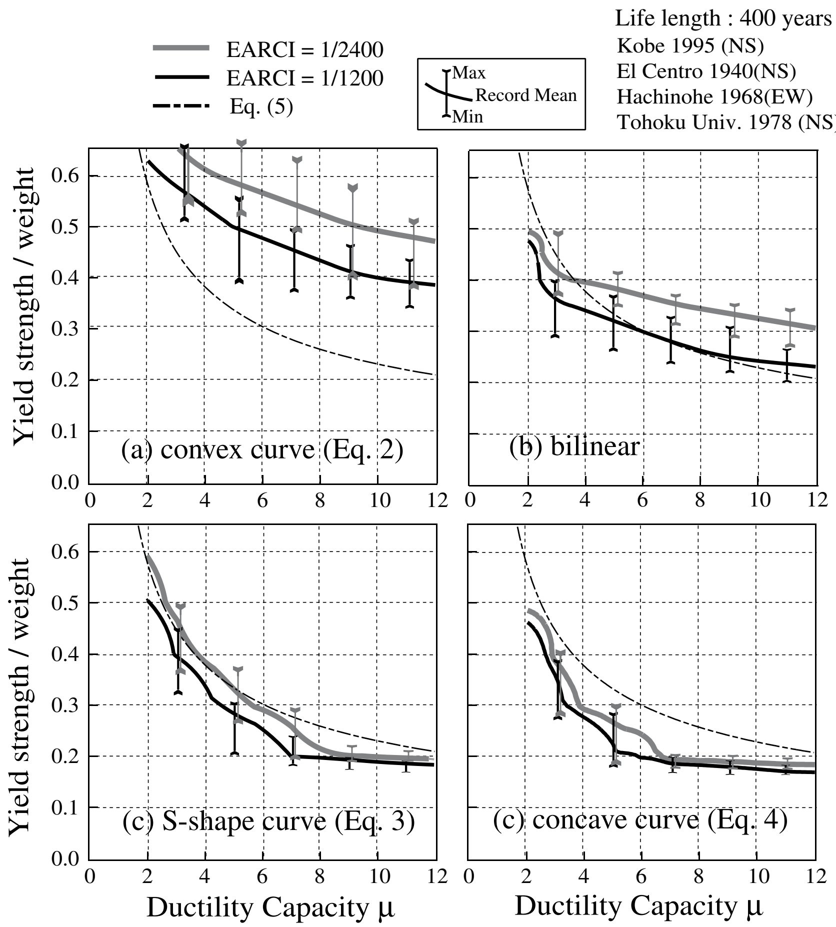

Figure 5: Structural demand spectra based on different repairing cost models

6. CONCLUDING REMARKS

To estimate the seismic performance of a building through its life cycle, "Expected value of Annual Repairing Cost Index (EARCI)" was proposed as a measurement to evaluate the damage control performance. The procedure to calculate the EARC (unit: currency / year) was demonstrated by a very simple example. The concept of structural demand spectra based on life cycle economic loss was proposed. The structural demand spectra determined from the constant EARCI value was compared with the structural demand imposed by minimum requirement of safety. Using the simple procedure, the effects of the repairing cost model, a model to represent the relation between damage and repairing cost, on the EARCI was investigated. It is revealed that the structural demand determined by a specified EARCI is very sensitive to the repairing cost model.

The repairing cost model with non ductile elements require higher structural demand in particular to the system with low strength and high ductility.

7. REFERENCES

AIJ (1993):*Recommendations for Loads on Buildings* (*Second Revision*), Architectural Institute of Japan, Tokyo, Japan, 1993. (in Japanese)

DAN, K. and KANDA, J.,: Analysis of Earthquake Hazard using Distribution of Extreme Value with upper and lower Bound, Journal of Structural Engineering, Architectural Institute of Japan, Vol. 363, 1986. pp. 50-60. (in Japanese)

FEMA-273 (1997):*NEHRP Guidelines for the Seismic Rehabilitation of Buildings*, FEMA, Washington, D. C., USA, October 1997.

Otani, S. (1981), Hysteresis Model of Reinforced Concrete for Earthquake Response Analysis, Journal, Faculty of Engineering, University of Tokyo, Series B, Vol. XXXVI-II, No. 2, September 1981, pp. 407-441.

Park. Y. J. and Ang A. M. S., (1985), Mechanistic Seismic Damage Model of Reinforced Concrete, Journal of Structural Engineering, ASCE, Vol. 111, No. 1, 1985, pp. 722-739.

Shiohara, H., (1999):Life cycle Economic Loss Estimation of R/C Frame Structure Subjected to Multiple Earthquake Load Sequences, PEER Report 1999/10, University of California, Berkeley, pp. 161-173.

Takeda, T., M. A. Sozen, and N. N. Nielsen, (1970), Reinforced concrete response to simulated earthquakes, Journal, Structural Division, ASCE, Vol. 96, No. ST 12, 2557 - 2573.

METHODOLOGY AND SIMULATION MODELS FOR PERFORMANCE-BASED EARTHQUAKE ENGINEERING

Gregory G. DEIERLEIN[1] and Rohit KAUL[1]

ABSTRACT

Efforts underway to develop and implement computer simulation tools for performance-based earthquake engineering are presented. Part of a broader effort within the Pacific Earthquake Engineering Research center to develop enabling technologies for performance-based engineering, the response simulation tools provide the means to calculate engineering demand parameters and damage measures for performance assessment. Generalized hinge models provide one means of simulating the nonlinear response of reinforced-concrete beam columns, including strength and stiffness degradation under the combined effects of axial load, moment, and shear. The models are sufficiently robust to capture nonlinear response up to collapse, yet practical for simulation of large structures. Aspects of developing and implementing these models in an object framework are summarized.

OVERVIEW OF PBEE METHODOLOGY

Performance-Based Earthquake Engineering (PBEE) seeks to improve seismic risk decision-making through assessment and design methods that are more transparent, scientific, and informative to stakeholders than current prescriptive approaches. A key feature of PBEE is the definition of performance metrics that are relevant to decision making for seismic risk mitigation. Ideally, these metrics would be based on probabilistic estimates of losses due to earthquakes, including direct dollar losses (repair and restoration costs), loss in functionality (or downtime), and casualties.

One way to characterize PBEE is through the idealized "pushover curve" shown in Fig. 1. Typically plotted in terms of earthquake-induced base shear (vertical axis) and interstory drift (horizontal axis), the static pushover concept can be generalized to imply earthquake input intensity (on the vertical axis) and the resulting performance-metrics (on the horizontal axes). Structural engineers have traditionally calculated "performance" in terms of fairly narrow definitions described by simple response parameters such as structural deformations (e.g., interstory-drift, inelastic hinge rotations) and forces; but the goal of PBEE is to expand this interpretation to more direct performance metrics. The first generation of PBEE assessment procedures, such as FEMA 273 (1997), have attempted to relate structural response indices (interstory drifts, inelastic member deformations and member forces) to more performance-oriented descriptions such as Immediate Occupancy (IO), Life Safety (LS) and Collapse

[1] Dept. of Civil & Envr. Engrg., Stanford Univ., Stanford, CA 94306 (E-mail: ggd@stanford.edu)

Prevention (CP). However, the relationship between the structural indices and performance measures are approximate, determined in large part by calibration to expectations of performance provided by current building code provisions. The challenge remains to develop explicit methodologies to make more direct linkages between engineering response parameters (e.g., drift) and performance metrics (dollar loss, casualty rate, and downtime).

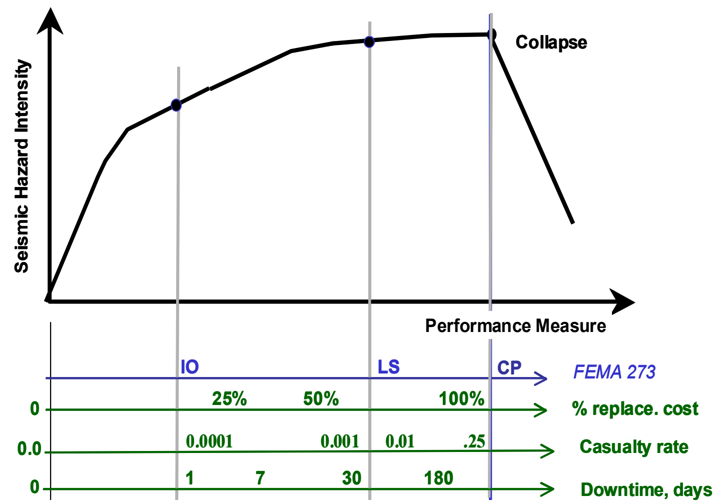

Figure 1. Idealized Pushover Representation of PBEE

Shown in Fig. 2 are the main parameters in a step-by-step PBEE assessment process under development in the Pacific Earthquake Engineering Research (PEER) center. The process begins with definition of a ground motion *Intensity Measure*, which defines in a probabilistic sense the salient features of the ground motion hazard that affect structural response. Today in the U.S., *Intensity Measures* are commonly defined by single parameter variables, e.g., peak ground acceleration/velocity or spectral acceleration/velocity, but work is underway in PEER and other organizations to look for improved *Intensity Measures* that correlate better with the resulting damage. Resulting measures could likely include multiple ground motion parameters, such as spectral acceleration coupled with duration. The next term, *Engineering Demand Parameters*, describe structural response in terms of deformations, accelerations, or other response quantities calculated by simulation of the building to the input ground motions. In cases where ground deformations or ground failures affect the response, the *Engineering Demand Parameters* would also include engineering indices of ground response. *Engineering Demand Parameters* are next related to *Damage Measures*, which describe the condition of the structure and its components.

A key consideration in defining the *Damage Measures* is to focus on the consequences of the damage. *Damage Measures* may include, for example, descriptions of the necessary repairs to structural and non-structural components associated with a calculated peak interstory drift or inelastic component deformation. *Damage Measures* would also describe potential life-safety implications of the damage associate with falling hazards, fire, blocked egress, etc. Finally, given a detailed probabilistic description of damage, the PBEE process culminates with the calculation of *Decision Variables*, which translate the damage into quantities that feed into risk management decisions. *Decision Variables* are described in terms of metrics

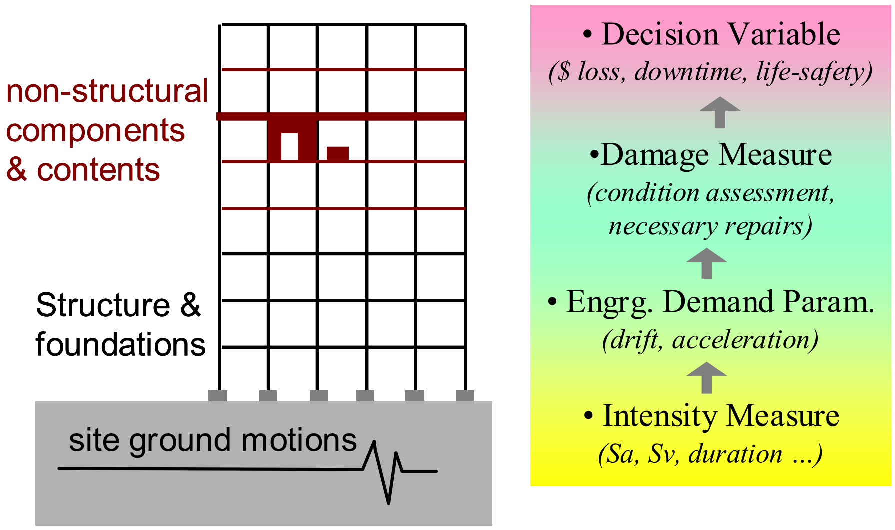

Figure 2. PBEE Assessment Variables

that describe direct dollar losses (repair, reconstruction, lost contents), facility downtime, and potential casualties.

OPENSEES – SIMULATION PLATFORM

Recognizing the central role of nonlinear simulation in structural performance assessment, PEER is developing a new software framework called *OpenSees* (*O*pen *S*ystem for *E*arthquake *E*ngineering *S*imulation), which utilizes modern computational, database, and information technologies. Developed in with a modular object oriented programming architecture, one of the central aims of *OpenSees* is to facilitate the integration of structural, geotechnical, non-structural component, and earthquake hazard/reliability models into a common platform. Through linkages to experimental databases and visualization tools, another goal is to relate quantitative *Engineering Demand Parameters* to more subjective *Damage Measures* and *Decision Variables*. For further details on *OpenSees* and information on obtaining source and executable codes, the reader is referred to the *OpenSees* website (http://opensees.berkeley.edu). The generalized-hinge element described in the next section provides an example of an implementation developed to fully utilize the object-oriented aspects afforded by the *OpenSees* architecture.

GENERALIZED HINGE BEAM-COLUMN MODEL

The PBEE methodology envisioned previously requires structural response models that accurately simulate structural response and track damage up through the onset of structural collapse. One type of beam-column element that the authors have developed and implemented in *OpenSees* is based on a stress-resultant plasticity formulation, which employs an axial-force moment interaction surface with inelastic hardening/softening models to capture stiffness and strength degradation. Local damage indices are defined to provide the basis to calibrate degradation parameters to test data. Work is on going to extend the formulation to incorporate shear effects, including moment, shear and axial strength degradation. Summarized below are the following aspects of this element: (a) essence of large deformation aspects of the formulation, (b) generalized hinge (concentrated plasticity) formulation of the beam-column element, (c) hardening/softening models, and (d) damage indices and hysteretic behavior. Details of the object oriented implementation in OpenSees are then described.

Large Deformations

Large deformation response is incorporated in the beam-column through an updated Lagrangian formulation, applied in the context of conventional beam-column assumptions (e.g., small strains, plane sections remain plane, etc.). The fundamental difference between this formulation and the conventional linear derivation, is in the nonlinear strain-displacement relationship defined by the following Lagrange strain, *e*,

$$e = \frac{du}{dx} + \frac{1}{2}\left[\left(\frac{du}{dx}\right)^2 + \left(\frac{dv}{dx}\right)^2\right] \tag{1}$$

where *u* and *v* are the axial and transverse member displacements measured with respect to the element coordinate axes. When applied in the standard stress-resultant form of the virtual work equation for a straight prismatic beam-column, the nonlinear terms in Eq. 1 lead to the following integrals in the virtual work equation,

$$\int_0^L P_x\left(d\delta u / dx\right)dx + \int_0^L M_z(d^2\delta v / dx^2)dx - \{\delta\Delta\}^T\{F\} = 0 \tag{2}$$

where P_x is the axial force, M_z is the bending moment, L is the member length, and F is the vector of element end forces resulting from the finite incremental displacements, u and v. When integrated and terms higher than second-order are eliminated, Eq. (2) leads to the following geometric stiffness matrix, K_g,

$$\left[K_g\right]\{\Delta\} = \begin{bmatrix} P/L & V/L & 0 & -P/L & -V/L & 0 \\ & 6P/5L & P/10 & -V/L & -6P/5L & P/10 \\ & & 2PL/15 & 0 & -P/10 & -PL/30 \\ & & & P/L & V/L & 0 \\ & Sym. & & & 6P/5L & -P/10 \\ & & & & & 2PL/15 \end{bmatrix} \begin{Bmatrix} u_i \\ v_i \\ \theta_i \\ u_j \\ v_j \\ \theta_j \end{Bmatrix} \tag{3}$$

where P and V are the axial and shear forces present in the element, and L is the member length. In an incremental/iterative analysis, K_g is combined with the elastic (K_e) or elastic-plastic (K_{ep}) matrix to form the total element stiffness matrix at the current equilibrium state. For calculating a displacement increment $\{d\Delta\}$ from a current converged state, with displacements measured with respect to that state, the incremental static equilibrium equation is $\{dF\} = [K_{ep} + K_g]\{d\Delta\}$.

One of the important challenges in a large-displacement analysis is the consistent recovery of element forces at the end of each displacement increment. As part of our research we investigated several methods and found that one, referred to as the "natural deformation" approach, to be the most accurate. In this approach the incremental vector of element end forces is calculated based on the natural displacement increments $\{d\Delta_n\}$, which (referring to Fig. 3) are the incremental deformations from configuration 1 to 2, measured with respect to the chord in configuration 2. The natural deformation increment $\{d\Delta_n\}$ differs from the total displacement increment $\{d\Delta\}$ in that it does not include the rigid body motion. Equations to calculate natural from total displacements are given by McGuire et al. (2001) and other texts on nonlinear analysis. Using the natural deformations, the force increment going from configuration 1 to 2 (Fig. 3) is given by $\{dF\} = [K_{ep} + K_g]\{d\Delta_n\}$, and the total resulting force in the current configuration 2 is simply the sum of the initial and incremental force, $\{^2F\} = \{^1F\} + \{dF\}$. Note that in the context of an inelastic analysis, the resulting force $\{^2F\}$ is still subject to plasticity corrections, as described in the next section.

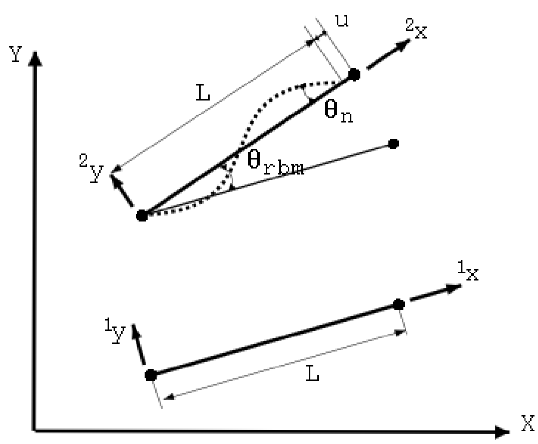

Figure 3. Element displacements

Rigid-Plastic Hinge Analysis

Formulation of the element with a generalized plastic hinge assumes that plastic zones are restricted to the element ends. The condition of plastic loading is determined from a yield criterion (or yield surface, *YS*), calculated as a function of the normalized member end forces, e.g., as shown in Fig. 4, for axial load and moment, $YS = fcn\,(P/P_n, M/M_n)$. Total member end deflections are distinguished between elastic and plastic, $\{d\Delta\}=\{d\Delta_e\}+\{d\Delta_p\}$, where the incremental member forces are related to either elastic or total deformations by the elastic or elastic-plastic tangent stiffness, respectively, i.e.,

$$\{dF\} = [K_e]\{d\Delta_e\} = [K_{ep}]\{d\Delta\} \qquad (4)$$

Assuming the normality criterion, plastic deformations are given as, $\{d\Delta_p\} = \lambda_p \{G\}$, where $\{G\}$ is the gradient to the yield

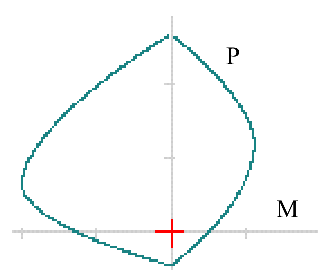

Figure 4. P-M yield surface for unsymmetric RC Section

surface and λ_p is a plastic deformation magnitude, related to the total displacement increment by the following,

$$\lambda_p=[\{G^T\}([K_e] + [K_h])\{G\}]^{-1}\{G^T\}[K_e]\ \{d\Delta\} \qquad (5)$$

The matrix $[K_h]$ is comprised of inelastic hardening/softening coefficients, which are determined through kinematic and/or isotropic manipulations of the yield surface. The hardening/softening results in the following force increment, which is a function of the plastic displacement, i.e.,

$$\{dF^*\} = [K_h]\{d\Delta p\} = [K_h]\{G\}\{\lambda_p\} \qquad (6)$$

Combining the above expressions and relationships, the elastic-plastic tangent stiffness is given by the following,

$$[K_{ep}] = [K_e] - [K_e]\{G\}\ [\{G^T\}([K_e] + [K_h])\{G\}]^{-1}\{G^T\}[K_e] \qquad (7)$$

This equation provides an inelastic tangent stiffness for the incremental loading step, which is a function of the elastic stiffness $[K_e]$, the hardening stiffness $[K_h]$, and the current yield surface gradients {G} based on the normalized forces at each end of the member.

Inelastic Force Recovery

The previous discussion dealt with a derivation of a consistent stiffness matrix for an element that is plastically loading. A second, and more important part of the inelastic solution (particularly for elements with softening), is the accurate recovery of element forces for a specified displacement increment. Summarized below are the major steps and considerations in this process, described in the context of one step from an incremental/iterative analysis.

Step 1 (trial incremental force): Given the incremental element displacement $\{d\Delta\}$, trial element forces are first computed, where the incremental force is calculated assuming elastic loading as $\{dF\} = [[K_e]+ [K_g]]\{d\Delta\}$. The resulting trial force point, equal to the sum of the previous equilibrium force point and the incremental force ($F_i = F_{i-1} + dF$), is then compared to the yield surface. If the force resultant is inside the surface, the response is elastic and the resulting element force is set equal to the trial force. If the force resultant is on or outside the element, the element is plastically loading, and the force recovery requires the additional steps 2 through 4.

Step 2 (hardening/softening): When the trial force point lies outside the surface, the portion of the incremental force dF associated with inelastic hardening/softening (dF^*) is calculated using Eq. 6. Depending on whether the element is hardening or softening, resultant $F_i + dF^*$ may be outside or inside the surface. The yield surface implementation allows for combined kinematic and isotropic behavior, so the yield surface translates and or expands/contracts, such that the force point $F_i + dF^*$ lies on the yield surface.

Step 3 (drift control): Once the location/size of the yield surface is updated (*step 2*), the trial force (F_i + dF) is recalculated, where the increment dF is calculated using Eq. 4. Due to curved convexity of the surface and depending on the hardening/softening stiffness, the resulting force point is usually outside the surface. Therefore, to satisfy the yield criteria, the trial force point is returned back to surface using a radial-return algorithm.

Step 4 (force balance): Steps 1 to 3 are applied to each end of a yielding member. Since each adjustment is independent, it is likely that the axial force is out of equilibrium between the two element ends. Therefore, an additional adjustment is made whereby the axial force at each end is revised to the average of that at the two ends. This usually causes the force point to drift off the yield surface, in which case a second "constant-P" return algorithm is then applied to return the force to the surface. Element shear forces are then computed based on the resulting member end moments.

Hardening/Softening behavior

Our current implementation models inelastic hardening/softening through uncoupled coefficients in $[K_h]$ where the parameters vary nonlinearly as a function of the corresponding plastic deformation component. So, for example, the hinge rotation hardening parameter, $K_{h\theta}$, is a function of θ_p, and the axial parameter, K_{hp}, is a function of Δ_p. Shown in Fig. 5 is an example of the nonlinear hardening/softening that can be achieved with this model. Note the shrinking of the P-M yield surface that occurs due to strain softening in the M-θ response.

We are currently extending this model to include more sophisticated damage indices that can serve as both *Engineering Demand Parameters* for component performance assessment and history parameters for the hardening/softening models. One example of the type of damage parameters we are considering is one by Mehanny and Deierlein (2001), which combines a peak and cumulative inelastic deformations based on a counting scheme that distinguishes between primary and follower loading cycles. A second modification is to introduce a

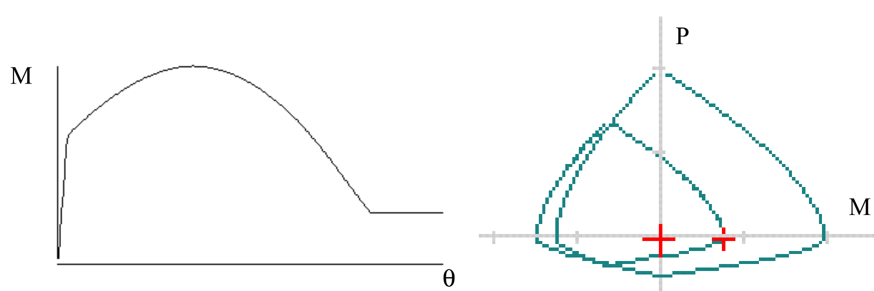

Figure 5. Force-displacement and yield surface in force space

method to account for stiffness degradation during “elastic” unloading, when the force point lies inside the yield surface.

OBJECT-ORIENTED IMPLEMENTATION

The beam-column implementation follows the standard element interface in *OpenSees* and an object-oriented design including abstract classes, inheritance, encapsulation, and overloaded methods. The following is a summary of the element class hierarchy shown in Fig. 6:

- *Element* is an abstract class in *OpenSees* from which all elements are derived.
- *Element2D02* is an abstract class specific to our element, which implements modeling attributes for geometric nonlinearity as described above.
- *InelasticYS2DGNL* is an abstract class derived from *Element2D02*, which implements the M-P interaction as described above. This class has pointers to two yield-surfaces (one for each end) and it inherits the geometric nonlinear capabilities from *Element2D02*.
- *Inelastic2DYS0** are final classes whose primary functions are to provide the appropriate “elastic” stiffness matrix to calculate $[K_{ep}]$ per Eq. 7. They provide calculation of stiffness properties between the two hinges to account for variations peculiar to specific types elements or behavior, e.g., composite steel-concrete beams, mild hysteretic degradation in the elastic domain, shear stiffness/strength degradation, incorporation of various damage indices, etc. In their current stage of development, some of these classes are experimental in that we are testing out different modeling strategies. We anticipate to consolidating the five classes shown into two or three. This ability to easily add, modify, and delete classes is one of the key virtues of the *OpenSees* platform for research.

Elements implemented through the *InelasticYS2GNL* class, each have two P-M *yield surfaces* with their own *hardening* models. The *hardening* models in turn point to hysteretic material models that provide plastic stiffness coefficients with respect to plastic axial deformations, plastic rotations, or other quantities. We are presently investigating ways to model shear critical behavior, either through a modification to the generalized end-hinges or through a separate shear spring, either of which approaches would employ an additional shear material model. The following is a description of the *yield surface* and *hardening* classes:

- *YieldSurfaceBC* is an abstract class and provides the interface between the specific yield surface description and the beam-column element. It implements methods to transform vectors and matrices between the element system and local yield-surface coordinates.
- *YieldSurfaceBC2D* is an abstract class that implements methods for two-dimensional (e.g., P-M) force point interpolations (e.g., drift control using radial or constant P return) and interactions with the hardening model. The final classes in the yield-surface hierarchy are

named after authors of published yield surface equations, including the *Orbison2D* and *Attalla2D* surfaces for steel sections (Attalla et al., 1994), the *ElTawil2D* and *ElTawil2DUnSym* surfaces for reinforced concrete sections (El-Tawil & Deierlein 2001), and the *Hajjar2D* surface for concrete filled tubes (Hajjar et al., 1997). The classes define the yield surface equations with an interface to *YieldSurfaceBC2D*, which provides yield surface gradient and force point drift calculations.

- *YS_HardeningModel* implements hardening rules associated with the translation and expansion/contraction of the yield-surface. It controls the isotropic and kinematic hardening ratio and the direction of surface translation. It also provides transformation between the displaced and undisplaced yield-surface coordinates.
- *YS_HardeningModel2D* is a specific implementation for cases with two hardening models, e.g., axial and flexural, and provides plastic stiffness as a function of cumulative plastic

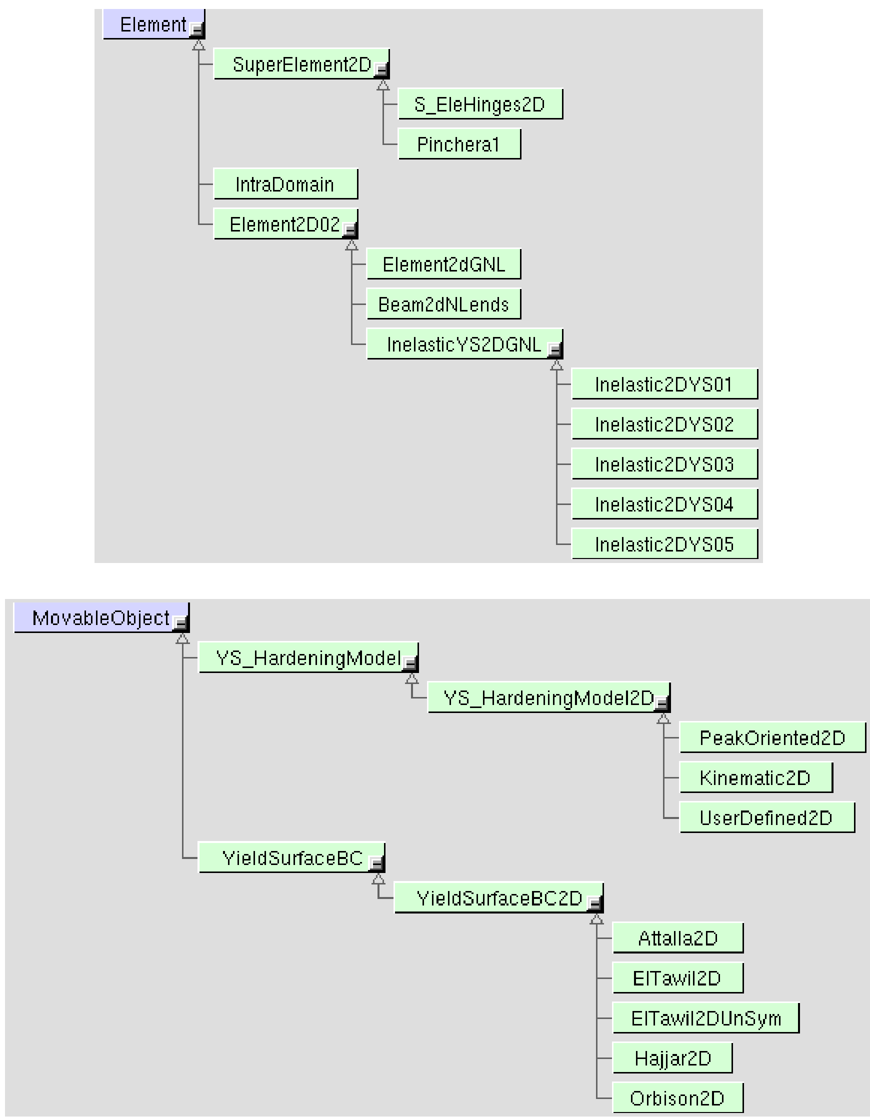

Figure 6. Element Class Hierarchy

deformations. The final classes in the hardening hierarchy implement alternative hardening model formulations.

FINAL REMARKS

This paper describes work in progress to develop and implement models to simulate inelastic response of reinforced concrete beam-columns. These and other models being implemented in the *OpenSees* software framework provide robust and extendable tools to calculate engineering demand parameters and damage indices for various input ground motions. The generalized hinge approach emphasizes models that are sufficiently refined and robust to accurately capture structural behavior up to collapse but still practical enough for application to large buildings and bridges. The plastic-hinge formulation described herein builds on concepts that are fairly well established. The current implementation includes several important extensions to this model, including a modular object-oriented implementation that allows for convenient extension of the models and rigorous hardening and force-recovery schemes that are stable for degrading hinges. Work is ongoing to calibrate and validate the models with test data and extend the models to capture P-M-V response.

ACKNOWLEDGMENTS

This paper is based on research supported by the Pacific Earthquake Engineering Research Center under NSF Award Number EEC-9701568.

REFERENCES

Attalla, M.R., Deierlein, G.G., McGuire, W. (1994), "Spread of Plasticity - A Quasi-plastic Hinge Approach", *Jl. of Struct. Engrg.*, ASCE, NY, 120(8), pp. 2451-2473.

El-Tawil, S., Deierlein, G.G. (2000), “ Analysis Models for Mixed Steel-Concrete Space Frames Part I – Beam-Column Element Formulation, Pt I – Implementation and Verification” *Jl. of Struct. Engrg.*, ASCE, 127 (6) June 2001, pp. 647-666.

FEMA (1997), *NEHRP Guidelines for the Seismic Rehabilitation of Buildings*, FEMA Report 273/4, Washington, DC.

Hajjar J. F. and Gourley B.C. (1997). “A cyclic nonlinear model for concrete filled tubes I: formulation”, *Jl. of Struct. Engrg.*, ASCE, 736-744

McGuire, W., Gallagher, R., Ziemian, R. (2001), *Matrix Structural Analysis*, 2nd Edition, J. Wiley, N.Y.

Mehanny, S.S., Deierlein, G.G., (2001) “Seismic Collapse Assessment of Composite RCS Moment Frames,” *Jl. of Struct. Engrg.*, ASCE, 127(9).

EFFECT OF IMMEDIATE OCCUPANCY DESIGN ON PERFORMANCE OF RC FRAMES AT COLLAPSE PREVENTION LEVEL

M. N. FARDIS[1] and T. B. PANAGIOTAKOS[1]

ABSTRACT

The paper examines how provision of the required deformation capacity at the Collapse Prevention (CP) performance level is affected by fulfillment of the criteria for structural and non-structural performance under the Hazard Level for which the goal is Immediate Occupancy (IO) after the event. Regular multistory RC frames and the columns of soft-story buildings are considered. Conclusions are drawn for the effect of design parameters, such as column axial load level (and tributary mass), concrete strength and design spectra at IO and CP level. Columns of soft-story buildings designed for IO under the corresponding hazard level meet marginally the deformation capacity demands at the CP level. In regular frames drift control and ULS proportioning of members at IO level provide a large margin against exceedance of member ultimate deformation under the CP earthquake, especially in columns.

1. INTRODUCTION

In Performance-based Seismic Engineering the "Basic Performance Objective" for buildings of normal occupancy involves verification of up to four Performance Levels under the corresponding Earthquake (or Hazard) levels. Hazard levels typically include the 475yr earthquake, for which present codes aim at Life Safety, and an about 1.5-times stronger "Maximum Considered" earthquake (MCE), for which Collapse Prevention should be achieved. Emphasis is placed on lower Hazard Levels, for which Immediate Occupancy after the event should be ensured. Some aspects of the design (member sizes and amount of reinforcement) will be controlled by the criteria of one Performance Level and other aspects by another. Satisfaction of the criteria at any Performance Level depends on the balance between demand and capacity, which often depend on the same factors. For example, the amount of reinforcement determines not only the capacity of an RC member, but its seismic demand as well, as its effective "elastic" stiffness is a function of its reinforcement. The same applies to member sizes and concrete strength. As another example, mass is important for seismic demands but, as it also generates the axial load in columns, it affects their strength and deformation capacity too.

The goal of the paper is to study how provision of the required deformation capacity at the

[1] *Structures Laboratory, Department of Civil Engineering, University of Patras, P.O. Box 1424, GR26500, Patras, Greece*

Collapse Prevention Performance Level may be indirectly controlled by fulfilment of the criteria for structural performance (Ultimate Limit State - ULS) and non-structural performance (drift) under the Hazard Level for which Immediate Occupancy (IO) after the earthquake is the goal. Section 2 focuses on columns, which are the critical elements for Collapse Prevention (CP). To include the effect of (tributary) mass on column deformation demand (through the period, etc.) and capacity (via the column axial load), columns are assumed to support a rigid superstructure, as in multistory buildings with a soft (open) ground story. Section 3 focuses on multistory regular RC frame buildings with typical bay length, story height and floor loads and masses. To allow a large member of parametric studies, analysis of the frames for lateral loads is equivalent static, assuming points of inflection at member midlengths. The equal displacement rule is adopted for estimation of inelastic member deformations and P-δ effects are considered.

Numerical applications are based on the spectra in Appendix I: "Tentative Guidelines for Performance-based Seismic Engineering" of the 1999 SEAOC Blue Book for the Hazard Levels appropriate for Immediate Occupancy ("Earthquake I") and Collapse Prevention ("Earthquake IV") in US Zone 4. The performance criteria for the "Immediate Occupancy" Performance Level is member yielding (attainment of the Ultimate Limit State and R=1), while those for the Collapse Prevention Performance Level is attainment of member ultimate deformation capacity (which corresponds to a "near collapse" Performance Level for the structure).

2. PERFORMANCE OF COLUMNS IN BUILDING WITH SOFT-STORY

2.1 Definitions, assumptions and basic data

A series of columns is considered here, supporting with double fixity a rigid superstructure. The net (story) height is h_{st}. The system responds to horizontal motion as a SDOF one and may be considered idealisation of a multistory frame with stiff and strong infills in all stories above the ground story. Each column has: a) square cross section with side h_c and area $A_g=h_c^2$; b) tension and compression reinforcement at a ratio $\rho=\rho'=\rho_c$, with distance d' from the corresponding extreme fibre (depth to reinforcement $d=h_c-d'$) and bar diameter d_b; c) confinement reinforcement at a ratio ρ_{sx} in each horizontal direction with confinement effectiveness ratio α after Sheikh & Uzumeri (1982) and the CEB/FIP Model Code 1990 ($\alpha=\alpha_s\alpha_n$, with $\alpha_s=(1-s_h/2b_o)^2$

and α_n=1-($b_o/n_h h_o+h_o/n_b b_o$)/3 for hoops at spacing s_h, with n_b legs or cross-ties parallel to side b_o of the confined core and n_h legs or cross-ties parallel to side h_o). The longitudinal and transverse steel bars have a yield strength of f_y and concrete a cylindrical compression strength of f'_c.

The axial force in each column is assumed to be due only to the weight W of its tributary mass m, producing in all columns the same axial load ratio $\nu=W/A_g f'_c$. If the column axial does not exceed the balance load, the column flexural capacity may be approximated as:

$$M_u = \rho_c A_g f_y (h_c - 2d') + 0.5 N h_c \left(1 - \frac{N}{A_g f'_c}\right) = A_g f'_c h_c \left[\rho_c \frac{f_y}{f'_c}\left(1 - 2\frac{d'}{h_c}\right) + 0.5\nu(1-\nu)\right] \tag{1}$$

The drift ratio at yielding of the column is taken equal to:

$$\theta_y = \frac{\phi_y h_{st}}{6} + 0.0025 + \frac{0.25 d_b f_y^2}{E_s (h_c - 2d')\sqrt{f'_c}} \tag{2}$$

In Eq. (2) ϕ_y is the yield curvature (from first principles); f_y, E_s (steel Elastic modulus) and f'_c are in MPa. The second term accounts for the effects of shear and the third is the end rotation due to anchorage slip beyond the member end. Eq. (2) was fitted by Panagiotakos & Fardis (2001) to about 1000 test results of RC members with a coefficient of variation of 37%.

If the effective yield-point rigidity of the column is taken equal to:

$$EI_{ef} = \frac{M_u}{\theta_y}\frac{h_{st}}{6} \tag{3}$$

the effective lateral stiffness (without P-Δ effects) and the corresponding yield-point period are:

$$K_{ef} = 12\frac{EI_{ef}}{h_{st}^3} = \frac{2M_u}{\theta_y h_{st}^2} \tag{4}$$

$$T_y = 2\pi\sqrt{\frac{m}{K_{ef}}} = 2\pi h_{st}\sqrt{\frac{\nu A_g f'_c}{2g\frac{M_u}{\theta_y}}} \tag{5}$$

In concrete structures the yield-point period is normally near or above the transition period T_s between the acceleration- and velocity-controlled parts of the elastic spectrum. Then the equal displacement rule applies in good approximation and the peak inelastic displacement of a SDOF system may be taken equal to the 5%-damped elastic spectral displacement S_d at period T_y. If the acceleration spectrum falls as 1/T for $T>T_s$, the displacement demand is:

$$S_d = \left(\frac{T_y}{2\pi}\right)^2 \min\left(S_{as}g, \frac{S_{a1}g}{T_y}\right) = h_{st} \min\left(S_{as}h_{st}\frac{\nu A_g f'_c \theta_y}{2M_u}, \frac{S_{a1}}{2\pi}\sqrt{\frac{g}{2}\frac{\nu A_g f'_c \theta_y}{M_u}}\right) \tag{6}$$

In Eq. (6) S_{as} and S_{a1} (in g's) are the 5%-damped elastic spectral accelerations in the constant acceleration region and at T=1 sec respectively. The drift ratio demand at the Hazard Level chosen for the Collapse Prevention Performance Level is:

$$\theta_{CP} = \frac{S_d}{h_{st}} \tag{7}$$

with S_d from Eq. (6) and the values of S_{as}, S_{a1} corresponding to the CP Hazard Level.

At Collapse Prevention the drift ratio capacity to be compared with the demand from Eq. (7) may be taken equal to the ultimate drift (taken here at loss of 20% of lateral load capacity) of the column in double fixity. This ultimate drift is taken here equal to:

$$\theta_{cap} = 0.0086\left(0.2^{\nu}\right)\left(\frac{\max(0.01, \rho'\frac{f_y}{f'_c})}{\max(0.01, \rho\frac{f_y}{f'_c})} f'_c\,(\text{MPa})\right)^{0.275}\left(\frac{L_s}{h_c}\right)^{0.45} 1.1^{100\alpha\rho_{sx}\frac{f_y}{f'_c}} \tag{8}$$

Eq. (8) is a special case of an empirical equation fitted by Panagiotakos & Fardis (2001) to the results of about 900 flexure-controlled tests carried to ultimate deformation. It applies to beams or columns with hot-rolled ductile reinforcing steel under cyclic loading. The new variables in Eq. (8) are: ρ, ρ': ratios of the tension and compression steel; L_s: member shear span $=0.5h_{st}$ in columns with double fixity (see 1st paragraph of Section 2.1 for ρ_{sx} and factor α).

2.2 Effect of fulfillment of IO criteria on column performance at CP level

In Performance-Based Seismic Engineering buildings are typically required to remain elastic at the Immediate Occupancy Performance Level. To this end their members are proportioned at the Ultimate Limit State (ULS) for the elastic load effects of the earthquake chosen for Immediate

Occupancy, i.e. with R=1. Interstory drift limits are also imposed for that Hazard Level, and for all others. Fulfilment of IO drift limits is checked assuming cracked concrete sections, with effective rigidities typically taken as 50% of the uncracked gross concrete section rigidity, E_cI_g. Therefore drift limits control member cross-sectional dimensions, and member ULS verification for elastic response to the IO earthquake determines the reinforcement.

For the SDOF system of columns of Section 2.1 the conventional effective lateral stiffness is equal to $K_o=0.5(12E_cI_g/h_{st}^3)=0.5(E_cA_g/h_{st})(h_c/h_{st})^2$. The drift is then computed for a period T:

$$T = 2\pi\sqrt{\frac{m}{K_o}} = 2\pi\frac{h_{st}}{h_c}\sqrt{\frac{2h_{st}\nu f_c'}{gE_c}} \tag{9}$$

The drift demand to be compared to the IO limit, $\theta_{lmt}h_{st}$ (θ_{lmt}: drift ratio limit), is calculated as the ratio of the elastic base shear of the IO earthquake to the conventional lateral stiffness K_o:

$$\theta_{lmt}h_{st} \geq \frac{S_{aIO}\nu A_g f_c'}{K_o} \tag{10}$$

in which S_{aIO} (in g's) is the 5%-damped elastic spectral acceleration of the IO earthquake at the period of Eq. (9). The value of h_c should observe the smaller of the following two limits:

$$h_c \geq h_{st}\sqrt{\frac{2S_{asIO}}{\theta_{lmt}}\frac{\nu f_c'}{E_c}} \tag{11}$$

$$h_c \geq \frac{S_{a1IO}}{\theta_{lmt}}\sqrt{\frac{gh_{st}}{2}\frac{\nu f_c'}{E_c}} \tag{12}$$

Eqs. (11) or (12) apply if the value of T from Eq. (9) is less or greater, respectively, than the transition period $T_{sIO}=S_{a1IO}/S_{asIO}$ of the spectrum of the IO earthquake.

The bending moment at the column ends is calculated, with the applicable value of S_{aIO} (g's), as:

$$M_{IO}=0.5h_{st}S_{aIO}W \tag{13}$$

The steel ratio required for a factored capacity φM_u at least equal to M_{IO} is calculated via Eq. (1).

The drift capacity and demand are compared at the CP Level, with the column depth h_c and the steel ratio $\rho=\rho'=\rho_c$ determined from drift control and the ULS verification in flexure with axial load at the IO level. The following typical values are used in the parametric study: f_y=420MPa, d'=40mm, d_b=16mm, f'_c=30Mpa, $\alpha\rho_{sx}$=0.001(corresponding to $\rho_{sx}\approx0.005$), while the axial load ratio $\nu=W/A_g f_c'$ varies. The Earthquake I spectral accelerations in Appendix I of the SEAOC '99 Blue Book for Zone 4 sites and soil SD are selected for the IO hazard level: S_{asIO}=0.4, S_{a1IO}=0.24. The drift ratio limit at IO is that specified for Earthquake I in Appendix I for Special Moment Resisting Frames: θ_{lmt}=0.005. The capacity factor φ of ACI318 for flexure with axial load is applied in the ULS proportioning of the reinforcement. All drift and ULS calculations at IO use the nominal values of f'_c and f_y; demand and capacity calculations at the CP Performance Level are based on the expected values of steel and concrete strengths, assumed equal to: $f_{ym}=1.15f_y$ and $f'_{cm}=f'_c$+8MPa. The parametric analysis is performed for two values of h_{st}: h_{st}=3.0m and h_{st}=7.5m. For these values of h_{st} Eqs. (11), (12) yield conventional cracked section periods of 0.39sec and 0.63sec, respectively, compared to $T_{sIO}=S_{a1IO}/S_{asIO}$= 0.6sec.

For the IO demand parameters used in this parametric analysis, Eqs. (11) and (12) give, for the same value of ν, column depths for h_{st}=7.5m about 2.5 times those required for h_{st}=3m. As shown in Fig. 1(a), drift control at the IO performance level requires quite large column depths, even for low to medium values of the axial load ratio ν. The reinforcement ratio required for the ULS in flexure with axial load is also high, especially for h_{st}=3m. Due to this heavy reinforcement the effective yield point rigidity from Eq. (2) is relatively large and the corresponding yield point stiffness T_y from Eq. (5) is shown in Fig. 1(d) to be of the same order as the cracked section elastic period of Fig. 1(c), computed conventionally from Eqs. (9), (11) or (12), with an effective rigidity of $0.5E_cI_g$. For the values of h_c, $\rho=\rho'=\rho_c$ and T_y shown in Figs. 1(a), (b), (d), the drift capacity-demand ratio at the CP Level is given in Fig. 1(e) for the CP spectral accelerations in Appendix I of the SEAOC '99 Blue Book for Zone 4 sites over stiff soil (SD) (S_{asCP}=1.65, S_{a1CP}=0.96). Fig. 1(e) gives capacity-demand ratios consistently greater than 1.0, except for values of ν above the balance load.

In Fig. 2 the value of ν is fixed at 0.2 while the Hazard Level for which the IO Performance Level is pursued varies and that at CP is fixed. The values of S_{asCP} and S_{a1CP} are maintained equal to those in Appendix I of the SEAOC '99 Blue Book for Zone 4 and SD soil, while the ratio

$S_{asIO}/S_{asCP}=S_{a1IO}/S_{a1CP}$ varies. In Appendix I this ratio equals 0.25 for soil SD, but varies from 0.19 for SA to 0.44 for S_{asIO}/S_{asCP} and soil SE. The other parameters have the same values (h_{st}=3m or 7.5m, $\alpha\rho_{sx}$=0.001, f'_c=30MPa, f_y=420MPa, d'=40mm, d_b=16mm).

As the earthquake level at which drift and ULS requirements are imposed for IO increases, column depth (Fig. 2(a)) and reinforcement ratio (Fig. 2(b)) increase less than proportionally with the IO earthquake level. The capacity-demand ratio at the CP performance level is about proportional to the IO earthquake. The required concrete cross sectional area $A_g=h_c^2$ increases about proportionally to the IO earthquake level. However, as ρ_c increases also with the IO earthquake, the total amount of steel, $2\rho_cA_g$, increases more than proportionally with the IO earthquake level. So the additional safety against CP achieved by increasing the IO earthquake is gained at a higher incremental material cost.

Figs. 2(c) and (d) present the conventional and the "actual" yield point periods, T and T_y. The "conventional" period of the cracked structure is not much longer than the "actual" one. The difference disappears for the very high steel ratios needed for high IO earthquake levels. For h_{st}=3.0m the yield point period T_y in Figs. 1(d), 2(d) is less than the transition period T_{sCP}=0.58sec for SD soil. Then the equal displacement rule employed may underestimate mean inelastic deformation demands and the results in Figs. 1(e), (f) and 2(e), (f) for h_{st}=3.0m may be on the unconservative side.

As confinement affects only the demand in the straightforward way of the last term in Eq. (8), no parametric analysis results are shown for $\alpha\rho_{sx}$. The capacity-demand ratio increases by a factor of about 2.5 if $\alpha\rho_{sx}$, increases from typical value of 0.001 to a high value of 0.005.

3. MULTISTORY RC FRAME BUILDINGS.

3.1 Scope, definitions and assumptions.

An idealised multistory RC frame is considered with: a) n_{st} stories of the same height h_{st}; b) square columns with side h_c, constant throughout the building; c) a two-way system of beams of uniform span L_b, the same in both directions; and d) distributed dead load and live loads at floor levels uniform throughout the building. Beam width, b_w, is considered constant in all storeys, but beam depth, h_b, may vary from one story to another. The slab is considered to contribute to the moment of inertia of the beams with an effective flange width according to ACI318-95.

Equivalent lateral forces due to the earthquake are distributed over the height according to a linear mode shape. An interior bay of the frame is considered. Inflection points due to the earthquake loads are assumed to be at beam mid-span and at column midheight. The columns of the bottom story are assumed fixed at grade level. In the calculations of displacements the finite size of beam-column joints is considered but joints are assumed rigid. P-Δ effects are considered. The fundamental period of the building is estimated through the Rayleigh quotient for the story elastic horizontal displacements due to the equivalent lateral forces with (inverted) triangular distribution. Axial forces in the columns are considered to be due to gravity loads alone, but column bending due to these loads is neglected. Beam bending moments due to gravity loads are computed on the basis of the loads from the beam tributary area in the two-way slab system, considering the beams as fixed against rotation at both ends.

3.2 Member proportioning to fulfil drift and ULS criteria at the IO performance level

The procedure for sizing members and proportioning their reinforcement to satisfy drift and ULS requirements at the IO performance level is a generalization of the procedure of Sect. 2.2. ACI318 Ch.21 minimum and maximum reinforcement is enforced. The “capacity design” rule requiring the sum of column factored flexural capacities to exceed by 20% that of beams framing in the same joint is also applied (except at the roof), for a strong column / weak beam design.

The (uniform) column size h_c and the beam depths h_{bi} at each story are determined iteratively to satisfy the drift limitation everywhere. Rigidities of cracked members are taken as 50% of those of the uncracked gross concrete section, including the effective flange width of beams. Column depth h_c is chosen to fulfil the IO drift limit in the story with the minimum interstory drift among those violating this limit. In the rest of those stories beam depth is increased until the corresponding drift limitation is fulfilled. The estimate of the period and the resulting elastic spectral acceleration and displacement are revised during iterations. In every story beam depths are large enough to allow respecting the maximum steel ratio of ACI318-95 at the face of the column. Member depths are rounded up to the nearest 25mm (inch). Earthquake load effects are computed on the basis of the 5%-damped elastic spectral acceleration at a period consistent with the final member sizes. Proportioning of beam top and bottom reinforcement at column faces and of column reinforcement at the level of the beam soffit accounts for the flexural capacity reduction factors φ of ACI318. Reinforcement is tailored to the requirements of proportioning, to avoid member overstrengths that may affect their deformation demands or capacities.

3.3 Capacity-demand analysis at the Collapse Prevention Performance Level

Capacities and deformations at the CP level are compared in terms of chord rotations at the ends of beams and columns. The equal displacement rule is used for the estimation of inelastic displacements and extended to the estimation of member deformations (inelastic chord rotations at member ends) from an elastic analysis with a yield-point period T_y based on the effective yield-point member rigidities after Eq. (2) (with h_{st} replaced by the clear length of the beam or column). Since in beams the chord rotation capacity is more critical for hogging moment (as $\rho>\rho'$, cf. Eq. (8)), the beam chord rotation demand due to the simultaneously acting gravity loads in the beam is added to that due to the CP earthquake. In Eq. (8) L_s is one-half of the clear length of the member. Expected material strengths $f_{ym}=1.15f_y$ and $f_{cm}=f_c'+8$MPa are used in the calculations of member chord rotation demands and capacities.

The analyses of the frames are performed for: Story height $h_{st}=3$m; bay length in each direction 5m; dead load (including weight of framing) g=7kN/m^2; live load q=2kN/m^2; $f_y=420$MPa; d'=40mm; $d_b=16$mm, $b_w=0.25$m; factored gravity loads for ULS design of beams: 1.2g+1.6q; gravity loads simultaneously acting with the earthquake for ULS design of beams: 1.2g+0.5q (g for sagging moment) and for calculation of masses: g+0.2q; story drift limit: $\theta_{lmt}=0.005$ (for SMRF at IO performance level).

Table 1 gives the column depth h_c required for drift control and the resulting axial load ratio ν at grade level. Figs. 3 and 4 present the height-wise variation: a) of beam depth h_{bi} and of the resulting interstory drift ratio at the IO performance level; b) of top and bottom steel ratios ρ and ρ' in beams and of $\rho=\rho'=\rho_c$ in columns; c) of the interstory drift at the CP performance level; and d) of the chord rotation capacity-demand ratio for beams or columns. Results are presented for 4-, 6-, 8- and 12-story frames. They are given: a) in Figure 3 for f'_c= 20, 30, 40 and 50MPa (the only "free" design parameter) and SD soil ($S_{asIO}=0.4$, $S_{a1IO}=0.24$, $S_{aCP}=1.65$, $S_{a1CP}=0.96$); and b) in Fig. 4 for $f'_c=30$MPa and soils SB, SC, SD and SE.

Table 1: Column sizes of multistory buildings and axial load ratio at ground story.

		f_c' (MPa)				Soil type			
		20	30	40	50	SB	SC	SD	SE
4-story	h_c (m)	0.675	0.600	0.550	0.550	0.350	0.550	0.575	0.650
	$\nu=W/A_gf_c'$	0.058	0.054	0.051	0.042	0.159	0.064	0.059	0.046
6-story	h_c (m)	0.750	0.625	0.575	0.575	0.375	0.550	0.675	0.700
	$\nu=W/A_gf_c'$	0.070	0.075	0.070	0.058	0.208	0.097	0.064	0.060
8-story	h_c (m)	0.750	0.700	0.650	0.600	0.450	0.550	0.700	0.700
	$\nu=W/A_gf_c'$	0.094	0.079	0.073	0.071	0.192	0.129	0.079	0.079
12-story	h_c (m)	0.750	0.725	0.650	0.600	0.450	0.625	0.700	0.700
	$\nu=W/A_gf_c'$	0.141	0.111	0.109	0.106	0.288	0.150	0.119	0.119

The most important conclusion from Figs. 3 and 4 is that, unlike what happens in Figs. 1, 2, very satisfactory capacity-demand ratios are easily achieved at the CP performance level. These ratios are fairly uniform over the height of the building, have similar values for buildings with different number of stories and are systematically higher in columns than in beams. So drift control and the requirement for elastic behavior under the IO earthquake (plus a strong column-weak beam design) produce very satisfactory performance at the CP level. This applies also to the drifts under the CP earthquake, which are systematically below the 4% limit specified for the CP performance level in Appendix I of the SEAOC '99 Blue Book for SMRFs. The high capacity-demand ratios vis-a-vis the medium-low values in Figs. 3, 4 are due to: a) the sharing of story drift demands by beams and columns; b) for the columns, to their very low axial load ratio ν (see the values at ground story in Table 1), which is favorable for deformation capacity (cf. Eq. (8)).

Within the framework of this study concrete strength f_c' is the only "free" design parameter. Increasing f_c' allows some reduction in the member sizes needed for IO drift control, at the expense of higher reinforcement ratios. The increase in f_c' improves the capacity-demand balance in beams but has the opposite effect in columns, as the more slender columns possible for higher f_c' develop a larger proportion of the story drift and are subject to higher deformation demands.

The large differences in the IO and CP spectra across the different soil types in Appendix I of the SEAOC '99 Blue Book lead to widely different frame designs meeting the IO drift control and ULS requirements, with the soft soil designs requiring much heavier member sections and reinforcement than the rock-site ones. Nonetheless, these very different designs have similar and equally satisfactory CP performance as far as member deformations are concerned. Despite the less demanding displacement spectra of rock sites, interstory drifts under the CP earthquake are much larger for rock than soft soil, due to the larger flexibility and longer period of rock designs.

The fundamental period is indeed proportional to the number of stories, with the proportionality factor depending very much on the design, as affected by drift control for the "conventional" cracked period T, or by ULS proportioning of reinforcement for the actual yield-point T_y. Because steel ratios in frame members are not as high as in the columns of the soft-story system of Sect. 2, the yield-point period T_y exceeds the "conventional" one based on 50% of the rigidity of uncracked sections, by about 80% in the low-rise frames, to about 50% in the high-rise ones.

Member sizes in the high-rise buildings are not much heavier than in low-rise ones. Nonetheless, performance of high-rise buildings (i.e. deformation capacity-demand ratios and interstory drifts) is equal or better than in low-rise ones. The reason is that drift ratio demands in the high-rise buildings are essentially the same as in the low-rise ones: in the velocity-controlled range of the spectrum top drifts are proportional to period, period is proportional to building height and then story drift demand is almost independent of the number of stories.

ACKNOWLEDGMENT

This work has been funded by the European Commission, in TMR network “Innovative seismic design concepts for new and existing structures”, Contract: FMRX-CT96-0022 (DG12 - RSRF).

REFERENCES

Panagiotakos, T.B. and Fardis, M.N. (2001), Deformations of RC members at yielding and ultimate, *ACI Structural Journal*, 98, 2, 135-148.

SEAOC (1999). *Recommended lateral force requirements and commentary*, Structural Engineers Association of California, Sacramento.

Sheikh, S.A. and Uzumeri, S.M. (1982), Analytical model for concrete confinement in tied columns, *ASCE, J. of Structural Division*, 108, ST12, 2703-2722.

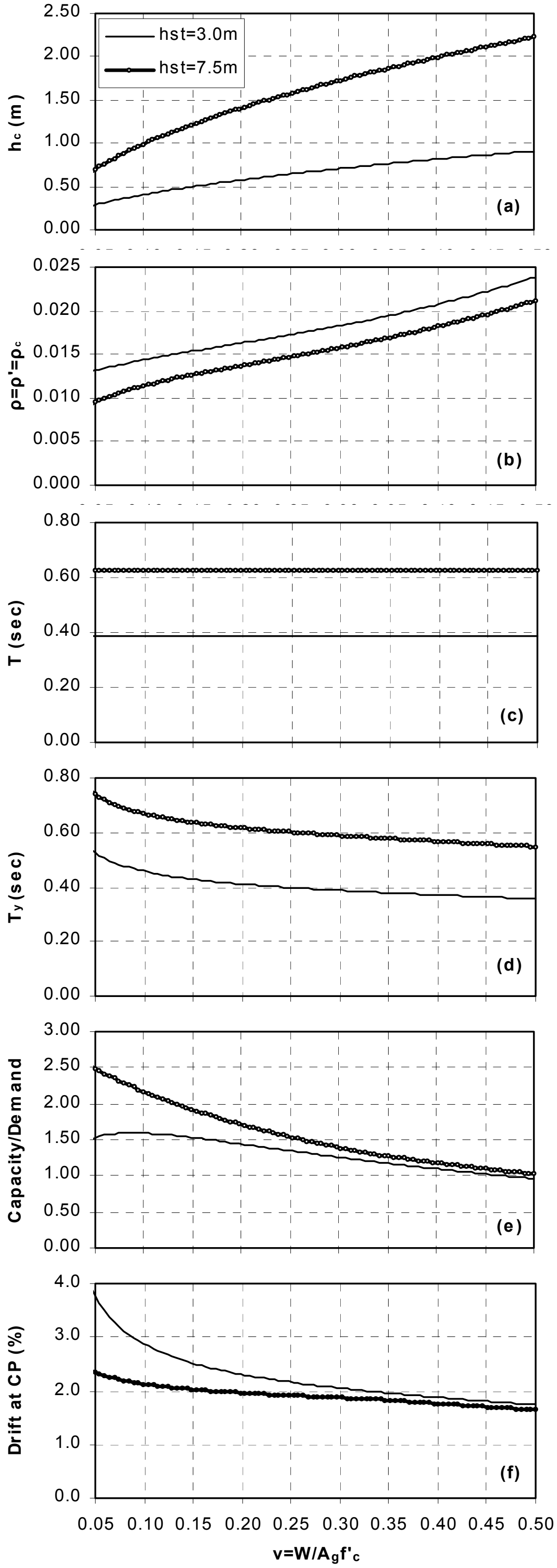

Fig.1. Columns of soft story system designed for the IO earthquake and checked for the CP one (soil SD).

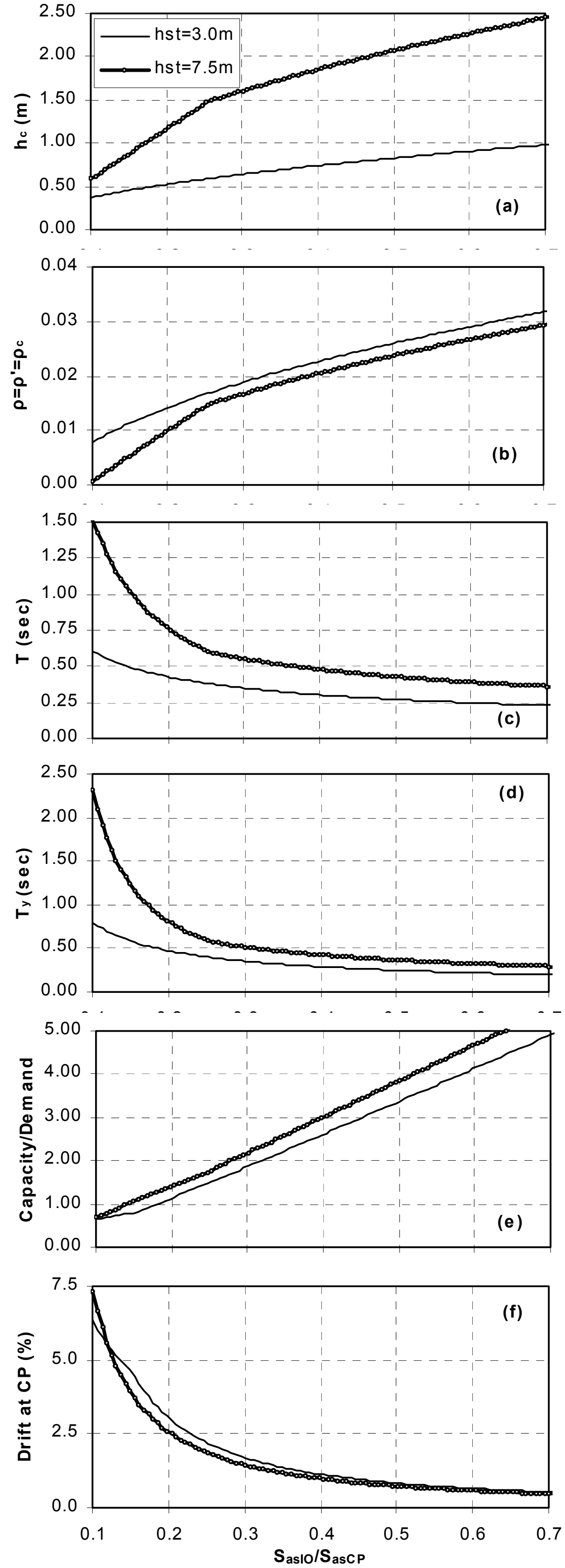

Fig.2. Effect of IO earthquake level on the design and CP performance of the columns of the soft-story system for soil SD.

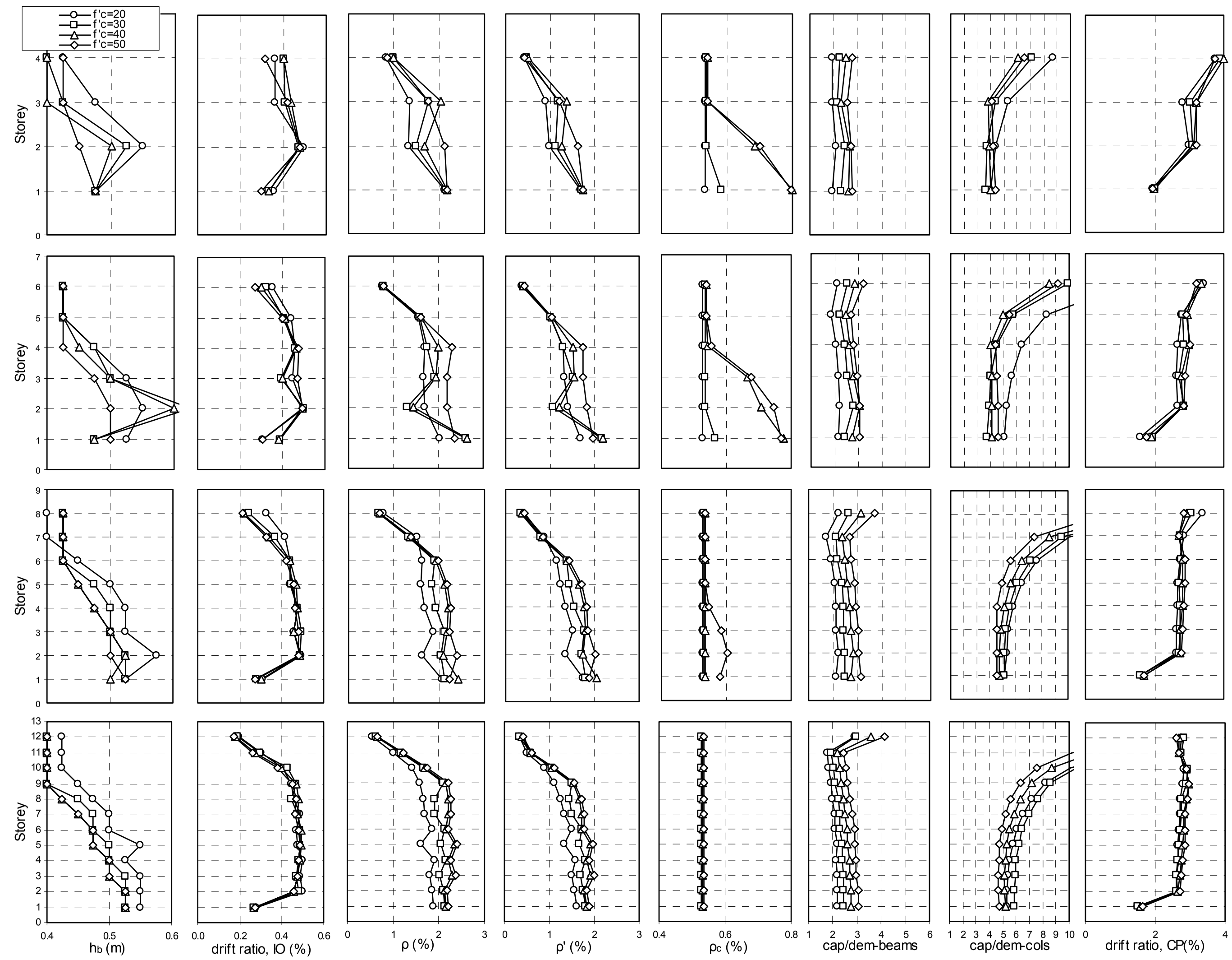

Fig.3. Design of multistory frame for IO earthquake and resulting performance at CP level as a function of concrete strength for soil SD.

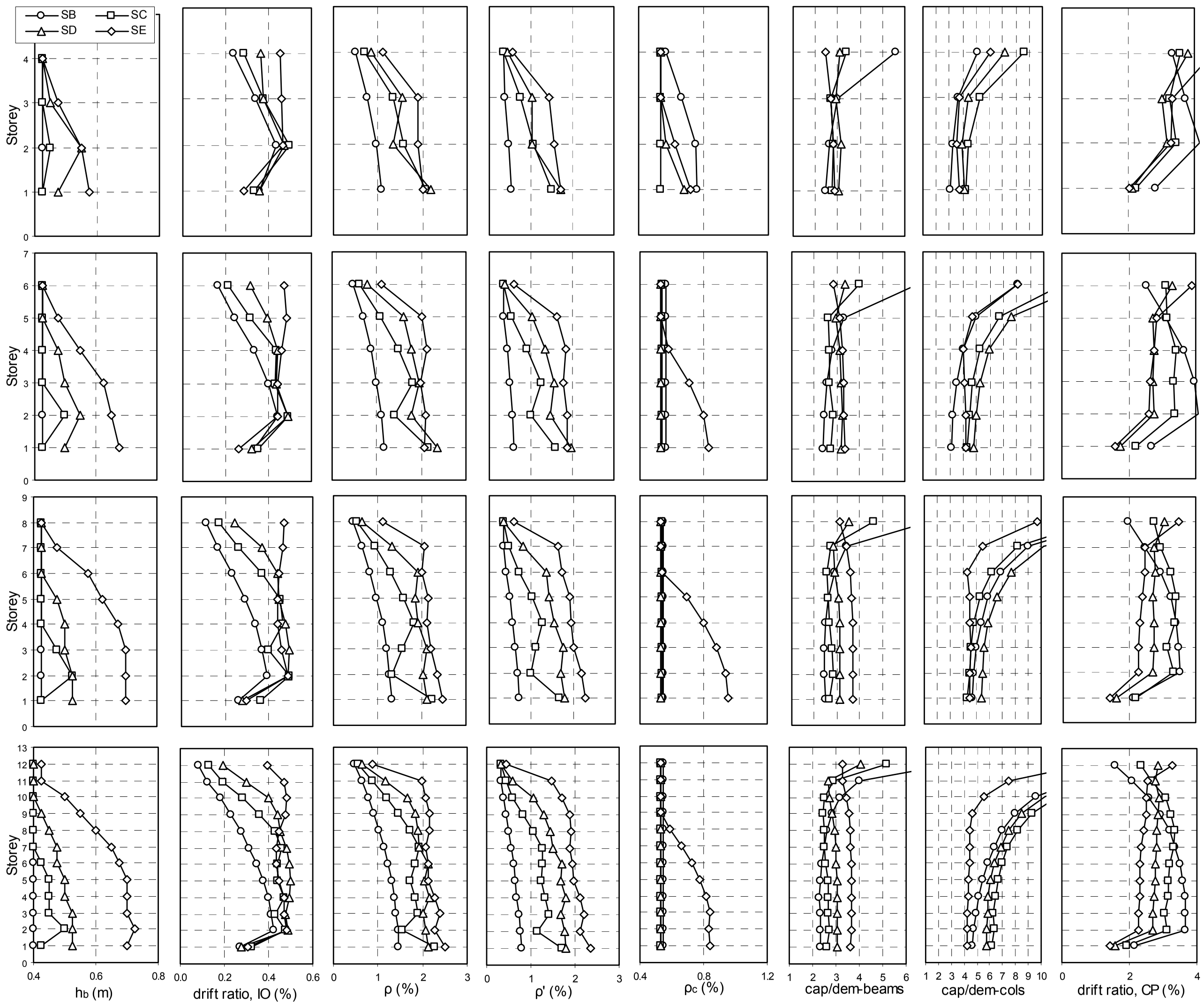

Fig.4. Design of multistory frame for IO earthquake and resulting performance at CP level as a function of soil type (f_c'=30MPa).

ATC 55: EVALUATION AND IMPROVEMENT OF INELASTIC SEISMIC ANALYSIS PROCEDURES

CRAIG D. COMARTIN[1]

ABSTRACT

The Applied Technology Council (ATC), with funding provided by the Federal Emergency Management Agency (FEMA), has initiated a project (ATC 55) to evaluate and improve the application of simplified inelastic analysis procedures for use with performance-based engineering methods for seismic design, evaluation, and rehabilitation of buildings. The objectives of this project are:

1. Improved understanding of the inherent assumptions and theoretical underpinnings of existing and proposed new simplified analysis procedures.
2. Recognition of the applicability, limitations, and reliability of various procedures.
3. Guidelines for practicing engineers to apply the procedures to new and existing buildings.
4. Direction for researchers on issues for future improvements of simplified inelastic analysis procedures.

This paper reports on the results of the first phase of the project. The focus is both on the current state of research for the development and enhancement of procedures as well as the state of practice in applying the procedures to real buildings. Issues include:

- Capacity spectrum vs. coefficient method
- Higher mode effects
- Uncertainty and reliability
- Equivalent SDOF and MDOF models
- Effects of degradation in stiffness and strength

The paper reviews the results of the first phase of the project which has included the assembly of basic information from researchers and practitioners. The objective of Phase I is to identify major issues for investigation during the subsequent two phases of the project. At the time of this writing (July 2001) the basic data has been assembled and the major issues formulated from a longer list of initial considerations. The second phase is currently being planned in detail. It is likely to include analyses of prototypical examples representing realistic buildings and behavior modes. The prototypes will be subject to nonlinear dynamic analyses to serve as benchmarks for assessing the relative merits of simplified dynamic (ESDOF and MDOF) and static (NSP) procedures. Various proposals for the improvement of procedures will also be investigated. The second phase culminates with the assembly of guidelines for the improved practical implementation of the simplified procedures. This will be followed in Phase III by a national workshop to present the results of the work and to gain focussed final input on particularly critical issues.

A dedicated project web site constitutes the primary communication activity for the project. Interested individuals can register at www.atcouncil.org. Access is unrestricted after registration. Documents cannot be changed on line but may be downloaded and returned with comments by email. Initially the site will contain a registration form, the detailed project work plan, a compilation of project issue summaries for review and comment, research and applications summary forms to allow researchers and practitioners to describe their relevant work. As work progresses, the results of the project will be posted to the web site for review and comment.

---

[1] *Comartin-Reis, Stockton, California*
comartin@comartin-reis.com

1. INTRODUCTION AND BACKGROUND

Knowledgeable engineers have long recognized that the response of buildings to strong ground shaking caused by earthquakes results in inelastic and nonlinear behavior. Until recently, most structural analysis techniques devised for practical application relied on linear procedures. In the last ten years there has been an emergence of simplified inelastic analysis procedures intended to provide engineers with more reliable and transparent tools for predicting seismic behavior of structures. These have facilitated the development of performance-based evaluation and design for new and existing buildings.

In 1996 the Applied Technology Council (ATC), with funding from the California Seismic Safety Commission, published the document*, ATC-40: The Seismic Evaluation and Retrofit of Concrete Buildings* (ATC, 1996). *FEMA 273/274: Guidelines and Commentary for the Seismic Rehabilitation of Buildings* were prepared by ATC (for the Building Seismic Safety Council) and issued in 1997. Both documents present similar performance-based engineering methods that rely on nonlinear static analysis procedures (NSPs). The two approaches are essentially the same when it comes to generating a "pushover" curve to represent the lateral capacity of a building. They differ, however, in the technique used to calculate the inelastic displacement demand for a given ground motion.

FEMA 273/274 documents a procedure known as the Coefficient Method. In the Coefficient Method, displacement demand is calculated by modifying elastic (or linear) predictions of displacement demand for anticipated differences between linear and nonlinear response, based in part, on statistically-based analytical investigations into nonlinear response behavior. (Krawinkler et al., 1992; Miranda and Bertero,1994; and Vidic et al., 1994).

ATC-40 details the Capacity Spectrum Method (Freeman et al., 1975). In this approach the pushover curve is plotted as a "capacity curve," a form in which plotting occurs in the domain of modal response acceleration vs. modal response displacement, as opposed to base shear versus roof displacement. Modal displacement demand is determined from the intersection of the capacity curve with a demand curve that consists of the smoothed response spectrum representing the design ground motion, modified to account for inelastic structural response behavior.

Structural engineers have applied nonlinear static procedures to the evaluation and rehabilitation of many structures in the past ten years. The use of NSPs has accelerated since the publication of ATC-40 and FEMA 273. There is consequently much information available on the practical application of these procedures. FEMA has recently issued *Case Studies: An Assessment of the NEHRP Guidelines for the Seismic Rehabilitation of Buildings* (BSSC, 1999). This document provides a summary of the application of the procedures of FEMA 273, including its NSP, to over 40 buildings by practicing engineers.

Additionally, several major institutions, including Stanford University and the University of California, Berkeley, have implemented guidelines for the rehabilitation of their existing buildings and design of new buildings using performance-based procedures and simplified inelastic analyses. Simplified dynamic analysis procedures have also been adapted to evaluate earthquake damaged structures (ATC, 1998abc). There is much information available on the issues encountered by practitioners when using the simplified dynamic analysis procedures. This information can be used to improve the future use of similar techniques.

In addition to the rather broad recent implementation of pushover methods in application to evaluation and upgrade of existing buildings, there has been very recent progress in applying these methods to the design of new buildings. An appendix to the 2000 edition of the *NEHRP Recommended Provisions for Seismic Regulation for Buildings and Other Structures* introduces pushover analysis as an alternative method for evaluation of strength and deformation demands on structures.

Concurrent to the development and initial applications of these performance-based methods, ongoing research portends important modifications, improvements, and alternatives to current NSPs. For example, several researchers have suggested that the Capacity Spectrum Method could be used to represent conventional (R, μ, T) methods of generating inelastic spectra (Fajfar, 1999; Chopra and Goel, 1999). Appendix I of the Structural Engineers Association of California (SEAOC) Blue Book (1999) covers performance-based design and includes a Direct Displacement-Based Procedure that applies principles of NSPs to the design of new buildings. Priestley (2000) describes a direct displacement procedure and compares it to other NSPs. The SAC Joint Venture, a partnership of SEAOC, ATC, and California Universities for Research in Earthquake Engineering, has extended the methods contained in FEMA 273 to explicitly account for uncertainty in both ground motion and structural response (SAC, 1999). The SAC procedures also incorporate practical application of incremental dynamic analysis to determine global structural stability (Luco and Cornell, 1999). Others are the studying the effects of strength and stiffness degradation, and higher mode effects on inelastic response.

The *ATC 40* document states explicitly that NSPs are relatively new and that future improvements and modifications are to be expected. In practice, engineers have found that in some cases different methods give substantially different estimates for displacement demand for the same building and ground motion, as well as the distribution of displacement demand throughout the structure (Aschheim et al., 1998; Maffei, 2000; Foutch, 2000). The disparities in displacement predictions highlight the need for comparison and further study of different approaches. Such study would provide guidance to structural engineers in the use of NSPs.

There has been a large national investment in performance-based engineering because of the tangible prospect to vastly improve seismic design practices. The future of performance-based engineering depends on reliable and credible inelastic analysis procedures. The proposed project defines a practical and effective way to resolve differences, incorporate new knowledge, and build consensus and guidance for improved use of nonlinear static analysis procedures as applied to both existing structure evaluation and upgrade, and new structure design.

2. PURPOSE AND OBJECTIVES

The objectives of the ATC 55 project are the development of practical recommendations for improved prediction of inelastic structural response of buildings to earthquakes (i.e., guidance for improved application of simplified inelastic analysis procedures) and the identification of important issues for future research. Specific anticipated outcomes are:

1. Improved understanding of the inherent assumptions and theoretical underpinnings of existing and proposed new simplified analysis procedures.
2. Recognition of the applicability, limitations, and reliability of various procedures.
3. Guidelines for practicing engineers to apply the procedures to new and existing buildings.
4. Direction for researchers on issues for future improvements of simplified inelastic analysis procedures.

The results of the project will culminate in a project document to be published by FEMA. This document will provide a comprehensive discussion of simplified inelastic seismic analysis of new and existing buildings. It will contain guidelines for applications of selected procedures including their individual strengths, weaknesses and limitations. The document will also contain illustrative examples and expert commentary on key issues. The document will serve to update and supplement existing publications including *FEMA 273/274, ATC 40,* and the *NEHRP Recommended Provisions*.

3. APPROACH

The technical approach on this project encompasses a variety of efforts, including: information and data gathering; data analysis and synthesis; identification and development of major issues impacting improved use of simplified inelastic analysis procedures; the planning and conduct of a national workshop to present and resolve major issues and identify research needs; the development of guidance to practicing engineers for improved use of existing and proposed procedures; and the documentation of project findings in suitable reports and engineering applications. In order to accomplish the project objectives expeditiously, the Project Team will conduct these activities in three distinct time phases. These are briefly described as follows:

Phase I – Assembly and Refinement of Key Issues

The focus of the first phase of the project will be the assembly and refinement of important issues relating to the improvement of inelastic seismic analysis procedures. Activities include the solicitation of input from researchers and practicing engineers. Study models of typical buildings will be developed to stimulate discussion, facilitate analytical studies, and provide example applications. As a result of the process key issues requiring analytical study will be identified for investigation in Phase II. This phase will be completed in the Summer of 2001.

Phase II – Resolution of Issues and Development of Practical Guidance

The second phase of the project will consist of analytical studies to explore selected key issues, the generation of written discussions on important topics, and the development of examples of the application of simplified inelastic analysis procedures. The phase will also include assembly of guidelines for the improved practical implementation of the simplified procedures. This work will be completed in early 2002.

Phase III – Presentation, Review, and Finalization of Project Report Document

The final phase of the work will include a national Workshop to present the results of the work and to gain focussed input on particularly critical issues. The final project document will incorporate the results of the Workshop. The Final report will be issued in 2002.

4. PERSONNEL AND MANAGEMENT

Chris Rojahn (Principal Investigator) manages the business aspects of the project, including contract funds. Craig Comartin (Project Director) is in charge of the technical activities. Bernadette Mosby coordinates the assistance provided by ATC staff and maintains project documents, information, and records.

The overall direction of the project work is the responsibility of the **Project Management Committee,** chaired by the Project Director and consisting of Chris Rojahn, Bill Iwan, Ron Hamburger, Bill Holmes, and Jack Moehle. Bob Hanson serves as FEMA's technical representative to this group. This committee establishes the goals of the project and the general strategy to meet them. All major project decisions are subject to the review and approval of this group. An advisory **Project Review Panel** provides independent expert review of the project work on a periodic basis.

A **Project Working Group,** lead by Joe Maffei and including Mark Aschheim and Mason Walters carry out most of the day-to-day activities for the project under the direction of the Project Director. A key aspect of the project is the active input of interested and qualified researchers and engineering practitioners. These participants, solicited at the beginning of the project, are to be informed of the progress of the work and provided opportunities for ongoing input.

5. ASSEMBLY ON INFORMATION ON RESEARCH AND PRACTICE

Work commenced on the project with the generation of a number of initial issues pertinent to the project objectives. These were assembled and described by the Working Group in a series Issue Summaries that are posted to a project web site www.atcouncil.org. The Working Group developed two forms to document the reaction and input of researchers and practitioners. These are also placed on the web, as was the overall project work plan. A short project summary is provided at the entry to the site. ATC has sent email announcements about the project website to a large number of potential contributors. Once at the site, individuals are asked to download any of the documents and fill out a form summarizing their comments.

To date nearly 400 individuals have registered at the site. Response to the web request for information has been small for researchers and practitioners alike. The Working Group, however, has contacted individuals directly to solicit information through emails, telephone conversations, and meetings. Information has been contributed by approximately 30 research. Data on the inelastic analyses of over 60 buildings has been contributed by practitioners. This information will be summarized in a Phase I Report that will be available soon at www.atcouncil.org.

At the beginning of Phase I a list of 42 issues relating to the development and application of inelastic analysis procedures was assembled. The Initial Issues Summary format comprised a succinct (one sentence) issue statement, an explanatory paragraph, pertinent references, and other appropriate information. The complete Initial Issues Summaries are available at www.atcouncil.org. .

Initial issues generally address the following:

Applicability

- Software limitations
- Three dimensional modeling
- Appropriateness of various analysis methods
- Variation in results using different procedures
- Uncertainty in ground motion and component capacity
- Global and component acceptability
- Differences between application to new buildings versus existing buildings
- Clarity and ease of use

Terminology

- Force-based versus displacement-based presentations
- Spectral presentation: Acceleration vs. Displacement vs. Period
- Different terminology used to express the same concepts
- Different meanings for the same terms
- Relating terminology between coefficient, capacity spectrum, and R-μ-T methods

Technical/Theoretical

- Inter-relationship of coefficient, capacity spectrum, and R-μ-T methods
- Relationship of effective damping to ductility
- Determination of initial stiffness and its effect
- Effect of Strength on Response
- Degradation of strength and stiffness
- Single-degree-of-freedom versus multi-degree-of-freedom and higher mode effects
- Ground motion parameters
- Probability and uncertainty
- Incremental dynamic analyses
- Load patterns for pushover analyses
- Variation in hysteretic parameters
- Limitations of various procedures
- Introduction of new methods

The intention of the Initial Issues Summaries was to form a basis for direction of the project. These were used to stimulate discussions with the researchers and practitioners as summarized in the previous sections. During the Phase I process the issues have been reviewed and consolidated to gain focus for the subsequent project work. In some most instances, this involved combining issues that were similar and organizing the results into logical groups. These logical groups form the major issues for future study and are summarized in the following subsections. Each Major Issue implies a primary project focus for the subsequent work. Secondary additional considerations are also listed. Finally, some issues are specifically designated as deferred for future study outside the scope of the current project.

5.1 Relative accuracy of procedures

Obviously, the user of any inelastic analysis procedure must be concern with the accuracy of the results. Many of the Initial Issues related to this concern. The "true" answer is particularly elusive for inelastic behavior of buildings subjected to strong ground shaking. Comparisons among various simplified procedures are not meaningful without a higher order benchmark. Regrettably, there is no accessible "right answer." Robust inelastic displacement records of real structures subject to actual strong ground shaking are virtually nonexistent. There is naturally a great deal of skepticism over the accuracy of nonlinear time history analyses of complex models. This is partially due to the difficulty in modeling complex inelastic component behavior. However, given this constraint on both THA's and simplified procedures (e.g. NSP's) using the same component models, the more rigorous analyses logically provides better, as opposed to "true", results. This currently is the best that can been done in judging the accuracy of inelastic analysis procedures.

There are many sources of variability including ground motion, behavior modes of components, modeling assumptions, etc. Simplified procedures tend to mask the sources of variability. Many engineers are not aware of the high degree of variability in ground motion, for example. Most accept the use of smooth response spectra as adequate for design purposes. It may be in many cases if the engineer understands the implications. This problem is exacerbated by the fact that there is generally a lack of good examples in literature. It is also important to note that research results must be carefully interpreted with regard to its inherent limitations. For example, it is not appropriate to extend directly the results of studies on bilinear elasto-plastic oscillators to strength degrading systems. In addition, much research is based on arbitrary parametric variations to a theoretical model. How do these models reflect the characteristics and variability of behavior of actual buildings?

Another related consideration is the relative applicability of simplified procedures. Some simplified procedures may have specific limitations. Some may be better than others for specific situations. There is also the question of when inelastic analysis is warranted in any form. Lower performance levels, for example, imply less inelastic behavior than higher levels and it may be that elastic procedures are adequate for this performance level.

Primary project focus

- Formulate prototypical examples based on real buildings.
- Establish benchmark inelastic time history analyses of prototypes.
- Include variability due to behavior mode.
- Incorporate variability of ground motion.
- Use a range of shaking intensity to generate a range of inelastic demand.
- Investigate results with and without P-Δ effects.
- Document the relative accuracy of the basic simplified procedures compared to benchmark.
- Apply selected modifications to simplified procedures and reassess accuracy.

Additional consideration

- Use actual recorded data to verify benchmark examples where available.
- Develop guidelines for the level of inelastic behavior actually warranting inelastic analysis.

Deferred for future study

- Consider variability attributable to engineering judgement with respect to modeling assumptions, component properties, etc.
- Investigate global and component acceptability criteria.

5.2 Fundamental bases and relationships

Most practicing engineers tend to select an inelastic analysis procedure as an adjunct to the use of a broader guideline or standard (e.g. FEMA 356, ATC 40). Although these documents represent an important step forward in the advancement of the state of the practice, they do not convey a complete understanding of basic principles underlying simplified procedure. They may be more "transparent" that past approaches, but are they deceptively so? The fundamentals of the various procedures affect applicability. In addition, procedures vary in complexity and basic assumptions associated with their application to specific buildings.

Primary project focus

- Explain the fundamental bases of each simplified procedures.
- Compare similarities and differences among procedures.

- Identify when complexity is warranted.

Additional consideration
- Modify/consolidate procedures for theoretical improvement

5.3 Behavior mode effects

The inelastic analysis procedures rely heavily on the initial strength and stiffness of the components of the structure. Yet, actual inelastic displacements are sensitive to changes in these parameters related to the characteristic behavior mode of the components and the corresponding ductility. These modes can result in a number of hysteretic categories including:
- elasto-plastic (unbonded braces),
- horizontally pinched (plywood shear walls),
- “Takeda-like” (flexurally controlled concrete and masonry), and
- vertically pinched (rocking walls or braced frames).

Besides strength and stiffness characteristics, cumulative component damage may decrease deformation acceptability. Strength and duration of ground shaking control this effect. There is little readily applicable research on this type of degradation. Consequently, the focus should probably be on strength and stiffness degradation (related to maximum displacement) leaving duration effects for future study.

Primary project focus
- Identify global behavior mode categories for prototypical examples based on predominant component behavior
- Select example buildings to represent prototypical behavior modes.

Additional consideration
- Investigate general effects of global strength and stiffness

Deferred for future study
- Duration effects

5.4 MDOF/Inelastic mechanism effects

Simplified procedures are affected by variability arising from assumptions about the degrees of freedom of motion in a structure. Most assume a predominant response in the first mode and specify a corresponding load pattern for a nonlinear static analysis. Simplified dynamic analyses using ESDOF oscillators also rely on force displacement relationships that neglect or simplify the effect of higher modes. These assumptions generate an anticipated inelastic mechanism for the structure independently of its actual dynamic response. The inelastic mechanism of a structure subject to shaking is dependent on its degrees of freedom of motion. Time history analyses typically indicate higher maximum inter-story shear forces than predicted using load distributions based on the first mode shape of a shear wall building in a nonlinear static analysis. Could this indicate a potential for an unanticipated inelastic mechanism forming at mid-height of the building? Although this has been speculated as a cause for damage observed in past earthquakes, there is a lack of conclusive documentation. Although there is a fair amount of research on this subject, it is not yet clear whether or when current procedures handle MDOF/inelastic mechanism effects adequately.

Three dimensional response can also be difficult to model for inelastic analysis. However, the focus for the project should be on two dimensional behavior as a logical area of initial work. Torsion and three-dimensional response are left for future study.

Primary project focus

- ♦ Identify typical inelastic mechanisms.
- ♦ Select examples with multiple possible inelastic mechanisms.
- ♦ Investigate the capability of simplified procedures in identifying inelastic mechanisms.
- ♦ Evaluate proposed enhancements to procedures to handle higher mode effects.

Additional consideration

- ♦ Distinguish between situations requiring simple procedures from those where more complex analysis is warranted.

Deferred for future study

- ♦ Plan torsion and other 3D effects.

5.5 Characterization of demand

Ground motion is a major source of variability in inelastic seismic analyses. Additionally, variability of inelastic demand increases with shaking intensity. Current guidelines for inleastic analysis do not provide extensive advice on characterizing ground motion and the implications of various alternatives. Simplified procedures handle ground motion differently. Current procedures may not be adequate for near fault motions. Researchers, for the most part, develop their own sets of input parameters when investigating inelastic procedures. Across the board, there is a lack of consistency and standards for ground motions utilized for inelastic analyses.

Primary project focus

- ♦ Develop standardized ground motion parameters for example analyses
- ♦ Include variation in shaking intensity
- ♦ Investigate capability of simplified procedures to handle near fault motions

Additional consideration

- ♦ Potential procedures for impulsive loading and near fault effects

Deferred for future study

- ♦ Duration effects

5.6 Practical guidance and education

It is clear from practitioners that there is a need for guidance and education about the application of inelastic procedures. There is a lot of good information in the technical literature but often it is not formulated in manner conducive to immediate application. There is a general lack of realistic examples of the application of procedures. As previously noted, practitioners are not well informed as to variability. There is a wide range of complexity associated with specific structures and the various alternatives. There is little guidance on the selection and implementation of appropriate procedures for given circumstances. Practitioners could benefit from a basic understanding of the principles involved. There is also a pervasive lack of consistency in terminology and nomenclature that hampers the educational process.

Primary project focus

- ♦ Develop accessible explanations of the basic principles and theories.
- ♦ Document thorough realistic example applications.
- ♦ Provide advice on selection of appropriate procedure based on specific project parameters.
- ♦ Develop step-by-step guidances for the application of the most generally useful procedures.
- ♦ Develop a comprehensive glossary of terms.
- ♦ Formulate and use a consistent nomenclature for simplified inelastic analysis.

Additional consideration

- ♦ Guidance on specialized applications
- ♦ Review of software capabilities

Deferred for future study

- ♦ Standards for application of each procedures
- ♦ Three dimensional effects

6. REFERENCES

Aschheim, M., Maffei, J., and Black, E., 1998, "Nonlinear Static Procedures and Earthquake Displacement Demands"*, Proceedings, Sixth U S National Conference on Earthquake Engineering*, Earthquake Engineering Research Institute, Oakland, California.

ATC, 1996, *The Seismic Evaluation and Retrofit of Concrete Buildings, Volume 1 and 2*, ATC-40 Report Applied Technology Council, Redwood City, California.

ATC, 1997a, *NEHRP Guidelines for the Seismic Rehabilitation of Buildings*, prepared by the Applied Technology Council (ATC-33 project) for the Building Seismic Safety Council; published by the Federal Emergency Management Agency, FEMA 273 Report, Washington, DC.

ATC, 1997b, *NEHRP Commentary on the Guidelines for the Seismic Rehabilitation of Buildings*, prepared by the Applied Technology Council (ATC-33 project) for the Building Seismic Safety Council; published by the Federal Emergency Management Agency, FEMA 274 Report, Washington, DC.

ATC, 1998a, *Evaluation of Earthquake Damaged Concrete and Masonry Wall Buildings - Basic Procedures Manual*, prepared by Applied Technology Council (ATC-43 project) for the Partnership for Response and Recovery; published by the Federal Emergency Management Agency, FEMA 206 Report, Washington, DC.

ATC, 1998b, *Evaluation of Earthquake Damaged Concrete and Masonry Wall Buildings - Technical Resources* prepared by Applied Technology Council (ATC-43 project) for the Partnership for Response and Recovery; published by the Federal Emergency Management Agency, FEMA 307 Report, Washington, DC.

ATC, 1998c, *Repair of Earthquake Damaged Concrete and Masonry Wall Buildings*, prepared by Applied Technology Council (ATC-43 project) for the Partnership for Response and Recovery; published by the Federal Emergency Management Agency, FEMA 308 Report, Washington, DC.

BSSC, 1999a, *Case Studies: An Assessment of the NEHRP Guidelines for the Seismic Rehabilitation of Buildings*, prepared by the Building Seismic Safety Council; published by the Federal Emergency Management Agency, FEMA 343 Report, Washington, DC.

Chopra, A.K., and Goel, R.K., 1999, "Capacity Demand Diagram Methods Based on Inelastic Design Spectrum", *Earthquake Spectra,* Vol. 15, No. 4, Earthquake Engineering Research Institute, Oakland, California.

Fajfar, P., 1999, "Capacity Spectrum Method Based on Inelastic Spectra, *Earthquake Engineering and Structural Dynamics.*

Freeman, S. A., Nicoletti, J. P., and Tyrell, J. V., 1975, "Evaluations of Existing Buildings for Seismic Risk: A Case Study of Puget Sound Naval Shipyard, Bremerton, Washington," *Proceedings, First U.S. National Conference of Earthquake Engineers*, Earthquake Engineering Research Institute, Berkeley, California.

Krawinkler, H., and Nassar, A.A., 1992, "Seismic Design Based on Ductility and Cumulative Damage Demands and Capacities," *Nonlinear Seismic Analysis and Design of Reinforced Concrete Buildings*, Elsevier Applied Science, London and New York.

Luco and Cornell, 1999, unpublished report for the FEMA-funded SAC Joint Venture project, Program to Reduce the Hazard of Steel Moment Frame Structures.

Maffei, J., 2000, "Suggested Improvements to Performance-Based Seismic Guidelines," *Proceedings, 12th World Conference on Earthquake Engineering*, Auckland, New Zealand.

Miranda, E., and Bertero, V.V., 1994, "Evaluation of Strength Reduction Factors for Earthquake Resistant Design", *Earthquake Spectra,* Vol. 10, No. 2, Earthquake Engineering Research Institute, Oakland, California.

Priestley, M. J. N., 2000, "Performance Based Seismic Design," *Proceedings, 12th World* Conference *on Earthquake Engineering*, Auckland, New Zealand.

SAC, 1999, *State of the Art Report Performance Prediction & Evaluation of Moment Resisting Steel Frame Structures,* 90% Draft, SAC Joint Venture, a partnership of the Structural Engineers Association of California, Applied Technology Council, and California Universities for Research in Earthquake Engineering.

SEAOC, 1999, *Recommended Lateral Force Requirements and Commentary*, Seismology Committee, Structural Engineers Association of California, Sacramento California.

Vidic, T., Fajfar, P., and Fischinger, M., 1999,"Consistent Inelastic Design Spectra: Strength and Displacement", *Earthquake Engineering and Structural Dynamics*.

SESSION B-1: COLUMNS AND NONSTRUCTURAL WALLS

Chaired by

♦ Sharon Wood and Masaomi Teshigawara ♦

AXIAL LOAD CARRYING CAPACITY OF R/C COLUMNS UNDER LATERAL LOAD REVERSALS

Daisuke KATO[1] and Koichi OHNISHI[2]

ABSTRACT

Recent earthquake resistant design concept of structures places explicit emphases on limit state design. Regarding reinforced concrete members three limit states have been discussed, i.e. operation limit state, repair limit state and safety limit state. The objective of this paper is to propose methods to evaluate limit deflections of reinforced concrete column members relating to safety limit state, which can be introduced in the performance based seismic design procedure. Conclusions were as follows : (1)Deflection angles to lose lateral load carrying capacity can be evaluated using Eqs.(1)(2) and coefficient m=2.3, (2)Deflection angles to lose axial load carrying capacity can be evaluated using Eqs.(1)(2) and coefficient m=3.6.

1. INTRODUCTION

Recent earthquake resistant design concept of structures places explicit emphases on limit state design. Regarding reinforced concrete members three limit states have been discussed, i.e. operation limit state, repair limit state and safety limit state. The objective of this paper is to propose methods to evaluate limit deflections of reinforced concrete column members relating to safety limit state, which can be introduced in performance based seismic design procedures.

Figure 1 shows an example of load-deflection relationship of a column specimen (specimen “C-5” reported by Kato(2001)) with high constant axial load (η=0.6). Two hollow circles represent important observed points relating to safety limit state; i.e. the point where restoring lateral force degraded to 80% of the maximum strength and the point where the specimen lost it’s axial load carrying capacity. The former point is assumed to represent the point where the specimen lost it’s design lateral load carrying capacity. On the other hand the specimen could not carry the scheduled axial load at the latter point. In other words the latter point is the last point measured in this loading test (after this point the loading was terminated).

The broken line in Fig. 1 represents evaluated skeleton curve which can be used in design procedures. Four solid circles represent characterized points of the column; i.e. cracking point, yielding point, point where the column loses the design lateral load (=yield strength) carrying capacity and point where the column loses the design axial load carrying capacity. It must be noted that the restoring lateral force of the last point was assumed to be 0 under conservative assumption although the specimen showed some residual restoring force in the loading test.

1 Department of Architecture, Faculty of Engineering, Niigata University, Niigata, Japan
Email: dkato@eng.niigata-u.ac.jp
2 Shiga Prefecture, Shiga, Japan

In this report evaluating methods of deflections of the last two points are discussed paying special attention to the last point which represents the axial load carrying capacity.

2. EVALUATING METHOD OF TWO LIMIT DEFLECTIONS

2.1 Analysis

Characterized points on the load deformation relationship can be calculated by basic flexural theory under the assumption that plane remains plane after bending. Figure 2 shows stress strain relationship of core concrete and assumed edge strain of core concrete at safety limit state.

Assuming edge strain of core concrete $m \cdot \varepsilon cp$ (εcp : strain at maximum stress point of confined concrete), plastic curvature at this point can be calculated replacing stress strain relationship by stress block shown in Fig. 2. Plastic deflection for this curvature can be given by assumed deformation mechanism of the column shown in Fig. 3. Consequently total deflection angle Rf can be given by Eqs. (1)(2) adding yield deflection angle Ry to plastic deflection angle mentioned above.

$$Rf = Ry + \varphi u \cdot D \qquad (1)$$

$$\Phi u = \begin{cases} (m \cdot \varepsilon p/je) \cdot (2/3)/e\eta & (0<e\eta<1/3) \\ (m \cdot \varepsilon p/je \cdot (2/3)/(5e\eta-4/3) & (1/3<e\eta<2/3) \end{cases} \qquad (2)$$

where D is depth of gross section of column, Je is core depth and $e\eta$ is equivalent axial load ratio discussed in section 2.2. Note that coefficient of the stress block $k1 \cdot k3$ was assumed to be 2/3. The coefficient m was obtained empirically with column specimens as described in Chapter 3.

2.2 Effects of varying axial load($e\eta$)

It is important to take effects of varying axial load on safety limit state into account. Figure 4(a) shows envelope curves of load deflection relationship of typical reinforced concrete column members with high axial load. Two examples are shown; i.e. a column with monotonic lateral loading and one with constant axial and cyclic lateral loading. It must be noted that behavior after yielding depend on the loading history, i.e. specimens with cyclic loading apt to show smaller deformation capacities comparing to those with monotonic loading. This is called cyclic loading effect in this study and previous study indicated that column specimens with constant axial load whose axial load ratio were higher than 1/3 showed the cyclic loading effect (Kato 1996).

Because behavior of a column with varying axial load and cyclic lateral loading is roughly similar to that with monotonic lateral loading, the behavior of the column with monotonic loading in Fig.4(a) can represent a column with varying axial load and cyclic lateral loading. Using experimental data equivalent axial load ratio $e\eta$ was proposed by Kato (Kato 1996), which can be used to obtain limit deflection of columns with varying axial load. In other words common design equation for limit deflection can be used for columns with constant axial load and those with varying axial load by this equivalent axial load ratio. Equivalent axial load ratio is expressed by Eq.(3) and Fig. 4(b) shows the relationship between maximum axial load ratio and equivalent axial load ratio.

$$
e\eta = \begin{cases} \eta p & 0 < \eta p \leq 1/3 \\ \eta p/5 + 4/15 - \eta s \quad (>0.33) & 1/3 < \eta p < 2/3/(1+\gamma) \\ (3+2\cdot\gamma)/5 \cdot \eta p - \eta s \quad (>0.33) & 2/3/(1+\gamma) \leq \eta p \leq 2/3 \end{cases} \qquad (3)
$$

γ = minimum axial load/maximum axial load (>0)

$\eta s = As\sigma y/(je \cdot je \cdot \sigma_B)$ (As:area of steel located at center of section)

2.3 Effects of shear strength (Rp)

Losing point of design lateral load carrying capacity of the column is not only determined by flexural behavior but shear failure after flexural yielding. In this study deflection angle to lose lateral load carrying capacity due to shear failure was assumed to be obtained as Rp value proposed by Architectural Institute of Japan (1990). Figure 5 shows this relationship. The Rp value was originally proposed as deformation capacity determined by shear failure after flexural yielding.

On the other hand effects of shear strength on losing point of axial load carrying capacity were not clearly understood. Further study is necessary on this point.

3. COMPARISON OF LIMIT DEFLECTION BETWEEN EXPERIMENT AND CALCULATION

3.1 Specimen Examined

Total number of 132 reinforced concrete column specimens tested in Japan were examined. Figure 6(a) shows frequency of subjected axial load of specimens with varying axial load and Fig. 6(b) shows that of specimens with constant axial load. Top part of each bar graph represents a number of specimens with data on neither deflection where restoring force degraded to 80% (Rexp,80%) nor that where the specimen lost it's axial load carrying capacity (Rexp,loss). In other words the loading was terminated before the restoring force degraded to 80% of the maximum strength in these specimens. Middle part of each bar graph represents a number of specimens with data on Rexp,80% only. In other words the loading was terminated before the specimen lost it's axial loading carrying capacity in these specimens. Consequently only 32 specimens (see Table 1) shown in the bottom part of each bar graph were available to evaluate axial load carrying capacity.

Figure 7 compares observed deflection angle when restoring force degraded to 80% of the maximum strength (Rexp,80%) with that where specimen lost the axial load carrying capacity (Rexp,loss) of 32 specimens. Most specimens lost axial load carrying capacities within 0.01 rad after the specimens lost lateral load carrying capacities.

3.2 Concrete Model for Core Concrete Confined by Transverse Reinforcement

In this study the concrete model proposed as a result of the New RC Projects (New RC Project 1993) was used for core concrete confined by square hoop reinforcement. This model was developed to match with a variety of experimental data conducted not only during the New RC Projects but by overseas researchers. The maximum strength of concrete and transverse reinforcement used in examined specimens was 132 and 1109 MPa, respectively. The maximum stress σp and the strain at the maximum strength εp of confined concrete are expressed as follows.

$$\sigma p=\sigma_B+\kappa \cdot \rho wh \cdot \sigma wy \tag{4}$$

$$\varepsilon p \begin{cases} \varepsilon c \cdot (1+4.7 \cdot (K-1)) & K \leq 1.5 \\ \varepsilon c \cdot (3.35+20 \cdot (K-1.5)) & K > 1.5 \end{cases}$$

$$\kappa=11.5 \cdot (dw/c) \cdot (1-0.5 \cdot s/je)$$
$$\varepsilon c=0.93(\sigma_B)^{1/4} \cdot 10^{-3} \qquad (\sigma_B\text{:MPa})$$
$$K=\sigma p/\sigma_B$$

where, σ_B denotes strength of plain concrete (MPa), c denotes length between effective supports of hoop, εc denotes axial strain at maximum point of plain concrete, ρwh denotes volumetric ratio of reinforcement to concrete core, je denotes core depth (mm), σwy denotes yielding strength of hoop (MPa, σwy<687MPa), dw and s denote diameter and spacing of hoop (mm).

3.3 Comparison between Calculation and Experiment

3.3.1 Deflection to lose design lateral load carrying capacity evaluated by previously proposed method (m=4.3)

Empirical equation to evaluate limit deflection to carry design lateral load was proposed by Kato (Kato 1996). Coefficient m, which was used to give edge strain of core concrete $m \cdot \varepsilon cp$, was obtained empirically and m=4.3 was proposed by Kato(Kato 1998) to estimate the average value of the deflection to carry design lateral load.

Figure 8 shows the relations between observed deflection angles when specimens lost lateral load carrying capacities (Rexp,80%) and calculation shown in Section 2.1 (Rf) using 32 specimens. As mentioned before Rf was given using the value of m=4.3 and equivalent axial load ratio $e\eta$. It must be noted that both vertical and horizontal axes were normalized by Rp value to eliminate the effect of deformation capacity determined by shear failure after flexural yielding. In other words the feasibility of the evaluating method of Rf should be discussed using the experimental data with Rf/Rp value of less than 1.

Figure 8 indicates that the calculation shows good estimation in the range of Rf/Rp<1. However in the range of Rf/Rp>1 the accuracy was found to be not good.

3.3.2 Deflection to lose design lateral load carrying capacity (m=2.3)

Figure 9 shows the relations between observed deflection angles when specimens lost lateral load carrying capacities (Rexp,80%) and calculation shown in Section 2.1 (Rf). It must be noted that vertical and horizontal axes were not normalized by Rp value in this case because the accuracy using Rp value was not good as shown in Fig. 8. In other words evaluating method using only Rf can be proposed by this figure. Coefficient m was chosen to match experimental data with calculation. Consequently the value of m=2.3 was obtained for average estimation. It may be added that reduction factor φ of 0.63 can be used for conservative design equation.

3.3.3 Deflection to lose axial load carrying capacity (m=3.6)

Figure 10 shows the relations between observed deflection angles when specimens lost axial load carrying capacities (Rexp,loss) and calculation shown in Section 2.1 (Rf). Vertical and horizontal axes were not normalized by Rp value either as discussion in Fig. 9. Coefficient m was chosen to match experimental data with calculation. Consequently the value of m=3.6 was obtained for average estimation. It may be added that reduction factor φ of 0.77 can be used for conservative design equation.

4. CONCLUSIONS

(1)Deflection angles to lose lateral load carrying capacity can be evaluated using Eqs.(1)(2) and coefficient m=2.3.

(2)Deflection angles to lose axial load carrying capacity can be evaluated using Eqs.(1)(2) and coefficient m=3.6.

REFERENCES

Architectural Institute of Japan (1990), *The design guidelines for earthquake resistant reinforced concrete buildings based on ultimate strength concept (in Japanese)*

Summary report on NEWRC project in 1992(1993), *c-7)state of the art report on characteristics of confined concrete, Research center on national land development, (in Japanese)*

Kato, D., Honda, Y., Suzuki, H. and Shiba, J. (1996)., *Confinement of Concrete of R/C Members under Varying Axial Load, The 11-th World Conference on Earthquake Engineering*

Kato, D., Shiba, J. and Matsuda, T. (1998)., *The deformation Capacities of R/C Columns under Varying Axial Load, Journal of Structural and Construction Engineering, No.506, pp.155-162 (in Japanese)*

Kato,D., Ohnishi, K., Otsuka, Y. and Doi, M. (2001)., *Tests of R/C Columns with Perpendicular Side Walls Subjected to Constant High Axial Load, Proceedings of the Japan Concrete Institute Vol.23.No.3, pp.163-168 (in Japanese)*

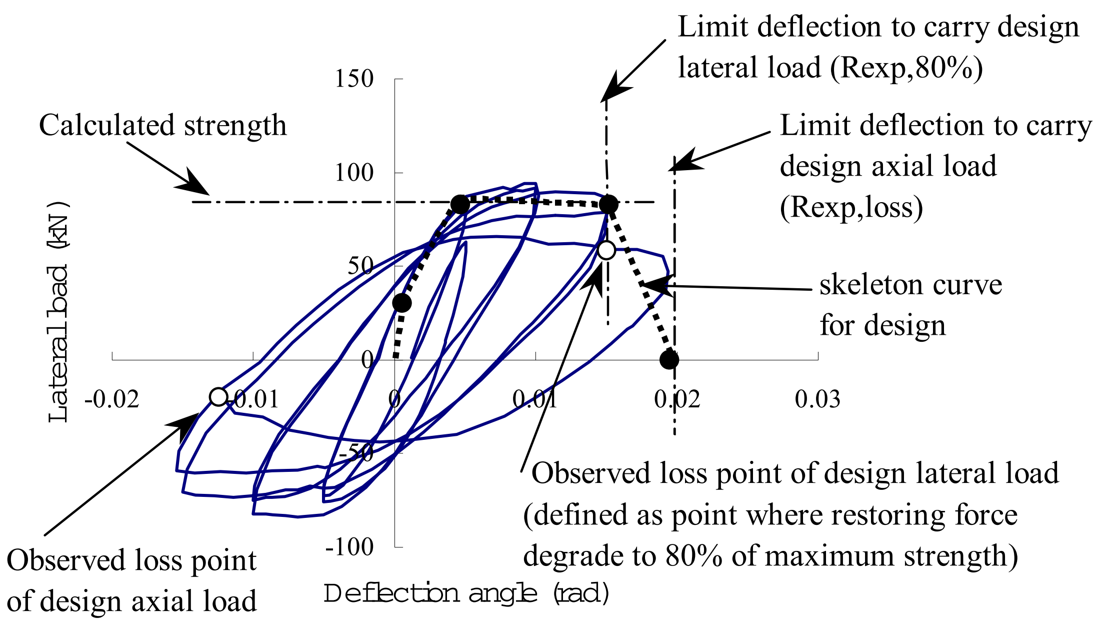

Figure 1 Example of load-deflection relationship of column with high axial load (Specimen C-2 by KATO(2001)) and evaluated skeleton curve for design

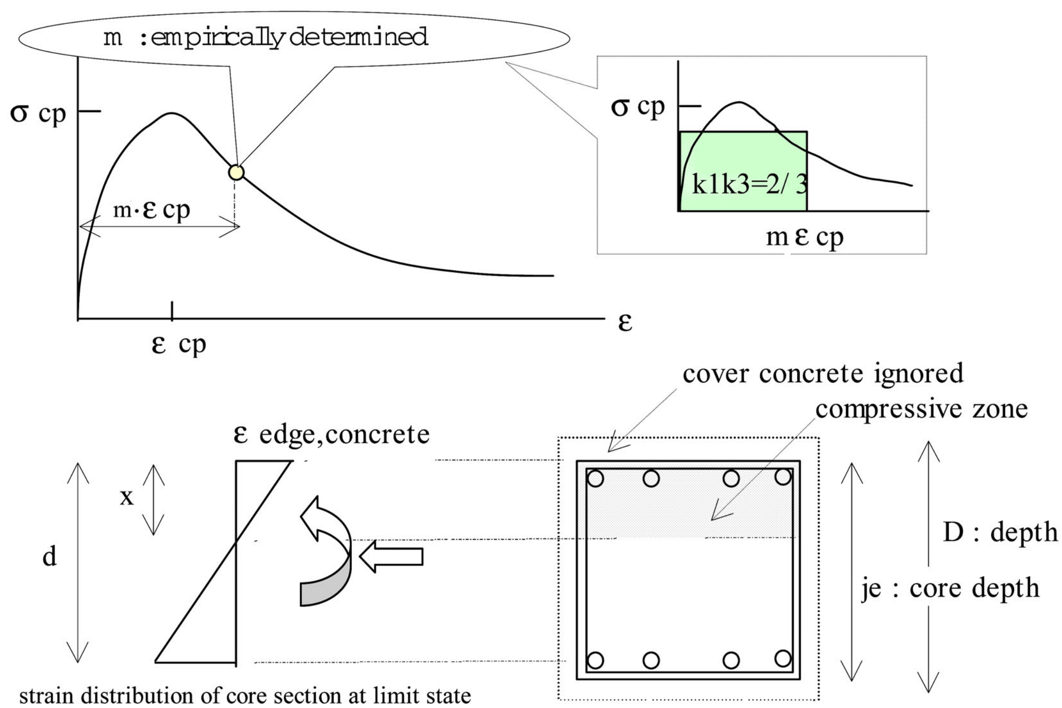

Figure 2 Stress-strain relationship of core concrete and assumed edge strain of core concrete at safety limit state

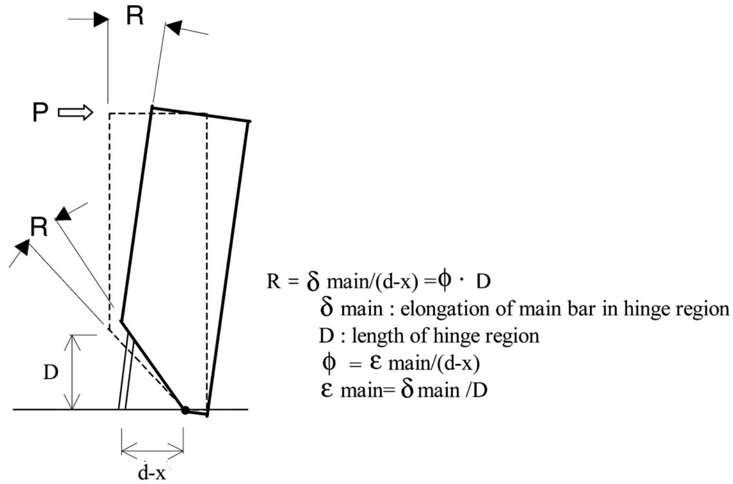

Figure 3 Deformation mechanism of column

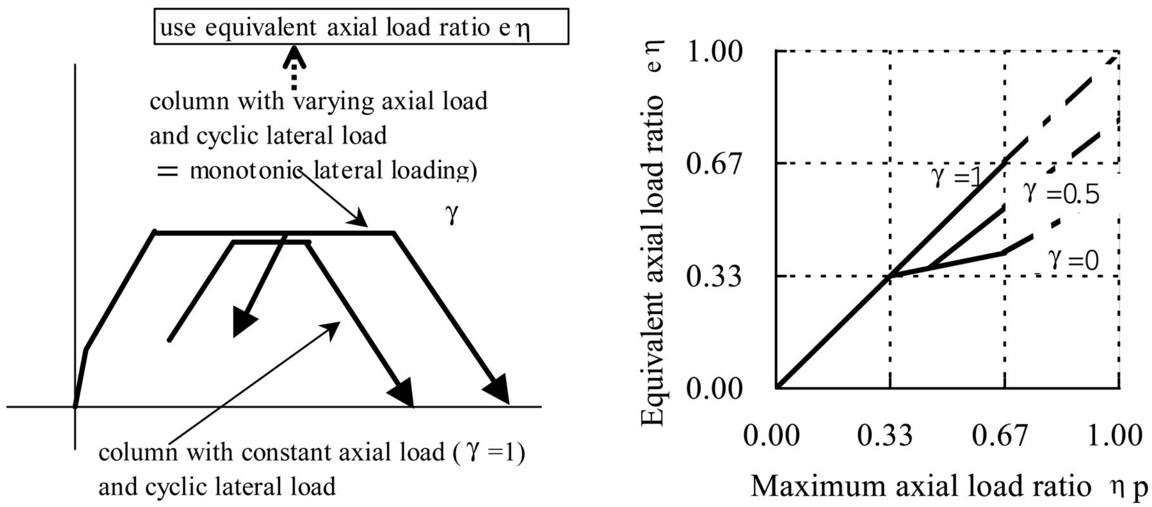

(a)Envelope curve of load-deflection relationship of columns (b)Equivalent axial load ratio

Figure 4 Effects of varying axial load on deformation capacity and equivalent axial load

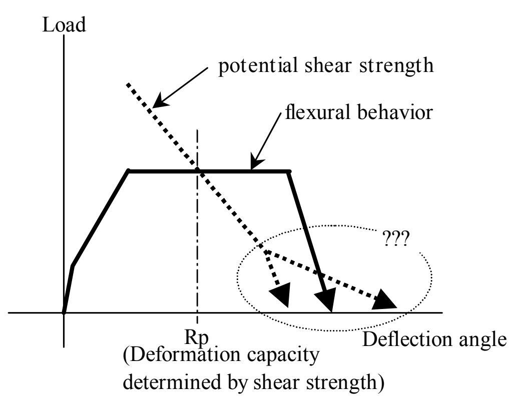

Figure 5 Effects of shear strength on deformation capacity

Table 1 Property of examined specimen

		Axial loading system		sum
		Constant	Varying	
Observed data	Both Rexp,80% & Rexp,loss value	25	7	32
	Rexp,80% value only	45	10	55
	None of the above	22	14	36
sum		92	31	123

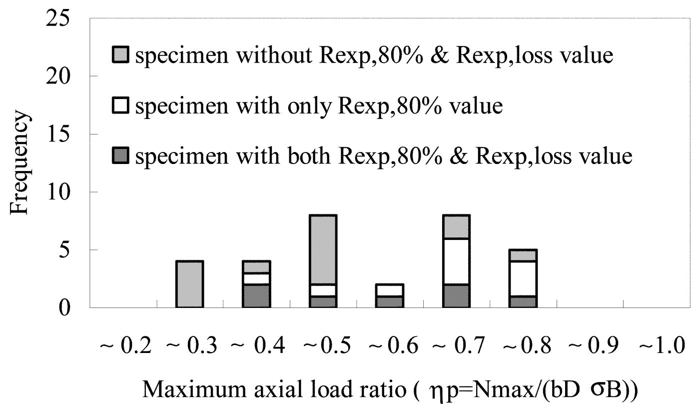

(a)specimen with varying axial load

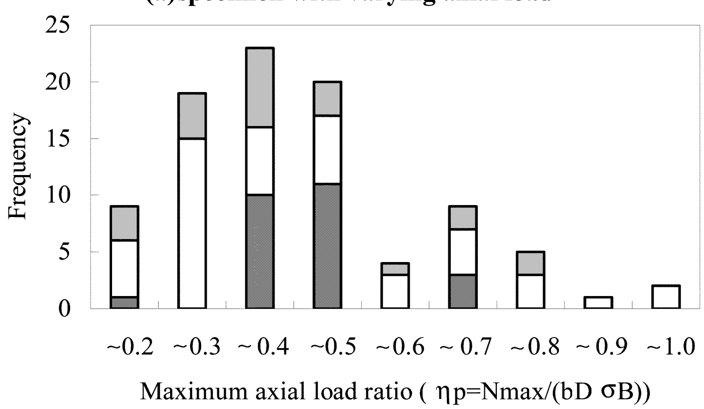

(b)specimen with constant axial load

Figure 6 Frequency of subjected axial load of examined specimens

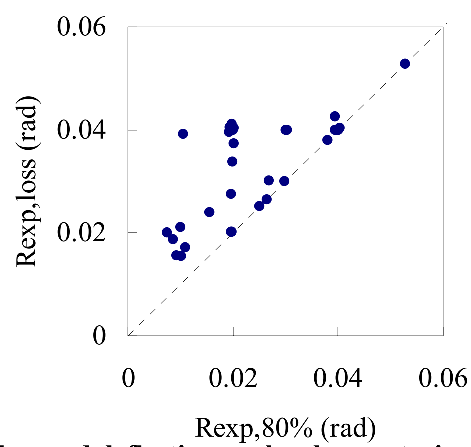

Figure 7 Relationship between observed deflection angle when restoring force degraded to 80% of the maximum strength (Rexp,80%) and that where specimen lost the axial load carrying capacity (Rexp,loss)

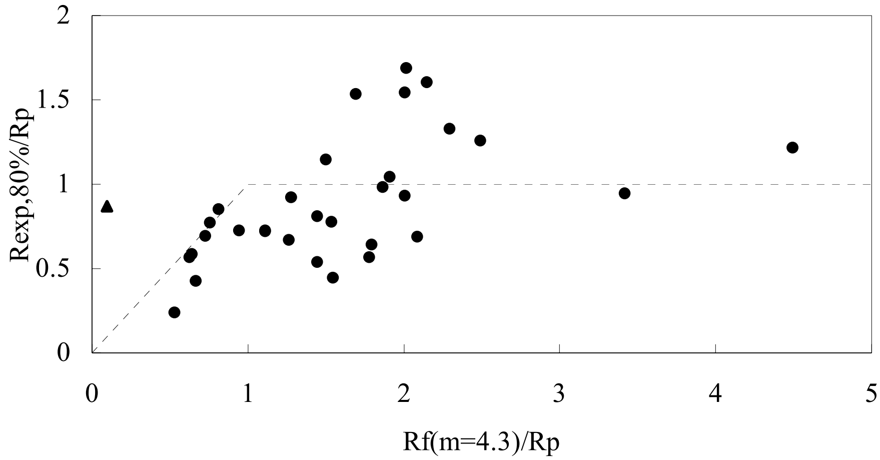

Figure 8 Comparison of deflection angle when specimen lost the design lateral load carrying capacity (assumed to be equal to Rexp,80% in this study) between experiment and calculation (m=4.3 was proposed for this point by KATO(1998))

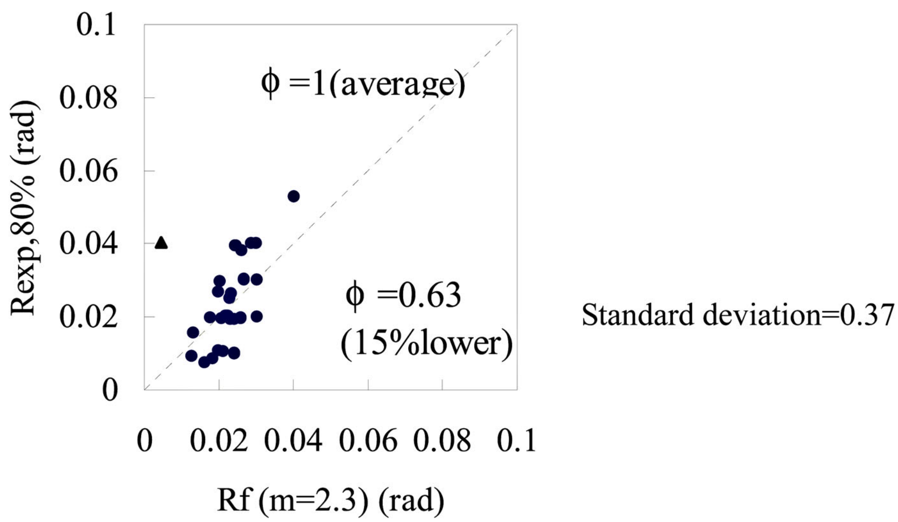

Figure 9 Comparison of deflection angle when specimen lost the design lateral load carrying capacity (assumed to be equal to Rexp,80% in this study) between experiment and calculation (m=2.3)

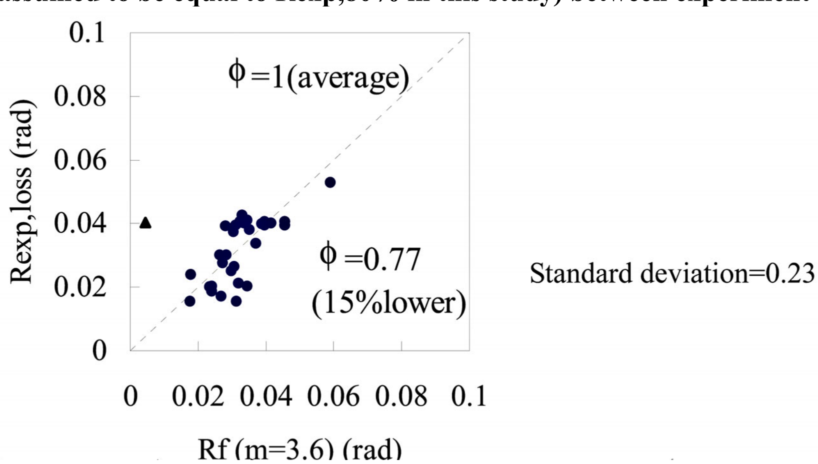

Figure 10 Comparison of deflection angle when specimen lost the axial load carrying capacity between experiment and calculation (m=3.6)

SEISMIC EVALUATION OF CUT AND COVER UNDERGROUND STRUCTURES

Antonio Bobet [1] and Julio A. Ramirez [2]

ABSTRACT

This paper describes the work conducted to date on the evaluation of the Daikai Station failure that occurred during the 1995 Great Hanshin event. The goal of the study is to evaluate the available tools and criteria to assess the seismic performance of cut and cover underground construction and propose modifications as needed. A series of numerical analyses have been carried out to investigate three specific issues: (1) the effects of the boundaries and the size of the mesh on the solution; (2) the contribution of interface elements between the soil and the structure; and, (3) the importance of the relative stiffness between the soil and the structure. The numerical study showed that: (1) the relative stiffness is a critical factor that controls the overall response of the soil-structure system; (2) the presence of the structure decreases the frequency of the response of the soil-structure system; and, (3) free field movements may not be produced due to the presence of the structure. In fact the response of the soil-structure system is a function of the relative stiffness of the structure compared to that of the ground. The analysis results show that a stiffer structure decreases the magnitude of the displacement field while a more flexible structure increases displacements. In the process of evaluating the collapse of the Daikai Station the failure mechanism of columns under inelastic shear reversals is being evaluated.

1. INTRODUCTION

The Daikai subway station, belonging to the Kobe Rapid Transit Line west of Kobe City, became the first reinforced concrete underground structure reported as having suffered complete collapse as a result of an earthquake (Figure 1). In addition, less severe damage was observed at many other locations along the line. In the Daikai station, more than 30 columns completely collapsed in a reported shear failure mode (Iida et al. (1996)). This caused the collapse of the ceiling slabs and a maximum subsidence of 3 meters of the national highway No. 28 running above the subway line.

The Daikai Station is the first underground structure not crossing an active fault that collapsed during an earthquake. Detailed analysis indicates that the middle column was grossly inadequate to resist lateral deformations. However, the Daikai failure is only a warning. The numerous examples of damage and even complete collapse of underground structures observed during the Great Hanshin Earthquake help define a problem that merits serious investigation. Of great concern to us is that there may be in the USA and Japan, underground structures under similar conditions to the Daikai Station. The problem is multi-faceted in that it requires that approaches be developed to both conduct the earthquake risk assessment of existing underground structures as well as the design of new ones, given certain ground motion characteristics. This calls for clearly defining structural performance

[1] School of Civil Engineering, Purdue University, 1284 Civil Eng. Bldg., West Lafayette, IN 47907-1284, USA (bobet@ecn.purdue.edu)

[2] School of Civil Engineering, Purdue University, 1284 Civil Eng. Bldg., West Lafayette, IN 47907-1284, USA (ramirez@ecn.purdue.edu)

not only in terms of safety, but serviceability as well, and as a function of possible disruptions of social and economic activities. This paper presents work completed during the first year of a project sponsored by the National Science Foundation under the US-Japan program. The project work has focused on load-transfer mechanisms between ground and structure and on deformation capacity of reinforced concrete columns.

Figure 1. Failure of Daikai Station

2. SEISMIC DESIGN PHILOSOPHY FOR UNDERGROUND STRUCTURES

The current seismic design philosophy is based on the notion that the effect of an earthquake on an underground structure, such as the Daikai station, is the imposition of a deformation that cannot be changed substantially by increasing the stiffness of the structure. Therefore, the strategy followed in the design is to provide sufficient ductility to handle the imposed deformation without collapse, rather than to try to resist inertial loads. The assumption that the underground structure conforms to the free field deformation of the ground is considered to be conservative because it ignores the stiffness of the underground structure. The degree of conservatism is considered to be dependent on the geometry of the structure and of the relative stiffness of the soil/structure system.

The above discussion leads directly to a displacement based design approach in these structures. A displacement-based design is predicated on the ability to properly estimate the ground displacement caused by the earthquake, and the effect of these displacements on the structure in terms of displacements as well. It is well known that this type of approach is useful because the calculated structural displacements, often expressed as the story drift ratio, can be related to levels of damage. For example, the inelastic deformation of structural and non-structural elements, behavior of “non-participating structural elements” that are deemed not to be part of the lateral load resisting system, global stability of the structure (P-Δ effects), damage to non-structural elements, and effects on the building occupants. A thorough discussion on this approach can be found elsewhere (Moehle, 92). A comparison between the displacement-based and the ductility based approaches (Moehle, 92), shows their parallel nature, and highlights the fact that in the ductility-based approach, readily calculated elastic forces define the ductility but do not provide a clear picture of the deformations. In the displacement-based approach, displacements are used directly to define element deformations.

It is also suggested, if strain limits for both concrete and steel are considered, a maximum drift ratio capacity on the order of 4%. In a building where maximum interstory drift ratio may be twice the roof drift ratio, the suggested maximum allowable roof drift ratio would be about 2%. It is also noted that roof drift ratios less than 2% would be desirable if the objective is to control nonstructural as well as structural damage. In walls with equal amounts of tension and compression reinforcement, the author suggested, that if a sufficient number is provided, a possible limit of 1% to the drift ratio would make confinement of the wall boundaries unnecessary. This same limit if applied to frame structures is suggested to permit neglecting P-Δ effects. The 1997 UBC limits the interstory drift ratios to a value between 2 and 2.5% depending on the period of the structure. In addition, a limit of 0.015 is placed on the extreme fiber compression strain.

3. FAILURE OF THE DAIKAI STATION

The Hyogoken-Nambu earthquake has brought into serious scrutiny the general appreciation that underground facilities are relatively safe structures during earthquake events. It can be argued that together with the damage observed in structural steel buildings, the damage of the underground structures represent the most startling revelations brought about by this event. The collapse of the one-story portion of the Daikai station shown in Figure 2, and depicted in Figure 3 as Section 1-1, has been related to the lack of deformation capacity of the central columns. A simple analysis based on the available static shear and flexural capacities of the critical middle column confirmed its shear critical nature.

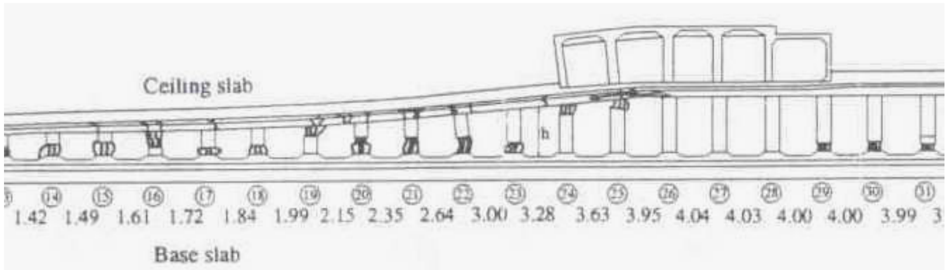

Figure 2. Schematic Damage of the Daikai Station

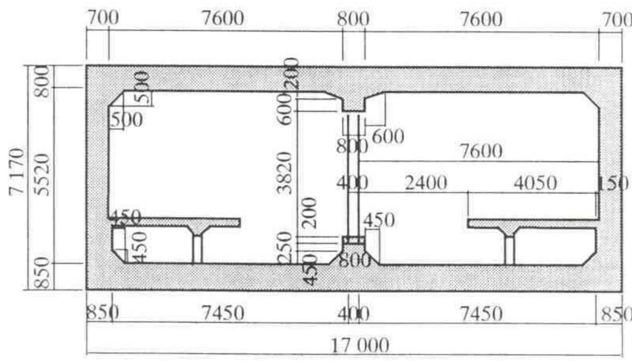

Section 1-1

Figure 3. Collapsed Cross Section

The results of the analysis lead to the conclusion that the maximum cross sectional distortion of the subway station could have been as low as 0.3% and as high as 1% for the structural shear failure of the middle column to occur. Observations during the Kobe event indicate that the strain in the "free field" soil could have been that high (Tokimatsu et al. 1996). Further analysis conducted by An and Maekawa also lead to the conclusion that the central columns failed first, which caused the collapse of the ceiling slab. However, questions relative to the load transfer from the soil to the structure, interface effects, significance of the overburden soil on the stability of the structure, and the deformation capacity in the inelastic range of reinforced concrete columns subjected to shear reversals under medium to high levels of axial load come to the forefront.

Figure 4. Damage in Two-Story Section of the Daikai Station

It must be noted that different levels of damage were observed within the Daikai station. As shown in Figure 2, the two-story portion of the station suffered some damaged but did not collapse. Figure 4 shows an example of the level of damaged observed in this part of the station. Other stations such as the Kamisawa and Sannomiya that suffered significant damage but did not collapse are examples of two and three story stations different from the collapsed one-story section of the Daikai station.

4. LOAD-TRANSFER MECHANISMS BETWEEN GROUND AND STRUCTURE

As part of the ongoing research project, a detailed numerical modeling of the structure and the soil has been performed with the Finite Element Method (FEM). A critical issue that has been addressed is the effect of the location and nature of the boundaries on the response of the soil-structure system. This is needed because the discretization of the continuum requires the existence of a finite domain with well-defined boundaries. If these boundaries do not exist naturally but are created artificially, it becomes necessary to determine appropriate conditions that simulate the physical behavior of the actual problem. This is not a trivial issue, and a large body of investigation has addressed this problem for the past fifty years (Waas, 1972; Desai and Christian, 1977; Wolf, 1985; Zheng and Takeda, 1995; Shawky and Maekawa, 1996; Wolf and Song, 1996; Akiyoshi et al., 1998; Athanasopoulos et al., 1999; Yazachi et al., 1999, among many others). The research shows that there are basically five types of boundaries that yield reasonable results with small errors compared to the "true" response:

(a) Free boundary (Zheng and Takeda, 1995): The soil can move freely in any direction
(b) Partially restrained movements at the boundary (Desai and Christian, 1977): The movements of the soil in one or more directions are restrained.
(c) Consistent boundary (Waas, 1972; Wolf and Song, 1996): Provides a response similar to the unbounded soil in a manner consistent with the finite element discretization; this approach is only suitable to solutions in the frequency domain.
(d) Superposition boundary (Wolf, 1985; Shawky and Maekawa, 1996): The solution is decomposed into its symmetric and anti-symmetric components, and thus the boundary is decoupled into a symmetric and anti-symmetric boundary with different constrains at each boundary.
(e) Viscous damper boundary (Akiyoshi et al., 1998; Athanasopoulos et al., 1999; Yazachi et al., 1999): It is based on the introduction of dampers to the boundaries of the mesh.

While all the methods have shown good results, it is important to realize that the consistent boundary requires a re-formulation of the algorithms of the finite element formulation, which is not possible with commercial software such as ABAQUS. The superposition boundary introduces additional complications with ABAQUS because it requires two layers of elements close to the boundary to impose the symmetric and anti-symmetric boundaries. Given the limitations of the implementation of some of the methods described, two types of boundaries have been investigated: free boundary, and viscous damper boundary.

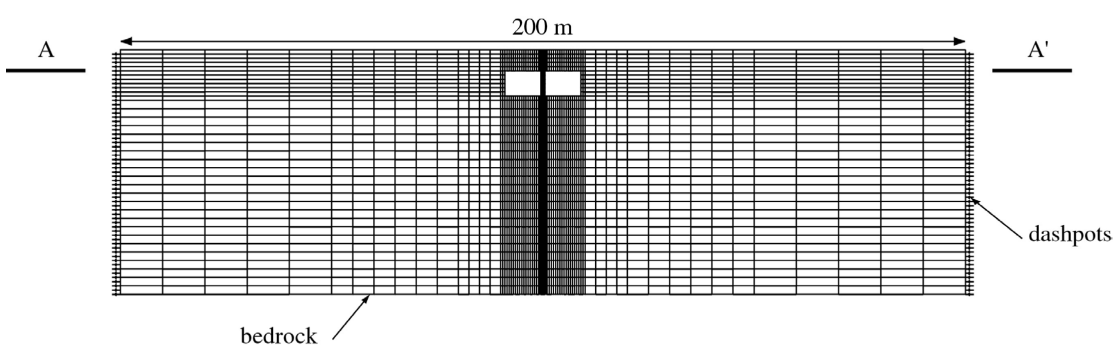

Figure 5. Mesh 200 m Long with Dashpots. Analysis (5)

A series of numerical analyses have been carried out to investigate the suitability of each of the two (free or viscous) boundary formulations given the nature of the problem and the software to be used. Five types of analyses have been conducted: (1) 1000 m long mesh without structure and free boundaries; the other four with the structure, as follows: (2) 1000 m long mesh with free boundaries; (3) 600 m long mesh with free boundaries; (4) 200 m long mesh with free boundaries; and (5) 200 m long mesh with dashpots at the boundaries. The length of the mesh in analysis (1) is large enough to provide the "free field" response of the soil in an area far from the boundaries. The goal of the simulations is to compare the response of the soil far from the structure with the response of the soil without the structure. If there is a region between the structure and the boundary where the soil recovers its free field response, then it can be concluded that the boundaries are placed far enough and they produce no disturbance, at least within an area near the structure. As an illustration, Figure 5 shows the mesh used for analysis (5). All the analyses have been carried out with the following parameters:

(a) Depth of the mesh down to bedrock, that appears at 58 meters below the surface.

(b) Ground modeled as a Drucker-Prager soil material, with the following properties: Unit weight, γ = 19.6 kPa; Young's Modulus, E = 30 MPa; Poisson's ratio, ν = 0.25; friction angle, $\phi=30^o$; dilation angle, $\psi = 3^o$; the ratio of the flow stress in triaxial tension to the flow stress in triaxial compression, k =0.8; Drucker Prager yielding stress, σ_c=20 kPa.

(c) Structure modeled as an elastic material with properties: Unit weight, γ = 23.5 kPa; Young's Modulus, E = 24000 MPa (e.g. concrete); Poisson's ratio, ν = 0.15.

(d) Interface elements between the structure and the ground, which allow for the opening of gaps and relative slippage between the structure and the soil. Coefficient of friction, μ = 0.4.

(e) Horizontal movements of the actual earthquake imposed at the base of the mesh (e.g. at bedrock).

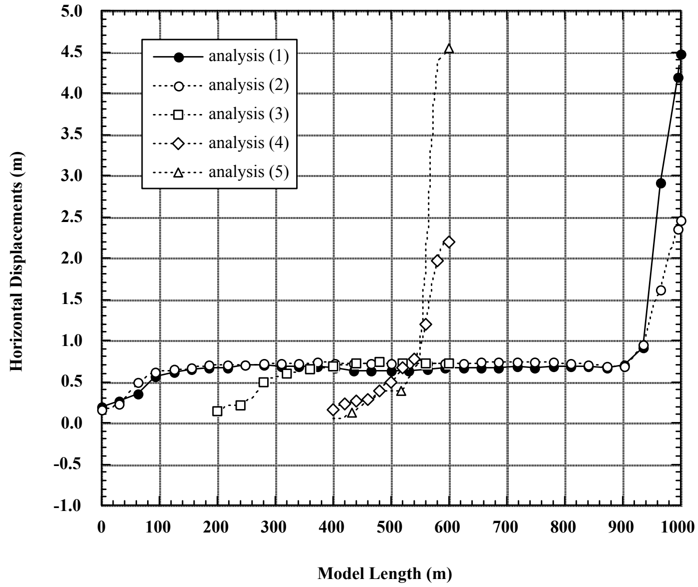

Figure 6. Comparison of maximum Horizontal Movements for Different Boundary Conditions, along Section A-A' (Figure 5)

Figure 6 shows a comparison between the maximum amplitudes of the horizontal movements along section A-A' (see Figure 5) for different boundary conditions and mesh lengths (i.e. results of analysis (1) through (5)). The only boundary conditions where the free field soil response is recovered between the structure and the boundaries are for the 1000 m long mesh and for the 600 m long mesh, although the 1000 m long mesh gives slightly better results. All the analysis have been run on a Sun Enterprise E6500 machine (28 CPUs running at 400 MHz and with 14 GB of system RAM from Engineering Computing Network, Purdue University). In this machine, it takes 15 hours to complete analysis (2), and 12 hours to complete analysis (3). Given that a small time increase improves the results, we have decided to use a 1000 m long mesh with free boundaries for all the detailed simulations.

Figure 7 shows the differential displacement history (i.e. difference between top and bottom horizontal displacements) of the central column of the structure during the earthquake. The maximum differential displacement of the central column is 0.084m, which represents a distortion of 1.5%. This distortion is large enough to produce failure of the column. Figure 7 also shows results of the simulation without interface elements. It is observed that the results are identical, which indicates that relative slippage between the structure and the soil plays a minor role on the load transfer mechanisms and compatibility deformations between the structure and the surrounding soil.

Another important issue under study is the effect of the relative stiffness between the underground structure and the soil. Two observations from this study: (1) the presence of the structure decreases the frequency of the response of the soil-structure system. (2) A stiffer structure decreases the response of the system, while a flexible structure increases the response of the system; naturally the force demand also changes.

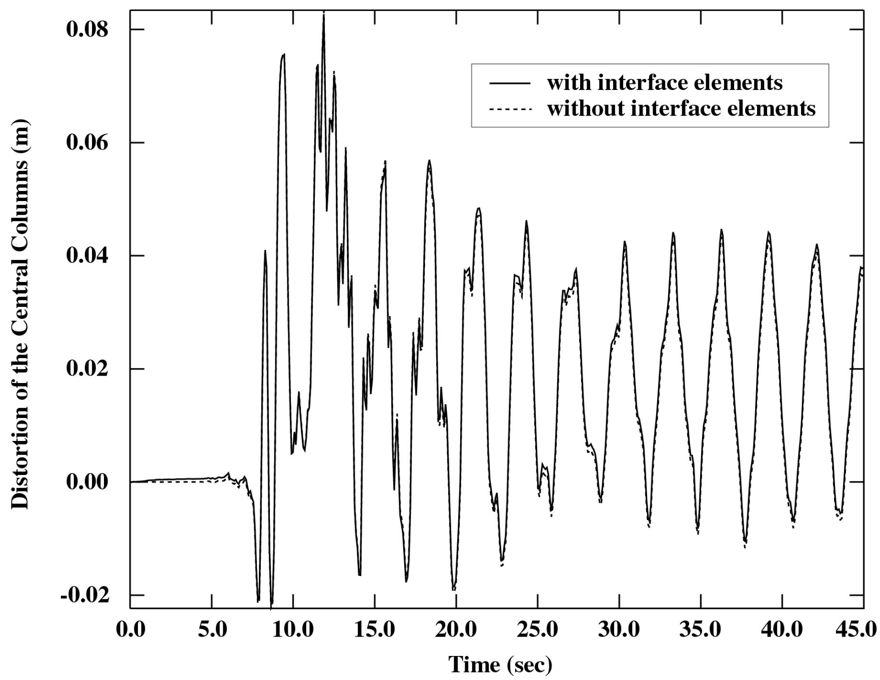

Figure 7. Analysis (2). Results with and without Interface Elements

The overall response of the soil-structure system, and thus the performance of the structure, is related to the stiffness/flexibility ratio of the ground-structure. We have defined the flexibility ratio as the ratio of the flexibilities of the ground and of the structure. The flexibility of the ground or the structure is defined as the ratio of the shear stress applied to either the ground or the structure to the displacement produced. For the case of the stiff structure, the flexibility ratio is 0.9 while for the flexible structure the ratio is 5.4. The results to date appear to follow the trend that for flexibility ratios less than one (structure stiffer than the ground), the response of the soil-structure system is smaller than the ground alone, while for flexibility ratios greater than one (structure more flexible tan the ground), the soil-structure system has a response larger than the ground alone.

5. DEFORMATION CAPACITY OF REINFORCED CONCRETE COLUMNS

A common design strategy for reinforced concrete buildings to sustain earthquakes is to allow their structures to dissipate energy through the process of permanently deforming some of their components. An alternative is to design the structure so that it remains elastic no matter what is the magnitude of the forces induced by the earthquake. The latter approach is expensive, risky, and essentially unpractical in cut and cover type structures. If permanent deformations are to be tolerated in the columns, as in the case of cut and cover structures such as the Daikai Station, the designer has to guarantee that they do not lose their integrity while being deformed permanently. Columns that do not have enough transverse reinforcement to carry the shear force associated with yielding of the longitudinal reinforcement do not meet this criterion: before they exhibit permanent deformations they would fail in shear.

A second possible behavior occurs when a column has sufficient shear strength and hence is displaced so much that it cannot recover its original shape after unloading, that is, when it is displaced beyond its "elastic" limit. Then, it may fail depending on the magnitude of the applied displacement and whether or not the direction of the load is reversed during the displacement process. Depending on the magnitude of the forces acting on it, such column may exhibit two different modes of failure. If the shear force acting on the column is relatively low, the column should be expected to fail after the outermost concrete is crushed and, subsequently, the longitudinal reinforcing bars buckle (Mode I). The displacement at which this type of failure takes place has been observed to decrease with increasing number of load reversals (El-Bahy et al., 1999). When the shear force acting on the column is high, a different type of failure is observed (Mode II). These columns fail in a relatively abrupt manner with successive shear reversals in the inelastic range of response at displacement levels below those that can be reached under monotonic loading (Wight et al. 1973; Priestley et al., 1994; Saatcioglu and Ozcebe, 1989). This type of failure seems to be associated with disintegration of the concrete in the core of the column. The meaning of the words "low" and "high" in this context is defined by the ranges of the experimental data examined. A component of this proposed study is devoted to the development of relatively simple analysis tools that can be used to take into account this phenomenon in the design and evaluation of concrete columns.

5.1 Shear Degradation Models

Several models for the failure mechanism of columns under shear reversals have been formulated (Aoyama, 1993; Moehle et al., 2000; Priestley et al., 1994 and 1996; and FEMA 273, 1997). In the models a common assumption is that the shear strength of a column decreases as the column is loaded under cyclic shear forces.

The initial shear strength of a column, where the main longitudinal steel yields, cannot be established because the maximum force that can be applied is limited to the force associated with the column's flexural strength. For the same reason, one cannot determine the rate at which the assumed degradation in the shear strength occurs. All one can determine through an experiment, in such cases, is the maximum displacement that can be reached before the lateral load that the column can carry decreases (Figure 8).

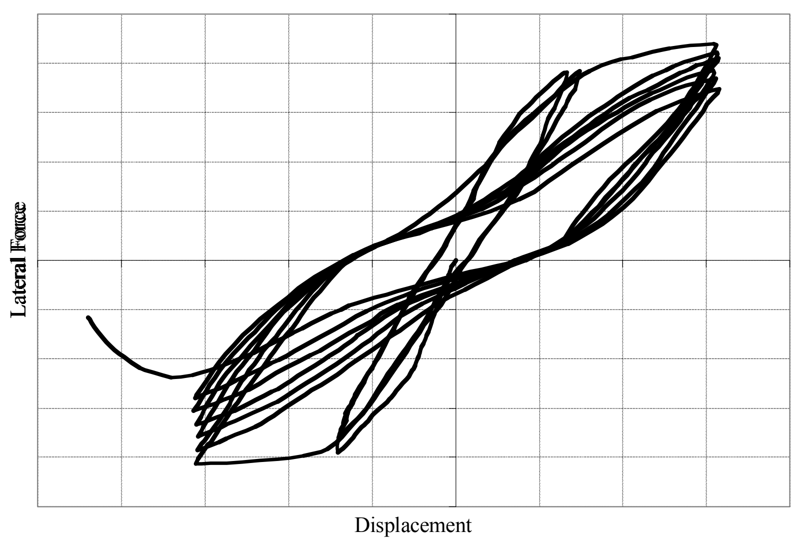

Figure 8. Lateral Force versus Displacement

A given maximum displacement can be reached through an infinite number of load "paths" or load sequences. It is reasonable to think that the deformation capacity of a given column may be a function of the way it is loaded. If the load is applied without changes in its direction, i.e. if the load is applied monotonically, there is no disintegration of the concrete in the core of the column. In fact, in most of the experiments where the flexural strength was attained prior to failure, the specimens were able to reach the displacement at which failure took place at least once before the strength started decreasing. Strength degradation can then be attributed to the effects of cycling, in combination with displacement levels. The question to be addressed is, therefore, the determination of the minimum level of displacement at which a reasonable number of cycles (a number representative of the response of structures under earthquakes) will cause failure.

6. SUMMARY OF FINDINGS AND FUTURE WORK

One of the most important contributions of the research performed in this period is the observation that free field movements may not be obtained due to the presence of the structure. In fact the response of the soil-structure system is a function of the relative stiffness of the structure compared to that of the ground. Our results show that a stiffer structure decreases the displacement field while a more flexible structure increases displacements. This observation can be used to address the failure of the Daikai Station and it may be useful to explain why other subway stations or other sections of the Daikai Station did not fail during the earthquake.

Current models for what has been called “shear strength degradation” ignore the number of load reversals as a variable. The available experimental data cannot be used to test such an assumption because in standard cyclic load tests displacement is increased gradually with increasing number of cycles. From the information obtained during such experiment it cannot be concluded whether failure was reached because of the number of times the load was reversed or because of the effect of the maximum applied displacement. In the next phase we will attempt to test systematically the available models, including a recent model proposed by Pujol et al. (2000), for columns under shear reversals, and special attention will be paid to the assumption that the number of load reversals is not relevant.

7. ACKNOWLEDGMENTS

This research is supported by the National Science Foundation, under grant CMS-0000136. The program manager is Dr. Peter Chang. This support is gratefully acknowledged.

In addition to the authors, the following personnel has been involved in the work: Mr. Hongbin Huo, a Ph.D. student from Purdue University, Professor Alfred Hendron and Dr. Gabriel Fernández, Research Engineer, from the University of Illinois at Urbana-Champain,

and Professor Koichi Maekawa, from University of Tokyo who has directed and coordinated the collaboration in this project between US and Japan researchers.

References

1. Akiyoshi, T., Sun, X. and Fuchida, K. (1998). General Absorbing Boundary Conditions for Dynamic Analysis of Fluid-saturated Porous Media, *Soil Dynamics and Earthquake Engineering,* 17, pp. 397-406.
2. An, X., and Maekawa, K. (1997). Failure Analysis of Underground RC Frame Subjected to Seismic Actions. Journal of Materials, Concrete Structures and Pavements, JSCE, No. 571, pp. 251-267.
3. Aoyama, H., (1993). Design Philosophy for Shear in Earthquake Resistance in Japan. *Earthquake Resistance of Reinforced Concrete Structures: A Volume Honoring Hiroyuki Aoyama*, Ed. Tsueno Okada, November 25, pp. 140-151.
4. Athanasopoulos, G.A., Pelekis, P.C. and Leonidou, E.A. (1999). Effects of Surface Topography on Seismic Ground Response in the Egion (Greece) 15 June 1995 Earthquake, *Soil Dynamics and Earthquake Engineering,* 18, pp. 135-149.
5. Desai, C.S. and Christian, J.T. (1977). *Numerical Methods in Geotechnical Engineering*, McGraw- Hill Book Company, New York.
6. Eberhard, M. and Parrish, M., (2000). Reinforced Column Test Database. *http://www.ce.washington.edu/~peera1*.
7. El-Bahy, A., Kunnath, S.K., Stone, W.C., and Taylor, A.W. (1999). Cumulative Seismic damage of Circular Bridge Columns: Benchmark and Low-Cycle Fatigue Tests. *ACI Structural Journal*, Vol. 96, No. 4, July-August, pp. 633-641.
8. FEMA 273 (1997). NEHRP Guidelines for the Seismic Rehabilitation of Buildings, *Federal Emergency Management Agency*, Washington DC, October 1997.
9. Iida H., Hiroto, T., and Yoshida, N. (1996). Damage to Daikai Subway Station. *Japanese Geotechnical Society*, Special Issue of Soils and Foundations, January 1996, pp. 283-300.
10. Moehle, J. P. (1992). Displacement-Based Design of RC Structures Subjected to Earthquakes. Earthquake Spectra, EERI, V. 8, No. 3, August, pp. 403-428.
11. Moehle, J.P., Elwood, K.J., and Sezen, H. (2000). Gravity Load Collapse of Building Frames During Earthquakes. *M. Uzumeri Symposium, Special Publication, American Concrete Institute.*
12. Priestley, M. J. N., Verma, R., and Xiao, Y. (1994). Seismic Shear Strength of Reinforced Concrete Columns. *Journal of Structural Engineering*, American Society of Civil Engineers (ASCE), Vol. 120, No. 8, August, pp. 2310-2329.
13. Priestley, M. J. N., Ranzao, G., Benzoni, G., Kowalsky, M. J. (1996). *Yield Displacement of Circular Bridge Columns*. University of California, San Diego.
14. Pujol, S., Sozen, M.A., Ramirez, J.A. (2000). Transverse Reinforcement for Columns of RC frames to Resist Earthquakes. *ASCE Journal of Structural Engineering*, Vol. 126, No. 4, April, pp. 461-466.
15. Richart, F. E., Brandtzaeg, A., and Brown, R.L. (1929). The Failure of Plain and Spirally Reinforced Concrete in Compression. *University of Illinois Eng. Exp. Station*, Bulletin No. 190, V. 26, No. 31, April, pp. 1-74.
16. Saatcioglu, M. and Ozcebe, G. (1989). Response of Reinforced Concrete Columns to Simulated Seismic Loading. *ACI Structural Journal*, Vol. 86, No. 1, pp.
17. Shawky, A. and Maekawa, K. (1996). Collapse Mechanism of Underground RC Structures during Hanshin Great Earthquake. *Proceedings of the First International Conference on Concrete Structures, Cairo, Egypt.*
18. Taylor, A.W. and Stone, W.C. (1993). A Summary of Cyclic Lateral Load Tests on Spiral Reinforced Concrete Columns. National Institute of Standards and Technology (NIST), *Report* NISTR 5285, United States Department of Commerce, Technology Administration.
19. Taylor, A.W., Kuo, C., Wellenius, K. and Chung, D. (1997). A Summary of Cyclic Lateral Load Tests on Rectangular Reinforced Concrete Columns. National Institute of

Standards and Technology (NIST), *Report* NISTR 5984, United States Department of Commerce, Technology Administration.
20. Tokimatsu, K., Mizuno, H., and Kakurai, M. (1996). Building Damage Associated with Geotechnical Problems. Japanese Geotechnical Society. Special Issue of Soils and Foundations, January, pp. 219-234.
21. Waas, G. (1972). *Linear Two-dimensional Analysis of Soil Dynamics Problems in Semi-infinite Layered Media*, Ph.D. thesis, Univ. of California, Berkeley.
22. Wight, J. K., and Sozen, M. A. (1973). Shear Strength Decay in Reinforced Concrete Columns Subjected to Large Deflection Reversals. *Structural Research Series No. 403*, University of Illinois at Urbana-Champaign, Civil Engineering Studies, 290 pp.
23. Wolf, J.P. (1985). *Dynamic Soil-Structure-Interaction Analysis*, Prentice-Hall, Englewood Cliffs, NJ.
24. Wolf, J.P. and Song, C. (1996). *Finite-Element Modeling of Unbounded Media*, John Wiley & Sons, Chichester, England.
25. Yazachi, M., Khalili, N. and Valliappan, S. (1999). Dynamic Soil-structure Interaction Analysis via Coupled Finite-element-boundary-element Method, *Soil Dynamics and Earthquake Engineering,* 18, pp. 499-517.
26. Zheng, J. and Takeda, T. (1995). Effects of Soil-structure Interaction on Seismic Response of PC-cable Stayed Bridge, *Soil Dynamics and Earthquake Engineering,* 14 pp. 427-437.

PERFORMANCE OF REINFORCED CONCRETE NON-STRUCTURAL WALL WITH SIMPLE ENERGY ABSORBING DEVICE

Akira TASAI[1] and Takashi TAGUCHI[2]

ABSTRACT

Recently, a structural control method that reduces the response in an earthquake is noticed and has gradually applied to the practical use. In this report, a structural control method using R/C non-structural walls was proposed. This method is composed of X-shape steel plates embedded into the R/C non-structural wall. The R/C non-structural wall as the hysteretic damper absorbs vibration energy by the steel plate's performance. The characteristics of the method were investigated by the real scale structural experiment. The earthquake response analysis is carried out in order to confirm the effectiveness of the method. The basic design data of the building with this method are accumulated by the parametric analysis.

1. INTRODUCTION

Many structural control methods have been used to the practical application. However, some kind of the method reduces the performance in the occupancy by installing to the opening. The authors propose a structural control method using R/C non-structural walls. This method is composed of X-shape steel plates embedded into the R/C non-structural wall, as shown in Figure 1. The steel plate deforms into plastic range proportionally to the story drift during an earthquake. The R/C non-structural wall as hysteretic dampers absorbs vibration energy by their hysteretic performance. Since particular installation is not necessary, this method has no influence to the architectural planning. Moreover, the method does not use special material or members. Concrete of the wall protects buckling of the embedded steel plate when subjected to the compression.

1 *Dept. of Architecture and Building Science, Faculty of Engineering, Yokohama National University, Yokohama 240-8501, Japan*
Email: tasai@arc.ynu.ac.jp
2 *Technology Promotion Department, Yahagi Construction Co., Ltd., Nagoya 461-0004, Japan*
Email: t-taguchi@yahagi.co.jp

Static characteristics of the R/C non-structural wall were investigated by the real size structural experiment. And the method to estimate the initial stiffness and yield shear of the wall was proposed. The earthquake response analysis was carried out in order to confirm the effectiveness of this method based on the experimental results. The basic design data of the building with this structural control method are accumulated by the parametric study.

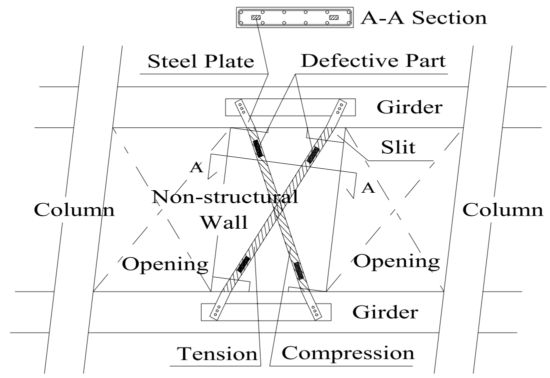

Figure 1 The Outline of the Method

2. OUTLINE OF REAL SCALE TEST

Three real scale non-structural wall specimens, whose shapes and dimensions are shown in Figure 2, were tested. The height, span and thickness of the R/C walls were 2000 mm, 1000 mm and 180 mm, respectively, supposing non-structural walls in apartment houses. Steel plates of 90 mm in width and 12 mm in thickness were embedded inside the wall in X shape, through the slits both at the bottom and at the top of the wall. The clearance of the slits was 25 mm, which was able to make the rotation of the wall free up to the 1/30 radian of the story drift.

The variable of the test was a shape of the embedded steel plate as shown in Table 1 and Figure 2. In specimen SD-11, normal steel plates with no defective parts were used, while in specimens SD-21 and SD-22, steel plates with defective parts of ellipse shape in vicinity of the slit were used to control the yielding of the plates. The area of the defective part was half of the total area of the plate and its length was 150 mm. In case of that length, within 1/100 radian of the story drift, the axial strain of the plate at the defective part was supposed not to reach 2 %, at which the strain hardening started. The surface of the plates was greased to remove the bond against the concrete of wall. Properties of the steel plate and concrete are shown in Table 2 and Table 3. The specimens were subjected to lateral shear reversals statically by the loading apparatus shown in Figure 3. The weight of the apparatus was cancelled by the axial hydraulic jack during the loading.

Table 1 The variable of the test

specimen	Steel Plate		Defective Part		
	Width (mm)	Thickness (mm)	Length (mm)	Width (mm)	Location* (mm)
SD-11	90.0	12.1	-	-	-
SD-21	89.9	12.1	150	45.1	150
SD-22	90.1	12.0	150	45.1	300

* : Distance between Slit and Center of Defective Part

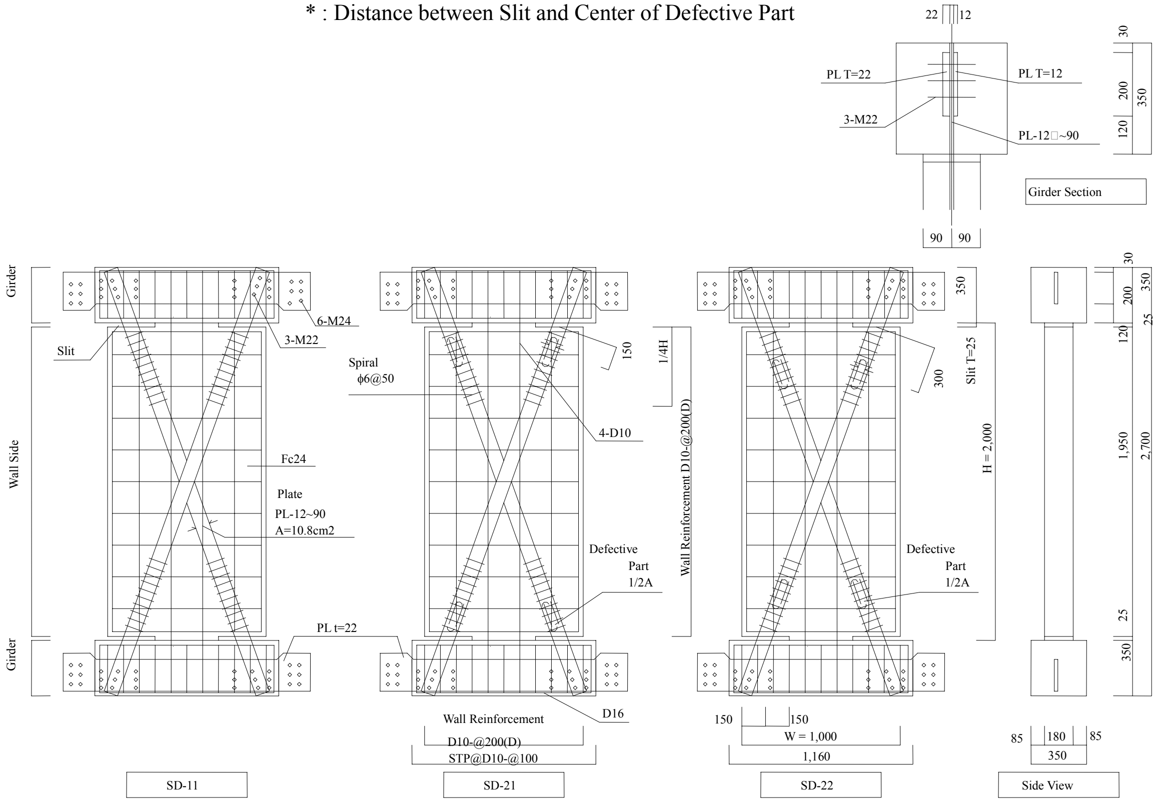

Figure 2 The real scale non-structural wall specimens

Table 2 Properties of the steel plate

Classification	Yield Stress (N/mm^2)	Tensile Strength (N/mm^2)	Strain at Strain Hardening (%)	Elongation at Fracture (%)
SS400	279.	441.	2.1	48.2
D10(SD295A)	382.	551.	2.3	19.3
D13(SD295A)	360.	524.	2.5	19.9

Table 3 Properties of the concrete

Compressive Strength (N/mm^2)	Split Tensile Strength (N/mm^2)	Slump (mm)	Max, Aggregate (mm)
40.4	2.7	185	20

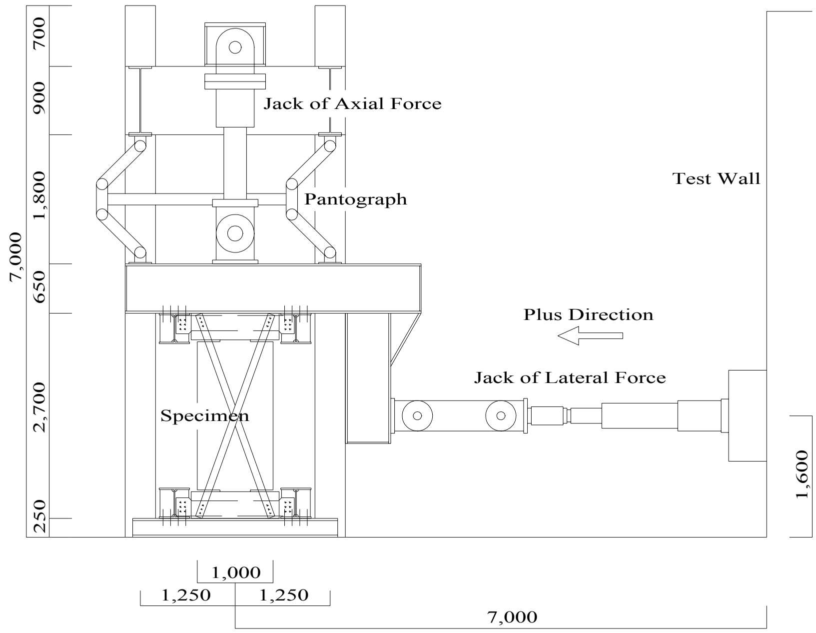

Figure 3 The loading apparatus

3. TEST RESULTS

Crack patterns of specimen SD-21 after the test are shown in Figure 4. In all specimens, only in the immediate vicinity of the slits were the cracks observed. The maximum width of the crack was 8 to 10 mm at 1/30 radian of the story drift. No visual damage generated in the R/C wall plate.

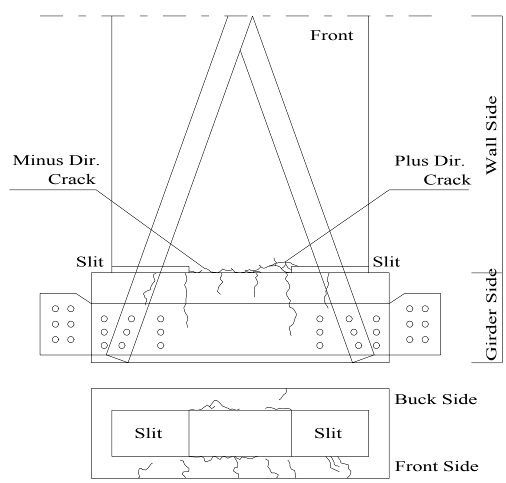

Figure 4 Crack patterns of specimen SD-21

The restoring force characteristics of specimens are shown in Figure 5. Marks in the figure indicate the tensile yielding at each location of the steel plates or wall reinforcement shown in Figure 6. Desirable energy absorbing performance was developed in all specimens. Buckling of the steel plates was not observed during the loading. Yielding at each location in Figure 6 at peak deformations of each loading cycles is illustrated in Figure 7. In specimen SD-11 with normal steel plate, yielding generated at all locations during the loading cycle of 1/100 radian. In specimen SD-21, yielding generated only in the defective part of the steel plate. In specimen SD-22, yielding at the defective part preceded but sequential yielding generated at other parts.

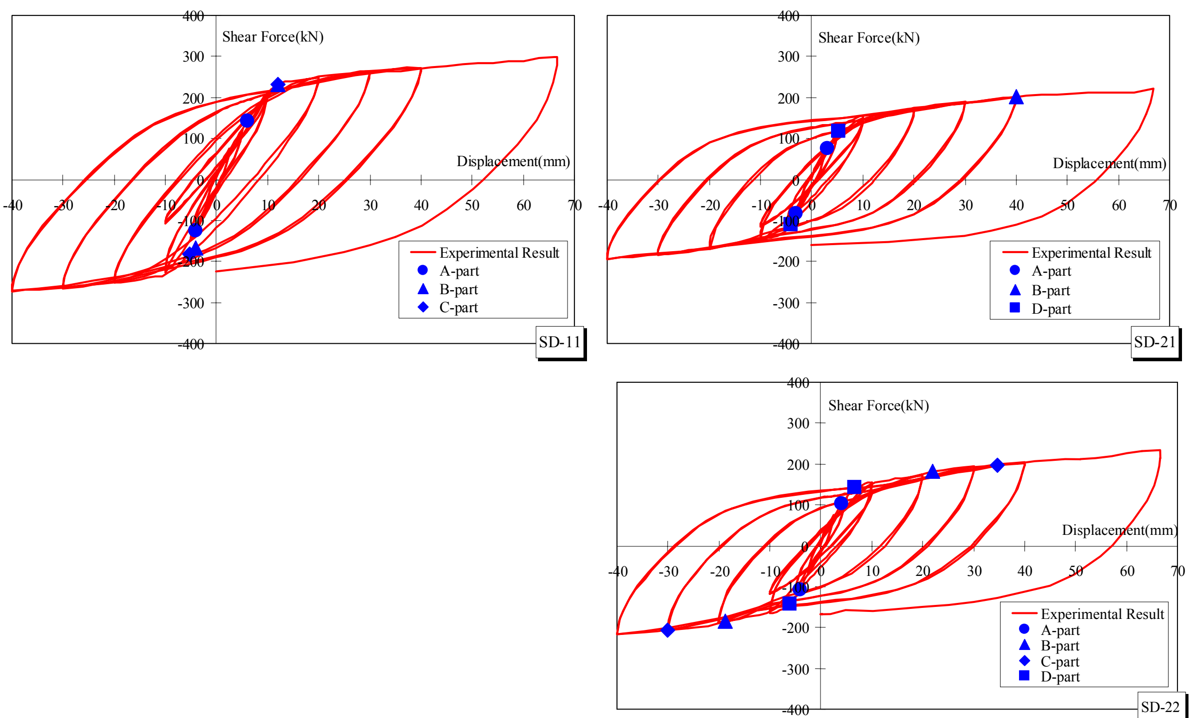

Figure 5　Restoring force characteristics

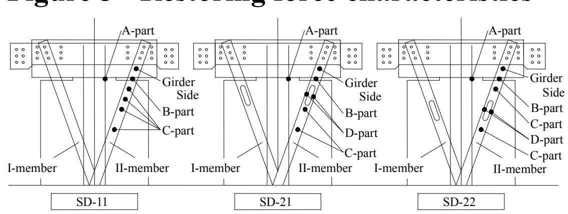

Figure 6　Marks

Absorbed energy E and equivalent viscous damping factor h_{eq} in each loading cycle are shown in Figure 8. The E of specimen SD-11 is superior to other specimens, but the h_{eq} of specimens SD-21 and SD-22 are larger than that of specimen SD-11. Energy absorbing performance did not deteriorated up to large deformation probably because little damage developed during the loading.

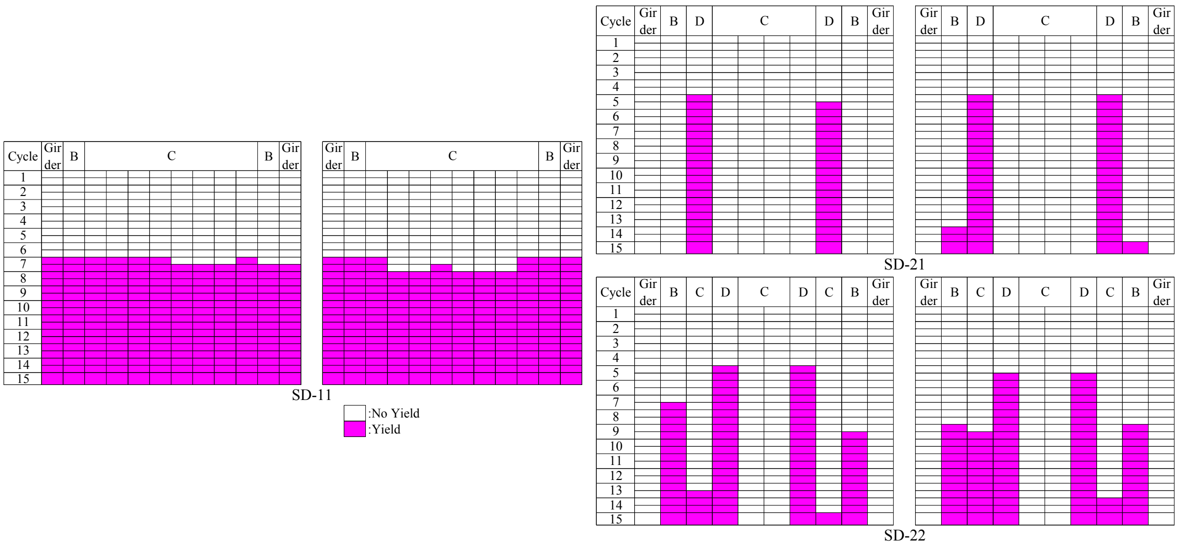

Figure 7　Development of Yielding in Steel Plates

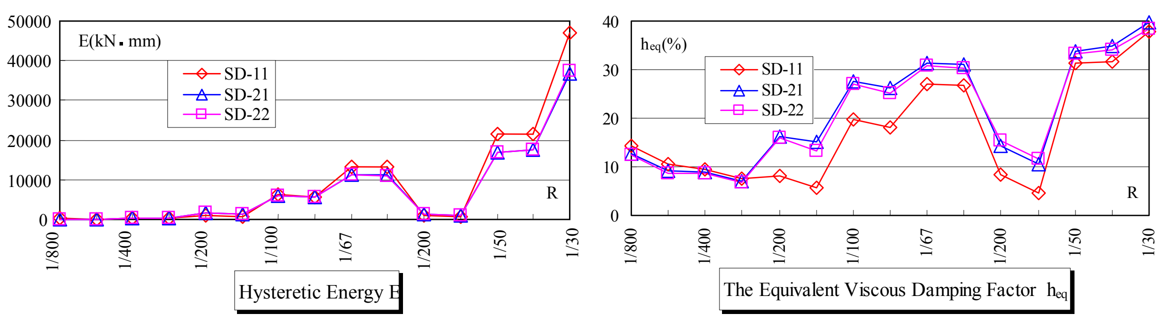

Figure 8　Absorbed energy E and equivalent viscous damping factor h_{eq}

4. RESPONSE ANALYSIS BASED ON TEST RESULTS

The effectiveness of the proposed method on the earthquake response of the building was analyzed based on the restoring force characteristics obtained by the experiment. Responses were compared between in the case of the R/C proto-type building and in the case adopted of the proposed method. The restoring force characteristic model in the analysis was determined based on the experimental results of the specimen SD-21. Three earthquake records, the NS component of El Centro record (1940), the EW component of Taft record (1952), and the NS component of JMA Kobe (1995) were used as input ground motions after their maximum velocities were corrected to 25 cm/sec or 50 cm/sec.

An outline of the R/C proto-type building is shown in Table 4 and Figure 9. The analysis was carried out in the X direction. The building was idealized to be 8 lumped mass model with equivalent shear stiffness obtained from the static elasto-plastic analysis for the proto-type frame. The Tri-linear type TAKEDA model was adopted as the hysteretic characteristics of each story (index for the unloading stiffness was assumed to be γ=0.4).

Table 4 An outline of the R/C proto-type building

Construction Site	Suzuka City
Use of the building	Apartment
Eaves height	22.81 m
Max height	24.71 m
Total floor area	5846.56 m^2
Building area	990.02 m^2
Construction	R/C Structure , 8-floors X direction : Frame Structure, 9 spans Y direction : Wall Structure , 1 span

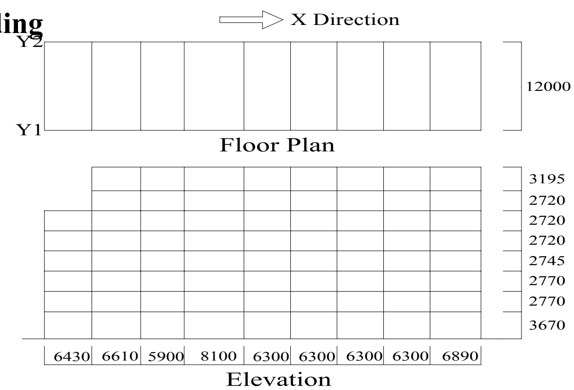

Figure 9 The R/C proto-type building

Two type models were adopted for the R/C non-structural wall. The first model was Tri-linear model whose absorbing hysteretic energy in loops between story drift angles of ±R=1/100 radians was equivalent to the experimental result. The second model was the Bi-linear model whose initial stiffness K and yield shear Qy were calculated by the following equations (1) and (2). In this model, the stiffness after yielding was assumed to be 0.2 times of the initial stiffness.

$$K = \frac{2W^2}{L^2} \cdot \frac{Es}{(L1/A)+(L2/A')} \qquad (1)$$

$$Qy = \frac{2A'\sigma yW}{L} \qquad (2)$$

H : Wall Height (2000 mm)
W : Steel Plate Distance between the Supports of the X-shape Plates (717.95 mm)
L : Steel Plate Length in Wall (2124.96 mm)
L1 : Steel Plate Length Except for Defective Part (1824.96 mm)
L2 : Steel Plate Length of Defective Part (150×2 mm)
A : Sectional Area of Steel Plate (1085.5 mm^2)
A' : Sectional Area of Steel Plate in Defective Part (540.6 mm^2)
Es : Young's Modulus of Steel Plate (205000N/mm^2)
Σy : Yield Stress of Steel Plate (279.0N/mm^2)
K : Initial Stiffness of R/C Non-Structural Wall (N/mm)
Qy : Yield Shear of R/C Non-Structural Wall (N)

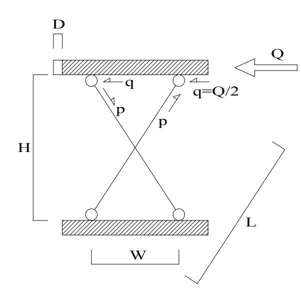

The comparison of the R/C non-structural wall models and experimental results is shown in Table 5 and Figure 10. In the both models, energy absorbing characteristics agreed with test results in the R=1/100 rad. However, in the Tri-linear model, absorbing energy was overestimated in the small displacement. Conversely, the Bi-linear model remained elastic in the small displacement. The analytical building model with the R/C non-structural walls was supposed to be installed with the non-structural wall at all stories and spans. At every story from the 1st to 6th floor,18 units of the wall were installed, and from the 7th to 8th floor, 16 units were installed. These non-structural walls were represented by an additional shear spring to the proto-type 8 lumped mass model in each story of the building.

Table 5　Comparison of the R/C non-structural walls model and experimental results

Wall Model	Story Drift Angle R	Hysteresis Energy / Equivalent Viscous Damping Factor	Experimental Result	Wall Model	Ratio to the Experimental Result
Tri-linear Model	1/800	E(kN mm)	96.5	0	0.00
		h_{eq}(%)	9.2	0	0.00
	1/400	E(kN mm)	248.6	490.1	1.97
		h_{eq}(%)	7.0	15.7	2.26
	1/200	E(kN mm)	1421.4	1755.5	1.24
		h_{eq}(%)	15.1	20.6	1.37
	1/100	E(kN mm)	5637.7	5755.1	1.02
		h_{eq}(%)	26.3	26.8	1.02
Bi-linear model	1/800	E(kN mm)	96.5	0	0.00
		h_{eq}(%)	9.2	0	0.00
	1/400	E(kN mm)	248.6	0	0.00
		h_{eq}(%)	7.0	0	0.00
	1/200	E(kN mm)	1421.4	1681.0	1.18
		h_{eq}(%)	15.1	21.6	1.43
	1/100	E(kN mm)	5637.7	4942.0	0.88
		h_{eq}(%)	26.3	23.7	0.90

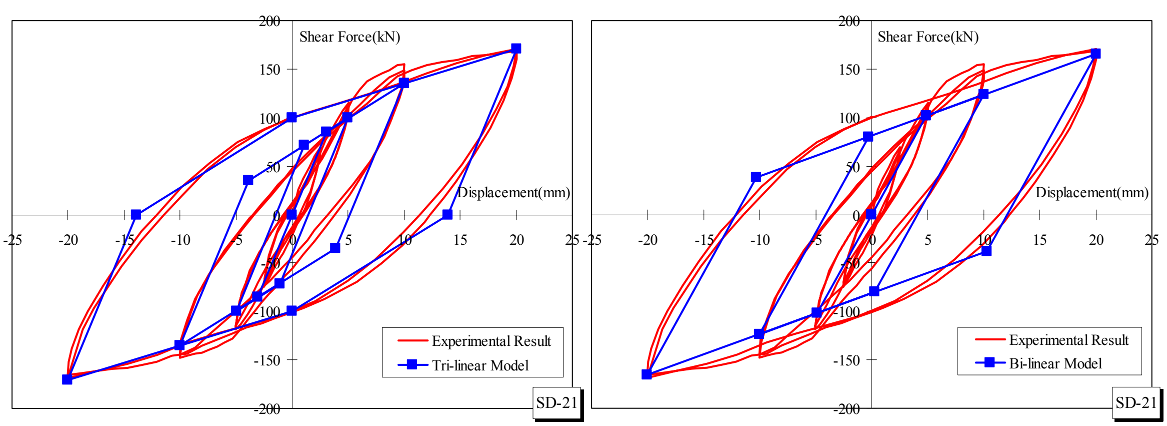

Figure 10　The experimental results and the R/C non-structural wall models

The analytical models and the dimensions of the proto-type building are shown in Figure 11 and Table 6, respectively. The dimensions of the R/C non-structural wall models are shown at Table 7. The damping of the proto-type building was assumed to be proportional to the varying instantaneous stiffness of the structure and assumed to be 3% for the first natural frequency. In the non-structural wall, only the hysteretic damping was considered.

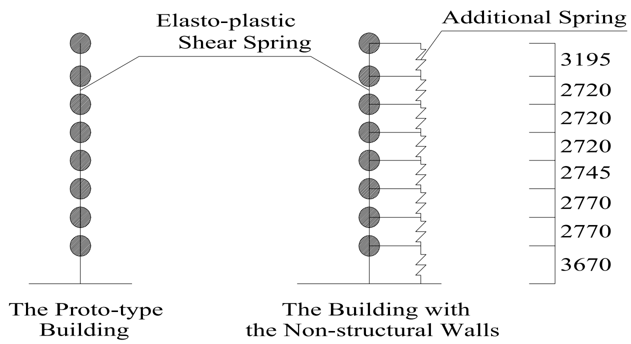

Figure 11 The analytical models

Table 6 The dimensions of the proto-type building

Floor	K1 (kN/mm)	Qy1 (kN)	α1	Qy2 (kN)	α2
8	1450.21	2026.75	0.1591	6052.57	0.0017
7	1915.40	2958.60	0.1735	9490.68	0.0022
6	2190.18	3664.72	0.1828	12679.82	0.0062
5	2459.07	4099.80	0.1935	15057.27	0.0109
4	2688.04	4584.21	0.1978	16705.15	0.0201
3	3035.70	4966.21	0.2012	18456.24	0.0197
2	3335.30	5849.21	0.1980	20249.90	0.0218
1	4516.03	7480.52	0.1722	23407.25	0.0013

K1:Initial Stiffness
Qy1:Cracking Shear
Qy2:Yield Shear
α1:Ratio of Secondary Stiffness to K1
α2:Ratio of Thirdly Stiffness to K1

Table 7 The dimensions of the R/C non-structural wall models

Wall Model	K (kN/mm)	Qy (kN)	α1	Qy2 (kN)	α2
Tri-linear	27.86	85.35	0.2587	135.34	0.1269
Bi-linear	20.93	101.91	0.2000	-	-

α1:Ratio of Secondary Stiffness to K
α2:Ratio of Thirdly Stiffness to K

The results of the analysis are shown in Table 8 and Figure 12. The first natural period of the case the non-structural wall was adopted was about 0.05 seconds shorter than the proto-type building. In the analysis of 25 cm/sec in the velocity of input ground motion, the maximum response story drift slightly reduced in the upper floor when the non-structural wall was adopted. In the analysis of 50 cm/sec, in cases of El Centro record and Taft record, the response story drift increased in the upper floors of the proto-type building. However, when the non-structural wall was adopted, the maximum value was reduced to about 0.7 times as proto-type building. The maximum response was within about R=1/100 rad. The significant effect to reduce the maximum response was not observed under the JMA Kobe record.

Between the two type wall models, remarkable differences in the response were not obtained. However, the response by the Bi-linear model was slightly larger than that by Tri-linear model. This reason was probably that the Bi-linear model remained in elastic range and no hysteretic energy was absorbed in the small displacement. In order to confirm the safety of the response, it is enough to use the Bi-linear model in the analysis.

Table 8 The analytical results

Analytical Model	First Natural Period (sec)	Adopted Seismic Record	25 cm/sec		50 cm/sec	
			Maximum Story Drift Angle R (story)	Ratio to the Proto-type Building	Maximum Story Drift Angle R (story)	Ratio to the Proto-type Building
Proto-type Building	0.595	ElCentro	1/183(4)		1/74(6)	
		Taft	1/213(5)		1/80(6)	
		JMA Kobe	1/137(4)		1/62(4)	
Building with the Tri-linear Model	0.549	ElCentro	1/190(4)	0.96	1/100(4)	0.74
		Taft	1/251(3)	0.85	1/109(5)	0.73
		JMA Kobe	1/158(2,3)	0.87	1/61(3)	1.02
Building with the Bi-linear Model	0.559	ElCentro	1/188(4)	0.97	1/97(4)	0.76
		Taft	1/209(4)	1.02	1/110(5)	0.73
		JMA Kobe	1/154(3)	0.89	1/61(3)	1.02

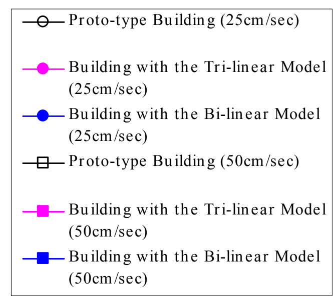

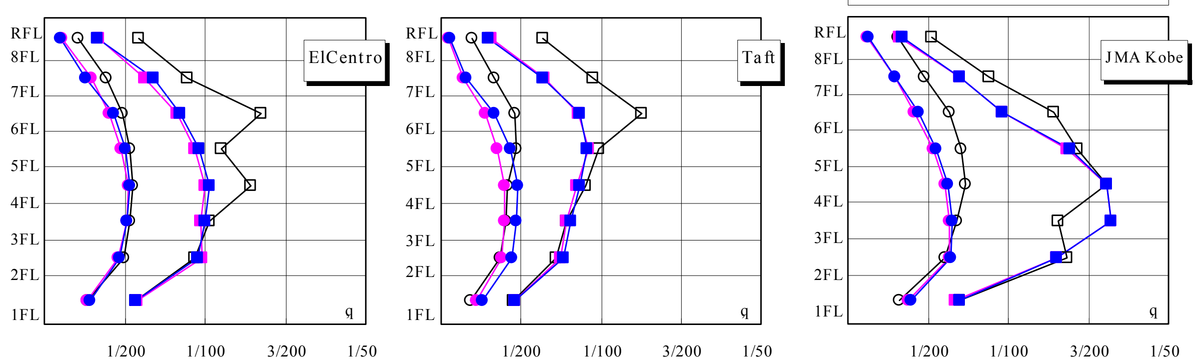

Figure 12 The analytical results (maximum story drift)

5. STUDY ON THE SECTIONAL AREA OF STEEL PLATE

In chapter 4, the size of the steel plate was 90mm in the width and 12mm in the thickness. In this chapter, the area of the steel plate A was chosen as a main variable of the analysis to study the effect of both stiffness and strength of the non-structural wall on the earthquake response. The yield stress σy of the steel plate was assumed to be 1.1 times of specified design strength as an average yield strength of real material.

Except for the area of the steel plate, the analytical model was the same as that in chapter 4. The area of the steel plate was changed by the thickness from 9 mm to 22 mm. The width of the steel plate was constant of 90mm and the defective part was half to the total area. The dimensions of each R/C non-structural wall model are shown in Table 9.

Table 9 The dimensions of the R/C non-structural wall models

Wall Model	σy (N/mm^2)	A (mm^2)	A' (mm^2)	K (kN/mm)	Qy (kN)
Plate Thickness 9	258.5	810.0	$\frac{A}{2}$	15.63	70.74
Plate Thickness 12		1080.0		20.84	94.33
Plate Thickness 16		1440.0		27.79	125.77
Plate Thickness 19		1710.0		33.00	149.35
Plate Thickness 22		1980.0		38.21	172.93

Table 10 The analytical results

Analytical Model	First Natural Period (sec)	Adopted Seismic Record	25 cm/sec		50 cm/sec	
			Maximum Story Drift Angle R (story)	Ratio to the Building with the Plate Thickness 12 Model	Maximum Story Drift Angle R (story)	Ratio to the Building with the Plate Thickness 12 Model
Building with the Plate Thickness 9 Model	0.568	ElCentro	1/187(4)	1.02	1/93(3)	1.04
		Taft	1/191(4)	1.09	1/112(4)	0.99
		JMA Kobe	1/150(3)	1.03	1/60(4)	1.02
Building with the Plate Thickness 12 Model	0.559	ElCentro	1/190(4)		1/97(4)	
		Taft	1/209(4)		1/111(5)	
		JMA Kobe	1/154(3)		1/61(4)	
Building with the Plate Thickness 16 Model	0.549	ElCentro	1/194(4)	0.98	1/99(4)	0.98
		Taft	1/248(4)	0.84	1/104(5)	1.07
		JMA Kobe	1/159(2)	0.97	1/59(3)	1.03
Building with the Plate Thickness 19 Model	0.542	ElCentro	1/191(4)	0.99	1/100(4)	0.97
		Taft	1/285(4)	0.73	1/104(4,5)	1.07
		JMA Kobe	1/165(2)	0.93	1/60(3)	1.02
Building with the Plate Thickness 22 Model	0.535	ElCentro	1/189(4)	1.01	1/100(4)	0.97
		Taft	1/286(4)	0.73	1/99(4)	1.12
		JMA Kobe	1/177(2)	0.87	1/61(3)	1.00

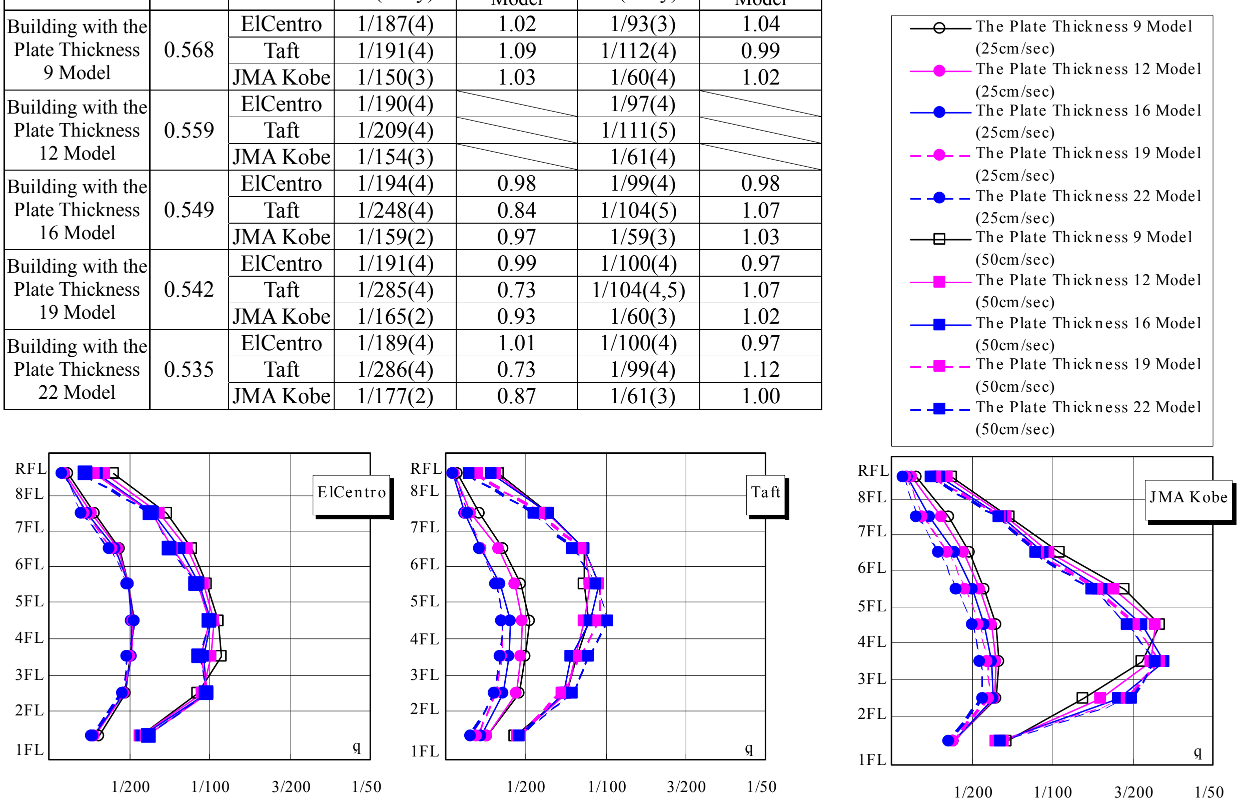

Figure 13 The analytical results (maximum story drift)

The results of the analysis are shown in Table 10 and Figure 13. In the analysis of 25cm/sec of Taft record and JMA Kobe record, the response story drift was relatively small in case of large sectional area of the steel plate. However, in the analysis of 25cm/sec of Taft record, the response displacement was relatively large. The response maximum story shear except for non-structural walls became smaller in the upper stories as the sectional area was larger. But in the first story, obvious effect of sectional area was not observed in the response shear. Although significant effect of the area of the steel plate on the response was not obtained, it seems that the steel plate with large sectional area generally reduces the story drift. It should be noted that extreme large strength of the non-structural wall generated large shear to the girder, which supported the wall. It is necessary to also consider the shear capacity of the girder attached the non-structural wall.

6. DISTRIBUTION OF THE R/C NON-STRUCTURAL WALLS ALONG HEIGHT

In the analysis of previous chapter, there was the case that the response story shear exceeds that of the proto-type building, when the non-structural wall was adopted. Therefore, adequate distribution of the non-structural walls in the quantity along the height of the building was studied in order to reduce both story drift and shear. The quantity of the non-structural walls was controlled by the areas of the embedded steel plates.

The analytical model was the same basically as that in previous chapters. The non-structural wall model was changed in its steel plate thickness in the range of 9~22mm in each story. The thickness was selected proportional to design story shear, initial story stiffness, and yield story shear of the proto-type building. The dimensions of the each non-structural wall models are shown in Table 11. In the Table, the model with constant plate thickness indicates the model with the plate thickness of 12mm described in chapter 5.

The results of the analysis are shown in Table 12 and Figure 14. In the model with variable plate thickness, the response maximum story drift was significantly smaller than that of the proto-type building and that of the model with constant plate thickness. Moreover, the maximum response story shear did not exceed that of the proto-type building. The proposed structural control method acts effectively when an adequate distribution of the non-structural walls along the height of the building is selected.

Table 11　The dimensions of the R/C non-structural wall models

Wall Model	Floor	Thickness (mm)	σy (N/mm^2)	A (mm^2)	A' (mm^2)	K (kN/mm)	Qy (kN)
Constant Plate Thickness	All	12	258.5	1080.0	$\frac{A}{2}$	20.84	94.33
Variable Plate Thickness	8	9		810.0		15.63	70.74
	7	12		1080.0		20.84	94.33
	6	13		1170.0		22.58	102.19
	5	15		1350.0		26.06	117.91
	4	17		1530.0		29.53	133.63
	3	19		1710.0		33.00	149.35
	2	21		1890.0		36.48	165.07
	1	22		1980.0		38.21	172.93

Table 12　The analytical results

Analytical Model	First Natural Period (sec)	Adopted Seismic Record	25 cm/sec		50 cm/sec	
			Maximum Story Drift Angle R (story)	Ratio to the Proto-type Building	Maximum Story Drift Angle R (story)	Ratio to the Proto-type Building
Proto-type Building	0.595	ElCentro	1/183(4)		1/74(6)	
		Taft	1/213(5)		1/80(6)	
		JMA Kobe	1/137(4)		1/62(4)	
Building with the Model with Constant Plate Thickness	0.559	ElCentro	1/190(4)	0.96	1/97(4)	0.76
		Taft	1/209(4)	1.02	1/111(5)	0.72
		JMA Kobe	1/154(3)	0.89	1/61(4)	1.02
Building with the Model with Variable Plate Thickness	0.546	ElCentro	1/188(5)	0.97	1/101(4)	0.73
		Taft	1/276(4)	0.77	1/99(5)	0.81
		JMA Kobe	1/174(3)	0.79	1/61(4)	1.02

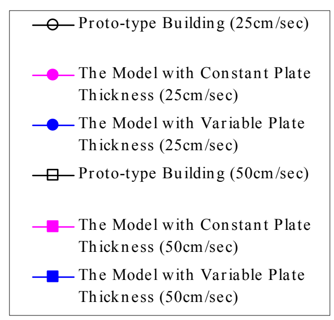

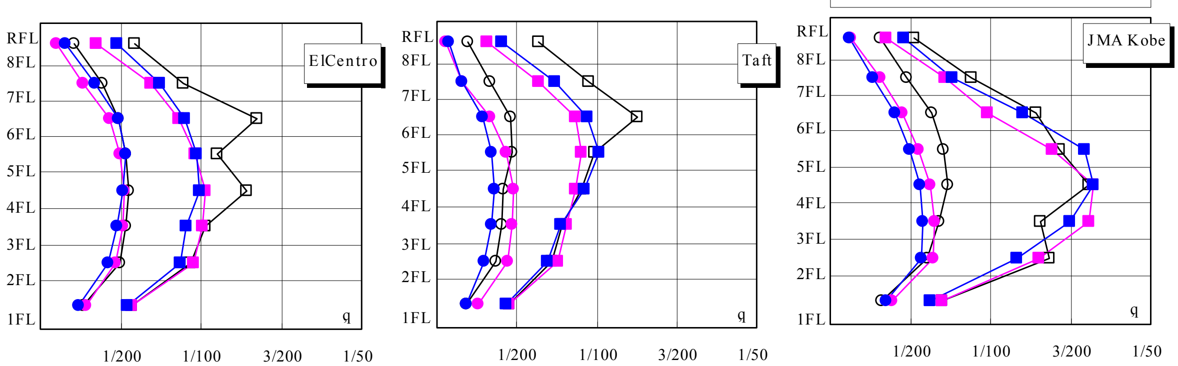

Figure 14　The analytical results (maximum story drift)

7. CONCLUSIONS

A structural control method using R/C non-structural walls with X-shape steel plates was proposed. The real scale structural experiment and the earthquake response analysis were carried out in order to confirm the effectiveness of the proposed method. The following conclusions were obtained.

Desirable energy absorbing performance was developed in all specimens. Buckling of the steel plates was not observed during the loading. Moreover, damage was observed only in the immediate vicinity of the slits.

This structural control method reduced the response story drift in large earthquakes. The Bi-linear model for the proposed R/C non-structural wall was effective to predict the earthquake response.

Although significant effect of the area of the steel plate on the response was not obtained, it seems that the steel plate with large sectional area generally reduces the story drift.

The proposed structural control method acted effectively when an adequate distribution of the non-structural walls along the height of the building was selected.

SHEAR RESISTANT PERFORMANCE OF VINYL-FIBER REINFORCED CONCRETE COLUMN

KITAYAMA Kazuhiro *1 and KOSAKA Hideo *2

ABSTRACT

It is known that vinyl-fiber contained in concrete is effective to enhance the ductility of concrete subjected to tensile force (generally called tension stiffening) and prevent explosion of concrete suffering from fire because numerous vapor paths are formed within concrete by melting of vinyl-fibers. In the paper, shear resistant performance of reinforced concrete columns mixed with vinyl-fibers was studied from the view of shear strength, deformation capacity and shear transfer mechanism. Vinyl-fiber contributed to restrain crack opening, confine core concrete in columns and ensure ductile behavior after shear strength, however hardly enhanced shear strength. Vinyl-fiber had no influence on truss mechanism, but was useful to maintain arch mechanism after shear strength because of its confining action to core concrete.

1. INTRODUCTION

Plain concrete cannot carry tensile force after occurrence of cracks because of its brittle characteristics. However, ductile deformation capacity will be provided for concrete by the mixture with steel- or vinyl-fibers. In the study, the availability of this improved concrete by mixing short vinyl-fibers, which seems to be useful for future reinforced concrete (RC) structures, was researched through column tests providing anti-symmetric bending moment at the top and bottom of a column. Shear resistant performance of vinyl-fiber reinforced concrete (called FRC) columns was studied by investigating shear strength, deformation capacity and shear resisting mechanism through tests. Vinyl-fiber concrete proves to be able to keep tensile strength up to large tensile deformation even after cracking. Light-weight vinyl-fiber reinforced concrete (called LFRC) column was also tested, which is beneficial to save resources and energy on the earth, to ascertain the applicability of LFRC to structural members of buildings in high seismicity zones.

2. OUTLINE OF TEST

*1 Associate Professor, Graduate School of Engineering, Tokyo Metropolitan University, Dr. Eng.
Email : kitak@arch.metro-u.ac.jp

*2 Graduate student, Tokyo Metropolitan University
Email : kskhdo@ecomp.metro-u.ac.jp

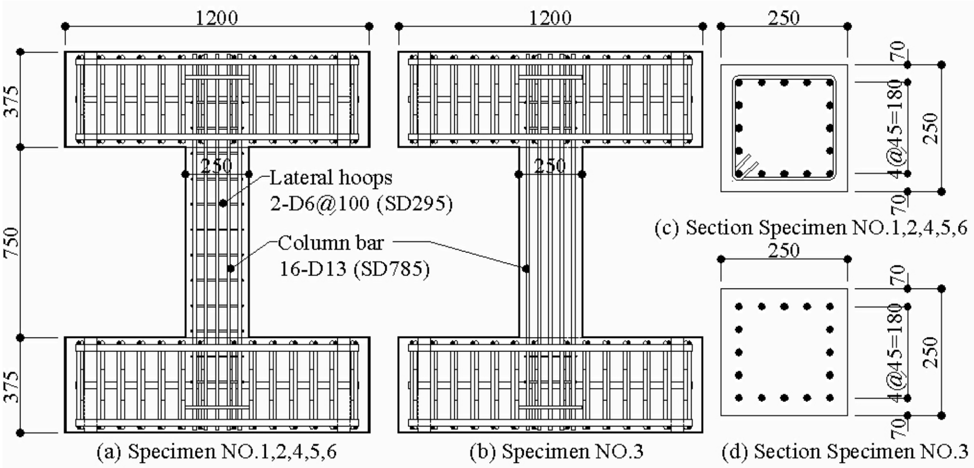

Fig. 1 Configurations and reinforcement details

Table 1 Properties of specimens, material properties and predicted strength

Specimen Number			1	2	3	4	5	6
Column section			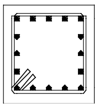		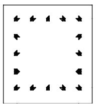		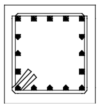	
Concrete		Types	FRC	FRC	FRC	FRC	RC	LFRC
		Compressive strength [MPa]	39.7	76.8	40.5	40.5	37.1	42.1
		Splitting tensile streng[MPa]	3 .4	5 .0	3 .4	3 .4	2 .8	2 .7
		Young's modulus [GPa]	30.0	33.5	29.0	29.0	27.6	16.1
Longitudinal bar		Arrangement	16-D13					
		Yield strength [MPa]	885					
		Gross ratio [%]	1.02					
Shear reinforcement		Arrangement	2-D6@100		none	2-D6@100		
		Yield strength [MPa]	343.4		none	343.4		
		ratio [%]	0.26		none	0.26		
Axial load (Comp. : positive)		N [kN]	784	735	784	-392	735	833
		Axial stress ratio	0.32	0.15	0.31	-0.15	0.32	0.32
Flexural strength		Q_{mu} [kN]	596.7	675.4	598.6	337.3	586.2	596.7
Shear strength	AIJ *1	Vu [kN]	209.3	251.6	153.7	199.1	153.0	202.1
	Arakawa *2	$Q_{su,min}$ [kN]	211.0	294.9	200.1	151.9	177.2	214.0
	Arakawa *3	$Q_{su,mean}$ [kN]	237.7	340.8	227.2	178.6	202.7	241.9

*1 AIJ provision (Ref.2), *2 Modified Arakawa minimum formula, *3 Modified Arakawa mean formula

2.1 SPECIMENS

Specimen configuration and reinforcing details are shown in Fig. 1. Properties of specimens and material properties of concrete and steel are summarized in Table 1. Six column specimens with one-third scale to actual frames were tested. Square column section (250 mm x 250 mm), shear span ratio of 1.5, the amount of longitudinal bars (16 deformed bars with 13 mm diameter) were common for all specimens. High-strength column longitudinal bars were arranged to cause shear failure prior to flexural yielding. Kind of concrete (plain, FRC and LFRC), nominal concrete compressive strength (35 MPa and 80 MPa), column

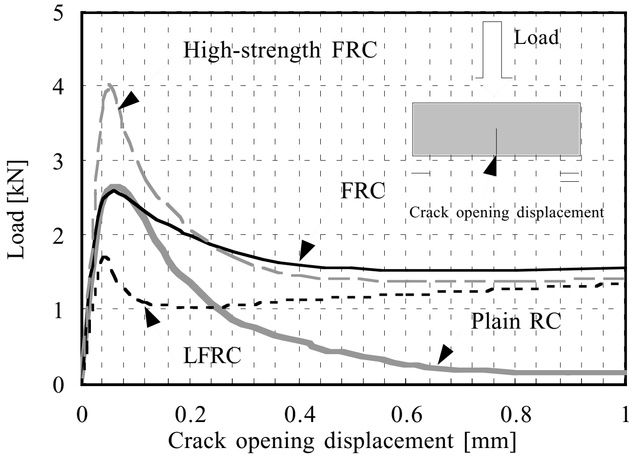

Fig. 2 Load- crack opening displacement relations tested by Kitsutaka

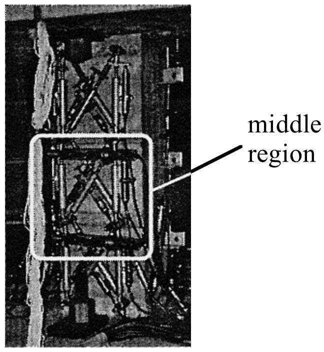

Fig. 3 Instrumentation for column

axial load (compression and tension) and the amount of shear reinforcement (none and 0.26 percent) were selected as test parameters. Control specimen No.1 was made of FRC with nominal concrete compressive strength of 35 MPa, had shear reinforcement ratio of 0.26 percent and was subjected to constant compressive axial stress of which ratio to concrete compressive strength was 0.32.

Short vinyl-fiber with 30 mm length and 0.66 mm diameter, whose fracture strength and Young's modulus was 900 MPa and 290GPa respectively, were used. The ratio of volume of vinyl-fibers to concrete was 1 percent taking account of workability of concrete mixing and casting. Compressive strength of FRC was 1.1 times greater than that of plain RC, while tensile strength by splitting test using cylinders with 100 mm diameter and 200 mm height was enhanced by vinyl-fiber mixture to 1.2 times that of plain RC. Weight of unit volume was 2.3 g/cm^3 for normal vinyl-fiber concrete and plain concrete, and 1.5 g/cm^3 for light-weight vinyl-fiber concrete. Artificial coarse aggregates with the diameter of 5 mm were used for LFRC. All kind of concrete was cast in horizontal position using wood form.

Load-crack opening displacement (COD) relations are shown in Fig. 2 for vinyl-fiber and plain concrete, which were obtained from simple beam tests conducted by Kamiyama and Kitsutaka [1] using 100mm-square and 400mm-length prisms with the notch of 50 mm depth at the center. Vinyl-fiber concrete and plain concrete was mixed by the same batch as FRC and RC column specimens. Vinyl-fiber concrete exhibited significant tension stiffening and ductile behavior due to fiber bridging across a crack while plain concrete showed brittle behavior after cracking.

2.2 LOADING METHOD AND INSTRUMENTATION

Reversed cyclic lateral shear force was applied to column specimens by an actuator so as to keep both stubs at the top and bottom of a column parallel through a pantograph. Constant compressive axial load except for Specimen No.4 was applied. Specimens were controlled by lateral drift angle for one cycle of 0.25 %, two cycles of 0.5 %, 1 %, 1. 5% and 2 % respectively, one cycle of 3 % and 4 %. However, monotonic lateral drift was forced up to the drift angle of 10% if shear resistant capacity degraded to less than half of shear strength.

Lateral drift of a column, and horizontal, vertical and diagonal local displacements of each region divided into three parts with equal height along a column were measured by displacement transducers as illustrated in Fig. 3. Strains of longitudinal bars and lateral hoops were measured by strain gauges.

2.3 PREDICTION OF STRENGTH

Flexural ultimate strength and shear strength were predicted before tests as listed in Table 1. Shear strength was computed according to provision of Architectural Institute of Japan (AIJ) [2]and modified Arakawa formulae. For the use of AIJ provision, judging from Fig. 2, the half of splitting tensile strength of vinyl-fiber concrete was taken into account to compute the contribution of truss action as expressed by Equation (3) mentioned later, where the term of σ_{ct} was replaced by $\frac{1}{2}\sigma_{cr}$ (σ_{cr} : splitting tensile strength of vinyl-fiber concrete). For modified Arakawa formulae, the contribution of shear reinforcement, i.e., $0.845\sqrt{p_w \sigma_{wy}}\, b \cdot j_t$ in unit of N (p_w : shear reinforcement ratio, σ_{wy} : yield strength of hoops in unit of MPa and $b \cdot j_t$: sectional area to resist shear effectively) was replaced by $0.845\sqrt{p_w \sigma_{wy} + \frac{1}{2}\sigma_{cr}}\, b \cdot j_t$.

3. TEST RESULTS

All specimens failed in shear without yielding of longitudinal bars. Crack patterns and shear

Table 2 Test results

Specimen Number			1	2	3	4	5	6
Flexural crack	Qmc	[kN]	159.6	107.5	158.7	-	134.3	143.2
Shear crack	Qsc	[kN]	246.3	264.4	232.9	-	206.2	143.2
Shear at hoop yielding	Qy	[kN]	247.2	294.5	-	141.3	223.0	185.7
	δy	[%]	0.77	0.80	-	1.00	0.65	0.50
Shear strength	Qmax	[kN]	247.5	299.7	238.9	166.8	225.3	185.7
	δmax	[%]	0.50	0.85	0.45	1.50	0.50	0.50
Limit state *1	Qu	[kN]	198.0	239.7	191.1	133.4	180.2	148.6
	δu	[%]	1.30	1.00	0.60	3.00	1.10	1.20

*1 Shear capacity and deformation at 20% degradation from shear strength in load-deformation envelope curve force-drift angle relations are shown in Fig. 4 and 5 respectively. Column shear force was corrected by taking P-delta effect due to column axial load into account. Test results are summarized in Table 2.

3.1 CRACK PATTERNS

Spall-off of shell concrete was prevented in FRC columns. At first, fine and short diagonal cracks occurred along the center of the column, then diagonal shear cracks were observed at both end regions for Specimen No.1 made of FRC. Bond splitting cracks along column longitudinal bars also developed under large drift loading. More diagonal cracks were observed in Specimen No.1 than Specimen No.5 made of plain concrete. In specimen No.3 made of FRC without shear reinforcement, primary diagonal shear crack occurred suddenly linking the top and the bottom of compressive zone at critical sections, and opened widely accompanying shear resistance decay. Number of cracks for Specimen No.3 was least among specimens. Crack patterns for Specimen No.6 made of LFRC were almost similar to those for Specimen No.1, however many fine cracks occurred over entire column surface.

3.2 SHEAR STRENGTH AND DUCTILITY

Shear strength was attained between drift angle of 0.5 % and 1 % immediately after development of primary diagonal shear crack except for Specimen No.4 subjected to tensile axial load at drift angle of 1.5 %.

Shear strength for Specimen No.1 made of FRC was enhanced to 1.10 times that for Specimen No.5 made of plain RC by the effect of vinyl-fibers. Shear resistant capacity for FRC Specimen No.1 decreased moderately after shear strength comparing with plain RC Specimen No.5.

Shear strength for Specimen No.3 made of FRC without shear reinforcement was almost same as that for FRC Specimen No.1 with lateral hoops, however shear resistant degradation was remarkable under cyclic loading after shear strength. This indicates that only use of vinyl-fiber of 1 percent content, without shear reinforcement, for RC columns failed in shear cannot contribute to maintain ductile behavior under earthquake loading.

Shear strength for Specimen No.2 made of high-strength FRC was only 1.21 times greater than that for Specimen No.1 although concrete compressive strength for former specimen was as high as 1.9 times that for later specimen.

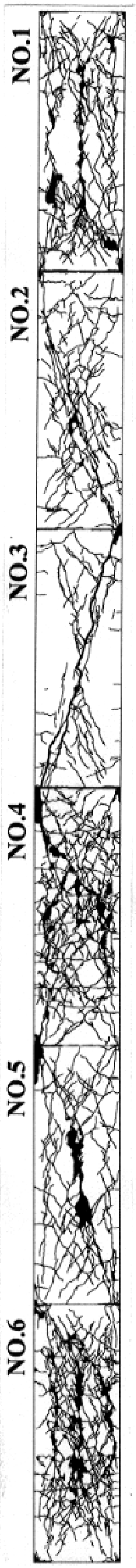

Fig.4 Crack patterns

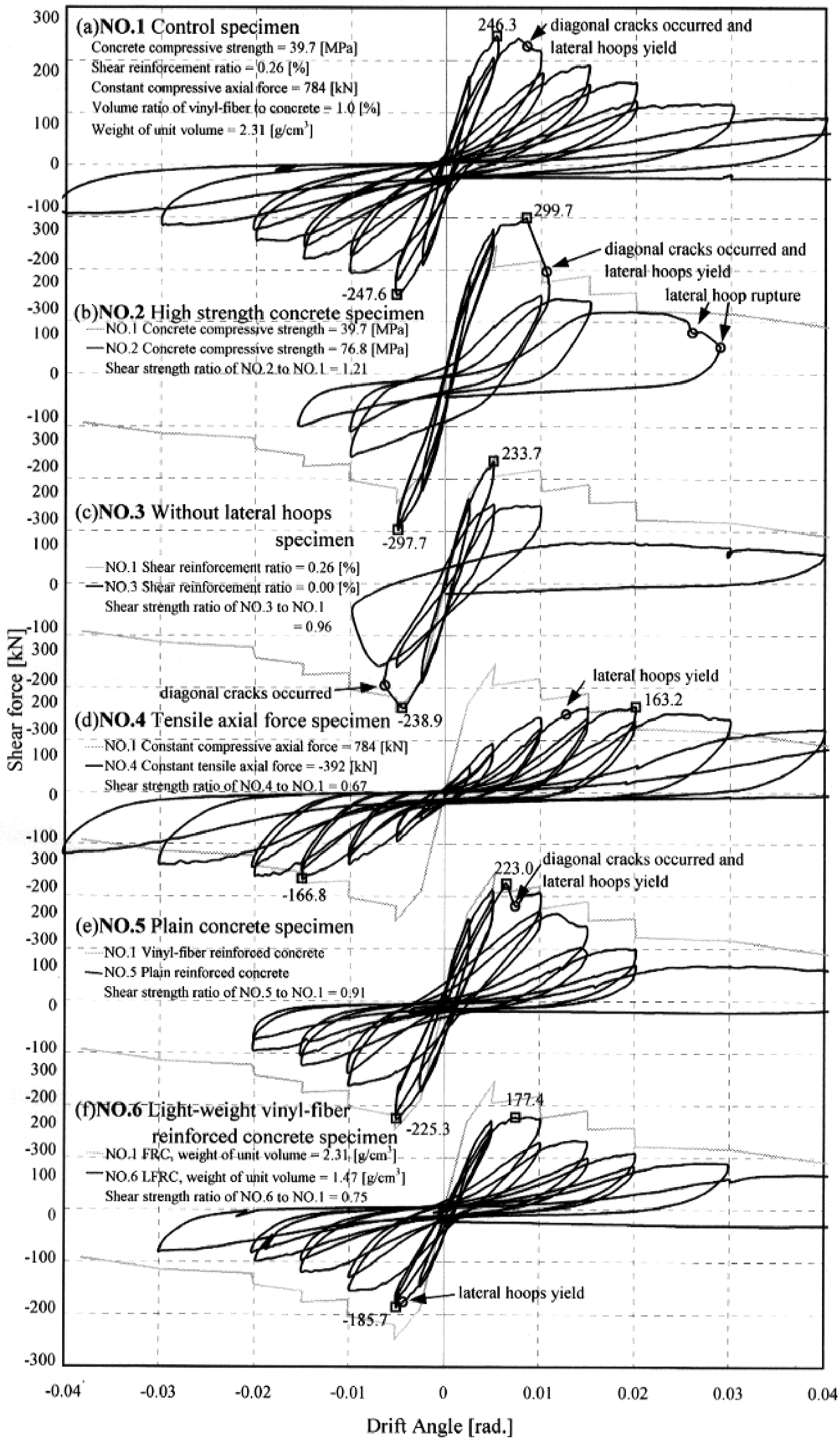

Fig. 5 Shear force - drift angle relations

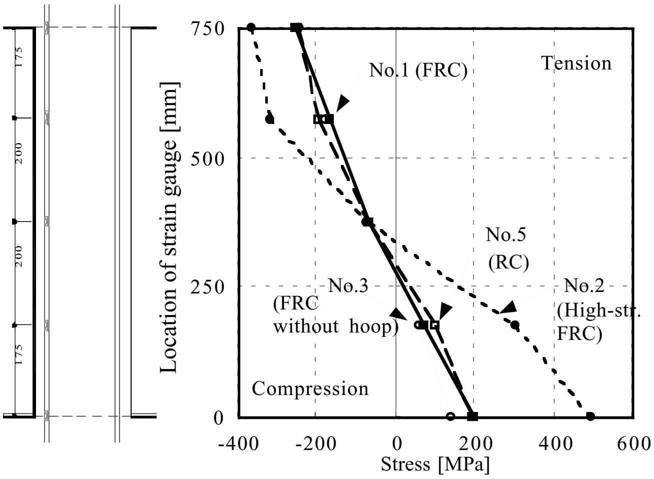

Fig. 6 Stress distribution along column bar

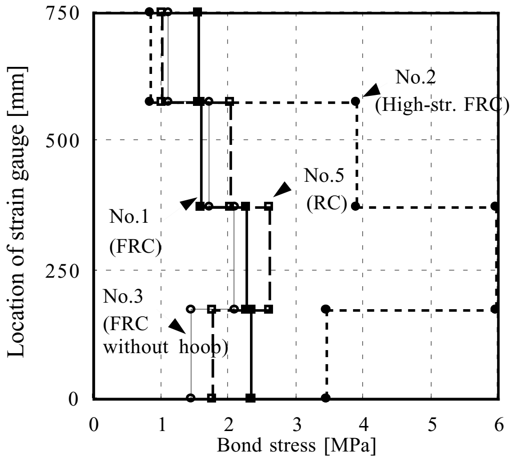

Fig. 7 Bond stress distribution along column bar

*0.86

For Specimen No.4 made of FRC subjected to axial tensile load, initial stiffness was very small comparing with FRC Specimen No.1 subjected to axial compressive load, and shear strength, which was attained at drift angle of 1.5 %, reduced to two-thirds that for Specimen No.1.

Initial stiffness for Specimen No.6 made of LFRC was only the half of FRC Specimen No.1 since the elastic modulus of light-weight vinyl-fiber concrete was approximately half of normal vinyl-fiber concrete. Shear strength for LFRC Specimen No.6 reached only three-quarters that for Specimen No.1.

3.3 STRAIN AND BOND STRESS DISTRIBUTION ALONG COLUMN BAR

Strain and bond stress distributions along column longitudinal bars are shown in Fig. 6 and 7 respectively. Bond stress was computed from strain difference between two adjacent strain-gauges. Column bars did not yield under cyclic loading. Maximum bond stress reached 2 to 3 MPa at drift angle of 1 % for normal-strength concrete specimens. It is supposed that columns failed in shear before bond stress reached the bond strength of 5.6 MPa computed according to AIJ provision [2].

On the other hand, for Specimen No.2 made of high-strength FRC, maximum bond stress was approximately two times that for other specimens, reaching 4 to 7 MPa at drift angle of 1 % which is almost equal to bond strength of 6.5 MPa computed from AIJ provision.

3.4 AXIAL DEFORMATION OF COLUMN

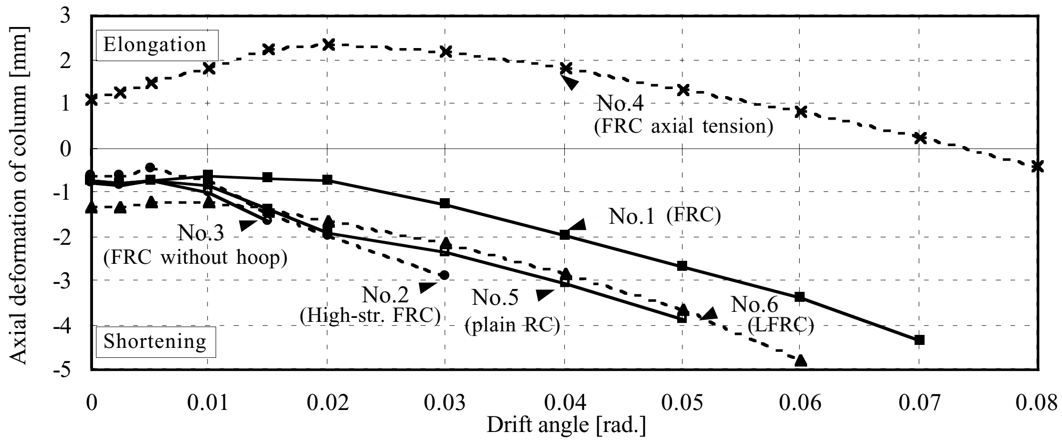

Fig. 8 Axial deformation in column

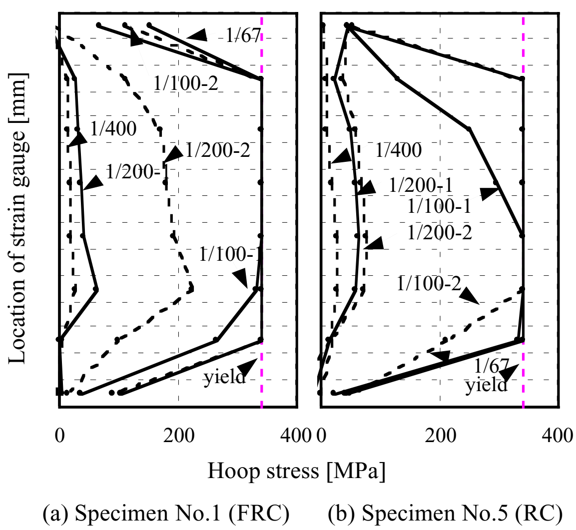

Fig. 9 Stress distribution of hoops parallel to loading direction

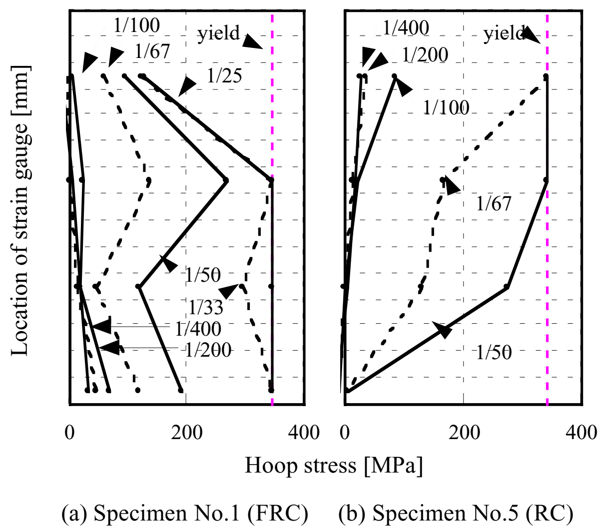

Fig. 10 Stress distribution of hoops perpendicular to loading direction

Column axial deformation is shown in Fig. 8. For FRC Specimen No.1, almost constant compressive deformation was held up to drift angle of 2 %, then axial deformation went to considerable shortening. On the contrary, column axial deformation for plain RC Specimen No.5 showed tendency of remarkable shortening after drift angle of 1 %. Vinyl-fibers contained in plain concrete was effective to prevent severe collapse of a column.

4. DISCUSSIONS

4.1 EFFECT OF VINYL-FIBER

1) Stress in lateral hoops

Stress distributions of lateral hoops parallel to loading direction are shown in Fig. 9 for

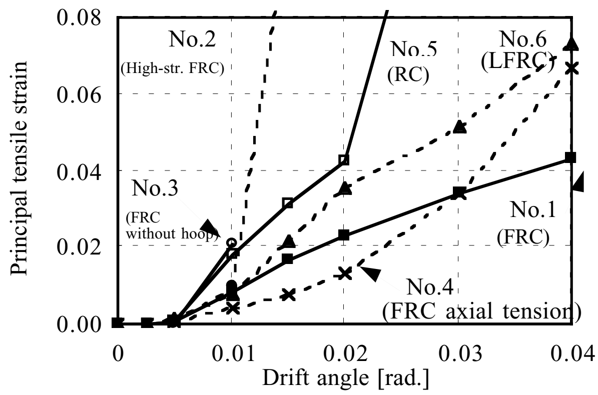

Fig. 11 Principal tensile strain in web concrete

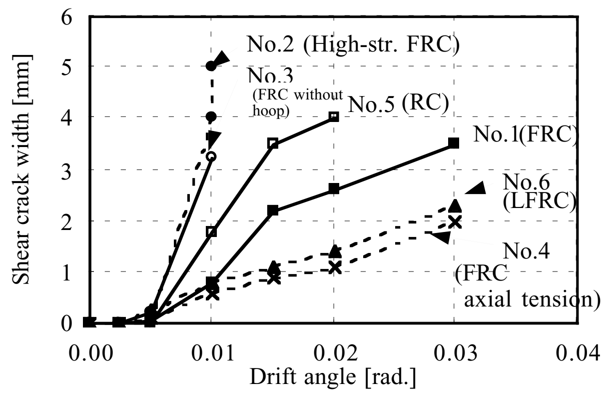

Fig 12 Shear crack width

FRC Specimen No.1 and plain RC Specimen No.5. Hoops except for those close to top and bottom RC stubs yielded at drift angle of 1 % for all specimens.

Stress distributions of lateral hoops perpendicular to loading direction are shown in Fig. 10. Hoop stress was approximately 50 MPa for both specimens at drift angle of 1 % just after column shear strength. At drift angle of 1.5 % exhibiting shear strength degradation, hoop stress was 100 MPa for FRC Specimen No.1 whereas ranged between 120 MPa and yield stress (343 MPa) for Specimen No.5. Vinyl-fibers contributed to restrain concrete lateral expansion caused by progress of shear failure.

2) Principal tensile strain of concrete

Principal tensile strains of web concrete within middle region of a column are shown in Fig. 11. Principal strain was computed from horizontal, vertical and diagonal displacement measured by displacement transducers set as illustrated in Fig. 3. Principal strains are picked at drift angle of 1 % among Specimens No.1, No.3 and No.5. Principal tensile strain for FRC Specimen No.1 was approximately half of that for FRC Specimen No.3 without shear reinforcement and plain RC Specimen No.5. This indicates that vinyl-fiber contained in plain concrete was efficient to reduce the increase in tensile strain. The strains were almost same for Specimens No.3 (no hoops) and No.5 (no fibers). The effect of vinyl-fibers of 1 percent content on restricting principal tensile strain in web concrete seemed to be equivalent with confining effect by steel hoops of 0.26 percent content. From above comparison, vinyl-fibers cooperated with steel hoops in shear resistant performance under descending branch of shear capacity.

3) Shear crack width

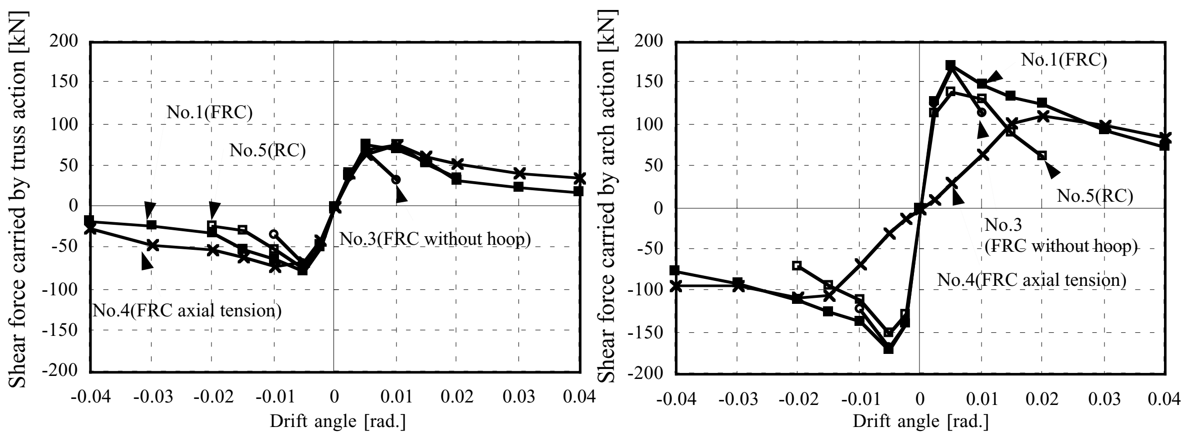

(a) Truss contribution (b) Arch contribution

Fig. 13 Truss and arch contributions to shear resistance

Maximum width of diagonal shear cracks is shown in Fig. 12 measured at peak displacement in each loading cycle. Crack widths for specimens made of normal concrete increased suddenly at drift angle of 1 %. The width for FRC Specimen No.1 was more restrained by vinyl-fibers than for plain RC Specimen No.5. Shear crack width for FRC Specimen No.4 subjected to tensile axial load was the smallest among specimens. The width for LFRC Specimen No.6 increased gradually and was smaller than for other specimens subjected to compressive axial load since many fine diagonal cracks occurred uniformly.

4.2 SHEAR RESISTING MECHANISM

Effect of vinyl-fibers mixed with plain concrete on shear resistant performance is discussed from studying on the contribution of truss and arch mechanism to shear resistance. Contribution of truss mechanism denoted as Q_{truss} was computed from Equation (1) by using measured bond stress along column longitudinal bars ;

$$Q_{truss} = n \cdot \psi \cdot \tau_b \cdot j_t \tag{1}$$

where n : number of column longitudinal bars in most outer layer, ψ : perimeter length of a column bar, j_t : distance between tensile and compressive column bars in opposite most outer layer and τ_b : bond stress along column bars which was obtained from tests as described at section 3.3. Contribution of arch mechanism denoted as Q_{arch} was taken by subtracting truss contribution from total shear capacity that was measured in the test as follows ;

$$Q_{arch} = Q_s - Q_{truss} \tag{2}$$

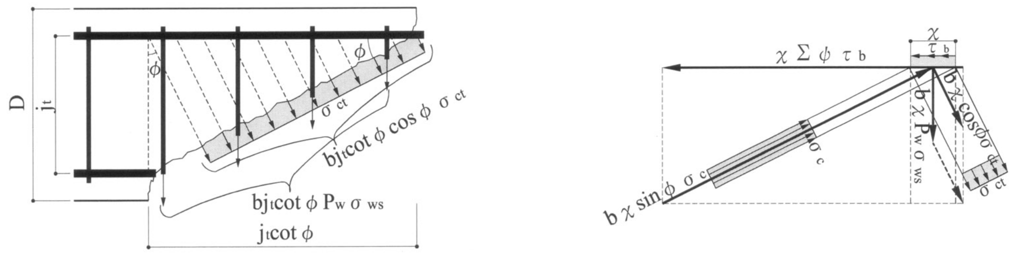

(a) Truss mechanism accounting for concrete tensile force across crack

(b) Force polygon for equilibrium at node

Fig. 14 Shear resisting mechanism of truss action in FRC

where Q_s is measured column shear capacity. Both contributions are shown in Fig. 13. Comparing with Specimens No.1 and No.5, truss contribution was almost same even after shear strength at drift angle of 1 %. This caused the difference of arch contribution between two specimens after shear strength, exhibiting that arch contribution for FRC Specimen No.1 decreased more moderately than for plain RC Specimen No.5. Vinyl-fibers did not enhance the resistance carried by truss mechanism in this test, however appeared to be efficient to maintain arch mechanism since reduction of concrete compressive strength due to tensile strain orthogonal to diagonal compressive strut may be prevented.

On the assumption that uniform compression field is formed in web concrete with the inclination of ϕ as shown in Fig. 14, shear resistance carried by truss mechanism is computed taking account of tensile stress of vinyl-fiber concrete as Equation (3) ;

$$Q_{truss} = b \cdot j_t \cot\phi \cdot \left(p_w \sigma_{ws} + \cos^2\phi \cdot \sigma_{ct}\right) \tag{3}$$

where b : column width, p_w : shear reinforcement ratio by lateral hoops, σ_{ws} : stress in lateral hoops, which was obtained from measured strains and σ_{ct} : tensile stress developed by vinyl-fiber concrete. Quantity of Q_{truss} in left-hand side of Equation (3) could be taken alternatively by Equation (1). Hence σ_{ct} can be computed from Equation (3) even after occurrence of diagonal shear cracks. Tensile stress carried by vinyl-fiber concrete across diagonal cracks is shown in Fig. 15 for FRC Specimen No.1 under axial compression and FRC Specimen No.4 under axial tension. In calculation of right-hand side of Equation (3), the inclination of diagonal uniform struts in web concrete was chosen from primary crack inclination observed in tests as $\phi = 26.6$ deg. $(\cot\phi = 2.0)$ for Specimen No.1 and $\phi = 39.8$ deg. $(\cot\phi = 1.2)$ for Specimen No.4.

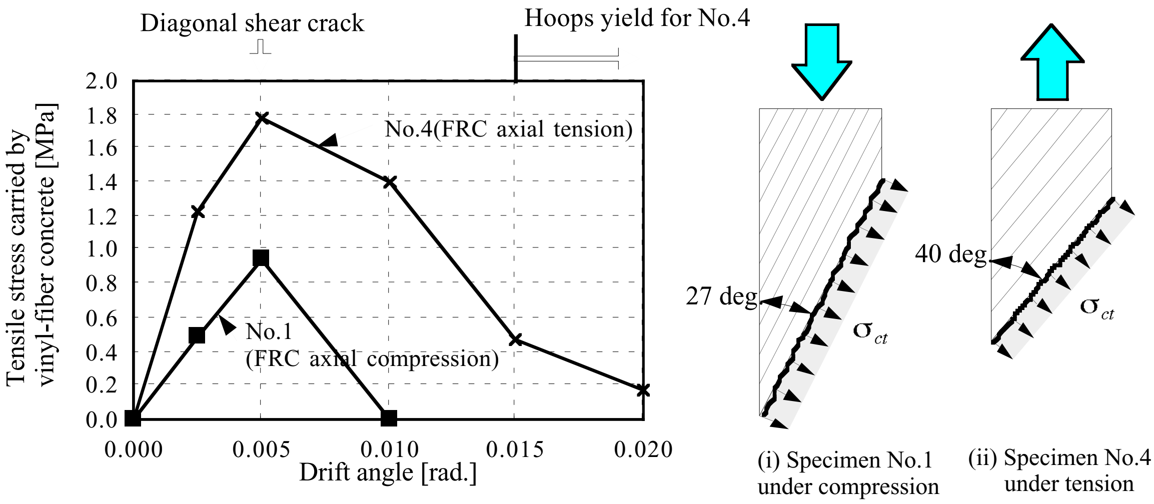

Fig. 15 Tensile stress carried by vinyl-fiber concrete across crack

Tensile stress carried by vinyl-fiber concrete reached the maximum value of 0.9 MPa for Specimen No.1 and 1.8 MPa for Specimen No.4 at drift angle of 0.5 % corresponding to occurrence of primary diagonal shear crack. Tendency of tensile stress after drift angle of 0.5 % was quite different between two specimens. Tensile stress in Specimen No.1 decreased considerably and contribution of vinyl-fibers disappeared after drift angle of 1 %, whereas tensile stress in Specimen No.4 diminished moderately and reached approximately zero stress at drift angle of 1.5 % when lateral hoops began to yield. This indicates that vinyl-fibers contained in plain concrete contributed to truss action in the column subjected to tensile axial load. However the point that vinyl-fibers developed the full effectiveness to transfer of tensile stress was not coincident with the point that lateral shear reinforcement developed full capacity, i.e., yielding.

5. CONCLUSIONS

Shear resistant performance of vinyl-fiber reinforced concrete columns was studied in the paper. Following concluding remarks were drawn.

(1) Vinyl-fiber contributed to restrain crack opening, confine core concrete in columns and ensure ductile behavior after shear strength, however hardly enhanced shear strength.

(2) Vinyl-fiber contained in a column subjected to axial compressive load had no influence on truss mechanism, but was useful to maintain arch mechanism after shear strength because of its confining action to core concrete.

(3) On the other hand, vinyl-fiber contributed to truss mechanism up to the onset of hoop yielding in a column subjected to axial tensile load.

(4) Both initial stiffness and shear strength in light-weight vinyl-fiber concrete column was inferior to those in normal-weight vinyl-fiber concrete column. In order to judge the applicability of LFRC to actual buildings, however, it is necessary to investigate the influence of reducing dead load, which is significant advantage of the use of light-weight vinyl-fiber concrete, on earthquake response of LFRC buildings.

ACKNOWLEDGMENT

The study reported in the paper was sponsored by a Grant-in-aid for Scientific Research of the Ministry of Education and Science (Head researcher : Professor T. Kabeyasawa, University of Tokyo) and a Grant-in-aid for Scientific Research of Japan Society for the Promotion of Science (Head researcher : Professor Y. Kitsutaka, Tokyo Metropolitan University). Authors wish to express their gratitude to Dr. S. Kishida and Mr. M. Tamura, research associates in Tokyo Metropolitan University in executing tests.

REFERENCES

[1] Kamiyama, C., Y. Kitsutaka and M. Tamura : A Study on Test Methods of Fracture Toughness in Various Concrete, *Proceedings of the Japan Concrete Institute*, Vol.23, No.3, pp.91-96, 2001, (in Japanese).
[2] Architectural Institute of Japan : Design Guidelines for Earthquake Resistant Reinforced Concrete Buildings Based on Inelastic Displacement Concept, 1999, (in Japanese).

SESSION B-2: SCALE EFFECTS, DATABASE ANALYSIS, AND DESIGN EQUATIONS

Chaired by

♦ Dawn Lehman and Daisuke Kato ♦

SCALE EFFECT ON FLEXURAL COMPRESSION BEHAVIOR OF REINFORCED CONCRETE COLUMNS

Minehiro Nishiyama*

ABSTRACT

A large-scale testing was conducted on prototype column units with 600x600 square cross section. Corresponding model column units with 250x250 square cross section were constructed and tested. The model units were considered to be 1/2.4-scale model of the prototype units based on the comparison of the section dimensions. Quasi-static horizontal load was applied to the top of the columns with axial load. Test results were discussed in terms of strength, ductility, failure modes and confining effect of transverse reinforcement.

1. INTRODUCTION

Cyclic loading tests on full-scale or large-scale reinforced concrete columns have been reported by a couple of institutions. In NIST (National Institute of Standards and Technology) reversed cyclic lateral load with constant axial load was applied to two full-scale reinforced concrete columns (NIST, 1989). Comparisons of the ultimate moment capacities, measured displacement ductilities, plastic hinge lengths, cyclic energy absorption capacity and the failure modes of the full-scale specimens are made with those observed from 1/6-scale model tests. PWRI (Public Works Research Institute, Japan) conducted reversed cyclic loading tests on full-scale reinforced concrete piers (PWRI, 1999). The test results were compared with the results obtained from small-scale test units in terms of load-displacement relationship, energy absorption, confining effect and so on. Their subjects were piers of highways and bridges not columns of buildings.

Lateral confining reinforcement has two advantages: (1) it increases the strength of core concrete and (2) it improves ductility. Extensive research has been carried out to investigate confining effect of transverse reinforcement, but most experimental research was on small model specimens. Some prototype tests have been conducted, which reported that the larger test units were, the less effective confinement was.

A large-scale testing was recently conducted in Kyoto University as a part of an extensive research project on “Enhancement of Earthquake Performance of Infrastructures based on Investigation into Fracture Process” promoted by Science and Technology Agency, Ministry of Education, Culture, Sports, Science and Technology, Japan. Four test units were designed so as to be a

**Department of Architecture and Architectural Systems, Kyoto University, Japan*
Email: mn@archi.kyoto-u.ac.jp

prototype of model test units which were also constructed and tested in Kyoto University five years ago. The model column test units with 250x250 column section was considered to be 1/2.4-scale model of the prototype test units with 600x600 section.

In this paper behavior under reversed cyclic loading of the prototype test units are compared with that of the model units in terms of strength, ductility and failure process. Focus is placed on confining effect of transverse reinforcement on flexural compression of concrete and equivalent plastic hinge length.

2. COLUMN TEST UNITS AND TEST PROCEDURES

2.1 Model Units

Four reinforced concrete column units with 250mm square cross section were constructed. The axial load, P_c, applied to the columns were $0.3f'_cA_g$ for D1N3 and D2N3, and $0.6f'_cA_g$ for D1N6 and D2N6, where f'_c and A_g denote the compressive strength of concrete and the gross sectional area of the columns, respectively. The longitudinal reinforcing steel for each column consisted of twelve 13mm diameter deformed bars with yield strength of 461MPa. The transverse reinforcements were 4mm diameter hoops from a round bar with yield strength of 486MPa. The mechanical properties of steel are summarized in Table 1. The cross sections and the dimensions of the columns, and the arrangement of longitudinal and transverse reinforcement in the columns are shown in Fig.1. The loading setup is shown in Fig.2.

Table 1 Mechanical properties of steel for model test units

	Yield strain (%)	Yield stress (MPa)	Tensile strength (MPa)	Young's modulus (10^5MPa)
D13	0.243	461	643	1.89
ϕ4	0.269	486	606	1.81

The design standard strength of concrete was 30MPa. The mix design for the concrete used was:

Aggregate (15mm max. size) ... 966 kg/m^3
Sand ... 790 kg/m^3
Portland Cement ... 378 kg/m^3
Superplasticiser ... 0.945 kg/m^3
Water ... 168 kg/m^3
Water/Cement ratio = 0.44

The average slump was 74mm. The compressive cylinder strength had reached f'_c=37.6MPa at the stage of testing the columns. All columns were cast vertically, compacted using vibrators, and were damp cured in the laboratory.

The volumetric ratio of confining reinforcement to confined core measured center-to-center was 1.04% for all specimens. The area of confining reinforcement placed in the column was 136% for the units under N=0.3f'_cA_g and 40% for the units under N=0.6f'_cA_g of that calculated according to Eq.8.26 of NZS3101:1995 using the measured material strengths and assuming that the capacity reduction factor ϕ=1. ACI318-99 requires 146% of the area of confining reinforcement placed in the columns.

Reversed cyclic horizontal load was statically applied to the column top by a hydraulic jack. For D1N3 and D1N6 which were subjected to one-directional loading, the first loading cycle consisting of two cycles to column rotation angle of ±1/400 was followed by a series of deflection controlled cycles in the inelastic range, also comprising two full cycles to each of the displacements to ±1/200, ±1/100, ±3/200, ±1/50, ±3/100 and ±1/25 in column rotation angle.

For D2N3 and D2N6 subjected to bi-directional loading, the first loading was applied up to +1/400 to the north-south direction with keeping the deflection of the east-west direction zero. Then, the top of the column is subject to horizontal displacements following the trace of a circle,

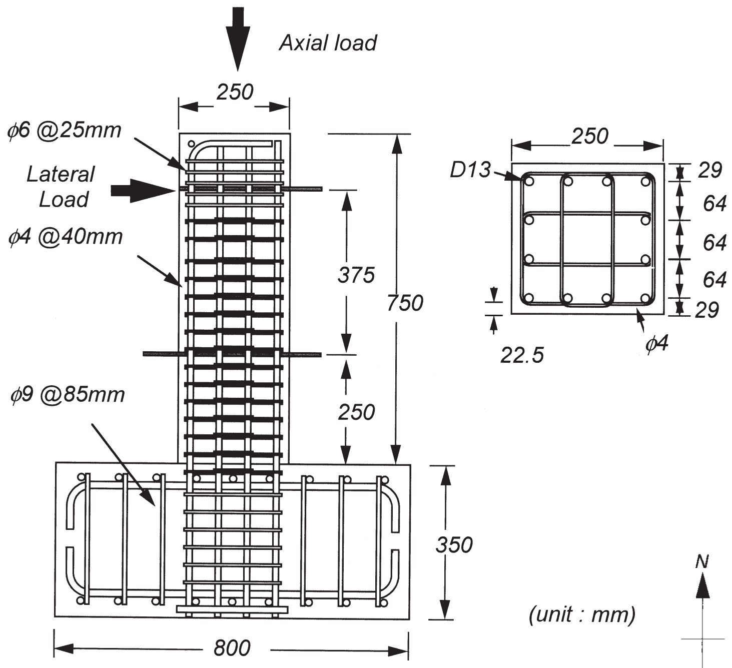

Figure 1 Model test units

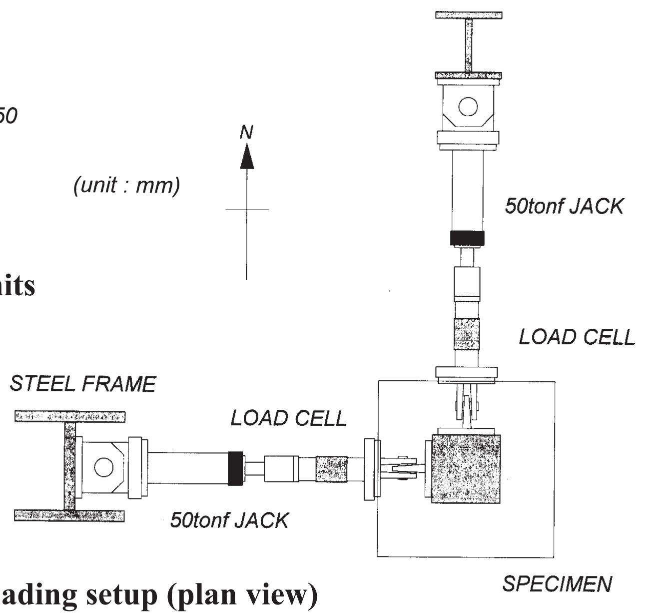

Figure 2 Loading setup (plan view)

followed by similar loadings with the north-south deflection increasing to 1/200, 1/100, 3/200, 1/50, 3/100 and 1/25.

2.2 Prototype Units

Four reinforced concrete column units with 600mm square cross section were constructed. The axial load, P_c, applied to the column was $0.6f'_cA_g$ for L1D60 and L1N60. For L1NVA and L2NVA the axial load applied was a function of flexural moment as shown below,

L1NVA: $$N/D^2 f_c' = 0.3 + 2.47\left(M_{NS}/D^3 f_c'\right) \quad (1)$$

L2NVA: $$N/D^2 f_c' = 0.3 + 2.47\left(M_{NS} - M_{EW}\right)/D^3 f_c' \quad (2)$$

where, M_{NS}, M_{EW}: flexural moment around N-S axis and E-W axis, respectively.

D: whole height of the column

The longitudinal reinforcing steel for each column consisted of twelve 25mm diameter deformed bars with yield strength of 388MPa. The transverse reinforcements were 13mm diameter hoops from a deformed bar with yield strength of 524MPa. The mechanical properties of steel are summarized in Table 2. The cross sections and the dimensions of the columns, and the arrangement of longitudinal and transverse reinforcement in the columns are shown in Fig.3. The loading setup is illustrated in Fig.4.

Table 2 Mechanical properties of steel for prototype test units

	Yield strain (%)	Yield stress (MPa)	Tensile strength (MPa)	Young's modulus (10^5MPa)
D25	0.211	388	588	1.84
D13	-	524*	673	1.94

*0.2% offset yield stress

The design standard strength of concrete was 36MPa. The mix design for the concrete used was:

Aggregate (20mm max. size) ... 964 kg/m^3
Sand ... 777 kg/m^3
Portland Cement ... 380 kg/m^3
Superplasticizer ... 0.76 kg/m^3
Water ... 182 kg/m^3
Water/Cement ratio=0.48

The average slump was 180mm. The compressive cylinder strength had reached f'_c=39.5 MPa at the time of testing. Young's modulus was 2.49x10^4 MPa. All columns were cast vertically, compacted using vibrators, and were damp cured in the laboratory.

The volumetric ratio of confining reinforcement to confined core measured center-to-center was

1.67% for all units. The area of confining reinforcement placed in the column was 62% of that calculated according to Eq.8-26 of NZS3101:1995 using the measured material strengths and assuming that the capacity reduction factor ϕ=1. ACI318-99 requires 84% of the area of confining reinforcement placed in the columns.

Reversed cyclic horizontal load was statically applied to the column top by a hydraulic jack. For L1N60 and L1D60 which were subjected to one-directional loading, the first cycle consisting of two cycles to column rotation angle of ±1/400 was followed by a series of deflection controlled cycles in the inelastic range, also basically comprising two full cycles to each of the displacements to ±1/200, ±3/400, ±1/100, ±1/50, ±3/100, ±1/25 and ±1/20.

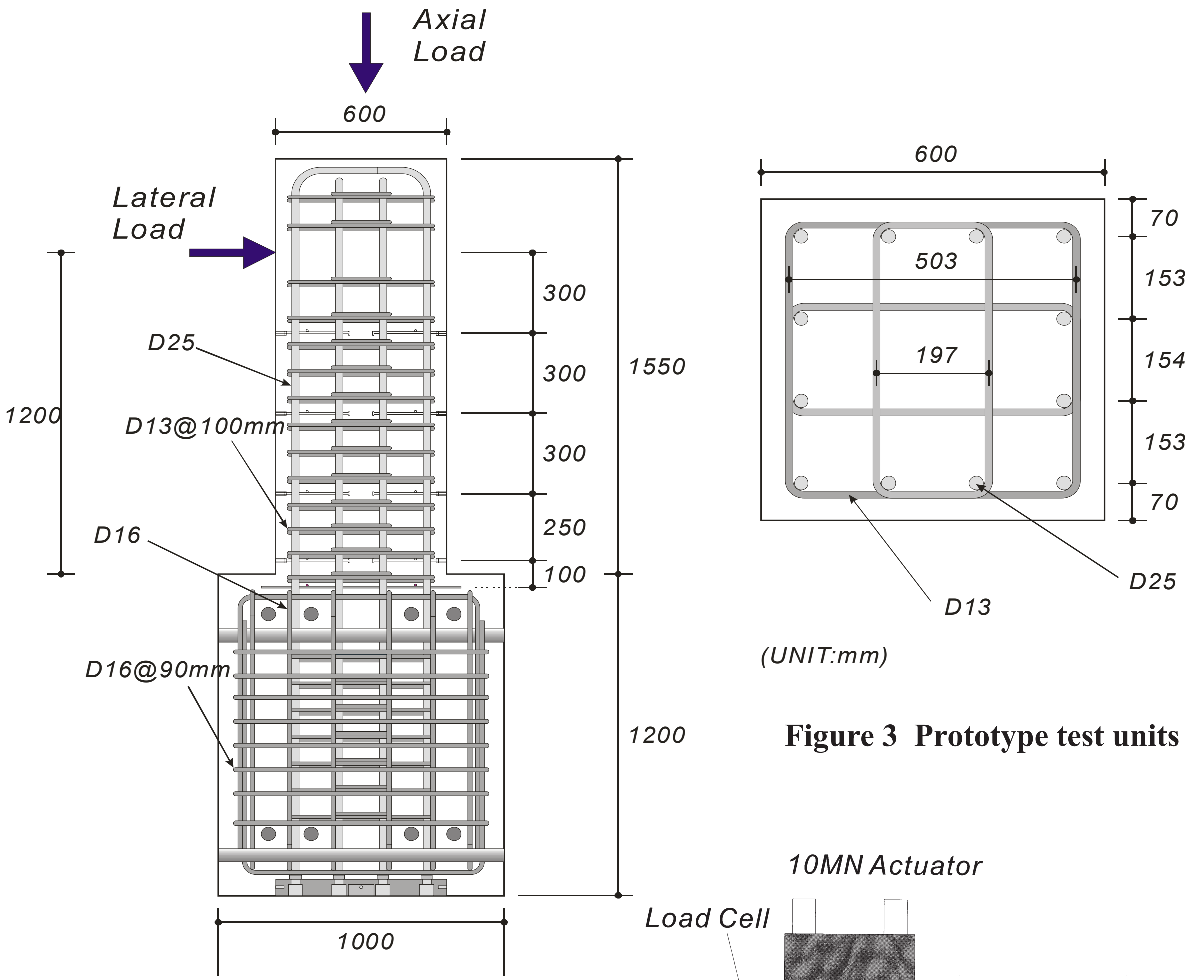

Figure 3 Prototype test units

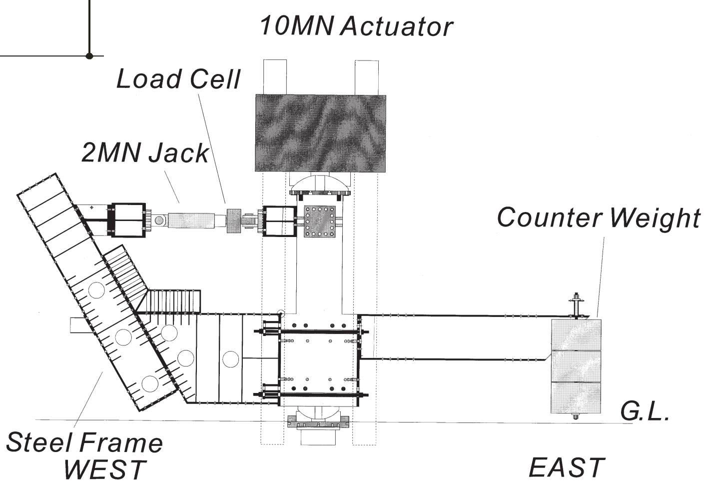

Figure 4 Loading setup (south view)

For L1NVA and L2NVA subjected to bi-directional loading, the top of the column is subject to horizontal displacements following the trace of a circle at the column rotation angle of 1/400, 1/200, 3/400, 1/100, 1/50, 3/100, 1/25 and 1/20.

All test units are summarized in Table 3 with the type of loading and the axial load level applied.

Table 3 Test units and loading

Test units		Loading	$N/A_g f'_c$
Model test units	D1N3	one-directional	0.3
	D1N6	one-directional	0.6
	D2N3	bi-directional (Circle)	0.3
	D2N6	bi-directional (Circle)	0.6
Prototype test units	L1D60	one-directional	0.6
	L1N60	one-directional	0.6
	L1NVA	bi-directional (Circle)	0~0.6
	L2NVA	bi-directional (Circle)	0~0.6

2.3 Scale Factors between Prototype Units and Model Units

Scale factors between the prototype and model units are summarized in Table 4. Because of limitations of materials available, scale factors for all aspects are not always 1/2.4.

Table 4 Scale factors

		Prototype	Model	Prototype/ Model
Dimensions	Section (mmxmm)	600x600	250x250	2.40
	Column height*1 (mm)	1200	625	1.92
	Shear span ratio	2.0	2.5	0.80
Concrete	Concrete strength (MPa)	39.5	37.6	1.05
	Max. aggregate size (mm)	20	15	1.33
Longitudinal rebar	Diameter (mm)	25	13	1.92
	Spacing between bars (mm)	154	64	2.41
	Reinforcement ratio	0.0113	0.0163	0.69
	Yield strength (MPa)	388	461	0.84
Transverse reinforcement	Diameter (mm)	13	4	3.25
	Pitch (mm)	100	40	2.50
	Volumetric ratio	0.0168	0.0104	1.62
	Yield strength (MPa)	524	486	1.08
	Reinforcing ratio, $p_w=A_s/bs$	0.00846	0.005	1.69
	$p_w\sigma_{wy}$ (MPa)	4.43	2.43	1.82

*1 From the top surface of the foundation to the loading point

3. TEST RESULTS

3.1 Load-displacement Relations and Failure Modes

Load-displacement curves for the test units are illustrated in Fig.5(a) and (b).

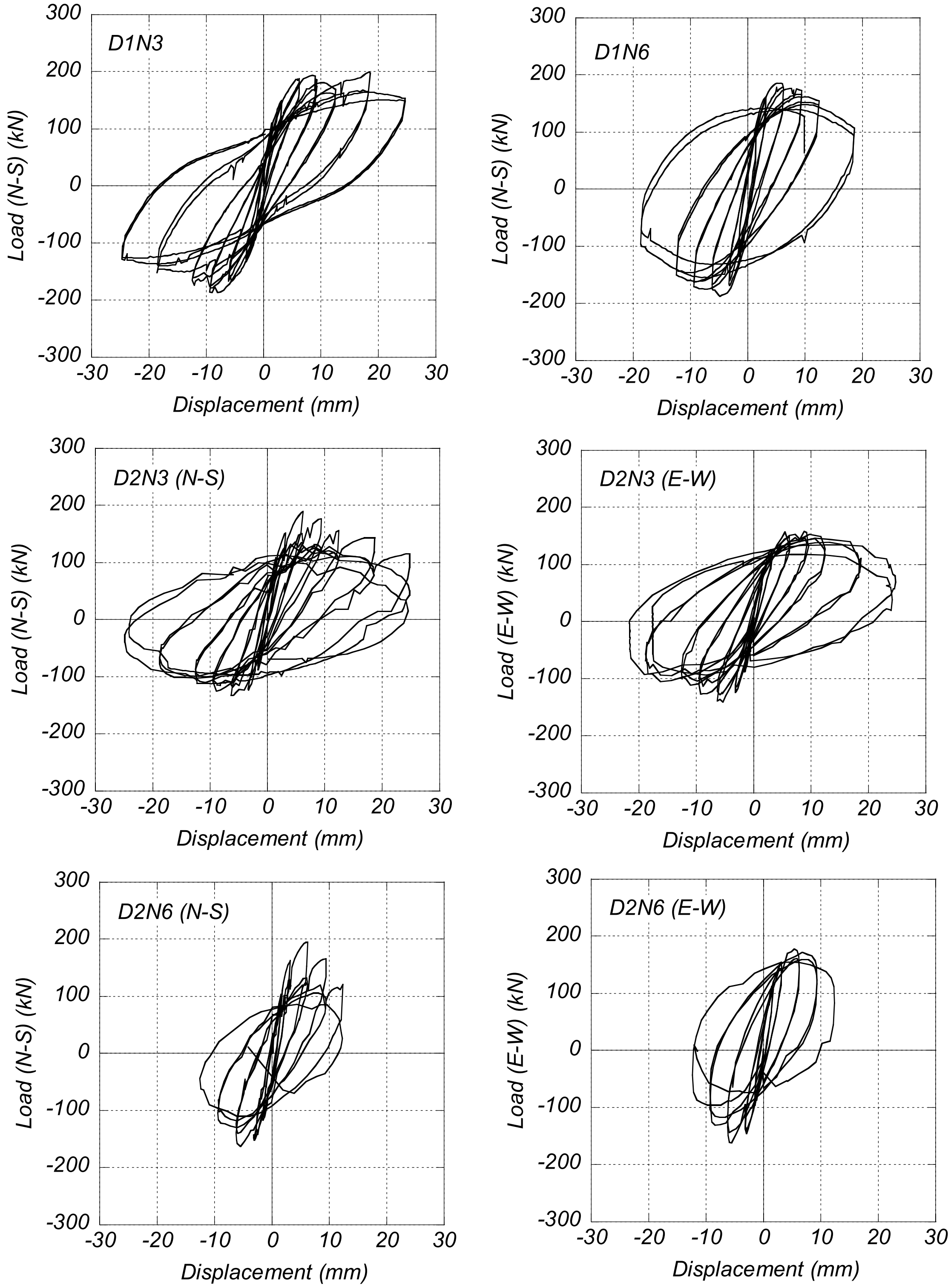

Figure 5(a) Load-displacement curves

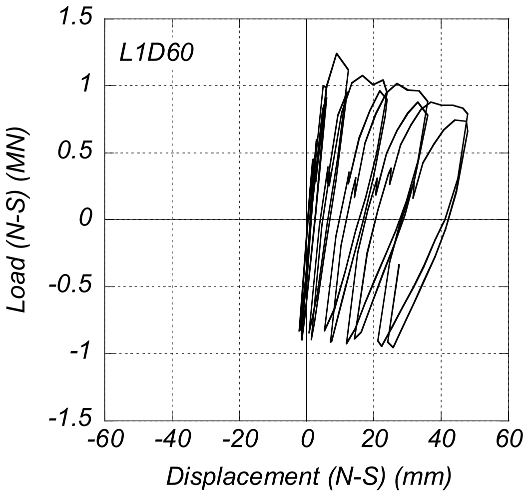

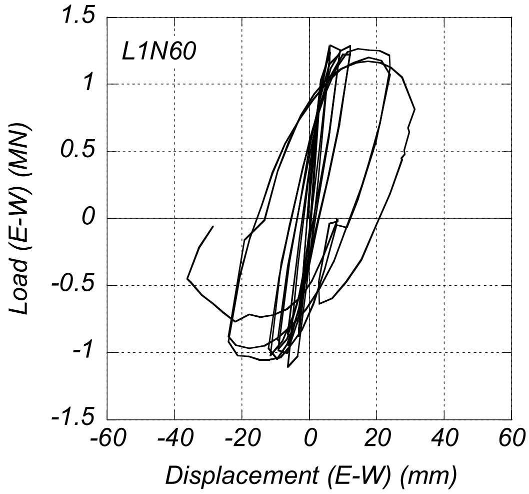

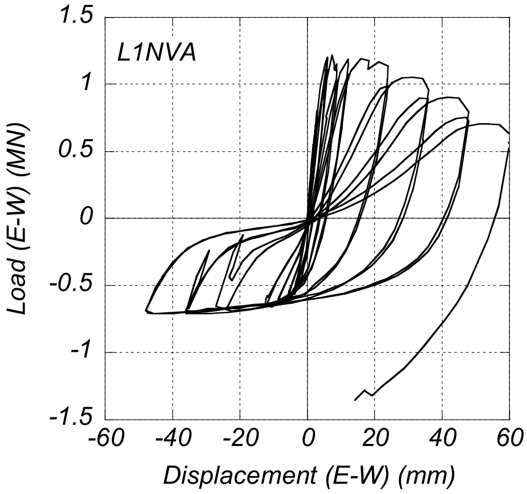

Figure 5(b) Load-displacement curves

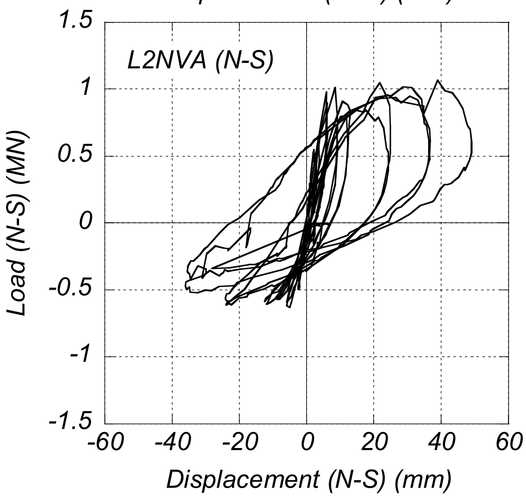

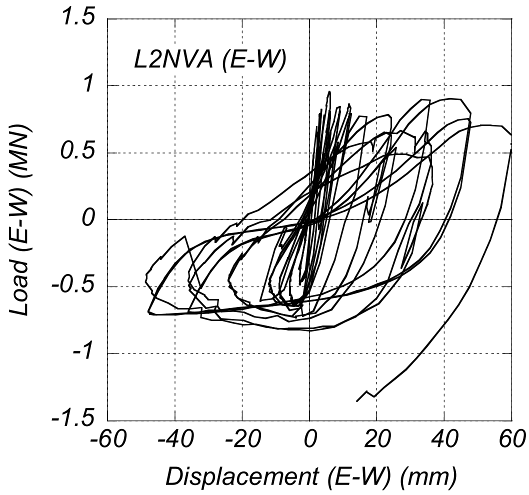

Failure modes of the model test units are summarized as follows;

D1N3...Buckling of longitudinal reinforcement was not observed. Cover concrete spalling was observed over the height of about 210mm from the column base.

D1N6...Slight buckling of longitudinal rebars was observed at the height of 110mm.

D2N3...All longitudinal rebars buckled at the height of about 110mm.

D2N6...Buckling was found on all longitudinal bars at the height of about 150mm.

Findings from the model unit tests;
1. The capacity reduction between the first loading cycle and the second loading cycle at a certain displacement larger than +3/200 was more significant than at the smaller displacement.
2. Axial load and bi-directional loading did not have large influence on the maximum capacity.
3. The larger the axial load was, the more significant capacity reduction was observed after the maximum capacity was attained. The bi-directional loading resulted in larger capacity reduction.

Loading sequences and failure modes of the prototype units are reported as follows;
L1D60...Because of insufficient capacity of a loading jack, load larger than 900kN was not applied in the negative direction. After column rotation angle of +4.0% was reached, loading to the positive direction only was carried out with the constant axial load of $0.6f'_cA_g$ on the column. However, loading was stopped due to a measuring apparatus trouble.

Cover concrete spalling was observed at the column base over 900mm from the column-foundation interface. Buckling of longitudinal rebars was not observed.

L1N60...When the axial load was applied, the top of the column moved 1mm in the direction perpendicular to the loading direction. As the reversed cyclic loading was proceeded the displacement to the perpendicular direction increased. Before the displacement in the loading direction reached +3.0%, the perpendicular-direction displacement reached 4.0%. Then, after unloading the load was applied to return the column top to the original position. After reloading column failure was observed at the column rotation angle of 3.0% when the axial load was not sustained.

Buckling of longitudinal reinforcement was observed at the north-east and north-west corners at the height of 300mm from the bottom.

L1NVA...Cover concrete at the north-east and north-west corners spalled off over the height of 900mm from the column base. Buckling of a longitudinal rebar was observed at the north-east corner at the height of 300mm.

L2NVA...Cover concrete on the south face completely spalled off over the height of 900mm. On the other sides all the longitudinal reinforcement were found buckled at the height of 150-300mm. One of the longitudinal reinforcement on the south side fractured at the height of 150mm.

In Figure 6, moment envelopes divided by the ultimate moment are plotted against column rotation angle for the model unit D1N6 and the prototype unit L1N60. These envelope curves are similar regardless of the scale.

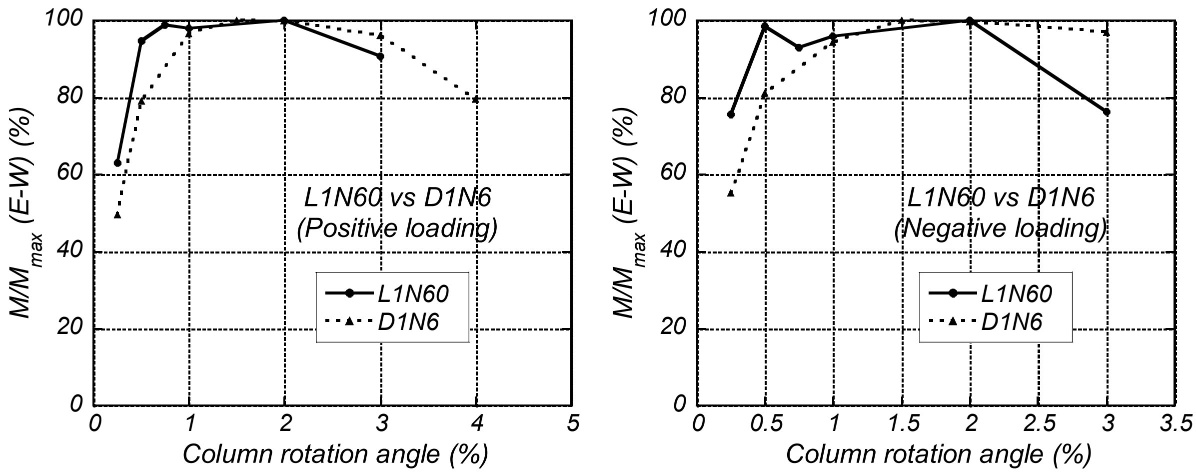

Figure 6 Envelope curves of moment-rotation angle relationships

3.2 Strength

The ideal theoretical flexural strength *Mi* of the columns calculated using the ACI318-99 equivalent stress block based on the measured material strengths are summarized in Table 5. The strength reduction factor ϕ was assumed to be unity. The flexural strengths *Me* obtained from the test results are also shown in Table 5.

For D2N3, D2N6 and L2NVA whose column tops are subjected to horizontal displacements following the trace of a circle, the peak moments in the orthogonal principal directions (N-S and E-W) are indicated. Generally the ACI method underestimates the experimental results.

Table 5 Maximum moment capacities obtained experimentally and by ACI methods

Test units	Experimental results, *Me* (kNm)		ACI Methods, *Mi* (kNm)		*Me/Mi*	
	Positive	Negative	Positive	Negative	Positive	Negative
D1N3	150.8	-137.4	105.0	-105.0	1.44	1.31
D1N6	143.4	-141.6	91.2	-91.2	1.57	1.55
D2N3	128.2	-96.6	105.0	-105.0	1.22	0.92
	96.4	-117.6	105.0	-105.0	0.92	1.12
D2N6	137.9	-126.0	91.2	-91.2	1.09	1.38
	113.1	-139.7	91.2	-91.2	1.24	1.53
L1D60	1567.0	-1078.7*1	1085.6	-1085.6	0.99	1.44
L1N60	1707.5	-1383.2	1085.6	-1085.6	1.57	1.27
L1NVA	1604.9	-1504.2	1085.6	-592.2	1.48	2.54
L2NVA	1628.5	-780.4	1085.6	-592.2	0.72	2.75
	1501.0	-1504.2	1085.6	-592.2	1.38	2.54

*1 Because of low capacity of hydraulic jack load could not be applied to the capacity of the test unit.

D1N6 vs L1N60

The experimental scale factor for the ultimate moments of D1N6 and L1N60 can be calculated as follows,

$$(M_{up}/M_{um})^{1/3} = (1707.5/143.4)^{1/3} = 2.2835 \quad (3)$$

The ratio of the compressive strengths of the prototype and model concretes, $f'_{cp}/f'_{cm} = 1.05$
The ratio of the yield strengths of the prototype and model concretes, $f_{yp}/f_{ym} = 0.84$
The ratio of the reinforcement ratios of the prototype and model concretes, $\rho_{cp}/\rho_{cm} = 0.69$

3.3 Equivalent plastic hinge length

Equivalent plastic hinge lengths were calculated based on the curvature measurements along the height of the columns. They are listed in Table 6.

Predicted plastic hinge length proposed by Paulay and Priestley (Paulay and Priestley, 1992) are 0.52D for the prototype and 0.75D for the model test units.

Table 6 Equivalent plastic hinge length

Test units		Plastic hinge length experimentally obtained	Plastic hinge length proposed by Paulay and Priestley
Model test units	D1N3	0.59D	0.75D
	D1N6	0.84D	
	D2N3	0.69D	
	D2N6	0.96D	
Prototype test units	L1D60	D	0.52D
	L1N60	0.8D	
	L1NVA	0.7D (+ve)	
		0.4D (-ve)	
	L2NVA	0.9D (+ve)	
		0.4D (-ve)	

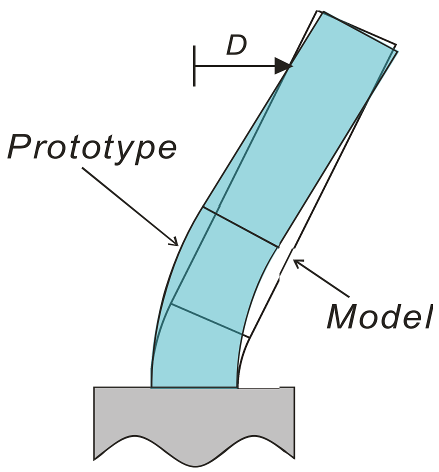

Figure 7 Deflection curves for the model and prototype test units

From the measurement deflection curves for the model and prototype test units can be described as illustrated in Fig. 7. The ratio of the flexural deformation at the base to the total deflection of the column in the model unit is larger than that of the prototype unit.

4. CONCLUSIONS

The following conclusions are derived from the experiments on the prototype and model test units:

1. Reversed cyclic loading tests on reinforced concrete columns were conducted to investigate scale effect on flexural compression behavior.
2. Moment envelopes divided by the ultimate moment, which was plotted against column rotation angle for the model unit D1N6 and the prototype unit L1N60 indicated that these envelope curves are similar regardless of the scale.
3. Generally the ACI method underestimates the ultimate moments obtained from the experimental results for the model and prototype test units.
4. The ratio of the flexural deformation at the base to the total deflection of the column in the model unit is larger than that of the prototype unit.
5. Further investigation is needed for reaching a conclusion that behavior of prototype test units can be predicted by model units.

5. REFERENCES

NIST (1989), *Inelastic Behavior of Full-Scale Bridge Columns Subjected to Cylcic Loading*, NIST Building Science Series 166.

Paulay, T. and Priestley, M. N. J. (1992), *Seismic Design of Reinforced Concrete and Masonry Buildings,* New York: John Wiley & Sons.

PWRI (1999), *Report on Corporative Research on Scale Effect on Seismic Performance of Reinforced Concrete Piers*, (in Japanese).

6. KEYWORDS

Scale effect, reinforced concrete, column, confinement, plastic hinge length, strength, ductility

Acknowledgment

The author would like to extend his sincere thanks Mr. Tetsuya Kuroyama, Mr. Nagayuki Matsuishi and Dr. Susumu Kono of Kyoto University for conducting the model and prototype tests.

THE SCALE EFFECTS ON THE REINFORCED CONCRETE COLUMNS WITH HIGH AXIAL LOAD

Hitoshi TANAKA[1], Tsuguo HIKIDA[2] and Hiroyuki NAKAJI[3]

ABSTRACT

In this study, focusing on the scale effects, some concentric compression loading tests were conducted using square columns to obtain the compressive stress-strain relationships of confined and unconfined concrete. As the main experimental variable, the sectional width of the tested square columns was varied from 194mm to 600mm. It was found that, due to the significant scale effect, the strength of columns was reduced more than predicted by any of the previously proposed models. Based on these experimental results, modification of a previous stress-strain model for confined and unconfined concrete was proposed so as to be able to take the sectional dimensions of column into account. The adequacy of the modified model was examined by comparing with the experimental results from this study and also from other sources.

It is noted that, when only the safety limit state is considered in the column design, the strength reduction due to the scale effect might not be so significant especially for the case of concrete columns confined by closely spaced lateral reinforcement. This is because the ultimate limit state of such confined concrete columns is dominated by the details of lateral confining reinforcement rather than the characteristics of plain concrete. However, the strength reduction of concrete due to the scale effect could become crucial if the serviceability limit state and the damage control limit state are considered in the design. This is because the column damage level under such limit states is predominantly determined by the characteristics of unconfined cover concrete and core concrete with little confining stress.

1. THE RIDDLE OF SCALE EFFECT ON CONFINED CONCRETE

It has been well known that the strength of plain concrete becomes smaller as the size of the test specimen becomes larger. For example, Neville proposed Eq. 1 to express the relationship between the concrete compressive strength of specimens with various sizes and that determined from the 15cm cubic concrete specimens (A.M. Neville,1966).

$$\frac{P}{P_{15}} = 0.56 + \frac{0.697}{\left(\dfrac{V}{2.36hd} + \dfrac{h}{d}\right)} \qquad (1)$$

1. *Professor of Disaster Prevention Research Institute, Kyoto University, Kyoto, Japan*

2. *ME student, Department of Architecture and Civil Engineering, Toyohashi University of Technology, Toyohashi, Japan*

3. *Assistant Prof., Department of Architecture and Civil Engineering, Toyohashi University of Technology, Toyohashi, Japan*

where

P = compressive strength of plain concrete specimen

P_{15} = compressive strength of concrete determined by 15cm cubes

V = volume of plain concrete specimen in cm^3

h = height of plain concrete specimen in cm

d = the least sectional dimension of plain concrete specimen

As can be seen from the test data plotted in Fig. 1 (A.M. Neville, 1966), the strength reduction factor for large scale specimens could likely be as small as 0.6. However, such a small value of strength reduction factor due to the scale effect is not introduced in any design code or stress-strain models proposed previously. As a good example, the stress-strain model expressed by Eqs. 2 to 13 is summarized below. This stress-strain model for confined concrete was developed by the working group which had been organized for the General Technology Development Project by the Ministry of Construction, Japan, (Ministry of Construction, Japan, March 1993). The modeling was conducted based on the data obtained from 54 cylindrical specimens and 117 square column specimens with section diameter or width of more than 20 cm, where the compressive strength of concrete determined by ϕ10cm cylinders were ranged from about 20 to 80 MPa. The adequacy of the stress-strain model was examined and confirmed by applying it to not only small size specimen but also some real scale specimens.

It is noted that, in the above model, the plain concrete strength of the square column specimens was assumed to be same as the compressive strength of concrete determined by ϕ10cm cylinders as can be seen from Eq. 4. This means that any significant strength reduction of plain concrete due to the scale effect was not recognized as far as the above test data were concerned. It is considered that the strength reduction of plain concrete due to the scale effect becomes less sensitive in the case of confined concrete because of the failure mechanisms of the confined concrete shown in Fig. 2.

When concrete columns are compressed beyond elastic range, shear sliding surfaces are formed inside the core concrete with the propagation of micro cracks. The shear sliding surfaces are either type A or type B (H. Tanaka, 1990). These types of failure modes are often observed in concentric loading tests on concrete cylinders and square columns. When these types of failure occur in the confined concrete specimens, the ultimate strength and ductility are quite dependent on the details of lateral reinforcement and the mechanical properties of reinforcing steel rather than the characteristics of the core concrete. This will be the reason why the strength reduction of plain concrete due to the scale effect becomes less sensitive in the case of the confined concrete specimens than in the case of the unconfined concrete specimens.

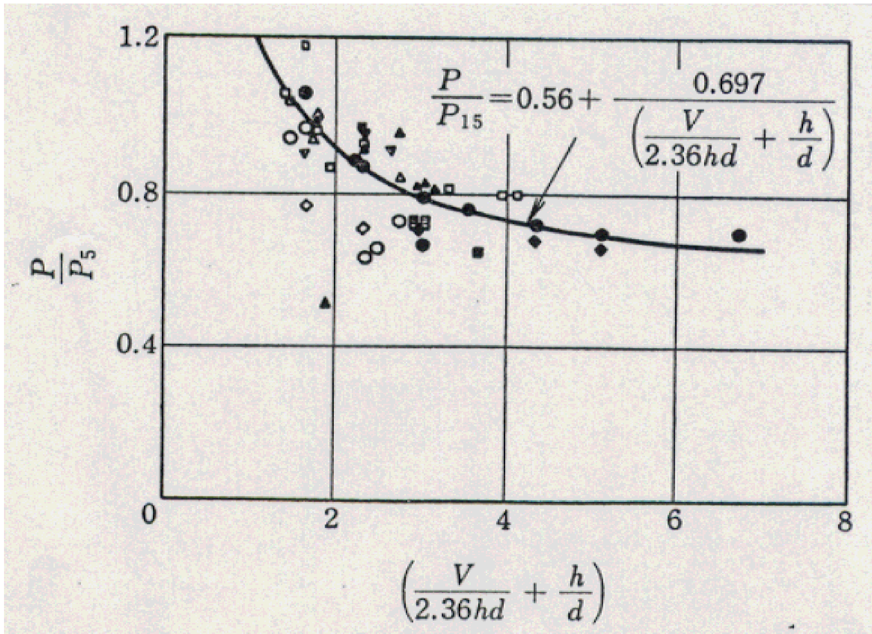

Fig.1 Strength Reduction of Concrete due to the Scale Effect
(A. M. Neville, 1966)

$$\frac{\sigma_c}{{}_c\sigma_{cB}} = \frac{AX + (D-1)X^2}{1 + (A-2)X + DX^2} \tag{2}$$

where

$${}_c\sigma_{cB} = \sigma_p + \kappa\rho_h\sigma_{hy} \tag{3}$$

$$\sigma_p = \mu_c\sigma_B = \begin{cases} 0.8\,{}_c\sigma_B, & \text{for circular section} \\ 1.0\,{}_c\sigma_B, & \text{for square section} \end{cases} \tag{4}$$

$$\kappa = \begin{cases} k_c\left(1 - \dfrac{s}{2D}\right)^2, & k_c = 2.09 \quad \text{for circular section} \\ k_s\left(\dfrac{d''}{C}\right)\left(1 - \dfrac{s}{2D_c}\right), & k_s = 11.5 \quad \text{for square section} \end{cases} \tag{5}$$

$$X = \frac{\varepsilon_c}{\varepsilon_{co}}, \quad A = \frac{E_c \varepsilon_{co}}{{}_c\sigma_{cB}}, \quad K = \frac{{}_c\sigma_{cB}}{\sigma_p} \tag{6}$$

$$\varepsilon_{co} = \varepsilon_o \begin{cases} 1 + 4.7(K-1), & K \le 1.5 \\ 3.35 + 20(K-1.5) & K > 1.5 \end{cases} \tag{7}$$

$$\varepsilon_o = 0.93\left({}_c\sigma_B\right)^{1/4} \times 10^{-3} \tag{8}$$

$$E_c = 4.1k\left({}_c\sigma_B / 100\right)^{1/3} \times 10^4 \times \left(\gamma / 24\right)^2 \tag{9}$$

$$k = \begin{cases} 1.0, & \text{for ordinary aggregates} \\ 1.2, & \text{for high elastic aggregates like limestone} \\ 0.9, & \text{for low elastic aggregates like light-weight aggregate} \end{cases} \tag{10}$$

$$D = \alpha + \beta_c \sigma_B + \gamma\sqrt{(K-1)_c \sigma_B / 23} \tag{11}$$

$$\alpha = 1.50 \qquad \beta = -1.68 \times 10^{-3} \tag{12}$$

$$\gamma = \begin{cases} 0.75, & \text{for square steel tube} \\ 0.50, & \text{for hoop reinforcement} \end{cases} \tag{13}$$

where

σ_c, ε_c : stress and strain of confined concrete, respectively

ρ_h : ratio of volume of lateral reinforcement to total volume of concrete core

${}_c\sigma_B$: compressive strength of concrete measured by ϕ100mm control cylinder

σ_p : plain concrete strength of actual structural members

${}_c\sigma_{cB}$: axial compressive strength of confined concrete in actual structural members

ε_{co} : strain at ${}_c\sigma_{cB}$

d" : diameter of lateral reinforcement or thickness of steel tube

C : length for evaluating effectively confined area (see Fig. 3)

s : spacing of lateral reinforcement (s = 0 for steel tube)

D_c : diameter or length of core section (see Fig. 3)

σ_{hy} : yield strength of lateral reinforcement or steel tube (when σ_{hy} >700MPa, σ_{hy} =700MPa)

When only the safety limit state is considered in the column design, the strength reduction due to the scale effect might not be so significant especially for the case of concrete columns confined by closely spaced lateral reinforcement. However, such strength reduction of concrete could become crucial if the serviceability limit state and the damage control limit state are considered in the design. This is because the column damage level under such limit states is predominantly determined by the characteristics of unconfined cover concrete and core concrete subjected to confining stress with comparatively minor level. From this reason, the experimental work and review of the previous studies on then scale effect were conducted as mentioned in the following sections, although this topic itself is quite old.

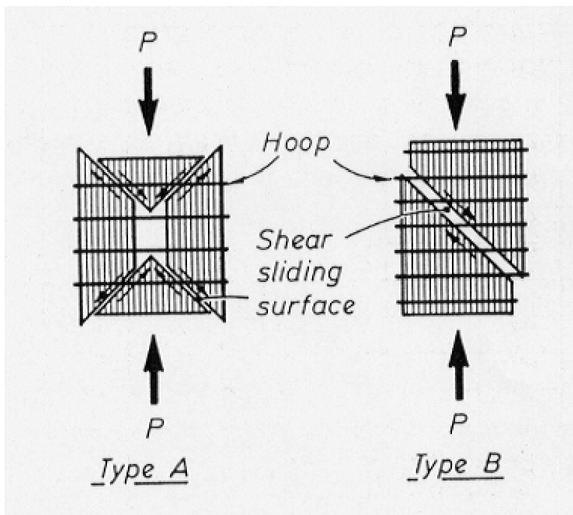

Fig. 2 Formation of Shear Sliding Surfaces in Core Concrete

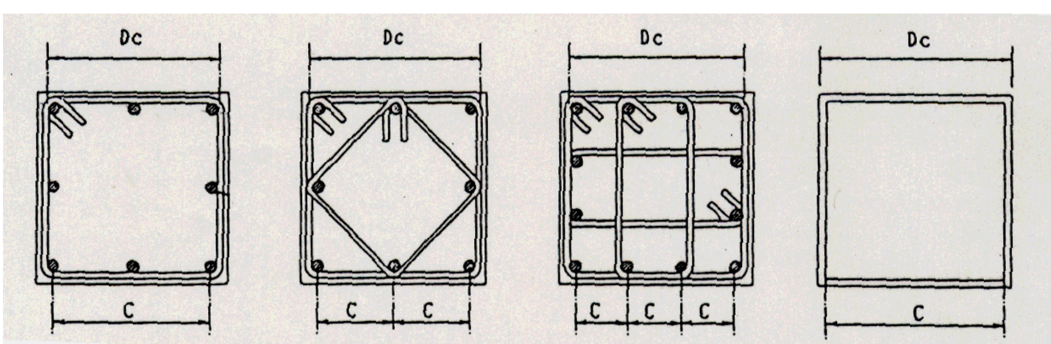

Fig. 3 Definition of C and D_c in Eq. 5

2. COLUMN TESTS TO EXAMINE THE SCALE EFFECT

2.1 Test Specimens and Testing Method

As listed in Tables 1, 18 unconfined square concrete columns were constructed and tested under monotonic concentric loading with low strain rate. 6 confined concrete columns were also constructed as shown in Table 2 and tested in a similar manner.

Dimensions of the concrete columns were varied as 600mm square section with 1200 mm in height, 400mm square section with 800 mm in height, and 194mm square section and 388 mm in height. Compressive strengths of concrete determined by ϕ100mm cylinders were from 20.3MPa to 134.0MPa. For confined concrete specimen, deformed bars with diameters of 6mm, 10mm and 13 mm were used for square hoop reinforcement. The volumetric ratio of hoop reinforcement to the total concrete core was about 1.0 % in all confined concrete specimens. The nominal yield strength of the hoop reinforcement was all 295MPa. To arrange hoop reinforcement, round bars with steel grade of 295MPa (measured yield strength = 351MPa) and diameter of 6mm were provided in longitudinal direction in each corner of the square hoop reinforcement. As an example, reinforcing arrangement for the confined concrete column with 600mm square section is shown in Fig. 4.

The axial load was applied by the 10MN servo-controlled jack and measured by the electric load cell attached to the jack head. The axial strain of the test column was measured at middle region of the test column with the gauge length of two-thirds of the test column height by two potentiometers placed symmetrically in each opposite side of the column section.

Table 1 Unconfined Test Columns and Measured Strengths

Dimensions of Test Columns	ϕ100mm cylinder strength of concrete, ${}_c\sigma_B$	Average Strength of Unconfined Column, σ_P	$\sigma_P / {}_c\sigma_B$
600×600×1200 mm	20.3 MPa	11.6 MPa (3columns)	0.57
	29.1 MPa	15.4 MPa (2columns)	0.53
400×400×800 mm	32.4 MPa	21.3 MPa (2columns)	0.66
400×400×800 mm	64.0 MPa	47.2MPa (2columns)	0.74
194×194×388 mm	32.4MPa	25.6 MPa (3columns)	0.79
194×194×388 mm	64.0MPA	49.9MPa (3columns)	0.78
194×194×388 mm	134.0MPA	108.0MPa (3columns)	0.81

Table 2 Confined Test Columns and Measured Strengths

Dimensions of Test Columns	ϕ100mm cylinder strength of concrete, ${}_c\sigma_B$	Hoop Reinforcement		Confined Concrete Strength, ${}_c\sigma_{cB}$ (${}_c\sigma_{cB}$ / ${}_c\sigma_B$)
		Rebar (SD295A)	Spacing	
600×600×1200 mm	29.1 MPa	D13	100mm	19.5 (0.67)
400×400×800 mm	32.4 MPa	D10	80mm	25.7 (0.79)
400×400×800 mm	64.0 MPa	D10	80mm	49.5 (0.77)
194×194×388 mm	32.4MPa	D6	77mm	26.0 (0.80)
194×194×388 mm	64.0MPA	D6	77mm	52.2 (0.82)
194×194×388 mm	134.0MPA	D6	77mm	88.1 (0.66)

note: measured yield strength of steel f_y=364MPa (D13), 373MPa (D10) , 396MPa (D6)

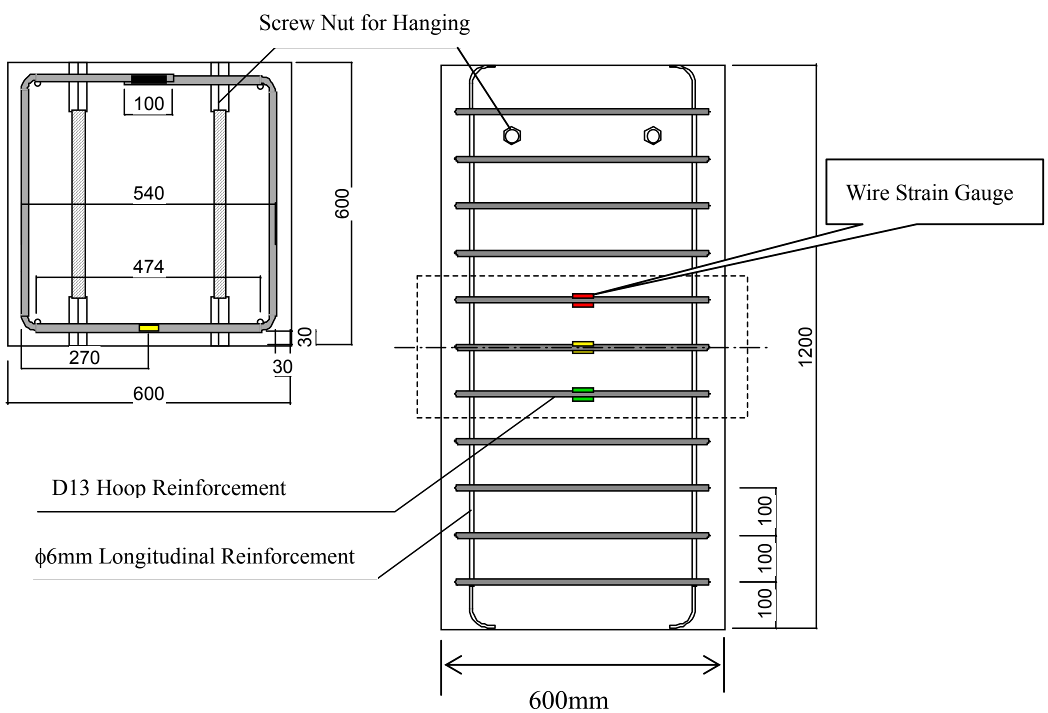

Fig. 4 Reinforcing Details of the Confined Concrete Column with 600mm Square Section

2.2 Test Results

Typical measured stress-strain relationships are shown in Fig. 5. It is noted that the strength of plain concrete is so significantly reduced as the sectional dimensions of the specimen increase. To evaluate the strength reduction of plain concrete due to the scale effect, regression analysis has been conducted and Eq. 14 was obtained as shown in Fig. 6.

$$\frac{\sigma_p}{{}_c\sigma_B} = -0.005818D_c + 0.913 \tag{14}$$

where D_c = width of square column section in cm

As far as the test results of this study are concerned, the strength reduction due to the scale effect was almost linear to the sectional dimensions of the square section. For reference, the strength reduction curve expressed by Eq. 15 proposed by Chang (K. Chang, 1997) is drawn in Fig. 6.

$$\frac{\sigma_p}{{}_c\sigma_B} = \frac{2.433}{B^{0.193}} \tag{15}$$

where B = width of square section of column in mm

Also shown in Fig. 6 is the curve determined by the combination of Eq. 1 by Neville and Eq. 16 by L'Hermite (R. L'Hermite, 1955) which converts the cubic concrete strength into cylindrical concrete strength.

$$\frac{{}_c\sigma_B}{W} = 0.76 + 0.2\log_{10}\frac{W}{196} \tag{16}$$

where W = compressive strength determined by concrete cube in kgf/cm^2.

2.3 Application of Strength Reduction Factor

Assuming that the plain concrete strength, σ_p, of the column specimens can be evaluated by Eq. 14, stress-strain relationship curves expressed by Eqs. 2 to 13 excluding Eq. 4 were drawn for the tested columns as shown in Fig.7. Also shown in Fig. 7 are the stress-strain curves determined by the Mander's model (J. B. Mander, 1988) and those modified using Eq. 14. It is noted that the theoretical stress-strain relationships modified using Eq. 14 have better agreement with the measured ones.

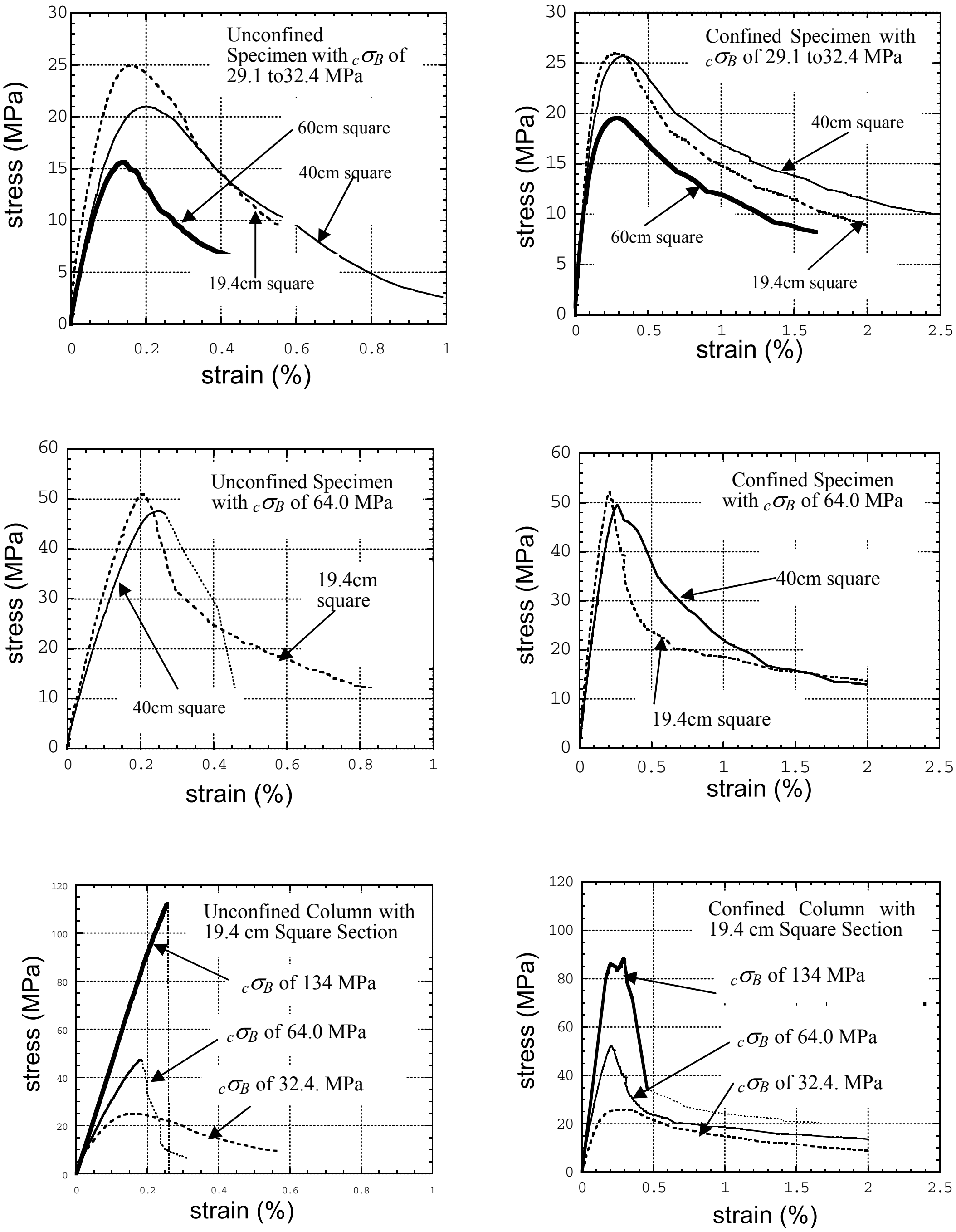

Fig. 5 Typical Measured Stress-Strain Relationships of Test Columns

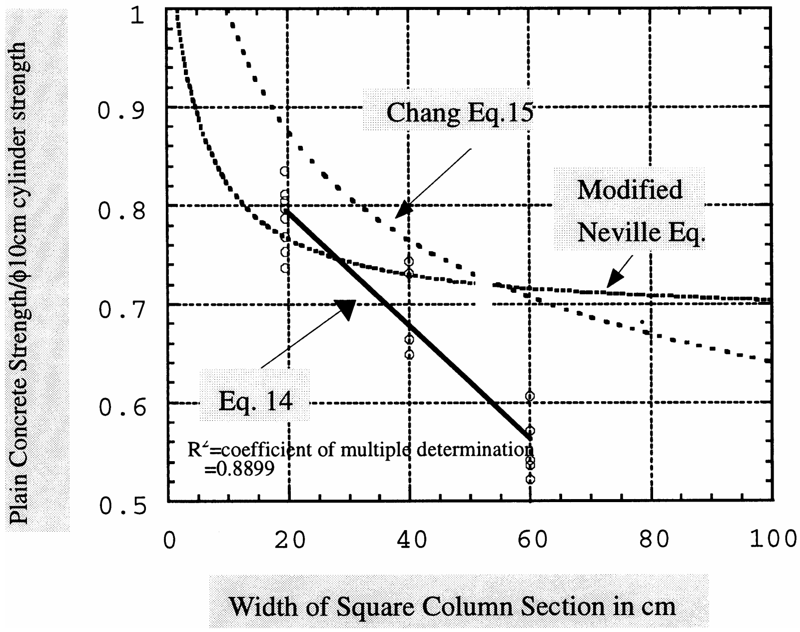

Fig. 6 Strength Reduction of Plain Concrete Specimen due to the Scale Effect

It was also found that the stress-strain curves determined by Eq.2 were adequate only when ${}_c\sigma_{cb}$ was less than about 80 MPa due to the mathematical characteristics of the function adopted in Eq. 2. A method to modify the Eq. 2 for the case of ${}_c\sigma_{cb}$ of more than 80 MPa is shown in the paper by Hikida et al. (Hikida, Tanaka, Nakji, 2001)

3. CONCLUSIVE REMARKS

In this study, focusing on the scale effects, concentric compression loading tests were conducted using square columns to obtain the compressive stress-strain relationships of confined and unconfined concrete. It was found that, due to the significant scale effect, the strength of columns was reduced more than predicted by any of the previously proposed models.

Based on those experimental results, modification of the previous stress-strain model for confined and unconfined concrete was proposed so as to be able to take the sectional dimensions of column into account. The adequacy of the modified model was examined by comparing with the experimental results from this study and also from other sources.

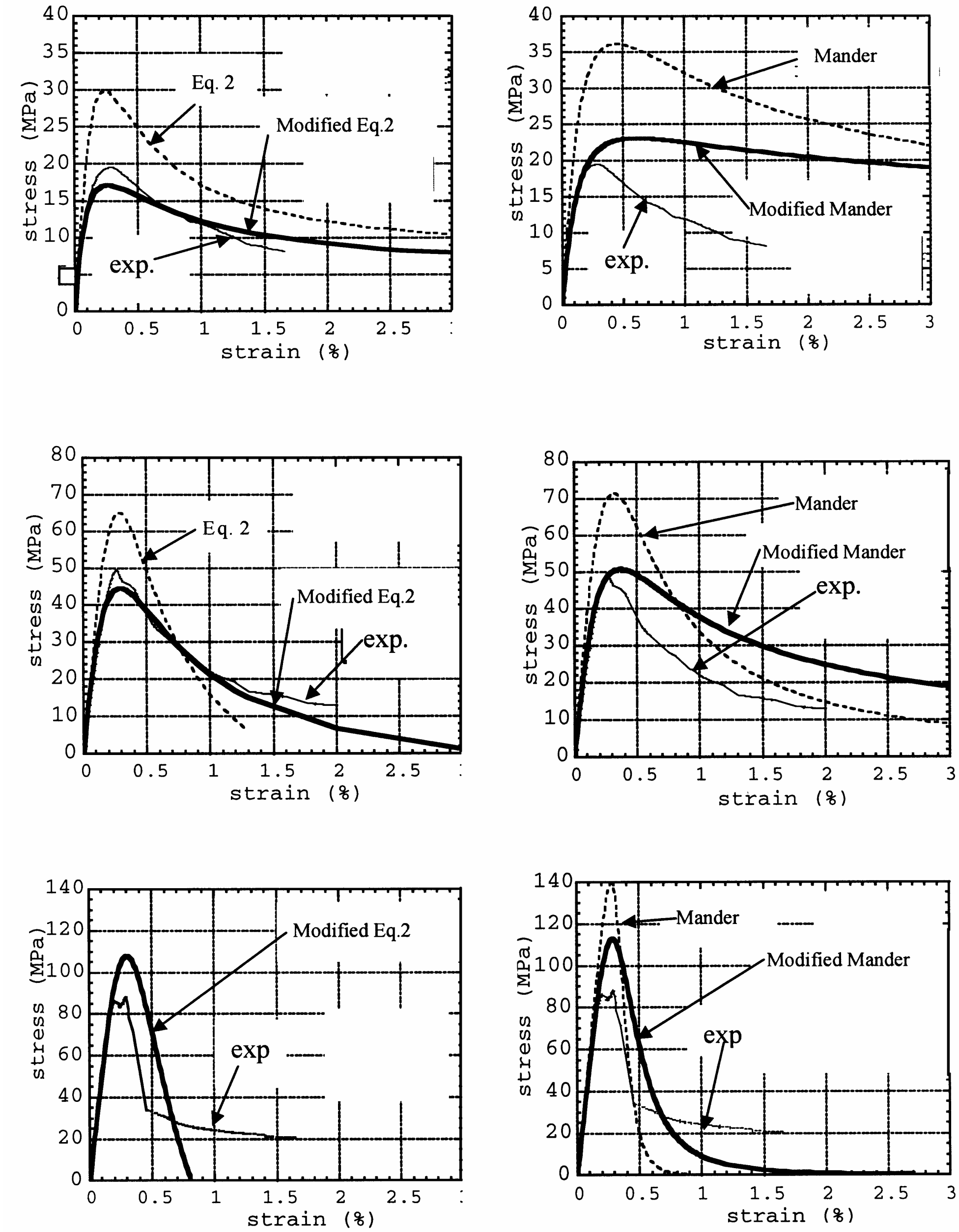

Fig. 7 Comparison between Theoretical and Measured Stress-Strain Curves

The strength reduction of concrete due to the scale effect could become crucial when the serviceability limit state and the damage control limit state are considered in the design. Hence, the scale effects on the strength and ductility of reinforced concrete members need to be more adequately taken into account in practical design.

REFERENCES

Chang, K. (March 1997). Study on the Compressive Strength and Deformability of Concrete Column with Real Scale (in Japanese) . Ph.D Thesis, Hirosima University, Japan.

L'Hermite, R. (1955). Idees Actuelles sur la Technologie du Beton, Documentation Technique du Batiment et des Travaux Publics, Paris.

Hikida, T., Tanaka, H. and Nakaji,H. (2001) Experimental study concerning the scale effects on the stress-strain models of confined concrete (in Japanese). The annual meeting of AIJ, Tokyo, Japan.

J. B. Mander, M. J. N. Priestley, and R. Park (August 1988). Theoretical Stress-Strain Model for Confined Concrete. *Journal of Structural Engineering*, Vol. 114, No. 8, pp. 1804-1826.

Ministry of Construction, Japan, (March 1993). General Technology Development Projects: Report on Development of Super-light Weight, Super-High Rise Technology for Reinforced Concrete Structure.

Neville, A. M. (Oct. 1966). A General Relation for Strengths of Concrete Specimens of Different Shapes and Sizes. Journal of ACI 63-10.

Tanaka, H.(June 1990). Effect of Lateral Confining Reinforcement on the Ductile Behaviour of Reinforced Concrete Columns, Research Report 90-2, Univ. of Canterbury, New Zealand, 458 pages.

ACCURACY OF SEISMIC PERFORMANCE METHODOLOGIES FOR RECTANGULAR REINFORCED CONCRETE COLUMNS

M. Parrish and M.O. Eberhard[1]

ABSTRACT

To implement Performance-Based Earthquake Engineering within a probabilistic framework, it will be necessary to account for inaccuracies in estimates of seismic performance. This paper describes the methodology used to quantify the accuracy of estimates of flexural strength, effective stiffness, and displacements at onset of spalling and longitudinal bar buckling. Statistics are reported for flexure-critical, rectangular reinforced concrete columns subjected to cyclic, lateral displacements. The ratio of measured-to-calculated strength had a coefficient of variation ranging from 9% to 18%, depending on the level of axial load and the concrete constitutive model. The effective stiffness was predicted less accurately, with coefficients of variation often above 25%. By accounting for the influence of axial-load ratio and transverse-reinforcement ratio on the plastic rotation at bar buckling, bar buckling displacement were estimated with a coefficient of variation of 28%.

1. INTRODUCTION

Structural engineers have always recognized that design and assessment methodologies need to account for uncertainties in structural properties and loading characteristics, as well as inaccuracies in the methodologies themselves. For example, the American Concrete Institute building code requirements provides a strength-reduction factor for each failure mode, whose value depends on the consequences of each type of failure and on variability of the actual strength from the computed strength (ACI 1999). Formal analyses of the calculated and measured resistances of reinforced concrete members (e.g., MacGregor et al. 1983) have led to recommendations for new strength-reduction factors for flexure, shear (e.g., MacGregor 1983) and bond (Darwin et al. 1998).

[1] *Department of Civil and Environmental Engineering, University of Washington, Seattle, USA*
Email: eberhard@u.washington.edu

To implement Performance-Based Earthquake Engineering (PBEE) within a probabilistic framework, the accuracy of various methods for predicting seismic performance needs to be evaluated. This paper provides reliability statistics for predictions of seismic performance of flexure-critical, rectangular reinforced concrete columns, subjected to cyclic loads. Statistics are reported for estimates of maximum flexural strength, effective stiffness at first yield, onset of concrete spalling and onset of bar buckling. Statistics were compiled by comparing the measured and calculated responses of columns extracted from a database of 204 tests of rectangular columns.

2. COMPILATION OF DATABASE

The results of more than 350 tests of spiral-reinforced and rectangular-reinforced concrete columns have been assembled to provide the basis with which to evaluate the assessment methodologies. The core of the database (199 tests) was assembled at the National Institute for Standards and Technology (Taylor and Stone 1993, Taylor et al. 1997). This database provided digital force-displacement histories for columns, as well as key material and geometric properties.

New tests have been added to the database, and the scope of information provided has been expanded to include more information about tie configurations, P-Δ effects and material properties. The database also includes the maximum displacement preceding observed spalling, bar buckling and failure, where such information was available. In addition, the columns were identified as flexure critical, flexure-shear critical or shear-critical based on column strength and on the reported observations of damage.

The resulting database, whose structure is shown in Figure 1, is available on the World Wide Web at *http//www.ce.washington.edu/~peera1*. Data is added intermittently to the site as new results become available. Regardless of the actual test configuration, the force-displacement data is provided as if the test had been performed on a cantilever column.

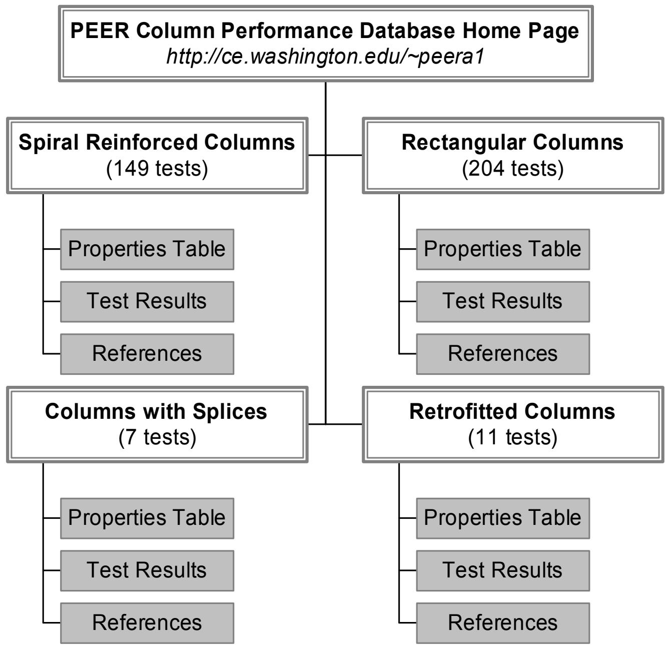

Figure 1. Structure of PEER Column Performance Database Website

3. PROCESSING OF COLUMN DATA

Of the 204 rectangular-reinforced columns in the database, only a subset was included in the reliability analyses of flexure-critical columns. Columns were included in the analyses only if the following conditions were met:

- Column was flexure-critical (no shear damage reported),
- Longitudinal reinforcement ratio was between 0.5% and 5%,
- Axial-load ratio (P/Agf'c) did not exceed 2/3,
- Largest column cross-sectional dimension was at least 150 mm,
- Test configuration could be analyzed as a cantilever (i.e., cantilever, double-curvature or double-ended configurations), and
- All important material properties were available.

The 130 column tests that satisfied the above criteria were used to evaluate methodologies for estimating flexural strength and effective stiffness. Of these tests, the maximum displacement at onset of spalling was reported for 76 tests, and the displacement at the onset of bar buckling was reported for 43 tests.

Based on the measured hysteretic behavior, lateral force-displacement envelopes were extracted and modified to account for the effect of the axial loads (P-Δ effect).

4. FORCE-DISPLACEMENT MODELING

For each column test, monotonic force-displacement relationships were computed for a variety of analytical models of flexural, shear and bond-slip deformations. The ability of various analytical models to predict column response was assessed by comparing key features of the measured and calculated force-displacement envelopes.

For the monotonically increasing portion of the force-displacement envelope, the contribution of flexural deformations to displacement was computed by integrating curvatures along the length of the column. Displacements due to bond-slip and shear deformation were then added. For larger displacements, the flexural contribution was calculated with plastic-hinge analysis. The following constitutive models were considered in the analyses:

Concrete

- Hognestad (1951)
- ACI Stress Bolck (318-99)
- Kent-Park (1971)
- Modified Kent-Park (1982)
- Mander, Priestley and Park (1988)
- Ravzi and Saatcioglu (1999)

Steel

- Elasto-Plastic
- Modified Burns-Seiss (1962)

Bond-Slip

- Uniform Bond Stress
- Lehman (1998)

5. FLEXURAL STRENGTH

It is important to compute column flexural strength accurately, because this property places an upper bound on column shear demand. The statistical properties of the ratio of measured-to-calculated are reported graphically in Figure 2 for four concrete models. In all cases, the Burns-Seiss model (1962) was used to model the stress-strain behavior of the steel, the Lehman (1998) recommendations were followed to model bond-slip deformation, and shear deformation was modelled as elastic. The mean and coefficient of variation (COV) for tests of 130 columns are reported for two ranges of axial-load ratio (P/Agf'c above or below 0.35) and two ranges of span-to-depth ratio (L/D above or below 3).

As shown in the figure, flexure strength could be computed accurately (COV ~10%) for low and moderate axial loads (regardless of L/D ratio) using any of the four models listed. For high axial loads, the values for the mean and COV for the Hognestad model were unacceptable, which is not surprising, because this model does not account for the effects of confinement. The accuracies of the other three models were similar.

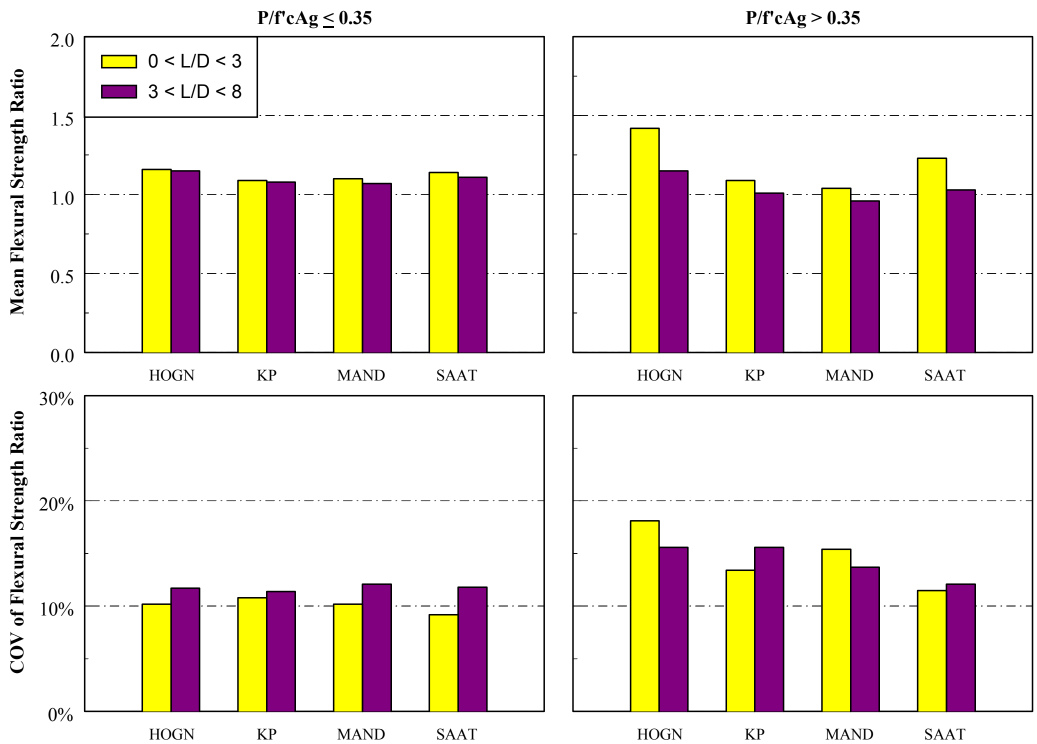

Figure 2. Accuracy of Estimates of Flexural Strength

6. EFFECTIVE STIFFNESS

Column stiffness is an important property, because this property controls the response of columns for small displacements (e.g., serviceability conditions). This property is also critical for estimating the yield displacement, and hence, the displacement ductility demand. As shown in Figure 3, effective stiffness was calculated at the force level corresponding to the point where the analytical model predicted that the longitudinal steel would first yield, or the concrete compressive strain reached a value of 0.0018.

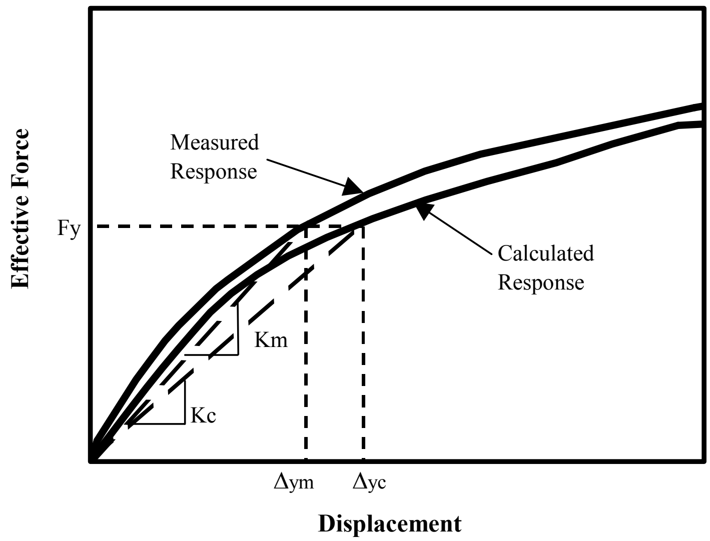

Figure 3. Procedure for Calculating Column Effective Stiffness

Statistics for the ratio of measured-to-calculated effective stiffness (K_m/K_c) are reported in Figure 4. These statistics were compiled following the same modelling assumptions that were followed to calculate flexural strength.

In general, the column stiffness was underestimated by the analysis, particularly for columns with L/D below 3. This observation suggests that the modelling methodologies underestimated the contribution of shear deformation, bond-slip deformation and/or joint deformation. All three of these factors contribute a larger proportion of the total column deformation for stocky columns than for slender ones. Parametric studies indicate that, although the mean value of the stiffness ratio can be increased by reducing the assumed bond stress, this reduction did not significantly lower the value of the coefficient of variation.

Both the Hognestad and Modified Kent-Park models gave unacceptable values for the mean and COV for high axial loads. The accuracy of the Mander et al., and Ravzi and Saatcioglu models produced better results.

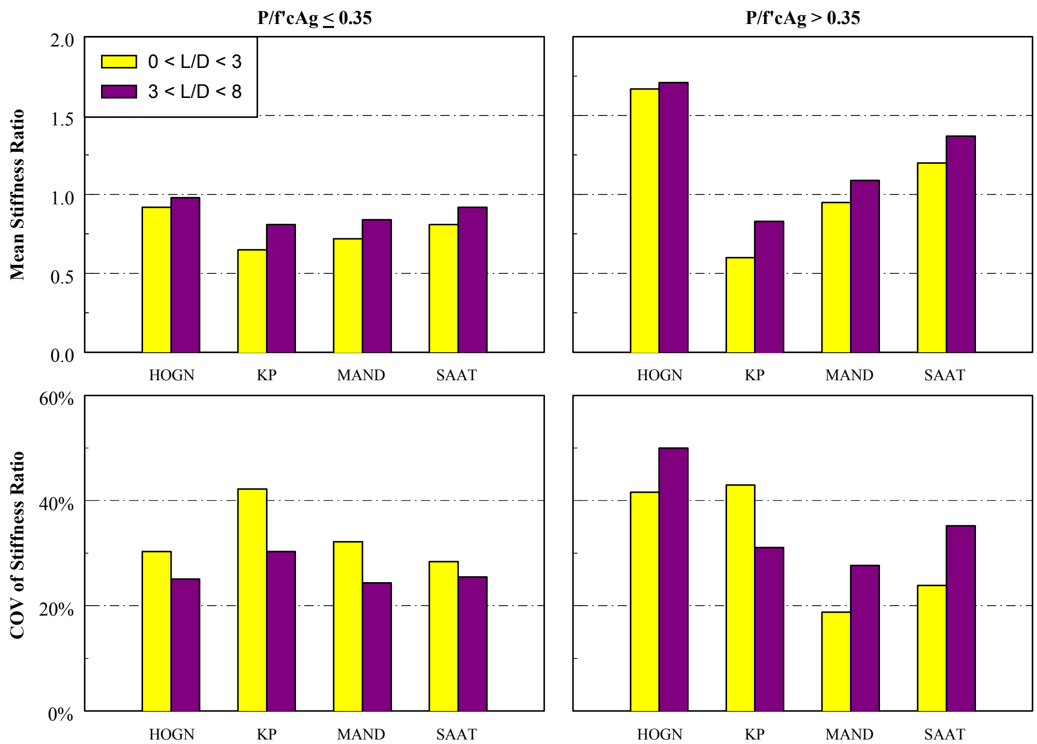

Figure 4. Accuracy of Estimates of Effective Stiffness

7. ONSET OF SPALLING

The onset of spalling is an important performance state, because spalling is the lowest level of damage likely to require repair for flexure-critical columns. For each test, Figure 5 reports the values of drift ratio, calculated compressive strain, displacement ductility (based on calculated yield displacement) and plastic rotation at the onset of concrete spalling. Yield displacements and concrete strains were calculated using the Mander et al. (1988) model for concrete, the Burns-Seiss model for steel, the Lehman bond model (1998) and an elastic model for shear deformations. The mean concrete compressive strain was 0.0057 with a COV of 46%.

Spalling displacements were estimated using a strain value of 0.005. The resulting ratio of measured displacement to calculated displacement at spalling had a mean of 0.89 and a COV of 43%. The value of all of the other three parameters decreased with increasing axial load, so in these cases, displacements were estimated using linear relationships based on axial-load ratio (Fig. 5). For these estimates, the

COV of the measured-to-calculated displacement ratios was above 50%.

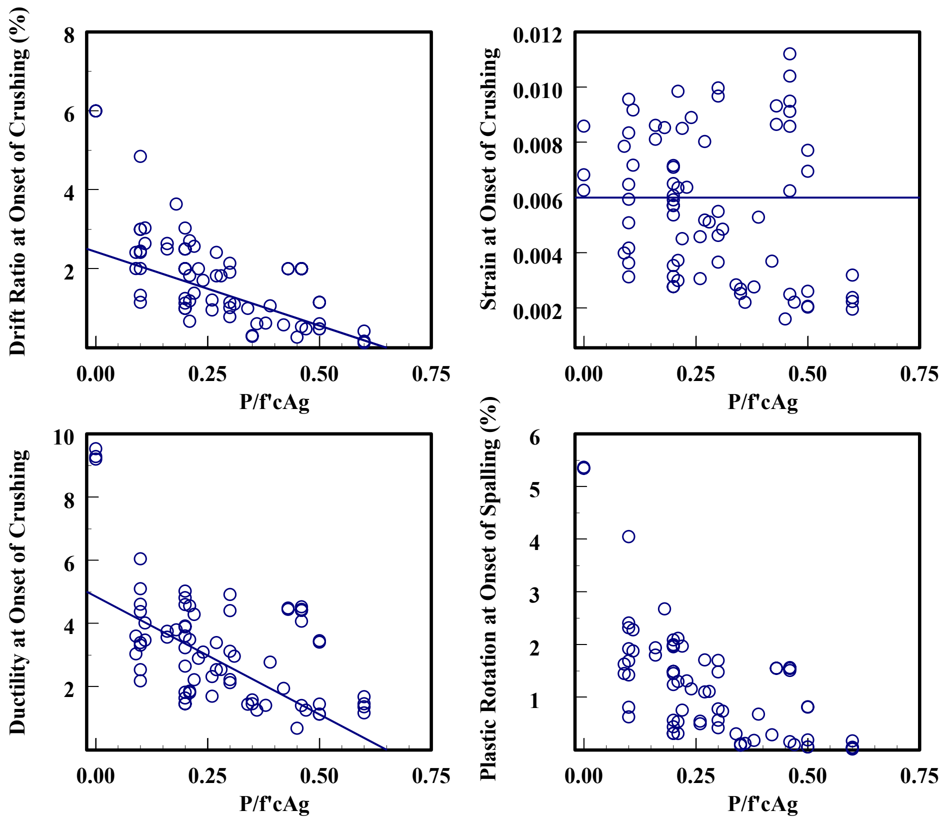

Figure 5. Column Deformation at Onset of Spalling

The values of the COVs were large, as expected, because various researchers identify the onset of spalling at various levels of damage. In addition, displacement histories often increase by 50% or more from one set of cycles to the next. Even if each researcher identifies the onset of spalling at the same level of damage, considerable uncertainty remains in identifying the displacement level needed to cause damage.

8. ONSET OF BAR BUCKLING

The onset of longitudinal bar buckling is another important damage state, because repair strategies can be expensive to implement in this case. In addition, occupants may feel unsafe if a building reaches this level of damage. Figure 6 reports the values of key deformation parameters at the onset of buckling. The values of all the parameters tend to decrease with increasing axial-load ratio, and to a lesser extent, the values increase with increasing amount of transverse reinforcement.

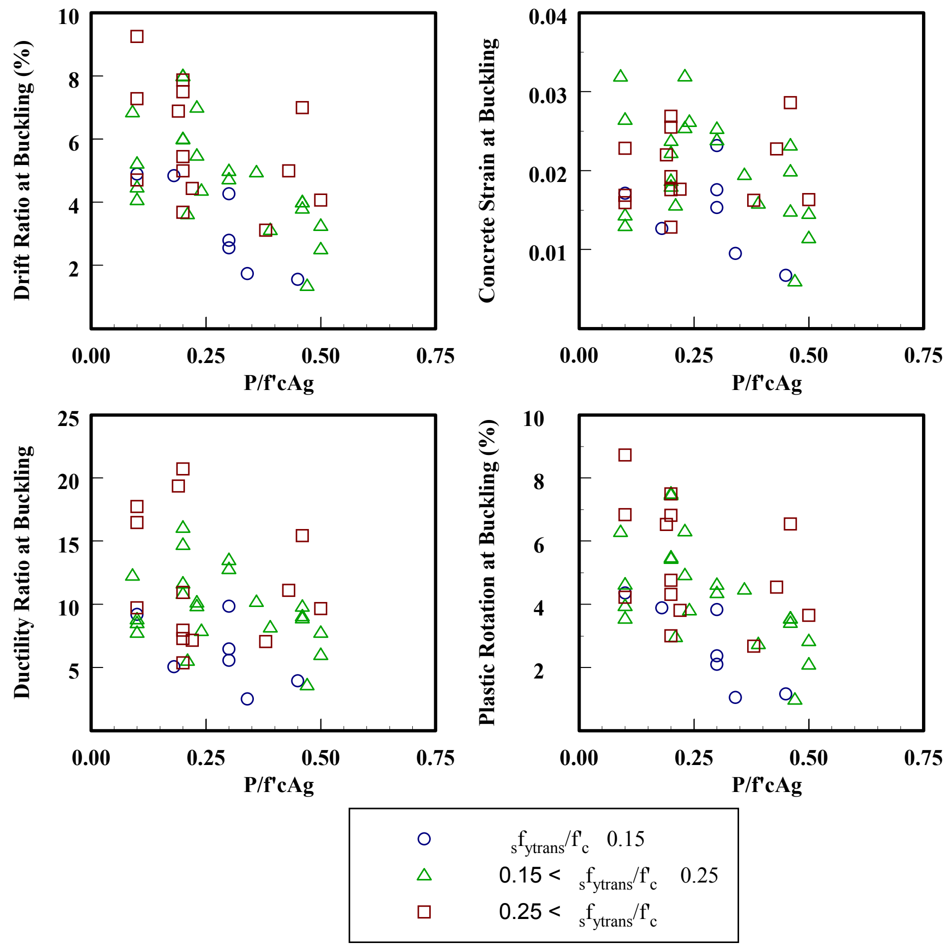

Figure 6. Column Deformation at Onset of Bar Buckling

Based on the trends apparent in Fig. 6, the displacement at onset of bar buckling, $\Delta_{buckling}$, was estimated based on the plastic rotation as follows:

$$\Delta_{buckling} = \Delta y + 0.02 * L * (1 - P/Agf'c) * (1 + 8\ \rho_s f_{ytrans}/f'_c) \qquad (1)$$

where Δy is the calculated displacement at first yield of the longitudinal reinforcement, L is the length of the cantilever, $P/A_g f'_c$ is the axial-load ratio, ρ_s is the transverse reinforcement ratio, f_{ytrans} is the yield strength of the transverse reinforcement, and f'_c is the concrete cylinder strength. In Equation (1), the quantity $\rho_s f_{ytrans}/f'_c$ is limited to 0.3. The resulting ratio of measured-to-calculated displacement for bar buckling had a mean of 1.11 and a COV of 28%.

9. CONCLUSIONS

By analysing measured force-deformation envelopes and damage reports for numerous column tests, it was possible to systematically study the accuracy of performance models for flexure-critical, rectangular concrete columns.

For low and moderate levels of axial-load ratio, the column flexural strength was estimated accurately, with means near 1.1 and coefficients of variation near 10%. As the axial-load ratio increased, the variation between calculated and measured strength increased, and selection of concrete model became important.

Effective stiffness was difficult to estimate accurately, because bond slip and shear deformation contributed significantly to total column deformation, particularly for small span-to-depth ratios. The ratio of measured-to-calculated effective stiffness varied according to the span-to-depth ratio, the axial-load ratio and the selected concrete stress-strain concrete model. For the two most complex models considered, the coefficient of variation for the stiffness ratio fell in the range of 20% to 35%.

The onset of spalling was estimated based on the calculated concrete compressive strain, and the onset of longitudinal bar buckling was estimated based on the plastic rotation. The coefficients of variation for the resulting ratios of measured-to-calculated displacement were 28% for spalling and 43% for buckling. The high magnitude of these coefficients of variation result, in part, from the inaccuracy of the performance models. The high variability also stems from variations in observer interpretation of damage, and from limitations in load histories, which usually increase in large increments from one set of cycles to the next.

10. REFERENCES

ACI Committee 318 (1999). Building Requirements for Structural Concrete (ACI 318-99) and Commentary (ACI 318R-99), American Concrete Institute. Farmington Hills, MI, USA.

Darwin, D., E.K. Idun, J. Zuo and M.L. Tholen (1998). Reliability-Based Strength Reduction Factor for Bond, *ACI Journal*, 95:4:434-443.

Hognestad, E. (1951). *A Study of Combined Bending and Axial Load in Reinforced Concrete Members*, University of Illinois Engineering Experimental Station Bulletin Series, Report No. 399, November.

Lehman, D.E. and J.P. Moehle. (1998), *Seismic Performance of Well-Confined Concrete Bridge Columns*, Pacific Earthquake Engineering Research Center, Report PEER-1998-01, University of California, Berkeley, USA.

Mander, J.B., M.J.N. Priestley and R. Park (1988). Theoretical Stress-Strain Model for Confined Concrete, *Journal of the Structural Division*, ASCE, 114:8:1804-1826.

MacGregor, J.D. (1983). Load and Resistance Factors for Concrete Design, *ACI Journal*, 80:4:279-287.

MacGregor, J.D., S.A. Mirza and B. Ellingwood (1983). Statistical Analysis of Resistance of Reinforced and Prestressed Concrete Members, *ACI Journal*, 80:3:16-182.

Park, R., M.J.N. Priestley and W.D. Gill. (1982). Ductility of Square-Confined Concrete Columns, *Journal of the Structural Division*, ASCE, 108:ST4:929-950.

Park, R. and T. Paulay. (1975). *Reinforced Concrete Structures*, New York, John Wiley and Sons.

Razvi, S. and M. Saatcioglu. (1999). Confinement Model for High-Strength Concrete, *Journal of the Structural Division*, ASCE,125:3:281-289.

Taylor, A.W., C. Kuo, K. Wellenius and D. Chung. (1997). *A Summary of Cyclic Lateral-Load Tests on Rectangular Reinforced Concrete Columns*, National Institute of Standards and Technology, Report NISTIR 5984.

Taylor, A.W. and W.C. Stone. (1993). *A Summary of Cyclic Lateral-Load Tests of Spiral Reinforced Concrete Columns*, National Institute of Standards and Technology, Report NISTIR 5285.

9. KEYWORDS

Accuracy, Assessment, Buckling, Column, Database, Reinforced Concrete, Performance, Spalling

SHEAR DESIGN EQUATION FOR RC MEMBERS CONSIDERING DUCTILITY DEMAND AND DETAILING

Toshikatsu ICHINOSE[1]

ABSTRACT

Reinforced concrete (RC) beams or columns often fail in shear after inelastic cyclic loading. This paper firstly reviews an analytical research based on Coulomb criterion. Second, an experimental research on the effect of loading excursions is reviewed. Third, experimental researches on the effects of loading excursion and of hoop detailing (hoop spacing both in longitudinal and transverse directions) are reviewed. Finally, the paper summarizes a shear design equation adopted in Japanese Design Guidelines where ductility demand and hoop detailing are considered.

1. INTRODUCTION

Shear failure after inelastic cyclic loading is often observed in reinforced concrete (RC) beam or column whose shear strength is slightly larger than its flexural strength. In the AIJ Design Guidelines (1999), this kind of failure is attributed to the two reasons: (1) reduction of effective compressive strength of concrete due to intersecting flexural-shear cracks, and (2) reduction of aggregate interlocking due to wide flexural-shear cracks (Ichinose 1992). The effects of hoop detailing are also considered in the Guidelines. Priestley et al. (1994) expressed the strength degradation by reducing the contribution of concrete to shear strength. Pujol et al. (2000) described the effect using Coulomb criterion. Kinugasa et al. (1994) experimentally showed that the degradation is largely dependent on loading history and attributed the phenomena to the incompklete closing of flexural-shear cracks. The objective of this paper is to summarize some of the experimental and analytical works on the topic.

[1] *Department of Systems Management and Engineering, Nagoya Inst. of Tech., Nagoya, Japan.*

Email: ichinose@archi.ace.nitech.ac.jp

2. COULOMB CRITERION UTILIZED BY PUJOL ET AL. (2000)

Pujol et al. (2000) presented a simple and effective method to calculate transverse reinforcement for given ductility demand. They assumed that represents shear failure of core concrete is represented by Coulomb criterion shown by the inclined solid line in Fig. 1 or

$$v_u = k_1 f'_c + \frac{3}{4}\sigma \tag{1}$$

where v_u = unit shear strength;

f'_c = compressive strength of concrete;

σ = unit stress acting perpendicular to the potential failure plane; and

k_1 = empirical factor representing cohesion.

The factor k_1 is assumed to decrease as ductility demand increases as shown in Fig. 2, where γ = maximum drift ratio and λ = shear span ratio.

The stress circle in Fig. 1 is determined by the following three parameters:

σ_a = mean axial stress on the core due to axial force and tensile reinforcement;

σ_t = mean stress exerted on the concrete by the hoop bars assumed to have yielded; and

v = mean shear stress in the core (= shear force divided by core area).

The proposed method can be useful for many situations, but the applicability to a member failing without yielding of transverse reinforcement is doubtful because one cannot estimate σ_t in such a case. The applicability is also questionable to the other extreme case where transverse reinforcement ratio is so small that the effect of the shear span ratio is large at small drift ratio.

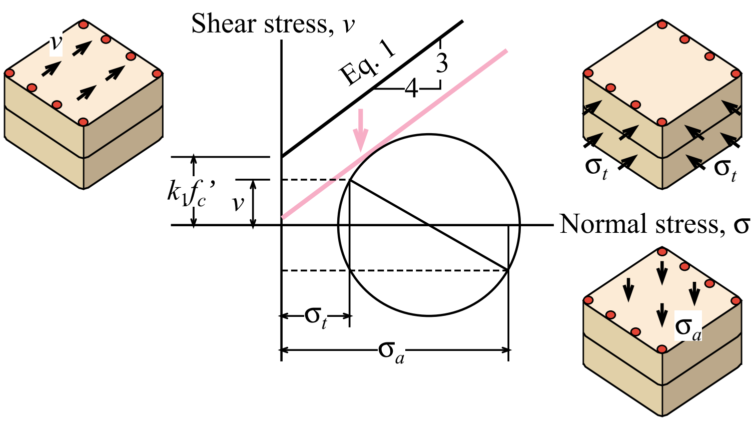

Fig. 1 Coulomb criterion used by Pujol et al. (2000)

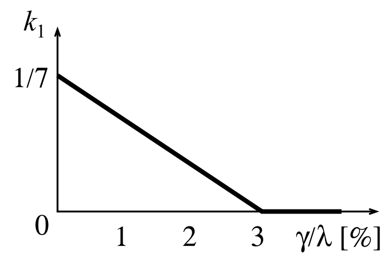

Fig. 2 Cohesion factor proposed by Pujol et al. (2000)

3. EFFECTS OF LOADING EXCURSION --- KINUGASA ET AL. (1994)

Kinugasa et al. (1994) tested ten specimens with identical detailing under different loading excursions. Shear reinforcement ratio, $A_w/(s.b)$ was 0.75 %. Selected results are shown in Fig. 3. One can have the following observations.

(a) Under the cyclic loading shown in Fig. 3a, the specimen showed large ductility.

(b) Cyclic loadings of an amplitude 80×10^{-3} rad. shown in Fig. 3b caused large stiffness degradation but small strength degradation.

(c) Cyclic loadings of an amplitude 120×10^{-3} rad. shown in Fig. 3c caused large stiffness degradation as well as large strength degradation.

(d) Incremental cyclic loadings shown in Fig. 3d caused large strength degradation from an

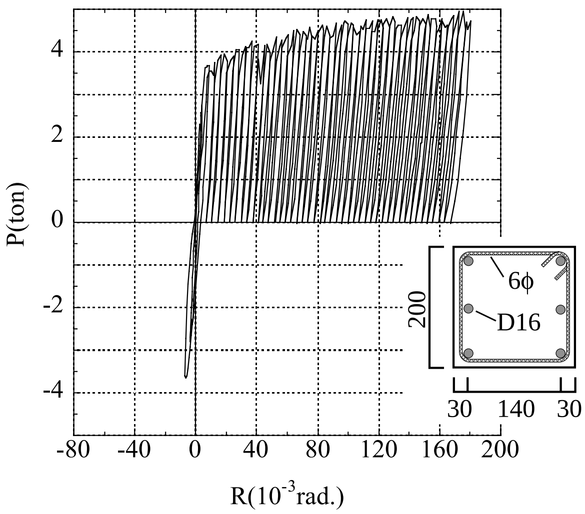

(a) Cyclic unloadings

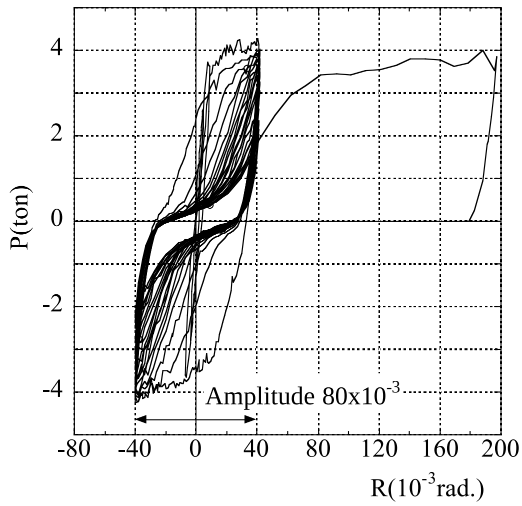

(b) Cyclic loadings at 40×10^{-3} rad.

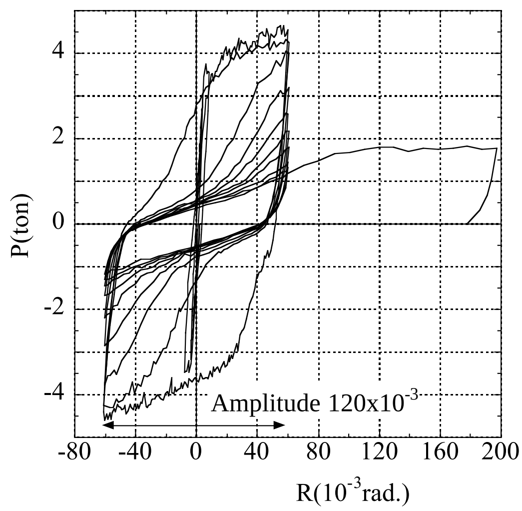

(c) Cyclic loadings at 60×10^{-3} rad.

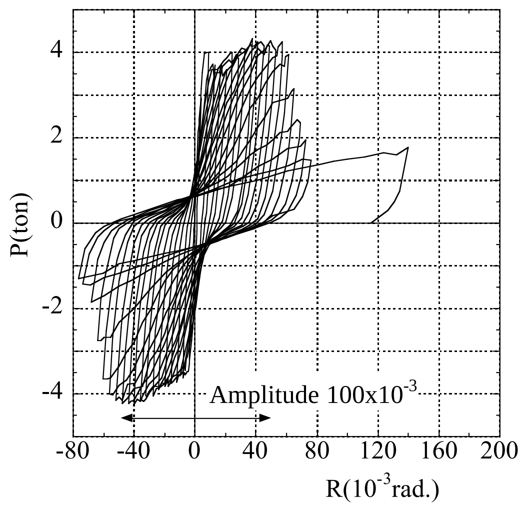

(d) Incremental cyclic loadings

amplitude $100x10^{-3}$ rad. which is between Figs. 3b and 3c.

(e) A large cyclic loading shown in Fig. 3e affected the response in the negative deflection but not in the positive deflection. However, the strength degradation started about the same deflection angle as Fig. 3d both in positive and negative deflections.

(f) Cyclic loadings between positive and zero deflections shown in Fig. 3f caused considerable strength degradation. Note that the degradation started when the amplitude of the deflection angle was $100x10^{-3}$ rad., which is similar to that of Fig. 3d.

In short, a threshold of deflection angle amplitude seems to exist for strength degradation irrespective of loading types.

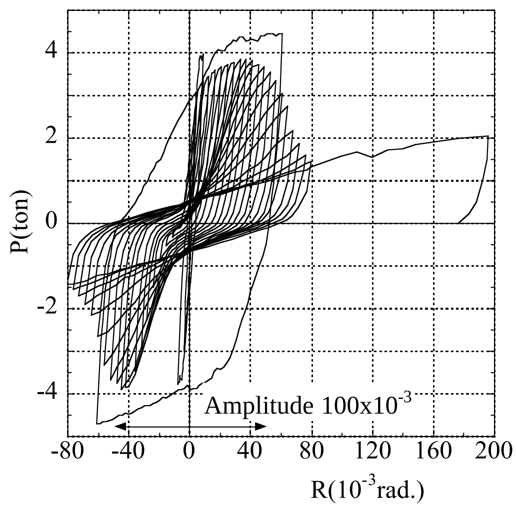

(e) A large cyclic loading followed by incremental cyclic loadings

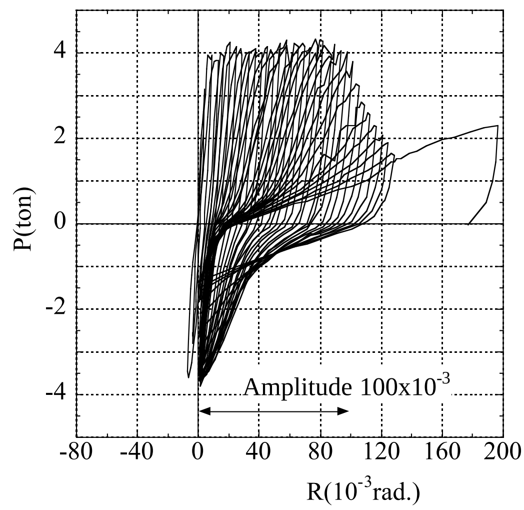

(f) Cyclic loadings between positive and zero deflections

Fig. 3 Load-deflection relationship obtained by Kinugasa et al. (1994)

4. EFFECTS OF DETAILING --- ICHINOSE ET AL. (1995 AND 2001)

Ichinose et al. (1995) conducted tests of RC members having sections shown in Fig. 4. The parameters were (a) with or without cross ties and (b) the spacing of ties. Materials (concrete and reinforcing bars) and shear reinforcement ratio, $A_w/(s.b)$ = 1.7 %, were identical for all the specimens. They failed in shear without yielding of flexural nor shear reinforcement. The observed shear strengths are listed in Table 1, where the difference is as large as 30%.

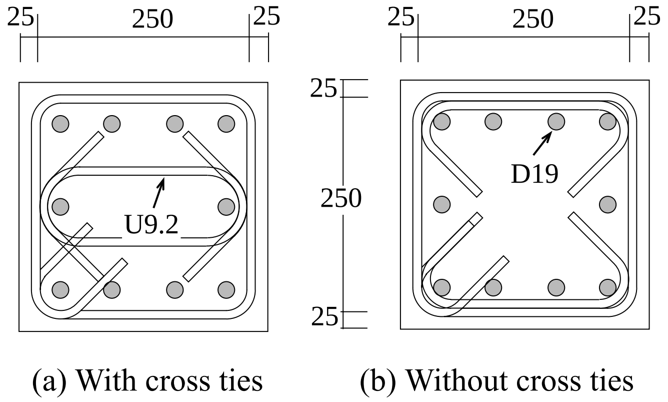

Fig. 4 Specimens' sections (unit: mm)

Table 1 Observed shear strength

Specimen		Strength
With cross-ties	s = 50	422 kN
	s = 150	365 kN
Without cross-ties	s = 50	353 kN
	s = 150	318 kN

Ichinose et al. (2001) conducted cyclic loading of specimens with shear reinforcement ratio, $A_w/(s.b)$ = 1.3 %, which failed in shear after flexural yielding as shown in Fig. 5. The specimen did not have cross-ties. The shear strengths predicted by the equations of either Priestley et al. (1994) or Pujol et al. (2000) for largest ductility demand greatly overestimated the observed strengths. It seems that these equations are not valid for members with large shear reinforcement ratio.

Average transverse strains in the core concrete were measured using piano wires and displacement meters fixed to the ties. Figure 6 shows an example of deflection vs. average transverse strains relationships. Note that the strain started to increase significantly before strength degradation started. The strain at the center of the section was about 1.3 or 1.4 times of those near the sides. The strains of the ties were also measured using wire strain gages, which showed that they

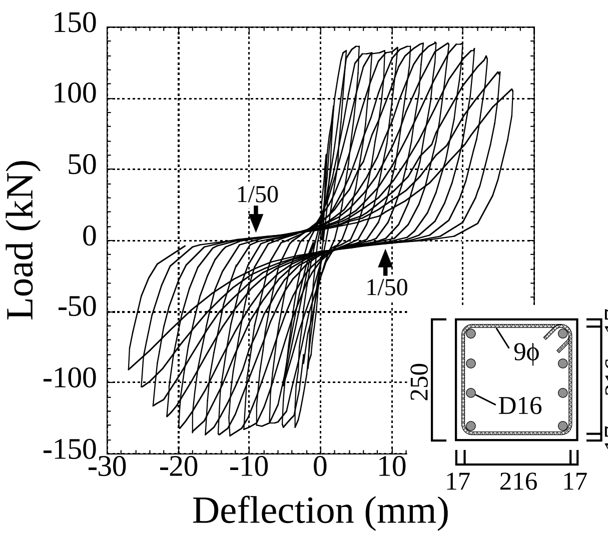

Fig. 5 Load-deflection relationship

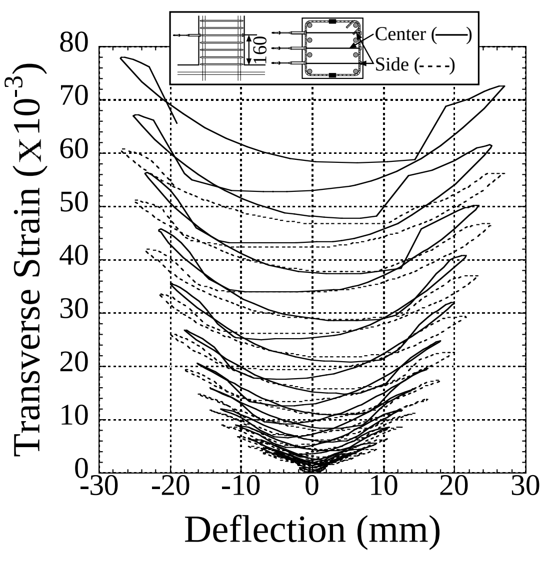

Fig. 6 Transverse strain of concrete

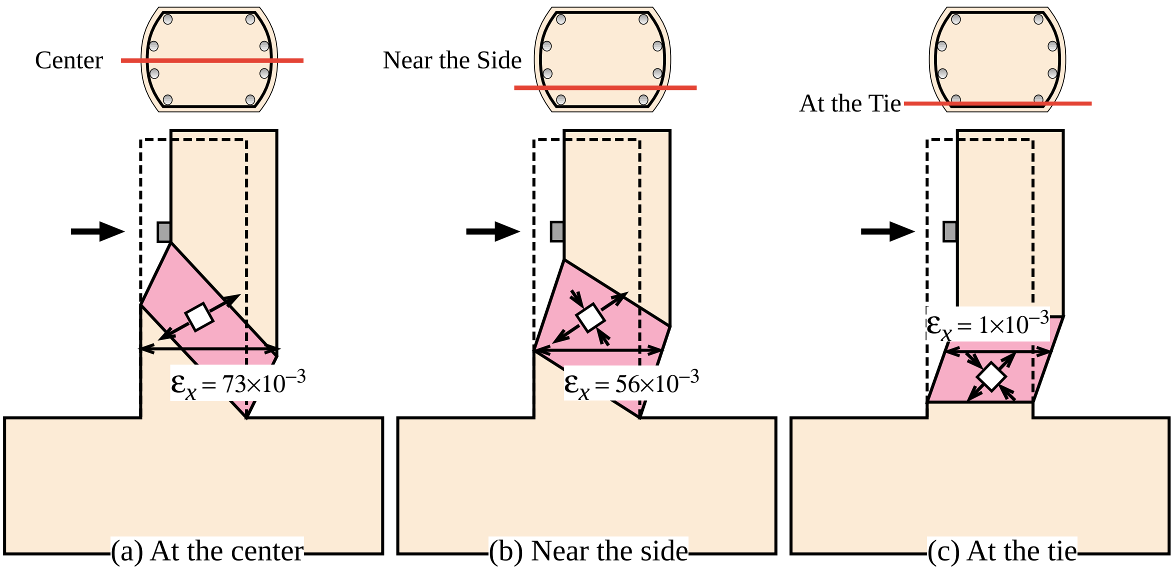

Fig. 7 Shear deformation at three sections

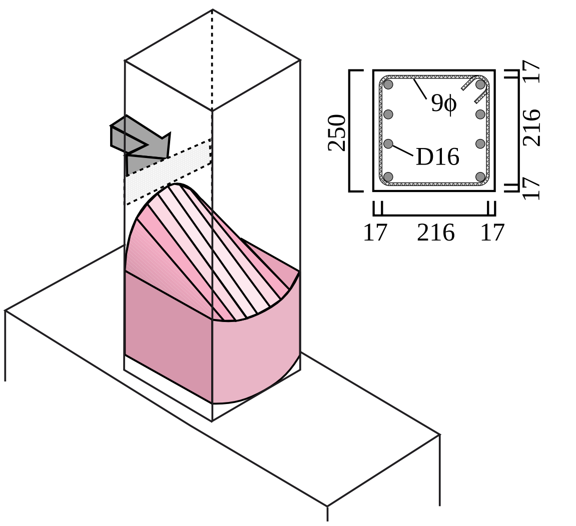

Fig. 8 Three-dimensionally shaped deformed zone of a specimen without cross ties

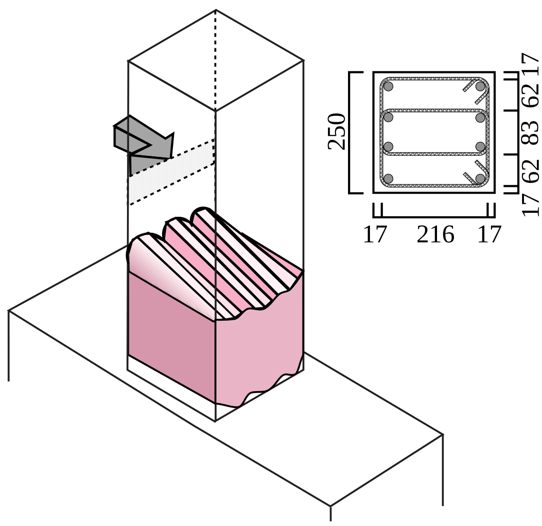

Fig. 10 Deformed zone of a specimen with cross ties

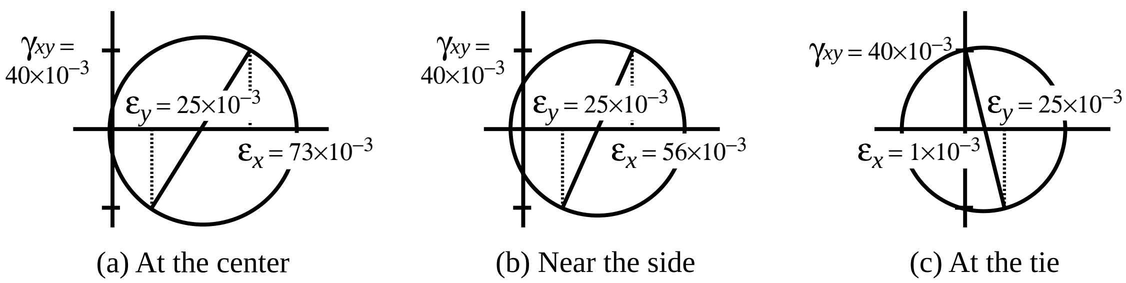

Fig. 9 Mohr's strain circles in deformed zone without cross ties

did not reach the yield strain; and after the strength degradation started, the strains of the ties decreased till 1.0 x 10^{-3}, which is 1/50 of the strain at the center of the section. Shear deformation and axial deformation are also measured using displacement meters.

The compatibility condition requires that the shear deformation should have occurred as shown in Fig. 7. This means that the deformed zone was three-dimensionally shaped as shown in Fig. 8. Assuming that the height of the deformed zone is equal to the depth of the core, one may obtain the Mohr's strain circles indicated in Fig. 9. Note that the principal compressive strain at the center (Fig. 9a) was smaller than that near the side (Fig. 9b) and was much smaller than that at the tie (Fig. 9c). This indicates that the inclined compressive stress at the center was much smaller than that at the tie; in other words, truss action was ineffective at the center. Ichinose et al. (2001) conducted similar measurement in a specimen with cross ties and found that the strain distribution was more uniform than in a specimen without them forming a deformed zone shown in Fig. 10.

5. AIJ DESIGN GUIDELINES (1999)

The foregoing discussions indicate that the compressive stress field should be like Fig. 11. The field is simplified as shown in Fig. 12. The minimum effective area at the center of hoop spacing, $A_{\min}$ in Fig. 12b, is given by the following equation:

$$A_{\min} = \left(1 - \frac{s}{2j_e} - \frac{b_s}{4j_e}\right) \cdot b_e j_e = \lambda \cdot b_e j_e \qquad (2)$$

where s and b_s are longitudinal and transverse spacing of hoops, respectively; and b_e and j_e are width and depth of core concrete (measured center-to-center of peripheral hoops), respectively;

Architectural Institute of Japan (1999) published design guidelines based on the inelastic displacement concept, which prescribe the upper limit of shear strength for members with large transverse reinforcement ratio considering ductility demand and detailing as follows:

$$V_u = \frac{\nu f'_c}{2} A_{\min} \tag{2}$$

where f'_c is compressive strength of concrete in MPa; ν is an effectiveness factor for concrete strength defined as shown in Fig. 13, and $A_{\min}$ is an effective area given by Eq. 2.

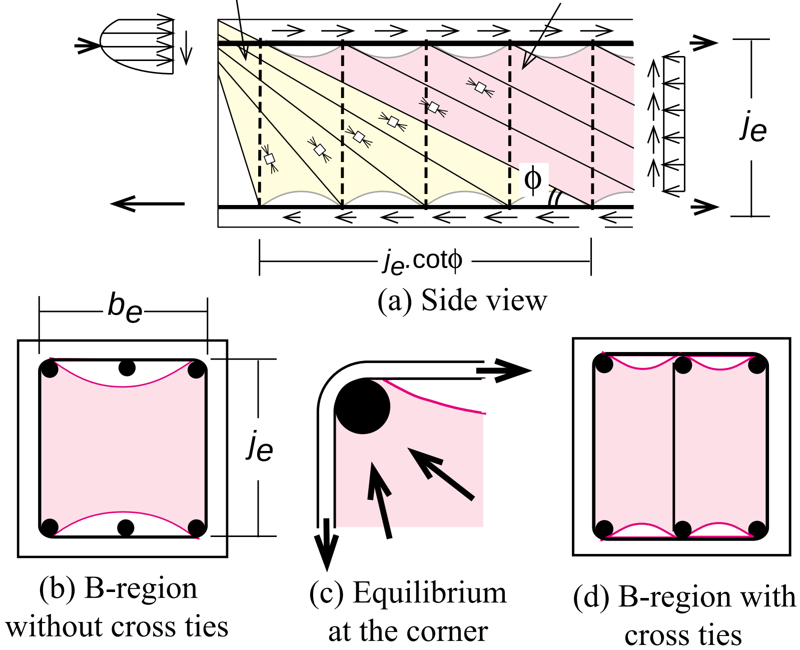

Fig. 11 Compressive stress field

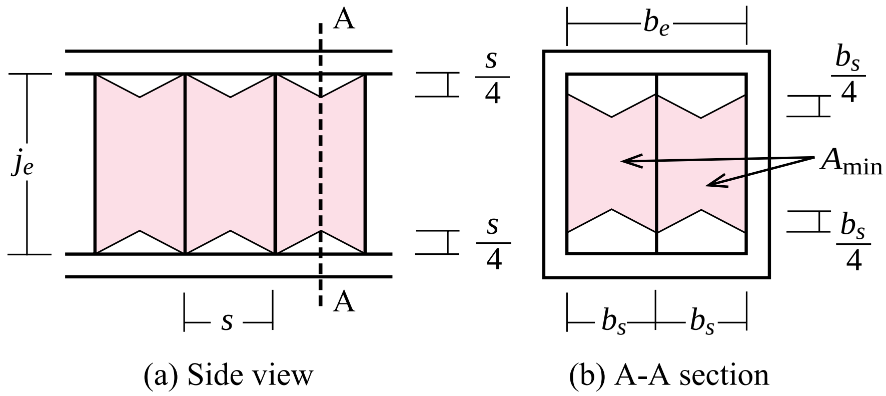

Fig. 12 Simplified stress field

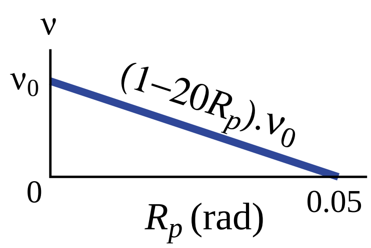

Fig. 13 Effectiveness factor

($\nu_0 = 3.68 f_c'^{-1/3}$ and R_p = rotation demand in hinge region.)

Figure 14 shows the comparison between the observed and predicted plastic deflection angles ($R_p = R_u - R_y$), where n_0 indicates the ratio of the axial force to the compressive strength of each specimen. The plotted data cover transverse reinforcement ratio = 0.1 to 2.0 %, shear span ratio = 1.0 to 3.0, and concrete strength = 15 to 80 MPa. The design equation gives conservative prediction. However, correlation is not good enough. For example, the effects of axial compressive stress on the core, which is reported important by Pujol et al. (2000), is neglected in the equation, and should be discussed in the future. The effects of loading excursion should also be carefully considered when comparing the observed and predicted deflection angles.

6. CONCLUSIONS

1) The method proposed by Pujol et al. (2000) assumes that the cohesion in Coulomb criterion decreases as ductility increases, and is effective for calculating transverse reinforcement. However, the applicability to members with large transverse reinforcement ratio is doubtful.
2) Experiments by Kinugasa et al. (1994) indicate that a threshold of deflection angle amplitude seems to exist for strength degradation irrespective of loading types.

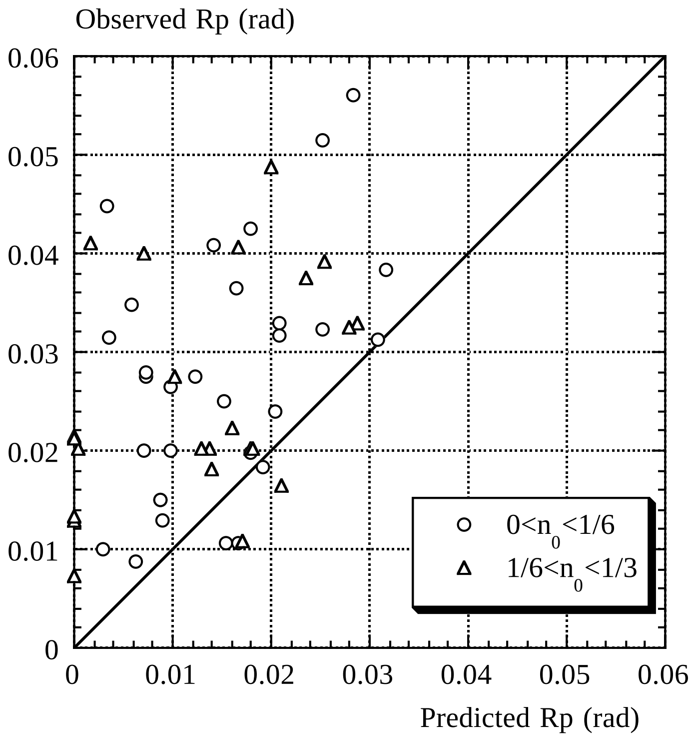

Fig. 14 Observed and predicted plastic deflection angle

3) Experiments by Ichinose et al. (1995 and 2001) indicate that hoop spacing both in longitudinal and transverse directions affects the shear strength and deformation pattern when transverse reinforcement ratio is large.

4) AIJ design guidelines (1999) prescribe the upper limit of shear strength for members with large transverse reinforcement ratio considering ductility demand and detailing. The guidelines give conservative prediction for ductility capacity.

Acknowledgements: Grateful thanks are due to Drs. Kinugasa and Sakata for providing digital data of Figs. 3 and 14.

REFERENCES

Architectural Institute of Japan (1999). *Design Guidelines for Earthquake Resistant Reinforced Concrete Buildings Based on Inelastic Displacement Concept*, Tokyo, Japan. (in Japanese)

Ichinose, T. (1992): “A shear design equation for ductile RC members,” *Earthquake Engineering and Structural Dynamics*, Vol. 21. 197-214.

Ichinose, T. and Hanya, K. (1995): “Three Dimensional Shear Failure of R/C Beams", *International Conference on Concrete under Severe Condition,* Vol. 2, 1737-1747

Ichinose, T., Imai, M., Okano, T., and Ohashi, K. (2001): “Three-Dimensional Shear Failure of RC Columns after Cyclic Loading,” *Modeling of Inelastic Behavior of RC Structures under Seismic Loads, Committee Report*, ASCE, 546-561

Kinugasa, H. and Nomura, S. (1994): ”Failure mechanism under reversed cyclic loading after flexural yielding,” *Concrete research and technology*, 5(2), 85-97, (in Japanese)

Priestley, M. J. N., and Benzoni, G. (1994): “Seismic shear strength of reinforced concrete columns,” *J. Struct. Engineering,* ASCE, 120 (8), 2310-2329

Pujol, S., Sozen, M., and Ramirez, J. (2000): “Transverse Reinforcement for Columns of RC Frames to Resist Earthquakes.” *Journal of Structural Engineering*, ASCE, 126 (4), 461-166

SESSION B-3: PERFORMANCE OF BEAM-COLUMN JOINTS AND FRAMES

Chaired by

♦ Marc Eberhard and Minehiro Nishiyama ♦

INFLUENCE OF JOINT SHEAR STRESS DEMAND AND DISPLACEMENT HISTORY ON THE SEISMIC PERFORMANCE OF BEAM-COLUMN JOINTS

S.G. WALKER, C.M. YEARGIN, D.E. LEHMAN, AND J.F. STANTON[1]

ABSTRACT

Beam-column joints in reinforced concrete frames subjected to earthquakes may be highly stressed in shear and susceptible to damage. This potential for damage is particularly high in older frames, which typically contain no transverse joint shear reinforcement, were not designed to limit the joint shear stress demand, and may have high beam bar bond demands. To evaluate the seismic response of older joints, seven reinforced concrete beam-column joints, representative of joints in frames constructed prior to 1970, were subjected to reversed lateral load. The test matrix was designed to study the influence of joint shear stress demand and displacement history. In the experimental phase of the program, two test series were performed on nominally identical specimens. The first series consisted of four specimens, with a target joint shear stress of $0.75\sqrt{f'_c}$ MPa ($9\sqrt{f'_c}$ psi), but subjected to different displacement histories. In the second series, three specimens with a target joint shear stress of $1.29\sqrt{f'_c}$ MPa ($15.5\sqrt{f'_c}$ psi) were subjected to displacement histories matching three of those used in the first series. During the testing the damage was monitored and local deformations were measured. The data were used to correlate engineering parameters with important joint damage states.

1 INTRODUCTION

In reinforced concrete moment frames subjected to seismic loading, the joints are stressed in shear. Even in modern buildings, in which the joints contain transverse reinforcement, the shear stresses are large enough that they often control the size of the column. However, in buildings constructed before the mid 1970s, the joints typically contained no reinforcement, and the buildings' behavior is more likely to be adversely affected by poor response of the joints. Despite this vulnerability of older frames, previous joint shear investigations have focused almost exclusively on developing reinforcing schemes for modern joints, and relatively little is known about unreinforced joints. This paucity of information causes difficulties for engineers faced with the problem of evaluating older buildings for possible retrofit.

The overall goal of the research described here was to investigate the response of joints typical of those found in older buildings. This was achieved by conducting laboratory experiments on beam-column joint sub-assemblages. In order to make the results useful in the context of Performance-Based Engineering (PBE), an effort was made during the

[1] *Department of Civil and Environmental Engineering, University of Washington, Seattle Washington, USA*
Email: delehman@u.washington.edu

experiments to correlate identifiable damage states, such as first spalling of the concrete, with engineering parameters, such as story drift. This was done because economic decisions about repair are usually made on the basis of damage, yet engineering predictions are commonly expressed in terms of parameters such as strain. To be useful for PBE, damage states and engineering parameters must be linked.

The joints in older frame structures display a wide range of characteristics (Mosier 2000), and not all could be studied here. For example, beams were often offset from the columns lines, bottom beam bars may have been spliced, or simply butted, within the column, and the joint shear stress varied widely, because the column frequently changed size over the height of the building. In this study, the beams and columns were the same width and were aligned with each other, and all the beam bars were continuous through the joints.

2 TEST MATRIX, SPECIMEN, MATERIALS, SETUP, AND PROCEDURE

Little experimental information is available on the response of unreinforced joints, so a test program was conducted to provide data. Of the many parameters that influence behavior,

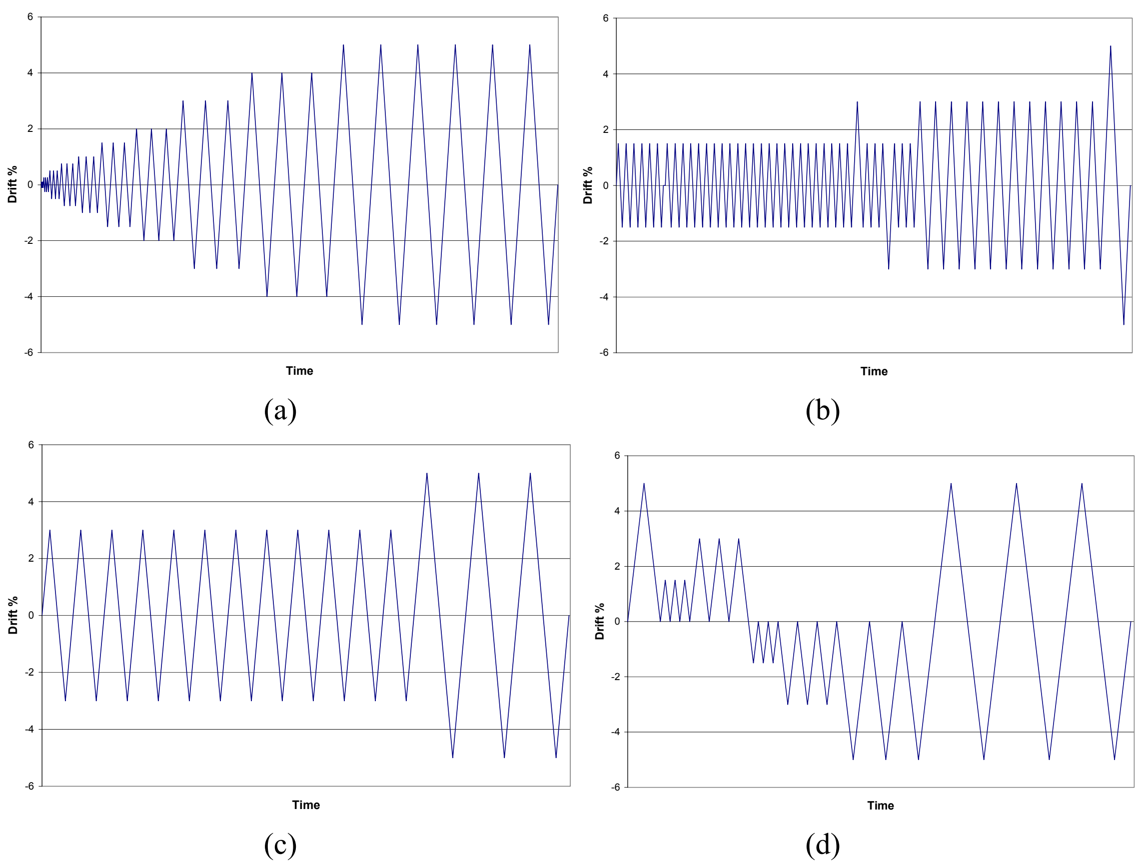

Figure 1 Displacement Histories: (a) PEER, (b) CD15, (c) CD30, (d) NFPD

Mosier (2000) had identified the joint shear stress demand and the displacement history as the most important. Thus, these parameters were varied in the tests, while others, such as the bond stress demand and column axial load, were kept as close to constant as possible. The test matrix of seven specimens is shown in Table 1. The specimen naming system consists of a four-letter name that describes the displacement history, and a two-digit extension that defines the target joint shear stress demand.

The four displacement histories (PEER, CD15, CD30 and PADH) are illustrated in Figures 1a-d. Each figure shows the drift as a function of the cycle number. The label PEER refers to the standard PEER Center displacement history, in which three cycles are applied at each of several increasingly large displacements. This history mimics those that have been used in many previous studies, and permits comparison with other work conducted by PEER. The CD15 and CD30 displacement histories consisted of many cycles at a **C**onstant **D**isplacement amplitude of +/-1.5% or 3.0% drift, with the goal of determining the effect of a long duration earthquake. The constant displacement cycles were followed by an asymmetric series of cycles intended to demonstrate the effect of loading in one direction on the strength in the other. The **P**ulse **A**symmetric **D**isplacement **H**istory (PADH) was intended to reflect the pulse characteristics of a near-fault ground motion. It was also useful for developing behavioral rules for analytical models, which require a monotonic envelope and information about response to asymmetric load cycles. Response to the PADH history proved to be a rich source of information.

Table 1 Test Matrix

Test Series	Specimen	Displacement History	Joint Shear Stress Mpa (psi)
14	PEER-14	PEER	$0.14f'_c$ or $0.75\ (9)\sqrt{f'_c}$
	CD15-14	CD15	$0.14f'_c$ or $0.75\ (9)\sqrt{f'_c}$
	CD30-14	CD30	$0.14f'_c$ or $0.75\ (9)\sqrt{f'_c}$
	NFPD-14	NFPD	$0.14f'_c$ or $0.75\ (9)\sqrt{f'_c}$
22	PEER-22	PEER	$0.22f'_c$ or $1.29(15.5)\sqrt{f'_c}$
	CD30-22	CD30	$0.22f'_c$ or $1.29(15.5)\sqrt{f'_c}$
	NFPD-22	NFPD	$0.22f'_c$ or $1.29(15.5)\sqrt{f'_c}$

The target joint shear levels of 0.14 and 0.22 f'_c corresponded to approximately 0.75 and 1.29 $\sqrt{f'_c}$ MPa (9 and 15.5 $\sqrt{f'_c}$ in psi). These values were selected because they correspond approximately to the average joint shear stresses found by Mosier (2000) in his study of existing buildings, constructed before 1967 and between 1967 and 1979 respectively. The higher value also corresponds approximately to the nominal strength attributed by ACI 318-99 to a Type II joint with standard reinforcement. Exact joint shear stresses were constrained by the availability of bar sizes and strengths.

The beam bars were selected so that the ratio of the column width to beam bar diameter, hc/db, was 20 in all cases, in order to limit the bond demand. The column/beam flexural strength ratio was kept between 1.5 and 1.8, and the column axial load was $0.1f'_cA_g$ (based on measured f'_c).

Figure 2 shows the geometry and reinforcement of a typical test specimen for each test series. The exterior dimensions of the specimens were determined based upon the dimensions selected from the existing construction study [Mosier 2000] using a scale factor of 2/3. The beam and column reinforcement depended on the joint shear factor, ratio of the column width to beam bar diameter, h_c/d_b and the moment strength ratio, $\sum M_c/\sum M_b$. The size of the beam reinforcement was dictated by the h_c/d_b ratio. The beam reinforcement was designed to reach the target joint shear factor at yield of the reinforcement. The column reinforcement was designed to meet the moment strength ratio, $\sum M_c/\sum M_b$.

Material samples were tested to determine concrete compressive and tensile strengths as well as steel stress-strain relationships. The concrete and longitudinal beam bar material properties are summarized in Table 2. The target f'_c was 35 MPa (5000 psi), f_y was assumed to be 462 MPa (67 ksi) and the clear cover was 38 mm (1.5"). A complete description of the testing methods and results can be found in (Walker 2001).

Table 2 Target and Actual Material Properties

Specimen	f_c' (psi) (Day of Test)	No. 7	
		f_y (ksi)	f_u (ksi)
Target	5,000	67	84
PEER -14	4,465	61	99
CD15-14	4,600	61	99
CD30-14	6,100	61	99
NFPD-14	6,200	61	99
PEER-22	5,533	75	126
CD30-22	5,570	69	111
NFPD-22	5,259	75	126

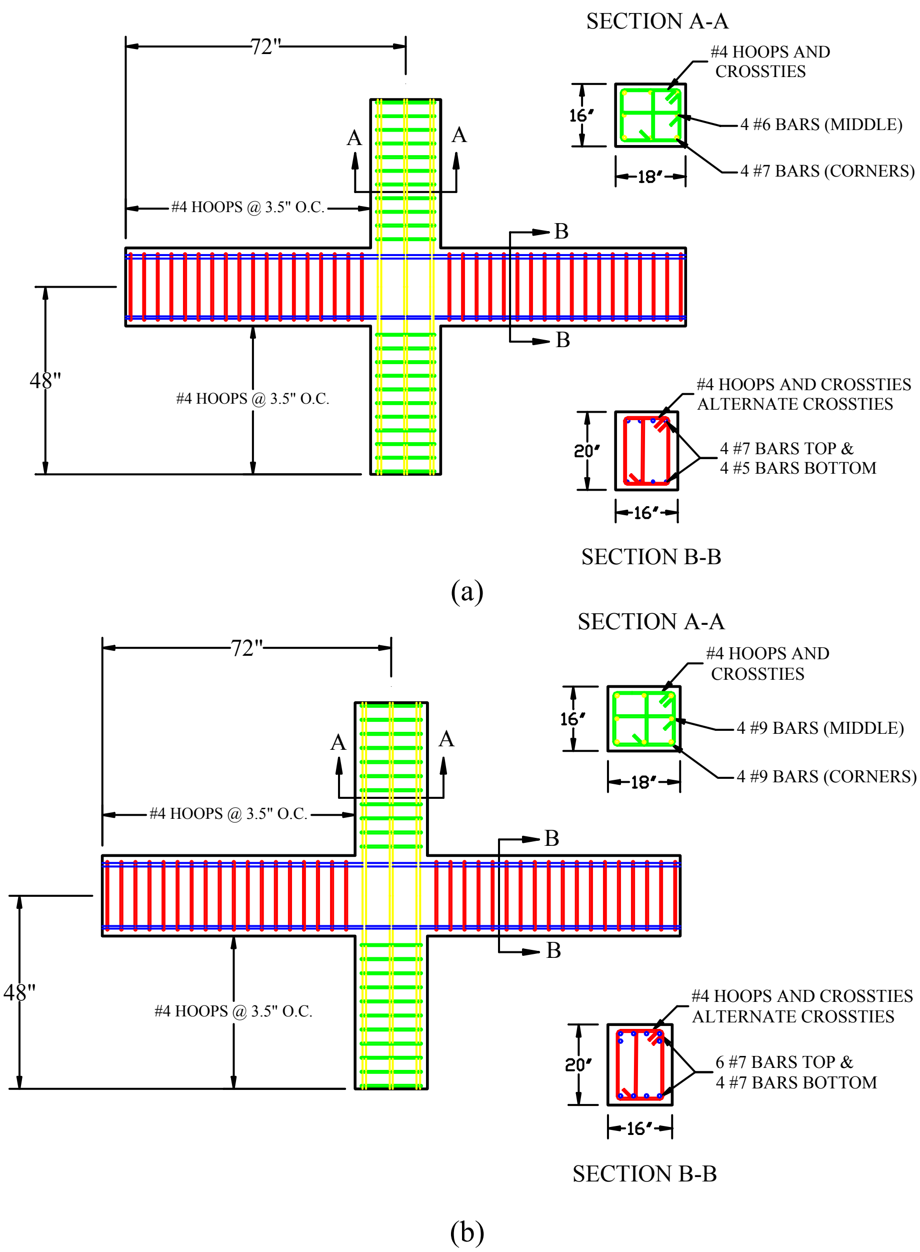

Figure 2 Geometry and Reinforcement for (a) Test Series 14 (b) Test Series 22

The specimens were instrumented to measure global loads and displacements, local deformation modes, and internal steel strains. Instrumented regions included the regions of the beams and columns that were expected to sustain damage and the joint region. Internal strain gauges were used to monitor axial strains on the beam and column longitudinal reinforcement. This measurement is important in the assessment of the bond stress distribution of the beam bars along the joint region. To minimize disruption to the joint deformation, and therefore the bonding characteristics of the bars, the strain gauges were placed in small grooves that had been made at the rib of the bar. Details of the instrumentation can be found in (Walker 2001).

Each specimen was subjected to a constant axial load and reversed cyclic lateral load. Figure 3 shows the test setup. The lateral load was applied to be beams using two 110 kip actuators by imposing equal displacements in opposite directions to each beam in a cyclic manner. The actuators were connected to the beams with four bolts through beam ducts placed during casting. The column was restrained laterally both in-plane and out-of plane. Both supports were bolted to the specimen through ducts placed during casting. The axial load was applied at the top of the column by stressing two post-tensioning rods that were placed on either side of the specimen. A steel crossbeam, which was seated in a spherical rocker bearing, transferred the axial load to the column.

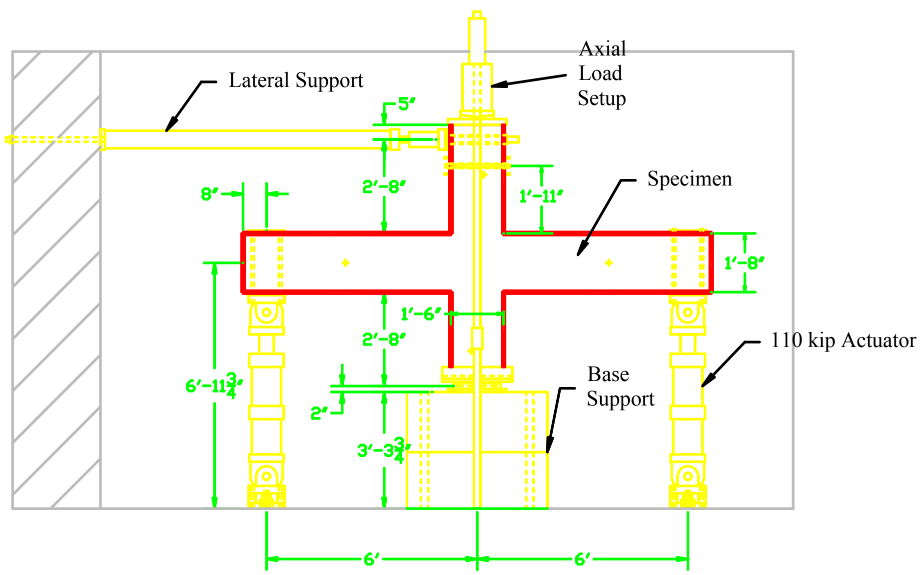

Figure 3 Test Setup

3 EXPERIMENTAL OBSERVATIONS

Component damage may be indicative of the level of seismic demand and required repair effort in performance-based seismic evaluation. During testing, the damage states were monitored for use in the development of such evaluation methodologies.

During testing of each specimen, the following damage states were noted: (1) onset of cracking, (2) measurable residual crack widths, (3) beam bar yielding, (4) spalling of the joint cover, and (5) degree of damage to the core joint concrete. In this section, these damage states are described and indicated on the force-displacement response histories for each specimen, where applicable (Figure 5). The influence of the study parameters, namely joint shear stress demand and displacement history, on the occurrence of each damage state and the force-drift response envelopes is also evaluated.

3.1 Cracking

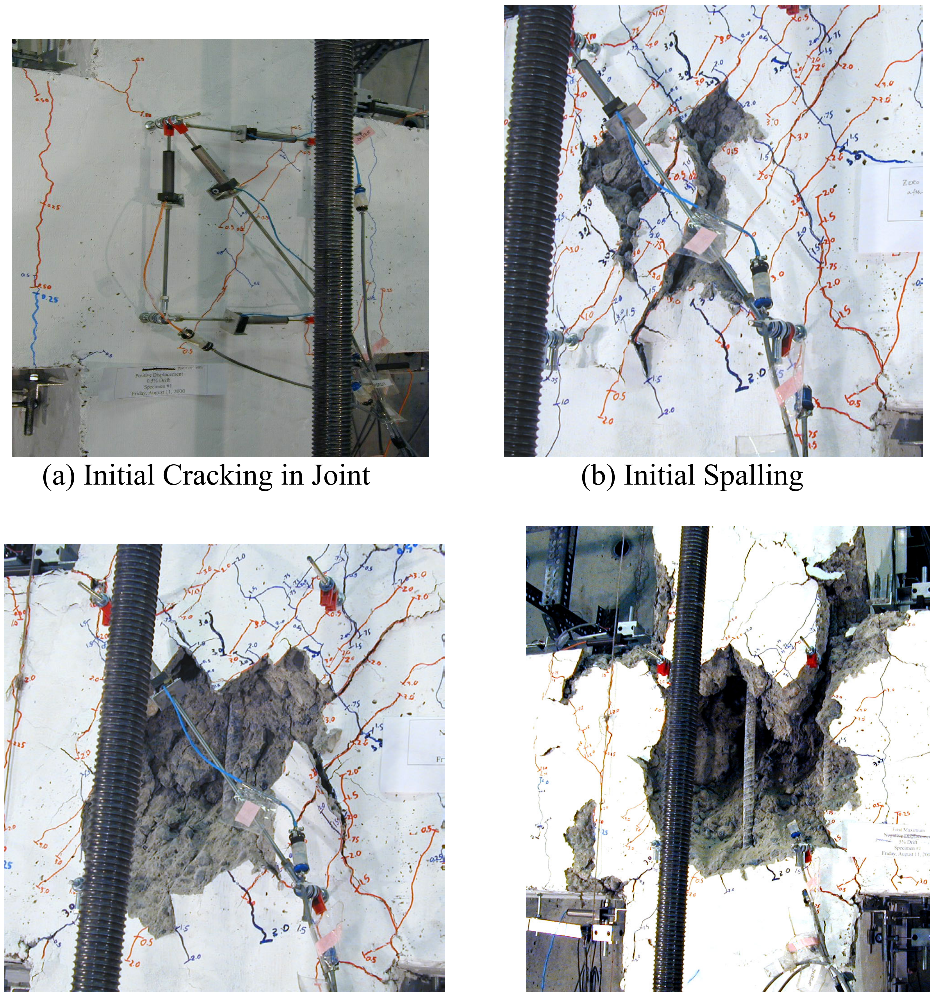

(a) Initial Cracking in Joint (b) Initial Spalling

(c) Exposure of Center Column Bar (d) End of Test

Figure 4 Important Damage Stages (Shown for Specimen PEER-14)

Joint cracks were marked and monitored during testing. The new cracks and crack extensions were marked and measured at the first positive and negative peaks of every three cycles. Residual crack widths were measured at the end of the three cycles.

Monitoring the progression of damage at the peaks prevented precise observation of initiation of joint cracking. Because only the PEER displacement history utilized small drift cycles, the PEER specimens offer the closest approximation to the actual onset of joint cracking. For Specimens PEER-14 and PEER-22, cracking was not noted during the 0.25% drift cycles but was noted after the application of the first positive cycle to 0.5% drift. The joint shear stresses corresponding to 0.5% drift for Specimens PEER-14 and PEER-22 were 2.9 MPa (420 psi) and 3.1 MPa (450 psi), respectively. When normalized with respect to the square root of the measured concrete strength, the values are $0.50\sqrt{f'_c}$ MPa ($6.2\sqrt{f'_c}$ psi) and $0.51\sqrt{f'_c}$ MPa ($6.0\sqrt{f'_c}$ psi), respectively.

Residual crack widths in the joint were not measurable until the 1.5% drift cycles for the PEER-14, CD15-14, and PEER-22 specimens. Since cover spalling occurred prior to the end of the first set of cycles, joint residual crack widths were not measured for the other specimens.

3.2 Yielding

Specimen yielding was measured using strain gauges that were attached to the longitudinal beam reinforcing bars. Yielding occurred at approximately 1.1% drift for the Series-14 specimens and 1.5% drift for the Series-22 specimens. Differences due to displacement history were not distinguishable.

3.3 Damage to Joint Cover Concrete

Damage to the cover concrete initiated at the center for the joint (Figure 4b). The number of cycles applied to cause cover spalling are summarized in Table 3. In the table, a full reversed cycle to the positive and negative peak drifts is given a value of 1; a cycle only to the positive or negative peak drift is given a value of 0.5.

Table 3 Number of Drift Cycles Applied to Cause Initial Cover Spalling

Specimen	0.1%	0.25%	0.50%	0.75%	1.0%	1.5%	2.0%	3.0%
PEER-14	3	3	3	3	3	3	3	0.5
CD15-14	3	-	-	-	-	10		
CD30-14	3	-	-	-	-	-	-	1
PEER-22	3	3	3	3	3	3	0.5	
CD30-22	3	-	-	-	-	-	-	0.5

To determine the influence of the joint shear stress on the occurrence of joint cover spalling, the PEER specimens were compared. Cover spalling occurred during the first positive 3% drift cycle for Specimen PEER-14 and occurred during the first positive cycle to 2% drift for Specimen PEER-22. The results indicate that a larger joint shear stress demand results in an earlier occurrence of cover spalling.

A similar analysis was made to evaluate the influence of displacement history on the occurrence of joint concrete spalling. Specimens PEER-14, CD15-14 and CD30-14 were compared. Spalling occurred at 3% drift in Specimen PEER-14 after 22 cycles and at 1.5% drift in Specimen CD15-14 after 13 cycles. However, both PEER-14 and CD30-14 spalled at 3% drift although they had a different number of cycles applied up to that point. These results indicate that spalling is a function of both the number of cycles and the displacement amplitude.

3.4 Damage to Joint Core Concrete

During testing it was not possible to observe damage to the joint core concrete directly. Since it was possible to evaluate exposure of the center column longitudinal bar for all specimens, this common damage state was recorded for all specimens and used to indicated that extent of damage to the core concrete. An example of this damage state is indicated in Figure 4c. The number of cycles at each drift level that were applied prior to exposure of the center column longitudinal bar are summarized in Table 4.

Table 4 Number of Drift Cycles Applied to Expose Center Column Longitudinal Bar

Specimen	0.1%	0.25%	0.50%	0.75%	1.0%	1.5%	2.0%	3.0%	4.0%	5.0%
PEER-14	3	3	3	3	3	3	3	3	0.5	
CD15-14	3	-	-	-	-	36	-	5.5		
CD30-14	3	-	-	-	-	-	-	6		
PADH-14	3	-	-	-	-	3	-	3	-	1.5
PEER-22	3	3	3	3	3	3	3	0.5		
CD30-22	3	-	-	-	-	-	-	3.5		
PADH-22	3	-	-	-	-	3	-	3	-	1

To establish the influence of the joint shear stress demand on the joint damage, Specimens PEER-14 and PEER-22 were compared. Exposure of the center column longitudinal bar was observed during the 4%-drift cycles for Specimen PEER-14 and the 3%-drift cycles for Specimen PEER-22. The results indicate that the deformation at which joint core concrete damage is occurs is influenced by the joint shear stress demand.

By comparing specimens with similar levels of joint shear demand but similar displacement histories, the influence of displacement history on joint damage was assessed. The center longitudinal column bar of Specimen PEER-14 was exposed after application of the displacement history to the first cycle to 4% drift. The same damage state was observed in

Specimen CD30-14 after 6.5 cycles to 3% drift. Comparison of the two specimens indicates that joint concrete damage is influenced by both the number of cycles and drift amplitude.

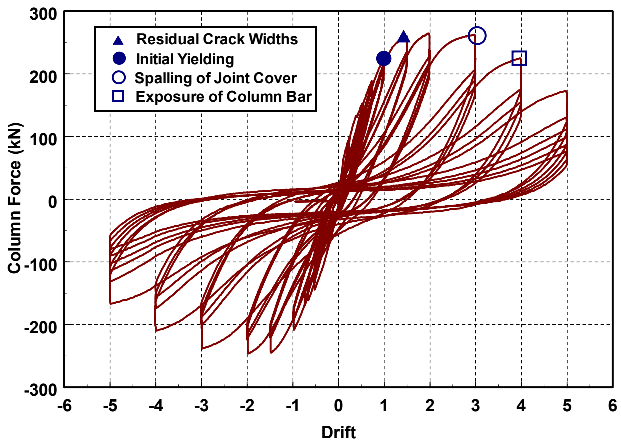

(a) Specimen PEER-14

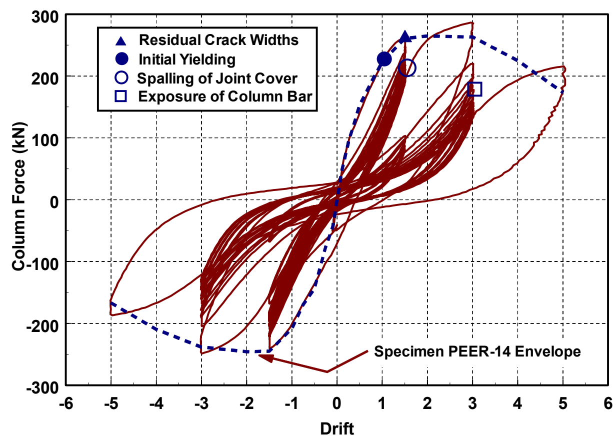

(b) Specimen CD15-14

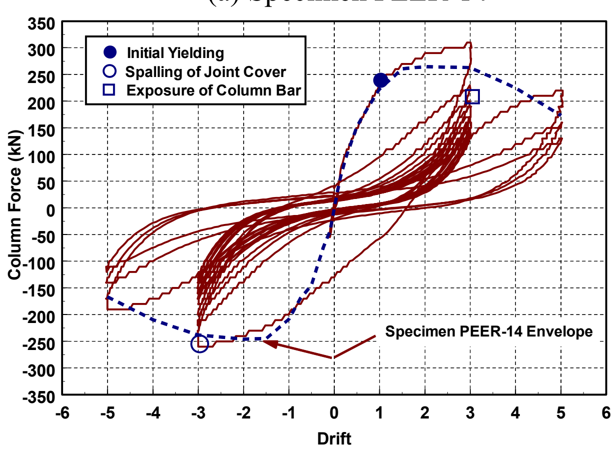

(c) Specimen CD30-14

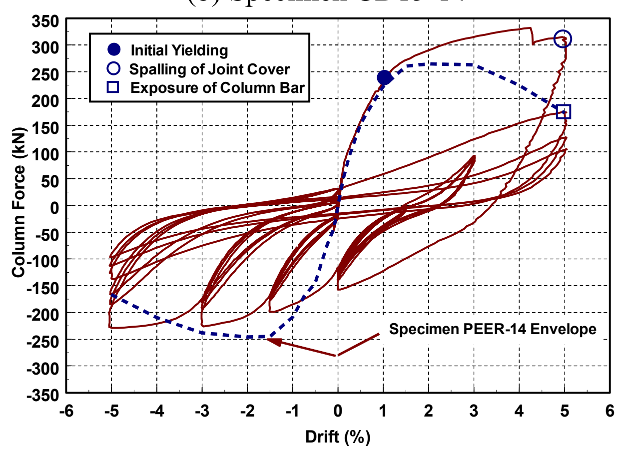

(d) Specimen PADH-14

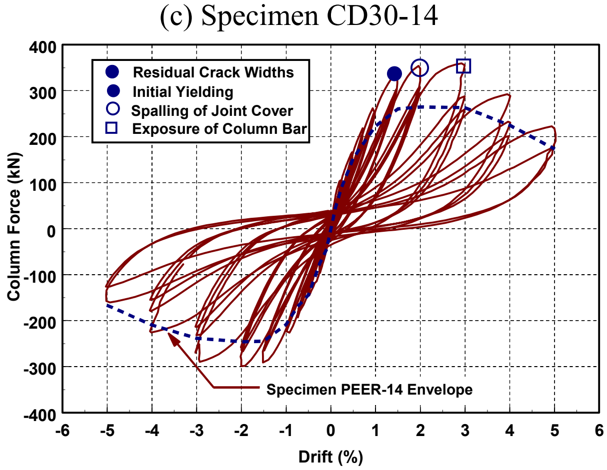

(e) Specimen PEER-22

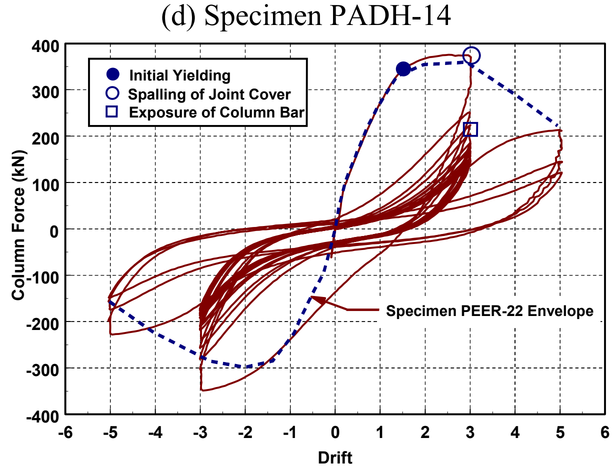

(f) Specimen CD30-22

Figure 5 Force-Drift Response of Specimens

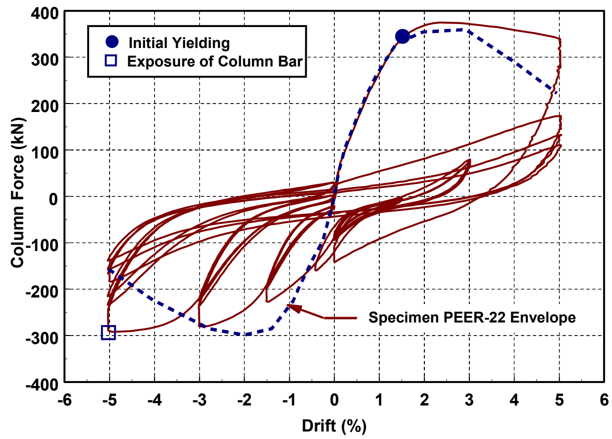

(g) Specimen PADH22

Figure 5 Force-Drift Response of Specimens (cont'd)

3.5 Significant Reduction in Lateral Load Carrying Capacity

Testing continued until the specimen exhibited at least a 20% loss of lateral strength of the force-drift envelope from peak strength. Most specimens were tested significantly past this state. Figure 5d shows the damage state at the end of testing. Significant damage to the joint concrete is evident. All of the column longitudinal bars are exposed. In many cases, the beam bars were exposed as well. At the end of testing, buckling of the column longitudinal bars was observed. In all cases the specimens maintained their column axial load.

4 FORCE-DRIFT RESPONSE ENVELOPES

The force-drift response envelopes were studied to determine the influence of the study parameters on the force-drift response. The envelopes were normalized with respect to the column shear force, V_y, and the specimen drift corresponding to initial yielding of the beams. In general, the envelopes correspond to the response for the first positive cycle at each drift level. However, the envelopes for the PADH specimens correspond to the first cycle to 5% drift. These envelopes provide monotonic response curves for each test series.

To evaluate the effects of the displacement history on the response, the normalized response envelopes for each test series were studied (Figures 6a and 6b). The response envelopes of the Test Series-14 specimens are similar at displacement ductilities less than or equal to 1.5. The response envelopes of the Test Series-22 specimens are similar at displacement ductilities less than or equal to 2. At larger displacement ductilites, the response envelopes differ. Differences in the behavior of the specimens are most notable between the monotonic curve, provided by the PADH specimen, and the other curves. The results indicate that although the response envelopes depend on the cyclic displacement history they more strongly depend on if the application of drift is monotonic or cyclic.

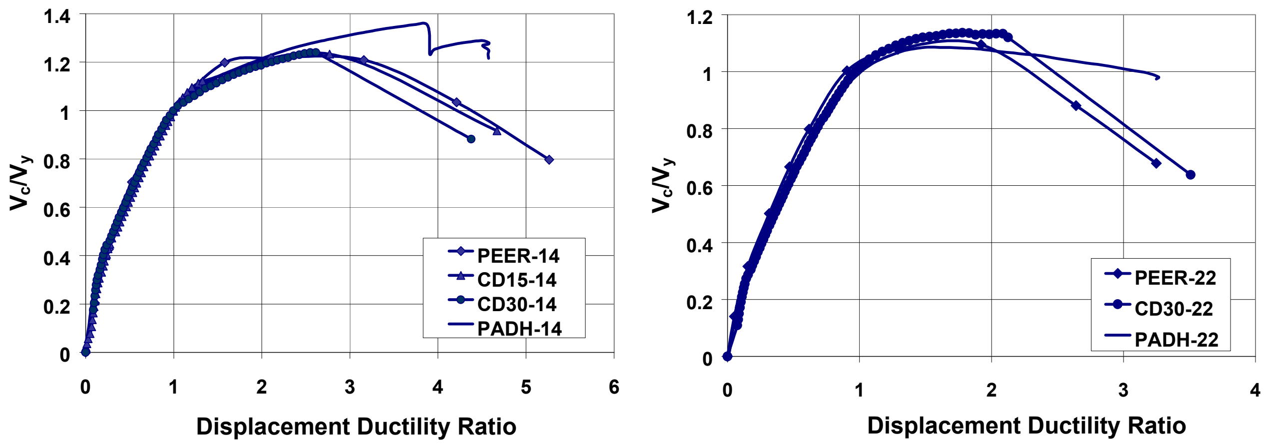

Figure 6 Normalized Response Envelopes for (a) Test Series 14 and (b) Test Series 22

The differences in the response envelopes that result from the joint shear stress demands are shown in Figure 7 for the PADH specimens. The results for the CD30 specimens and the PEER specimens were similar and are described in (Walker 2001). An increase in the joint shear stress demand results in a decrease in the normalized column shear force (likely due to limited strain hardening in the beams) and a smaller displacement ductility.

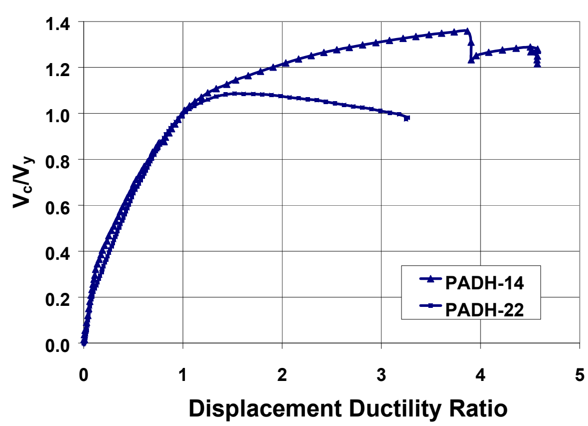

Figure 7 Normalized Response Envelopes for PADH Specimens

5 CONCLUSIONS

An experimental research program was developed to determine the influence of joint shear stress demand and displacement history on beam-column joints without transverse reinforcement. Seven joints were tested in two test series. Each test series studied a single level of joint shear stress. Joint shear stresses of approximately $9\sqrt{f'_c}$ and $15\sqrt{f'_c}$ (psi) were used. Within each test series, nominally identical specimens were subjected to different displacement histories.

The test results were used to evaluate the influence of the test parameters on the occurrence of important damage states and the force-displacement response. The following summarizes some of the important preliminary findings:

1. The joint shear stress demand influences joint damage. In particular, a higher joint shear stress leads to more significant damage for a given displacement history.

2. The cyclic deformation history influences the joint damage and response. Full, symmetric cycles were found to be more damaging than asymmetric half cycles. For the specimens tested, cycling at or below 1.5% drift did not result in significant damage or have a significant influence on the peak lateral strength. Cycling at or above 3% drift resulted in significant damage.

3. The axial load of the specimens ($0.1f'_cA_g$) was sustained regardless of the joint shear stress demand or displacement history.

The research results from this work will help engineers to evaluate reinforced concrete frame buildings for seismic retrofit. At present, the only guidelines for joint behavior are those for new construction, but these are inappropriate because they were developed for joints with transverse reinforcement. Because joint-by-joint retrofit is generally expensive, engineers tend also to investigate global solutions, such as introducing a shear wall to limit the lateral drift demand. However, even if the wall carries the lateral load, the frame joints must still accommodate the necessary deformations without losing their capacity to carry vertical load. The test results with a displacement history that consisted of many cycles of moderate drift provide some guidance to the designer in this issue.

6 ACKNOWLEDGEMENTS

The research was supported primarily by the Pacific Earthquake Engineering Research Center, a program of the National Science Foundation, under Award Number EEC-9701568. The authors would like to acknowledge the work of Greg Mosier, whose research served as the basis for this experimental research project. The help of numerous students and the laboratory staff at the University of Washington is also acknowledged.

7 CITED REFERENCES

Mosier G. (2000) Seismic Assessment of Reinforced Concrete Beam-Column Joints, Master of Science Thesis, Department of Civil Engineering, University of Washington, December 2000.

Walker S. (2001) Seismic Performance of Existing Reinforced Concrete Beam-Column Joints, Master of Science Thesis, Department of Civil Engineering, University of Washington, June 2001.

SEISMIC EVALUATION OF SUBASSEMBLAGES CONSISTING OF EXTERIOR COLUMN AND HALFSPAN BEAMS IN LOWER PART OF RC HIGH-RISE BUILDING

Masaru TERAOKA[1], Yoshikazu KANOH[2], Kazuya HAYASHI[3] and Naoki TAKAMORI[4]

ABSTRACT

One-fourth scale RC subassemblages consisting of 3-story exterior column and halfspan beams, representing the lower part of a 30-story building, were tested to investigate seismic behavior, and the information useful for seismic design was obtained. The column was subjected to high fluctuating axial force inducing significant P-Δ effect but the subassemblages exhibited sufficient seismic resistance. It is concluded that the P-Δ effect and the movement of inflectional points of the columns must be taken into account in high-rise building design while they are neglected in the conventional design.

1. INTRODUCTION

The lower part of exterior columns in high-rise building frames are subjected to high fluctuating axial force due to overturning moment during earthquake. In the exterior columns of RC frames, the non-linear characteristics including stiffness, cracking resistance capacities and yield capacities are significantly changing under the interaction of fluctuating axial force, bending moment and shear force. Addressing these subjects, non-linear analysis considering the effect of fluctuating axial force on RC frame (Isozaki et al. 1987) and experimental study on exterior beam-column joints under tensile force on column (Kaku et al. 1989) have already been reported. But the problem has not been adequately clarified, because sufficient data for non-linear behavior of column subjected to fluctuating axial force has not been provided in the former study and the experimental data is few in the latter study. Therefore in this study, focusing on the behavior of the exterior columns mentioned above, experiment on subassemblages consisting of 3-story exterior column and halfspan beams which represent the lower part of 30-story RC building, was conducted to investigate the seismic behavior and to obtain the information useful for seismic design. The results of the study have been partially reported (Teraoka et al. 1993).

[1] *Technology Development Division, Fujita Corporation, Kanagawa, Japan, E-mail: teraoka@fujita.co.jp*
[2] *Professor emeritus, Meiji University*
[3] *Technology Development Division, Fujita Corporation, Kanagawa, Japan, E-mail: kahayashi@fujita.co.jp*
[4] *Technology Development Division, Fujita Corporation, Kanagawa, Japan, E-mail: takamori@fujita.co.jp*

Six one-fourth scale subassemblages consisting of 3-story exterior column and halfspan beams, were constructed and tested under lateral load reversals with fluctuating axial compression and tension load on the column. The cross sectional properties and overall geometry are presented in Table 1 and Fig. 1. The main parameters considered in the test were (a) the range of the maximum and the minimum axial load on the column part (b) the amount of beam main rebars, (c) the anchorage method of beam main rebars in a exterior

Table 1 Cross sectional properties of test subassemblages

Test Structures	σ_0	Beam $b_b \times D_b$	Beam Main Rebars*	Beam Anchorage Method	Beam Stirrup	Column $b_c \times D_c$	Column Main Rebars	Column Hoop
EF-1	+0.65F_c ~ −0.15F_c	160 x 200	2-D10 / 2-D13	L Type+Rein.	Ⅲ-5φ @60	200 x 200	12-D10 + 4-D13 Core Rebars	◘-5φ @55
EF-2				U Type				
EF-3				L Type+Rein.				(EF-3,6 1F HZ ◘-D6 @55)
EF-4			4-D13		(EF-4 Ⅲ-5φ @45)			
EF-5	+0.5F_c ~ −0.035F_c		2-D10 / 2-D13					
EF-6								

Notes: σ_0=Axial Load Level at 4th Floor Column=$N/(b_cD_c)$; *Top/Bottom Rebars; Rein.=Reinforcing; HZ=Hinge Zone; Refer Table 2 Regarding Stirrup and Hoop Design; Dimensions are in mm

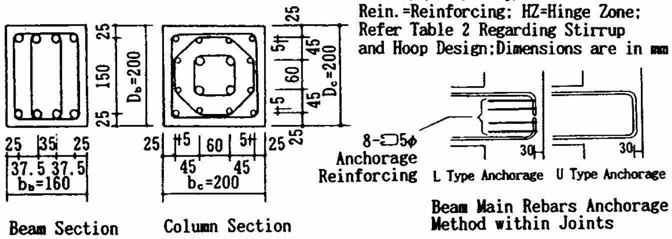

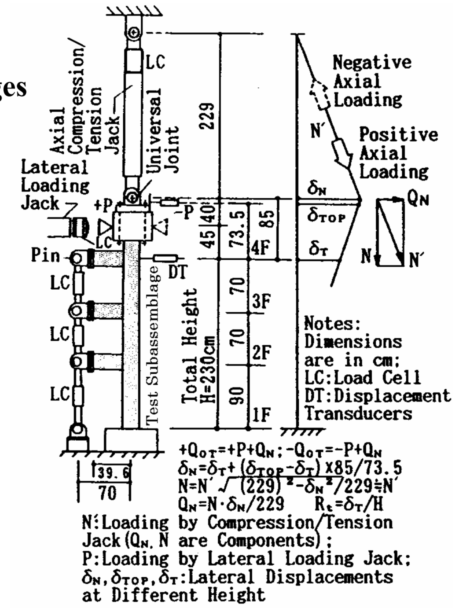

Fig. 1 Test subassemblage with loading system

Table 2 Design criteria of members

During Positive Loading (Assumed beam sideway mechanism)	During Negative Loading* (Assumed story mechanism)

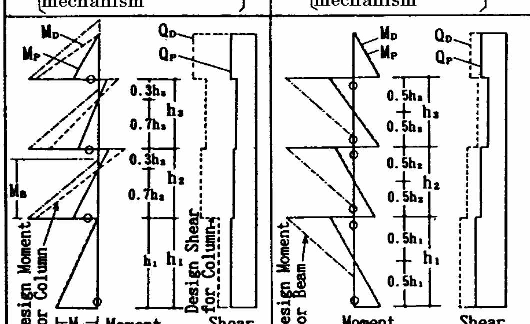

		Multiplication Factors A, B
During Positive Loading	Bending (A)	1.0 (1F), 2.5 (2~4F)
During Positive Loading	Shear (B)	1.5 (1F), 2.5 (2~4F)
During Negative Loading	Bending (A)	1.0 (1F), 1.0 (2~4F)
During Negative Loading	Shear (B)	1.5 (1F), 1.4 (2~4F)

M_c, M_B: Column, Beam Flexural Capacity According to AIJ
——: Bending Moment M_P and Shear Force Q_P at Plastic Hinge Mechanism
– – –: Bending Moment $M_D=A\cdot M_P$ and Shear Force $Q_D=B\cdot Q_P$ Used in Design [A, B: Multiplication Factors Presented at Right Side]
*When Beam Flexural Capacity is higher than Column Yield Moment Capacity, then Moments are Distributed According to Stiffness in Column
Note: Stirrup and Hoop are Designed Based on Ohno-Arakawa-Shibata's Equation

Table 3 Mechanical properties of materials

Reinforcement: Re-bar	Area (cm^2)	σ_y (t/cm^2)	σ_u (t/cm^2)	E_s (t/cm^2)	e (%)
D13	1.27	4.91	6.69	2086	16.2
D10	0.71	3.46	5.03	1886	20.5
D6	0.32	3.18	4.39	1596	29.3
5φ	0.20	2.94	4.69	2085	35.9

Concrete: σ_B (kg/cm^2)	ε_B (%)	E_c (t/cm^2)	σ_t (kg/cm^2)
458	0.27	322	40.5

Notes: Max. Coarse Aggr. Size 10 mm

Table 4 Program of loading

R_t (10^{-3})	Cycles
2.5	±3
5.0	±3
10.0	±3
20.0	±3
30.0	±2
50.0	±1

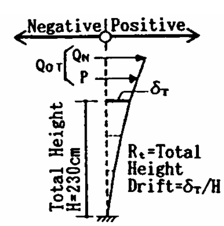

beam-column joint, and (d) the amount of transverse reinforcement in the bottom region (plastic hinge zone) of the 1st floor column.

The test subassemblages were designed according to the assumed collapse mechanism and multiplication factors presented in Table 2. The mechanical properties of materials are listed in Table 3. The mold for the test subassemblages was placed flat on the ground laying column part in the horizontal plane. Concrete was cast monolithically from the same batch. The axial and lateral loading systems and the principal instrumentation are presented in Fig. 1. The relationship between the fluctuating axial load (N) applied to the column and the lateral load (Q_{ot}) at top level are presented in Fig. 2. The program of lateral loading is presented in Table 4.

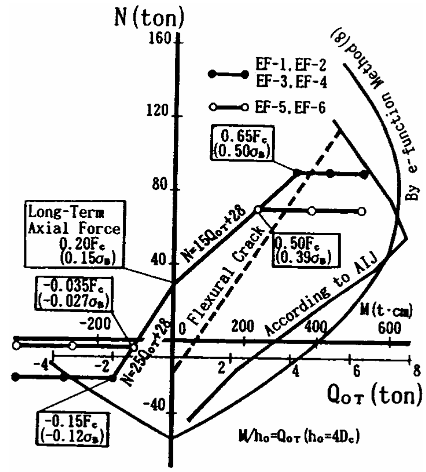

Fig. 2 Axial load (N) – lateral load (Q_{ot}) relationship

3. TEST RESULTS

The hysteretic relationship between Q_{ot} and total height drift angle R_t (top displacement/total height of the test subassembly) is presented in Fig. 3. The crack patterns at R_t=1/100 rad. and at the end of test are presented in Fig. 4. It can be seen from Fig. 3 that during positive loading (see Fig. 1 and Table 4), after attainment of maximum lateral load carrying capacities, all the hysteresis loops showed significant slip and unstable behavior. This is due to the P-Δ effect and compression failure progressed at the lower end of the columns. On the other hand, under negative loading (see Fig. 1 and Table 4) all the test subassembly showed stable response with increasing resistance until the end of test.

During positive loading, the maximum lateral load was attained at Rt=1/100~2/100 rad. After that, the rapid decrease in resistance in the case of EF-1~EF-4, subjected to high axial loading, was notable in comparison with EF-5 and EF-6 subjected to low axial loading.

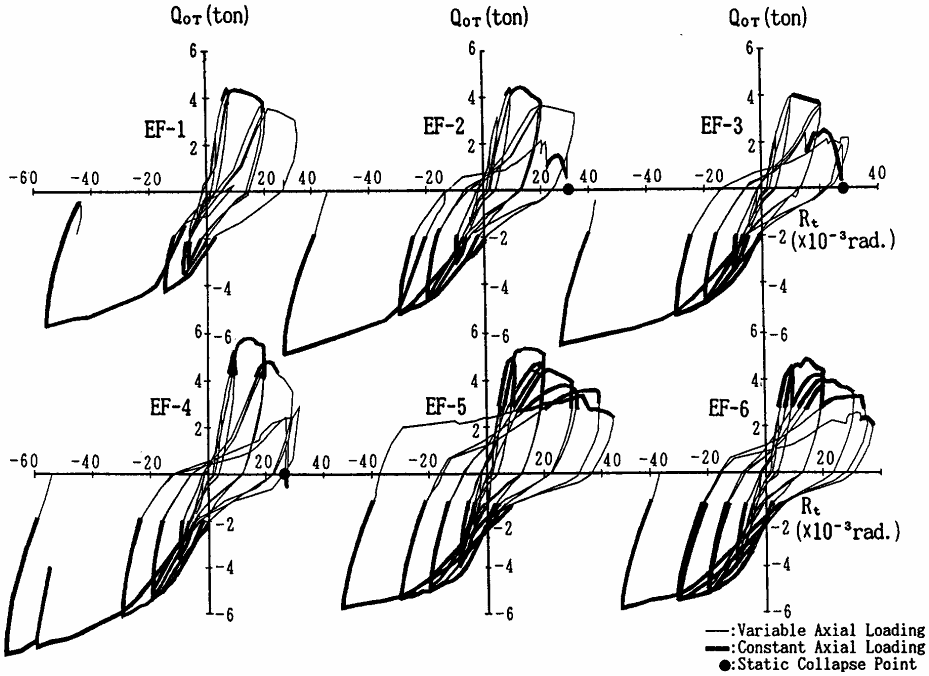

Fig. 3 Lateral load (Q_{ot}) - total height drift angle (R_t) relationship

EF-1~EF-4 sustained constant axial load of 91 tons due to the formation of sideway mechanism and exhibited stable hysteresis response until R_t=2/100 rad., but after that compression failure was observed at the lower end of each story column due to the repeated reversal loadings. Finally, compression failure progressed at the bottom end of the 3rd story columns due to the growth of bow-shaped overall deflection mode (Uetani and Tagawa 1993, 1997) . Consequently, the resistance of frames decreased rapidly and they approached the static collapse point (the point where lateral load becomes zero due to post-bifurcation behavior effect and decrease of resistance) at R_t ≒ 3/100 rad. EF-5 and EF-6 sustained constant axial load of 70 tons due to the formation of beam sideway mechanism and exhibited stable hysteresis response until the end of the test (R_t ≒ 4/100 rad.), when the lower end of the 1st floor column of EF-5, and the lower end of 1st and 3rd story columns of EF-6 showed notable compression failure.

The amount of transverse reinforcement at the lower end of the 1st floor column of EF-3 and EF-6 were larger in comparison to EF-1 and EF-5, but EF-3 and EF-6 showed slightly lower resistance during positive loading and slightly higher resistance during negative loading in comparison with EF-3 and EF-6. Final collapse mechanisms of EF-5 and EF-6 differed each other slightly.

EF-4 provided with higher amount of beam main rebars exhibited higher resistance in comparison with the other test subassemblages. EF-1 and EF-2 differed each other in anchorage method of beam main rebars within joints, but their Q_{ot}-R_t relationship and collapse mechanism were almost the same. In addition, all joint panels of test subassemblages did not collapse until the end of the test.

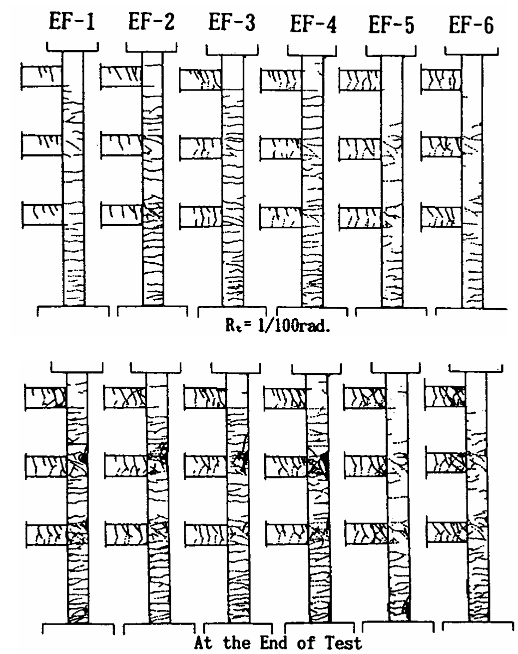

Fig. 4 Crack patterns

In the design of RC high-rise building frames based on the Japanese conventional methods, the maximum interstory drifts are normally limited to 1/100rad for the severe earthquake. Test results of Q_{ot}-R_t relationships showed stable hysteresis even at 2/100 rad. range, which indicated that the designated high-rise building possessed sufficient seismic resistance.

4. ANALYSIS

The analytical model used in this study is shown in Fig. 5. One-dimensional finite element method (FEM, stiffness method) and limit analysis were used for the prediction of response behavior. In the FEM, elastic stiffness of members were estimated by incremental equations which include elastic stability functions and bowing functions and tangential stiffness of members were estimated by incremental equations which were derived by using plastic flow rule and Ziegler's modification of Prager's kinematic hardening rule (Inoue and Ogawa 1974). The limit analysis was carried out considering the influence of P-Δ effects and assuming the weak beam-strong column mechanism.

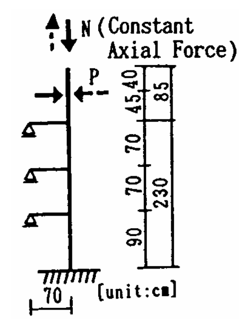

Fig. 5 Analytical model

In the FEM, after applying maximum compressive or tensile axial loading to the column, lateral displacement at top level was imposed. In Fig. 6, the stiffness and strength of constituent members used for FEM are presented. The moment-rotation (M-θ) relationship of beams was assumed by using the elastic stiffness, stiffness degradation ratio (α_y) at yield point proposed by Sugano (1973), and flexural strength of beam calculated by approximate equation in AIJ 1988. The moment-rotation (M-θ) and axial load-axial strain (N-ε) relationships of columns were assumed by using the secant stiffness at yield point (Isozaki et al. 1987) and the ultimate flexural strength (Kanoh et al. 1985). In the limit analysis, the same values for flexural capacity of members used in the FEM were used and it was verified that the assumed collapse mechanism totally coincided with analytical results.

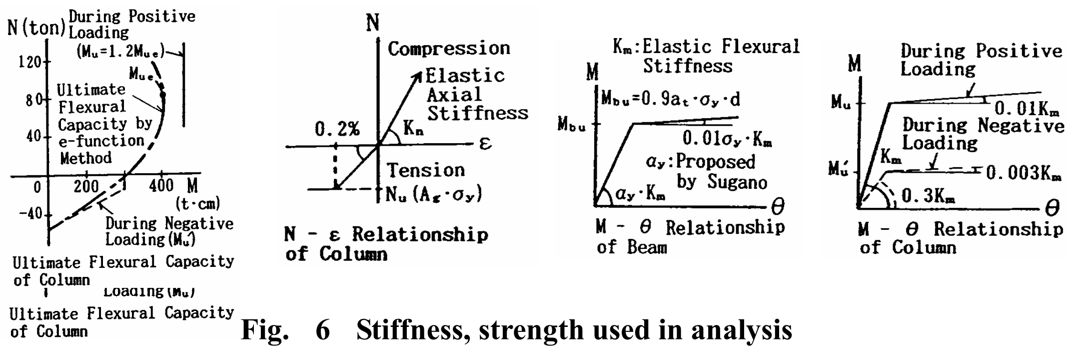

Fig. 6 Stiffness, strength used in analysis

5. BEHAVIOR OF SUBASSEMBLAGES

5. 1 Envelope curves of Q_{ot}-R_t

The measured and calculated envelope curves of Q_{ot}-R_t relations are compared in Fig. 7. The results obtained from the FEM analysis approximately agreed with the tested structural response curves at initial stiffness during positive and negative loading, the decrease in lateral resistance due to P-Δ effect during positive loading, the increase in lateral resistance due to strain-hardening in the main rebars and P-Δ effect during negative loading. The values obtained by limit analysis approximately agreed with the measured envelope curves after the collapse mechanism was formed. During positive loading, the EF-1~EF-4 experienced progressive collapse resulting in a rapid decrease in resistance in the region of R_t>2/100 rad. and showed disagreement with the results obtained by the both analytical methods, because the both analytical methods did not take account of the post-bifurcation behavior.

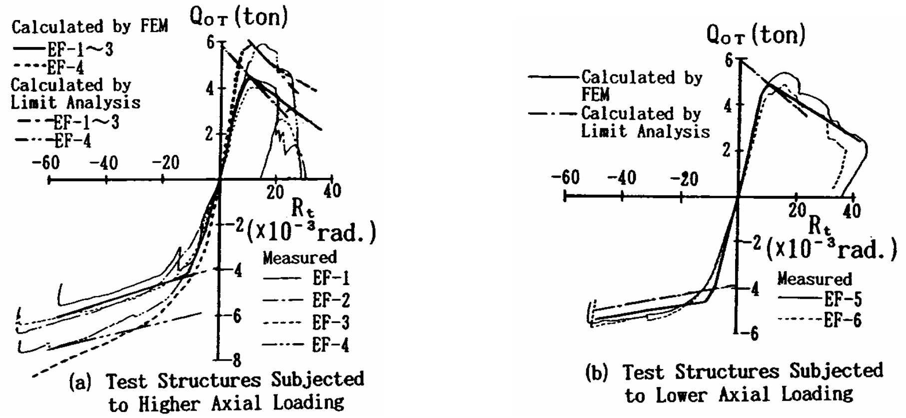

Fig. 7 Comparison of $Q_{ot} - R_t$ envelope curves

5. 2 Overall horizontal deflection shapes of subassemblages

Typical examples of overall horizontal deflection shapes of frames up to R_t=2/100 rad. are presented in Fig. 8(a). During positive loading, all test subassemblages exhibited the deflection shape as of a cantilever beam type, because column stiffness became relatively higher than beam stiffness, while during negative loading they exhibited the deflection shape as of a bending resisting frame type because column stiffness became relatively lower than beam stiffness. Those deflection shapes were remarked in the case of test subassemblages subjected to higher fluctuating axial loading. Those deflection shape characteristics would not appear in multi-span frames due to the interaction of external and internal columns.

The measured and calculated deflections over the height of the subassemblage agree reasonably well at R_t=1/100 rad. , but not so well at R_t=2/100 rad. as shown in Fig. 8 (b). This may be indicating that the assumption made in the analysis regarding the stiffness degradation of members was not adequate. Also, it may be due to that the degradation in the rotational characteristics of plastic hinges was not considered as mentioned in Fig. 6.

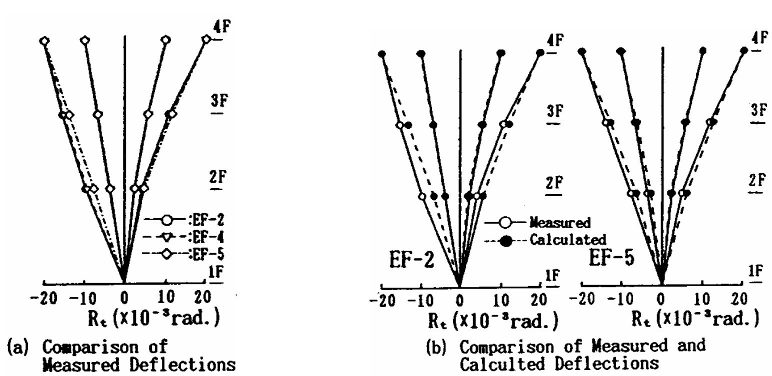

Fig. 8 Overall horizontal deflection shapes of subassemblages

5. 3 Bifurcation behavior in the over-height of column

Transition of deflection shapes of EF-3 and EF-5 during positive loading is presented in Fig. 9. For EF-3, the relationship between beam-end moment (M_{bi}) in each floor and total height drift angle (R_t) is presented in Fig. 10. From the figures, it is observed that the deflection shapes are stable for EF-5 subjected to lower axial loading but are unstable for EF-3 subjected to higher axial loading. In the region of Rt>2/100 rad. for EF-3, as the result of growing bow-shaped overall deflection mode, the bifurcation phenomenon appears in the over-height of column. Therefore the moments of the beam-ends at 2nd and 3rd floor decreased without increasing lateral rotation angle due to the enforced return of column deflection. According to the symmetry limit theory of frames (Uetani and Tagawa 1993,1997), a bow-shaped overall deflection mode never appears at any level of the deflection amplitude in case of $N<N_{cr}$.

$$N_{cr} = \pi^2 \cdot (\alpha_v \cdot E) \cdot I_c \Big/ (h)^2 ,$$

where N is axial compressive load, N_{cr} is critical value of axial compressive load, which is obtained as the buckling load of the equivalent elastic frame, α_v is degradation factor of stiffness during positive loading in column, E is young's modulus of concrete in column, I_c is second moment of cross section in column and h is length between the bottom of 1st column and the axial loading point (in this test, h is 315cm).

In this test, α_v is nearly equal 0.2 for EF-3 and 0.3 for EF-5 in final loading stage (see fig.11). For EF-3, critical load N_{cr} is nearly 88 tonf, which is smaller than the axial load at loading point (N=91tonf) and at 1st column ($N_1 \fallingdotseq$ 105tonf). But for EF-5, N_{cr} is 132 tonf, which is larger than the axial load at loading point (N=70tonf) and at 1st column (N1 ≒ 85tonf). So that the bifurcation phenomenon may appear for EF-3, but may not appear for EF-5.

Bow-shaped mode deflection would be hard to appear in low–rise multi-span frames due to the interaction of external and internal columns, but would be easy to appear in high–rise multi-story frame due to the increasing axial force. Further research effort is required on getting the general conditions for suppression of bow-shaped mode deflection in super high-rise RC frames subjected seismic loading.

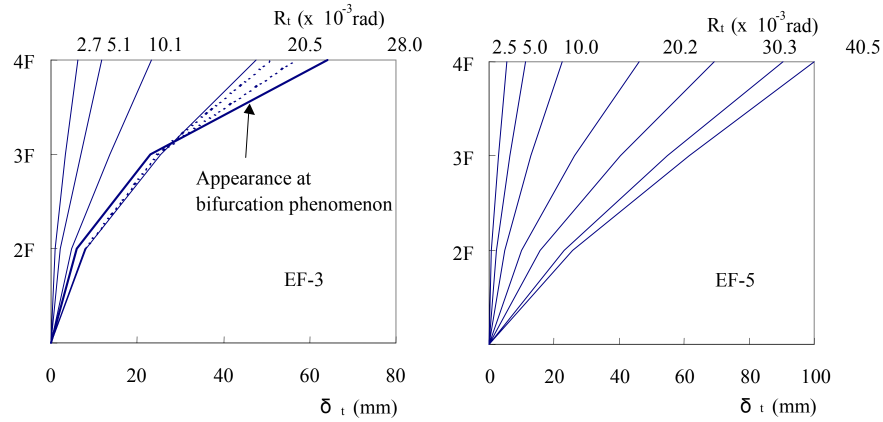

Fig.9 Deflection shapes of EF-3 and EF-5 during positive loading

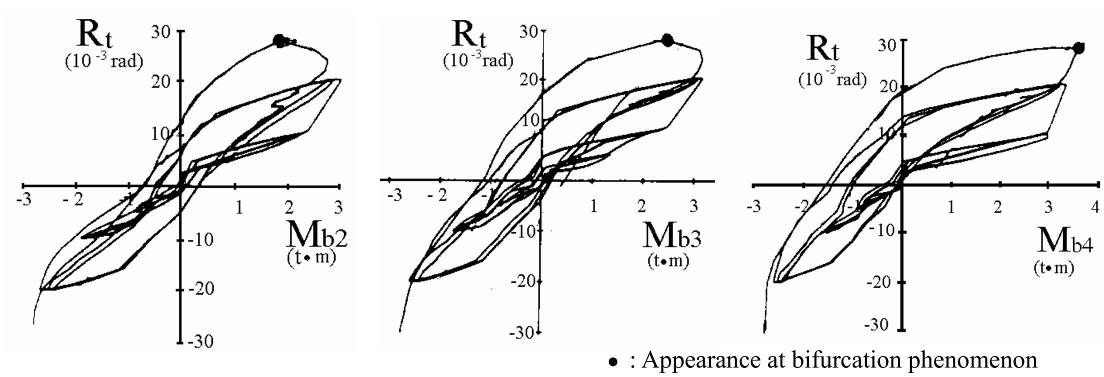

Fig. 10 M_{bi} - R_t hysteresis loops of EF-3

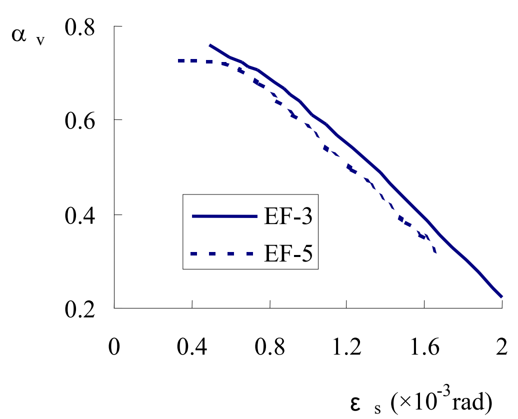

Fig.11 Relationship between stiffness degradation ratio (α_v) and axial average strain (ε_s) of column during positive loading

5.4 Moment distribution, state of hinge formation and movement of inflectional point

Figure 12 illustrates the comparison of measured and calculated moment distribution. The values calculated by the two methods are in close agreement. In comparison with measured values, the calculated values at the lower end of columns are smaller in the case of EF-2 during positive loading at 2/100 rad. and during negative loading at 1/100 and 2/100 rad., and in the case of EF-5 during positive loading at 2/100 rad.

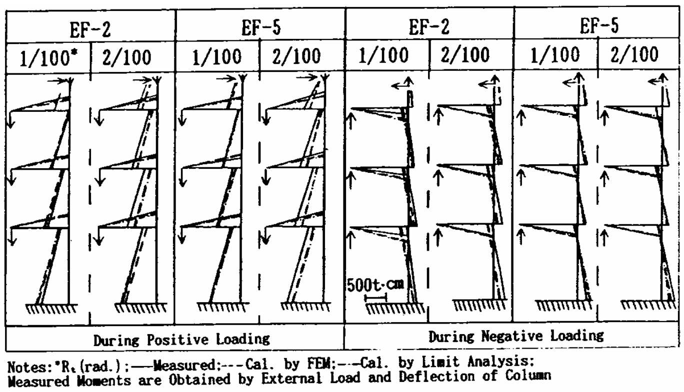

Fig. 12 Comparison of measured and calculated moment distribution

Figure 13 illustrates the state of hinge formation in the frames. The occurrence of hinges in subassemblages during testing are assessed as follows. At first, the measured strain was substituted to the Ramberg-Osgood model to get stress in main rebars in a column and at beam ends. And then, the stress condition of member sections at flexural capacity were calculated by e-function method (Umemura 1951). Finally, the judgement of hinge formation was made by comparison between the measured and calculated stress condition. At R_t=2/100 rad., a comparison between test results and calculated results by the FEM was made. Both test and calculated results indicated the weak beam-strong column mechanism except in the case where the test subassemblages were subjected to higher tensile axial loading. In addition, at the end of testing, hinges were developed at lower ends of the 2nd and 3rd story columns resulting in total-complete collapse. The relationship between the ratio of inflectional point heights (I_p) and total height drift angle (R_t), in the 1st floor and 3rd floor columns is shown in Fig. 14. When plastic hinges occurred at the lower ends of column and at beam ends with lateral displacement at R_t ≒ 1/100 rad., the collapse mechanism was formed and the I_p tended to converge in some constant values. However, the I_p showed a small increase during positive loading and some decrease during negative loading by the P-Δ effect with the increase of lateral displacement. The calculated values approximately agreed with measured values.

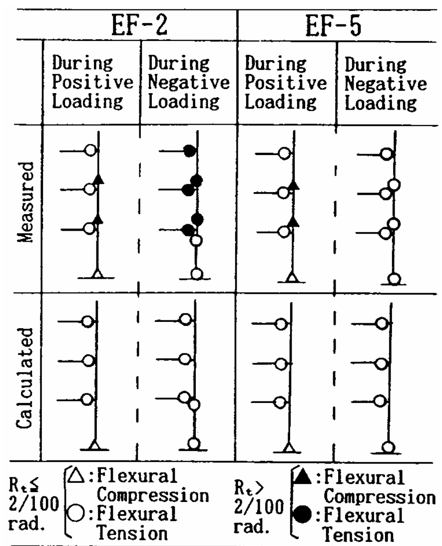

Fig. 13 State of hinge formations

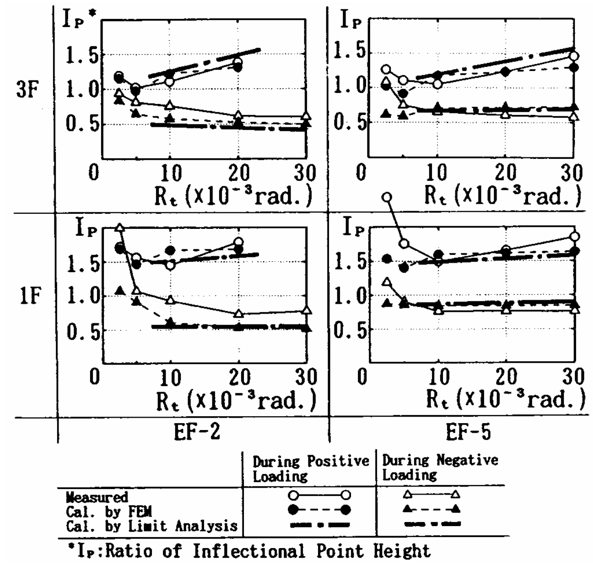

Fig. 14 Moment of inflection point height

6. BEHAVIOR OF BEAMS AND COLUMNS

6.1 Beam

Figure 15 illustrates the lateral load (Q_b) – deformation angle (R_b) of the 2nd and 3rd floor beams. The hysteresis loops progressed gradually in the positive direction with repeated and incremental loading and this tendency is most remarkable in the upper floors. This may be due to the different deflection shape which appeared under positive and negative loading. The initial stiffness agree closely with the calculated values. Except for EF-4 under negative loading, the stiffness at yield point and the yield capacities in flexure are almost identical to the values calculated by the equation proposed by Sugano (1973) and the approximate equation in AIJ (1988).

For EF-4 under negative loading, the yield capacities in flexure at beam-end do not reach the magnitude of the calculated values according to the approximate equation in AIJ (1988). This may be due to not only the overall horizontal deflection shape of subassemblage but also the lack of anchorage capacity of beam rebars in a beam-column joint. The latter cause may be induced by the relaxation of the restraint for the beam-column joints due to high axial tension loading on column.

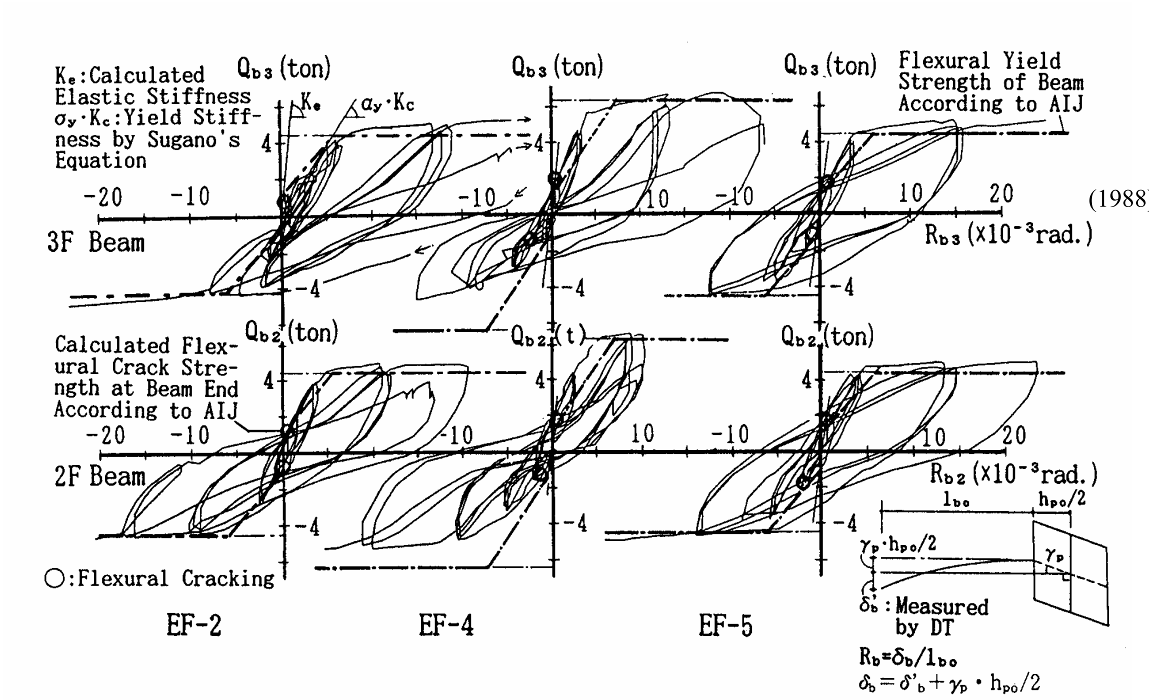

Fig. 15 $Q_b - R_b$ hysteresis loops

6.2 Column

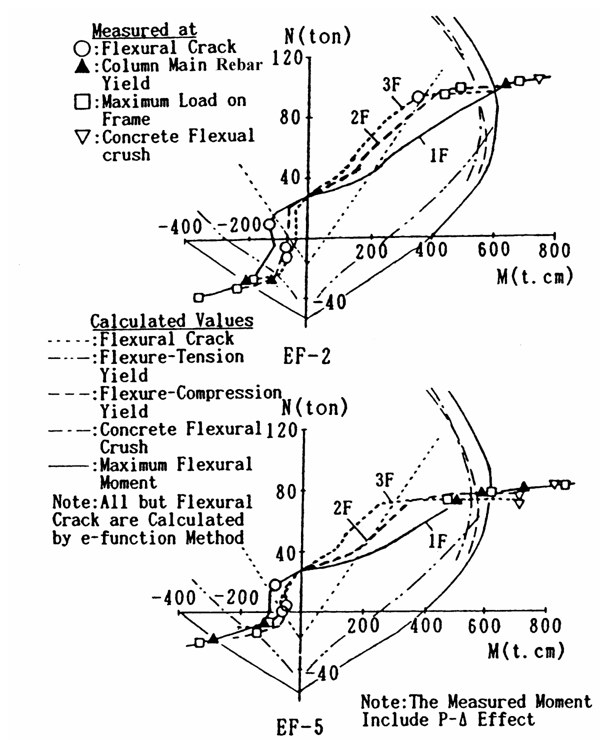

Fig.16 Axial load – bending moment correlation

Fig. 16 illustrates the correlation between axial force at each floor level and the corresponding bending moment at the lower end of column. The correlated curves include the values of flexural cracking moment, main rebar yield moment, maximum flexural moment of column as shown in the figure. The measured values of flexural cracking and yield moments approximately agree to their calculated values. As the strain-hardening of column main rebars and the effect of core concrete confinement by transverse reinforcement in the first floor progress, the measured maximum capacity show higher values than the calculated ones. This phenomenon agrees with the assumption that during compressive axial loading the ultimate moment is 1.2 times higher than that obtained by the e-function method, which was made in the analysis.

Figure 17 illustrates lateral load (Q_{c1}) – deformation angle (R_{c1}) response in the 1st floor column. During positive loading, envelope curves of Q_{c1}-R_{c1} relationships are in close agreement with the calculated values by the FEM. But during negative loading, the stiffness at near yield point calculated by the FEM, shows higher values in comparison to the measured ones. This seems to be due to the fact that the variation in column stiffness under fluctuating tensile axial loading was not estimated adequately.

Figure 18 illustrates axial load (N_1) – axial displacement (δ_{ax1}) response in the 1st floor columns. The measured envelope curves of N_1-δ_{ax1} relationships are in fairly good agreement with the calculated value by the FEM.

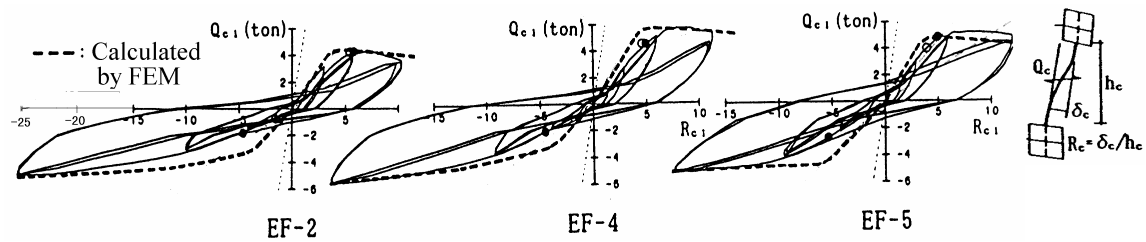

Fig.17 Q_{c1} – R_{c1} relationship

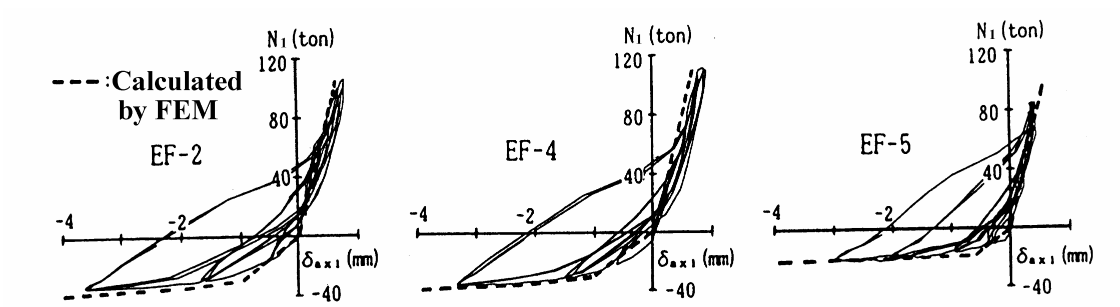

Fig.18 N_1 –δ_{ax1} relationship

7. CONCLUSIONS

In this study, the tested subassemblages showed stable hysteresis even at 2/100 rad. range, which was much higher than the usually accepted design value (1/100 rad.) for the severe earthquake. This indicates that the high-rise building designed based on the Japanese conventional methods possesses sufficient seismic resistance. But also the study indicated that it was necessary to take into account the P-Δ phenomenon to adequately assess the total frame behavior when columns are subjected to high compressive axial force. Further considerations must be made for the P-Δ phenomenon and strain-hardening of columns when subjected to high tensile axial force and for the movement of inflectional points due to the variation in flexural stiffness of beams and columns under fluctuating axial force on exterior column in order to adequately design structural members. These structural behaviors can be adequately predicted by FEM taking into account the material and geometrical nonlinearities and by the limit analysis taking into account the P-Δ effect.

REFERENCES

Architectural Institute of Japan (1988). *AIJ Standard for Structural Calculations of Reinforced Concrete Structures*, : 615 (in Japanese).

Inoue K. and Ogawa K. (1974). Nonlinear Analysis of Strain-Hardening Frames Subjected to Variable Repeated Loading. *Technology Reports of Osaka Univ.* . No. 1222: 763-781.

Isozaki Y. et al.. (1987). Elastic-Plastic Analysis of Reinforced Concrete Frame in Consideration of Fluctuation of Axial Forces on Columns. *Journal of Structural and Construction Engineering (Transaction of AIJ)*. No. 372 : 31-43 (in Japanese).

Kaku T. , Asakusa H. and Aoki. M. (1989). Ductility Estimation of Exterior Beam-Column Subassemblages in Reinforced Concrete Frames. *Journal of Structural and Construction Engineering (Transaction of AIJ)*. No. 401 : 87-96 (in Japanese).

Kanoh Y. , Kobayashi K. Teraoka M. et al.. (1985). Investigation on the Strength and Deformation Capability of Reinforced Concrete Columns under High Axial Compressive Stress (Part 1). *Summaries of Technical Papers of Annual Meeting, AIJ(Structure)* : 445-446 (in Japanese).

Sugano S. (1973). Study on Restoring Force Characteristics in RC Members (Test on Strength and Stiffness of Beam and Column at Yield and Shear Wall without Opening). *Journal of the Japan Concrete Institute*, Vol. 11, No. 2 : 1-9 (in Japanese).

Teraoka M. , Kanoh Y. et al.. (1993), Experimental Study on Subassemblages Consisting of Exterior Column and Halfspan Beams in Lower Part of RC High-Rise Building Subjected to Seismic Loading. *Transaction of the Japan Concrete Institute,* Vol. 15 : 361-368

Uetani, K. and Tagawa, H. (1993), Bifurcation behavior analysis of multistory planar frame models subjected to one-way top horizontal displacement. *Journal of Structural and Construction Engineering (Transaction of AIJ)*. No. 453 : 101-110 (in Japanese).

Uetani, K. and Tagawa, H. (1998), Criteria for suppression of deformation construction of building frames under severe earthquakes, Engineering Structures. Vol.20, Nos 4-6 : 372-383.

Umemura H. (1951). Plastic Deformation and Ultimate Flexure Capacity of Reinforced Concrete Beam *Journal of the Architectural Institute of Japan (AIJ)*. No. 42 : 59-70 (in Japanese).

KEYWORDS: RC high-rise building, seismic design, exterior column, experiment, subassemblage, high fluctuating, P-Δ effect, moment of inflectional point of column, bifurcation behavior, one-dimensional finite element method, limit analysis

PERFORMANCE OF PRECAST INDUSTRIAL BUILDINGS DURING THE 1999 EARTHQUAKES IN TURKEY

M. POSADA[1] and S.L. WOOD[2]

ABSTRACT

Precast frame buildings are used throughout Turkey for industrial facilities. One-story warehouses are the most common structural configuration; however, low-rise commercial and manufacturing facilities are also constructed using precast concrete members. These structural systems are economical to construct and provide large open areas needed for manufacturing. Many precast industrial building collapsed during the recent earthquakes in Turkey. This paper summarizes the observed damage in one-story warehouses and investigates the relationship between structural stiffness and the observed damage.

1. INTRODUCTION

Precast construction was introduced in Turkey in the 1960s. During the 1990s, approximately 90% of the warehouse and light industrial facilities were constructed using precast members (Karaesmen, 2001). The most common structural system for these facilities is based on a structural configuration that was developed in Western Europe to carry gravity loads only (Ersoy et al. 1999). Turkish engineers modified the connection details so that the precast buildings have the capacity to resist lateral loads. However, each producer of precast elements has developed a unique set of connection and reinforcement details, and the details vary appreciably from producer to producer.

Precast buildings sustained considerable damage during the 1999 earthquakes in Turkey. Structural damage and collapse (Fig. 1) was common throughout the epicentral region (Ataköy, 1999; EERI, 2000). The objective of this investigation was to document the observed damage and determine the likely causes. Researchers from the University of Texas, Kocaeli University, Boğaziçi University, the Middle East Technical University, Purdue University, and the University of Minnesota visited more than 50 precast industrial buildings in the epicentral region of the August 1999 Kocaeli and November 1999 Düzce earthquakes. Their observations, and the results of a parametric study to identify the causes of the observed structural damage, are summarized in this paper.

[1] *Graduate Research Assistant, Ferguson Structural Engineering Laboratory, University of Texas, Austin, Texas, USA.*
[2] *Professor of Civil Engineering, Ferguson Structural Engineering Laboratory, University of Texas, Austin, Texas, USA. Email: swood@mail.utexas.edu*

Figure 1: Photographs of Damaged Precast Buildings near Adapazarı

2. CHARACTERISTICS OF ONE-STORY INDUSTRIAL BUILDINGS

Although two- to four-story precast buildings were observed in the epicentral region, this paper will focus on single-story structures. Single-story structures represent the most common form of precast construction and the overwhelming majority of the structures that sustained damage during the 1999 earthquakes. The single-story buildings tended to be rectangular in plan with one to four bays in the transverse direction and ten to thirty bays in the longitudinal direction. Transverse bay widths ranged from 10 to 25 m, and longitudinal bay widths ranged from 6 to 8 m. Story heights also ranged from 6 and 8 m.

Figure 2 shows an elevation of a typical one-story building with two bays in the transverse direction. The columns are supported by precast socket footings, and are assumed to be fixed at grade level. Flexural hinges were observed at the base of columns in many buildings, which confirms this assumption. No evidence of foundation rotation or damage was observed.

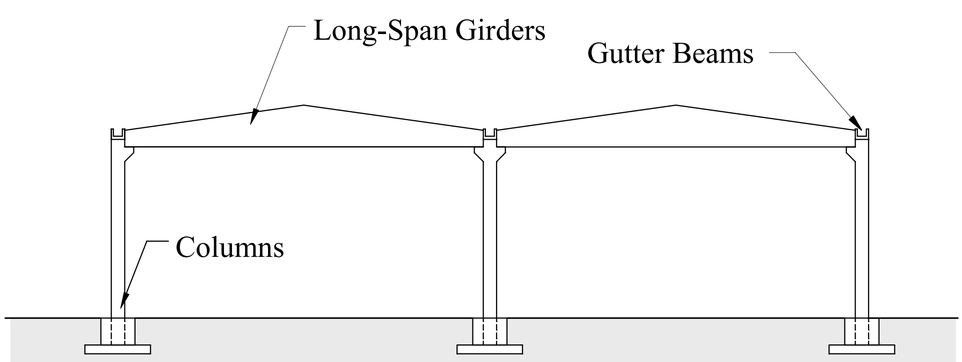

Figure 2: Transverse Elevation of Typical Precast Warehouse

Long-span roof girders are oriented along the transverse axis of the building. The depth of these girders often varies along their length, forming the triangular shape shown in Fig. 2. Beams with U-shaped cross sections are oriented along the longitudinal axis of the building. These beams function as gutters to collect water from the roof. Purlins span between the roof girders at regular intervals. Typically five to eight purlins ran between adjacent roof girders.

In one-story construction, the precast girders, gutter beams, and purlins were pinned at both ends. Vertical dowels extended up from the supporting member and the horizontal elements were cast with vertical holes near their ends to accommodate these dowels. The holes were filled with grout in most buildings. In some cases the dowels were threaded, and nuts were installed before grouting. Typically, lightweight materials, such as metal decking or asbestos panels, were used to form the roof. Clay tile infill was used in most cases for the exterior walls, but precast concrete wall panels were also used.

The typical, one-story industrial building depends entirely on the cantilevered columns for lateral strength and stiffness. Even when precast wall panels were used for cladding, the connection details were developed such that the wall panels did not contribute to the lateral stiffness of the building.

Three types of structural damage were frequently observed in the one-story industrial buildings: flexural hinges at the base of the columns; axial movement of the roof girders which led to pounding against the supporting columns or unseating of the roof girders; and out-of-plane movement of the roof girders which led to tilting of the beams and rotation off the supports.

3. BUILDING CODE PROVISIONS

The current Turkish Building Code (1998) uses the structural behavior factor, R, to convert elastic spectral accelerations to design spectral accelerations. The code defines four structural systems for cast-in-place reinforced concrete buildings, four systems for precast concrete buildings, and four systems for structural steel buildings. The structural behavior factors range from 8 for reinforced concrete or structural steel moment-resisting frames to 4 for precast concrete shear walls. The structural system used for the typical one-story industrial buildings described in the previous section is assigned a structural behavior factor of 5. The design base

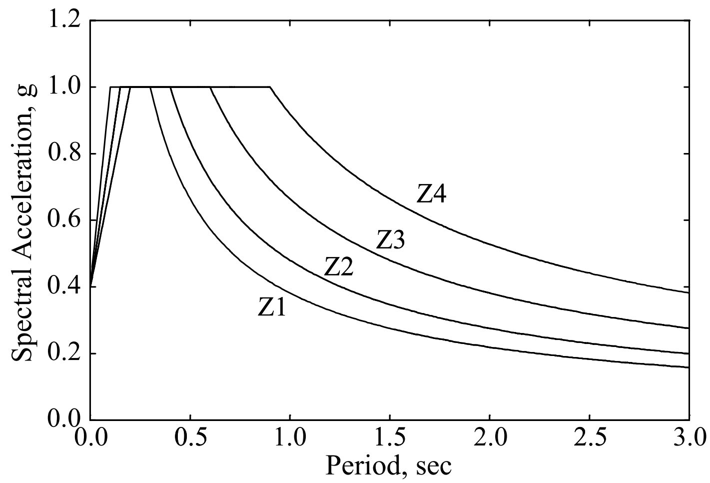

Figure 3: Elastic Response Spectra for Seismic Zone 1 (Damping Factor = 0.05)

shear also depends on the effective peak ground acceleration, the intended use of the building, the soil characteristics at the site, and the period of the building.

Elastic response spectra corresponding to the four soil categories identified in the building code are shown in Fig. 3. The effective peak ground acceleration used to calculate these spectra corresponds to the zone of highest seismic risk in Turkey.

With the exception of buildings with very short periods, the design spectral accelerations are determined by dividing the elastic spectral accelerations shown in Fig. 3 by the structural behavior factor. Inter-story drift ratios are calculated using the lateral forces corresponding to the design spectral accelerations and must not exceed the limits given below:

$$\frac{(\Delta_i)_{\max}}{h_i} \leq 0.0035 \quad (1)$$

$$\frac{(\Delta_i)_{\max}}{h_i} \leq \frac{0.02}{R} \quad (2)$$

where $(\Delta_i)_{max}$ is the maximum inter-story displacement, h_i is the height of the corresponding story, and R is structural behavior factor. For typical one-story industrial buildings, the maximum calculated story drift ratio is controlled by Eq. 1 and is limited to 0.35%. An investigation of four damaged one-story buildings in Adapazarı (Ataköy, 1999) indicated that all four buildings failed to satisfy this stiffness criterion.

4. INFLUENCE OF COLUMN STIFFNESS ON STRUCTURAL PERFORMANCE

A parametric study was conducted to relate the behavior of one-story precast industrial buildings to the column stiffness. An 80 by 200 m building in Adapazarı, which sustained light damage during the Kocaeli earthquake, was selected as the prototype structure for this study. The transverse bay widths were 20 m, the longitudinal bay widths were 7.5 m, and the story height was 7 m.

A linear model of the framing system in the transverse direction was developed. The base of each column was fixed and the connections between the columns and roof girders were pinned such that vertical loads and shear were resisted, but the flexural resistance at the ends of the beams was negligible.

For the purpose of the parametric study, column dimensions were varied from 40 by 40 cm to 80 by 80 cm. These dimensions correspond to the smallest and largest precast columns that were observed in the epicentral region. The cross-sectional dimensions and mass of the girders, gutter beams, purlins, roofing materials, and cladding in the prototype building were used in all analyses. The variation of the calculated fundamental period with the assumed column dimensions is given in Table 1.

Table 1: Column Sizes Considered in Parametric Study

Column Dimensions		Calculated Period
Depth	Width	
cm	cm	sec
40	40	1.10
40	45	1.05
45	40	0.93
45	45	0.88
50	40	0.80
50	45	0.76
50	50	0.73
50	55	0.70
55	50	0.64
55	55	0.61
60	55	0.54
60	60	0.52
65	65	0.45
70	70	0.40
80	80	0.31

4.1 Ground Motion Records

Each of the buildings considered in the parametric study was analyzed using fifteen ground motion records (Table 2). Most of the recording stations were within 50 km of the epicenters of the 1999 earthquakes, and all were within 20 km of the surface trace of the faults (EERI, 2000). The ground motion records were divided into two groups depending on the soil conditions at the recording station. Records from Bolu, Düzce, and Yarimca were used to determine the spectral characteristics for soft soil, while records from Arcelik, Gebze, İzmit, and Sakarya were used to determine the spectral characteristics for stiff soil sites.

Elastic acceleration and displacement response spectra corresponding to a damping ratio of 2% were calculated for each ground motion record. Mean, maximum, and minimum spectra are plotted in Fig. 4 and 5 for the soft soil and stiff soil/rock sites, respectively. Although statistical information is not shown in the plots, the maximum and minimum values were typically less than 1.2 standard deviations from the mean value for the range of periods considered.

Table 2: Ground Motions Considered in the Parametric Study

Station	Component	Peak Acceleration g	Epicentral Distance km	Soil Conditions
Düzce (DZC)	180 270	0.41 0.51	10**	Soft Soil
İzmit (IZT)	090 180	0.23 0.17	12*	Rock
Yarimca (YPT)	240 330	0.30 0.32	22*	Soft Soil
Sakarya (SKR)	090	0.41	35*	Stiff Soil
Bolu (BOL)	000 090	0.74 0.81	42**	Soft Soil
Gebze (GBZ)	000 270	0.27 0.14	50*	Stiff Soil
Arcelik (ARC)	000 090	0.21 0.13	60*	Stiff Soil
Düzce (DZC)	180 270	0.32 0.37	110*	Soft Soil

* Approximate distance to epicenter of Kocaeli earthquake.

** Approximate distance to epicenter of Düzce earthquake.

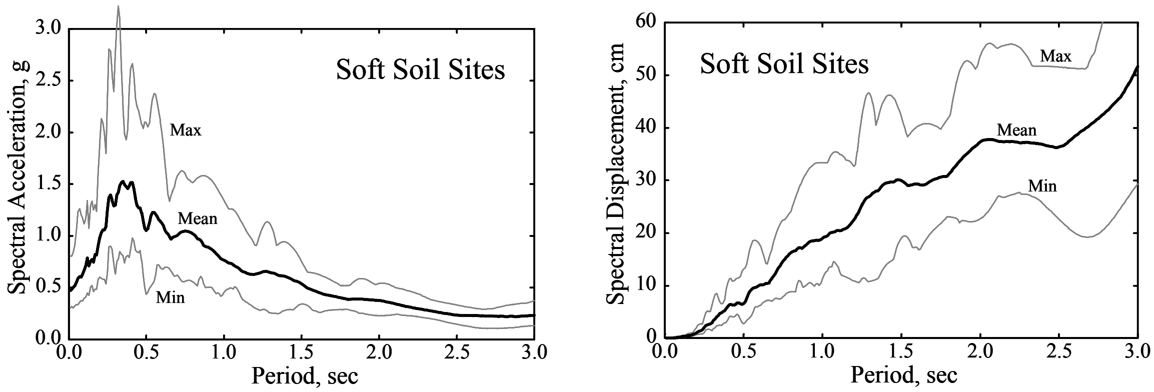

Figure 4: Mean, Maximum, and Minimum Values of Elastic Response Spectra for Ground Motions Recorded on Soft Soils (Damping Factor = 0.02)

In general, the minimum spectral displacements from the soft soil sites were approximately equal to the maximum spectral displacements from the stiff soil/rock sites. For periods less than 0.25 sec, the maximum spectral accelerations from the stiff soil/rock sites were nearly the same as the maximum spectral accelerations from the soft soil sites. However, for periods greater than 0.5 sec, the maximum spectral accelerations from the stiff soil/rock sites were approximately equal to the minimum spectral accelerations from the soft soil sites.

4.2 Displacement Capacity of Idealized Buildings

The displacement capacity of the idealized columns was determined by first calculating the moment-curvature response of each of the cross sections listed in Table 1. Reinforcement ratios of 1, 2, and 3% were used in the analysis. The assumed arrangement of the longitudinal reinforcement is shown in Fig. 6.

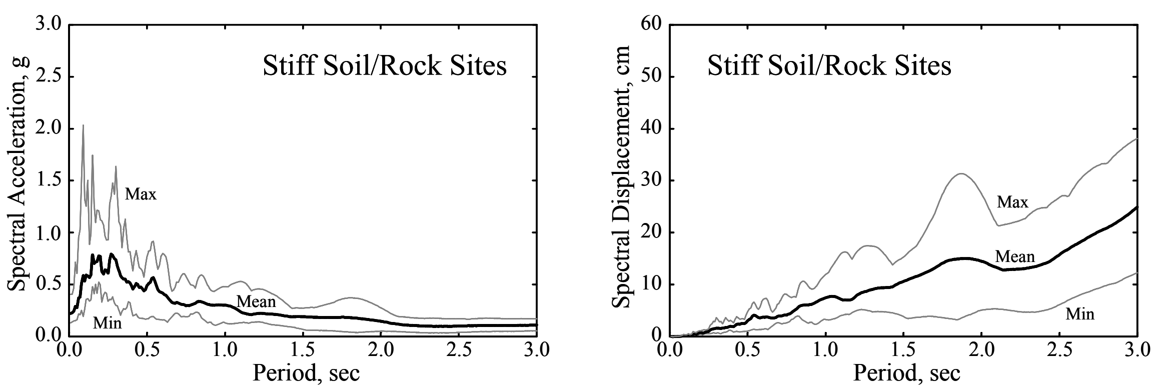

Figure 5: Mean, Maximum, and Minimum Values of Elastic Response Spectra for Ground Motions Recorded on Stiff Soils (Damping Factor = 0.02)

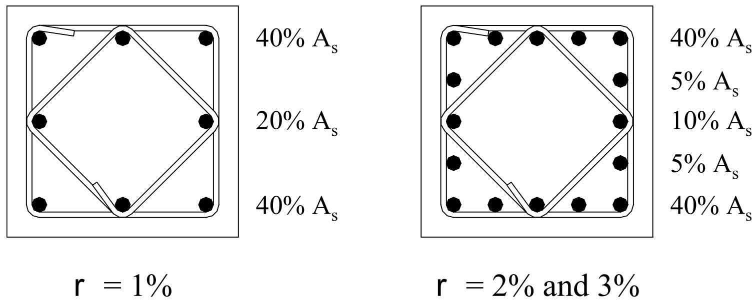

Figure 6: Assumed Arrangement of Reinforcing Bars for Parametric Study

The behavior of the concrete was modeled using the stress-strain relationship developed by Hognestad (1951), a concrete compressive strength of 30 MPa, an initial modulus of elasticity of 26,000 MPa, and a limiting compressive strain of 0.003. The stress-strain relationship for steel was assumed to be linear to the yield point. The yield plateau was assumed to extend to a strain of 0.01, and strain hardening was considered for strains between 0.01 and 0.10. The yield stress of the steel was assumed to be 420 MPa, the tensile strength was 500 MPa, and the modulus of elasticity was 204,000 MPa. The contribution of the transverse reinforcement in confining the column core was ignored because ties with 90-degree hooks were used throughout the epicentral region.

Because the cantilevered columns provided all the lateral stiffness for the one-story buildings, the yield displacement and displacement capacity could be calculated using Eq. 3 and 4.

$$\Delta_y = \frac{\phi_y \cdot L^2}{3} \tag{3}$$

$$\Delta_u = \Delta_y + \left(\phi_u - \phi_y\right) \cdot \ell_p \cdot \left(L - \frac{\ell_p}{2}\right) \tag{4}$$

where Δ_y is the yield displacement at the roof, ϕ_y is the yield curvature, Δ_u is the displacement capacity at the roof, ϕ_u is the curvature capacity, L is the height of the one-story building, and ℓ_p is the height of the equivalent plastic hinge. The plastic hinge length was assumed to be one-half the depth of the cross section for all cases (Moehle, 1992).

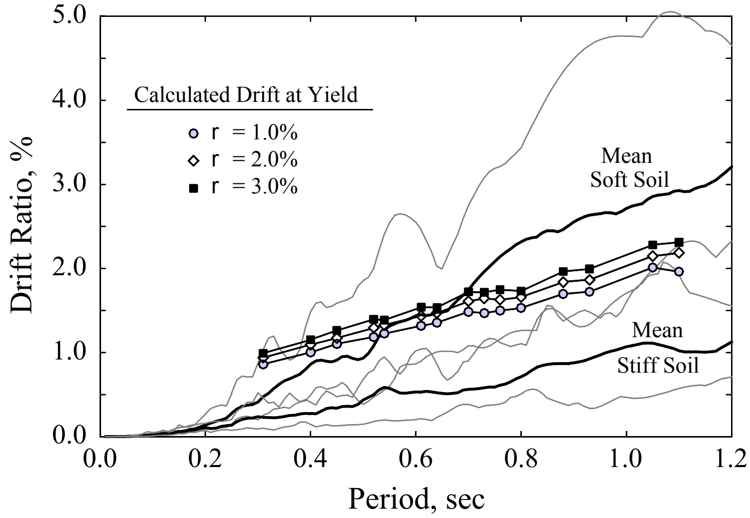

Figure 7: Comparison of Drift Demand with Calculated Drift at Yield

4.3 Comparison of Drift Demand and Capacity

The inelastic displacement demands in the one-story buildings during the 1999 earthquakes were approximated using the elastic displacement demands calculated using a damping factor of 2% (Shimazaki and Sozen, 1984). The elastic displacement demands from the fifteen ground motion records are compared with the calculated yield displacements in Fig. 7. Similarly to Fig. 4 and 5, mean, maximum, and minimum response spectra are plotted for the two groups of ground motions. All displacements are plotted in terms of the drift ratio: the roof displacement divided by the building height.

The data in Fig. 7 indicate that all of the buildings considered in the parametric study had the ability to resist the displacements induced by the composite maximum response spectrum for the stiff soil/rock sites without yielding. However, the data in Fig. 7 also indicate that idealized buildings with calculated periods larger than 0.7 sec would yield when subjected to the mean response spectrum for the soft soil sites and all the idealized buildings would yield when subjected to the composite maximum response spectrum for the soft soil sites. These results were not sensitive to the amount of longitudinal reinforcement in the columns.

The calculated drift capacities of the idealized buildings are compared with the response spectra for soft soil sites in Fig. 8. Idealized buildings with periods greater than 0.8 sec are likely to be pushed beyond their displacement capacity by the mean ground motion at the soft soil sites.

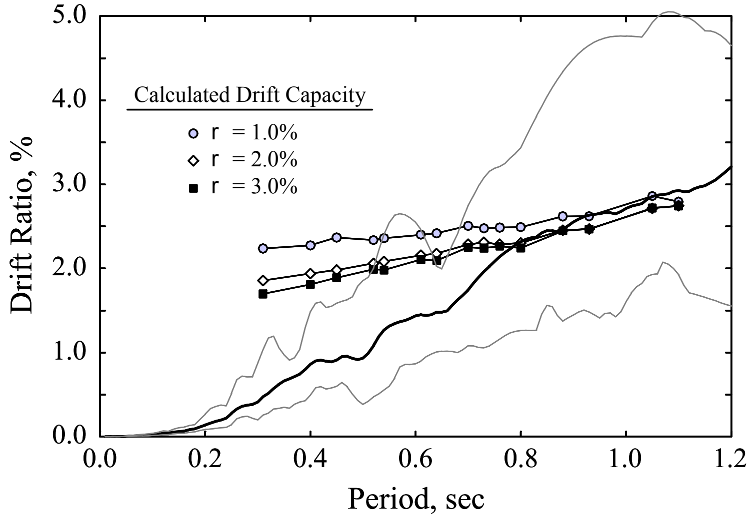

Figure 8: Comparison of Drift Demand from Soft Soil Sites with Calculated Drift Capacity

Only buildings with periods less than 0.5 sec are likely to survive the maximum composite response spectrum without reaching their displacement capacity.

As indicated in Table 1, a period of 0.8 sec corresponds to a building with 50 by 40-cm columns. The overwhelming majority of the buildings visited in the epicentral region were constructed with columns this size or smaller. A period of 0.5 sec corresponds to a building with 60 by 60-cm columns. Less than 5% of the single-story buildings visited had columns larger than this size.

The calculations summarized in this section agree with observations from the field. The building inventories in Gebze and Adapazarı were very similar in terms of construction quality. The buildings in Gebze appeared to be undamaged, while a large number of buildings collapsed in Adapazarı. The earthquake demand was likely to be significantly different in the two cities due to the soil conditions. Buildings that experienced satisfactory performance when founded on stiff soil were likely to collapse when founded on soft soil deposits.

4.4 Comparison with Turkish Building Code

Each of the idealized buildings was also analyzed using design response spectra defined in the Turkish Building Code (1998) for soil classifications Z3 and Z4. A period of 0.7 sec corresponded to the stiffness at which the idealized building located on a site with soft soil conditions (Z4) would satisfy the drift criterion in the building code (Eq. 1). The critical period is increased to approximately 0.75 sec if the idealized building is located on a site with Z3 soil conditions. The data shown in Fig. 8 indicate that buildings with fundamental periods in this range would likely experience drift levels near capacity for the mean response spectrum, and would be pushed beyond capacity for the composite maximum spectrum for soft soil.

5. CONCLUSIONS

This paper has focused on one aspect of the seismic behavior of one-story, precast, industrial buildings in Turkey: the flexural response of the transverse frames. Large variations in the performance of precast industrial buildings were observed in the epicentral regions of the 1999 Kocaeli and Düzce earthquakes. Column dimensions and connection details are considered to have a critical influence on the performance of this type of structure. Because the structural system is not redundant, inelastic action in any column can lead to unseating of the roof girders and collapse of the roof. Drift must be controlled for this type of structural system to reliably survive future earthquakes. The design provisions in the Turkish building code and typical column dimensions observed in the epicentral region do not appear to be sufficient to control damage on soft soil sites.

6. ACKNOWLEDGMENTS

The assistance of Şevket Özden (Kocaeli University), Sami And Kılıç (Boğaziçi University), Uğur Ersoy, Erhan Karaesmen, Güney Özcebe, and Tuğrul Tankut (Middle East Technical University), Julio A. Ramirez and Mete A. Sözen (Purdue University), Catherine W. French and Arturo E. Schultz (University of Minnesota), Michael E. Kreger and Eric B. Williamson (University of Texas) and numerous engineers at GÖK, Pekintaş, Set Betoya, and Yapı Merkezi, are gratefully acknowledged.

The work described in this paper sponsored by the US National Science Foundation under grant CMS-0085337. The opinions expressed in this paper are not necessarily those of the sponsor.

7. REFERENCES

Ataköy, H. (1999). 17 August Marmara Earthquake and the Precast Concrete Structures Built by TPCA Members, Turkish Precast Concrete Association, Ankara, Turkey.

Code for Buildings to be Built in Disaster Areas (1998). Ministry of Construction, Ankara, Turkey. (In Turkish).

Earthquake Engineering Research Institute (2000). 1999 Kocaeli, Turkey, Earthquake Reconnaissance Report. *Earthquake Spectra.* Supplement A to Vol. 16.

Ersoy, U., T. Tankut, and G. Özcebe (1999). Damages Observed in the Precast Framed Structures in the 1998 Ceyhan Earthquake and their Rehabilitation. Department of Civil Engineering, Middle East Technical University, Ankara, Turkey.

Hognestad, E. (1951). A Study of Combined Bending and Axial Load in Reinforced Concrete Members. *Bulletin*, 399, University of Illinois Engineering Experiment Station, Urbana, Illinois.

Karaesmen, E. (2001). Prefabrication in Turkey: Facts and Figures. Department of Civil Engineering, Middle East Technical University, Ankara, Turkey.

Moehle, J.P. (1992). Displacement-Based Design of RC Structures Subjected to Earthquakes. *Earthquake Spectra*, 8(3):403-428.

Shimazaki, K. and M.A. Sozen (1984). Seismic Drift of Reinforced Concrete Structures. *Research Reports*, Hazama-Gumi Ltd., Tokyo. (In Japanese).

EXPERIMENTAL STUDY ON SEISMIC PERFORMANCE OF REINFORCED CONCRETE WALL COLUMNS WITH SMALL OPENINGS

Masaomi TESHIGAWARA[1] and Haruhiko SUWADA[2]

ABSTRACT

The small openings which are provided for the use of an air-conditioner, a ventilation duct, and equipment apparatus is needed for a wall column in a medium and high-rise wall frame RC structure with flat beams (FB Structure) building. It is reported the experiment in that the effect of those small openings in the wall column on the strength, ductility of wall column with small openings are studied using 1/2 scaled model.

1. INTRODUCTION

The main purpose of this study is to understand the maximum strength, the deformation capacity, and failure mechanism of the wall columns with small openings, which are used for air conditioner, duct, ventilation and applications of equipment in the buildings of medium and high-rise framed-wall reinforced concrete structure with flat beams (the following, FB buildings).

2. THE TEST SPECIMEN

The test specimens are 1/2-scaled models of wall column at the 1st story in longitudinal direction of the 11-story FB buildings, which are designed in trial. The flexural yielding is preceded to shear failure for No. 1 test specimen and the shear failure is assumed on preceded to flexural yielding for No.2. The axial force ratio (N/BDF_c) is determined to be 0.2 and ratio of flatness (D/B) to be 4 is the index of the limitation for deformation capacity rank 1 in medium and high-rise framed-wall reinforced concrete structure construction design guidelines (the following, guideline). In the combination between axial force ratio and ratio of flatness, deformation rank 1 that means drift angle of 1/50rad and more are proposed as shown in Figure 1. Shear span ratio (M/QD) is set at 2.5 and the shearing stress at $0.1F_c$. Each of them is upper limit in usual design range. The reinforcing bar arrangement of test specimens is shown in Figure 2. The detailed data of test specimens and the list of calculated

[1] *Structural Research Group, Building Research Institute, Japan*
Email: teshi@kenken.go.jp
[2] *Building Department, National Institute for Land and Infrastructure Management, Ministry of Land, Infrastructure and transport, Japan*
Email: suwada-h92h9@nilim.go.jp

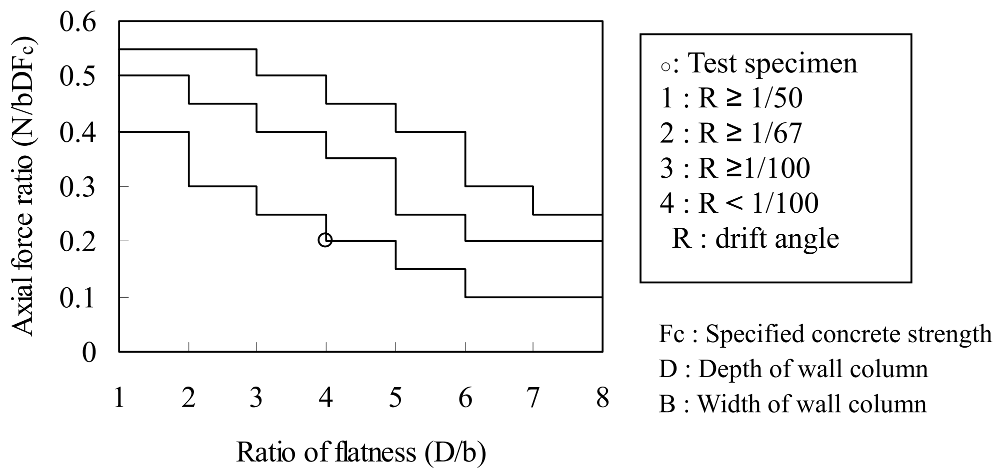

Figure 1: Deformation capacities [H.Hiraishi, 1992]

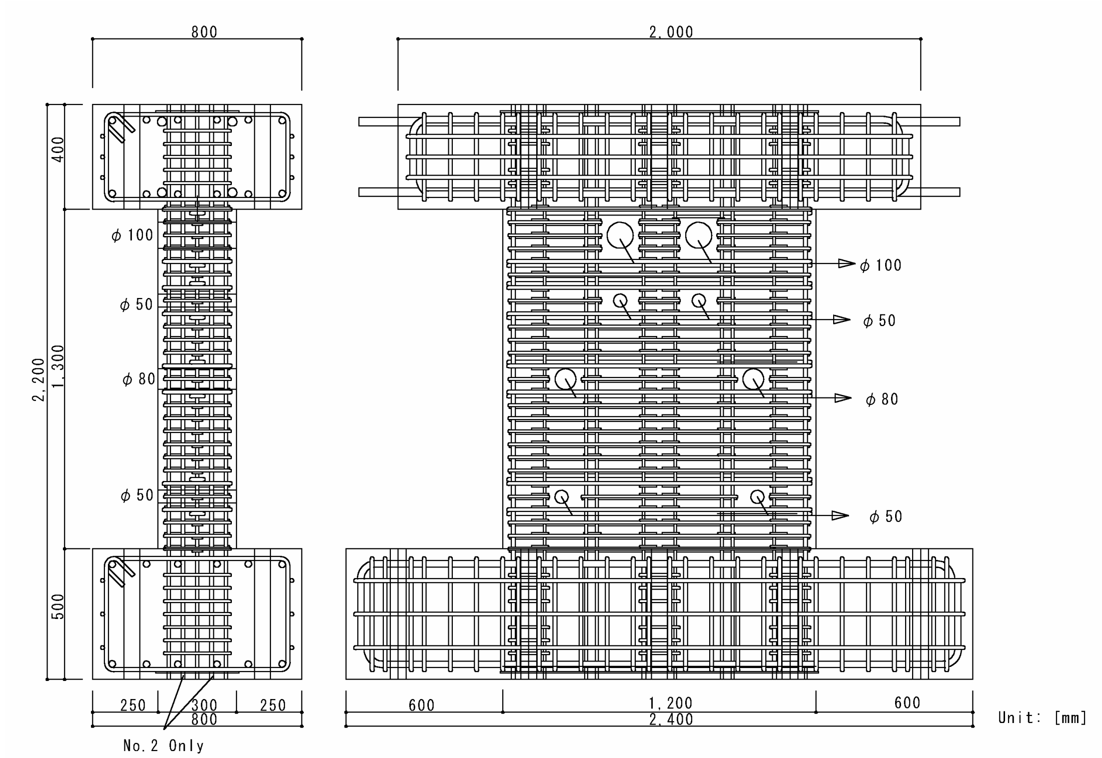

Figure 2: The reinforcement bar arrangement of test specimens

value for various strengths are shown in table 1 and table 2, respectively. In the calculation of the ultimate strength, the effect of the opening reduction is not considered. The flexural, and shear strengths are calculated by equation (1) and (2), respecting.

$$M_u = 0.9a_t \cdot \sigma_y \cdot D + 0.4a_w \cdot \sigma_{wy} \cdot D + 0.5N \cdot D\left(1 - \frac{N}{b \cdot D \cdot F_c}\right) \tag{1}$$

Where:

a_t : cross-section aria of effective tension longitudinal reinforcement (mm^2)

σ_y : nominal yield strength of effective tension longitudinal reinforcement (N/mm^2)

D : depth (mm)

a_w : cross-section aria of longitudinal reinforcement (mm^2)

σ_{wy} : nominal yield strength of longitudinal reinforcement (N/mm^2)

N : axial force (N)

F_c : design compression strength of concrete (N/mm^2)

$$Q_{su} = \left(\frac{0.053\, p_{te}^{\ 0.23} (F_c + 18)}{M/(Q \cdot d) + 0.12} + 0.85 \sqrt{p_{we} \cdot \sigma_{wy}} + 0.1 \sigma_{oe} \right) b_e \cdot j \qquad (2)$$

Where :

P_{te} : ratio of tension reinforcement ($100\Sigma a_t/b_e \cdot D$)

M/Qd : shear span ratio (d : effective depth)

P_{we} : ratio of shear reinforcement ($a_w/(b_e \cdot s)$)

σ_{wy} : nominal yield strength of shear reinforcement (N/mm^2)

σ_{0e} : average axial stress (N/mm^2)

b_e : width (mm)

j : distance between tension and compression ($(7/8)d$) (mm)

The position of small openings is determined by guidelines. With the regulation as shown in figure 3, the distance between the edge of small opening and that of wall column is set at 400mm. Shear reinforcement bars cut for small openings are additionally arranged at the upper and lower sides of openings.

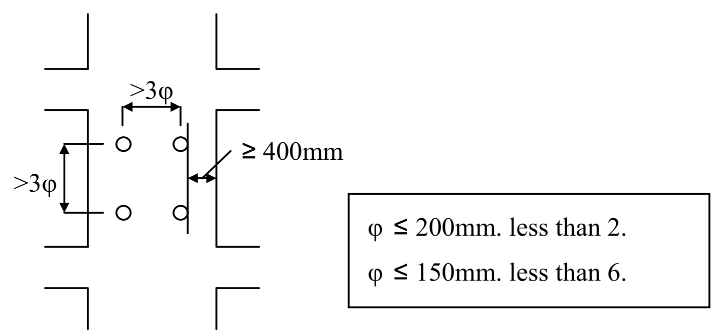

Figure 3: Position of small openings

Table 1: Details data of test specimens

Specimen	b (mm)	D(mm)	D/b	M/Qd*	N/(bDFc)	longitudinal bar: Size and Part	longitudinal bar: Grade	shear reinforcement: Size and Part	shear reinforcement: Grade
No.1	300	1200	4	1.31	0.2	3-D13 (at extreme edge) 16-D10 (at general part)	SD295A	D10@50 D6@50 (for sub tie) D13(at edge the opening)	SD345
No.2	300	1200	4	1.31	0.2	5-D13 (at extreme edge) 16-D10 (at general part)	Super high strength SD785	D10@50 D6@50 (for sub tie) D13(at edge the opening)	SD345

* : d is effective depth (0.95D)

Table 2: List of the calculated value for various strengths

Specimen	Bending strength M_u(kN・m)	Bending strength Q_{mu}(kN)	Shear strength Q_{su}(kN)	Q_{su}/Q_{mu}	Shear stress at collapse mechanism τ_u(N/mm^2)	Design compression strength of concrete F_c(N/mm^2)	τ_u/F_c
No.1	1268.8	845.9	1008.8	1.19	2.83	27	0.10
No.2	2194.2	1462.8	1045.9	0.71	4.89	27	0.18

3. MATERIALS

A coarse aggregate used in concrete has 13mm diameter or less, and the specified design compression strength is 27N/mm^2. Reinforcing bars used in the specimen are shown in table 1. The test results of material properties of concrete and reinforcing bar are shown in table 3. The reason why the high-strength reinforcing bars are employed as main reinforcing bars in No.2 test specimen is to precede shear failure.

Table 3: Material properties of concrete and reinforcing bar

Concrete	E_s(N/mm^2)	σ_B(N/mm^2)	ε_y(%)
F_c=27N/mm^2	2.09×10^4	28.7	0.22
Reinforcing bar	**E_s(N/mm^2)**	**σ_y(N/mm^2)**	**ε_y(%)**
D6-345(Confiment steel)	1.69×10^5	351.1	0.41
D10-295(Longitudinal bar of No.1)	1.73×10^5	355.5	0.20
D10-345(Shear reinforcement)	1.73×10^5	408.2	0.24
D10-785(Longitudinal bar of No.2)	1.95×10^5	859.7	0.45
D13-295(Longitudinal bar of No.1)	1.74×10^5	345.2	0.20
D13-345(Opening reinforcement)	1.74×10^5	370.6	0.21
D13-Super high strength(Longitudinal bar of No.2)	1.84×10^5	1371.2	0.83

4. THE LOADING METHOD

A constant axial force(N/bDσ_B = 0.2) was applied by a 3000kN actuator. The oil jacks were installed on either side of a loading beam for lateral loading. Cyclic lateral force are applied to the specimen.

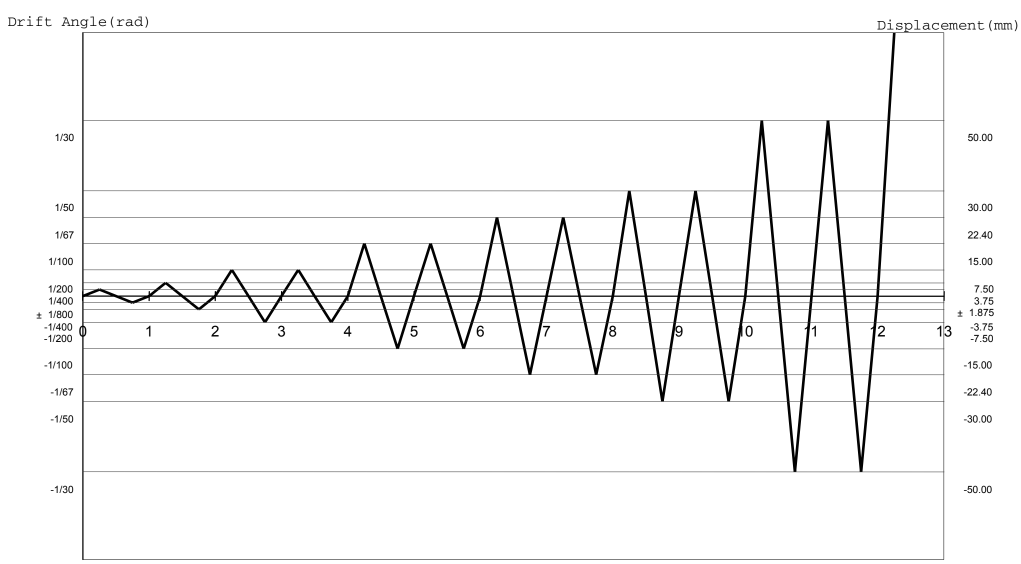

Figure 4: Loading cycle

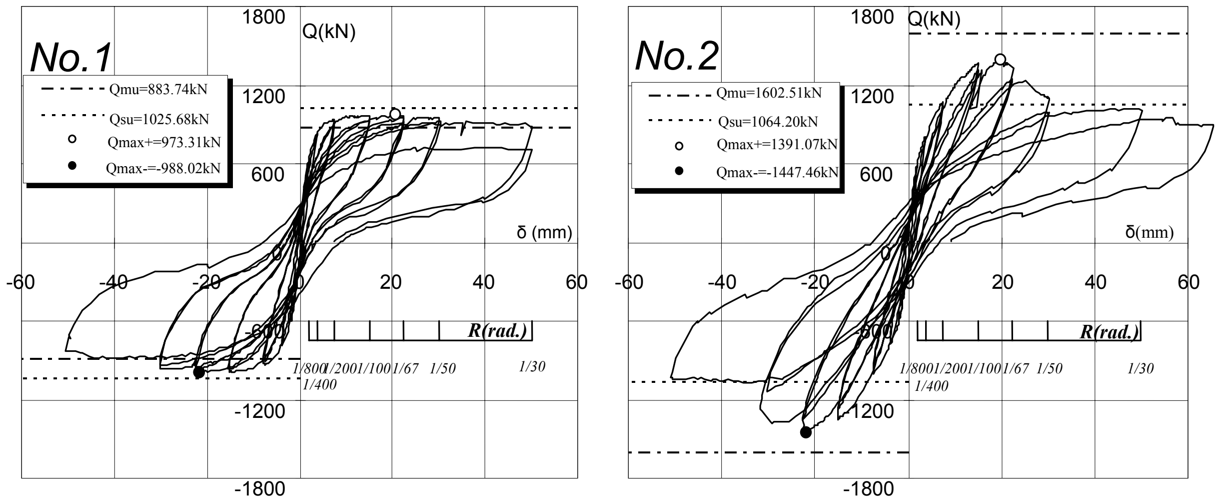

Figure 5: Shear force and displacement relationships

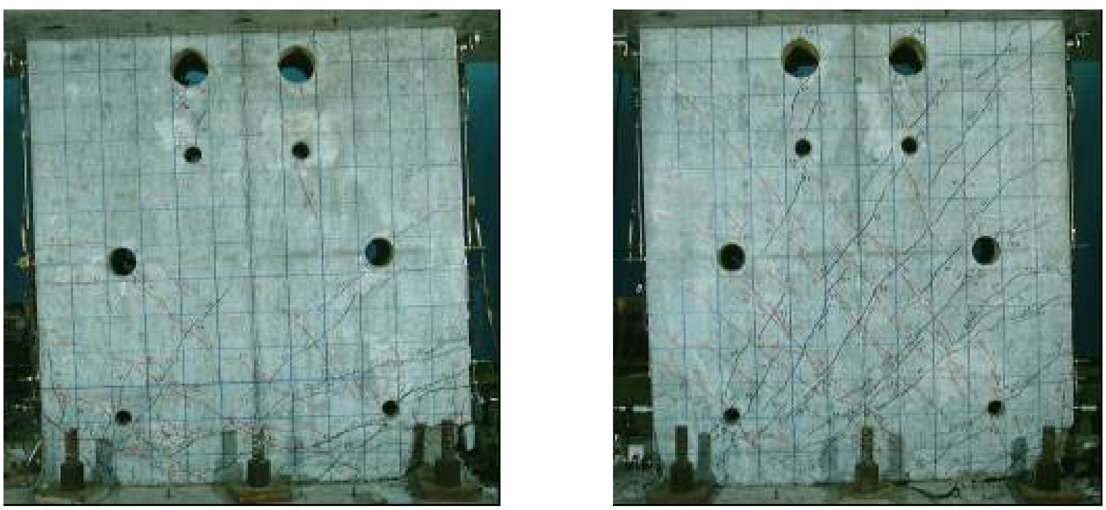

a) No.1　　　　b) No.2

Photo 1: Damage condition under the drift angle of +1/30

5. TEST RESULTS

The load-deformation relation and the damage condition under the drift angle of +1/30 are shown in figure 4 and photo.1, respectively. No.1 showed the stable manner till the drift angle of +1/30rad. after flexural yielding observed at the drift angle of 1/200rad. Afterwards, the main reinforcing bars were buckled, at the unloading from drift angle of 1/30rad., and when it approaches to drift angle of -1/30rad., they broke, and the lateral load capacity decreased in No.1 test specimen. In No.2 test specimen, on the way to drift angle of +1/67rad., the welded part between the main reinforcing bars and embedding plate broke on the moment of yielding of the main reinforcing bars (After the experiment, the bottom stub was shaved for confirmation.) The lateral strength decreased before shear failure. On the contrary, maximum strength greatly exceeded calculated shear strength, which used the material testing result of reinforcement and concrete, and it was 1.36 times in the positive side and 1.31 times in negative. Previous research for the wall columns reported that experimental value of shear strength exceeded calculated value by more than 1.4 times (Hiraishi, et al, 1992). By the outcomes of this experiment, shear strength can be evaluated to be safe even if ultimate strength was calculated without the consideration of opening effects. And every specimen showed no clear progress or collapse of cracks around openings until the drift angle of 1/30rad. Each of them showed the failure mechanism, which was the spalling out of concrete from confinement area in wall columns toe. It is presumed that openings of these specimens don't affect a lot on the stress transfer mechanism of wall columns. And the test result showed that the deformation capacity of these specimens is more than drift angle of 1/50rad. These results are equivalent to drift angle of deformation capacity rank 1 of a no opening wall column. The cracking widths both at the peak of loading and in unloading to the drift angle of 1/100 were measured by "a crackscale". As a result, the cracking widths of drift angle of 1/100rad. at the peak of loading and in unloading were 0.75mm-0.1mm in No. 1, and 0.7mm-0.01mm in No.2. The numerical values were less than residual cracking width (0.3mm) regulated as the serviceability limit. The result shows that the influence on the cracking width would be small when the specimen has openings.

6. CONCLUSION

The following results were derived from this study. The deformation capacity of wall columns with small openings is more than drift angle of 1/50rad. Shear bearing is more than 1.31 times as much as calculated shear strength without consideration of openings.

7. ACKNOWLEDGEMENT

The authors express their sincere thanks and appreciation to the members of the R/D committee for medium and high-rise framed-wall reinforced concrete structure with flat beams for their excellent experimental studies.

8. REFERENCES

H. Hiraishi, et al. (1992). Evalution of seismic capacity of wall columns in high-rise reinforced concrete frame structures, *Journal of Structural and Construction Engineering, Architectural Institute of Japan (AIJ)*, No.439.

SESSION B-4: AXIAL FAILURE OF COLUMNS

Chaired by

♦ James Jirsa and Hitoshi Tanaka ♦

AN ECONOMICAL AND EFFICIENT METHOD OF STRENGTHENING REINFORCED CONCRETE COLUMNS AGAINST AXIAL LOAD COLLAPSE DURING MAJOR EARTHQUAKE

Toshimi Kabeyasawa[1],

Akira Tasai[2] and Shun'ichi Igarashi[3]

ABSTRACT

A new method of strengthening reinforced concrete columns against axial failure was developed and verified through seismic tests. The purpose of the strengthening was specially focused on the maintenance of axial load capacity to prevent total collapse of a structure under very large lateral deformation of the columns. A total of eight specimens, which represents reinforced concrete columns designed by the old building code of Japan or Turkey, were tested under constant gravity load and cyclic lateral load. Some of the columns were strengthened using polyester sheet by which the cost of retrofit would remarkably be reduced from existing technology. The columns strengthened by the new method could maintain the relatively high gravity load until more than ten percent inter-story drift, which was ten times or more than that of the specimen without strengthening. A series of axial tests on concrete prisms and cubes confined with the sheet in various types were also tested, based on which the hysteresis relations and axial load resistance mechanism of the columns were interpreted. It may be concluded from the tests and analysis that the new method is efficient, effective, economical and ready for use in seismic retrofit of existing buildings.

1. INTRODUCTION

A lot of casualties have been caused due to the collapse of building structures even by recent major earthquakes in the countries with advanced earthquake engineering technologies. Although research themes in earthquake engineering are being oriented to innovative technology for new structures, continuous efforts are still important to reduce loss-of-life by developing an economical way of retrofit for existing buildings. To prevent the casualties due to structural failure during major earthquakes, it is primarily important to maintain capacity

[1] *Earthquake Research Institute, The University of Tokyo.*
Email: kabe@eri.u-tokyo.ac.jp
[2] *Yokohama National University*
Email: sanada@eri.u-tokyo.ac.jp
[3] *Square Inc, Japan*
Email: kura@kenken.go.jp

of the column against gravity load even in the cases that the response would exceed the limit state expected from design earthquake intensity. In some cases of old reinforced concrete buildings, the columns would not be capable of bearing the gravity load at the earthquake induced displacement due to inadequate amount of confining hoops or shear reinforcement. In these cases, the buildings would collapse in the weak story or totally like so-called pancake, which have been still observed after recent earthquake disasters. The development of an economical and simple strengthening method would be very worthwhile to prevent these brittle columns from the gravity load collapse. In this paper, a new method of strengthening reinforced concrete columns against axial failure was developed and verified through seismic tests on the column specimens[1]. The purpose of the strengthening was specially focused on the maintenance of axial load capacity of the columns until the excessive lateral deformation induced by seismic loads.

2. TEST ON CONFINED PRISMS AND CUBES

The concrete prisms or cubes confined with the polyester sheet were tested to investigate the basic stress-strain relation of confined concrete. The thickness and number of layers of the sheet were varied systematically. The concrete prism and cube were made using the same concrete with column specimens, the compressive strength of which was 18.25MPa. The height was 300mm commonly and the shapes of the base were also varied as: (a) R-type, rectangular of 210 mm×75mm, (b) S-type, square of 150 mm×150mm, and (c) C-type, circular with diameter of 150mm. The prism and cube specimens with the sheet layers are shown in Figure 1.

The thickness of the used sheets was 0.5mm(A), 0.9mm(B) and 1.2mm(C). The number of the sheet layers was varied as 1, 2, 3 for 0.5mm(A), 2, 3 for 0.9mm(B), and 2 for 1.2mm(C). The results from the tensile test of the sheets were listed in Table 1. The measured strengths were a little less than the nominal strengths. The observed elongation strain at the maximum strength were in proportion to the thickness varying from 0.11 to 0.21, whereas the nominal value is commonly 0.15. The observed stress strain relations were shown in Figure 2.

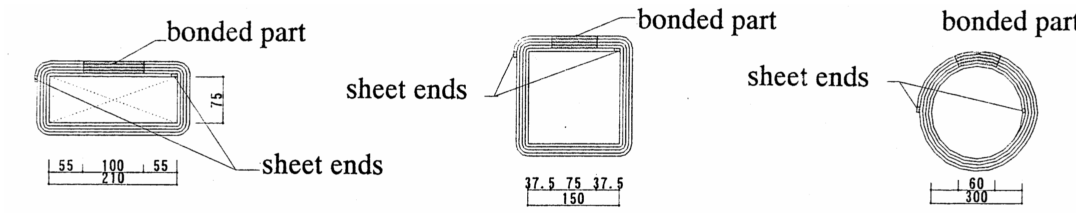

(a) rectangular R-type **(b) square S-type** **(c) circular C-type**

Figure 1 Prism and cube specimens confined with sheet

Table 1 Results of the tensile test of the polyester sheet

Mark	Thickness (mm)	Weight (g/m^2)	Nominal Strength (N/mm)	Nominal Elongation Strain	Measured Strength (N/mm)	Measured Elongation Strain
A	0.50	310	105	0.15	90	0.11
B	0.90	550	183	0.15	164	0.14
C	1.20	860	278	0.15	263	0.21

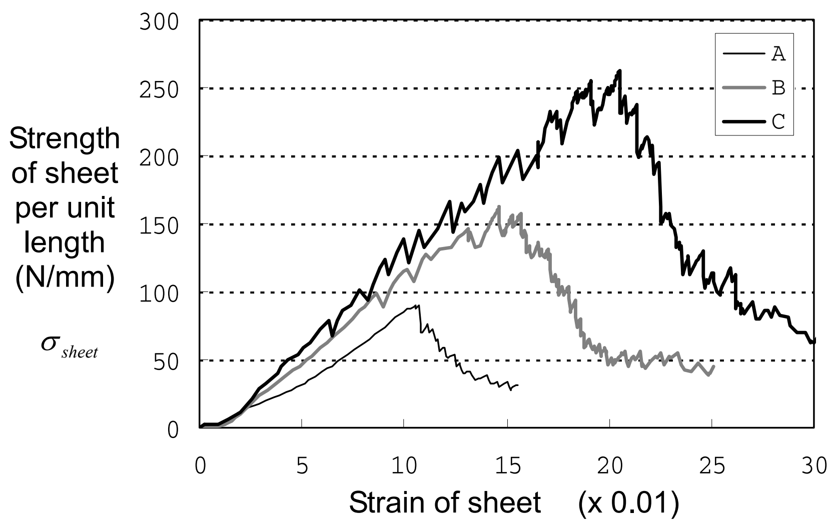

Figure 2 Tensile stress-strain relations of the polyester sheet for strengthening

The stress strain relations from the compression tests of the prisms and cubes are shown in Figure 3. The specimens failed in compression at the first peak strains of 0.003 to 0.007. The specimens without sheet failed after the peak. The axial stress of the specimens with sheet decreased after the first peak down to 5 MPa to 15 MPa at the strain of 0.01 to 0.05, and then recovered gradually with progress of the axial strain. The stress reached the second peak up to 30 MPa at the strain of 0.1 to 0.3, where the sheet ruptured with a vertical gap.

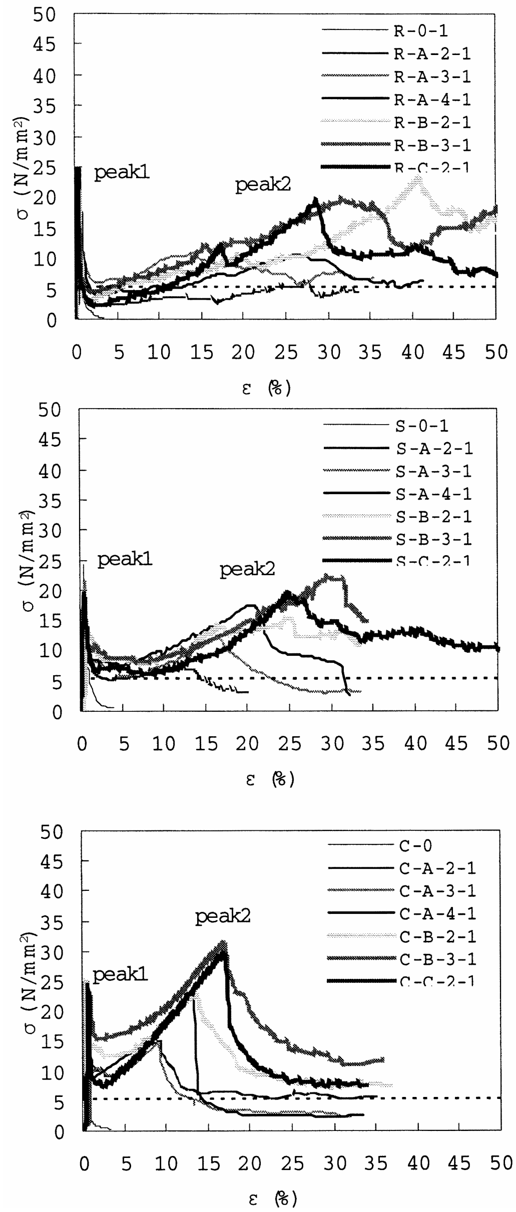

Figure 3 Compressive stress-strain relations of the prisms confined with equivalent sheet ratios

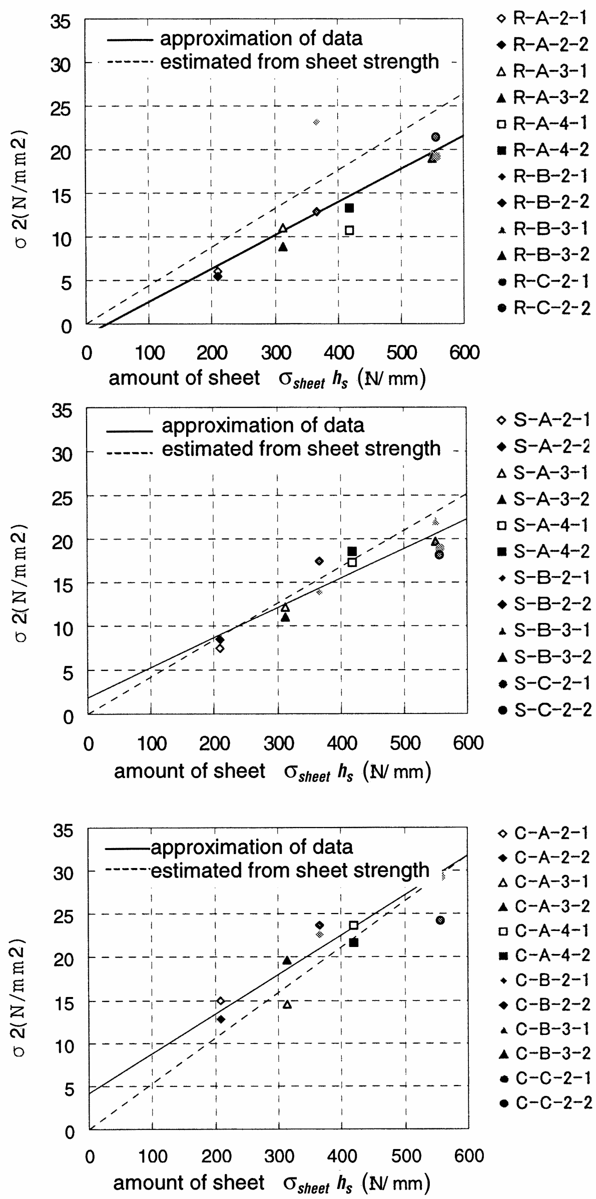

Figure 4 Relations of the second peak strengths and the amount of sheet

The measured strengths were analyzed with the amount of the sheet, which is the sheet strength measured from the tensile test and multiplied with number of layers. The amount sheet was not effective to the first peak strength (σ_1), which was determined essentially by the unconfined concrete strength. The second peak strength (σ_2) had clear relations with the amount of the sheet, as shown in Figure 4, where the horizontal axial is the amount of the sheet in . The observed second peak strength were in proportion to the amount of the sheet regardless of number of layers in case of each specimen types (R, S, C). The increment of the second peak strength to the amount of the sheet was almost equal in cases of R, rectangular, and S, square, whereas it was 1.6 times larger generally in case of C, circular. The least square linear relations were shown in solid lines in the figures.

The relations were analyzed as follows reflecting the amount of the sheet and the shapes of the specimens. The normal stress for expansion or passive confinement stress σ_ℓ can be related with the measured second peak stress σ_2 as:

$$\sigma_\ell = k \cdot \sigma_2 \qquad (1)$$

Under the normal stress of σ_ℓ in the cube with the radius of r_e, the passive tensile stress of the sheet per unit thickness in the tangential direction are in the form as:

$$\sigma_{sheet} = \cdot\, r_e \cdot \sigma_\ell \,/\, h_s \qquad (2)$$

where, h_s is the sheet thickness, therefore $\sigma_{sheet}\, h_s \cdot$ is the sheet strength per unit height. From the equations (2) and (3), the observed peak can be related to the amount of the sheet introducing the effective factor α on the effective working stress of the sheet:

$$\sigma_2 = \frac{\alpha}{k \cdot r_e} \cdot \sigma_{sheet}\, h_s \qquad (3)$$

If simply α=1.0 and k =1/4 are assumed, the dashed line for the cube (type C) could be derived from above equation, which is a fair approximation for the measured strengths. As for the rectangular (type R) and square (type S) prisms, the same values were assumed and the effective radius was defined simply replacing the section as equivalent circular, which has the same peripheral length of the rectangular and the square, resulting: r_e= 90.7mm or 210mm x75mm rectangular, r_e =95.5mm for 150mm×150mm square. The approximation was also shown in Figure 4 with dashed lines, where a fair correlation can be derived, although a slight overestimate is observed especially in cases of rectangular specimens. In that case, the effective factor α may be introduced, for example α = 2/3 with k = 1/4, for the estimation of the lower bounds.

3. METHOD OF THE COLUMN TEST

Tested were eight one-half scale reinforced concrete column specimens, five of which were strengthened using polyester fiber sheet, as listed in Table 2 with sectional dimensions, reinforcement details and sheet strengthening details. The two types of column sections for the specimens were designed representing those in old buildings in Turkey or Japan: A-type was rectangular section of 420mm×150mm with 1260mm height based on Turkish style, as shown in Figure 5 and B-type was square section of 300mm×300mm with 900mm height in Figure 5(b) based on Japanese code before 1971. The specimens were subject to constant axial load and cyclic anti-symmetric bending and shear. Therefore, the shear span ratio was 1.5 for both types. Two methods of the sheet confinement were used as shown in Figure 6: (a) Norimaki (Rolled-Sushi) type by the sheet width of the inner column height in the paste state and (b) Bandage-type for obliquely winding sheet of the 30cm width to the test specimen, which became equivalent to three layers. The polyester fiber sheet can be wound to the column by manpower, and the parts of the sheet were bonded each other by the epoxy urethane adhesive. An original and innovative feature in the method, which is different from the conventional strengthening, such as with carbon fiber sheet, is that the sheet is deliberately unbonded to the concrete surface so that the sheet would be prevented from local rupture with inelastic deformation of the concrete column. The strengthening could be finished within one hour for a specimen, which was very easy, although curing time of about 24 hours was required afterwards.

The specimens A-2, A-4, and B-2 were strengthened with sheet before the loading test, while the specimens A-3, A-5, B-3 were subjected to seismic loading without strengthening and damaged to some extent, and then strengthened with sheet and subjected to seismic loading again up to larger deformation. The latter method simulated the case of utilization in the post-earthquake quick strengthening. The degree of the damage at the first loading was that the shear crack width is progressing and the lateral and axial load capacity started to decay. The axial load was once released for strengthening. For the specimens A-3 and B-3, the horizontal displacement was restored to the origin, whereas A-5 was strengthened with relatively large residual displacement.

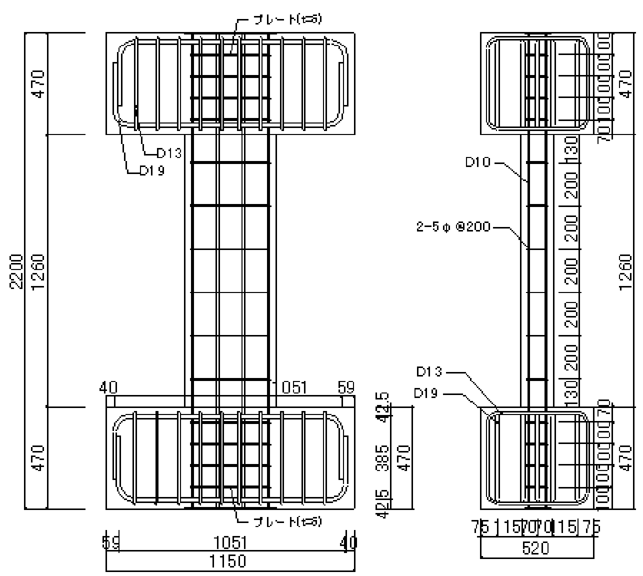

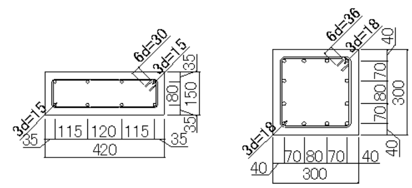

(a) Turkey-type (b) Japan-type

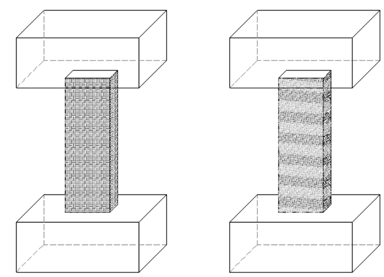

(a) Norimaki-type (b) Bandage-type

Figure 5 Dimensions and reinforcement detail of the specimens

Figure 6 Confinement method

Table 2 List of the specimens with sectional dimensions and strengthening methods

Specimen	Size (mm)	Axial Load (kN)	Main bar (MPa)	Hoop (MPa)	Sheet strengthening		
					stage	layers	type
A-1	420*150 H=1260	334	8-D10 p_g=0.009 (σ_y=349)	5φ@200 p_w=0.0013 (σ_y=289)	-	-	-
A-2					before test	4	Norimaki
A-3					after damage*	3	Bandage
A-4					before test	2	Norimaki
A-5					after damage**	3	Bandage
B-1	300*300 H=900	477	12-D13 p_g=0.017 (σ_y=338)	5φ@160 p_w=0.0008 (σ_y=289)	-	-	-
B-2					before test	4	Norimaki
B-3					after damage*	3	Bandage

* strengthened after damage without residual deformations
** strengthened after damage with the relatively large residual deformation

The target strength of concrete was 17.65 MPa (180kgf/cm^2), while the compressive strength s_c from the cylinder test was 18.25 MPa at the strain of 0.0021. The initial Young modulus was 29GPa. Deformed bars of D10 and D13 (SD345) were used for the main bars and rolled bar of 5ϕ for hoops. Yield strengths from the material test were 349, 338 and 289 MPa for D10, D13 and 5ϕ, respectively. The nominal tensile strength of the polyester fiber sheet was 278 N/mm with thickness of 1.2mm, whereas the strength from the tensile test result was 263N/mm at the strain of 0.21, as shown in Figure 3. Anti-symmetric cyclic seismic load was applied with the constant axial load N: N=333kN for type A and N=476kN for type B, both of which co*rresponded* to the axial force ratio of about 0.3 for the gross section of the column A_c, i.e., $N/(A_c s_c)=0.3$.

4. RESULTS OF THE COLUMN TEST

The specimens A-1 and B-1 without sheet could not bear the axial force and horizontal force after the shear cracking and succeeding typical tensile shear failure at relatively small drift angles. The maximum crack width was 5.0mm for A-1 and 11mm for B-1 at the final stage. On the other hand, in the final states of the specimens A-2 and B-2 strengthened with sheet shown in Photo 1, the axial deformation progressed up to 240mm, the axial strains of 0.18 for A-2 and 0.27 for B-2, maintaining the constant load, where the stroke of the vertical jacks reached their limits. The relationship between the shear force Q and the horizontal displacement d of A-1, A-2 and B-1, B-2 are shown in Figure 7 and Figure 8, respectively.

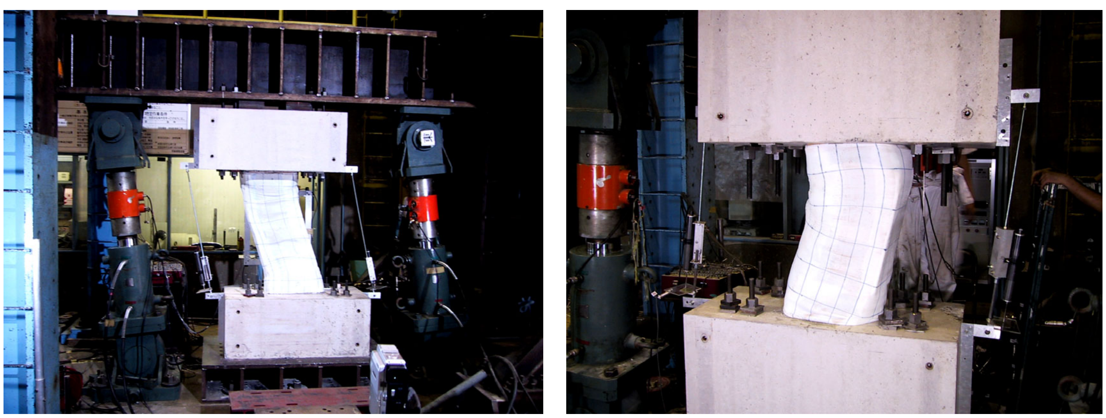

(a) Specimen A-2 **(b) Specimen B-2**

Photo 1. Final states of the specimens with and without sheet

In the specimens confined with sheet, the first brittle behavior was substantially similar to those of the specimens without sheet, although the shear failure was retarded so that the strength and the deformability at the shear failure were also improved slightly. However, the axial load capacity and the lateral load carrying capacity of the specimens with sheet decayed temporarily but recovered with the progress of the axial deformation. Though the axial deformation progressed gradually, the stable behavior was observed under the constant axial load of 0.3.

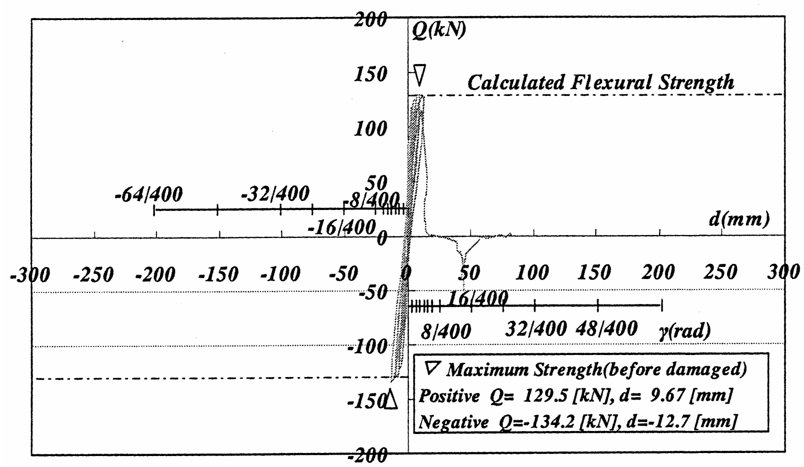

(a-1) Specimen A-1 without sheet

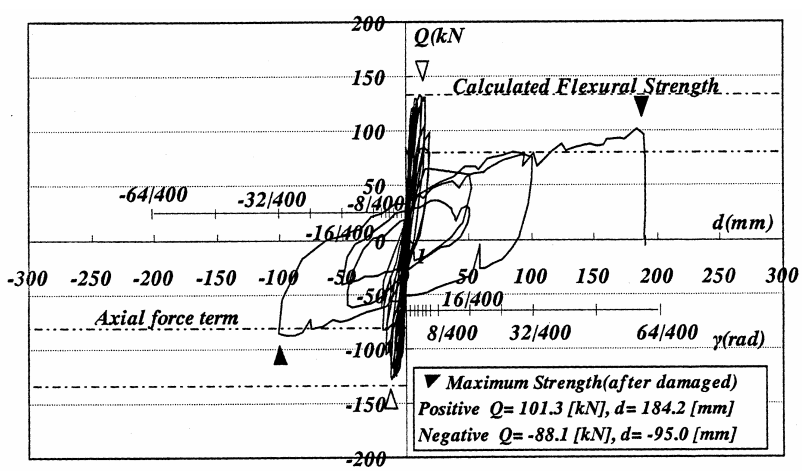

(a-2) Specimen A-2 with sheet

Figure 7 Hysteresis relations between shear force and lateral displacement

The relations between the axial force and the axial deformation are shown in Figure 9. Compared for the A type specimens, the specimen A-1 without sheet could support only half of the constant load N at maximum after the shear failure, whereas for the specimen A-2 with sheet, the force decreased down to 0.6N, but recovered at the axial strain of 0.07 and could support the constant load until the end of testing. As for the B type, more stable behavior was observed such that the axial load reduced to 0.8N but recovered at the axial strain of 0.08 and was sustained until the end of testing without decay.

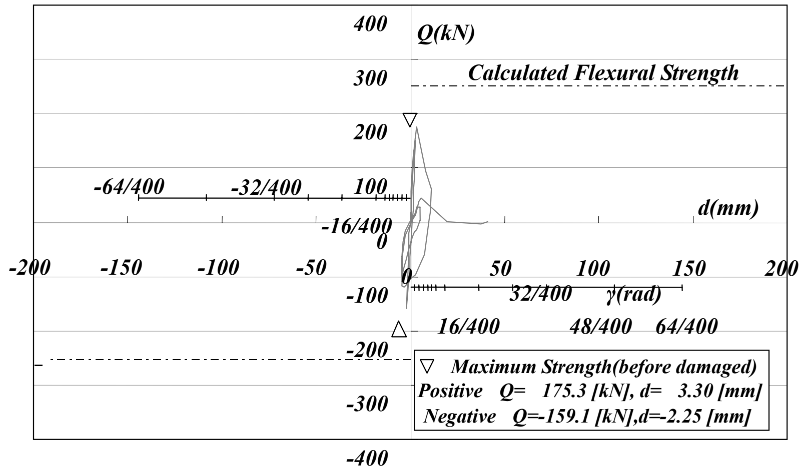

(b-1) Specimen B-1 without sheet

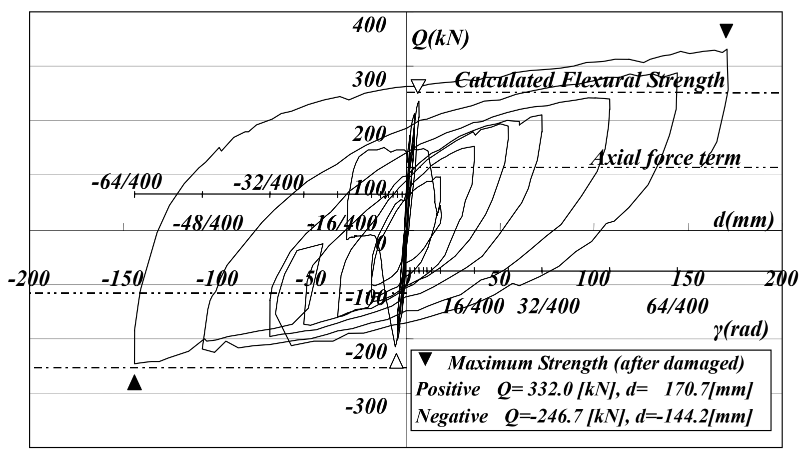

(b-2) Specimen B-2 with sheet

Figure 8 Hysteresis relations between shear force and lateral displacement

Figure 10 shows the hysteresis relations of the specimen B-3, which was strengthened after the shear cracking was generated. The lateral resistance recovered gradually up to 100(kN) as in the case of the specimen B-3 with the progress of the axial deformation. The specimen B-3 with the bandage type, the sheet ratio of which was equivalent to three layers, maintained the axial force until the end of testing, therefore, it may be concluded that the three layers would be sufficient.

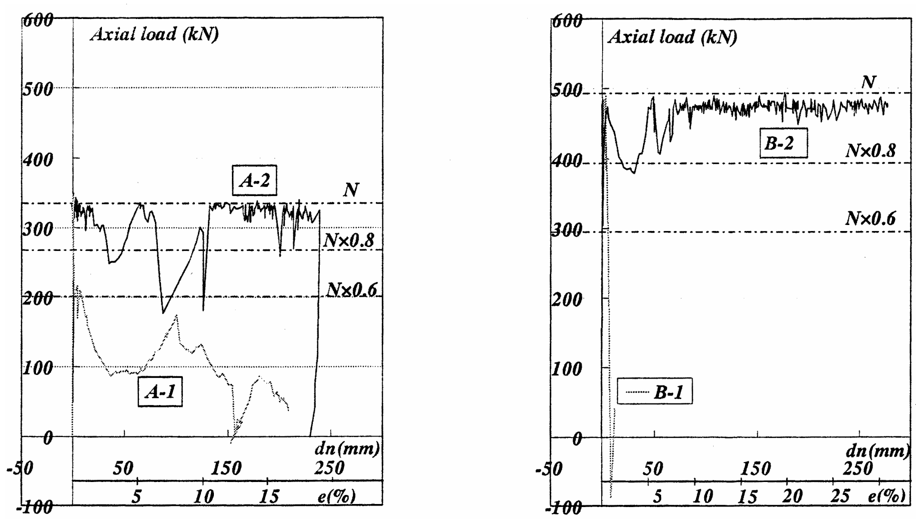

(a) Specimen A-1 and A-2 **(b) Specimen B-1 and B-2**

Figure 9 Axial load and axial deformation

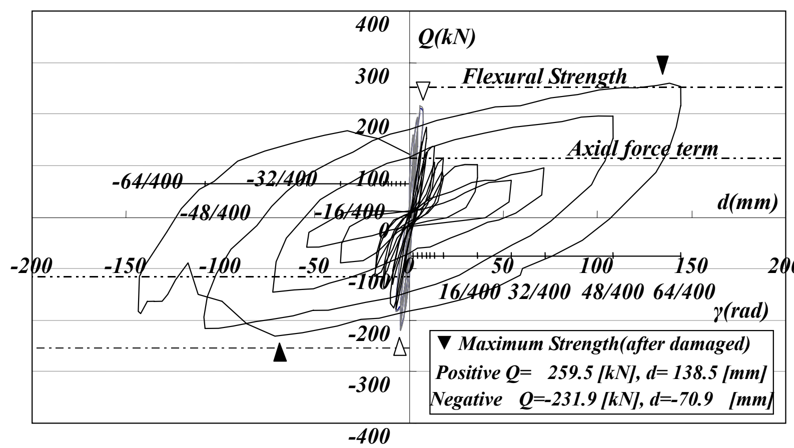

Figure 10 Hysteresis of Specimen B-3 strengthened after shear cracking

As for other A-type specimens with sheet, the effect of the sheet was not so remarkable as in the specimen A-2, though the specimen A-3 maintained axial force stably up to 16/400 rad. and the specimen A-4 up to R=8/400 rad. The unstable behavior beyond these drifts was due to the local rupture of the sheet at the end region, and the accidental out-of-plane deformation which were observed clearly in case of A-type with rectangular section. As for the specimen A-5, the control of displacement after shear failure was poor by which the large residual

deformation was produced up to R=10/400. The strengthening and reloading was done with the residual deformation so that the stable behavior was not observed.
The elongation of the sheet along the perimeter was measured at the peak of loading cycles. The elongation strains tends to be larger up to 0.10 in the end regions for both A and B types, whereas the elongation strain in the mid-height of A type remains within 0.02. The elongation of the sheet became remarkable after shear cracking, and rapidly progressed when the axial force reduced temporarily. The elongation strain of the sheet was around 0.10 for both-types of specimens, even in the case that the rupture of the sheet was observed. On the other hand, the maximum tensile strength was measured at 0.21 in the tensile test of the sheet as shown in Figure 3. This indicates that the sheet still had the allowances averagely and the rupture occurred locally.

5. EXAMINATION OF CAPACITY

Flexural capacity and shear capacity were calculated for the specimens without sheet based on the design equation[3], which are illustrated in the restoring force characteristics in Figures 7 and 9. The contribution of the axial force term (=0.4ND, D: column depth) to the calculated flexural capacity is also shown in the figure. The calculated shear strengths for both A and B types were lower than the flexural strengths. However, the specimen A-1 failed in shear right after yielding, while B-1 failed before yielding. The observed shear capacity was higher than the calculated.

The observed behavior of the specimen with sheet after shear failure may be interpreted based on the stress-strain relation of prism with sheet by the uniaxial compression test shown in Figure 4. Effective compressive strength of the concrete strut decreased after the initial shear fracture so that the horizontal resistance decreased. Effective compression strength of the concrete recovered with the increase of the axial deformation and peripheral strain. The sheet also worked effectively for the shear resistance mechanism, while the axial deformation was stabilized. The horizontal resistance was limited by flexural capacity, because the shear strength was sufficiently provided by the sheet. As for the A-type specimens, the main reinforcing bars buckled so that the main bars were not effective to the flexural strength and the horizontal resistance force was equivalent to the contribution of axial force. As for the B-type, which was stable against out-of-plane deformation, the main bar was thick so that the flexural strength could be expected to recover approximately close to the calculated value with the effective main bars. One of the reasons why the strength could be higher than the calculated maximum was that the shear span became smaller due to the large axial compressive deformation.

6. CONCLUSIONS

A new method of strengthening columns in existing reinforced concrete buildings was developed using the polyester fiber sheet. The effectiveness was verified through the static loading test on the column specimens and the prism test, from which the following conclusions could be drawn.

(1) The stress-strain relations of prism confined with sheet showed ductile behavior after the first peak of unconfined concrete. The second peak stresses were clearly proportional to the amount of sheet, which can be estimated fairly based on the passive confinement.
(2) The columns specimens strengthened with sheet failed in shear after shear cracking similarly to the specimens without sheet. However, as for the specimens with sheet, the lateral resistance and the axial load capacity were recovered remarkably with the progress of axial deformation, while those of the specimens without sheet decayed rapidly after the shear failure.
(3) The sheet strengthening improved the deformation capacity up to the lateral drift of about R=64/400 rad. under relatively high constant axial load ratio of 0.3.
(4) In the B-type specimens with square cross section, the strengthening was generally more effective on the strength and deformability than in the case of the B-type specimens with rectangular cross section.
(5) Both confinement details, Norimaki-type and Bandage-type, were effective. The post-damage strengthening was effective as well as the pre-damage strengthening, if the residual deformation was not large.
(6) The failure of the specimens with sheet was mainly due to the local rupture at the end

regions, in case that occurred. Therefore, it would be more effective to provide the sheet densely in the hinge region.

It was verified that the strengthening method using the polyester sheet was surprisingly effective to the maintenance of the axial load capacity and could be applied in practice as an economical, effective and efficient way of retrofit. Further studies are needed, such as development of rational calculation method for the minimum amount of sheet to ensure required deformation capacity, and experimental and analytical verification on the overall behavior of the structure strengthened with the sheet.

ACKNOWLEDGEMENT

The tests were conducted in the Structural Testing Laboratory at Yokohama National University. Cooperative works of Mr. Hiroshi Koizumi formerly with ERI, Ms. Yasuko Osugi, ERI, Mr. Daichi Tanabe and Mr. Rei Tamura, YNU, in the tests and the data analyses are gratefully acknowledged. The strengthening method reported herein has been international patent pending by Square Inc., Japan.

REFERENCES

[1] Koizumi, H., Kabeyasawa, T., Tasai, A., Igarashi, S., “A study on sheet strengthening reinforced concrete columns against axial load collapse during major earthquake (in Japanese),” Proceedings of the Japan Concrete Institute, Vol. 23, July 2001.

[2] Tanabe, D., Osugi, Y., Tasai, A., Kabeyasawa, T., “Effect of sheet strengthening on the axial ductility of reinforced concrete columns at large lateral drift (in Japanese),” Proceedings of the Japan Concrete Institute, Vol. 23, July 2001.

[3] Architectural Institute of Japan, “*AIJ Design Guidelines for Earthquake Resistant Reinforced Concrete Building Structures Based on Ultimate Strength Concept,*” 1990.

KEYWORDS

gravity load bearing capacity, seismic strengthening, reinforced concrete building, polyester sheet, confinement, deformation capacity, collapse, life safety.

THE USE OF A SEISMIC DAMAGE PARAMETER IN PERFORMANCE-BASED EARTHQUAKE ENGINEERING OF CONCRETE BUILDINGS

Mario E. Rodriguez

National University of Mexico
Mexico City, Mexico
Email: mrod@servidor.unam.mx

US-Japan Workshop in PBEE for Reinforced Concrete Buildings, Seattle, August 17-18, 2001

ABSTRACT

This paper describes, with emphasis on performance-based earthquake engineering concepts, a seismic damage parameter previously proposed in the literature. This paper also explores the use of this parameter for performance-based seismic design of reinforced concrete buildings.

INTRODUCTION

Several earthquakes during the last decade have shown the need of revising traditional procedures for earthquake-resistant design of structures. This has lead to several attempts of using performance-based engineering concepts. Examples of application in the USA of these concepts are ATC-40 (1996) and FEMA 273-274 (1997). Typically, these documents are based on the use of capacity and demand diagrams. The capacity of a structure is obtained using non-linear static analysis procedures. The seismic demands are obtained by estimating peak displacements of a building using any of several methods for the evaluation of peak displacement response of the analogous non-linear single-degree-of-freedom (SDOF) system. These methods have been described and are discussed in detail elsewhere (Freeman, 1978; Chopra and Goel, 1999; Fajfar, 1999; Aschheim and Black, 2000).

Several shortcomings of the use of capacity and demand diagrams have been discussed in the literature (Krawinkler, 1995; Chopra and Goel, 1999; Fajfar, 1999). In particular, it has been shown that the use of elastic design spectra for equivalent linear systems leads to unconservative estimation of seismic deformation of inelastic structures (Chopra and Goel, 2001). Also, as in usual seismic design procedures, the capacity and demand diagrams ignore the effect of multiple inelastic cycles that a structure is subjected to during an earthquake. It is of interest that some attempts have been made in the literature to consider earthquake duration in usual seismic design procedures (Fajfar, 1992).

It must also be pointed out that the aim of performance-based seismic design is controlling damage and loss of function of structures during earthquakes. In addition, it has been emphasized that "there are may uncertainties associated with the generation of site-specific input and with the analytical models presently employed to represent structural behavior" (Gupta and Krawinkler, 2000). It follows that it would be desirable to have a seismic design procedure that is simple and based on a direct measure of damage. This paper explores the use of such a measure in performance-based earthquake engineering of concrete buildings and is based on the use of a seismic damage parameter previously proposed by the author (Rodriguez, 1994; Rodriguez and Aristizabal, 1999).

PROPOSED SEISMIC DAMAGE PARAMETER

The reader is referred elsewhere (Rodriguez, 1994) for a detailed derivation of the proposed seismic damage parameter I_D. Only a brief description of this derivation, emphasizing some concepts related to performance-based seismic design, is given in the following.

The force-deformation relation of a non-linear multistory structure represented by an equivalent SDOF system is shown in Fig 1. The ordinates correspond to the resistance function R* per unit of equivalent mass M* and the abscissas correspond to the roof displacement δ (Rodriguez, 1994). The natural circular frequency of the equivalent SDOF system is ω^*, which is assumed to be equal to the natural circular frequency ω of the analogous SDOF system. The equivalent SDOF system reaches a maximum displacement ductility ratio μ_m, which is defined as

$$\mu_m = \frac{\delta_m}{\delta_y} \qquad (1)$$

where δ_m and δ_y are the maximum and yielding roof displacements, respectively. It is also assumed that μ_m and the displacement ductility ratio of the analogous SDOF system, μ, are equal. The hysteretic energy per unit of equivalent mass dissipated by the equivalent SDOF non-linear system is defined as E^*_H.

The parameter δ_d shown in Figure 1 is defined as the maximum roof displacement in the multistory building associated with an acceptable building performance during an earthquake. Figure 1 shows the force-deformation relationship of an equivalent SDOF elastic system with the same dynamic parameters as those of the equivalent SDOF non-linear system, and with a maximum roof displacement equal to δ_d. Also, the parameter E^*_λ shown in Figure 1 is defined as the total energy per unit of equivalent mass that the equivalent SDOF elastic system absorbs in a complete cycle ($+\delta_d$ and $-\delta_d$). This energy is evaluated as

$$E^*_\lambda = \omega^{*\,2}\,\delta_d^2 \qquad (2)$$

The proposed parameter I_D is defined as

$$I_D = \frac{E^*_H}{E^*_\lambda} \qquad (3)$$

The physical meaning of I_D can be thought of as the number of complete cycles in the equivalent SDOF elastic system (when forced to displace to its extreme acceptable roof displacement $+\delta_d$ and $-\delta_d$) that are required for absorbing an amount of energy equal to the hysteretic energy E^*_H.

It is of interest to note that since E^*_λ is explicitly related to a building displacement, the definition of I_D involves not only a ratio of energy terms in a structure (Equation 3) but also involves important building displacements as shown later. While I_D is a ratio of energy terms involving building displacements, the well known Park and Ang (1985) damage parameter (I_{PA}) is a linear combination of displacement terms and hysteretic energy in a SDOF system as can be seen in the Park-Ang equation, which is given by

$$I_{PA} = \frac{u}{\mu_u \, u_y} + \beta \, \frac{E_H}{F_y \, \mu_u \, u_y} \qquad (4)$$

where u is the actual dynamic displacement, u_y is the yield displacement, and μ_u is the ultimate ductility factor under monotonic loading. F_y is the lateral strength of the system, and E_H is the dissipated hysteretic energy. The parameter β is a constant that depends on structural characteristics.

It is of interest to discuss another form of Equation (3) that was proposed in the original derivation of the parameter I_D. In this other form of Equation (3), D_{rm} is the maximum roof drift ratio in a multistory building subject to an earthquake ground motion, and is defined as

$$D_{rm} = \frac{\delta_m}{H} \qquad (5)$$

where H is the height of the building. Also, D_{rd} is defined as the maximum acceptable roof drift ratio in a building associated to an acceptable building performance in an earthquake.

The alternative expression for I_D in Equation (3) is defined as (Rodriguez, 1994):

$$I_D = \gamma^2 \left(\frac{D_{rm}}{D_{rd}} \right)^2 \qquad (6)$$

where γ is given by:

$$\gamma = \frac{1}{\mu} \sqrt{\frac{E_H}{F_y \, u_y}} \qquad (7)$$

The parameter γ is a normalized hysteretic energy coefficient and has also been used by Fajfar (1992) for a seismic design procedure considering the effect of cumulative seismic damage. Values of γ up to 2 have been reported in the literature when analyzing several strong input ground motions (Fajfar, 1992; Rodriguez, 1994). According to Fajfar (1992), γ is a relatively stable parameter. It follows that the ratio D_{rm}/D_{rd} is of relevant importance for evaluating the proposed parameter I_D. If D_{rd} is assumed constant, the above finding and equation (6) indicate that I_D would be directly proportional to D_{rm} squared, which suggests the importance of controlling displacements for minimizing seismic damage.

To illustrate the use of parameter I_D, Figure 2 (Rodriguez and Aristizabal, 1999) shows results of the evaluation of this parameter for the following records. The record obtained in the soft soil area of Mexico City during the 1985 earthquake (SCT), Sylmar (SYL) record obtained in the 1994 Northridge earthquake, and Kobe-JMA record obtained in the Kobe earthquake in 1995 (KOB). The last two records are considered representative of near-fault ground motions, which are characterized by a pulse with very high energy input.

In the results shown in Figure 2 parameter D_{rd} was assumed equal to 0.01. Global drift ratio D_{rm} was calculated assuming several values for μ, a participation factor for the first mode equal to 1.5, and an interstory height, h, equal to 2.7 m. In the evaluation of D_{rm} the building height H of analyzed buildings was assumed equal to nh, where n is the number of floors in a building. Parameter n was related to the fundamental period of the building, T, with the following approximated equation

$$n = T\ \lambda \qquad (8)$$

where λ is a parameter that generally depends on the type of structural system and on the amplitude of seismic excitation.

Typically, when using Equation (8) for RC frame buildings on hard soils subjected to small amplitude seismic excitation the parameter λ is taken equal to 10. This parameter is reduced to a factor $10/\sqrt{2}$ when considering that during earthquakes the lateral stiffness reduces to one half of initial lateral stiffness. In addition, for buildings on soft soil such as those of Mexico City, the soil-structure interaction (SSI) problem should be considered. Bazan et al (1992) have shown that the seismic response of SSI systems can be obtained using seismic response results of the fixed-base case with a SSI period equal to1.3T. With this finding the above mentioned value of λ reduces to 5.5, which was used for obtaining the I_D values for the SCT record shown in Figure 2.

For the I_D values corresponding to the Sylmar record shown in Figure 2, it was considered that the analyzed buildings were frame or dual systems and λ was assumed equal to $10/\sqrt{2}$. For the Kobe-JMA record it was considered that the analyzed buildings were structural wall systems and λ was assumed equal to $20/\sqrt{2}$.

It is relevant mentioning that a good correlation has been observed between overall building damage during several studied earthquakes and parameter I_D (Rodriguez and Aristizabal, 1999).

It is of interest that a plot of I_D as a function of fundamental period and the corresponding hysteretic energy spectra have similar shapes. The implication of this property is that maximum demands of hysteretic energy of an analogous SDOF system around a characteristic period also correspond to maximum demands of parameter I_D in a building around the same period. For example, Figure 2 shows that peak I_D demands for the SCT record correspond to structures around a characteristic period equal to 2.0 sec.

THE USE OF THE PROPOSED SEISMIC DAMAGE PARAMETER IN PERFORMANCE-BASED EARTHQUAKE ENGINEERING OF CONCRETE BUILDINGS

An interesting feature of parameter I_D is that it explicitly considers earthquake duration in a simple way. This is taken care of by parameter γ. This feature is ignored in current approaches for performance-based earthquake engineering such as those used in ATC-40 (1996) and FEMA 273-274 (1997). It is of interest that Fajfar (1992) has proposed using approximate values of the parameter γ for defining equivalent displacement ductility factors which consider earthquake duration and that can be directly used in usual design procedures.

In addition to earthquake duration, parameter I_D uses maximum building displacement (D_{rm}) and maximum acceptable building displacement (D_{rd}). This gives grounds for proposing the following procedure of performance-based seismic design of buildings.

In a first step, appropriate values of parameters μ and D_{rd} are defined by relating these parameters to a target performance level. For instance, it is commonly assumed that design provisions in the Uniform Building Code (1997) correspond to a Life Safety performance level associated to a ground motion having 10% probability of exceedance in 50 years. In this case, appropriates values for μ and D_{rd} that correspond to this performance level should be used.

A second step in the proposed design procedure is assuring that the selected ground motion be representative of the target earthquake hazard.

Finally, appropriate target values of parameter I_D also must be selected. Parameter I_D has been evaluated for 15 records, considering simplistic approximations for the evaluation of the seismic response of typical, regular RC multistory buildings and assuming only one value for D_{rd} (Rodriguez and Aristizabal, 1999). The results of this evaluation suggest values for I_D that correspond to several performance levels depending on the selected value for D_{rd} . To arrive at reliable values of I_D for use in a seismic design procedure a more complete calibration of I_D is needed considering a larger set of earthquake records, different levels of acceptable maximum building displacements, and several structural systems.

CONCLUSIONS

A seismic damage parameter previously proposed in the literature has been used in this paper as a basic tool for a proposed performance-based seismic design of reinforced concrete buildings. In this approach important parameters involved in the seismic response of buildings are considered. These are maximum displacement demand and maximum acceptable displacements in a building, as well as earthquake duration. The later parameter is not considered in existing procedures of performance-based seismic design of RC buildings such as those in ATC-40 (1996) and FEMA 273-274 (1997). Further studies are needed for defining specific values of the proposed seismic damage parameter and corresponding involved parameters in order to relate these parameters and selected performance levels.

REFERENCES

Aschheim, M. and Black E.F., 2000. Yield point spectra for seismic design and rehabilitation. Earthquake Spectra, Vol 16 (2), 317-335.

ATC 40, 1996, Seismic evaluation and retrofit of concrete buildings, California Seismic Safety Commission, Report SSC 96-01, Applied Technology Council, Redwood City, CA.

Bazan E., Diaz-Molina I., Bielak J., and Bazan N., 1992. Probabilistic Seismic Response of Inelastic Building Foundation Systems. Proc. Tenth World Conf. on Earthquake Eng., Madrid, Spain, Vol 3, 1559-1565.

Chopra A.K., and Goel R.K., 1999. Capacity-Demand-Diagram methods based on inelastic design spectrum. Earthquake Spectra, Vol 15 (4), 637-656.

Chopra A.K., and Goel R.K., 2001. Direct displacement-based design: Use of inelastic vs elastic design spectra. Earthquake Spectra, Vol 17 (1), 47-64.

Fajfar, P., 1992. Equivalent ductility factor, taking into account low-cycle fatigue. Earthquake Engineering and Structural Dynamics. Vol. 21, 837-848.

Fajfar, P, 1999, Capacity Spectrum method based on inelastic demand spectra. Earthquake Engineering and Structural Dynamics, Vol 28, 979-993

FEMA 273, 1997, NEHRP Guidelines for the Seismic Rehabilitation of Buildings, FEMA, Washington, DC

FEMA 274, 1997, NEHRP Commentary on the Guidelines for the Seismic Rehabilitation of Buildings, FEMA, Washington, DC

Freeman, S, 1978, Prediction of response of concrete buildings to severe earthquake motion. Douglas Mc Henry International Symposium on Concrete and Concrete Structures, ACI Special Publication 55, ACI, Detroit, MI

Gupta, A. and Krawinkler, H., 2000. Estimation of seismic drift demands for frame structures. Earthquake Engineering and Structural Dynamics, Vol 29, 1287-1305

International Conference of Building Officials (ICBO), 1997. Uniform Building Code, CA

Krawinkler, H. 1995. New trends in seismic design methodology. Proc 10th European Conference on Earthquake Engineering, Vol 2, Balkema, Rotterdam.

Park, Y.J., and Ang, A., 1985. Mechanistic seismic damage model for reinforced concrete. Journal of Structural Engineering, ASCE 111, 722-739

Rodriguez, M. 1994. A Measure of the Capacity of Earthquake Ground Motions to Damage Structures. . Earthquake Engineering and Structural Dynamics, Vol 23, No 6, 627-643.

Rodriguez, M. and Aristizabal, J.C., 1999. Evaluation of a seismic damage parameter. Earthquake Engineering and Structural Dynamics, Vol 28, 463-477.

.

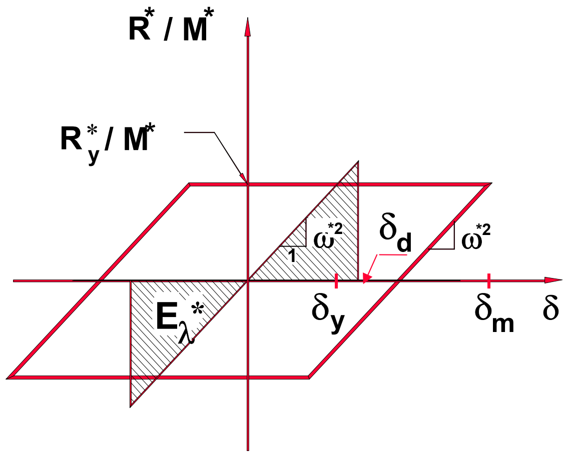

Figure 1. Force-deformation relations for a non-linear and equivalent linear structure

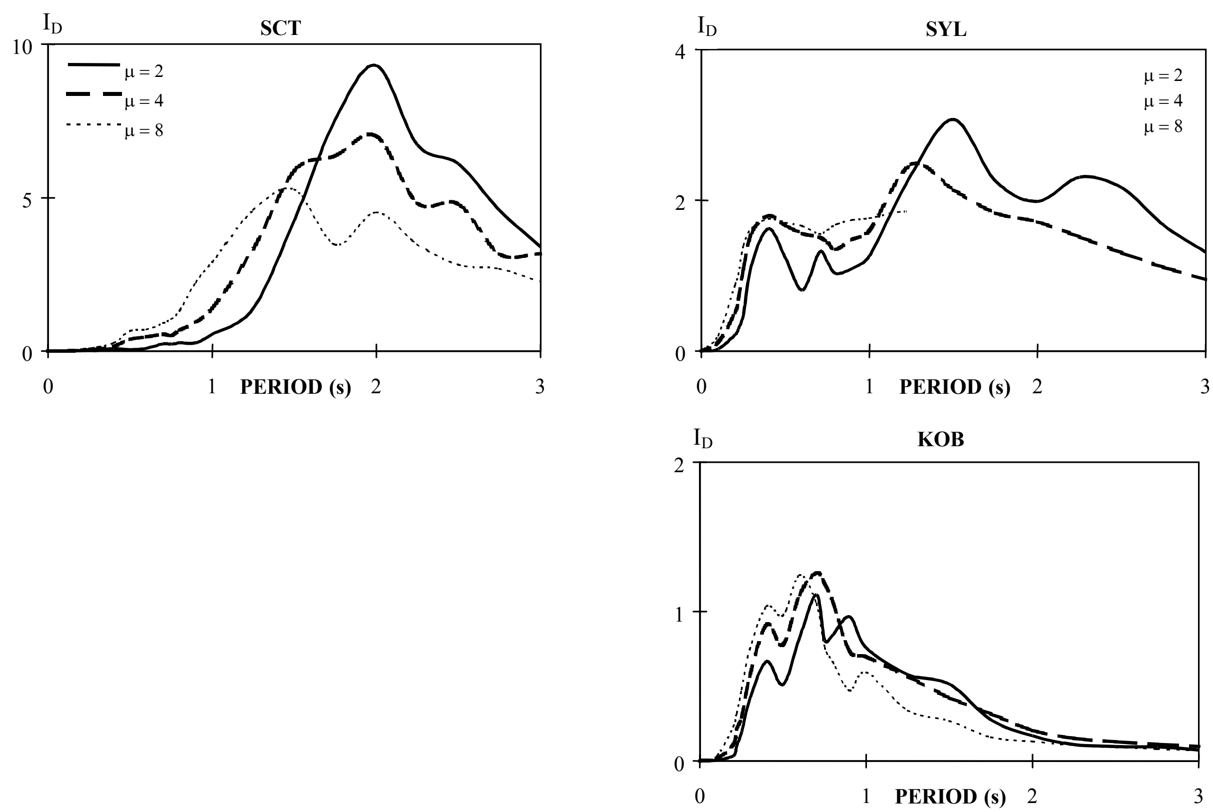

Figure 2. Measure of seismic damage for SCT, SYL, and KOB records

SHAKE TABLE TESTS ON THE GRAVITY LOAD COLLAPSE OF REINFORCED CONCRETE FRAMES

K. J. Elwood and J. P. Moehle[1]

ABSTRACT

While collapse is recognized as an important limit state in most performance-based earthquake engineering methodologies, work is needed on understanding the process by which collapse occurs and developing tools to accurately predict collapse. The study described herein provides insight into some of the factors influencing the collapse of reinforced concrete frames during earthquakes. Data from shake table tests are presented and compared with results of an axial failure model.

1. INTRODUCTION

Experimental research and post-earthquake reconnaissance have demonstrated that reinforced concrete columns constructed in the western United States prior to seismic building code changes in the mid-1970's are vulnerable to shear failure during earthquakes. Such damage can also lead to a reduction in axial load capacity, although this process currently is not well understood. The resulting redistribution of gravity loads to the neighboring elements may play a role in progressing the collapse of the building frame. Shake table tests were conducted in an effort to investigate the process of column shear and axial load failures and the effect such failures have on the rest of the building frame.

The project described herein is limited to the study of two-dimensional frames. Obviously, out-of-plane frames and slab systems will contribute to the capacity of a building to resist gravity load collapse, however, the response of two-dimensional building frames must be well understood before the whole building system can be realistically considered. This study is further limited to reinforced concrete frames with columns that can be characterized by a low ductility capacity and a brittle shear failure mode. The shear failure is accompanied by significant lateral strength degradation, and may be followed by a loss of axial load capacity.

[1] *Pacific Earthquake Engineering Research Center, U.C. Berkeley, CA, USA*
Email: moehle@peer.berkeley.edu

"Short" columns or piers, characterized by a brittle shear failure prior to yielding of the longitudinal reinforcement, are not directly considered in this study.

2. DESIGN OF SHAKING TABLE TESTS

2.1 Specimen Design and Construction

Shake table tests were designed to observe the process of dynamic shear and axial load failures in reinforced concrete columns when an alternative load path is provided for load redistribution. The test specimens comprised three columns fixed at their base and interconnected by a beam at the upper level (Figure 1). The central column had wide spacing of transverse reinforcement to result in shear and axial load failure of that column during testing. As the central column failed, shear and axial load would be redistributed to the adjacent ductile columns.

Two test specimens were constructed and tested. The first specimen supported a mass of 67 kips, producing column axial load stresses roughly equivalent to those expected for a seven-story building. The second specimen also supported a mass of 67 kips, but pneumatic jacks were added to increase the axial load carried by the central column from 28.7 kips ($0.10f'_cA_g$) to 68.2 kips ($0.24\ f'_cA_g$), thereby amplifying the demands for redistribution of axial load when the central column began to fail.

The shear-critical center column was designed as a one-half scale reproduction of the 9'-8" tall, 18"x18" square-cross-section columns tested by Sezen (2000) and Lynn (1994). From those previous tests, it was expected that the center column would sustain flexural yielding prior to developing shear failure. Axial load failure was expected to be more gradual for the column with low axial load and more sudden for the column with higher axial load. The remaining frame elements (i.e. the beams, outside columns, and footings) were not scaled from prototype designs, but instead were designed to achieve the desired response. Table 1 summarizes the critical properties of the frame specimens illustrated in Figure 1.

For a building containing columns susceptible to combined flexure-shear-axial load failure, as considered in this study, it is reasonable to expect that some components would experience limited yielding before the columns failed in shear. Hence, the outside columns of the frame were designed to yield before shear failure of the center column. Furthermore, preliminary analysis of the frame showed that if the outside columns were allowed to remain elastic, or nearly elastic, then the lateral response of the frame following shear failure of the center column would only entail elastic vibration of the remaining intact elements. This response did not seem realistic for such an extreme loading condition and was not of interest to the current study. To achieve the desired response, the outside columns were designed to have a yield displacement and yield moment approximately equal to two-thirds of those of the center column.

Table 1: Properties for Shake Table Test Specimens

f'_c (columns and beam, Specimen 1)	3.56 ksi
f'_c (columns and beam, Specimen 2)	3.47 ksi
f_y (center column longitudinal bars)	69.5 ksi
f_y (outside column longitudinal bars)	61.5 ksi
f_y (center column transverse bars)	100 ksi
Mass	67 kips
Center column axial load (Specimen	28.7
Center column axial load (Specimen	67.2
ρ_l (center column)	2.5 %
ρ_l (outside column)	2.0 %
ρ_h (center column)	0.18%

A circular section with closely spaced spiral reinforcement was chosen for the outside columns in order to ensure the columns were capable of resisting large ductility demands without any threat of axial failure. This choice of section also provided a more gradually yielding load-displacement relationship compared with a square section, a desirable characteristic since the three-column frame is intended to represent part of a larger building frame which would also be expected to have a gradually yielding load-displacement relationship.

Once the strength and stiffness of the outside columns were chosen, capacity design procedures were used to design the beams and footings. Pushover analyses were conducted to displacements corresponding to three levels of damage to the center column (i.e., just before shear failure, just after shear failure, and after axial load failure) to determine the critical demands for the beams. Due to the lack of analytical tools to accurately model the shear failure of reinforced concrete components, the shear failure was crudely modeled by removing the lateral stiffness of the center column once a specified shear demand (corresponding to shear failure) was reached. The demands after axial failure of the center column were roughly determined by "pushing" the frame, modeled without a center column, to a displacement ductility greater than 6 (equal to the maximum displacement ductility observed to cause axial load failure in the columns tested by Sezen (2000)). To ensure all of the damage is concentrated in the columns, the estimated column strengths were multiplied by 1.5 for the pushover analyses (resulting in higher demands in the beams), and a very conservative strength reduction factor of 0.5 was used in the design of the beams and footings.

Since the bending stiffness of the beam will influence the shedding of axial load after failure of the center column, the beam stiffness must be appropriately chosen. For this purpose, a seven-story building in Van Nuys, California (described in detail in Browning et al. (2000)) was used as the prototype building. After axial failure of a column, a longitudinal frame of the building could be approximately modeled as shown in Figure 2. If each of the floors is considered identical in stiffness and load, then the columns continuing above the failed column will carry zero axial load and the deflection of the second story at point A can be approximated by considering only the beams, columns and loads of the second story as shown in Figure 2. The deflection of point A using such a model is approximately 0.18 inches.

The stiffness of the beam in the three-column frame was selected to give an equivalent scaled deflection of 0.09 inches after axial failure of the center column for the first test specimen. The width of the beam was chosen as 5 feet to provide support for the 50 kips of lead mass required to achieve the appropriate axial stress in the center column. The beam reinforcement was selected such that the ratio of the yield strength of the beam to the maximum moment demand from plastic analysis after axial failure of the center column was 0.63 for the Specimen 1 and 1.22 for Specimen 2.

Particular attention was paid to the connection between the 5' wide beam and the columns. The moment developed over the width of the wide beam must be transferred to the narrow columns. A similar condition arises in buildings with wide beams due to restricted story heights or one-way joist systems. Transverse torsional beams were provided, as shown in Figure 1, to ensure the moments could be transferred without torsional cracking of the beam.

The test specimens were constructed in an upright position in a casting site adjacent to the earthquake simulator. Reinforcement cages were assembled and instrumented with strain gauges. Normal-weight aggregate concrete (nominal maximum aggregate size of 10 mm) was cast in two lifts. Specimens were wet-cured for 14 days and then stored in the laboratory until testing (age at testing was 151 days for Specimen 1 and 184 days for Specimen 2). Companion cylinders were stored with the specimens and were tested near the day of the shaking table tests according to ASTM procedures. Resulting mean compressive strengths are in Table 1.

2.2 Test Setup

Each test specimen was moved to the earthquake simulator prior to testing. Because it was important to track the redistribution of horizontal and vertical load from the central column to the side columns, the specimens were supported on force transducers that monitored axial load, shear, and moment (Figure 1). Specimens were aligned with the intended shaking direction on top of the force transducers and bolted in place after placement of hydrostone to ensure a level surface. Specimens were shored while lead weights (total of 67 kips) were placed to simulate gravity loads and inertial mass. The lead weights were supported at one end on a steel shim to fix the position and on the other end by a rubber shim to allow deformation of the concrete test specimen beneath the lead weights. The weights were then bolted in position so the moved in unison with the test specimen.

The planar frame specimens were to be subjected to unidirectional horizontal base motions. An out-of-plane bracing system was developed to restrain motion out of the plane of the specimen; otherwise the bracing system allowed unrestrained in-plane horizontal and vertical motion.

The two specimens were identical except for the axial load on the columns. Since a mass larger than 67 kips could not be reliably controlled by the shake table, the additional axial load for the second test was attained by prestressing using a pneumatic jack on either side of the center column (Figure 3). The air cylinder of the pneumatic jacks allows the center column to shorten without loosing more than 10% of the prestress load.

Instrumentation consisted of displacement transducers to measure global vertical and horizontal displacements of the mass and local deformations of the center column, accelerometers to measure vertical and horizontal accelerations of the mass, strain gages on selected reinforcing bars, and the force transducers under each column as discussed previously.

2.3 Base Motion

Both specimens were subjected to one horizontal component from a scaled ground motion recorded during the 1985 Chile Earthquake (Figure 4). Several factors led to the selection of this ground motion record. First, the record needed enough intensity to fail the center column in shear. Secondly, the maximum displacement ductility demand on the frame needed to be limited to avoid failure of the outside columns. Thirdly, a ground motion of long duration was of interest to observe the mechanics of axial failure while the specimen was still subjected to strong ground shaking. Finally, the choice of ground motion record was significantly restricted by the displacement and velocity capacity of the shake table (5 inches and 25 in./sec, respectively).

3. TEST RESULTS

Selected results from the shake table tests are plotted in Figures 5-8. To aid in understanding the relationships among the plots, symbols have been placed at significant points in the response histories.

The triangular marker indicates the approximate time (16.7 sec) at which the center column shear for Specimen 2 begins to drop off relative to the center column shear for Specimen 1. Also at this time, the center column axial load for both specimens drops by approximately 10 kips. This drop in load coincides with the development of significant cracks in the outside and center columns, and, hence, is thought to be caused by redistribution of gravity loads as the lengths of the columns change owing to flexural response.

The square marker indicates the pulse (at 24.9 sec) that initiates the axial failure of Specimen 2. The continuation beyond this point of the plots in Figure 8 is only possible because an alternative load path was provided and the axial load in the center column could be redistributed to the outside columns. Figures 6 and 7 demonstrate that by the time indicated by the square marker the center column shear capacity for Specimen 1 has only just begun to degrade, while the center column shear capacity of Specimen 2 has degraded to less than one-half of the ultimate center column shear attained. Figure 9 shows the state of both columns at the time indicated by the square marker. At this time, a large shear crack is apparent in Specimen 1, while Specimen 2 has experienced severe local distortions.

The diamond marker indicates the approximate time (29.8 sec) at which the minimum center column axial load is reached for the first time. By this point the center column shear capacity has all but disappeared for both specimens. The center column axial load for both specimens remains nearly constant after this time despite the continuation of strong ground shaking. Figure 10 shows the state of both columns at the end of the tests. It is surprising to many that a column such as that shown in Figure 10a can support 84% of its initial axial load (see Figure 5).

The behavior of the center column during axial failure for Specimen 2 is characterized by the region between the square and the diamond markers in Figure 8. The figure suggests that there are two mechanisms by which the vertical displacements increase: first, large pulses that cause a sudden increase in vertical displacement after a critical drift is attained; and second, smaller oscillations that appear to "grind down" the failure plane. It is interesting to note for the first mechanism discussed above that the axial load drops immediately prior to the sudden increase in vertical displacements, and increases immediately after the increase in vertical displacements. Data such as those presented in Figure 8 are being used in ongoing studies to help understand the mechanisms leading to axial failure.

4. SHEAR-FRICTION AXIAL FAILURE MODEL

4.1 Capacity Model

Moehle et al. (2000) used a shear-friction model to represent the general observation from experimental tests that the drift ratio at axial failure of a shear-damaged column is inversely proportional to the magnitude of the axial load. Considering a free-body diagram of the upper portion of a column under shear and axial load, the classic shear-friction equation from ACI 318 ($V_{sf} = N\mu$), and several simplifying assumptions, Moehle et al. (2000) developed the following equation for the axial capacity of a shear-damaged column:

$$P = \frac{A_{sw} f_y h}{s} \tan\theta \left(\frac{\cos\theta + \mu \sin\theta}{\sin\theta - \mu \cos\theta} \right) \quad (1)$$

where P is the axial load capacity of the column, h is width of the column, θ is the angle of the shear failure plane, μ is the effective coefficient of friction, and A_{sw}, f_y, and s are the area, yield strength, and spacing of the transverse reinforcement, respectively.

Relationships for inclination θ of the shear failure plane versus the magnitude of the axial load, and the effective coefficient of friction μ versus the drift ratio were developed based on experimental data from Lynn (1996) and Sezen (2000). These relationships can be combined with Equation (1) to produce relations among column axial load, column transverse reinforcement, and drift ratio at loss of axial load capacity, as shown in Figure 11. This figure supports the observation from the experimental tests that the drift ratio at axial failure of a shear-damaged column is inversely proportional to the magnitude of the axial load. Note that the curves are not extended beyond drift ratios of 0.01 or 0.06 since the experimental database did not contain results outside this range. While useful as a design chart for determining drift capacities, Figure 11 must only be used with a full appreciation for the accuracy of the results as discussed in Moehle et al. (2000) and the limitation that the results are based on unidirectional, pseudo-static tests.

4.2 Comparison with Shake Table Data

Figure 12 plots the results from the shake table tests along with the drift capacity curve for the center column based on the model discussed above. The high yield strength of the transverse reinforcement wire results in the high transverse reinforcement constant ($(A_{sw}f_y h/s)/P_o$ = 0.039). The maximum drift ratio experienced by the center column was used to plot the data points from the shake table tests shown in Figure 12.

The data point for Specimen 1 lies below the drift capacity curve indicating that the shear-friction model predicts no axial failure for the test column with low axial load. The data point for Specimen 2 lies above the drift capacity curve indicating that the shear friction model predicts that axial failure would occur for the test column with moderate axial load.

Since an alternative load path for the gravity loads is provided in the test specimen, the axial load in the failing center column is not lost all at once (see Figure 8). This makes it difficult to establish a single point to be defined as "axial failure". Hence, there is no confirmation whether the shear-friction model correctly predicts the drift ratio at the instant of axial failure. Further comparison of static test data (Sezen (2000) and Lynn (1996)) to the dynamic test data may help to isolate the point at which axial failure begins.

4.3 Implementation of Shear-Friction Model for Analysis

In its current form the shear-friction model only provides a capacity curve to predict the drift ratio of a column at axial failure. In order to use this model in the analytical prediction of the shake table test results, the model must be implemented in an analytical platform with a complete force-displacement relationship. The OpenSees platform developed at PEER has been selected for this purpose.

A material model is under development, which will detect when shear failure has occurred in the element and then trace the element axial load and drift until the drift capacity curve defined by the shear-friction model has been exceeded (that is, the onset of axial failure). Before axial failure is detected, the axial stiffness of the undamaged column is used (AE/L). How to model the strength and stiffness degradation after axial failure is a subject of ongoing studies, however, Figure 8 suggests that a coupling between horizontal and vertical displacements is necessary.

5. CONCLUSIONS

Shake table tests were conducted to observe the process of dynamic shear and axial load failures in reinforced concrete columns when an alternative load path is provided for load redistribution. The test results show that the axial stress on the column influences the behavior of the column during ground shaking, particularly after shear failure. A column with an axial stress of $0.24f'_c$ failed to maintain its gravity loads, while another column with an axial stress of $0.10f'_c$ only saw minor gravity load redistribution. An axial failure model based on shear friction compared favorably with the test results and is being implemented into an analytical platform.

ACKNOWLEDGMENTS

This work was supported in part by the Pacific Earthquake Engineering Research Center through the Earthquake Engineering Research Centers Program of the National Science Foundation under Award number EEC-9701568. This support is gratefully acknowledged. The experimental studies were conducted in the research laboratories of PEER at the University of California, Berkeley.

KEYWORDS

Reinforced concrete; Buildings; Columns; Shear; Axial load; Collapse; Design; Earthquakes; Experimentation, Shake table

REFERENCES

ACI Committee 318 (1999) *Building Code Requirements for Structural Concrete (318-99) and Commentary (318R-99),* American Concrete Institute, Farmington Hills, Michigan.

Browning, J., Li, Y. R., Lynn, A. C., and Moehle, J. P. (2000) Performance Assessment of a Reinforced Concrete Frame Building, *Earthquake Spectra*, Earthquake Engineering Research Institute, Vol. 16, No. 3, August 2000, pp. 541-555.

Lynn, A. C., Moehle, J. P., Mahin, S. A., and Holmes, W. T. (1996) Seismic Evaluation of Existing Reinforced Concrete Columns, *Earthquake Spectra*, Earthquake Engineering Research Institute, Vol. 12, No. 4, November 1996, pp. 715-739.

Moehle, J. P., Elwood, K.J., and Sezen, H., (2001) "Gravity load collapse of building frames during earthquakes", *Second US-Japan Workshop on Performance-Based Design Methodology for Reinforced Concrete Building Structures*, September, 2000, Sapporo, Japan, PEER report 2001. Berkeley, Calif.: Pacific Earthquake Engineering Research Center, University of California.

Sezen, H. (2000) Evaluation and Testing of Existing Reinforced Concrete Columns, *CE 299 Report*, Dept. of Civil and Environmental Engineering, UC Berkeley.

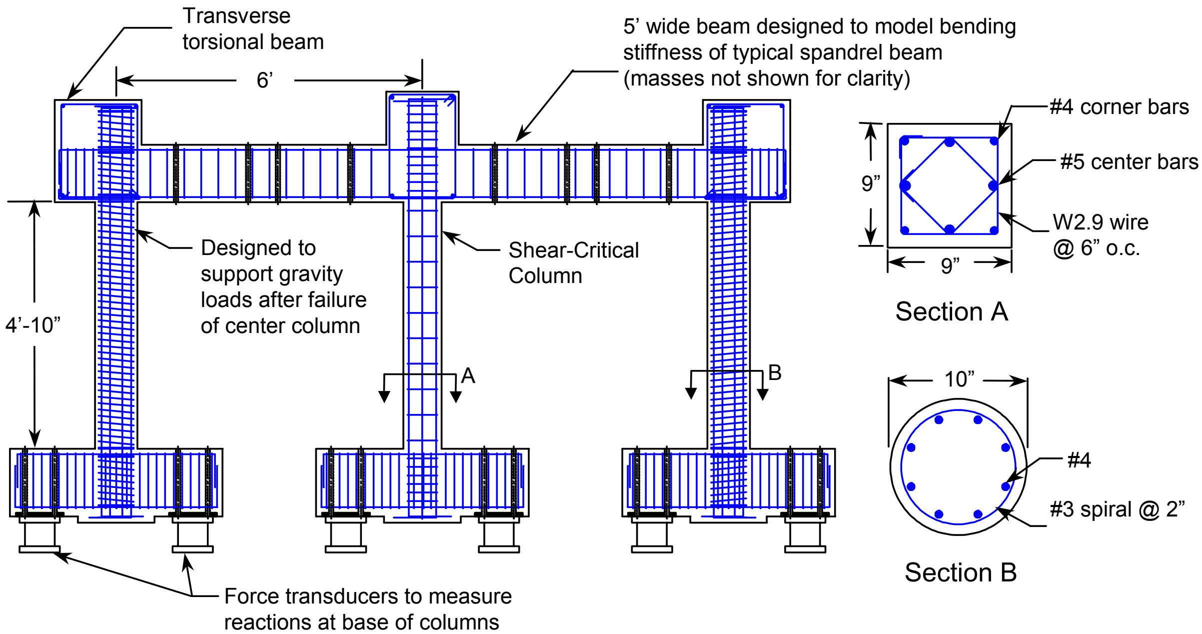

Figure 1: Shake table test specimen

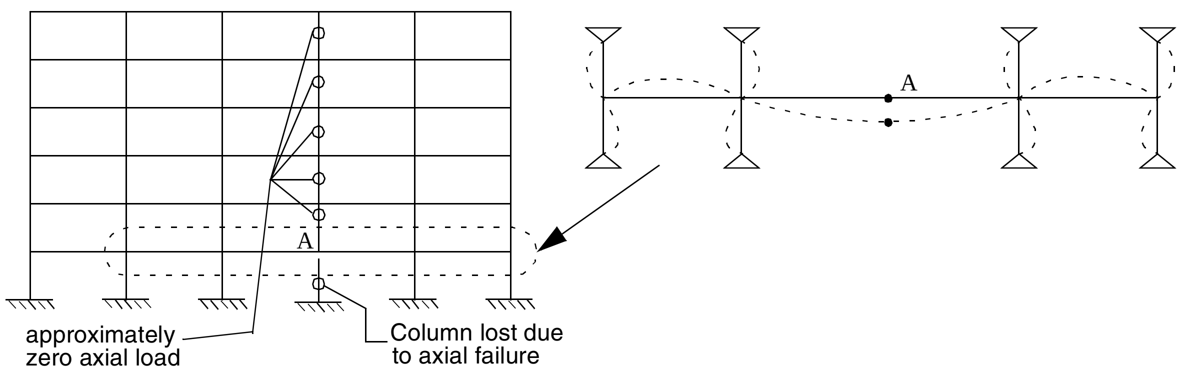

Figure 2: Model for determining beam stiffness

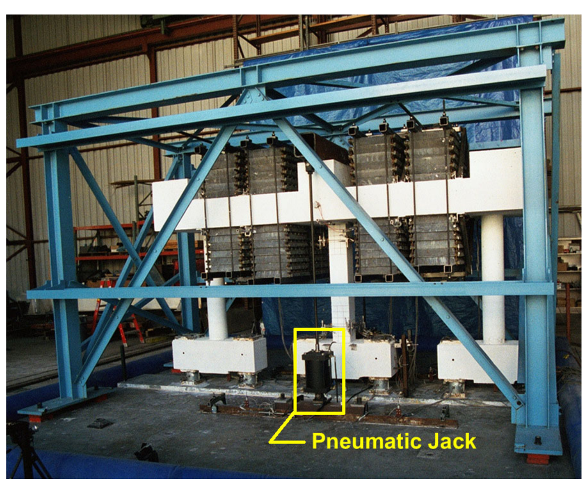

Figure 3: Loaded test specimen on shaking table

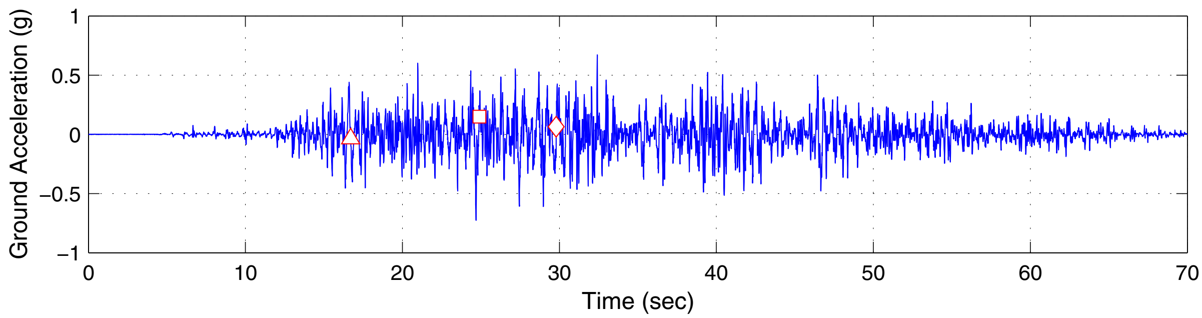

Figure 4: Table acceleration record (scaled Chile, 1985)

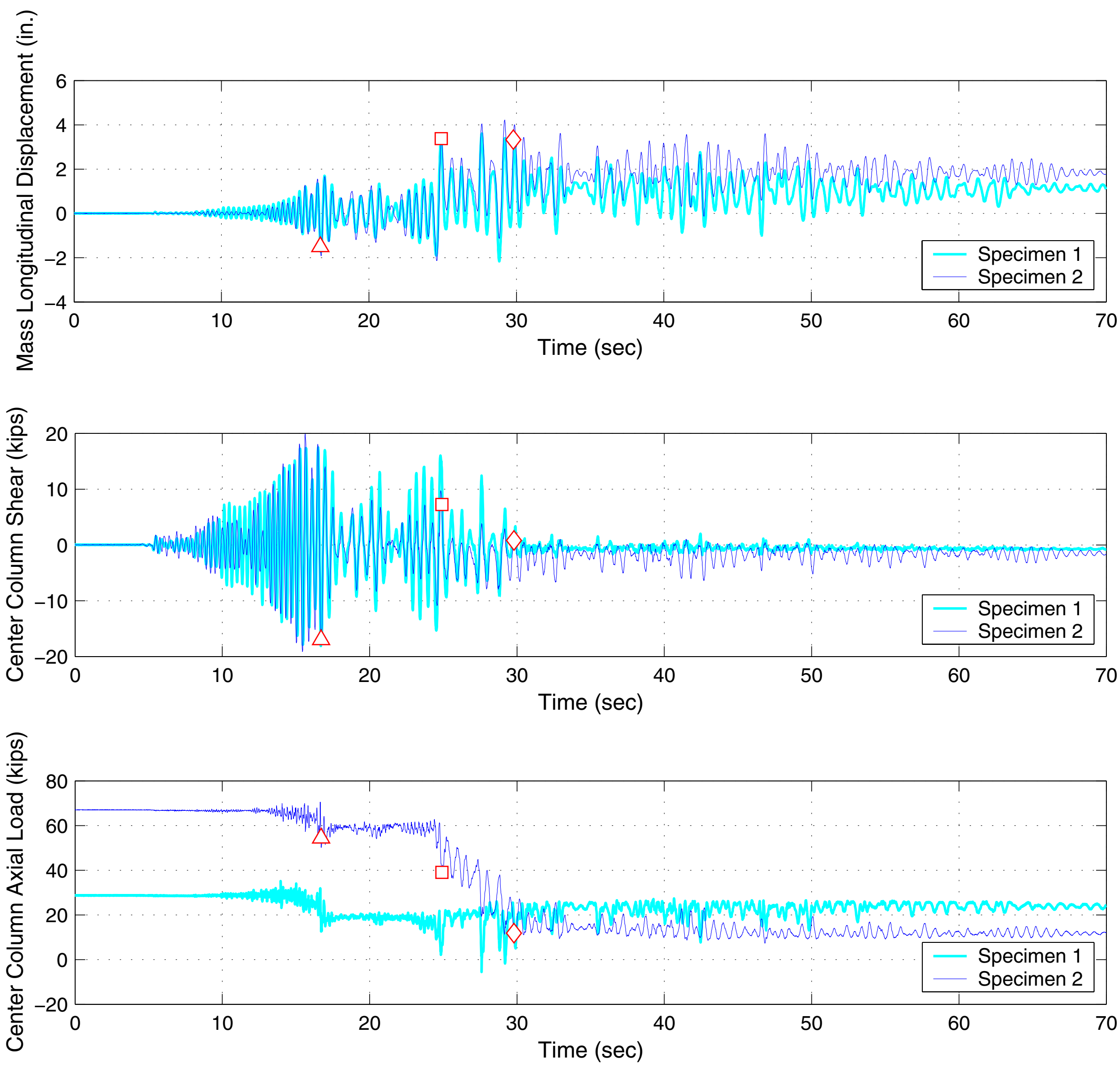

Figure 5: Response time histories for shake table tests
(Specimen 1: *$P = 0.10f'_cA_g$*; Specimen 2: *$P = 0.24f'_cA_g$*)

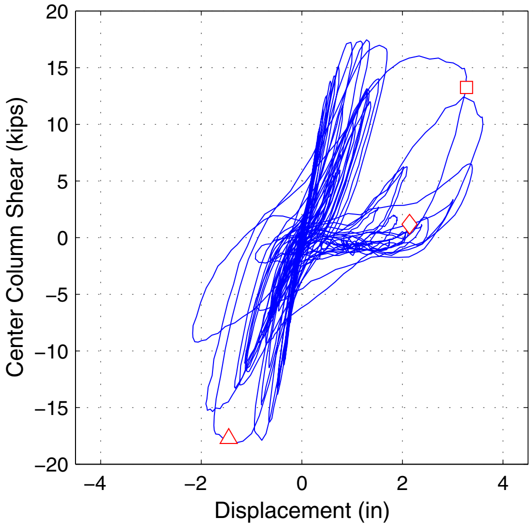

Figure 6: Specimen 1 center column shear hysteretic response

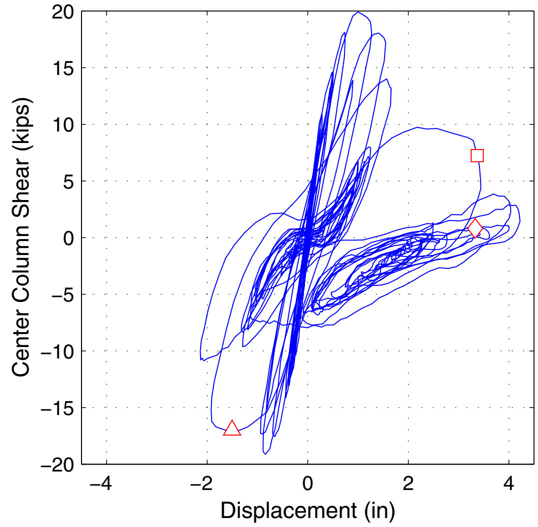

Figure 7: Specimen 2 center column shear hysteretic response

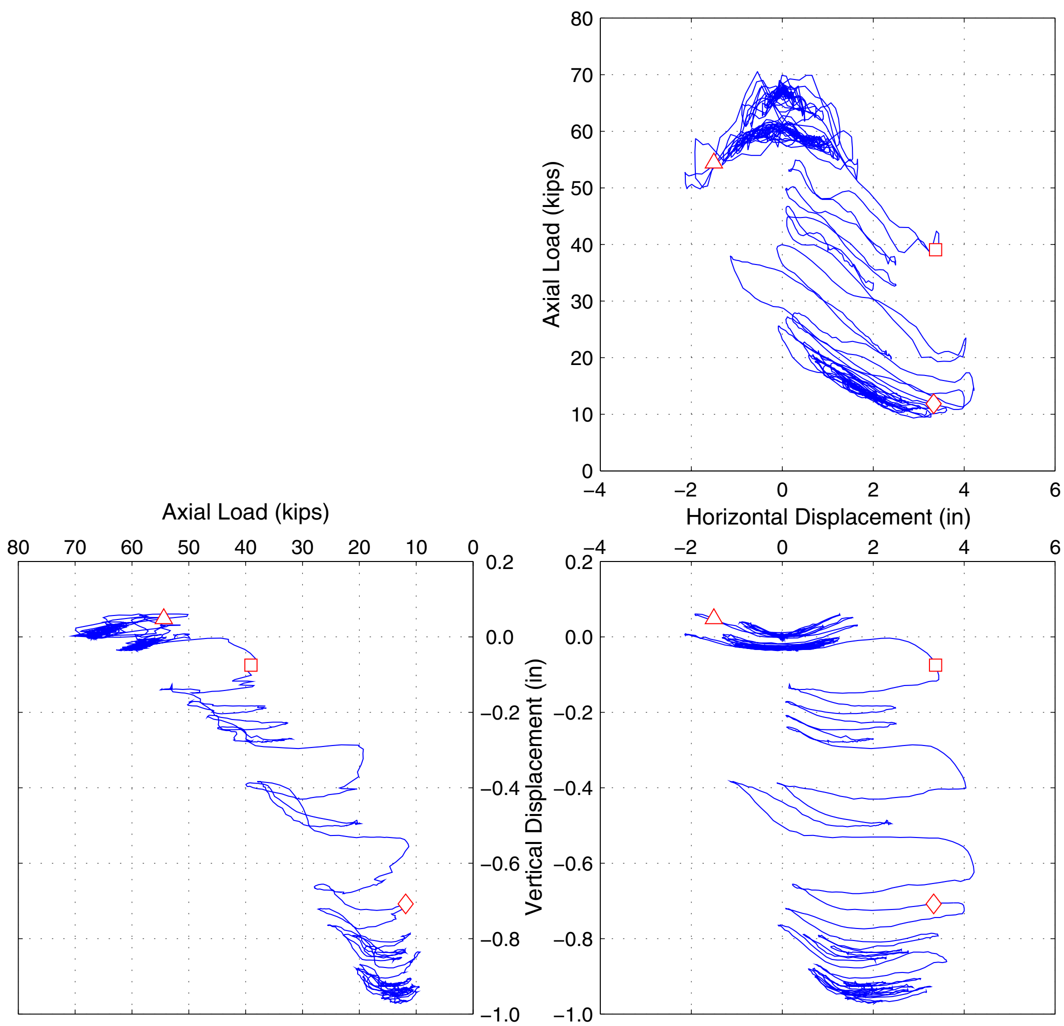

Figure 8: Relations between center column axial load, vertical displacement, and horizontal displacement of top of center column for specimen 2

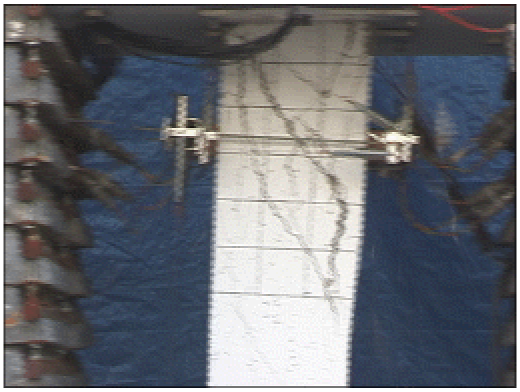

Figure 9a: Top of center column, Specimen 1 at 24.9 sec

Figure 9b: Top of center column, Specimen 2 at 24.9 sec

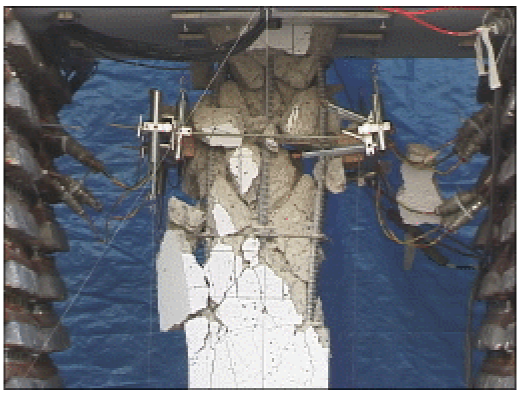

Figure 10a: Top of center column, Specimen 1 at end of test

Figure 10b: Top of center column, Specimen 2 at end of test

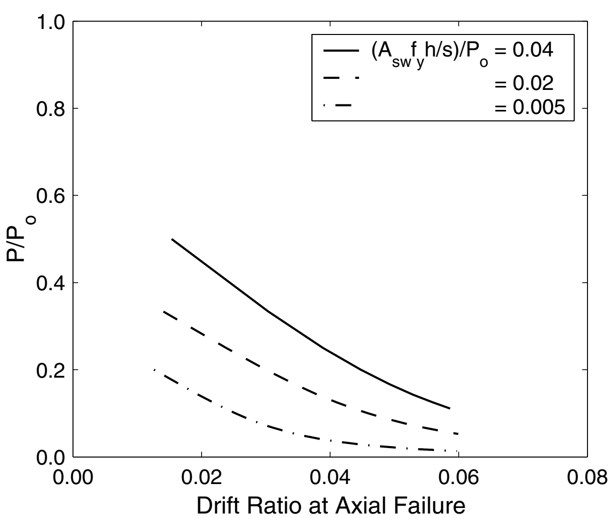

Figure 11: Drift capacity curves based on shear-friction model

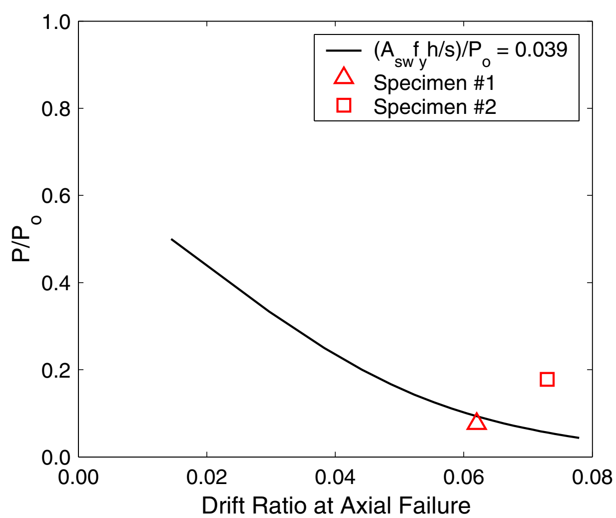

Figure 12: Comparison of shear-friction model with test data

CLOSING PRESENTATION

Chaired by

♦ Anil K. Chopra and Peter Fajfar ♦

THE NEED FOR FIELD DATA IN DEVELOPING PBEE

James O. JIRSA[1]

ABSTRACT

The use of analytical programs to predict the response of structures is gaining acceptance in design offices and for justifying designs to building officials. Programs have been developed for analyzing structures under catastrophic loadings as well as for assessing serviceability. What is missing is a means of verifying the reliability of the analysis. There have been a few structures instrumented in areas affected by severe earthquakes or where severe exposure conditions are encountered but very little useful data is available for calibrating the assumptions on which the analyses are based. Perhaps nowhere is the problem more apparent than in the rehabilitation of existing structures where it is necessary to understand not only the response of the original structure but also the response of the system after rehabilitation. The purpose of this discussion is to examine means by which critical data can be acquired so that performance based engineering can be developed from a sound base of technical data.

1. WHAT HAVE WE LEARNED?

Structural damage and failures that have been observed in the past 20 years illustrate the problems that need to be addressed. Hazards in the large inventory of inadequate buildings in densely populated, industrial regions may be present for a variety of reasons.

- Construction practices dictated by culture and tradition.
- Lack of code provisions addressing key problems—more often the lack of enforcement or adoption of codes that reflect improved knowledge of building response.
- Level of training of design and construction workforce.
- Economic and zoning issues.

Some review of the experiences following earthquakes in Turkey and Mexico City may help to define these issues.

[1] ***Department of Civil Engineering, University of Texas at Austin, Austin, TX 78712, Email: jirsa@uts.cc.utexas.edu***

1.1 Turkey

The inadequacies of many low to medium-rise reinforced concrete buildings in Turkey (and Greece) have been well documented following recent earthquakes. Most low and medium-rise, residential and commercial reinforced concrete structures are designed to resist lateral forces through frame action. These structures have flexible columns and flat plate floor systems. Columns typically have large aspect ratios. In many cases, all the columns are oriented with the weak axes in the same direction. The use of "non-structural" infills above the ground floor stiffens the structure and changes the lateral force-resisting system. The columns at the first level often fail in a brittle manner. In upper stories, frames are infilled with masonry walls (hollow tiles or aerated concrete blocks) of varying strength and stiffness. The effect of the infills on frame response is generally not taken into account in design. Many buildings may have been constructed without engineering design or inspection during construction. Detailing of joints and connections, transverse reinforcement, development and splice lengths, and cover over bars is often inadequate. Floors are sometimes added without design or permit. It is interesting to note that new buildings are still being constructed that are no different from those that have performed poorly in recent earthquakes in the region. In some cases, the owners purposely build them outside the jurisdiction of building officials.

Because the upper floors of the structure are stiff, energy is dissipated through large deformations of the columns at the ground level. These columns generally do not have sufficient moment or shear capacity to resist the forces generated during a moderate to severe earthquake. The elements do not have adequate transverse reinforcement to maintain moment and shear capacity under large deformations. Continuity of reinforcement between elements is often lacking and bars may not be adequately anchored or spliced in critical locations. In addition, concrete materials are generally low strength and plain (undeformed) mild steel reinforcement is frequently used. Corrosion may cause further reductions in the bar cross-sections in many older buildings. Modifications to the structural frame or to the infill walls made by owners or occupants may also reduce the lateral resistance.

The structures are often irregular in plan because of the column orientation and/or the presence of infill walls. Plan irregularities may produce unsymmetrical frame behavior and result in torsion effects on the structure. As noted above, the elevation may be irregular as well since the ground floor is usually open space reserved for commercial purposes, storage, or parking and the upper floors may not have the same plan—especially when stories are added.

There is a clear need to reduce the risk posed by these existing buildings through an extensive rehabilitation program. However, it may be even more important to change practices within the regulatory, design, and construction communities that control the building processes. Rehabilitation techniques employed should be consistent with the capabilities of local contractors and the resources of the owners and/or occupants. To reduce the risk for as much of the population as possible, reliable and cost-effective rehabilitation approaches will be needed.

1.1 Mexico City

Many of the buildings damaged in the 1985 earthquake were slab-column frames. In general, they were quite flexible and suffered collapses when large lateral deformations weakened the slab-column connections and resulted in punching shear failures. Others failed because the column and joint detailing was inadequate for the deformation demands imposed. Because Mexico City lies in an ancient lakebed, foundation conditions are unique and difficult. The dynamic characteristics of the lakebed resulted in damage to structures that had periods close to the natural period of the lakebed—generally structures in the 3 to 10 story range. In many cases, the long duration of shaking produced damage that reduced the stiffness of the structure and lengthened the period so that it approached that of the lakebed.

Many different rehabilitation techniques were implemented in Mexico City after the 1985 earthquake. Foundation rehabilitation was time-consuming and costly and was avoided if possible. Many of the new lateral force resisting systems did not appear to be compatible with existing lateral force systems and they resulted in increased forces on the foundation.

Control of rehabilitation work was not monitored closely by building officials or owners. In many cases, structures that were undamaged or only lightly damaged during the earthquake were "rehabilitated by calculation." Designers demonstrated adequate performance by calculating the response of structures that appeared to be little different in geometry, construction quality, and building type from others that collapsed or were heavily damaged. Since there have been no large earthquake in Mexico City since 1985, there is no way of knowing how the rehabilitated—or non-rehabilitated--buildings will perform.

However, the Mexico City experience did provide a demonstration of the psychological aspects of rehabilitation and field experience. Structures that involved strengthening techniques neither visible from the outside nor apparent to the occupants did not instill the same confidence in the seismic behavior of the building, as did those that were visible and the function was clear. Seeing that changes had been made in the lateral force resisting system through the addition of braces composed of steel sections or cables resulted in the occupants returning rapidly and willingly to the building. It is interesting to note that architects and engineers were unprepared for the reactions. They had expected that the users would find the external bracing ugly. Instead, the occupants took comfort in looking out of windows that had views obstructed by braces. The braces were a reassuring reminder that a change for the better had been made. The cable braces permitted the Mexico City to strengthen many two-story school buildings in a short time and children returned to schools were no longer of concern to their parents. The importance of visual and direct transfer of knowledge should not be underestimated. It is likely that design drawings would not have made the same impression that seeing the braces did.

Another interesting aspect of the activity in Mexico City was the rehabilitation of badly damaged structures that did not appear to be worth salvaging. However, zoning ordinances had changed since the buildings were constructed, and now required that in the construction of new buildings, adequate parking had to be provided for all occupants. In considering the economics of demolition and reconstruction, the cost of providing parking in a new structure made repair of a damaged building a feasible, and often less costly, option.

2. WHY FIELD STUDIES?

Analytical programs for structural response are based largely on the data that has been obtained from laboratory studies of members or subassemblies of beams and column or walls—some have included portions of slabs to better simulate a real structure. The prediction of the response of such test elements is generally quite good. However, when the program is applied to a real structure, there is no way to judge the reliability of the results. In the few cases where response data is available, measured response has been difficult to duplicate through analysis. The brief overview of the situation in Turkey and Mexico City illustrates why such comparisons are likely to be disappointing. It is difficult to make assumptions for analysis when a number of variables that could influence analysis are not included in the programs, such as--

- Different non-structural elements may be present in existing buildings—partial or full infill walls, curtain walls, utilities, appurtenances.
- Irregularity either by virtue of the plan itself or by virtue of unsymmetrical lateral force-resisting systems that produce torsional effects in the structure.
- Differences between details, materials, and construction quality assumed in design and those in the real structure.
- Modifications made by owners.

Most of the data and knowledge available on structural response has been obtained through laboratory studies. While there are a number of laboratories around the world that are capable of conducting tests at large or full-scale, very few have the capability to test structures with multiple bays and stories. In most cases, non-structural elements are not included and the materials and construction quality may not reflect field practice. To implement performance-based engineering, the ability to predict response reliably under any load or environmental condition is fundamental. The data obtained from laboratory studies is not likely to provide the information needed for credible calibration of analytical procedures.

Data is needed from field tests with loads intentionally imposed to produce failure and from installation of sensors to monitor performance during the service life of the structure including natural loads or unintentionally applied overloads.

The difficulty in conducting field tests to failure is identifying candidate structures. Buildings scheduled for demolition are the most likely candidates, however, careful planning will be needed to take advantage of such situations. Field test equipment must be available on short notice and personnel need to be trained to move onto a site quickly and conduct tests in a short time so that the owner and contractor are not adversely impacted by the field study. The development of new sensors and data acquisition systems that provide vast recording and remote transmitting capabilities make field testing more feasible than it has been in the past. At the very least, our profession should be actively seeking to employ the new technologies on a regular basis and should be making a united, concerted effort to convince potential sponsors of building research (and owners of candidate structures) of the need for field studies.

3. ADDITIONAL ROLES OF FIELD STUDIES

While a major reason for promoting field studies is the gathering of data for calibration of design and analysis programs, there are a number of other issues that justify such studies. The use of nearly identical framing systems and construction techniques throughout Turkey and Greece is favorable for implementing design and rehabilitation approaches that-

- Are cost-effective.
- Can be monitored by building officials during construction to achieve desired quality.
- Provide reassurance to occupants that the life safety of buildings has been improved.

For example, field or large-scale laboratory tests of a few selected typical structures or elements of those structures to failure will provide critical data that would otherwise have to be assumed conservatively. Similar structures could then be rehabilitated using several different techniques and tested to failure as well. Such an approach would--

- Provide a means of calibrating evaluation techniques and improvements in performance that various rehabilitation or strengthening techniques provide.
- Demonstrate proper design and construction procedures to be followed by engineers, contractors, and owners doing their own rehabilitation or repair work. Field tests could also demonstrate the consequences of not following suggested procedures.
- Provide the public, and owners who construct their own buildings, with direct evidence that improvements can be made that will make the structures they occupy safer.

Such field tests are likely to attract considerable attention and will make participation in a rehabilitation program easier for all parties—engineers, contractors, and owners/occupants.

4. IS PBE A REALISTIC APPROACH?

Performance-based design and engineering offers great promise as an alternative to the approaches that have governed building design for the past 50 years. However, when one considers the loss of life and property that has accompanied recent earthquakes all over the world, the lack of sophisticated design techniques cannot be cited as contributing to most of those losses. Lack of knowledge of appropriate design procedures and enforcement of those procedures is more likely to be a key factor. It is imperative that we use our ability to develop advanced design procedures to find ways of converting such knowledge to design and construction guidelines that can be used to reduce the risks posed by unsophisticated buildings constructed without the benefit of trained engineers and skilled contractors. The knowledge and insight we gain in developing complex procedures should provide us with the capacity to reduce the risk in buildings ranging from simple one-room homes to high-rise office complexes. Our profession owes it to our clientele—the people who suffer when our buildings fail.

PEER REPORTS

PEER reports are available from the National Information Service for Earthquake Engineering (NISEE). To order PEER reports, please contact the Pacific Earthquake Engineering Research Center, 1301 South 46th Street, Richmond, California 94804-4698. Tel.: (510) 231-9468; Fax: (510) 231-9461.

PEER 2002/08 *Component Testing, Stability Analysis and Characterization of Buckling-Restrained Unbonded Braces™.* Cameron Black, Nicos Makris, and Ian Aiken. September 2002.

PEER 2002/07 *Seismic Performance of Pile-Wharf Connections.* Charles W. Roeder, Robert Graff, Jennifer Soderstrom, and Jun Han Yoo. December 2001.

PEER 2002/06 *The Use of Benefit-Cost Analysis for Evaluation of Performance-Based Earthquake Engineering Decisions*. Richard O. Zerbe and Anthony Falit-Baiamonte. September 2001.

PEER 2002/05 *Guidelines, Specifications, and Seismic Performance Characterization of Nonstructural Building Components and Equipment*. André Filiatrault, Constantin Christopoulos, and Christopher Stearns. September 2001.

PEER 2002/02 *The Third U.S.-Japan Workshop on Performance-Based Earthquake Engineering Methodology for Reinforced Concrete Building Structures*. July 2002.

PEER 2002/01 *Nonstructural Loss Estimation: The UC Berkeley Case Study. Mary C. Comerio and John C. Stallmeyer.* December 2001.

PEER 2001/16 *Statistics of SDF-System Estimate of Roof Displacement for Pushover Analysis of Buildings.* Anil K. Chopra, Rakesh K. Goel, and Chatpan Chintanapakdee. December 2001.

PEER 2001/15 *Damage to Bridges during the 2001 Nisqually Earthquake.* R. Tyler Ranf, Marc O. Eberhard, and Michael P. Berry. November 2001.

PEER 2001/14 *Rocking Response of Equipment Anchored to a Base Foundation.* Nicos Makris and Cameron J. Black. September 2001.

PEER 2001/13 *Modeling Soil Liquefaction Hazards for Performance-Based Earthquake Engineering.* Steven L. Kramer and Ahmed-W. Elgamal. February 2001.

PEER 2001/12 *Development of Geotechnical Capabilities in OpenSees.* Boris Jeremic. September 2001.

PEER 2001/11 *Analytical and Experimental Study of Fiber-Reinforced Elastomeric Isolators*. James M. Kelly and Shakhzod M. Takhirov. September 2001.

PEER 2001/10 *Amplification Factors for Spectral Acceleration in Active Regions.* Jonathan P. Stewart, Andrew H. Liu, Yoojoong Choi, and Mehmet B. Baturay. December 2001.

PEER 2001/09 *Ground Motion Evaluation Procedures for Performance-Based Design.* Jonathan P. Stewart, Shyh-Jeng Chiou, Jonathan D. Bray, Robert W. Graves, Paul G. Somerville, and Norman A. Abrahamson. September 2001.

PEER 2001/08 *Experimental and Computational Evaluation of Reinforced Concrete Bridge Beam-Column Connections for Seismic Performance*. Clay J. Naito, Jack P. Moehle, and Khalid M. Mosalam. November 2001.

PEER 2001/07 *The Rocking Spectrum and the Shortcomings of Design Guidelines.* Nicos Makris and Dimitrios Konstantinidis. August 2001.

PEER 2001/06 *Development of an Electrical Substation Equipment Performance Database for Evaluation of Equipment Fragilities*. Thalia Agnanos. April 1999.

PEER 2001/05 *Stiffness Analysis of Fiber-Reinforced Elastomeric Isolators.* Hsiang-Chuan Tsai and James M. Kelly. May 2001.

PEER 2001/04 *Organizational and Societal Considerations for Performance-Based Earthquake Engineering.* Peter J. May. April 2001.

PEER 2001/03 *A Modal Pushover Analysis Procedure to Estimate Seismic Demands for Buildings: Theory and Preliminary Evaluation.* Anil K. Chopra and Rakesh K. Goel. January 2001.

PEER 2001/02 *Seismic Response Analysis of Highway Overcrossings Including Soil-Structure Interaction.* Jian Zhang and Nicos Makris. March 2001.

PEER 2001/01 *Experimental Study of Large Seismic Steel Beam-to-Column Connections.* Egor P. Popov and Shakhzod M. Takhirov. November 2000.

PEER 2000/10 *The Second U.S.-Japan Workshop on Performance-Based Earthquake Engineering Methodology for Reinforced Concrete Building Structures.* March 2000.

PEER 2000/09 *Structural Engineering Reconnaissance of the August 17, 1999 Earthquake: Kocaeli (Izmit), Turkey.* Halil Sezen, Kenneth J. Elwood, Andrew S. Whittaker, Khalid Mosalam, John J. Wallace, and John F. Stanton. December 2000.

PEER 2000/08 *Behavior of Reinforced Concrete Bridge Columns Having Varying Aspect Ratios and Varying Lengths of Confinement.* Anthony J. Calderone, Dawn E. Lehman, and Jack P. Moehle. January 2001.

PEER 2000/07 *Cover-Plate and Flange-Plate Reinforced Steel Moment-Resisting Connections.* Taejin Kim, Andrew S. Whittaker, Amir S. Gilani, Vitelmo V. Bertero, and Shakhzod M. Takhirov. September 2000.

PEER 2000/06 *Seismic Evaluation and Analysis of 230-kV Disconnect Switches.* Amir S. J. Gilani, Andrew S. Whittaker, Gregory L. Fenves, Chun-Hao Chen, Henry Ho, and Eric Fujisaki. July 2000.

PEER 2000/05 *Performance-Based Evaluation of Exterior Reinforced Concrete Building Joints for Seismic Excitation.* Chandra Clyde, Chris P. Pantelides, and Lawrence D. Reaveley. July 2000.

PEER 2000/04 *An Evaluation of Seismic Energy Demand: An Attenuation Approach.* Chung-Che Chou and Chia-Ming Uang. July 1999.

PEER 2000/03 *Framing Earthquake Retrofitting Decisions: The Case of Hillside Homes in Los Angeles.* Detlof von Winterfeldt, Nels Roselund, and Alicia Kitsuse. March 2000.

PEER 2000/02 *U.S.-Japan Workshop on the Effects of Near-Field Earthquake Shaking.* Andrew Whittaker, ed. July 2000.

PEER 2000/01 *Further Studies on Seismic Interaction in Interconnected Electrical Substation Equipment.* Armen Der Kiureghian, Kee-Jeung Hong, and Jerome L. Sackman. November 1999.

PEER 1999/14 *Seismic Evaluation and Retrofit of 230-kV Porcelain Transformer Bushings*. Amir S. Gilani, Andrew S. Whittaker, Gregory L. Fenves, and Eric Fujisaki. December 1999.

PEER 1999/13 *Building Vulnerability Studies: Modeling and Evaluation of Tilt-up and Steel Reinforced Concrete Buildings.* John W. Wallace, Jonathan P. Stewart, and Andrew S. Whittaker, editors. December 1999.

PEER 1999/12 *Rehabilitation of Nonductile RC Frame Building Using Encasement Plates and Energy-Dissipating Devices.* Mehrdad Sasani, Vitelmo V. Bertero, James C. Anderson. December 1999.

PEER 1999/11 *Performance Evaluation Database for Concrete Bridge Components and Systems under Simulated Seismic Loads.* Yael D. Hose and Frieder Seible. November 1999.

PEER 1999/10 *U.S.-Japan Workshop on Performance-Based Earthquake Engineering Methodology for Reinforced Concrete Building Structures.* December 1999.

PEER 1999/09 *Performance Improvement of Long Period Building Structures Subjected to Severe Pulse-Type Ground Motions*. James C. Anderson, Vitelmo V. Bertero, and Raul Bertero. October 1999.

PEER 1999/08 *Envelopes for Seismic Response Vectors.* Charles Menun and Armen Der Kiureghian. July 1999.

PEER 1999/07 *Documentation of Strengths and Weaknesses of Current Computer Analysis Methods for Seismic Performance of Reinforced Concrete Members.* William F. Cofer. November 1999.

PEER 1999/06 *Rocking Response and Overturning of Anchored Equipment under Seismic Excitations.* Nicos Makris and Jian Zhang. November 1999.

PEER 1999/05 *Seismic Evaluation of 550 kV Porcelain Transformer Bushings.* Amir S. Gilani, Andrew S. Whittaker, Gregory L. Fenves, and Eric Fujisaki. October 1999.

PEER 1999/04 *Adoption and Enforcement of Earthquake Risk-Reduction Measures.* Peter J. May, Raymond J. Burby, T. Jens Feeley, and Robert Wood.

PEER 1999/03 *Task 3 Characterization of Site Response General Site Categories*. Adrian Rodriguez-Marek, Jonathan D. Bray, and Norman Abrahamson. February 1999.

PEER 1999/02 *Capacity-Demand-Diagram Methods for Estimating Seismic Deformation of Inelastic Structures: SDF Systems*. Anil K. Chopra and Rakesh Goel. April 1999.

PEER 1999/01 *Interaction in Interconnected Electrical Substation Equipment Subjected to Earthquake Ground Motions.* Armen Der Kiureghian, Jerome L. Sackman, and Kee-Jeung Hong. February 1999.

PEER 1998/08 *Behavior and Failure Analysis of a Multiple-Frame Highway Bridge in the 1994 Northridge Earthquake.* Gregory L. Fenves and Michael Ellery. December 1998.

PEER 1998/07 *Empirical Evaluation of Inertial Soil-Structure Interaction Effects.* Jonathan P. Stewart, Raymond B. Seed, and Gregory L. Fenves. November 1998.

PEER 1998/06 *Effect of Damping Mechanisms on the Response of Seismic Isolated Structures.* Nicos Makris and Shih-Po Chang. November 1998.

PEER 1998/05 *Rocking Response and Overturning of Equipment under Horizontal Pulse-Type Motions.* Nicos Makris and Yiannis Roussos. October 1998.

PEER 1998/04 *Pacific Earthquake Engineering Research Invitational Workshop Proceedings, May 14–15, 1998: Defining the Links between Planning, Policy Analysis, Economics and Earthquake Engineering.* Mary Comerio and Peter Gordon. September 1998.

PEER 1998/03 *Repair/Upgrade Procedures for Welded Beam to Column Connections.* James C. Anderson and Xiaojing Duan. May 1998.

PEER 1998/02 *Seismic Evaluation of 196 kV Porcelain Transformer Bushings.* Amir S. Gilani, Juan W. Chavez, Gregory L. Fenves, and Andrew S. Whittaker. May 1998.

PEER 1998/01 *Seismic Performance of Well-Confined Concrete Bridge Columns.* Dawn E. Lehman and Jack P. Moehle. December 2000.